

# **Characterisation and quantification of microstructure, physicochemical and functional properties of oven and forced convection continuous tumble roasted cereal grains**

by

**Letitia Schoeman**



*Dissertation presented for the degree of  
Doctor of Philosophy (Food Science) in the  
Faculty of AgriSciences at  
Stellenbosch University*

The financial assistance of the National Research Foundation (NRF) towards this research is hereby acknowledged. Opinions expressed and conclusions arrived at are those of the author and are not necessarily to be attributed to the NRF

**Supervisor:** Prof Marena Manley  
**Co-supervisor:** Dr Anton du Plessis

March 2017

## DECLARATION

By submitting this dissertation electronically, I declare that the entirety of the work contained therein is my own, original work, that I am the sole author thereof (save to the extent explicitly otherwise stated), that reproduction and publication thereof by Stellenbosch University will not infringe any third party rights and that I have not previously in its entirety or in part submitted it for obtaining any qualification.

This dissertation includes two original papers published in peer-reviewed journals and four unpublished publications. The development and writing of the papers (published and unpublished) were the principal responsibility of myself and, for each of the cases where this is not the case, a declaration is included in the dissertation indicating the nature and extent of the contributions of co-authors.

Letitia Schoeman

March 2017

## ABSTRACT

The use of roasted cereal grains in foods can improve organoleptic properties, enhance shelf life, ease incorporation into ready-to-eat products and increase antioxidant activity. Structural, physicochemical and functional changes will inevitably occur during roasting and this study aimed to investigate these properties. X-ray micro-computed tomography ( $\mu$ CT) was used as a non-destructive technique for characterising and quantifying microstructural changes in individual cereal grains induced by conventional oven and forced convection continuous tumble (FCCT) roasting at 180°C for 140 s. X-ray  $\mu$ CT uses differences in X-ray attenuation arising from differences in density within a sample.

X-ray tomograms of the raw and roasted wheat and maize kernels were obtained, using a General Electric Phoenix model V|Tome|X L240 X-ray  $\mu$ CT system with a source voltage of 60 kV and an electron current set at 240  $\mu$ A. Analysis of the whole kernel and regions-of-interest (ROIs) was performed with VGStudio Max 2.2 three-dimensional (3D) software. Qualitative results were depicted as two-dimensional (2D) transmission images and 3D volumes. Internal structural changes were observed as a loss of endosperm integrity, detected as a decrease in attenuation. For both cereal grains oven roasting was associated with a larger increase in kernel volume (wheat=4.47%; maize=10.76%) than FCCT roasting (wheat=1.57%; maize=3.41%), as well as larger relative density decreases (wheat=2.76%; maize=6.33%) in comparison to FCCT roasting (wheat=0.55%; maize=1.92%). During FCCT roasting the material density (excluding air) remained unaffected.

Structural changes can strongly influence physicochemical and functional properties. Kernel hardness and hectolitre mass (HLM) can be helpful to assess the milling yield, which was not affected ( $P>0.05$ ) by either roasting methods. Scanning electron microscopy (SEM) illustrated the starch-protein morphology, where both roasting methods resulted in a partially disintegrated protein network and swollen and/or ruptured starch granules in the oven-roasted samples. Quantification of these structural differences included crystallinity determinations using X-ray diffraction (XRD), thermal properties using differential scanning calorimetry (DSC) and pasting properties employing a Rapid Visco Analyser (RVA). The reduction in crystallinity for both FCCT (wheat=0.12%; maize=0.45%) and oven (wheat=0.16%; maize=1.83%) roasting was consistent with the decrease in gelatinisation enthalpy ( $\Delta H$ ). Only partial gelatinisation occurred in both the oven (wheat=17.16%; maize=25.27%) and FCCT-roasted (wheat=10.14%; maize=16.23%) samples.

Oven roasting caused more adverse changes in most of the measured properties, being a more destructive process. With FCCT roasting the samples are continuously moving, resulting in an even heat transfer in comparison to oven roasting where the samples are stationary. FCCT roasting maintained more of the favourable characteristics, i.e. microstructure, hardness and milling yield and will thus result in a more acceptable final product.

This study demonstrated the capability of X-ray  $\mu$ CT in combination with image analysis as a non-invasive technique to study microstructural changes in cereal grains, induced by roasting, both in a qualitative and quantitative manner and at a relatively high spatial resolution of 12 micron. The results integrate qualitative and quantitative information that could be useful for understanding structure-property relationships in terms of further processing and utilisation, e.g. the development of value-added products with improved digestibility and viscosity or delayed staling phenomenon.



## UITTREKSEL

Die gebruik van geroosterde grane in voedsel kan organoleptiese eienskappe verbeter, rakleef tyd verleng, byvoeging in gereed-vir-eet produkte en ontbytgrane vergemaklik en antioksidant aktiwiteit verhoog. Dit is onvermydelik dat strukturele, fisies-chemiese en funksionele veranderinge sal plaasvind tydens rooster en dus was die doel van die studie om hierdie eienskappe te ondersoek. X-straal mikro-berekende tomografie ( $\mu$ BT) was gebruik as 'n nie-vernietigende tegniek vir die karakterisering en kwantifisering van mikrostrukturele veranderinge in individuele grane, geïnduseer deur konvensionele oond- en geforseerde konveksie aaneenlopende tuimel (GKAT) rooster by 180°C vir 140 s. X-straal  $\mu$ BT gebruik verskille in X-straal attenuasie, wat voortspruit uit verskille in digtheid in 'n monster.

X-straal tomogramme van die rou en geroosterde koring en mieliepitte is verkry met 'n General Electric Phoenix model V|Tome|X L240 X-straal  $\mu$ BT sisteem met 'n bronspanning van 60 kV en 'n elektronstroom gestel op 240  $\mu$ A. Analise van die heelpit en areas-van-belang (AVBs) is uitgevoer met VGStudio Max 2.2 drie-dimensionele (3D) sagteware. Kwalitatiewe resultate is uitgebeeld as twee-dimensionele (2D) transmissiebeelde en 3D volumes. Interne strukturele veranderinge is waargeneem as 'n verlies van endosperm integriteit, bespeur as 'n afname in attenuasie. Vir beide grane is oond rooster geassosieer met 'n groter toename in pitvolume (koring=4.47%; mielie=10.76%;) as vir GKAT rooster (koring=1.57%; mielie=3.41%), sowel as 'n groter afname in relatiewe digtheid (koring=2.76%; mielie=6.33%) in vergelyking met GKAT rooster (koring=0.55%; mielie=1.92%). Gedurende GKAT rooster het die materiaal digtheid (lug uitgesluit) onveranderd gebly.

Strukturele veranderinge kan fisies-chemiese en funksionele eienskappe beïnvloed. Pit hardheid en hektolitermassa (HLM) is nuttig om maalopbrengs te evalueer, wat nie geaffekteer is ( $P>0.05$ ) deur beide rooster metodes. Skandeer-elektronmikroskopie (SEM) het die stysel-proteïen morfologie geïllustreer, waar beide rooster metodes tot 'n gedeeltelike gedisintegreerde proteïen netwerk en geswelde en/of gebarste stysel granules in die oond geroosterde monsters gelei het. Kwantifisering van hierdie strukturele veranderinge het kristalliniteit-bepalings met X-straal diffraksie (XSD), termiese eienskappe met differensiële skandeer kalorimetrie (DSK) en plak eienskappe met behulp van 'n Rapid Visco Analyser (RVA) ingesluit. Die afname in kristalliniteit vir beide GKAT (koring=0.12%; mielie=0.45%) en oond (koring=0.16%; mielie=1.83%) rooster was konsekwent met die afname in gelatinisasie entalpie ( $\Delta H$ ). Slegs gedeeltelike gelatinisasie het in beide die oond (koring=17.16%; mielie=25.27%) en GKAT geroosterde (koring=10.14%; mielie=16.23%) monsters plaasgevind.

Oond rooster het meer ongunstige veranderinge in meeste van die gemete eienskappe veroorsaak, wat 'n meer vernietigende proses impliseer. Met GKAT rooster beweeg die monsters voortdurend, wat lei tot 'n eweredige hitte-oordrag in vergelyking met oond rooster waar die monsters stilstaande is. Tydens GKAT rooster het meeste van die gunstige eienskappe, soos

mikrostruktuur, hardheid en maalopbrengs behoue gebly en dit sal aanleiding gee tot 'n meer aanvaarbare eindproduk.

Hierdie studie demonstreer die vermoë van X-straal  $\mu$ BT in kombinasie met beeld-analise as 'n nie-vernietigende tegniek om mikrostrukturele veranderinge in graan, veroorsaak deur rooster, in beide 'n kwalitatiewe en kwantitatiewe wyse en teen 'n relatiewe hoë ruimtelike resolusie van 12 mikron te bestudeer. Die resultate integreer kwalitatiewe en kwantitatiewe inligting wat nuttig is vir die begrip van struktuur-eienskap verhoudings in terme van verdere verwerking en gebruik, byvoorbeeld vir die ontwikkeling van toegevoegde waarde produkte met verbeterde verteerbaarheid en viskositeit of vertraagde verouderingsverskynsel.

## ACKNOWLEDGEMENTS

Firstly I would like to thank my heavenly Father, who blessed me with this opportunity and for granting me the health, motivation and strength to succeed. Without Him it would not have been possible. All glory goes to Him.

Additionally I would like to express my most sincere gratitude to the following people and institutions for their contribution towards the successful completion of this study:

Professor Marena Manley, my supervisor, for her professional supervision, guidance, advice, motivation and confidence in my abilities. Her attention to detail, passion for cereal science and insight were invaluable to the completion of this study. There are not enough words to express my gratitude;

My co-supervisor, Dr Anton du Plessis, for his advice on X-ray  $\mu$ CT and assistance with skeletonization;

Doctor Paul Williams for his support and encouragement and the willingness to go the extra mile whenever help or advice was needed;

Stephan le Roux from the Central Analytical Facility (CAF) for assistance in the use of the X-ray  $\mu$ CT system and help and advice with data analysis;

Johan du Plooy from Agricol for allowing me to use the forced convection continuous tumble (FCCT) roaster at their facility, free of charge;

Prof Martin Kidd, from the Centre of Statistical Consultation, Stellenbosch University, for his advice in planning the experiments and for his valuable statistical analysis;

The National Research Foundation (NRF) for a bursary;

The Winter Cereal Trust for a bursary and the provision of funding to attend the annual Winter Cereal Trust meetings in Pretoria (2014-2016);

Stellenbosch University for a merit bursary and arrangement of workshops by the Postgraduate and International Office (2014-2016);

The Faculty of AgriSciences for awarding me the postgraduate travel award to attend the 29<sup>th</sup> EFFoST International Conference in Athens, Greece (10-12 November 2015);

SAAFoST for awarding me the Brian Koeppen Memorial Scholarship, which made it possible to attend the IUFoST 18th World Congress of Food Science and Technology in Dublin, Ireland (21-25 August 2016);

Sasko, a division of Pioneer Foods, Essential Grains, Research and Development for the use of their facilities and equipment; especially Kim O’Kennedy and Carien Roets for their valued assistance and generosity

Dawie de Villiers from the Department of Chemistry for his assistance with DSC analysis;

Gratitude goes to Dr Remy Bucher, from iThemba Labs, for XRD analysis;

Anchen Lombard for her assistance with travel arrangements;

All the staff and postgraduate students of the Food Science Department, thank you for your motivation and support;

The cereal science research group: Anina Guelpa, Jason Zhang, Shuaibu Bala, Sandra Balet, Irene Orina, Kate Sendin, Terry-Lee Kammies, Megan Kleyn and Pholisa Dumalisile for their continuous interest and kind support;

My parents, sister, grandfather, family and friends whose unconditional love, never-ending support, encouragement and patience have meant more to me than words can express. Thank you for the many hours spent listening to my seminars! I am truly grateful for your prayers and continuous interest in my work; and

Wynand van der Westhuizen for always believing in me; your unwavering love, patience and support, as well as your endless encouragement, has kept me motivated throughout this journey.

“Trust in the Lord with all your heart and lean not on your own understanding;  
in all your ways acknowledge him, and he will make your paths straight.”

(Proverbs 3:5-6)

## TABLE OF CONTENTS

<b>DECLARATION</b>	i
<b>ABSTRACT</b>	ii
<b>UITTREKSEL</b>	iv
<b>ACKNOWLEDGEMENTS</b>	vi
<b>LIST OF FIGURES</b>	xvii
<b>LIST OF TABLES</b>	xxi
<b>LIST OF ABBREVIATIONS</b>	xxiii
<b>CHAPTER 1: Introduction</b>	1
References	6
<b>DECLARATION BY THE CANDIDATE</b>	13
<b>CHAPTER 2: Literature review 1 (X-ray micro-computed tomography (<math>\mu</math>CT) for non-destructive characterisation of food microstructure)</b>	14
Abstract	14
Introduction	15
Fundamental principles of X-ray CT	16
Background	16
Experimental setup and image acquisition	16
X-ray CT systems	19
Image processing and analysis	20
Image processing and segmentation	21
Image analysis	22
3D and 2D interpretation and visualisation of X-ray CT images	23
2D vs. 3D analysis	24
3D modelling	26
Information provided by X-ray $\mu$ CT: Qualitative and quantitative	27
Qualitative X-ray CT data analysis	27
Quantitative X-ray CT data analysis	27
Image texture analysis	28
Principles	28
Applications	29
Food applications	29
Meat and fish	35
Dairy products	35

<i>Fruit and vegetables</i> .....	35
<i>Cereals and cereal products</i> .....	37
<i>Coffee beans and nuts</i> .....	38
<i>Confectionary</i> .....	39
<i>Dough and baked products</i> .....	39
<b>Limitations</b> .....	40
<i>Time and financial constraints</i> .....	40
<i>Imaging artefacts</i> .....	40
<i>Operator dependency</i> .....	41
<b>Conclusion</b> .....	41
<b>References</b> .....	41
<b>DECLARATION BY THE CANDIDATE</b> .....	50
<b>CHAPTER 3: Literature review 2 (Cereal grain roasting methods and applications: a review)</b> .....	51
<b>Abstract</b> .....	51
<b>Introduction</b> .....	51
<b>Maize</b> .....	53
<i>Background</i> .....	53
<i>Morphology</i> .....	53
<b>Wheat</b> .....	54
<i>Background</i> .....	54
<i>Morphology</i> .....	54
<b>Traditional and current roasting methods</b> .....	55
<i>Sand roasting</i> .....	56
<i>Fluidised bed roasting (FBR)</i> .....	56
<i>Flame roasting</i> .....	57
<i>Microwave roasting</i> .....	58
<i>Gun and oven puffing</i> .....	59
<i>Continuous roasting</i> .....	59
<i>Forced convection continuous tumble (FCCT) roasting</i> .....	60
<b>Effect of roasting on food and especially cereal grains</b> .....	62
<i>Nutrition</i> .....	63
<i>Sensory</i> .....	64
<i>Microstructure</i> .....	65
<b>Roasting applications</b> .....	65

<i>General</i> .....	65
<i>Cereal grains</i> .....	66
<b>Conclusion</b> .....	74
<b>References</b> .....	74
<b>DECLARATION BY THE CANDIDATE</b> .....	84
<b>CHAPTER 4: Non-destructive characterisation and quantification of the effect of conventional oven and forced convection roasting on the three-dimensional microstructure of whole wheat kernels using X-ray micro-computed tomography (<math>\mu</math>CT)</b> .....	85
<b>Abstract</b> .....	85
<b>Introduction</b> .....	86
<b>Materials and methods</b> .....	88
<i>Wheat samples</i> .....	88
<i>Roasting</i> .....	89
<i>X-ray micro-computed tomography (<math>\mu</math>CT) image acquisition</i> .....	89
<i>Image processing and analysis</i> .....	90
<u>Segmentation and defining regions-of-interest (ROIs)</u> .....	91
<u>Quantitative measurements</u> .....	91
<i>Experimental design</i> .....	92
<i>Statistical analysis</i> .....	92
<b>Results and discussion</b> .....	93
<i>Visual assessment</i> .....	93
<i>Qualitative image analysis</i> .....	95
<u>Porosity, internal cracks and cavities (2D analysis)</u> .....	95
<u>Porosity, internal cracks and cavities (3D analysis)</u> .....	99
<i>Quantitative analysis</i> .....	99
<u>Volumes-of-interest (VOIs)</u> .....	100
<u>Porosity analysis</u> .....	101
<u>Expansion ratio (ER)</u> .....	101
<u>Density analysis</u> .....	102
<b>Conclusion</b> .....	104
<b>References</b> .....	105
<b>DECLARATION BY THE CANDIDATE</b> .....	110



<b>CHAPTER 5: Oven and forced convection continuous tumble (FCCT) roasting: effect on physicochemical, structural and functional properties of wheat</b>	111
<b>Abstract</b>	111
<b>Introduction</b>	111
<b>Materials and methods</b>	115
<i>Wheat samples</i>	115
<i>Tempering of test run for FCCT roasting</i>	116
<i>Roasting</i>	116
<i>Grinding of wheat samples</i>	116
<i>Experimental design</i>	117
<i>Physicochemical analyses</i>	118
<u>Weight loss</u>	118
<u>Bulk density and puffing index (PI)</u>	118
<u>Moisture content</u>	118
<u>Milling and flour yield</u>	118
<u>Hectolitre mass (HLM)</u>	119
<u>Crude protein</u>	119
<u>Particle size index (PSI)</u>	119
<i>Structural analyses</i>	120
<u>Scanning electron microscopy (SEM)</u>	120
<u>X-ray diffraction (XRD)</u>	120
<i>Functional analyses</i>	120
<u>Water absorption capacity (WAC), water solubility index (WSI) and flour dispersibility (FD)</u>	120
<u>Differential scanning calorimetry (DSC)</u>	121
<u>Pasting properties and <math>\alpha</math>-amylase activity</u>	121
<u>Rheology: Mixograph and Alveograph</u>	122
<i>Statistical analysis</i>	123
<b>Results and discussion</b>	123
<i>Physicochemical analyses</i>	123
<u>Weight loss</u>	123
<u>Bulk density and puffing index (PI)</u>	125
<u>Moisture content</u>	125
<u>Milling and flour yield</u>	126

<u>Hectolitre mass (HLM)</u> .....	126
<u>Crude protein</u> .....	127
<u>Particle size index (PSI)</u> .....	127
<i>Structural analyses</i> .....	128
<u>Scanning electron microscopy (SEM)</u> .....	128
<u>X-ray diffraction (XRD)</u> .....	130
<i>Functional analyses</i> .....	131
<u>Water absorption capacity (WAC), water solubility index (WSI) and flour dispersibility (FD)</u> .....	131
<u>Differential scanning calorimetry (DSC)</u> .....	132
<u>Pasting properties and <math>\alpha</math>-amylase activity</u> .....	133
<u>Rheology: Mixograph and Alveograph</u> .....	136
<b>Conclusion</b> .....	137
<b>References</b> .....	138
<b>DECLARATION BY THE CANDIDATE</b> .....	146
<b>CHAPTER 6: Effect of oven and forced convection continuous tumble (FCCT) roasting on the microstructure and dry milling properties of white maize</b> .....	147
<b>Abstract</b> .....	147
<b>Introduction</b> .....	148
<b>Materials and methods</b> .....	150
<i>Maize samples</i> .....	150
<i>Roasting</i> .....	150
<i>X-ray micro-computed tomography (<math>\mu</math>CT) image acquisition</i> .....	151
<i>Image processing and analysis</i> .....	151
<u>Segmentation and defining ROIs</u> .....	153
<u>Quantitative measurements</u> .....	153
<i>Dry milling properties</i> .....	154
<i>Statistical analysis</i> .....	155
<b>Results and discussion</b> .....	155
<i>Visual assessment</i> .....	155
<i>Qualitative image analysis</i> .....	157
<u>Internal cracks, cavities, pores and porosity (2D analysis)</u> .....	157
<u>Porosity, cavities and pores (3D analysis)</u> .....	159
<i>Quantitative microstructural analysis</i> .....	160

<u>Volume-of-interest</u> .....	160
<u>Percentage object volume (POV)</u> .....	163
<u>Porosity (cavities and pores)</u> .....	163
<u>Expansion ratio (ER)</u> .....	165
<u>Endosperm ratios</u> .....	166
<u>Relative density analysis</u> .....	166
<i>Dry milling properties</i> .....	169
<b>Conclusion</b> .....	169
<b>References</b> .....	170
<b>DECLARATION BY THE CANDIDATE</b> .....	175
<b>CHAPTER 7: Physicochemical, structural and functional properties of oven and forced convection continuous tumble (FCCT) roasted maize</b> .....	176
<b>Abstract</b> .....	176
<b>Introduction</b> .....	176
<b>Materials and methods</b> .....	180
<i>Maize samples</i> .....	180
<i>Tempering of test run sample before FCCT roasting</i> .....	180
<i>Roasting</i> .....	181
<i>Grinding of maize samples</i> .....	181
<i>Experimental design</i> .....	181
<i>Physicochemical analyses</i> .....	181
<u>Weight loss</u> .....	181
<u>Bulk density and puffing index (PI)</u> .....	181
<u>Moisture content</u> .....	181
<u>Crude protein</u> .....	182
<u>Particle size index (PSI)</u> .....	182
<i>Structural analyses</i> .....	183
<u>Scanning electron microscopy (SEM)</u> .....	183
<u>X-ray diffraction (XRD)</u> .....	184
<i>Functional analyses</i> .....	185
<u>Water absorption capacity (WAC) and water solubility index (WSI)</u> .....	185
<u>Flour dispersibility (FD)</u> .....	185
<u>Differential scanning calorimetry (DSC)</u> .....	185
<u>Pasting properties and <math>\alpha</math>-amylase activity using the RVA</u> .....	185

<i>Statistical analysis</i> .....	187
<b>Results and discussion</b> .....	187
<i>Physicochemical analyses</i> .....	187
<u>Weight loss</u> .....	187
<u>Bulk density and puffing index (PI)</u> .....	187
<u>Moisture content</u> .....	188
<u>Crude protein</u> .....	188
<u>PSI (c/f)</u> .....	189
<i>Structural analyses</i> .....	189
<u>Scanning electron microscopy (SEM)</u> .....	189
<u>X-ray diffraction (XRD)</u> .....	193
<i>Functional analyses</i> .....	195
<u>Water absorption capacity (WAC) and water solubility index (WSI)</u> .....	195
<u>Flour dispersibility (FD)</u> .....	195
<u>Differential scanning calorimetry (DSC)</u> .....	196
<u>Pasting properties and <math>\alpha</math>-amylase activity using the RVA</u> .....	198
<b>Conclusion</b> .....	200
<b>References</b> .....	201
<b>CHAPTER 8: General discussion and conclusions</b> .....	209
<b>References</b> .....	216
<b>APPENDICES</b> .....	219
<b>Appendix A: X-ray <math>\mu</math>CT acquisition and reconstruction process of wheat kernels</b> .....	219
<b>Appendix B: Qualitative image analysis of wheat kernels</b> .....	220
<b>Appendix C: Preliminary roasting trials</b> .....	226
<b>Appendix D: X-ray <math>\mu</math>CT instrumentation</b> .....	227
<b>Appendix E: Optimising X-ray <math>\mu</math>CT scanning parameters</b> .....	229
<b>Appendix F: Stacking of X-ray <math>\mu</math>CT slices</b> .....	230
<b>Appendix G: Image and histogram analysis</b> .....	231
<b>Appendix H: Segmentation and defining regions-of-interest</b> .....	233

<i>Segmentation</i> .....	226
<i>Regions-of-interest</i> .....	228
<i>Reference standard as ROI</i> .....	228
<i>Germ as ROI</i> .....	229
<i>Floury and vitreous endosperm as ROI</i> .....	231
<b>Appendix I: Quantitative measurements</b> .....	244
<b>Appendix J: Qualitative image analysis of maize kernels</b> .....	246
<b>Appendix K: 2D and 3D interpretation and visualisation of X-ray <math>\mu</math>CT images</b> .....	248
<b>Appendix L: Clipping</b> .....	253
<b>Appendix M: Stress cracks</b> .....	255
<b>Appendix N: Cavity analysis</b> .....	256
<b>Appendix O: Pore network analysis</b> .....	260
<b>Appendix P: Porosity (pores and cavities) analysis in three dimensions</b> .....	263
<b>References</b> .....	266

## LIST OF FIGURES

<b>Figure 2.1.</b> Schematic illustration of the measurement principle of X-ray CT. An object is exposed to collimated X-rays, generated by the X-ray tube and the detector converts the X-rays into digital radiographs.....	17
<b>Figure 2.2.</b> Representation of (a) the reconstruction process where a 3D volume is created from the 2D projection images and the illustration of (b) the stacking of 2D slices to obtain (c) a 3D image and (d) a clipped image.....	18
<b>Figure 2.3.</b> Schematic illustration of a typical image processing and analysis procedure used e.g. when analysing a maize kernel. Images with a resolution of 12 $\mu\text{m}$ were obtained from a source voltage of 60 kV and an electron current set at 240 $\mu\text{A}$ (General Electric Phoenix V Tome X L240 $\mu\text{CT}$ instrument).....	21
<b>Figure 2.4.</b> Illustration of the different X-ray image views (horizontal, frontal and sagittal) of a maize kernel. Two-dimensional views are shown on the left and the corresponding section in the 3D view on the right. These images were produced using a General Electric Phoenix V Tome X L240 $\mu\text{CT}$ instrument with settings of 60 kV and 240 $\mu\text{A}$ and a voxel size (resolution) of 12 $\mu\text{m}$ ....	24
<b>Figure 2.5.</b> Stack of seven polymer discs, used for the density calibration, along with eight maize kernels with (a) showing the floral oasis, used for mounting, and (b) with the mounting material removed. Two-dimensional X-ray $\mu\text{CT}$ slice images of a (c) hard and (d) soft maize kernel illustrating distinct, large cavities (marked with white circles) present in mostly the floury endosperm. Cavities are shown as black in X-ray images.....	37
<b>Figure 2.6.</b> Three-dimensional visualisation of the volume size distribution (indicated by the colour scale bar) of the porosity (cavities and pores) in a maize kernel (a) before and (b) after roasting. In the raw kernel separate cavities and pores are illustrated by different colours. In the roasted kernel the cavities and pores are interconnected, respectively, thus representing the cavity (yellow) and pore (blue) networks.....	38
<b>Figure 3.1.</b> Structure of a maize kernel displaying the location of the basic constituents (Anonymous., 1996a).....	54
<b>Figure 3.2.</b> Illustration of the internal structure of a wheat kernel (Anonymous., 1996b).....	55
<b>Figure 3.3.</b> A schematic diagram of a fluidised bed roaster (Murthy <i>et al.</i> , 2008).....	57
<b>Figure 3.4.</b> Raw and puffed cereal grains with the expanded structure clearly visible from the puffed kernels (Mariotti <i>et al.</i> , 2006).....	60
<b>Figure 3.5.</b> Illustration of (a) the main components and (b) internal set-up of the forced convection continuous tumble (FCCT) roaster.....	62
<b>Figure 3.6.</b> Key factors influencing cereal product quality. The figure shows the variables involved and the systematic approaches to obtain an optimal procedure that integrates raw materials and processing to obtain an acceptable end product (adapted from Poutanen <i>et al.</i> 2014).....	63

<b>Figure 3.7.</b> Scanning electron micrographs of raw (R), sand under roasted (S1), hot air under roasted (H1), sand optimum roasted (S2), hot air optimum roasted (H2), sand over roasted (S3) and hot air over roasted (H3) wheat (Murthy <i>et al.</i> , 2008).....	69
<b>Figure 4.1.</b> Flow diagram of experimental design for determining the effect of oven and FCCT roasting on the microstructure of whole wheat kernels using X-ray $\mu$ CT and image analysis.....	93
<b>Figure 4.2.</b> Digital (Canon SX40 digital camera, Canon, Ohtaku, Tokyo, Japan) images of the same wheat kernels before and after roasting with (a) and (b) raw, (c) and (d) FCCT-roasted, (e) and (f) raw, and (g) and (h) oven-roasted. The cross-sectional digital images of (i) raw, (j) FCCT-roasted and (k) oven-roasted kernels reveals the internal structure.....	94
<b>Figure 4.3.</b> Grey scale 2D tomographic images of the different views (frontal, horizontal and sagittal) of whole wheat kernels before and after FCCT and oven roasting (average dimensions: length= $6.02 \pm 0.38$ mm; width= $3.32 \pm 0.27$ mm; depth= $3.22 \pm 0.32$ mm).....	97
<b>Figure 4.4.</b> 2D slice images (centre slice) of the spatial distribution of the porous network in wheat kernels before and after roasting, with the voids (total air) selected as ROI. The air filled pores and cavities are displayed in yellow and outlined with blue, while the kernel matrix is grey (average dimensions: length= $6.02 \pm 0.38$ mm; width= $3.32 \pm 0.27$ mm; depth= $3.22 \pm 0.32$ mm).....	98
<b>Figure 4.5.</b> 2D images (a-c) [(a) horizontal, (b) sagittal and (c) frontal views] and 3D volume rendering (d) of the porosity in a raw wheat kernel. In the 3D volume the visualisation of the porosity volume size distribution is characterised in yellow and the kernel structure (material) is represented as transparent (kernel dimensions: length=5.46 mm; width=2.59 mm; depth=2.70 mm).....	99
<b>Figure 4.6.</b> Illustration of the use of the Volume analyser tool on a (a) raw sample where the whole kernel was selected as VOI ( $28.12 \text{ mm}^3$ ) and (b) oven-roasted sample where the air (yellow) was selected as VOI ( $5.44 \text{ mm}^3$ ) (kernel dimensions: length=6.24 mm; width=3.56 mm; depth=3.27 mm).....	101
<b>Figure 4.7.</b> Histograms illustrating the grey value distribution in images of whole (a) FCCT-roasted and (b) oven-roasted kernels and the air selected as ROI in (c) FCCT-roasted and (d) oven-roasted kernels. The top three values in the tables indicate the minimum, maximum and mean grey values, respectively.....	103
<b>Figure 5.1.</b> A simplified flow diagram of the roasting and analyses procedures used. HLM= hectolitre mass; PSI= particle size index; SEM= scanning electron microscopy; XRD= X-ray diffraction; WAC= water absorption capacity; WSI= water solubility index; FD= flour dispersibility; DSC= differential scanning calorimetry; RVA= Rapid Visco Analyser.....	117
<b>Figure 5.2.</b> Scanning electron micrographs of a cross section of (a) control, (b) FCCT-roasted and (c) oven-roasted wheat kernels, illustrating the (1) whole kernel at a lower magnification (scale bar = 200 $\mu\text{m}$ ) and (2) endosperm and (3) aleurone layer at a higher magnification (scale bar = 10 $\mu\text{m}$ ). Large A-type and small B-type starch granules are identified with arrows in the endosperm region. P=protein matrix; F= fragmented protein strands.....	129

<b>Figure 5.3.</b> XRD traces of the control, FCCT and oven-roasted wheat flour samples. The prominent peaks for A-type crystallinity are indicated with dashed vertical lines.....	130
<b>Figure 5.4.</b> RVA pasting profiles of a representative (a) control, (b) FCCT-roasted and (c) oven-roasted whole wheat flour. The RVA viscograms reports the viscosity as a function of time together with the temperature ramp.....	134
<b>Figure 6.1.</b> Flow diagram of experimental design for determining the effect of oven and FCCT roasting on the microstructure of whole maize kernels using X-ray $\mu$ CT and image analysis.....	152
<b>Figure 6.2.</b> Digital images (Canon SX40 digital camera, Canon, Ohtaku, Tokyo, Japan) of the same maize kernels before and after roasting: (a) and (b) raw, (c) and (d) FCCT-roasted, (e) and (f) raw, and (g) and (h) oven-roasted kernels. The cross-sectional digital images of (i) raw, (j) FCCT-roasted and (k) oven-roasted kernels reveals the internal structure, depicting the floury and vitreous endosperm regions as well as the germ (dashed arrow).....	156
<b>Figure 6.3.</b> Grey scale tomographic images of the different views (sagittal and horizontal) of the whole maize kernels, before and after FCCT and oven roasting. Differences in the grey level intensities indicate density variations (light grey = high density; darker grey = low density) while the black areas represent air voids.....	158
<b>Figure 6.4.</b> Detailed 2D tomogram representations of pores (dashed arrow) and cavities (solid arrow) as observed in the frontal slice images of a (a) raw, (b) FCCT-roasted and (c) oven-roasted maize kernel.....	159
<b>Figure 6.5.</b> Semi-transparent 3D X-ray $\mu$ CT volumes (12 $\mu$ m resolution) of cavities, pores and porosity (cavities and pores combined) before and after roasting. The colour scale bar indicates the volume size distribution ( $\text{mm}^3$ ) of the cavities and pores, where larger voids are magenta and smaller ones blue. In the raw kernels cavities and pores are separate (shown by different colours) whereas in the roasted kernels the voids are interconnected (shown as one colour).....	161
<b>Figure 6.6.</b> Three-dimensional (3D) skeletonization images illustrating the topology and thickness of the pore network in (a) raw, (b) FCCT-roasted and (c) oven-roasted maize kernels. The segments of the skeletons are colour coded based on their thickness, according to the colour scale bar ranging from 0 (dark blue) to 1 (red). Blue represents thin segments and red thick segments, where a thickness of 1 is equal to 10 $\mu$ m.....	162
<b>Figure 6.7.</b> A semi-transparent 3D volume illustrating the density differences of the maize constituents, where the less dense area (floury endosperm) is shown with partial transparency and the more dense regions (germ and vitreous endosperm) in grey.....	167
<b>Figure 7.1.</b> Illustration of a simplified flow diagram of the roasting and analyses procedures used. PSI= particle size index; SEM= scanning electron microscopy; XRD= X-ray diffraction; WAC= water absorption capacity; WSI= water solubility index; FD= flour dispersibility; DSC= differential scanning calorimetry; RVA= Rapid Visco Analyser.....	182



**Figure 7.2.** Photograph of (a) the maize kernels mounted on aluminium stubs with double-sided carbon tape and placed into the sample holder; (b) the LEO 1430VP scanning electron microscope (Zeiss, Germany).....184

**Figure 7.3.** Representation of a longitudinal digital slice image and SEM micrograph of (a) a control maize kernel revealing the transition (encircled region) phase from the vitreous (left) to the floury (right) endosperm. Figures (b) and (c) represent a digital longitudinal slice image and SEM micrograph of a FCCT and oven-roasted kernel, respectively. S= starch granules; P= protein matrix; V= vitreous endosperm; F= floury endosperm; E= elongated strands; C= cavity and R= ruptures. The scale bar (20 µm) is given in the lower left corner of the micrographs.....192

**Figure 7.4.** XRD traces of the control, FCCT and oven-roasted maize flour samples. Dashed vertical lines indicate the location of the prominent peaks for A-type crystallinity. Solid lines indicate the development of new peaks that resembles V-type crystallinity in the roasted samples.....194

**Figure 7.5.** RVA pasting profiles of a representative control, FCCT-roasted and oven-roasted maize flour. The RVA viscogram reports the viscosity as a function of time together with the temperature ramp.....200

## LIST OF TABLES

<b>Table 2.1.</b> An overview of X-ray $\mu$ CT applications related to various food commodities and types.....	30
<b>Table 3.1.</b> Applications of roasted wheat (Lazar <i>et al.</i> , 1974).....	69
<b>Table 3.2.</b> Summary of the literature available on the roasting methods, conditions and the purpose of roasting cereal grains.....	70
<b>Table 4.1.</b> Summary of the scanning parameters used for image acquisition.....	90
<b>Table 4.2.</b> Mean and percentage increase/decrease in microstructural parameters of wheat kernels before and after roasting.....	100
<b>Table 5.1.</b> Relative wheat hardness scale.....	119
<b>Table 5.2.</b> Effects of roasting on the physicochemical characteristics of whole wheat.....	124
<b>Table 5.3.</b> WAC, WSI and FD of the control and roasted whole wheat flours.....	131
<b>Table 5.4.</b> DSC thermal characteristics of the control and roasted whole wheat flours.....	133
<b>Table 5.5.</b> RVA pasting properties of the control and roasted whole wheat flours.....	135
<b>Table 5.6.</b> Mixograph and Alveograph indices of the control and roasted whole wheat flours.....	135
<b>Table 6.1.</b> Mean volumes-of-interest (VOIs), percentage object volumes (POVs), expansion ratios (ERs) and vitreous-to-floury endosperm ratios (V:F <sub>s</sub> ) of the two roasting methods.....	163
<b>Table 6.2.</b> Mean relative densities of the different maize kernel constituents and the weight of the raw, FCCT and oven-roasted kernels.....	168
<b>Table 6.3.</b> Dry milling properties of the raw and roasted maize samples.....	169
<b>Table 7.1.</b> Details of the RVA standard profile 1.....	186
<b>Table 7.2.</b> Details of the RVA stirring number profile.....	186
<b>Table 7.3.</b> Physicochemical properties of the control and roasted maize samples.....	187
<b>Table 7.4.</b> WAC, WSI and FD properties of the control and roasted whole maize flours.....	196
<b>Table 7.5.</b> DSC thermal characteristics of the control and roasted maize flours.....	198
<b>Table 7.6.</b> RVA pasting properties of the control and roasted whole maize flours.....	199

## LIST OF ABBREVIATIONS

%	Percentage
°C	Degrees Celsius
°C/min	Degrees Celsius per minute
$\Delta H$	Gelatinisation enthalpy
$\Delta T$	Gelatinisation temperature range
$\mu A$	Microampere
$\mu CT$	Micro-computed tomography
$\mu m$	Micrometre
$\mu L$	Microliter
2D	Two-dimensional
3D	Three-dimensional
AACC	American Association of Cereal Chemists
AFM	Atomic force microscopy
ANOVA	Analysis of variance
a.u.	Arbitrary units
Ca	Calcium
CAF	Central Analytical Facility
CAT	Computerised Axial Tomography
CCD	Charged-coupled-device
c/f	Coarse-to-fine ratio
CLSM	Confocal laser scanning microscopy
cP	Centipoise
CT	Computed tomography
DFI	Direct Fourier Inversion
dH <sub>2</sub> O	Deionised water
DSC	Differential scanning calorimetry
e.g.	<i>exempli gratia</i> (for example)
<i>et al.</i>	<i>et alibi</i> (and elsewhere)
EM	Electron microscopy
ER	Expansion ratio
Eq.	Equation
FBP	Filtered back projection
FBR	Fluidised bed roasting
FCCT	Forced convection continuous tumble
FD	Flour dispersibility
Fig.	Figure

Fe	Iron
FE	Finite element
FOV	Field-of-view
g	Gram
g/cm <sup>3</sup>	Gram per cubic centimetre
GLCM	Grey level co-occurrence matrix
h	Hour
H1	Hot air under roasted
H2	Hot air optimum roasted
H3	Hot air over roasted
HLM	Hectolitre mass
HTC	Hard-to-cook
HTST	High-temperature-short-time
HU	Hounsfield unit
Hz	Hertz
i.e.	<i>id est</i> (that is)
IVDV	Intensification of Vaporisation by Decompression to the Vacuum
K	Potassium
Kg	Kilogram
kg hL <sup>-1</sup>	Kilogram per hectolitre
kV	Kilovolt
keV	Kilo-electronvolt
L	Extensibility
LM	Light microscopy
LPG	Liquefied petroleum gas
mA	Milliampere
mb	Moisture base
mg	Milligram
Mg	Magnesium
min	Minute
mL	Millilitre
mm	Millimetre
mm <sup>3</sup>	Cubic millimetre
MRI	Magnetic resonance imaging
ms	Milliseconds
n	Number of samples
MTI	Mixing tolerance index
Na	Sodium

OSVR	Object structure volume ratio
P	Stability
PI	Puffing index
P/L	Curve configuration ratio
POV	Percentage object volume
PSI	Particle size index
P <sub>temp</sub>	Pasting temperature
PTFE	Polytetrafluoroethylene
R	Raw
RI	Reconstitution index
ROFEX	Rosendorf fast electron beam X-ray tomography
ROI, ROIs	Region-of-interest, Regions-of-interest
rpm	Revolutions per minute
RVA	Rapid Visco Analyser
RVE	Representative volume element
s	Seconds
S	Strength
S1	Sand under roasted
S2	Sand optimum roasted
S3	Sand over roasted
SAGL	South African Grain Laboratory
SEM	Scanning electron microscopy
SN	Stirring number
T <sub>e</sub>	Endset temperature
TEM	Transmission electron microscopy
T <sub>o</sub>	Onset temperature
T <sub>p</sub>	Peak temperature
V <sub>b</sub>	Breakdown viscosity
V <sub>f</sub>	Final viscosity
V:F	Vitreous-to-floury endosperm ratio
VOI, VOIs	Volume-of-interest, Volumes-of-interest
V <sub>p</sub>	Peak viscosity
V <sub>s</sub>	Setback viscosity
V <sub>t</sub>	Through viscosity
W	Deformation energy
WAC	Water absorption capacity
WSI	Water solubility index
XRD	X-ray diffraction

Zn

Zinc

The language, style and referencing format used are in accordance with the requirements of the *International Journal of Food Science and Technology*. This dissertation represents a compilation of manuscripts where each chapter is an individual entity and some repetition between chapters has, therefore, been unavoidable.

## CHAPTER 1

### Introduction

The microstructure of food is an important feature that influences sensory aspects, i.e. appearance and texture and it conveys information on the processing and composition of the product (Chevallier *et al.*, 2014). Conventional methods for microstructural investigation include light microscopy (LM), electron microscopy (EM) and confocal laser scanning microscopy (CLSM) (Suresh & Neethirajan, 2015). These techniques have several drawbacks since they are time-consuming, destructive and sample preparation is necessary which may lead to the development of artefacts (Lim & Barigou, 2004). While these methods can be used to obtain high-resolution images, it is difficult to quantify shape, size and connectivity using these two-dimensional (2D) microscopic techniques (Ho *et al.*, 2013). To this end, a three-dimensional (3D) imaging method is required to quantitatively characterise food microstructure.

In recent years there has been renewed interest in the development of novel methods for microstructural investigations. X-ray micro-computed tomography ( $\mu$ CT) has especially gained interest due to the use of cutting-edge technology. X-ray  $\mu$ CT makes use of X-ray radiation which are capable of penetrating food material to visualise the internal structure (Ho *et al.*, 2013). This technique utilises differences in X-ray attenuation, arising primarily from differences in the density within a sample (Frisullo *et al.*, 2010a). X-rays are sent around and through the scanned sample, creating a 2D projection image. A series of 2D images are obtained by sample rotation and these images can be rendered into a 3D volume. Reconstruction is performed with special software which enables the investigation of cross-sections along any desired orientation of the plane of cut. High density materials attenuate the beam and areas of high attenuation appear light on the 2D slices obtained from angular projections.

X-ray  $\mu$ CT in combination with image analysis is an accurate, non-destructive and non-invasive imaging technique that can be used for high-resolution 3D visualisation and characterisation of the internal structure of a sample to obtain detailed qualitative and quantitative microstructural information (Maire *et al.*, 2001; Zhu *et al.*, 2012). It can be used to determine important processing parameters, influencing the quality of a product (Frisullo *et al.*, 2012b). Furthermore, X-ray  $\mu$ CT also enables precise dimensional measurements of internal features, volumes of regions-of-interest (ROIs), and more advanced analyses such as pore (void) or particle size distributions. X-ray  $\mu$ CT, which was at first mainly used for medical applications, is a relatively new technique in food analysis (Van Dalen *et al.*, 2003; Schoeman *et al.*, 2016). It has more recently also been explored in other fields such as material science (Landis & Keane, 2010; Salvo *et al.*, 2010), geology (Ketcham & Carlson, 2001; Cnudde & Boone, 2013), biology (Mizutani & Suzuki, 2012), industrial engineering (Du Plessis *et al.*, 2014) and archaeology (Du Plessis *et al.*, 2013).

Since X-ray  $\mu$ CT enables high-resolution 3D visualisation and characterisation of a sample, it is not surprising that in recent years this imaging technique has also been extended to the field of agriculture and food quality evaluation (Frisullo *et al.*, 2010a; Laverse *et al.*, 2012). It is rapidly becoming a useful technique for the non-destructive inspection of the internal quality of agricultural products and also to investigate food microstructure (Frisullo *et al.*, 2010a; Laverse *et al.*, 2012). This technique is relatively new in the field of food engineering, but has been successful in the characterisation of very porous food materials (Babin *et al.*, 2007).

There is a need for quantitative methods to accurately characterise food microstructure to determine structure-properties relationships (Lim & Barigou, 2004). X-ray  $\mu$ CT has proven to be a useful technique for the visualisation and quantitative analysis of cellular food products, e.g. aerated chocolates, muffins and mousses (Lim & Barigou, 2004), dough (Bellido *et al.*, 2006), extruded biopolymer foams (Trater *et al.*, 2005), bread (Cafarelli *et al.*, 2014), rice kernels (Van Dalen *et al.*, 2003; Mohorič *et al.*, 2009; Witek *et al.*, 2010), corn flakes (Chaunier *et al.*, 2007), porous cereal products (Van Dalen *et al.*, 2007), French fries (Miri *et al.*, 2006) and ice cream (Pinzer *et al.*, 2012). Other applications include studying ice crystals within frozen foods (Mousavi *et al.*, 2005), 3D pore space quantification in apple tissue (Mendoza *et al.*, 2007; Mendoza *et al.*, 2010), the role of sugar and fat in sugar-snap cookies (Pareyt *et al.*, 2009) and also investigation of the fat level and distribution in meat (Frisullo *et al.*, 2009; Frisullo *et al.*, 2010b).

Processing of food, whether it is milling of grain, gelatinisation of starch or heat denaturation of proteins, will result in changes at microscopic level (Kaláb *et al.*, 1995). Imaging techniques are capable of evaluating such composition and morphology modifications (Kaláb *et al.*, 1995). However, few studies have attempted to study the effect of roasting on the microstructure of cereal grains in an objective manner. Researchers often only report a few cross-sectional 2D images in combination with a qualitative discussion of the microstructure, without investigating the quantitative measurement of key properties (Owusu-Ansah *et al.*, 1984; Autio & Salmenkallio-Marttila, 2001; Gropper *et al.*, 2002). Due to the inadequacy of imaging techniques, like LM and EM, microstructure remained a grey area (Trater *et al.*, 2005).

To overcome the drawbacks of destructive 2D methods, non-invasive imaging techniques are increasingly explored for microstructural characterisation. X-ray  $\mu$ CT is a valuable imaging technique that can answer frequently asked questions such as: what does the internal structure of the sample look like, where are specific components situated and what are their actual measurements? X-ray  $\mu$ CT empowers researchers with both quantitative and qualitative information and permits the characterisation of images in 3D and at an improved spatial resolution.

Since ancient times the importance of cereal grains have been recognised (Hernández *et al.*, 2014). Maize (*Zea mays* L.) and wheat (*Triticum aestivum* L.) are two of the most important staple food crops in the world and in conjunction with rice, they provide 30% of the food calories to 4.5 billion people in 100 developing countries (Hellin *et al.*, 2012). These cereal grains are important sources of protein, carbohydrates, vitamins, minerals and phytochemicals (Oboh *et al.*, 2010). The



use of these grains for human consumption is very diverse and range from staple food in undeveloped countries to specialised foods in developing countries. White maize is usually preferred for human consumption and yellow maize for animal feed (Esteve Agelet *et al.*, 2012).

Nowadays, greater emphasis is placed on microstructure to obtain a better understanding of the physical and rheological behaviour of foods, as well as the textural, sensory and functional properties (Laverse *et al.*, 2012). The identity and quality of food is greatly affected by microstructural elements such as starch granules, air (porosity), protein assemblies and food biopolymer matrices (Aguilera, 2005). This correlation could be advantageously used to improve the quality of a product and also to tailor parameters that affect consumer acceptability. As a result of microscopic complexity, unambiguous methods that relate quality to food microstructure do not exist at present (Rizzolo *et al.*, 2014). Thus, there is a need to develop methods that directly measure the microstructural characteristics of food.

It is important to understand the structure of industrially important cereal grains since it plays an important role in various aspects of cereal technology, e.g. wheat milling and maize processing (Delcour & Hoseney, 2010). Two concepts of prime importance is insight into the 3D structure of cereal grains and the compartmentalisation of the various components in cereal grains (Delcour & Hoseney, 2010). Knowledge on food microstructure, physicochemical properties and functionality can be used to identify important processing parameters that may affect quality and from a food engineering perspective this information is very valuable (Frisullo *et al.*, 2012b).

Roasting is an essential thermal process which leads to the improvement of colour, flavour, texture and appearance, and ultimately enhances the overall palatability of the product (Uysal *et al.*, 2009). The main purpose of roasting is to improve and alter quality and safety. Cereals are traditionally roasted to improve nutritional and sensory properties, enhance shelf life and to improve the processing efficiency of a subsequent step (Kikugawa *et al.*, 1983; Asep *et al.*, 2008; Murthy *et al.*, 2008; Cämmerer & Kroh, 2009). Roasting is a high-temperature-short-time (HTST) process which inactivates contaminating microorganisms, destructive enzymes and growth inhibitors, while it retains nutrients (Srivastav *et al.*, 1990). Roasting will inevitably lead to a variety of changes and it is thus necessary to control the roasting time and temperature to obtain optimal characteristics, without burning the grains and compromising the flavour. Despite the availability of literature on the nutritional benefits of roasting cereal grains, little is known about the impact on the internal structure, physicochemical properties and functionality. The selection of appropriate roasting conditions is a major goal in roasting as it can be used to optimise these properties.

Different roasting techniques exists, i.e. fluidised bed (Murthy *et al.*, 2008), sand (Mridula *et al.*, 2007; Gujral *et al.*, 2011), microwave (Uysal *et al.*, 2009; Omwamba & Hu, 2010), pan (Ayatse *et al.*, 1983; Oboh *et al.*, 2010; Carrera *et al.*, 2015), oven (Krings *et al.*, 2006; Mariotti *et al.*, 2006) and flame (McNiven *et al.*, 1994; Mrad *et al.*, 2014) roasting. These methods, however, have various drawbacks as it may be unhygienic, tedious to operate or have low productivity (Murthy *et al.*, 2008). It can also be dangerous to the health of the operator (e.g. flame roasting) and the

roasted products may have non-uniform characteristics (Murthy *et al.*, 2008). Due to the negative aspects related to traditional and conventional roasting techniques there is a need for a reliable alternative. Forced convection continuous tumble (FCCT) roasting offers such an alternative (Anonymous, 2014). This roaster, based on forced convection roasting, uses superheated steam generated from the moisture inside the sample, in combination with the continuous tumbling movement of the screw conveyer inside the roasting drum, to create even heat transfer and a more uniformly roasted product.

Dietary guidelines recommend an increase in the consumption of whole grain cereal products due to the health benefits, i.e. reduction in the risk of chronic diseases, diabetes and cancer, associated with the consumption of these products (Ragaei & Abdel-Aal, 2006). Thus, the development of whole grain based ingredients and snack foods is favoured for the production of health-enhancing or functional foods (Salmenkallio-Marttila *et al.*, 2004). Currently, there is a growing interest in modification of cereal flours using innovative processing techniques, including high-pressure pulse-electric field, radio frequency, ohmic heating and microwave treatments (Ahmed *et al.*, 2007). There is evidence that whole grain cereals can be beneficial in terms of their health promoting effects when consumed in its roasted form (Sandhu *et al.*, 2015; Carrera *et al.*, 2015). The improved *in vitro* digestibility, antioxidant capacity and high dietary fibre content of roasted whole grains provides a fundamental basis for incorporating these grains into foods as health-enhancing ingredients (Carrera *et al.*, 2015; Oboh *et al.*, 2010). Modification of whole cereal grains, induced by roasting, may thus result in a higher quality end product.

Physicochemical and functional properties of foods are, however, strongly influenced by structure-property relationships (Frisullo *et al.*, 2012a). Thus, the usefulness of roasted whole grain and their flour will depend on their structural properties, as well as their functionality. Moreover, understanding the physicochemical properties, i.e. weight, bulk density, puffing index (PI), moisture, crude protein, hardness and milling characteristics is essential for further handling, processing and transportation, as well as for applications in food formulations. Scope thus exists to investigate the effect of roasting on the microstructural, physicochemical, functional and rheological characteristics of whole grains.

Structural changes induced by roasting comprise changes in the starch and protein components. These changes in the starch-protein morphology can be investigated using scanning electron microscopy (SEM). X-ray diffraction (XRD) studies revealed that roasting decreases the crystallinity content of maize, while the hydrolysis rate and starch digestibility and availability improved (Carrera *et al.*, 2015). Changes in the starch granule structure after roasting, in turn, affect the functional properties and rheological behaviour. Differential scanning calorimetry (DSC) can explain the effect of roasting on the thermal properties and gelatinisation characteristics (Carrera *et al.*, 2015).

Baked goods may benefit from a mixture of non-roasted and roasted flours when gelatinisation is needed but retrogradation must be limited for functionality and shelf-life purposes (Rothschild *et*

*et al.*, 2015). An increase in water absorption capacity (WAC) after roasting suggests that roasted flour can be used as means to control water migration in baked products (Mariotti *et al.*, 2006). Moisture content and moisture transfer plays a role in staling, thus roasted flour has the potential to retain more moisture and retard the staling phenomenon, resulting in a product that stays softer for longer (Mariotti *et al.*, 2006). A decrease in water solubility index (WSI) after roasting can be attributed to the formation of amylose lipid complexes, which reduces the water solubility (Gujral *et al.*, 2011). An increase in flour dispersibility (FD) after roasting may be useful for the production of instant convenience foods (Singh *et al.*, 2007).

Rheological changes in dough from roasted wheat flour can be attributed to starch modifications resulting in altered starch-protein and starch-starch interactions and protein aggregation. It is important to monitor rheological changes after thermal processing, since it can induce changes in starch and protein structure and availability (Baiano *et al.*, 2009). Flour quality is indicated by dough properties, which is one of the main intermediate steps in the transformation of flour to end products (Van Hung *et al.*, 2006). The ability of wheat flour to produce dough with desirable gas-holding properties is due to gluten, since it imparts elasticity and extensibility characteristics. Roasted wheat flour cannot be used for breadmaking alone and should be used in combination with regular wheat flour to improve the texture and functionality of end products (Van Hung *et al.*, 2006).

Roasted whole wheat and maize has potential as functional ingredients in food applications and have been successfully incorporated into various foods, i.e. bread (Baiano *et al.*, 2009), pasta (Baiano *et al.*, 2008), beverages (Youn & Chung, 2012) and porridges (Vivas *et al.*, 1987). A recent study on grain amaranth reported that roasting significantly increased the viscosity and would be preferred in the production of flour to be used as thickening agent (Muyonga *et al.*, 2014). During roasting starch granules may disintegrate and become more susceptible to hydration which is related to a higher viscosity. From a food scientist's perspective functionality, i.e. viscosity changes of raw materials are very important, since it can affect flow regimes, processing variables and end product quality. The Rapid Visco Analyser (RVA) is a viscometric tool that is widely used for studying starch pasting properties.

To date X-ray  $\mu$ CT has not been considered as a technique to provide information on the microstructure of roasted cereal grains. This study addresses this shortcoming and evaluated X-ray  $\mu$ CT for characterising the microstructure of roasted cereal grains. Due to the non-destructive capability of X-ray  $\mu$ CT, it enables investigation of the same grain in the raw and roasted state. When microscopy and images analysis are used in conjunction, they can become an even more powerful tool to examine microstructure (Barrera *et al.*, 2013). Few investigations have reported on the structural, physicochemical and functional properties of roasted cereal grains (Murthy *et al.*, 2008; Altan, 2014; Ranganathan *et al.*, 2014; Carrera *et al.*, 2015). A proper understanding of the effect of roasting on the microstructure and structure-property relationship of whole maize and

wheat is required to produce products with desired characteristics in terms of physiochemical and functional properties.

The aim of this study was thus to characterise and quantify the effect of two roasting methods, conventional oven roasting and innovative FCCT roasting, on the microstructural, physicochemical and functional properties of whole wheat and maize kernels using a series of destructive and non-destructive techniques. Specific objectives were to:

- provide a comprehensive literature review on X-ray  $\mu$ CT for food microstructure characterisation;
- review cereal roasting techniques and applications;
- investigate the feasibility of X-ray  $\mu$ CT as non-destructive technique for 2D and 3D visualisation of the structural changes induced by roasting in whole wheat and maize kernels;
- demonstrate the capability of X-ray  $\mu$ CT and image analysis as a useful technique for the quantification of microstructural parameters of raw and roasted whole wheat and maize kernels as well as that of selected ROIs;
- evaluate the influence of roasting on the grains' physicochemical properties, i.e. weight loss, bulk density, PI, moisture content, crude protein, hardness and milling characteristics;
- assess the impact of roasting on the wheat and maize starch-protein morphology and crystalline structure using SEM and XRD, respectively;
- examine functional properties of the roasted grains, i.e. WAC, WSI and FD, as well as thermal and pasting properties using DSC and the RVA, respectively; and
- determine the rheological properties of roasted whole wheat flour with a Mixograph and Alveograph.

In our study, we departed from the hypothesis that roasting, using different roasting methods (with similar time-temperature conditions) will result in differences in the microstructural, physicochemical and functional properties of whole wheat and maize kernels. This study will provide baseline information, which would help determine potential applications for roasted whole grain products in food systems.

## References

- Aguilera, J.M. (2005). Why food microstructure? *Journal of Food Engineering*, **67**, 3-11.
- Ahmed, J., Ramaswamy, H.S., Ayad, A., Alli, I. & Alvarez, P. (2007). Effect of high-pressure treatment on rheological, thermal and structural changes in basmati rice flour slurry. *Journal of Cereal Science*, **46**, 148-156.
- Altan, A. (2014). Effects of pretreatments and moisture content on microstructure and physical properties of microwave expanded hull-less barley. *Food Research International*, **56**, 126-135.
- Anonymous. (2014). Roastech [Internet document]. URL <http://www.roastech.com/contact.html>. Accessed 23/05/2014.

- Asep, E., Jinap, S., Tan, T.J., Russly, A., Harcharan, S. & Nazimah, S. (2008). The effects of particle size, fermentation and roasting of cocoa nibs on supercritical fluid extraction of cocoa butter. *Journal of Food Engineering*, **85**, 450-458.
- Autio, K. & Salmenkallio-Marttila, M. (2001). Light microscopic investigations of cereal grains, doughs and breads. *LWT-Food Science and Technology*, **34**, 18-22.
- Ayatse, J., Eka, O. & Ifon, E. (1983). Chemical evaluation of the effect of roasting on the nutritive value of maize (*Zea mays*, Linn.). *Food Chemistry*, **12**, 135-147.
- Babin, P., Della Valle, G., Dendievel, R., Lourdin, D. & Salvo, L. (2007). X-ray tomography study of the cellular structure of extruded starches and its relations with expansion phenomenon and foam mechanical properties. *Carbohydrate Polymers*, **68**, 329-340.
- Baiano, A., Fares, C., Peri, G., Romaniello, R., Taurino, A.M., Siciliano, P., Gambacorta, G., Lamacchia, C., Pati, S. & Notte, E.L. (2008). Use of a toasted durum whole meal in the production of a traditional Italian pasta: chemical, mechanical, sensory and image analyses. *International Journal of Food Science & Technology*, **43**, 1610-1618.
- Baiano, A., Romaniello, R., Lamacchia, C. & La Notte, E. (2009). Physical and mechanical properties of bread loaves produced by incorporation of two types of toasted durum wheat flour. *Journal of Food Engineering*, **95**, 199-207.
- Barrera, G.N., Calderón-Domínguez, G., Chanona-Pérez, J., Gutiérrez-López, G.F., León, A.E. & Ribotta, P.D. (2013). Evaluation of the mechanical damage on wheat starch granules by SEM, ESEM, AFM and texture image analysis. *Carbohydrate Polymers*, **98**, 1449-1457.
- Bellido, G.G., Scanlon, M.G., Page, J.H. & Hallgrimsson, B. (2006). The bubble size distribution in wheat flour dough. *Food Research International*, **39**, 1058-1066.
- Cämmerer, B. & Kroh, L.W. (2009). Shelf life of linseeds and peanuts in relation to roasting. *LWT-Food Science and Technology*, **42**, 545-549.
- Carrera, Y., Utrilla-Coello, R., Bello-Pérez, A., Alvarez-Ramirez, J. & Vernon-Carter, E.J. (2015). In vitro digestibility, crystallinity, rheological, thermal, particle size and morphological characteristics of pinole, a traditional energy food obtained from toasted ground maize. *Carbohydrate Polymers*, **123**, 246-255.
- Chaunier, L., Della Valle, G. & Lourdin, D. (2007). Relationships between texture, mechanical properties and structure of cornflakes. *Food Research International*, **40**, 493-503.
- Chevallier, S., Réguerre, A.-L., Le Bail, A. & Della Valle, G. (2014). Determining the cellular structure of two cereal food foams by X-ray micro-tomography. *Food Biophysics*, **9**, 219-228.
- Cnudde, V. & Boone, M. (2013). High-resolution X-ray computed tomography in geosciences: a review of the current technology and applications. *Earth-Science Reviews*, **123**, 1-17.
- Delcour, J. & Hosney, R.C. (2010). *Principles of Cereal Science and Technology*. Pp. 1-12. St. Paul, Minnesota, USA: AACC International Press.

- Du Plessis, A., Seifert, T., Booysen, G. & Els, J. (2014). Microfocus X-ray computed tomography (CT) analysis of laser sintered parts. *South African Journal of Industrial Engineering*, **25**, 39-49.
- Du Plessis, A., Steyn, J., Roberts, D.E., Botha, L.R. & Berger, L.R. (2013). A proof of concept demonstration of the automated laser removal of rock from a fossil using 3D X-ray tomography data. *Journal of Archaeological Science*, **40**, 4607-4611.
- Esteve Agelet, L., Ellis, D.D., Duvick, S., Goggi, A.S., Hurburgh, C.R. & Gardner, C.A. (2012). Feasibility of near infrared spectroscopy for analyzing corn kernel damage and viability of soybean and corn kernels. *Journal of Cereal Science*, **55**, 160-165.
- Falcone, P., Baiano, A., Zanini, F., Mancini, L., Tromba, G., Montanari, F. & Nobile, M. (2004). A novel approach to the study of bread porous structure: phase-contrast X-ray microtomography. *Journal of Food Science*, **69**, 38-43.
- Falcone, P.M., Baiano, A., Zanini, F., Mancini, L., Tromba, G., Dreossi, D., Montanari, F., Scuor, N. & Nobile, M.A.D. (2005). Three-dimensional quantitative analysis of bread crumb by X-ray microtomography. *Journal of Food Science*, **70**, 265-272.
- Frisullo, P., Barnabà, M., Navarini, L. & Del Nobile, M. (2012a). *Coffea arabica* beans microstructural changes induced by roasting: an X-ray microtomographic investigation. *Journal of Food Engineering*, **108**, 232-237.
- Frisullo, P., Conte, A. & Del Nobile, M. (2010a). A novel approach to study biscuits and breadsticks using X-ray computed tomography. *Journal of Food Science*, **75**, 353-358.
- Frisullo, P., Laverse, J., Barnabà, M., Navarini, L. & Del Nobile, M. (2012b). Coffee beans microstructural changes induced by cultivation processing: an X-ray microtomographic investigation. *Journal of Food Engineering*, **109**, 175-181.
- Frisullo, P., Laverse, J., Marino, R. & Del Nobile, M. (2009). X-ray computed tomography to study processed meat microstructure. *Journal of Food Engineering*, **94**, 283-289.
- Frisullo, P., Marino, R., Laverse, J., Albenzio, M. & Del Nobile, M. (2010b). Assessment of intramuscular fat level and distribution in beef muscles using X-ray microcomputed tomography. *Meat Science*, **85**, 250-255.
- Gropper, M., Moraru, C.I. & Kokini, J.L. (2002). Effect of specific mechanical energy on properties of extruded protein-starch mixtures. *Cereal Chemistry*, **79**, 429-433.
- Gujral, H.S., Sharma, P. & Rachna, S. (2011). Effect of sand roasting on beta glucan extractability, physicochemical and antioxidant properties of oats. *LWT-Food Science and Technology*, **44**, 2223-2230.
- Hellin, J., Shiferaw, B., Cairns, J.E., Matthew Reynolds, M., Ortiz-Monasterio, I., Banziger, M., Sonder, K. & La Rovere, R. (2012). Climate change and food security in the developing world: potential of maize and wheat research to expand options for adaptation and mitigation. *Journal of Development and Agricultural Economics*, **4**, 311-321.



- Hernández, O., Fraga, J., Jiménez, A., Jiménez, F. & Arias, J. (2014). Characterization of toasted cereal flours from the Canary Islands (gofios). *Food Chemistry*, **151**, 133-140.
- Ho, Q.T., Carmeliet, J., Datta, A.K., Defraeye, T., Delele, M.A., Herremans, E., Opara, L., Ramon, H., Tijssens, E. & Van Der Sman, R. (2013). Multiscale modeling in food engineering. *Journal of Food Engineering*, **114**, 279-291.
- Kaláb, M., Allan-Wojtas, P. & Miller, S.S. (1995). Microscopy and other imaging techniques in food structure analysis. *Trends in Food Science & Technology*, **6**, 177-186.
- Ketcham, R.A. & Carlson, W.D. (2001). Acquisition, optimization and interpretation of X-ray computed tomographic imagery: applications to the geosciences. *Computers & Geosciences*, **27**, 381-400.
- Kikugawa, K., Arai, M. & Kurechi, T. (1983). Participation of sesamol in stability of sesame oil. *Journal of the American Oil Chemists' Society*, **60**, 1528-1533.
- Krings, U., Johansson, L., Zorn, H. & Berger, R.G. (2006). In vitro DNA-protective activity of roasted wheat germ and fractions thereof. *Food Chemistry*, **97**, 712-718.
- Landis, E.N. & Keane, D.T. (2010). X-ray microtomography. *Materials Characterization*, **61**, 1305-1316.
- Lassoued, N., Babin, P., Della Valle, G., Devaux, M.-F. & Réguerre, A.-L. (2007). Granulometry of bread crumb grain: contributions of 2D and 3D image analysis at different scale. *Food Research International*, **40**, 1087-1097.
- Laverse, J., Frisullo, P., Conte, A. & Nobile, M. (2012). X-ray microtomography for food quality analysis. In: *Food Industrial Processes—Methods and Equipment*. Pp. 339-362. InTech Open Publishers.
- Lim, K.S. & Barigou, M. (2004). X-ray micro-computed tomography of cellular food products. *Food Research International*, **37**, 1001-1012.
- Maire, E., Buffière, J.-Y., Salvo, L., Blandin, J., Ludwig, W. & Letang, J. (2001). On the application of X-ray microtomography in the field of materials science. *Advanced Engineering Materials*, **3**, 539-546.
- Mariotti, M., Alamprese, C., Pagani, M.A. & Lucisano, M. (2006). Effect of puffing on ultrastructure and physical characteristics of cereal grains and flours. *Journal of Cereal Science*, **43**, 47-56.
- McNiven, M.A., Hamilton, R.M.G., Robinson, P.H. & DeLeeuw, J.W. (1994). Effect of flame roasting on the nutritional quality of common cereal grains for non-ruminants and ruminants. *Animal Feed Science and Technology*, **47**, 31-40.
- Mendoza, F., Verboven, P., Ho, Q.T., Kerckhofs, G., Wevers, M. & Nicolaï, B. (2010). Multifractal properties of pore-size distribution in apple tissue using X-ray imaging. *Journal of Food Engineering*, **99**, 206-215.
- Mendoza, F., Verboven, P., Mebatsion, H.K., Kerckhofs, G., Wevers, M. & Nicolaï, B. (2007). Three-dimensional pore space quantification of apple tissue using X-ray computed microtomography. *Planta*, **226**, 559-570.

- Miri, T., Bakalis, S., Bhima, S. & Fryer, P. (2006). Use of X-ray micro-CT to characterize structure phenomena during frying. In: *Proceedings of the IUFOST, 13th World Congress of Food Science and Technology*, Nantes, France. Pp. 735-747. 17-21 September.
- Mizutani, R. & Suzuki, Y. (2012). X-ray microtomography in biology. *Micron*, **43**, 104-115.
- Mohorič, A., Vergeldt, F., Gerkema, E., Van Dalen, G., Van Den Doel, L., Van Vliet, L.J., Van As, H. & Van Duynhoven, J. (2009). The effect of rice kernel microstructure on cooking behaviour: a combined  $\mu$ -CT and MRI study. *Food Chemistry*, **115**, 1491-1499.
- Mousavi, R., Miri, T., Cox, P. & Fryer, P.J. (2005). A novel technique for ice crystal visualization in frozen solids using X-ray micro-computed tomography. *Journal of Food Science*, **70**, 437-442.
- Mrad, R., Debs, E., Maroun, R.G. & Louka, N. (2014). Multiple optimization of chemical components and texture of purple maize expanded by IVDV treatment using the response surface methodology. *Food Chemistry*, **165**, 60-69.
- Mridula, D., Goyal, R., Bhargav, V. & Manikantan, M. (2007). Effect of roasting on texture, colour and acceptability of soybean for making *sattu*. *American Journal of Food Technology*, **2**, 265-272.
- Murthy, K.V., Ravi, R., Keshava Bhat, K. & Raghavarao, K.S.M.S. (2008). Studies on roasting of wheat using fluidized bed roaster. *Journal of Food Engineering*, **89**, 336-342.
- Oboh, G., Ademiluyi, A.O. & Akindahunsi, A.A. (2010). The effect of roasting on the nutritional and antioxidant properties of yellow and white maize varieties. *International Journal of Food Science & Technology*, **45**, 1236-1242.
- Omwamba, M. & Hu, Q. (2010). Antioxidant activity in barley (*Hordeum vulgare* L.) grains roasted in a microwave oven under conditions optimized using response surface methodology. *Journal of Food Science*, **75**, C66-C73.
- Owusu-Ansah, J., Van De Voort, F. & Stanley, D. (1984). Textural and microstructural changes in corn starch as a function of extrusion variables. *Canadian Institute of Food Science and Technology Journal*, **17**, 65-70.
- Pareyt, B., Talhaoui, F., Kerckhofs, G., Brijs, K., Goesaert, H., Wevers, M. & Delcour, J.A. (2009). The role of sugar and fat in sugar-snap cookies: structural and textural properties. *Journal of Food Engineering*, **90**, 400-408.
- Pinzer, B., Medebach, A., Limbach, H., Dubois, C., Stampanoni, M. & Schneebeli, M. (2012). 3D-characterization of three-phase systems using X-ray tomography: tracking the microstructural evolution in ice cream. *Soft Matter*, **8**, 4584-4594.
- Ragae, S. & Abdel-Aal, E.-S.M. (2006). Pasting properties of starch and protein in selected cereals and quality of their food products. *Food Chemistry*, **95**, 9-18.
- Ranganathan, V., Nunjundiah, I.T. & Bhattacharya, S. (2014). Effect of roasting on rheological and functional properties of sorghum flour. *Food Science and Technology International*, **20**, 579-589.



- Rizzolo, A., Vanoli, M., Cortellino, G., Spinelli, L., Contini, D., Herremans, E., Bongaers, E., Nemeth, A., Leitner, M. & Verboven, P. (2014). Characterizing the tissue of apple air-dried and osmo-air-dried rings by X-CT and OCT and relationship with ring crispness and fruit maturity at harvest measured by TRS. *Innovative Food Science & Emerging Technologies*, **24**, 121-130.
- Salmenkallio-Marttila, M., Heiniö, R.-L., Myllymäki, O., Lille, M., Autio, K. & Poutanen, K. (2004). Relating microstructure, sensory and instrumental texture of processed oat. *Agricultural and Food Science*, **13**, 124-137.
- Salvo, L., Suéry, M., Marmottant, A., Limodin, N. & Bernard, D. (2010). 3D imaging in material science: application of X-ray tomography. *Comptes Rendus Physique*, **11**, 641-649.
- Sandhu, K.S., Godara, P., Kaur, M. & Punia, S. (2015). Effect of toasting on physical, functional and antioxidant properties of flour from oat (*Avena sativa* L.) cultivars. *Journal of the Saudi Society of Agricultural Sciences*, <http://dx.doi.org/10.1016/j.jssas.2015.06.004>.
- Schoeman, L., Williams, P., Du Plessis, A. & Manley, M. (2016). X-ray micro-computed tomography ( $\mu$ CT) for non-destructive characterisation of food microstructure. *Trends in Food Science & Technology*, **47**, 10-24.
- Singh, J., Kaur, L. & McCarthy, O. (2007). Factors influencing the physico-chemical, morphological, thermal and rheological properties of some chemically modified starches for food applications—a review. *Food Hydrocolloids*, **21**, 1-22.
- Srivastav, P., Das, H. & Prasad, S. (1990). Effect of roasting process variables on in-vitro protein digestibility of bengalgram, maize and soybean. *Food Chemistry*, **35**, 31-37.
- Suresh, A. & Neethirajan, S. (2015). Real-time 3D visualization and quantitative analysis of internal structure of wheat kernels. *Journal of Cereal Science*, **63**, 81-87.
- Trater, A.M., Alavi, S. & Rizvi, S.S.H. (2005). Use of non-invasive X-ray microtomography for characterizing microstructure of extruded biopolymer foams. *Food Research International*, **38**, 709-719.
- Uysal, N., Sumnu, G. & Sahin, S. (2009). Optimization of microwave–infrared roasting of hazelnut. *Journal of Food Engineering*, **90**, 255-261.
- Van Dalen, G., Blonk, H., Van Aalst, H. & Hendriks, C.L. (2003). 3-D imaging of foods using X-ray microtomography. *GIT Imaging and Microscopy*, **3**, 18-21.
- Van Dalen, G., Nootenboom, P. & Van Vliet, L.J. (2007). 3D imaging, analysis and modelling of porous cereal products using X-ray microtomography. *Image Analysis and Stereology*, **26**, 169-177.
- Vivas, N., Waniska, R. & Rooney, L. (1987). Thin porridges (atole) prepared from maize and sorghum. *Cereal Chemistry*, **64**, 384-389.
- Wang, S., Austin, P. & Bell, S. (2011). It's a maze: the pore structure of bread crumbs. *Journal of Cereal Science*, **54**, 203-210.

- Witek, M., Węglarz, W., De Jong, L., Van Dalen, G., Blonk, J., Heussen, P., Van Velzen, E., Van As, H. & Van Duynhoven, J. (2010). The structural and hydration properties of heat-treated rice studied at multiple length scales. *Food Chemistry*, **120**, 1031-1040.
- Youn, K.-S. & Chung, H.-S. (2012). Optimization of the roasting temperature and time for preparation of coffee-like maize beverage using the response surface methodology. *LWT-Food Science and Technology*, **46**, 305-310.
- Zhu, L.J., Dogan, H., Gajula, H., Gu, M.H., Liu, Q.Q. & Shi, Y.C. (2012). Study of kernel structure of high-amylose and wild-type rice by X-ray microtomography and SEM. *Journal of Cereal Science*, **55**, 1-5.

**Declaration by the candidate:**

With regard to Chapter 2 (pp. 14-49), the nature and scope of my contribution were as follows:

<b>Nature of contribution</b>	<b>Extent of contribution (%)</b>
Literature search and writing of chapter	75

The following co-authors have contributed to Chapter 2 (pp. 14-49):

<b>Name</b>	<b>e-mail address</b>	<b>Nature of contribution</b>	<b>Extent of contribution (%)</b>
Prof Marena Manley	mman@sun.ac.za	Research inputs, editorial suggestions and proofreading	15
Dr Anton du Plessis	anton2@sun.ac.za	Recommendations on X-ray $\mu$ CT applications and proofreading	5
Dr Paul Williams	pauljw@sun.ac.za	Literature recommendations and proofreading	5

Signature of candidate: L. Schoeman

Date: 30/11/2016

**Declaration by co-authors:**

The undersigned hereby confirm that

1. the declaration above accurately reflects the nature and extent of the contributions of the candidate and the co-authors to Chapter 2 (pp. 14-49),
2. no other authors contributed to Chapter 2 (pp. 14-49) besides those specified above, and
3. potential conflicts of interest have been revealed to all interested parties and that the necessary arrangements have been made to use the material in Chapter 2 (pp. 14-49) of this dissertation.

<b>Signature</b>	<b>Institutional affiliation</b>	<b>Date</b>
Prof Marena Manley	Department of Food Science, Stellenbosch University	30/11/2016
Dr Anton du Plessis	CT Scanner Facility, Stellenbosch University	30/11/2016
Dr Paul Williams	Department of Food Science, Stellenbosch University	30/11/2016

Declaration with signature in possession of candidate and supervisor.

## CHAPTER 2

### Literature review 1

#### **X-ray micro-computed tomography ( $\mu$ CT) for non-destructive characterisation of food microstructure\***

##### **Abstract**

Food microstructure can be visualised by a wide range of microscopic techniques, however these methods are usually destructive and require sample preparation. X-ray micro-computed tomography ( $\mu$ CT) provides an alternative as it is non-invasive, non-destructive and requires no sample preparation. It characterises structures three-dimensionally, allowing evaluation of microstructural changes at resolutions as high as a few hundred nanometres. After the discovery of X-rays in 1895, X-ray computed tomography (CT) was developed and introduced into clinical practices in the 1970s. The first X-ray  $\mu$ CT food application, to detect the maturity of green tomatoes, followed in 1991. This review aims to provide an overview of the basic principles of X-ray  $\mu$ CT, the different systems, image processing and analysis as well as image texture analysis. Food applications are highlighted and the review concludes with future trends of X-ray  $\mu$ CT. The controlled production and stability of microstructure is of great interest to the food industry. Both laboratory  $\mu$ CT and synchrotron systems are becoming more common and thus will lead to imaging in three dimensions at a micron scale playing a much bigger role in future food studies. Limitations include operator dependency, time and cost constraints and imaging artefacts. Technological and computational progress, however, encourages the growth of this technique in food science.

**Keywords:** Food microstructure; X-ray micro-computed tomography; Non-destructive; Three-dimensional; Food applications

---

\*Published as: Schoeman, L., Williams, P., Du Plessis, A. & Manley, M. (2016). X-ray micro-computed tomography ( $\mu$ CT) for non-destructive characterisation of food microstructure. *Trends in Food Science and Technology*, **47**, 10-24.

## Introduction

Food microstructure influences the physical, sensory and textural properties of products. This requires better evaluation and understanding of the structural organisation of food in order to produce products with desired organoleptic and physical characteristics. Also, food science research often demands knowledge of the true three-dimensional (3D) microstructure. Food microstructure can be defined as the spatial organisation of structural components of food and their interactions (Herremans *et al.*, 2013a). Current techniques used to obtain information on food microstructure are mostly invasive and entail sample preparation (e.g. light and electron microscopy) or are limited to specific applications (e.g. magnetic resonance imaging (MRI) and atomic force microscopy (AFM)) (Frisullo *et al.*, 2012). X-ray micro-computed tomography ( $\mu$ CT) is an innovative radiographic imaging technique that enables non-destructive and non-invasive 3D imaging, at resolutions higher than 1  $\mu$ m, and analysis aimed at the internal examination of the structural arrangement of products (Landis & Keane, 2010). The same sample can thus be scanned numerous times under different conditions. This is especially of value in food research where information on microstructural changes over time is required. X-ray  $\mu$ CT also enables scanning of the entire sample due to its large field-of-view without any sample preparation (Léonard *et al.*, 2008). X-ray  $\mu$ CT enables samples to be studied in their natural state at atmospheric temperature and pressure. Besides being used in the millimeter to micron (X-ray  $\mu$ CT) resolution range, recently sub-micrometer or nanometer (X-ray nano-CT) pixel resolution has become possible (Herremans *et al.*, 2011). X-ray CT thus enables 3D microstructural investigation of samples in a near-native state and at unprecedented resolution.

X-ray CT has numerous applications and a number of reviews have been published to demonstrate the versatility of this technique in fields such as, geosciences (Cnudde & Boone, 2013), material science (Landis & Keane, 2010; Maire & Withers, 2014) and biology (Mizutani & Suzuki, 2012). The success of X-ray  $\mu$ CT in medical science and other sciences encourages its use in food science. There is a need for quantitative techniques that can accurately characterise food products with the aim of establishing an intrinsic relationship between microstructure and food quality (Lim & Barigou, 2004) and to comprehend and control structure-property interactions (Herremans *et al.*, 2013a). The ability to measure and visualise food microstructure in 3D is important to understand these properties (e.g. sensorial perception) in association with processing conditions (Pinzer *et al.*, 2012). Modification of structural features by processing can be used to design products with desired attributes. As a result of microscopic complexity, straightforward techniques, with the ability of relating quality to microstructure, are non-existent today and the only way of advancing is to develop techniques that can directly measure microstructural parameters (Herremans *et al.*, 2013a). Although evidence exists of a good relationship between the microstructure and texture of foods, techniques are needed at-line and on-line to non-destructively measure the microstructural properties (Herremans *et al.*, 2013a).

This review demonstrates the ability of X-ray  $\mu$ CT as a non-destructive and non-invasive technique to investigate the 3D microstructure of a range of food products. The first section will introduce the theory and basic principles, followed by an overview of image processing and analysis for both quantitative and qualitative analyses. X-ray  $\mu$ CT systems are briefly reviewed. The last section considers applications in food and agricultural related fields, limitations and future trends.

## **Fundamental principles of X-ray CT**

### *Background*

X-ray radiation was first discovered in 1895 by Wilhelm Conrad Röntgen (Kotwaliwale *et al.*, 2014) with X-ray computed tomography (CT) introduced into clinical practices in 1972 with a typical resolution of 300  $\mu$ m (Kalender, 2011). Further development of instrumentation and improvement in computing power led to true 3D imaging of internal structures rapidly extending to other fields.

X-ray CT originates from Computerised Axial Tomography (CAT or CT) scans (Landis & Keane, 2010). The South African born American physicist, Alan M. Cormack was awarded the Nobel Prize for Physiology or Medicine in 1979 for the development of CAT scanning (De Beer, 2005). CT scanning is an extension of projection radiography capable of producing two-dimensional (2D) images of a sample's internal structure. The limitation of radiography is that features can only be studied within the 2D plane, resulting in a loss of information and consequently the misinterpretation of an image. X-ray CT or  $\mu$ CT overcomes this drawback by linking data from a sequence of 2D absorption images that is recorded by rotating a sample around an axis (Landis & Keane, 2010). Mathematical principles can then be used to reconstruct the series of 2D radiographs into 3D digital images. Cormack, in conjunction with Godfrey Hounsfield, first employed the mathematical transformation algorithms generated by John Radon in 1907 to create 3D reconstructed images for the medical examination of patients (De Beer, 2005).

The basic principles of X-ray CT imaging are thus absorption physics (related to 2D projection images) and reconstruction mathematics (relevant to the generation of a 3D volume from a series of 2D images) (Landis & Keane, 2010). For greater depth and breadth on the principles and the technique, the reader is referred to more comprehensive work (Maire & Withers, 2014; Kalender, 2011).

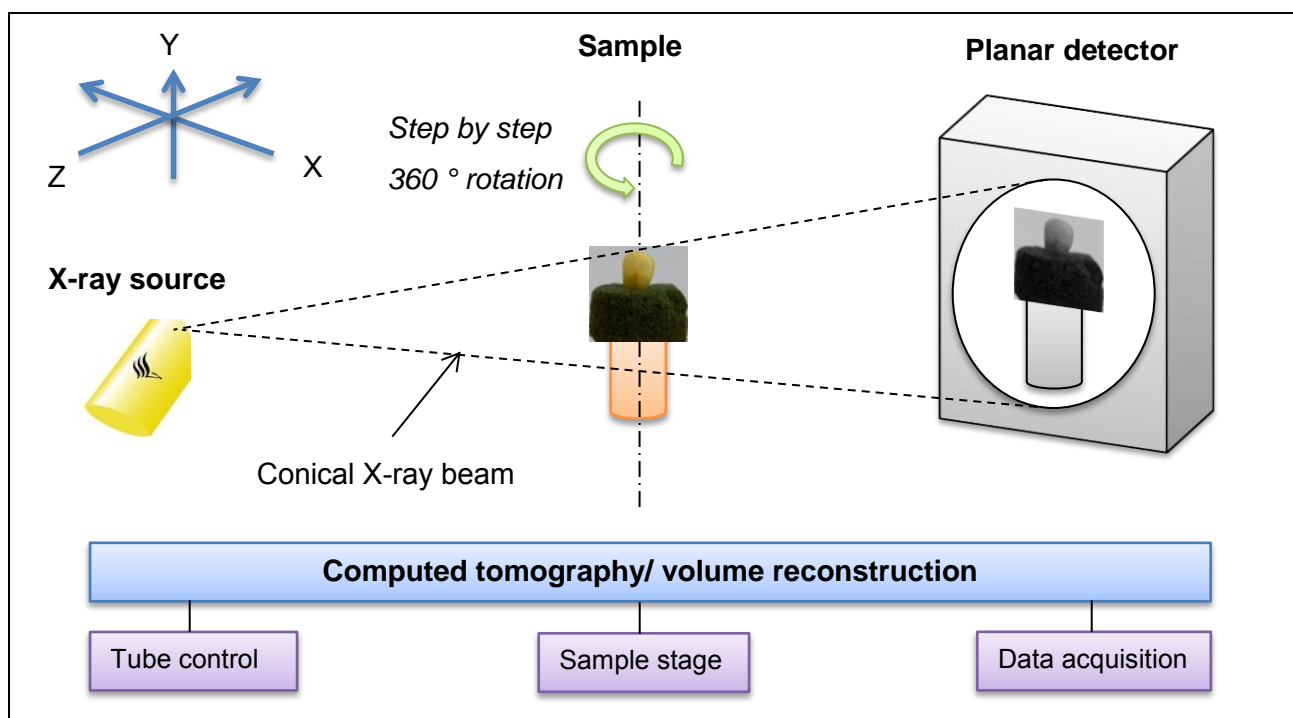
### *Experimental setup and image acquisition*

X-ray CT evaluates the internal structure of a sample by means of a X-ray source and a detector in order to obtain information from a projected slice (Kotwaliwale *et al.*, 2014). The principle is based on image contrast that is produced by variations in the X-ray attenuation that includes absorption and scattering (Lim & Barigou, 2004). When an X-ray beam passes through a sample it is attenuated. The differences in attenuation are attributable to density and compositional differences

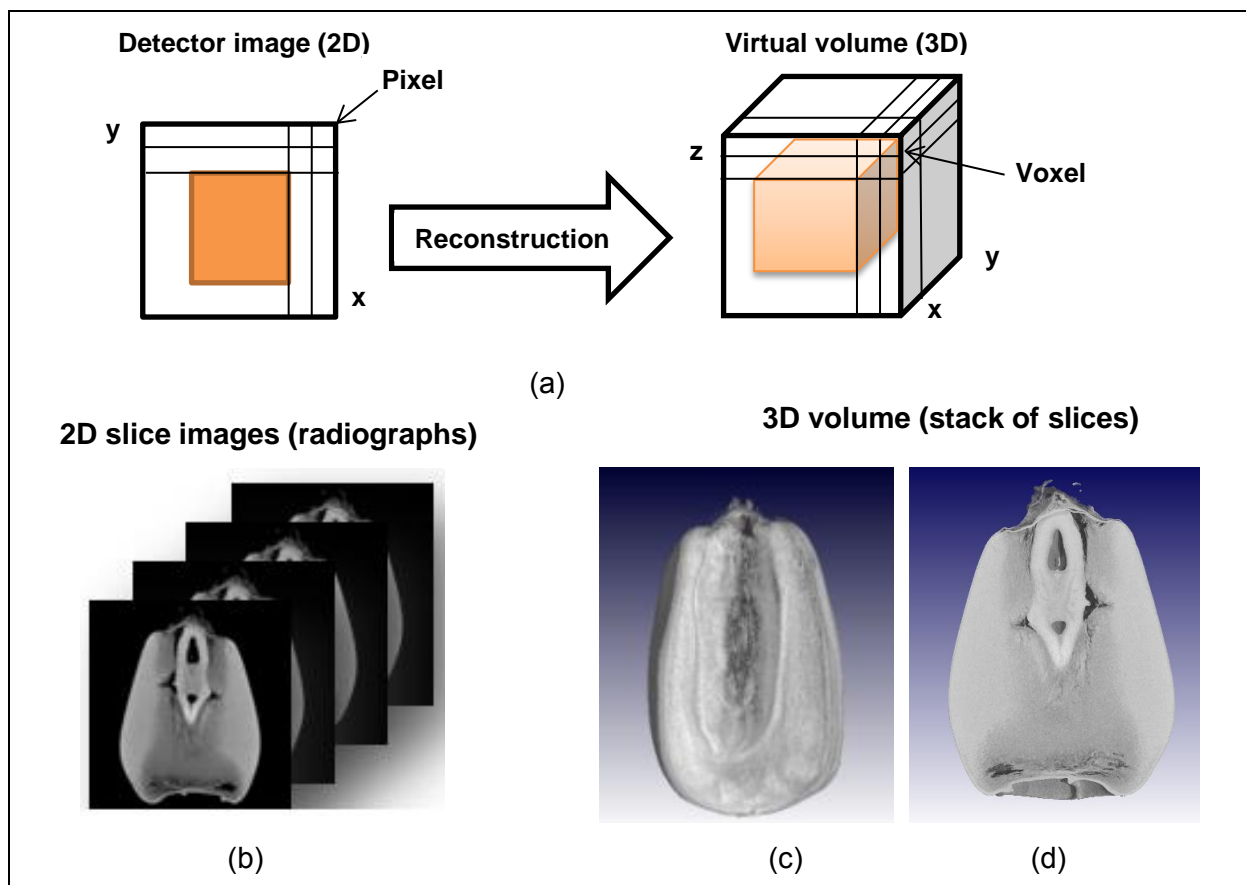
within a sample. Thus the transmission level of the X-ray is determined by the mass as well as the absorption coefficient of a sample.

During image acquisition an X-ray beam, which is collimated, is directed toward a sample, the detector measures the remnant attenuated radiation and the response is transferred to a computer. This radiation type has the ability to penetrate a sample in varying degrees (Cnudde & Boone, 2013). Before scanning, instrumental conditions such as beam energy and current, sample-to-detector distance and exposure time, must be optimised.

During scanning a sample is rotated on a translation stage while illuminated with X-rays (Baker *et al.*, 2012). The X-rays pass through the object in many different directions and along different pathways to create an image illustrating variation in density at numerous points in a 2D slice (Lim & Barigou, 2004). As the sample rotates, a series of 2D radiographs or projection images are acquired (Frisullo *et al.*, 2009). The total angle of rotation depends on the geometry of the beam and the sample, but is typically  $180^\circ$  in the case of a parallel beam (e.g. synchrotron) or  $360^\circ$  when a cone-beam is used (e.g. laboratory system) (Baker *et al.*, 2012). Figure 2.1 schematically demonstrates the acquisition principle. The detector records the object that is transversed by the conical X-ray beam. The ratio of distance from the tube to the detector and to the sample determines the magnification. Data from numerous X-ray radiographs are processed with a computer to reconstruct a 3D volume (Fig. 2.1).



**Figure 2.1.** Schematic illustration of the measurement principle of X-ray CT. An object is exposed to collimated X-rays, generated by the X-ray tube and the detector converts the X-rays into digital radiographs.



**Figure 2.2.** Representation of (a) the reconstruction process where a 3D volume is created from the 2D projection images and the illustration of (b) the stacking of 2D slices to obtain (c) a 3D image and (d) a clipped image.

Tomograms, which are the 3D representation of a sample's internal structure and composition, can be extracted from these 3D volumes. This image is comprised of volume elements (voxels) that represent the X-ray absorption at a specific point (Landis & Keane, 2010) (Fig. 2.2 (a)). The images can be presented as virtual slices at various depths and in various directions or the sample can be viewed as a whole. Dedicated software packages enable manipulation and analysis of the data as well as reconstruction of cross-sections along any orientation. Image contrast is due to differences in X-ray absorption and is caused by density and compositional variation in the sample. It is the association between X-ray absorption and object density that enables the 3D internal structure to be visualised (Landis & Keane, 2010). Thus, the images obtained could be considered a map of the X-ray spatial distribution, where the brighter regions correspond with a higher density (Frisullo, *et al.*, 2009).

Different types of reconstruction algorithms have been developed which can be divided into direct and iterative approaches (Landis & Keane, 2010). Direct methods are most often used and include filtered back projection (FBP) and direct Fourier inversion (DFI) (Landis & Keane, 2010). Due to the fact that reconstruction is such a computational intensive procedure and the high



commercial value of a rapid reconstruction algorithm, these algorithms are usually patented and not freely available (Landis & Keane, 2010).

## **X-ray CT systems**

The earliest CT scanners made use of a linear array of photodetectors which resulted in image acquisition and reconstruction occurring slice-by-slice (fan beam configuration). Subsequent applications of 2D detectors enabled faster scan times through the acquisition of 2D projection images (cone beam configuration) (Fig. 2.1) (Landis & Keane, 2010). For these two beam configurations the spot size of the X-ray source influences the image quality, where a smaller spot size leads to less blurring and thus a more accurate image (Landis & Keane, 2010). The development of high resolution digital detectors and micro-focus sources, in recent years, enabled the construction of tomographic systems that have spatial resolutions down to 0.7  $\mu\text{m}$  (Baker *et al.*, 2012).

During image acquisition an X-ray beam, produced by the X-ray tube, transverses through the sample after which it is recorded by the detector; usually an X-ray CCD (charged-coupled-device) camera where an enlarged radiograph (projection) is produced (Lim & Barigou, 2004). The focus of the tube limits the spatial resolution while the actual resolution is dependent on the magnification and object size (Lim & Barigou, 2004). The spatial resolution can be varied by altering the distance of the sample between the source and the detector. This varies the resolution from a few millimetres down to one micron and the acquisition time usually ranges from 20-60 minutes. Time resolution thus remains a concern for most imaging methods; the higher the spatial resolution the longer the image acquisition time (Turbin-Orger *et al.*, 2015). Optimum resolution also depends on sample size, e.g. a 100 mm sample will have a resolution of 100  $\mu\text{m}$  whereas a 10 mm sample will have a resolution of 10  $\mu\text{m}$  (i.e. samples size/spatial resolution ratio of  $10^3$ ).

A noteworthy advance in CT imaging was the use of synchrotron radiation, which led to major enhancements (Landis & Keane, 2010). The high flux of the X-ray beam, high-speed detectors and the rapid reconstruction algorithms of this system, enable 3D images to be created at speeds that nearly approaches real-time (Landis & Keane, 2010). Modern synchrotron X-ray  $\mu\text{CT}$  systems are known for its improved image quality and reduction in data collection time, in contrast to traditional systems (Baker *et al.*, 2012). This is because of the X-ray beam features: the monochromaticity, beam geometry and the high spatial coherence and high intensity (Baker *et al.*, 2012). Due to the much higher resolution of synchrotron X-ray images, compared to those of conventional X-rays, it can more effectively be used to reveal fine details of also soft tissue. In addition, the fast acquisition times enables real-time analysis.

Because of these different properties and imaging features, a synchrotron system is a good tool for investigating food applications. Such systems have been used for the study of bread (Babin *et al.*, 2006), cereal products (Guessasma & Hedjazi, 2012) and pome fruits (Mebatsion *et al.*,

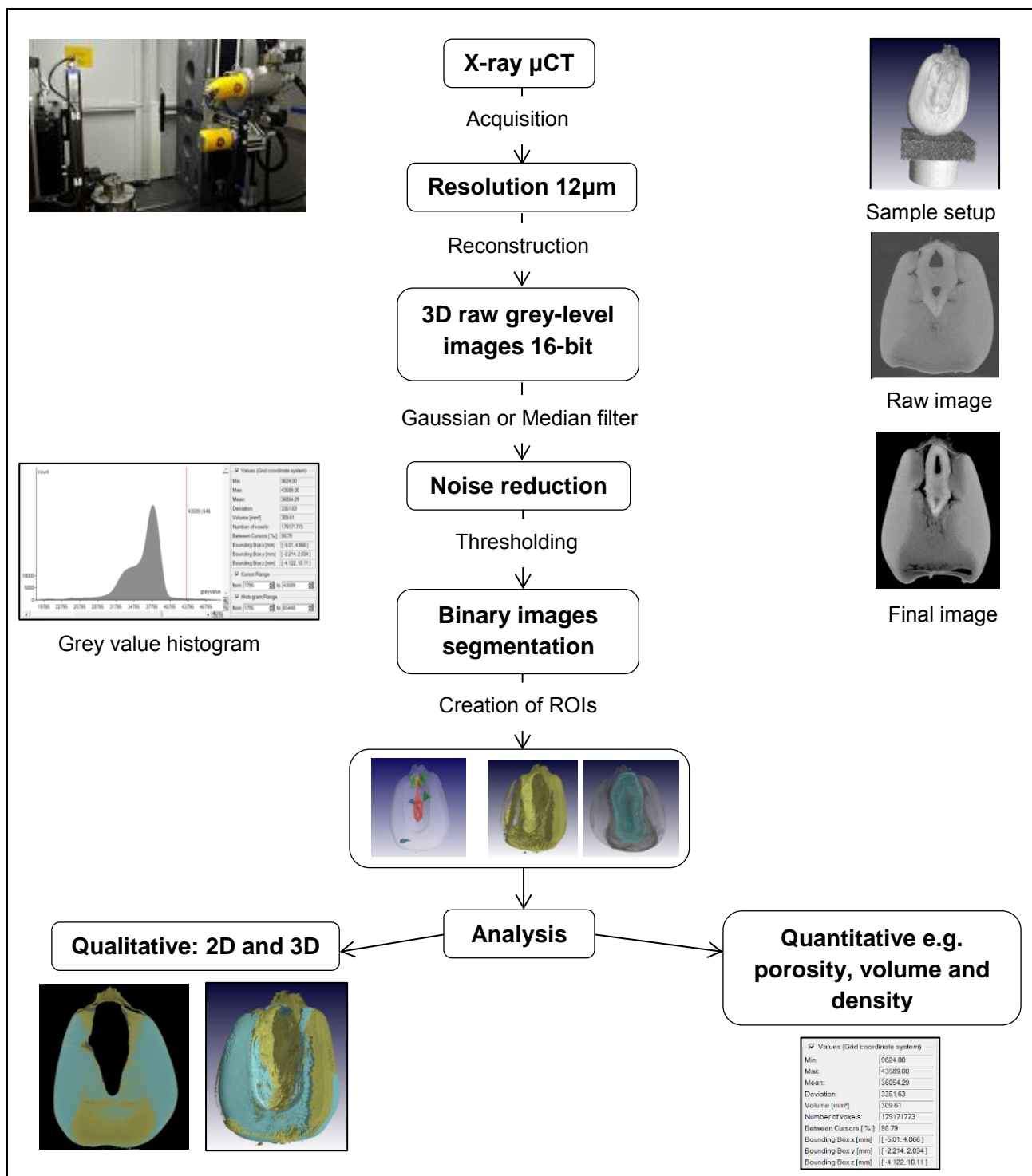
2009). Modern laboratory setups, based on cone-beam geometry, also have the ability to generate high-resolution images and phase-contrast properties but are limited compared to synchrotron imaging (Baker *et al.*, 2012). Synchrotron CT is usually restricted to very small samples, ranging from 5-10 mm (Landis & Keane, 2010).

A newer, faster technique exists with great potential for fast in-line imaging (Donis-González *et al.*, 2014b). The ultrafast Rossendorf fast electron beam X-ray tomograph (ROFEX) scanner relies on an electron beam gun to generate an electron beam, which is focussed onto an X-ray production target. An electromagnetic deflection system allows the X-ray beam to be swept across the target, consequently producing X-rays from the moving focal spot. In this way radiation moves through a sample and a detector captures the radiation intensity signals. Images can be captured at a rate of up to 7000 frames  $s^{-1}$ . ROFEX CT technology can easily be applied in-line to automatically sort agricultural produces, due to its rapid scanning capabilities.

Both modern and laboratory CT systems provide high quality images. Thus, there is no ideal setup for every sample type and therefore a compromise should be found to obtain maximum information (Baker *et al.*, 2012). The convenience of conventional laboratory systems will lead to increased use, but there will always be a gap for the unique characteristics of synchrotron sources (Landis & Keane, 2010).

### **Image processing and analysis**

Image processing and analysis is required to visualise CT data and to extract suitable information from the image. For microstructural analysis information from the sample volume, density, porosity, object surface to volume ratio, particle size and sample thickness can be obtained. X-ray CT and image analysis are non-destructive tools capable of scanning a whole sample to provide information on pore volume and size distributions and density variations (Léonard *et al.*, 2008). A typical image processing and analysis procedure, when e.g. a maize kernel would be imaged and analysed, is schematically illustrated in Figure 2.3.



**Figure 2.3.** Schematic illustration of a typical image processing and analysis procedure used e.g. when analysing a maize kernel. Images with a resolution of 12  $\mu$ m were obtained from a source voltage of 60 kV and an electron current set at 240  $\mu$ A (General Electric Phoenix V|Tome|X L240  $\mu$ CT instrument).

### *Image processing and segmentation*

Image reconstruction maps are estimates of the attenuation coefficients and are dependent on the density variation in a sample. During image processing the images are initially smoothed using

filters (e.g. Gaussian or Median) to reduce random noise. This step is followed by segmentation where the volume is partitioned into voxel groups of each region-of-interest (ROI) in the sample (Baker *et al.*, 2012). Thus the grey scale slices are transformed into a binary layout that consists only of solid (black) and void (white) pixels (Chawanji *et al.*, 2012). The purpose of using ROIs is to separate a volume data set into individual parts, allowing analyses to be restricted to specific areas of a data set. In Figure 2.3, 3D reconstructed X-ray  $\mu$ CT images of a maize kernel and its selected ROIs, i.e. cavities, floury endosperm and germ are illustrated.

Segmentation is usually done using thresholding techniques, i.e. (1) selecting a global threshold that is relevant to all the voxels; (2) locally adaptive thresholds; (3) region-growing techniques; and (4) clustering by iterative techniques (Baker *et al.*, 2012). Voxels containing grey values lower or higher than this threshold value are regarded as background or sample material respectively. It is essential to eliminate errors and unwanted information before starting with analysis. Pre-processing is usually done before image analysis to reduce noise and to correct detector defects. Correction steps usually applied include filtering or smoothing and beam-hardening corrections to suppress random noise and beam-hardening artefacts, respectively (Frisullo, *et al.*, 2009). Filtering is also applied to eliminate artefacts, to increase the visibility of different phases and to enhance the edges of a sample (Baker *et al.*, 2012). After segmentation, a cleaning step is typically applied to remove small quantities of pixels that are considered artefacts i.e. the partial volume effect (Baker *et al.*, 2012). This effect is the result of one pixel containing numerous phases. The cleaning methods are either topological (based on sample connectivity) or morphological (erosion and dilation tools) (Baker *et al.*, 2012).

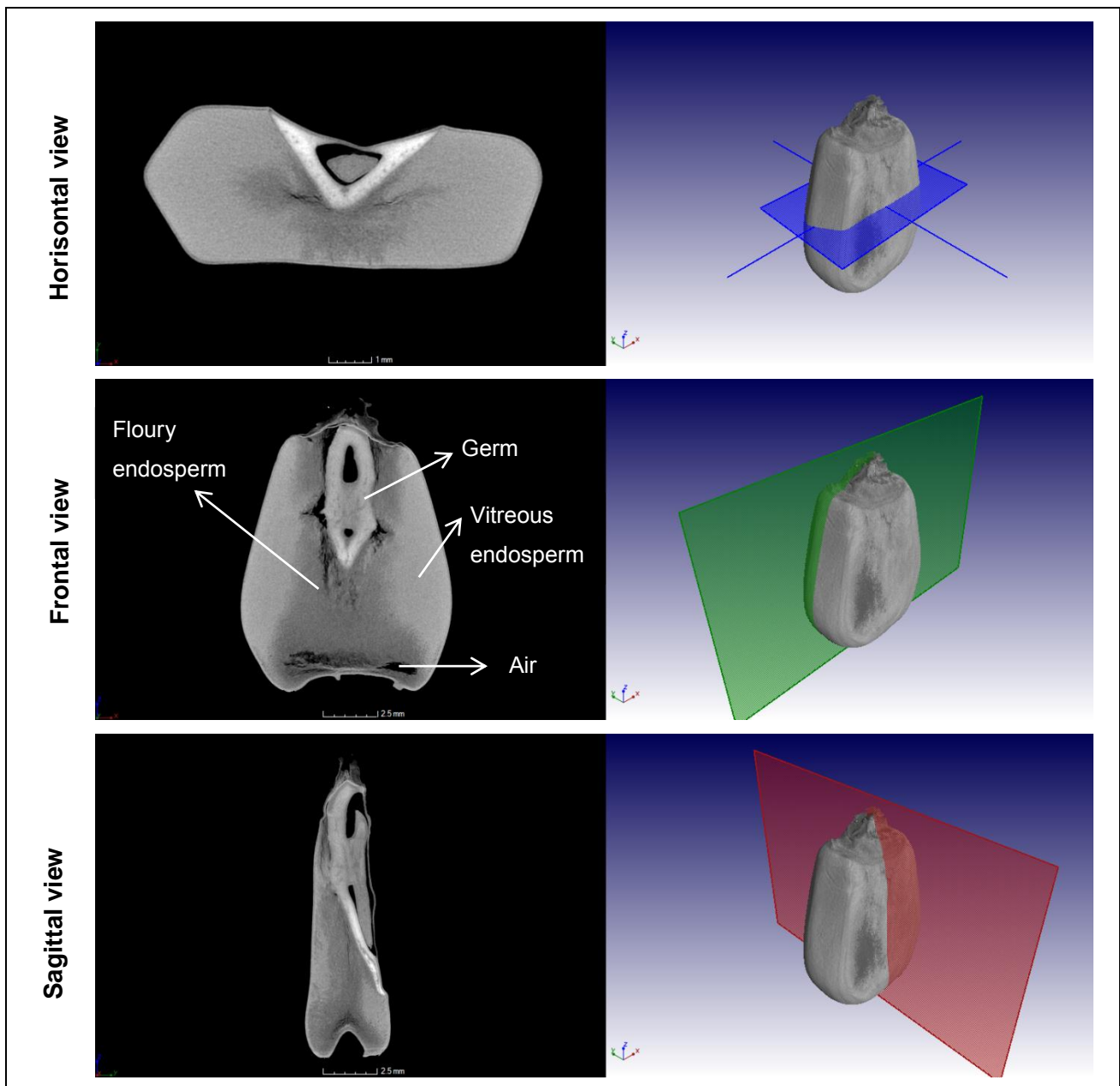
### *Image analysis*

Image analysis is used to qualitatively and quantitatively extract visual information and morphometric parameters to characterise the microstructure of a product (Herremans *et al.*, 2013b). The objective of image analysis is to describe an image on the basis of information that could be extracted from the images or image sequences. Analysing an image in its original form is very time-consuming because of the immense size, therefore it is often reduced to smaller selected ROIs (Jayas *et al.*, 2000). When performing quantitative analysis, representativeness should be taken into consideration (Ramírez *et al.*, 2010). It is thus important that a representative volume element (RVE) is obtained from the sample or ROI. A RVE is a heterogeneous material volume, which is large enough to be statistically representative of the entire sample or ROI. It must therefore include all microstructural variances (e.g. voids and inclusions) present in the sample. A sample (or ROI) with a wide data spread and large structural elements will have a larger RVE than a sample with a narrow distribution and smaller structural features (Ramírez *et al.*, 2010). To ensure representativeness, each ROI should thus be a RVE.

The internal structure of various products can be studied and the distribution of regions varying in density can be visualised through virtual slicing of the 3D rendered volume (Baker *et al.*, 2012). This is only possible if the X-ray attenuation of the ROIs is significantly different to provide adequate contrast. A benefit of X-ray  $\mu$ CT is that image analyses is not restricted to one individual slice at a time, but covers the volume in all three dimensions. Volume data contains an incessant set of voxels that are organised in a 3D grid structure. Voxels are volumetric pixels and thus the 3D equivalent of pixels. The x and y axis represents the vertical and horizontal pixel coordinates (2D), whereas the z axis characterises the 3D spatial dimension. Each voxel signifies a particular area of the sample where the grey value offers information on the density properties in this region. The information from several 2D slices can be merged to create a 3D image that allows volumetric observations and measurements of the 3D microstructure. In contrast to conventional microscopy techniques, X-ray  $\mu$ CT provides both 2D and 3D images of the whole sample and the internal ROIs (Lim & Barigou, 2004).

### *3D and 2D interpretation and visualisation of X-ray CT images*

A 3D map of X-ray absorption can be obtained from the projection images (Landis & Keane, 2010). Different features can be identified from these images due to the variation in absorption of different materials (Landis & Keane, 2010). Three-dimensional CT maps can be viewed in various planes. Figure 2.4 illustrates this approach with a 2D tomogram of a maize kernel. The brightness in the images is correlated to the X-ray absorption, where the brighter regions correspond to a higher absorption (higher grey value) and the dark areas correlate to a lower absorption (lower grey value). From the grey value histogram the lower grey values corresponding to surrounding air and internal void space and higher values corresponding to solid material can be identified. This is valuable for phase analysis and is often used to segment an image into different ROIs. A grey value histogram for a maize kernel has separate peaks each corresponding to a different phase i.e. solid or air (Fig. 2.3). This tool enables segmentation to be done based on thresholding. A threshold is selected where all the pixels lower than the threshold are equal to zero (black) and those larger are equal to one (white) (Landis & Keane, 2010).



**Figure 2.4.** Illustration of the different X-ray image views (horizontal, frontal and sagittal) of a maize kernel. Two-dimensional views are shown on the left and the corresponding section in the 3D view on the right. These images were produced using a General Electric Phoenix V|Tome|X L240  $\mu$ CT instrument with settings of 60 kV and 240  $\mu$ A and a voxel size (resolution) of 12  $\mu$ m.

### 2D vs. 3D analysis

Qualitative assessment of spatial relationships can be performed effectively with 3D renderings (Landis & Keane, 2010). The data acquired from image analysis is a 3D image of a scanned sample comprised of numerous slices. Each slice has a certain number of voxels and each voxel can be related to a Hounsfield Unit (HU) or CT number (Furnols *et al.*, 2009). The HU is regarded as the average attenuation in the corresponding section in the sample on a Hounsfield scale (Furnols *et al.*, 2009). The high resolution of CT and the intrinsic contrast, allows differentiation of



material densities. The image intensity, expressed in HU, represents the attenuation capabilities of a sample (Donis-González *et al.*, 2014b). Thus, differences in the physical density are observed as changes in the CT number. Low-density objects (e.g. air) have a low HU (-1000) and high-density samples (e.g. solid material) a high HU (up to 3000 HU) (Donis-González *et al.*, 2014b). Water has an attenuation of 0 HU and air a value of -1000 HU. Changes in the HU-values between different ROIs are highly correlated with deviations in sample density, thus X-ray CT is sensitive enough to enable accurate quantification of internal density deviations.

Much research in food science demands an understanding of the true 3D morphology to investigate the internal structure of a food product. A 3D approach enables essential and reliable information on microstructure and spatial distribution to be obtained, and it provides insight into the overall structure and morphology of a sample. A 3D model of a sample can be rendered from the reconstructed 2D images. The model can be sliced in any direction and at any depth to enable visualisation of the internal structure. This makes X-ray CT ideal for non-invasive imaging of the internal features of food, especially foods with a delicate structure, giving X-ray CT a leading edge over other methods (Lim & Barigou, 2004).

Software packages enable analysis of images and 3D visualisation with the ability to rotate and cut the sample on a computer screen (Lim & Barigou, 2004). Numerous parameters can be obtained from a 3D model such as air volume, surface-to-volume ratio, connectivity, cell wall thickness and degree of anisotropy (Lim & Barigou, 2004). The section on quantitative X-ray CT data analysis will further expand on this topic.

In 2D analysis the information extracted is usually limited. Considering the 2D slice images in Figure 2.4, a multiphase composition can be observed as the maize kernels are made up of a germ, floury (soft) and vitreous (hard) endosperm and air space. These components can be distinguished owing to the difference in X-ray absorption. This difference manifests itself through the variation in the grey scale intensities and therefore it appears visually as distinct phases. From reconstructed 2D images density differences can be visualised and qualitative information can be obtained. Two-dimensional images is not always fully representative of the true 3D structures, for example where the shapes and sizes of vesicles or pores in a sample is reliant on the location of the 2D section (Baker *et al.*, 2012).

With 2D X-ray imaging only one image is acquired per sample, in contrast to CT where a transverse 2D image (slice) is reconstructed making use of information from more than one 2D projection image obtained at various angles. Thus, 2D X-ray  $\mu$ CT images are capable of demonstrating variation in the size and geometry of certain features such as pores or cavities. The geometry of individual components in a food structure can thus be quantified by size, shape, orientation and position. More information can be provided from a series of CT slices of the same sample than from modern microscopy procedures (e.g. SEM) (Lim & Barigou, 2004). With 3D

analysis ROIs can be selected, the sample can be viewed from any arbitrary angle and it can be cut and sliced to examine the 2D sections in any orientation.

### *3D modelling*

As a result of increased computing power,  $\mu$ CT data can also be used to model the microstructure of materials, perform numerical simulations and to predict mechanical properties. The microstructure of food is a 3D description of the morphology, where the quantification of a sample's microstructure begins with a geometric model. A 3D model of the microstructure of a product can be built and image analysis techniques can be used to attain quantitative data on a number of properties such e.g. cell wall-thickness, spatial size distribution, voidage, connectivity and degree of anisotropy (Lim & Barigou, 2004). The development of different finite element (FE) methods, which are numerical methods capable of predicting material properties from accurate structural knowledge in mechanical modelling, has been well demonstrated for composite materials (Maire *et al.*, 2003). More recently it has been applied to food science for the mechanical modelling of cereal products in order to predict texture (Guessasma *et al.*, 2011). FE modelling can be divided into four stages: definition of geometry and meshing; input of material properties; stress distribution of the REV; and lastly the REV being submitted to a virtual standard mechanical test (Guessasma, *et al.*, 2011).

X-ray CT can simulate food samples and create models by combining object measurements with the 3D microstructure (Baker *et al.*, 2012). As a result of the strong contrast between the matter within the sample and the voids, X-ray tomography is capable of providing 3D images of the structure of porous foods (Lim & Barigou, 2004). Even though the application of X-ray CT 3D simulations in food science is in its early stages, tomographic imaging as a foundation for modelling structures has become commonplace. In a novel method by Mebatsion *et al.* (2009) 3D microstructural modelling of pome fruit tissue was performed using synchrotron radiation. Herremans *et al.* (2014b) made use of multiscale modelling to understand the changes in gas concentrations, respiration and fermentation rates in apples during the development of a disorder.

A review on multiscale modelling explains the underlying physical and computational concepts and provides an overview of the applications in food engineering (Ho *et al.*, 2013). Modelling the microstructural evolution and fracture of brittle confectionery wafer has been studied in a recent publication which combined X-ray  $\mu$ CT and FE methods (Mohammed *et al.*, 2014). This study demonstrated that an FE model can predict the product properties with a high level of accuracy in order to optimise industrial processes. The most accurate way of accounting for the structure when modelling cellular samples is to use the 3D information obtained by X-ray  $\mu$ CT to develop a FE model of the real microstructure (Maire *et al.*, 2003). A drawback of using FE computations, obtained from X-ray  $\mu$ CT, is that these computations are both time- and memory-consuming



(Mohammed *et al.*, 2014). It is always aimed to find a compromise between computing time and the accuracy of results.

### **Information provided by X-ray $\mu$ CT: Qualitative and quantitative**

A range of commercial and open source software is available for extracting qualitative and quantitative information from a data set (Landis & Keane, 2010). Furthermore, animations illustrating evolutionary processes add value to the investigations in a manner, not possible with 2D analyses. Initially, very few studies have attempted to study food microstructure in an objective manner, since researchers often just report a few cross-sectional images in combination with a qualitative discussion of the microstructure, without investigating the quantitative measurement of key properties. Studies have shown that X-ray  $\mu$ CT has been established as an accurate method for the visualisation of the microstructure of materials with pixel sizes close to, and below 1  $\mu\text{m}$  (Van Dalen *et al.*, 2007; Verboven *et al.*, 2008). In favourable conditions, X-ray CT delivers unparalleled data with a great level of detail that is not easily matched by any other technique (Baker *et al.*, 2012). Even though 2D slice images provides qualitative and some quantitative value, it is the digital nature and quantitative possibilities of 3D volumes that is the most compelling characteristic of tomographic data (Landis & Keane, 2010).

#### *Qualitative X-ray CT data analysis*

Qualitative analysis is essential to distinguish between diverse classes of a commodity or to detect anatomical and physiological changes. Furthermore, the cell structure of products can be observed giving an indication of the connectivity between cells. 3D rendered images enable the visualisation of the morphology and microstructure such as the pore shape, size and distribution.

Qualitative data analysis offers a powerful tool for improving the understanding of sample structure relationships and the spatial distribution throughout the sample. Qualitative 3D modelling is possible as a result of the added spatial dimension. CT images illustrate similarity in samples through the grey values; similar grey values correspond to similar densities.

#### **Quantitative X-ray CT data analysis**

Besides 3D visualisation of the reconstructed volume through 3D rendering procedures, image processing also enables the quantitative analysis of data volumes (Baker *et al.*, 2012). Various microstructural parameters, i.e. size distribution of void cells, wall thickness, volume fractions, porosity, dimensions, and connectivity along with density information can be obtained from data sets. In food science, the geometry and organisation of structural components i.e. ice crystals, pores, fractures and areas of internal disorders can be examined using X-ray  $\mu$ CT.

Over the past decade software for morphological quantitative tomographic data sets has significantly advanced and commercially available software is the result of industry demand (e.g.

Avizo-VSG, VGStudio Max, ImageJ and MAVI-Fraunhofer ITWM) and several research groups have developed their own toolboxes for IDL® (Interactive Data Language) and Matlab® software (e.g. Blob3D, Pore3D, 3DMA and Quant3D) (Baker *et al.*, 2012).

Once a segmented volume, with the various ROIs, has been defined measurements can be performed. For example, the number of bubbles, the bubble volume and size can be determined in an aerated chocolate (Haedelt *et al.*, 2007). The quantification of structural parameters enables the objective relationship between microstructure and other properties. The microstructure of a sample can be quantified by applying 2D and 3D algorithms that results in morphometric parameters and geometric 3D models of microstructures (Herremans *et al.*, 2013b). X-ray  $\mu$ CT enables the visualisation and quantification of 3D microstructures at scales down to a sub-micron level (Baker *et al.*, 2012). Herremans *et al.* (2013b) describes the 3D microstructural parameters that can be used for the quantification of microstructure.

### **Image texture analysis**

Image texture analysis is regarded as an essential feature in the food industry for quality evaluation (Zheng *et al.*, 2006). One should, however, not confuse the concept of texture in computer vision (image texture analysis) and texture of food products (Zheng *et al.*, 2006). Food texture is described by properties such as hardness, elasticity, viscosity and chewiness in contrast to image texture that refers to coarseness, fineness, smoothness and graininess. Image texture is regarded as the spatial arrangement of the brightness values of pixels and is comprised of four different texture feature categories, i.e. statistical texture, structural texture, model-based texture and transform-based texture (Zheng *et al.*, 2006). Statistical texture makes use of statistical methods obtained from higher-order pixel grey values. Structural texture is based on structural primitives conducted from the grey values of pixels. Model-based texture is achieved by computing coefficients from a model based on the association of the grey values between a pixel and its neighbouring pixels. Transform based texture is based on the use of statistical measurements from images which is transformed with specific techniques. Of the above mentioned the most frequently used technique in the food industry, for quality grading, is statistical texture because of its high accuracy and reduced computation time.

### **Principles**

Images consist of basic components known as pixels. Each pixel includes two kinds of information, i.e. the brightness value as well as the locations in the coordinates that are allocated to the images (Zheng *et al.*, 2006). Brightness is a colour feature, while the latter correlates to shape or size features. Another image feature is texture and it corresponds to both the above mentioned features (Zheng *et al.*, 2006). One of the most widely used statistical texture analysis methods is grey level co-occurrence matrix (GLCM) and this method extracts textural features by statistical methods

from the co-occurrence matrix. Information on the distribution of grey level intensities in relation to the relative position of pixels with equal intensities is provided by a GLCM (Paliwal *et al.*, 2003).

### *Applications*

Texture is regarded as an important image feature that can be used for describing image properties and it has a wide range of applications, which includes food quality evaluation. From the texture in images, changes in the intensity values of the pixels can be observed, since a change in intensity might indicate a change in geometric structure (Zheng *et al.*, 2006). In the food industry, texture can be an indicator of quality as it can reflect the cellular structure of food. For instance, texture can be used to reflect beef tenderness (Li *et al.*, 1999). The food industry is regarded as one of the top ten manufacturers using computer vision for image texture analysis as its application includes a wide range of foodstuffs i.e. vegetables (Thybo *et al.*, 2004), cereal grains (Paliwal *et al.*, 2003) and fruits (Kondo *et al.*, 2000).

### **Food applications**

In recent years, X-ray  $\mu$ CT has become more commonplace in food science for evaluating quality and microstructure, enabling a better understanding of the physical structure of a sample. X-ray  $\mu$ CT has been investigated on an extensive range of commodities (fish, meat, fruit and vegetables, dairy, cereals, coffee beans, nuts, confectionary and baked products) and applications (internal disorders, microstructural characterisation and quantification, infestation detection, visualise pore structure and pore size distribution; estimate and evaluate a specific ingredient or component).

Reliable microstructural information on foods undergoing chemical and physical processes has successfully been obtained using X-ray  $\mu$ CT (Léonard *et al.*, 2008). This tool is however still relatively new in the field of food processing (Lim & Barigou, 2004). In the food industry 3D X-ray microstructural applications are gaining popularity in order to understand the functionality of food components and ingredients (Chawanji *et al.*, 2012; Pareyt *et al.*, 2009), and to determine internal quality, especially to detect internal defects in agricultural products (Kotwaliwale *et al.*, 2014).

X-ray  $\mu$ CT is particularly well suited to investigate the dynamics of structural changes in food, provided that it takes the time resolution constraints into account. Examples include the 3D characterisation of three-phase systems to track the microstructural evolution in ice cream (Pinzer *et al.*, 2012) and to study bread dough aeration dynamics (Trinh *et al.*, 2013). Challenges encountered in such applications are illustrated by Turbin-Orger *et al.* (2015) who examined the evolution of cellular structures in fermenting wheat flour dough, specifically looking at the growth and setting of gas bubbles. An overview of X-ray  $\mu$ CT applications related to the various commodities in the food industry is given in Table 2.1.

**Table 2.1.** An overview of X-ray  $\mu$ CT applications related to various food commodities and types

Food commodity/ type	Tube voltage and current	Spatial resolution	Application	Reference
<b>Meat and fish</b>				
Chicken nuggets	100 keV, 98 $\mu$ A	14.06 $\mu$ m	Microstructural characterisation	(Adedeji & Ngadi, 2011)
Cured pork	130 keV	6.2 pixels/mm	Quantification of salt concentrations	(Vestergaard <i>et al.</i> , 2004)
Dry cured ham	80, 120 and 140 kV, 250 mA	1.1 pixels/mm	Prediction of salt and water content	(Fulladosa <i>et al.</i> , 2010)
Freshwater fish	-	-	Fillet composition measurement	(Romvári <i>et al.</i> , 2002)
Lamb	-	-	Carcass composition and meat quality traits	(Karamichou <i>et al.</i> , 2006)
Pork	140 kV, 145 mA	-	Lean meat prediction using a density model	(Picouet <i>et al.</i> , 2010)
Pork	-	-	Fat deposition and distribution	(Kolstad, 2001)
Pork	80, 110 and 130 kV, 106 mA	0.3, 0.5 and 0.6 pixels/mm	Sodium quantification	(Håseth <i>et al.</i> , 2008)
Pork	140 kV, 145 mA	-	Estimation of lean meat content	(Furnols <i>et al.</i> , 2009)
Processed meat	82 kVp, 125 $\mu$ A	15 $\mu$ m	Intramuscular fat level and distribution	(Frisullo <i>et al.</i> , 2009)
Salmon	80, 110 and 130 kV, 106 mA	2.56 pixels/mm	Salt and fat distributional analysis	(Segtnan <i>et al.</i> , 2009)
Salmon	150 keV, 164 $\mu$ A	-	Ice recrystallisation	(Syamaladevi <i>et al.</i> , 2012)
Sausages	100 kVp, 100 $\mu$ A	17.3 $\mu$ m	Microstructural analysis and the relationship with hardness	(Santos-Garcés <i>et al.</i> , 2013)
<b>Dairy</b>				
Cheese	120 kV, 150 mA	0.424 and 0.431 pixels/mm	Quantitative determination of eye formation	(Schuetz <i>et al.</i> , 2013)
Cheese	120 kV, 150 mA	0.423-0.508 pixels/mm	Quantitative determination of eye formation	(Guggisberg <i>et al.</i> , 2013)

Cream cheese	100 kVp, 100 $\mu$ A	2 $\mu$ m	Microstructural characterisation	(Laverse <i>et al.</i> , 2011b)
Eggshell	85 kV, 70 $\mu$ A	1.5 $\mu$ m	Quantification of microstructure	(Riley <i>et al.</i> , 2014)
Ice cream	75 kV	6 $\mu$ m	Tracking microstructural evolution	(Pinzer <i>et al.</i> , 2012)
Mayonnaise	100 kVp, 100 $\mu$ A	2 $\mu$ m	Microstructural characterisation	(Laverse <i>et al.</i> , 2012)
Milk powder	45 keV, 177 $\mu$ A	2 $\mu$ m	Microstructure of loose-packed and compacted milk powders	(Chawanji <i>et al.</i> , 2012)
Yogurt	100 kVp, 100 $\mu$ A	2 $\mu$ m	Fat microstructure	(Laverse <i>et al.</i> , 2011a)
<b>Fruit and vegetables</b>				
Apples	40 keV	9.89 $\mu$ m	Microstructural visualisation of different cultivars	(Ting <i>et al.</i> , 2013)
Apples	85 and 58 keV	82.6 and 4.8 $\mu$ m	Quantitative microstructural engineering	(Herremans <i>et al.</i> , 2014b)
Apples	80 keV, 100 $\mu$ A and 49 keV, 201 $\mu$ A	4.8 $\mu$ m	Comparison of X-ray CT and MRI to detect watercore disorder	(Herremans <i>et al.</i> , 2014a)
Apples	63 kV, 156 $\mu$ A	8.5 $\mu$ m	Investigation of the multifractal properties of pore-size distribution	(Mendoza <i>et al.</i> , 2010)
Apples	58 keV	4.8 $\mu$ m	Characterisation of 'Braeburn' browning disorder	(Herremans <i>et al.</i> , 2013b)
Bananas	60 kV, 167 $\mu$ A	15 $\mu$ m	Effect of far-infrared radiation on the microstructure	(Léonard <i>et al.</i> , 2008)
Cucumbers, pineapples, cherries and chestnuts	120 keV, 170 and 240 mA	1.289 pixels/mm	Internal characterisation of agricultural products	(Donis-González <i>et al.</i> , 2014b)
Kiwi fruit	60 kV, 167 $\mu$ A	4.87 $\mu$ m	Microstructural characterisation	(Cantre <i>et al.</i> , 2014)
Mango	150 keV, 3mA	-	Linking X-ray absorption with physicochemical properties	(Barcelon <i>et al.</i> , 1999)
Nectarines	80 kV, 40 mA	-	Woolly breakdown	(Sonego <i>et al.</i> , 1995)
Pears	53 kV, 0.21 mA	-	Investigating core breakdown	(Lammertyn <i>et al.</i> , 2003)

Pomegranate	200 kV, 100 $\mu$ A	71.4 $\mu$ m	Quantification and characterisation of internal structure	(Magwaza & Opara, 2014)
Tomatoes	-	-	Determining maturity	(Brecht <i>et al.</i> , 1991)
<b>Cereals and cereal products</b>				
Cereal powders	50 kV, 800 $\mu$ A	6.46 $\mu$ m	Internal microstructural characterisation to study process structure relationships	(Hafsa <i>et al.</i> , 2014)
Cornflakes	-	15 $\mu$ m	Relationships between texture, mechanical properties and structure	(Chaunier <i>et al.</i> , 2007)
Crackers, coated biscuit shells and wheat based soup	50 kV, 100 $\mu$ A	15 and 18 $\mu$ m	Imaging and analysis of porous cereal products	(Van Dalen <i>et al.</i> , 2007)
Maize	40 kV	-	Analysis of maize kernel density and volume	(Gustin <i>et al.</i> , 2013)
Maize	60 kV, 240 $\mu$ A	13.4 $\mu$ m	Estimation of maize kernel hardness using a density calibration	(Guelpa <i>et al.</i> , 2015)
Maize	150 kV, 70 $\mu$ A	8 $\mu$ m	Investigating <i>Fusarium</i> infection	(Williams, 2013)
Rice	46 kV, 75 $\mu$ A	3.91 $\mu$ m	Study of high-amylose and wild-type rice kernel structure	(Zhu <i>et al.</i> , 2012)
Rice	50 kV, 100 $\mu$ A	9.1 $\mu$ m	Effect of kernel microstructure on cooking behaviour	(Mohorič <i>et al.</i> , 2009)
Rice	50 kV, 100 $\mu$ A	9.1 $\mu$ m	Structural and hydration properties of heat-treated rice	(Witek <i>et al.</i> , 2010)
Wheat	140 kV, 96 mA	3.42 pixels/mm	Imaging and automated detection of <i>Sitophilus oryzae</i> (Coleoptera: Curculionidae) pupae	(Toews <i>et al.</i> , 2006)

Wheat	13.5 kV, 185 $\mu$ A and 26 kV, 11 $\mu$ A	60 pixels/mm	Dual energy X-ray imaging for classifying vitreousness	(Neethirajan <i>et al.</i> , 2007)
Wheat, barley, flax seed, peas and mustard	-	120 and 200 $\mu$ m	Analysis of the pore network	(Neethirajan & Jayas, 2008)
Wheat, barley, flax seed, peas and mustard	420 kV, 1.8 mA	120 $\mu$ m	Explanation of airflow resistance	(Neethirajan <i>et al.</i> , 2006)
Cereal food foams	17.6 keV and 50 kV	6.5, 7.5, 16.2 and 25.8 $\mu$ m	Determination of cellular structure	(Chevallier <i>et al.</i> , 2014)
<b>Coffee beans and nuts</b>				
Chestnut	120 kV, 170 mA	1.42 and 2.52 pixels/mm	Postharvest assessment of internal decay	(Donis-González <i>et al.</i> , 2014a)
Coffee beans	29 kVp, 175 $\mu$ A	2.8 $\mu$ m	Microstructural changes induced by roasting	(Frisullo <i>et al.</i> , 2012)
Coffee beans	19 and 20 keV	9 $\mu$ m	Evaluation of microstructural properties	(Pittia <i>et al.</i> , 2011)
Pecan nuts	120 kV, 33mA	-	Insect behaviour	(Harrison <i>et al.</i> , 1993)
Pecan nuts	4-50 kVp, 1 mA	-	X-ray attenuation coefficients of pecan components	(Kotwaliwale <i>et al.</i> , 2006)
<b>Confectionary</b>				
Chocolate	-	-	Characterisation of the structure of bubble-included chocolate	(Haedelt <i>et al.</i> , 2007)
Chocolate	37 kV, 228 $\mu$ A	13.3 $\mu$ m	Microstructural characterisation	(Frisullo <i>et al.</i> , 2010b)
Foams	100 kV, 96 $\mu$ A	10-20 $\mu$ m	Microstructure of foams	(Lim & Barigou, 2004)
Sugar gels	49 keV, 201 $\mu$ A	4 $\mu$ m	Microstructure–texture relationships	(Herremans <i>et al.</i> , 2013a)
<b>Dough and baked products</b>				
Biscuits	80 kV, 180 $\mu$ A	22.5 $\mu$ m	Impact of flavour solvent on biscuit	(Yang <i>et al.</i> , 2012)

			microstructure	
Bread	59 kV, 149 $\mu$ A	16-20 $\mu$ m	Pore structure of bread crumbs	(Wang <i>et al.</i> , 2011)
Bread	50 kV, 100 $\mu$ A	6 $\mu$ m	Effect of crumb morphology on water migration and crispness retention	(Hirte <i>et al.</i> , 2012)
Bread	49 keV, 200 $\mu$ A	5.9 $\mu$ m	Microstructural properties of extruded crisp bread	(Gondek <i>et al.</i> , 2013)
Bread	18 keV	15 $\mu$ m	Bubble growth and foam setting during breadmaking	(Babin <i>et al.</i> , 2006)
Bread	12 keV	14 $\mu$ m	3D quantitative analysis	(Falcone <i>et al.</i> , 2005)
Bread	75 kV, 220 $\mu$ A	30 $\mu$ m	Characterisation of structural patterns	(Van Dyck <i>et al.</i> , 2014)
Bread	-	10 $\mu$ m	Granulometry of bread crumb grain	(Lassoued <i>et al.</i> , 2007)
Bread (gluten-free)	45 kVp, 177 $\mu$ A	-	Structural characterisation	(Demirkesen <i>et al.</i> , 2014)
Bread and biscuits	59 kVp, 167 $\mu$ A	15 $\mu$ m	Microstructural analysis	(Frisullo <i>et al.</i> , 2010a)
Bread dough	50-65 keV, 200-285 $\mu$ A	7.1-10.8 $\mu$ m	Aeration dynamics during pressure step-change mixing	(Trinh <i>et al.</i> , 2013)
Bread	50 kV, 800 $\mu$ A	22.1 $\mu$ m	Characterising cellular structure of bread crumb and crust	(Besbes <i>et al.</i> , 2013)
Cake	40 kV, 250 $\mu$ A	23.29 $\mu$ m	Structural parameters and starch crystallisation	(Sozer <i>et al.</i> , 2011)
Sugar-snap cookies	68 kV, 0.51 mA	91 $\mu$ m	Effect of fat and sugar	(Pareyt <i>et al.</i> , 2009)
Wheat flour dough	70 kV, 109 $\mu$ A	10 $\mu$ m	Investigation of bubble size distribution	(Bellido <i>et al.</i> , 2006)
Wheat flour dough	17.6 keV	5 and 15 $\mu$ m	Growth and setting of gas bubbles	(Turbin-Orger <i>et al.</i> , 2015)



### *Meat and fish*

Most X-ray  $\mu$ CT applications on meat considered the estimation of fat and its distribution. Fat contributes to palatability (juiciness, taste and texture) of meat products. Chemical extraction methods are time-consuming, expensive, and destructive and make use of flammable solvents harmful to the environment and health. Frisullo *et al.* (2009) investigated the fat distribution (qualitative) as well as the content (quantitative) in salamis by means of the percentage object volume (POV), structure thickness and object structure volume ratio (OSVR). Validation of the X-ray  $\mu$ CT technique with chemical analysis showed no statistical differences. It was also possible to determine the microstructure of fat and protein simultaneously (quantitatively and qualitatively). Conventional chemical techniques only quantify chemical components one at a time.

The intramuscular fat content and distribution in various beef meat joints and breeds could be accurately determined ( $r = 0.92-0.99$ ,  $P < 0.001$ ) using the POV as determined with X-ray  $\mu$ CT and the soxhlet extraction as reference method (Frisullo *et al.*, 2010c). Although this method is expensive, it provides more information regarding the fat distribution thus enabling a more accurate description of the meat quality.

### *Dairy products*

The dairy industry has been using X-ray  $\mu$ CT for a number of analyses as detailed in Table 2.1. More recently, complex products such as cream cheese (Laverse *et al.*, 2011b) and mayonnaise (Laverse *et al.*, 2012) were evaluated for a variety of characteristics. Pinzer *et al.* (2012) used X-ray  $\mu$ CT to track the microstructural evolution during temperature variation in ice cream by means of time-lapse studies.

The microstructure of milk powders, both loose-packed and compacted as well as spray-dried skimmed and whole milk powders was examined by Chawanji *et al.* (2012). This allowed the quantification of the proportion of interstitial and occluded air voids. This is of importance as the packing density is portrayed by the air voids and directly impacts the transportation and storage costs. Furthermore, the microstructural details such as the shape and size of the particles and internal voids could be characterised. It was found that the disparity in the air voids of the loose-packed and compacted samples were due to the powder particle shape, size and surface properties.

### *Fruit and vegetables*

The fruit and vegetable industry suffers great losses, as approximately 25 to 30% of the production is discarded after harvest due to undetectable internal quality defects and safety problems. Fresh fruit and vegetable quality is measured in terms of external factors (i.e. colour, shape, size and surface mould) as well as internal disorders that is the result of physiological and anatomical changes (e.g. moisture loss, senescence, bruising, decay, insect injury, discolouration and

microorganism attack) (Donis-González *et al.*, 2014b). One of the most important advantages of X-ray imaging is that defects or internal disorders can be identified and visualised in  $\mu$ CT images, before they can be seen on the product itself. However, in spite of the extensive research effort, internal characterisation of fresh fruit and vegetables using X-ray imaging is still uncommon in the industry.

Since the first application of X-ray  $\mu$ CT in the early 1990's, the detection of maturity in green tomatoes (Brecht *et al.*, 1991), numerous investigations have been performed on fruit and vegetables making it the most prominent field of application. X-ray  $\mu$ CT has mainly been used to determine factors that negatively impact quality such as anatomical and physiological deviations within the tissue of fruit and vegetables i.e. decay, insect infestations, internal disorders and cell breakdown. The earliest applications in horticulture focussed mostly on fruit such as mangoes and peaches, with little reported on vegetables.

An X-ray imaging inspection method to detect an internal disorder, spongy tissue, in mangoes was developed in 1993 (Thomas *et al.*, 1993). Differences between the healthy and affected fruit were indicated by variances in the grey values of the X-ray images. Spongy tissue appeared as darker regions, whereas the sound fruit were correlated to lighter areas. Density differences were also used to discriminate between sound mangoes (lighter regions) and fruit infested with weevils (dark areas) (Thomas *et al.*, 1995).

A few studies compared MRI and X-ray  $\mu$ CT. Herremans *et al.* (2014b) investigated the effect of watercore disorder on different apple cultivars. Despite the better contrast in the MRI images, 89% of the fruit was correctly classified using X-ray  $\mu$ CT in comparison to the 79% classification accuracy with MRI. These techniques were also used to study the spatial distribution of core breakdown in 'Conference' pears (Lammertyn *et al.*, 2003). Both were capable of differentiating between unaffected tissue, brown tissue and cavities. However, MRI appeared to produce a better contrast between unaffected and affected tissue.

A more recent study by Donis-González *et al.* (2014b) investigated the internal attributes of fresh agricultural products: pickling cucumbers (internal defects), pineapples (translucency defects) and cherries (pit presence and infestation) using traditional and ultrafast X-ray  $\mu$ CT imaging. The authors found that changes in the internal tissue of agricultural commodities, caused by various factors (e.g. insect damage, disorders or void presence), leads to significant changes in the HU. This value either increased or declined with respect to healthy tissue.

There is potential for non-destructive inline sorting of agricultural products using X-ray  $\mu$ CT. This will enable detection of internal quality characteristics (after validation under commercial conditions) at a relatively early stage and prevent fruit with short shelf life from entering the supply chain (Donis-González *et al.*, 2014b). With the 3D advantage and the ability to visualise the internal structure, improved knowledge of products are obtained that could result in a better understanding of the environmental effects on the fruit and vegetable structure. Even though larger

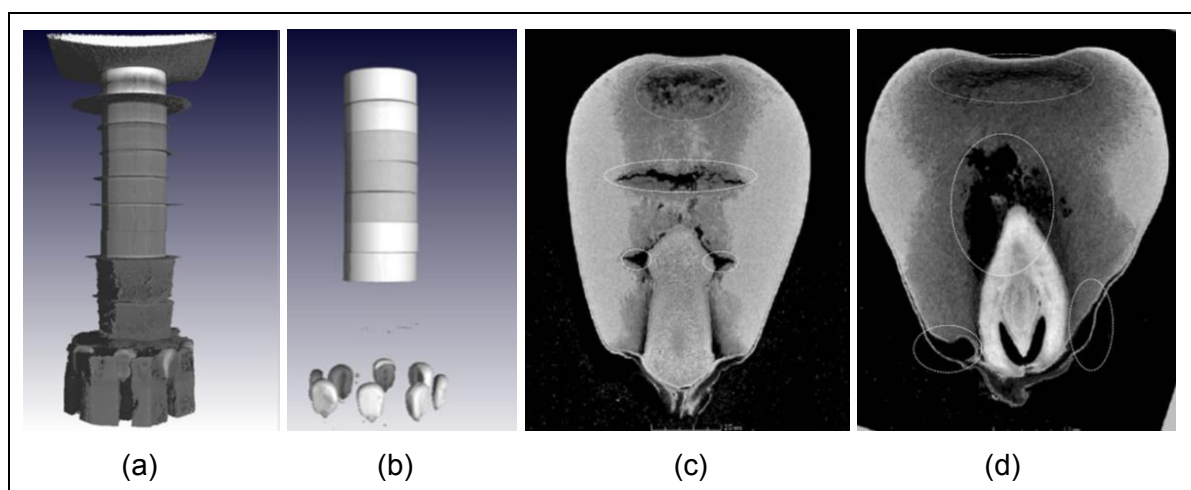
samples sets should be used, it is restricted because of the high cost of performing X-ray CT analysis. Nevertheless, X-ray  $\mu$ CT can serve as a valuable technique for the development of future prediction models for internal quality.

### *Cereals and cereal products*

Several papers have been published on the cellular structure of cereal grains and cereal products (Table 2.1). Neethirajan *et al.* (2006) investigated the airflow resistance of various grains in grain bulks. They observed that the ratio of total airspace to the total number of air paths is the best predictor for the difference in airflow resistance in grain bulks (Neethirajan *et al.* 2006).

Maize plays a vital role in the diet of the African population. The development of fungal infection during storage in silos is a concern as the presence of fungus renders the entire stock unsuitable for use and this consequently has an impact on the economy (Williams, 2013). With visual assessment, the fungal damage is only detectable at an advanced stage of infection. With X-ray CT it was possible to visualise infestation earlier, when the damage is still not present on the exterior of a product.

With X-ray  $\mu$ CT both quantitative (e.g. volume, density) and qualitative (e.g. hardness classification) analyses of whole maize kernels could be performed (Gustin *et al.*, 2013; Guelpa *et al.*, 2015). Guelpa *et al.* (2015) constructed an X-ray  $\mu$ CT density calibration for whole maize kernels, using polymer discs of known densities as calibration standards (Fig. 2.5). Larger cavities were much more prominent in the floury endosperm of the soft hybrids, resulting in lower kernel densities. Floury endosperm density was also lower than that of the vitreous endosperm.

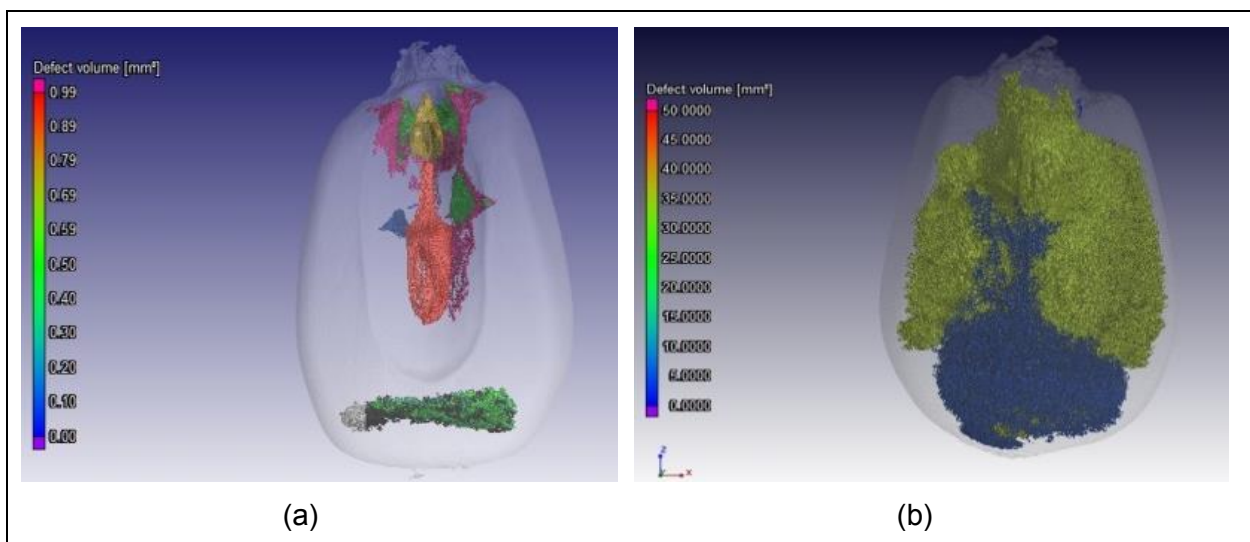


**Figure 2.5.** Stack of seven polymer discs, used for the density calibration, along with eight maize kernels with (a) showing the floral oasis, used for mounting, and (b) with the mounting material removed. Two-dimensional X-ray  $\mu$ CT slice images of a (c) hard and (d) soft maize kernel illustrating distinct, large cavities (marked with white circles) present in mostly the floury endosperm. Cavities are shown as black in X-ray images.

### Coffee beans and nuts

During coffee processing, roasting forms one of the most important steps as this affects the sensorial and textural characteristics of the roasted beans. A few studies focussed on the microstructural and morphological alterations of coffee beans induced by roasting (Table 2.1). Roasting had a significant impact on the microstructure as it led to the development of a porous bean structure (Pittia *et al.*, 2011). Pore shapes, sizes and distributions are relatively easy to measure with X-ray  $\mu$ CT. Because of the rupture of the bonds in the internal structure during roasting, the total pore volume and porosity increased and density decreased with an increase in the roasting time (Frisullo *et al.*, 2012). X-ray  $\mu$ CT could help to achieve a better understanding of the impact of roasting on the microstructural evolution of coffee beans, which may influence stability along with grinding and brewing performances. Three-dimensional volumes can be used to visualise and quantify the increase in porosity (cavities and pores) as illustrated in Figure 2.6 for a maize kernel before and after roasting.

Donis-González *et al.* (2014b) investigated the internal decay and internal characteristics of chestnuts using the ultrafast ROFEX-scanner. In a similar study postharvest non-invasive assessment of internal decay in fresh chestnuts was performed using a medical CT scanner (Donis-González *et al.*, 2014a).



**Figure 2.6.** Three-dimensional visualisation of the volume size distribution (indicated by the colour scale bar) of the porosity (cavities and pores) in a maize kernel (a) before and (b) after roasting. In the raw kernel separate cavities and pores are illustrated by different colours. In the roasted kernel the cavities and pores are interconnected, respectively, thus representing the cavity (yellow) and pore (blue) networks.

### *Confectionary*

Applications where the microstructure of products is highly correlated to the physical and sensory attributes, to either evaluate consumers' acceptance (Haedelt *et al.*, 2007) or to develop food products with desired properties (e.g. mechanical and organoleptic) (Lim & Barigou, 2004), have also been assessed using X-ray  $\mu$ CT. Table 2.1 details X-ray  $\mu$ CT applied to confectionary. Many confectionary products exhibit a cellular foam structure (e.g. mousse, muffins, chocolate and biscuits) that needs to be characterised so that the relationship between structure and mechanical properties can be determined. X-ray CT applied in confectionary applications enables real-time, non-destructive analysis of complex aerated products. In a novel approach by Haedelt *et al.* (2007), X-ray CT was used to characterise the structure of bubble-included chocolate produced using different gasses. This enabled the visualisation and interpretation of the bubble distribution, bubble size and number of bubbles in the chocolate and was related to sensory responses.

### *Dough and baked products*

Good quality bread is influenced by the quality of the dough and the processing parameters. X-ray CT is ideal for the characterisation of the internal structure of porous products (Table 2.1). It can be applied to analyse the dough and the finished product. Knowledge on food microstructure can be used to identify key processing parameters that may influence quality. Functional, technological and physicochemical properties is influenced by structure-property relationships e.g. in solid foams like bread, cakes and biscuits the consumer acceptance is strongly associated with the texture. Several results have been published on the cellular structure of dough, bread and other baked products using either laboratory X-ray CT devices (Agbisit *et al.*, 2007; Hirte *et al.*, 2012; Wang *et al.*, 2011) or synchrotron sources (Lassoued *et al.*, 2007).

Most of the studies addressing bread microstructure focused on the visualisation of the porous structure where quantitative analysis entailed cell shape, cell wall thickness, void fraction, fineness, crumb porosity, anisotropy, pore size distribution and the geometry and orientation of pore networks. These investigations emphasised the important role the pore networks play and has improved the understanding thereof. A novel X-ray  $\mu$ CT study investigated the bubble size distribution in wheat flour dough (Bellido *et al.*, 2006), opening the possibility of gaining more knowledge on the aeration phenomenon in wheat flour dough.

This technique enables examination at microscopic level, which is useful to the food industry, as the accurate calculation of the number, dimension and distribution of pores could lead to the improvement of sensorial attributes. As is often the case with making use of novel technology, most are only feasibility studies, performed on laboratory scale and not in a commercial environment. Thus, there is room for future investigations and developments in the technique.

## Limitations

Even though some of the limitations of X-ray  $\mu$ CT are intrinsic to the technique, others are currently being addressed and are likely to have a reduced influence in future.

### *Time and financial constraints*

The use of this technique in industry is still limited due to time and financial constraints (Kotwaliwale *et al.*, 2014). Even though modifications in the hardware has considerably reduced the time that is needed for a scan, it remains a concern (Kotwaliwale *et al.*, 2014). Guelpa *et al.* (2015) reported that it took up to 30 minutes to scan single maize kernels at a resolution of 13.4  $\mu\text{m}$ , whereas a two hour scan time was needed to obtain a 6  $\mu\text{m}$  resolution. Several studies which compare the performance of X-ray  $\mu$ CT against other imaging techniques, i.e. MRI, has revealed that X-ray is less costly and more convenient (Lammertyn *et al.*, 2003). Most X-ray  $\mu$ CT investigations on food, to date, have been feasibility studies performed on a limited number of samples because of the costs involved. Large data volumes (gigabytes) call for considerable computer resources, with considerable storage capacity, for visualisation and analysis. In addition to image acquisition being time-consuming, image analysis is also a very lengthy procedure and is therefore a real limitation in the use of this technique. Segmentation of one image could take up to three hours, whereas further quantitative measurements to derive the main characteristics could take another hour. The time taken to analyse images is, however, dependent on the complexity of the sample, the number of ROIs created and the type of quantitative measurements required.

### *Imaging artefacts*

Images may contain errors which could be as a result of the sample shape, leading to shading effects or optical errors. Three major artefacts can occur during image acquisition: beam hardening, the cone-beam effect and phase-contrast artefacts (Cnudde & Boone, 2013). Fortunately, beam hardening artefacts can be compensated for by making use of filters or correction tools. However, many procedures for the compensation of beam hardening artefacts or the removal of other artefacts may influence the image quality by reducing the spatial resolution (Baker *et al.*, 2012).

Besides the three main artefacts, others may also occur i.e. ring artefacts, streak artefacts and artefacts caused by movement of the sample during acquisition (Cnudde & Boone, 2013). Angle artefacts occur because of the loss of resolution in a 2D CT image due to the limited number of available projection images. Thus, imaging artefacts complicate data acquisition and interpretation. (Cnudde & Boone, 2013).



### *Operator dependency*

There is no fixed or generally accepted protocols for X-ray  $\mu$ CT, because of the variety in sample sizes, shape as well as composition (Cnudde & Boone, 2013). Certain parameters such as the tube voltage, current and exposure time can thus be chosen arbitrarily and this ultimately affects the result. Furthermore, different X-ray  $\mu$ CT setups will produce different results in terms of image quality. Besides image acquisition, image analysis is also reliant on the operator's judgement especially in the segmentation step of a volume (Cnudde & Boone, 2013). Because of the partial volume effect and image noise, this step is very dependent on the operator. However, when volumes of similar samples are analysed, the error is constant and thus comparison of these samples are possible (Cnudde & Boone, 2013). The quantitative results obtained from 3D analysis should rather be considered as relative than absolute results (Cnudde & Boone, 2013).

### **Conclusion**

X-ray  $\mu$ CT is an essential development in imaging technology, which has eliminated some of the shortcomings of traditional imaging by enabling the non-invasive, 3D and quantitative characterisation of food microstructure. Consequently, it has become an increasingly popular device to investigate food microstructure. X-ray  $\mu$ CT now offers characterisation of food properties non-destructively on a micro-scale on which bases decisions in the processing environment can be made. X-ray  $\mu$ CT is likely to be increasingly used to develop classification algorithms to sort food, especially fresh agricultural commodities, on the basis of their internal characteristics. Ideally, a commercial sorting system using  $\mu$ CT could be developed. However, this will remain a challenge as high throughput requirements will have to be met. With improvements in instruments and computational power, it is expected that X-ray imaging and  $\mu$ CT would become more applicable. It is foreseen that the interest of X-ray  $\mu$ CT will continue to increase and that this technique will become indispensable for food quality evaluation and product development. High-resolution X-ray  $\mu$ CT can be used for many food science applications and its potential is only starting to be explored. It is hoped that this overview is an inspiration for new investigations that will benefit from further use of this breakthrough technology.

### **References**

- Adediji, A. A. & Ngadi, M. O. (2011). Microstructural characterization of deep-fat fried breaded chicken nuggets using X-ray micro-computed tomography. *Journal of Food Process Engineering*, **34**, 2205-2219.
- Agbisit, R., Alavi, S., Cheng, E., Herald, T. & Trater, A. (2007). Relationships between microstructure and mechanical properties of cellular cornstarch extrudates. *Journal of Texture Studies*, **38**, 199-219.

- Babin, P., Della Valle, G., Chiron, H., Cloetens, P., Hoszowska, J., Pernot, P., Réguerre, A., Salvo, L. & Dendievel, R. (2006). Fast X-ray tomography analysis of bubble growth and foam setting during breadmaking. *Journal of Cereal Science*, **43**, 393-397.
- Baker, D. R., Mancini, L., Polacci, M., Higgins, M. D., Gualda, G. A. R., Hill, R. J. & Rivers, M. L. (2012). An introduction to the application of X-ray microtomography to the three-dimensional study of igneous rocks. *Lithos*, **148**, 262-276.
- Barcelon, E. G., Tojo, S. & Watanabe, K. (1999). Relating X-ray absorption and some quality characteristics of mango fruit (*Mangifera indica* L.). *Journal of Agricultural and Food Chemistry*, **47**, 3822-3825.
- Bellido, G. G., Scanlon, M. G., Page, J. H. & Hallgrimsson, B. (2006). The bubble size distribution in wheat flour dough. *Food Research International*, **39**, 1058-1066.
- Besbes, E., Jury, V., Monteau, J.Y. & Le Bail, A. (2013). Characterizing the cellular structure of bread crumb and crust as affected by heating rate using X-ray microtomography. *Journal of Food Engineering*, **115**, 415-423.
- Brecht, J. K., Shewfelt, R. L., Garner, J. C. & Tollner, E. (1991). Using X-ray-computed tomography to nondestructively determine maturity of green tomatoes. *HortScience*, **26**, 45-47.
- Cantre, D., East, A., Verboven, P., Trejo Araya, X., Herremans, E., Nicolaï, B. M., Pranamornkith, T., Loh, M., Mowat, A. & Heyes, J. (2014). Microstructural characterisation of commercial kiwifruit cultivars using X-ray micro computed tomography. *Postharvest Biology and Technology*, **92**, 79-86.
- Chaunier, L., Della Valle, G. & Lourdin, D. (2007). Relationships between texture, mechanical properties and structure of cornflakes. *Food Research International*, **40**, 493-503.
- Chawanji, A., Baldwin, A., Brisson, G. & Webster, E. (2012). Use of X-ray micro tomography to study the microstructure of loose-packed and compacted milk powders. *Journal of Microscopy*, **248**, 49-57.
- Chevallier, S., Réguerre, A.L., Le Bail, A. & Della Valle, G. (2014). Determining the cellular structure of two cereal food foams by X-ray micro-tomography. *Food Biophysics*, **9**, 219-228.
- Cnudde, V. & Boone, M. (2013). High-resolution X-ray computed tomography in geosciences: a review of the current technology and applications. *Earth-Science Reviews*, **123**, 1-17.
- De Beer, F. (2005). Characteristics of the neutron/X-ray tomography system at the SANRAD facility in South Africa. *Nuclear Instruments and Methods in Physics Research Section A: Accelerators, Spectrometers, Detectors and Associated Equipment*, **542**, 1-8.
- Demirkesen, I., Kelkar, S., Campanella, O. H., Sumnu, G., Sahin, S. & Okos, M. (2014). Characterization of structure of gluten-free breads by using X-ray microtomography. *Food Hydrocolloids*, **36**, 37-44.



- Donis-González, I. R., Guyer, D. E., Fulbright, D. W. & Pease, A. (2014a). Postharvest noninvasive assessment of fresh chestnut (*Castanea* spp.) internal decay using computer tomography images. *Postharvest Biology and Technology*, **94**, 14-25.
- Donis-González, I. R., Guyer, D. E., Pease, A. & Barthel, F. (2014b). Internal characterisation of fresh agricultural products using traditional and ultrafast electron beam X-ray computed tomography imaging. *Biosystems Engineering*, **117**, 104-113.
- Falcone, P. M., Baiano, A., Zanini, F., Mancini, L., Tromba, G., Dreossi, D., Montanari, F., Scuor, N. & Nobile, M. A. D. (2005). Three-dimensional quantitative analysis of bread crumb by X-ray microtomography. *Journal of Food Science*, **70**, 265-272.
- Frisullo, P., Barnabà, M., Navarini, L. & Del Nobile, M. (2012). *Coffea arabica* beans microstructural changes induced by roasting: an X-ray microtomographic investigation. *Journal of Food Engineering*, **108**, 232-237.
- Frisullo, P., Conte, A. & Del Nobile, M. (2010a). A novel approach to study biscuits and breadsticks using X-ray computed tomography. *Journal of Food Science*, **75**, 353-358.
- Frisullo, P., Laverse, J., Marino, R. & Del Nobile, M. (2009). X-ray computed tomography to study processed meat microstructure. *Journal of Food Engineering*, **94**, 283-289.
- Frisullo, P., Licciardello, F., Muratore, G. & Del Nobile, M. A. (2010b). Microstructural characterization of multiphase chocolate using X-ray microtomography. *Journal of Food Science*, **75**, 469-476.
- Frisullo, P., Marino, R., Laverse, J., Albenzio, M. & Del Nobile, M. (2010c). Assessment of intramuscular fat level and distribution in beef muscles using X-ray microcomputed tomography. *Meat Science*, **85**, 250-255.
- Fulladosa, E., Santos-Garcés, E., Picouet, P. & Gou, P. (2010). Prediction of salt and water content in dry-cured hams by computed tomography. *Journal of Food Engineering*, **96**, 80-85.
- Furnols, M. F., Teran, M. F. & Gispert, M. (2009). Estimation of lean meat content in pig carcasses using X-ray computed tomography and PLS regression. *Chemometrics and Intelligent Laboratory Systems*, **98**, 31-37.
- Gondek, E., Jakubczyk, E., Herremans, E., Verlinden, B., Hertog, M., Vandendriessche, T., Verboven, P., Antoniuk, A., Bongaers, E., Estrade, P. & Nicolaï, B. M. (2013). Acoustic, mechanical and microstructural properties of extruded crisp bread. *Journal of Cereal Science*, **58**, 132-139.
- Guelpa, A., Du Plessis, A., Kidd, M. & Manley, M. (2015). Non-destructive estimation of maize (*Zea mays* L.) kernel hardness by means of an X-ray micro-computed tomography ( $\mu$ CT) density calibration. *Food and Bioprocess Technology*, **8**, 1419-1429.
- Guessasma, S., Chaunier, L., Della Valle, G. & Lourdin, D. (2011). Mechanical modelling of cereal solid foods. *Trends in Food Science & Technology*, **22**, 142-153.

- Guessasma, S. & Hedjazi, L. (2012). On the fragmentation of airy cereal products exhibiting a cellular structure: mechanical characterisation and 3D finite element computation. *Food Research International*, **49**, 242-252.
- Guggisberg, D., Fröhlich-Wyder, M.T., Irmeler, S., Greco, M., Wechsler, D. & Schuetz, P. (2013). Eye formation in semi-hard cheese: X-ray computed tomography as a non-invasive tool for assessing the influence of adjunct lactic acid bacteria. *Dairy Science & Technology*, **93**, 135-149.
- Gustin, J. L., Jackson, S., Williams, C., Patel, A., Armstrong, P., Peter, G. F. & Settles, A. M. (2013). Analysis of maize (*Zea mays*) kernel density and volume using microcomputed tomography and single-kernel near-infrared spectroscopy. *Journal of Agricultural and Food Chemistry*, **61**, 10872-10880.
- Haedelt, J., Beckett, S. & Niranjana, K. (2007). Bubble-included chocolate: relating structure with sensory response. *Journal of Food Science*, **72**, 138-142.
- Hafsa, I., Cuq, B., Kim, S. J., Le Bail, A., Ruiz, T. & Chevallier, S. (2014). Description of internal microstructure of agglomerated cereal powders using X-ray microtomography to study of process–structure relationships. *Powder Technology*, **256**, 512-521.
- Harrison, R. D., Gardner, W. A., Tollner, W. E. & Kinard, D. J. (1993). X-ray computed tomography studies of the burrowing behavior of fourth-instar pecan weevil (*Coleoptera: Curculionidae*). *Journal of Economic Entomology*, **86**, 1714-1719.
- Håseth, T., Høy, M., Kongsro, J., Kohler, A., Sørheim, O. & Egelanddal, B. (2008). Determination of sodium chloride in pork meat by computed tomography at different voltages. *Journal of Food Science*, **73**, E333-E339.
- Herremans, E., Bongaers, E., Estrade, P., Gondek, E., Hertog, M., Jakubczyk, E., Nguyen Do Trong, N., Rizzolo, A., Saeys, W., Spinelli, L., Torricelli, A., Vanoli, M., Verboven, P. & Nicolaï, B. (2013a). Microstructure–texture relationships of aerated sugar gels: novel measurement techniques for analysis and control. *Innovative Food Science & Emerging Technologies*, **18**, 202-211.
- Herremans, E., Chassagne-Bercesb, S., Chanvrierb, H., Atoniukc, A., Kusztalc, R., Bongaersd, E., Verlindene, B., Jakubczyk, E., Estradeg, P. & Verbovena, P. (2011). Possibilities of X-ray nano-CT for internal quality assessment of food products. In: *Proceedings of the 11<sup>th</sup> International Congress on Engineering and Food (ICEF)*. 22-26 May 2011. Athens, Greece.
- Herremans, E., Melado-Herreros, A., Defraeye, T., Verlinden, B., Hertog, M., Verboven, P., Val, J., Fernández-Valle, M. E., Bongaers, E. & Estrade, P. (2014a). Comparison of X-ray CT and MRI of watercore disorder of different apple cultivars. *Postharvest Biology and Technology*, **87**, 42-50.

- Herremans, E., Verboven, P., Bongaers, E., Estrade, P., Verlinden, B. E., Wevers, M., Hertog, M. L. & Nicolai, B. M. (2013b). Characterisation of 'Braeburn' browning disorder by means of X-ray micro-CT. *Postharvest Biology and Technology*, **75**, 114-124.
- Herremans, E., Verboven, P., Defraeye, T., Rogge, S., Ho, Q. T., Hertog, M. L., Verlinden, B. E., Bongaers, E., Wevers, M. & Nicolai, B. M. (2014b). X-ray CT for quantitative food microstructure engineering: the apple case. *Nuclear Instruments and Methods in Physics Research Section B: Beam Interactions with Materials and Atoms*, **324**, 88-94.
- Hirte, A., Primo-Martín, C., Meinders, M. B. J. & Hamer, R. J. (2012). Does crumb morphology affect water migration and crispness retention in crispy breads? *Journal of Cereal Science*, **56**, 289-295.
- Ho, Q. T., Carmeliet, J., Datta, A. K., Defraeye, T., Delele, M. A., Herremans, E., Opara, L., Ramon, H., Tijskens, E. & Van Der Sman, R. (2013). Multiscale modeling in food engineering. *Journal of Food Engineering*, **114**, 279-291.
- Jayas, D., Paliwal, J. & Visen, N. (2000). Review paper: multi-layer neural networks for image analysis of agricultural products. *Journal of Agricultural Engineering Research*, **77**, 119-128.
- Kalender, W. A. (2011). *Computed Tomography: Fundamentals, System Technology, Image Quality, Applications*, 3rd ed. Germany: Erlangen Publishing.
- Karamichou, E., Richardson, R., Nute, G., McLean, K. & Bishop, S. (2006). Genetic analyses of carcass composition, as assessed by X-ray computer tomography, and meat quality traits in Scottish Blackface sheep. *Animal Science*, **82**, 151-162.
- Kolstad, K. (2001). Fat deposition and distribution measured by computer tomography in three genetic groups of pigs. *Livestock Production Science*, **67**, 281-292.
- Kondo, N., Ahmad, U., Monta, M. & Murase, H. (2000). Machine vision based quality evaluation of lyokan orange fruit using neural networks. *Computers and Electronics in Agriculture*, **29**, 135-147.
- Kotwaliwale, N., Singh, K., Kalne, A., Jha, S. N., Seth, N. & Kar, A. (2014). X-ray imaging methods for internal quality evaluation of agricultural produce. *Journal of Food Science and Technology*, **51**, 1-15.
- Kotwaliwale, N., Weckler, P. R. & Brusewitz, G. H. (2006). X-ray attenuation coefficients using polychromatic X-ray imaging of pecan components. *Biosystems Engineering*, **94**, 199-206.
- Lammertyn, J., Dresselaers, T., Van Hecke, P., Jancsó, P., Wevers, M. & Nicolai, B. (2003). MRI and X-ray CT study of spatial distribution of core breakdown in 'Conference' pears. *Magnetic Resonance Imaging*, **21**, 805-815.
- Landis, E. N. & Keane, D. T. (2010). X-ray microtomography. *Materials Characterization*, **61**, 1305-1316.

- Lassoued, N., Babin, P., Della Valle, G., Devaux, M.F. & Réguerre, A.L. (2007). Granulometry of bread crumb grain: contributions of 2D and 3D image analysis at different scale. *Food Research International*, **40**, 1087-1097.
- Laverse, J., Mastromatteo, M., Frisullo, P., Albenzio, M., Gammariello, D. & Del Nobile, M. (2011a). Fat microstructure of yogurt as assessed by X-ray microtomography. *Journal of Dairy Science*, **94**, 668-675.
- Laverse, J., Mastromatteo, M., Frisullo, P. & Del Nobile, M. (2011b). X-ray microtomography to study the microstructure of cream cheese-type products. *Journal of Dairy Science*, **94**, 43-50.
- Laverse, J., Mastromatteo, M., Frisullo, P. & Del Nobile, M. (2012). X-ray microtomography to study the microstructure of mayonnaise. *Journal of Food Engineering*, **108**, 225-231.
- Léonard, A., Blacher, S., Nimmol, C. & Devahastin, S. (2008). Effect of far-infrared radiation assisted drying on microstructure of banana slices: an illustrative use of X-ray microtomography in microstructural evaluation of a food product. *Journal of Food Engineering*, **85**, 154-162.
- Li, J., Tan, J., Martz, F. & Heymann, H. (1999). Image texture features as indicators of beef tenderness. *Meat Science*, **53**, 17-22.
- Lim, K. S. & Barigou, M. (2004). X-ray micro-computed tomography of cellular food products. *Food Research International*, **37**, 1001-1012.
- Magwaza, L. S. & Opara, U. L. (2014). Investigating non-destructive quantification and characterization of pomegranate fruit internal structure using X-ray computed tomography. *Postharvest Biology and Technology*, **95**, 1-6.
- Maire, E., Fazekas, A., Salvo, L., Dendievel, R., Youssef, S., Cloetens, P. & Letang, J. M. (2003). X-ray tomography applied to the characterization of cellular materials. Related finite element modeling problems. *Composites Science and Technology*, **63**, 2431-2443.
- Maire, E. & Withers, P. J. (2014). Quantitative X-ray tomography. *International Materials Reviews*, **59**, 1-43.
- Mebatsion, H. K., Verboven, P., Melese Endalew, A., Billen, J., Ho, Q. T. & Nicolaï, B. (2009). A novel method for 3-D microstructure modeling of pome fruit tissue using synchrotron radiation tomography images. *Journal of Food Engineering*, **93**, 141-148.
- Mendoza, F., Verboven, P., Ho, Q. T., Kerckhofs, G., Wevers, M. & Nicolaï, B. (2010). Multifractal properties of pore-size distribution in apple tissue using X-ray imaging. *Journal of Food Engineering*, **99**, 206-215.
- Mizutani, R. & Suzuki, Y. (2012). X-ray microtomography in biology. *Micron*, **43**, 104-115.
- Mohammed, I., Charalambides, M., Williams, J. & Rasburn, J. (2014). Modelling the microstructural evolution and fracture of a brittle confectionery wafer in compression. *Innovative Food Science & Emerging Technologies*, **24**, 48-60.

- Mohorič, A., Vergeldt, F., Gerkema, E., Van Dalen, G., Van Den Doel, L. R., Van Vliet, L. J., Van As, H. V. & Van Duynhoven, J. (2009). The effect of rice kernel microstructure on cooking behaviour: a combined  $\mu$ -CT and MRI study. *Food Chemistry*, **115**, 1491-1499.
- Neethirajan, S. & Jayas, D. S. (2008). Analysis of pore network in three-dimensional (3D) grain bulks using X-ray CT images. *Transport in Porous Media*, **73**, 319-332.
- Neethirajan, S., Jayas, D. S. & Karunakaran, C. (2007). Dual energy X-ray image analysis for classifying vitreousness in durum wheat. *Postharvest Biology and Technology*, **45**, 381-384.
- Neethirajan, S., Karunakaran, C., Jayas, D. & White, N. (2006). X-ray computed tomography image analysis to explain the airflow resistance differences in grain bulks. *Biosystems Engineering*, **94**, 545-555.
- Paliwal, J., Visen, N., Jayas, D. & White, N. (2003). Cereal grain and dockage identification using machine vision. *Biosystems Engineering*, **85**, 51-57.
- Pareyt, B., Talhaoui, F., Kerckhofs, G., Brijs, K., Goesaert, H., Wevers, M. & Delcour, J. A. (2009). The role of sugar and fat in sugar-snap cookies: structural and textural properties. *Journal of Food Engineering*, **90**, 400-408.
- Picouet, P. A., Teran, F., Gispert, M. & Font i Furnols, M. (2010). Lean content prediction in pig carcasses, loin and ham by computed tomography (CT) using a density model. *Meat Science*, **86**, 616-622.
- Pinzer, B., Medebach, A., Limbach, H., Dubois, C., Stampanoni, M. & Schneebeli, M. (2012). 3D-characterization of three-phase systems using X-ray tomography: tracking the microstructural evolution in ice cream. *Soft Matter*, **8**, 4584-4594.
- Pittia, P., Sacchetti, G., Mancini, L., Voltolini, M., Sodini, N., Tromba, G. & Zanini, F. (2011). Evaluation of microstructural properties of coffee beans by synchrotron X-ray microtomography: a methodological approach. *Journal of Food Science*, **76**, 222-231.
- Ramírez, C., Young, A., James, B. & Aguilera, J. M. (2010). Determination of a representative volume element based on the variability of mechanical properties with sample size in bread. *Journal of Food Science*, **75**, E516-E521.
- Riley, A., Sturrock, C., Mooney, S. & Luck, M. (2014). Quantification of eggshell microstructure using X-ray micro computed tomography. *British Poultry Science*, **55**, 311-320.
- Romvári, R., Hancz, C., Petrás, Z., Molnár, T. & Horn, P. (2002). Non-invasive measurement of fillet composition of four freshwater fish species by computer tomography. *Aquaculture International*, **10**, 231-240.
- Santos-Garcés, E., Laverse, J., Gou, P., Fulladosa, E., Frisullo, P. & Del Nobile, M. (2013). Feasibility of X-ray microcomputed tomography for microstructure analysis and its relationship with hardness in non-acid lean fermented sausages. *Meat Science*, **93**, 639-644.
- Schuetz, P., Guggisberg, D., Jerjen, I., Fröhlich-Wyder, M., Hofmann, J., Wechsler, D., Flisch, A., Bisig, W., Sennhauser, U. & Bachmann, H.P. (2013). Quantitative comparison of the eye

- formation in cheese using radiography and computed tomography data. *International Dairy Journal*, **31**, 150-155.
- Segtnan, V. H., Høy, M., Sørheim, O., Kohler, A., Lundby, F., Wold, J. P. & Ofstad, R. (2009). Noncontact salt and fat distributional analysis in salted and smoked salmon fillets using X-ray computed tomography and NIR interactance imaging. *Journal of Agricultural and Food Chemistry*, **57**, 1705-1710.
- Sonego, L., Ben-Arie, R., Raynal, J. & Pech, J. (1995). Biochemical and physical evaluation of textural characteristics of nectarines exhibiting woolly breakdown: NMR imaging, X-ray computed tomography and pectin composition. *Postharvest Biology and Technology*, **5**, 187-198.
- Sozer, N., Dogan, H. & Kokini, J. L. (2011). Textural properties and their correlation to cell structure in porous food materials. *Journal of Agricultural and Food Chemistry*, **59**, 1498-1507.
- Syamaladevi, R. M., Manahiloh, K. N., Muhunthan, B. & Sablani, S. S. (2012). Understanding the influence of state/phase transitions on ice recrystallization in atlantic salmon (*Salmo salar*) during frozen storage. *Food Biophysics*, **7**, 57-71.
- Thomas, P., Kannan, A., Degwekar, V. & Ramamurthy, M. (1995). Non-destructive detection of seed weevil-infested mango fruits by X-ray imaging. *Postharvest Biology and Technology*, **5**, 161-165.
- Thomas, P., Saxena, S., Chandra, R., Rao, R. & Bhatia, C. (1993). X-ray imaging for detecting spongy tissue, an internal disorder in fruits of Alphonso mango (*Mangifera indica* L.). *Journal of Horticultural Science and Biotechnology*, **68**, 803-806.
- Thybo, A. K., Szczypiński, P. M., Karlsson, A. H., Dønstrup, S., Stødkilde-Jørgensen, H. S. & Andersen, H. J. (2004). Prediction of sensory texture quality attributes of cooked potatoes by NMR-imaging (MRI) of raw potatoes in combination with different image analysis methods. *Journal of Food Engineering*, **61**, 91-100.
- Ting, V. J., Silcock, P., Bremer, P. J. & Biasioli, F. (2013). X-ray micro-computer tomographic method to visualize the microstructure of different apple cultivars. *Journal of Food Science*, **78**, 1735-1742.
- Toews, M. D., Pearson, T. C. & Campbell, J. F. (2006). Imaging and automated detection of *Sitophilus oryzae* (Coleoptera: Curculionidae) pupae in hard red winter wheat. *Journal of Economic Entomology*, **99**, 583-592.
- Trinh, L., Lowe, T., Campbell, G. M., Withers, P. J. & Martin, P. J. (2013). Bread dough aeration dynamics during pressure step-change mixing: studies by X-ray tomography, dough density and population balance modelling. *Chemical Engineering Science*, **101**, 470-477.
- Turbin-Orger, A., Babin, P., Boller, E., Chaunier, L., Chiron, H., Della Valle, G., Dendievel, R., Réguerre, A. & Salvo, L. (2015). Growth and setting of gas bubbles in a viscoelastic matrix



- imaged by X-ray microtomography: the evolution of cellular structures in fermenting wheat flour dough. *Soft Matter*, **11**, 3373-3384.
- Van Dalen, G., Nootenboom, P. & Van Vliet, L. J. (2007). 3D Imaging, analysis and modelling of porous cereal products using X-ray microtomography. *Image Analysis and Stereology*, **26**, 169-177.
- Van Dyck, T., Verboven, P., Herremans, E., Defraeye, T., Van Campenhout, L., Wevers, M., Claes, J. & Nicolai, B. (2014). Characterisation of structural patterns in bread as evaluated by X-ray computer tomography. *Journal of Food Engineering*, **123**, 67-77.
- Verboven, P., Kerckhofs, G., Mebatsion, H. K., Ho, Q. T., Temst, K., Wevers, M., Cloetens, P. & Nicolai, B. M. (2008). Three-dimensional gas exchange pathways in pome fruit characterized by synchrotron X-ray computed tomography. *Plant Physiology*, **147**, 518-527.
- Vestergaard, C., Risum, J. & Adler-Nissen, J. (2004). Quantification of salt concentrations in cured pork by computed tomography. *Meat Science*, **68**, 107-113.
- Wang, S., Austin, P. & Bell, S. (2011). It's a maze: the pore structure of bread crumbs. *Journal of Cereal Science*, **54**, 203-210.
- Williams, P. J. (2013). Near infrared (NIR) hyperspectral imaging and X-ray computed tomography combined with statistical and multivariate data analysis to study *Fusarium* infection in maize. PhD in Food Science Thesis, University of Stellenbosch, South Africa.
- Witek, M., Węglarz, W. P., De Jong, L., Van Dalen, G., Blonk, J. C. G., Heussen, P., Van Velzen, E., Van As, H. & Van Duynhoven, J. (2010). The structural and hydration properties of heat-treated rice studied at multiple length scales. *Food Chemistry*, **120**, 1031-1040.
- Yang, N., Fisk, I. D., Linforth, R., Brown, K., Walsh, S., Mooney, S., Sturrock, C. & Hort, J. (2012). Impact of flavour solvent on biscuit micro-structure as measured by X-ray micro-computed tomography and the distribution of vanillin and HMF (HPLC). *European Food Research and Technology*, **235**, 1083-1091.
- Zheng, C., Sun, D. W. & Zheng, L. (2006). Recent applications of image texture for evaluation of food qualities—a review. *Trends in Food Science & Technology*, **17**, 113-128.
- Zhu, L.J., Dogan, H., Gajula, H., Gu, M.H., Liu, Q.Q. & Shi, Y.C. (2012). Study of kernel structure of high-amylose and wild-type rice by X-ray microtomography and SEM. *Journal of Cereal Science*, **55**, 1-5.

**Declaration by the candidate:**

With regard to Chapter 3 (pp. 51-83), the nature and scope of my contribution were as follows:

<b>Nature of contribution</b>	<b>Extent of contribution (%)</b>
Literature search and writing of chapter	80

The following co-authors have contributed to Chapter 3 (pp. 51-83):

<b>Name</b>	<b>e-mail address</b>	<b>Nature of contribution</b>	<b>Extent of contribution (%)</b>
Prof Marena Manley	mman@sun.ac.za	Research inputs, editorial suggestions and proofreading	20

Signature of candidate: L. Schoeman

Date: 30/11/2016

**Declaration by co-authors:**

The undersigned hereby confirm that

1. the declaration above accurately reflects the nature and extent of the contributions of the candidate and the co-authors to Chapter 3 (pp. 51-83),
2. no other authors contributed to Chapter 3 (pp. 51-83) besides those specified above, and
3. potential conflicts of interest have been revealed to all interested parties and that the necessary arrangements have been made to use the material in Chapter 3 (pp. 51-83) of this dissertation.

<b>Signature</b>	<b>Institutional affiliation</b>	<b>Date</b>
Prof Marena Manley	Department of Food Science, Stellenbosch University	30/11/2016

Declaration with signature in possession of candidate and supervisor.



## CHAPTER 3

### Literature review 2

#### Cereal grain roasting methods and applications: a review

##### Abstract

Roasting is usually performed to improve colour, flavour, texture and appearance of cereal grains, while it ultimately enhances the overall palatability of the end product. It also contributes to improving the processing efficiency of a following step and extending the shelf life of a product. In addition, it has the potential to increase the antioxidant activity and *in vitro* digestibility of cereal grains. Various roasting methods exist, i.e. sand, fluidised bed, flame, microwave, continuous and oven roasting. Some of these methods, however, have various drawbacks as it may be unhygienic, tedious to operate or result in low productivity. Uneven heat transfer during roasting may result in products with non-uniform characteristics. Some roasting methods can be dangerous to the operators' health and pose serious environmental hazards. This review presents a brief overview of traditional and current roasting methods, while some of the limitations and advantages are discussed. In addition, it evaluates the effect of roasting on nutritional, sensory and most importantly the microstructural properties of cereal grains. Some general roasting applications are considered as well as applications specific to cereal grains.

**Keywords:** Cereal grains; Roasting methods; Heat transfer; Roasting applications

##### Introduction

Worldwide, cereal grains form the staple diet of the majority of the population and it is also an important source of protein for human nutrition (Moore *et al.*, 1995; Shewry, 2007). In recent years, cereals and their constituents have been used in functional foods and nutraceuticals due to the fact that they are, apart from protein, also a good source of substances required for human health, i.e. dietary fibre, energy, vitamins and minerals (Charalampopoulos *et al.*, 2002).

Cereal-based products are derived from grains that have a well-organised microstructure (Autio & Salmenkallio-Marttila, 2001). The starch granule structure, cell wall thickness and size of the cells vary between different cereal grains and also between varieties. Processing causes changes in the microstructure of the grains which will affect the taste, texture, stability and appearance of the end product (Autio & Salmenkallio-Marttila, 2001). It is thus essential to understand the structure of commercially important cereal grains (Delcour & Hosney, 2010) as well as subsequent changes in their physicochemical, rheological and functional properties after processing.

Two concepts of prime importance are the compartmentalisation of the different components in cereal grains and insight into the three-dimensional (3D) structure (Delcour & Hosney, 2010).

The structural properties of these tissues and cells are vital in investigating the physiological and structural interaction in grains, that may have an effect on the quality and performance during processing (Autio & Salmenkallio-Marttila, 2001).

Different thermal processes, e.g. baking, extrusion, frying or roasting can be used to improve the flavour and texture of cereal grains (Salmenkallio-Marttila *et al.*, 2004). Roasting leads to the improvement of colour, flavour, texture and appearance of food and it ultimately enhances the nutritional value and overall palatability of the end product (Uysal *et al.*, 2009). In addition, roasting is capable of extending the shelf life and improving the processing efficiency of a subsequent step (Kikugawa *et al.*, 1983; Asep *et al.*, 2008; Murthy *et al.*, 2008; Cämmerer & Kroh, 2009). The beneficial effect of roasting and the characteristic quality changes are due to various reactions and alterations that develop during the roasting process (Mendes *et al.*, 2001). Physicochemical changes can be used to monitor the degree of roasting and to control the process to deliver a better quality roasted product.

Despite the availability of literature on the roasting of cereal grains, little is known about the effect on the structural and functional properties. A typical characteristic of roasted products is a more brittle and crumbly texture (Kahyaoglu & Kaya, 2006). Furthermore, roasting is also capable of reducing anti-nutritional components and aflatoxins (Huffman & Martin, 1994; Méndez-Albores *et al.*, 2004; Kabak, 2009) and increasing the antioxidant activity (Krings *et al.*, 2000; Gelmez *et al.*, 2009; Omwamba & Hu, 2010) and phenolic compounds (Chung *et al.*, 2011). Together with the desirable changes, undesirable modifications may also occur, such as the loss of certain nutrients (Ayatse *et al.*, 1983). In the food industry, thermal processing should take place at the minimum heating time, particularly when temperatures exceeding 100°C are used to reduce decomposition of vitamins and proteins (Andrejko *et al.*, 2011).

Various roasting methods exist, i.e. fluidised bed (Murthy *et al.*, 2008), sand (Sharma & Gujral, 2011), pan (Jain & Srivastav, 1993), microwave (Omwamba & Hu, 2010), flame (McNiven *et al.*, 1994) and oven (Caprez *et al.*, 1986; Zzaman & Yang, 2013) roasting. Some of these methods, however, have various drawbacks as it may be unhygienic, tedious to operate or result in low productivity (Murthy *et al.*, 2008). It can also be dangerous to the operators' health and the roasted products may have non-uniform characteristics (Murthy *et al.*, 2008).

Few studies have attempted to evaluate the influence of roasting on the microstructure of cereal grains in an objective manner. Researchers often only report a few cross-sectional images in combination with a qualitative discussion of the microstructure, without investigating the quantitative measurements of basic properties (Autio & Salmenkallio-Marttila, 2001; Gropper *et al.*, 2002; Owusu-Ansah *et al.*, 1984). In order to overcome the shortcomings of traditional imaging methods, non-invasive 3D imaging techniques are increasingly explored for microstructural characterisation. Schoeman *et al.* (2016) provided a comprehensive overview of X-ray micro-computed tomography ( $\mu$ CT) for non-destructive characterisation of food microstructure.

This review will firstly introduce maize and wheat as important cereal grains, after which some of the traditional and current roasting methods and their effect on nutritional, sensory and microstructural properties will be considered. Limitations of conventional roasting methods will be discussed with reference to more recently developed, less destructive roasting methods. Some general roasting applications will be addressed, followed by specific applications of cereal grain roasting.

## Maize

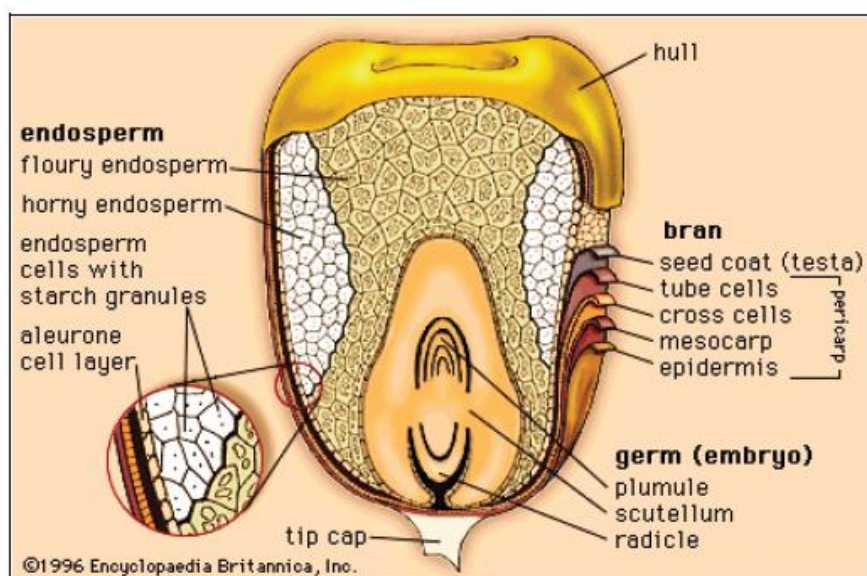
### *Background*

Maize (*Zea mays* L.), also known as corn, is considered a staple food and the cultivation, consumption and uses thereof are worldwide (Dowsell *et al.*, 1996). Maize is ranked first in the world with a production yield of over one billion ton in 2013, followed by rice and wheat (FAOSTAT, 2015). More than half of the annual maize production is used as feed for livestock and industrial materials, while the rest is used as food for human consumption. Besides from providing nutrients for humans and animals, maize also serves as a basic raw material for the production of starch, oil, protein, alcoholic beverages, food sweeteners and fuel (Wu & Guclu, 2013). Maize, as animal feed, also plays a vital role in the production of milk, meat and eggs (Watson, 1987). Maize is important in international trade and the top five exporting countries include United States, Argentina, France, China and Brazil (Wu & Guclu, 2013). In South Africa maize meal is mainly used for making porridge.

### *Morphology*

Maize, with an average kernel weight of 350 mg, is by far the largest of the common cereal grains (Delcour & Hoseney, 2010). The kernel consists of four main parts (Fig. 3.1): the bran (pericarp and seed coat) or hull, germ, endosperm and the tip cap. The tip cap forms the attachment part of the cob. Maize kernels may be solid or variegated and vary in colour. They can be yellow, white, blue, red, purple or dark brown (Delcour & Hoseney, 2010) with yellow being the most common colour, followed by white. The pericarp makes up 5 to 6% of the kernel and is coated with a wax layer (Delcour & Hoseney, 2010). Up to 14% of the kernel is made up by the germ and the remaining part (usually 80-85%) composes the endosperm (Watson, 1987). While the endosperm consists mostly of starch and protein, the germ comprises oil, protein, soluble solids, hormones and ash (Serna-Saldivar, 2010). Maize differs from wheat in that it contains both hard (vitreous) and soft (floury) endosperm in a single kernel in a certain ratio. Vitreous (translucent) endosperm is found near the sides or aleurone layer of a kernel, while the floury (opaque) endosperm is situated towards the centre of the kernel (Delcour & Hoseney, 2010; Watson, 1987). Few or no airspaces are found in the vitreous endosperm which is tightly compacted (Manley *et al.*, 2009). A protein

matrix holds the polygonal shaped starch granules together (Delcour & Hosney, 2010). In the floury endosperm, the many air spaces present lead to opacity.



**Figure 3.1.** Structure of a maize kernel displaying the location of the basic constituents (Anonymous., 1996a).

## Wheat

### Background

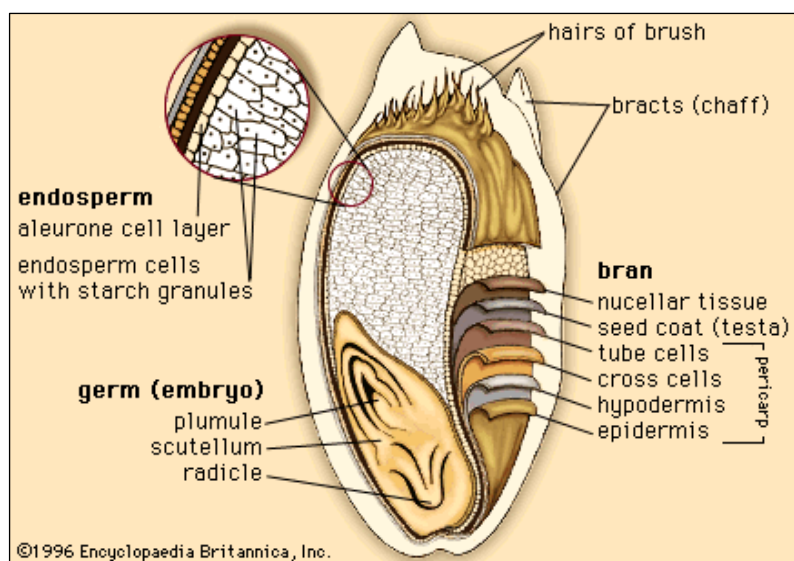
Wheat is grown on more land than any other crop, mainly because of its adaptability, since the wheat plant is tough and can grow in a variety of environmental conditions, and secondly because of the popularity of wheat-based products (Delcour & Hosney, 2010).

### Morphology

Wheat grain consists of separate tissues, each with a special function. Wheat germ is a unique source of highly concentrated nutrients as it comprises about 25% protein, 18% sugar, 48% oil and 5% ash (Delcour & Hosney, 2010). In the wheat kernel, the germ makes up 2.5 to 3.5% and consists of the embryonic axis as well as the scutellum, a storage organ (Delcour & Hosney, 2010). Due to the high nutritional value of the germ, it is a good enrichment element in many products like breads, cakes, biscuits and baby foods (Pomeranz *et al.*, 1970; İbanoğlu, 2002). Figure 3.2 illustrates the longitudinal view of a wheat kernel. On the dorsal side (side of the germ) the wheat kernel is rounded and it has a longitudinal crease over the ventral side (opposite germ) (Delcour & Hosney, 2010). The entire seed is surrounded by a pericarp which consists of various layers. The pericarp makes up 5% of the entire kernel and it contains 20% cellulose, 6% protein, 2% ash and 0.5% fat. The remaining part consists of non-starch polysaccharides. The seed coat is joined to the outer side of the tube cells and to the inner side of the nucellar tissue and varies

between 5 to 8  $\mu\text{m}$  in thickness. The nucellar tissue is bound tightly to the seed coat and the aleurone layer.

The endosperm comprises the aleurone layer and the starchy endosperm. The aleurone layer surrounds the entire kernel and covers the starchy endosperm and germ. The aleurone layer, nucellar tissue, seed coat and pericarp is removed during milling to form the bran (Delcour & Hoseney, 2010). Aleurone cells, that covers the endosperm, has thick walls, is cuboidal and free of starch at maturity. This layer is high in enzymatic activity, protein, lipids and vitamins. The starchy endosperm is made up of three types of cells: peripheral, prismatic and central cells (Delcour & Hoseney, 2010). The first type, located in the first row inside the aleurone layer, is very small cells and equal in diameter. The prismatic cells are elongated, while the central cells are more irregular in shape and size. Wheat endosperm cell walls consist of arabinoxylans, which contains small levels of  $\beta$ -glucans and other hemicelluloses. The cell walls vary in thickness with regard to location and it is thicker near the aleurone. Endosperm cells, which are filled with starch granules, are embedded in a protein matrix. Starch granules can be as large as 40  $\mu\text{m}$  across the flattened side and lenticular in shape, or it can be as small as 2 to 8  $\mu\text{m}$  in diameter and spherical in shape.



**Figure 3.2.** Illustration of the internal structure of a wheat kernel (Anonymous., 1996b).

### Traditional and current roasting methods

In the food industry roasting is generally performed to both improve and alter the quality of a product and to increase the processing efficiency of a following step (Youn & Chung, 2012). The extent of these beneficial features is influenced by the roasting conditions such as time and temperature as well as the roasting method. Roasting and popping of grain plays an essential role in the manufacturing of ready-to-eat products and foods with an extended shelf life (Jha, 2005). Roasting can be defined as a high-temperature-short-time (HTST) thermal process during which both heat and mass transfer takes place (Murthy *et al.*, 2008). Popping of grain occurs because of



the development of a high internal pressure that results in a change in volume and moisture content during roasting. Different roasting methods will have different effects on product quality.

### *Sand roasting*

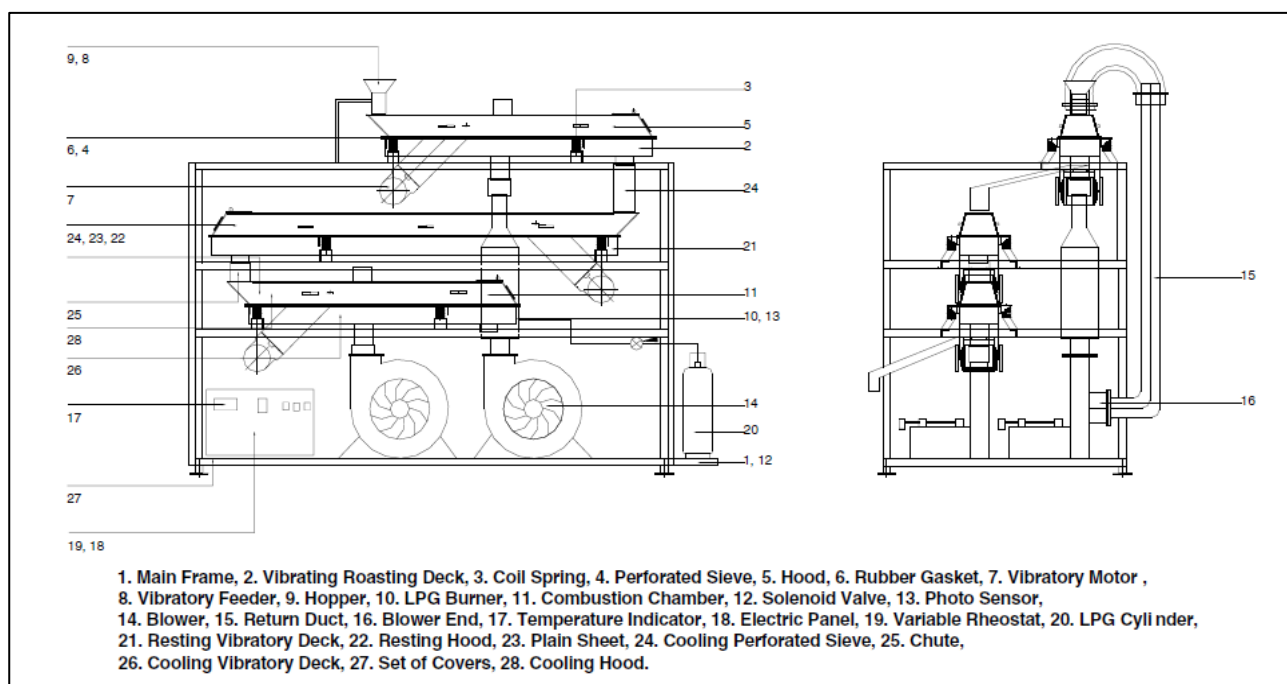
Sand roasting is a traditional method used in India, that involves roasting grain in a hot sand bed where conduction aids as the medium of heat transfer (Murthy *et al.*, 2008; Gujral *et al.*, 2011; Hoke *et al.*, 2005). The sand is heated by husk or wood chips and this poses a serious environmental hazard (Hoke *et al.*, 2005). Sand roasting results in low productivity as it is tedious to operate. In addition the roasting units are not very hygienic (Murthy *et al.*, 2008) and it is dangerous because the operators work directly in the presence of flame and smoke. Furthermore, sand roasting delivers products with non-uniform characteristics and the adherence of sand to the product leads to a high silica content. Gujral *et al.* (2011) reported that sand roasting (280°C; 15 s) of oats significantly lowered the bulk density resulting in decreases of 31-44%. This was attributed to the improved puffing effect or volumetric expansion. Another shortcoming is the lack of temperature control (Sharma & Gujral, 2010). Sand roasting is usually performed in a steel pan that is heated by liquefied petroleum gas (LPG) (Murthy *et al.*, 2008). Roasting temperatures vary between 250°C and 350°C and it is generally used to produce ready-to-eat products (Gujral *et al.*, 2011). Barley is widely consumed in India in its roasted form (Sharma & Gujral, 2011). The barley is sand roasted (250-300°C) for a short time, which will cause the grain to puff and expand and consequently split the husk. The husk is then removed and the grain is ground to flour, after which water and sugar is added to make a popular drink, known as *sattu*. An earlier study revealed large variation in the physical and functional characteristics, i.e. water absorption capacity and pasting and thermal properties of sand roasted barley cultivars (Sharma *et al.*, 2011). The barley puffed upon roasting and the hardness and colour difference were significantly lowered.

### *Fluidised bed roasting (FBR)*

The Central Food Technological Research Institute in India developed the fluidised bed roaster, which makes use of flue gas (Murthy *et al.*, 2008). It is primarily used for roasting cereals, oil seeds, spices and ingredients for ready-to-eat products. The structure of the grain can effectively be modified making use of this technique (fluidisation). Applications in the food industry that uses gas-solid fluidised beds include cooking, sterilisation and roasting. During fluidisation the solid particles are converted into a fluid phase and this is achieved by means of contact with a liquid or a gas (Shelton & Niranjana, 1993). The type of fluidising medium and the material properties will determine the form of fluidisation to be used (Murthy *et al.*, 2008).

Figure 3.3 illustrates a continuous fluidised bed roaster which consists of three decks: roasting, resting and cooling (Murthy *et al.*, 2008). The material is fed, at a constant rate, through a vibrating feeder. In the combustion chamber hot air is generated by burning LPG. The flue gas is

blended with fresh air and this mixture moves through a roasting deck at a controlled rate. An electric motor controls the amplitude and vibration rate of the roasting deck. To facilitate heat and mass exchange between the fluid and the solid, a quick and vigorous mixing step is required. Fluidisation has the following advantages: the equipment is simple to use, there is close gas-particle contact, uniform particle exposure and maintenance involves low costs (Heywood, 1978). The behaviour of a fluidised bed is not only related to air but it is also affected by the density and kernel size of the grain (Murthy *et al.*, 2008). According to Murthy *et al.* (2008) who performed a study on wheat roasting, FBR (280-350°C; 45-50s) is superior to traditional sand roasting (300 ±10°C; 25-30s) with regard to overall colour, since this method leads to more uniform heat transfer. Furthermore, FBR resulted in good expansion, a more uniform texture and it required less energy for size reduction. In another study FBR had a better puffing efficiency because the sample is more uniformly exposed to the heating medium in comparison to sand roasting (Chandrasekhar & Chattopadhyay, 1990). However, the fuel efficiency is limited during FBR (Hoke *et al.*, 2005).



**Figure 3.3.** A schematic diagram of a fluidised bed roaster (Murthy *et al.*, 2008).

### Flame roasting

Flame roasting is especially used where some foods are heat processed to destroy trypsin inhibitors, to increase the availability of nutrients or to eliminate mycotoxins (Hamilton & Thompson, 1992). Grain processing by means of roasting can influence digestibility in terms of the digestion rate (Campling, 1991). Flame roasting of cereal grains can lead to improved feed conversion and animal productivity by permitting optimal starch delivery for ruminal fermentation and it also allow more starch to escape fermentation to be digested in the small intestine (McNiven *et al.*, 1994). The effect of flame roasting on the nutritional quality of maize, barley, wheat and oats

was investigated earlier (McNiven *et al.*, 1994). For ruminant (e.g. cattle, sheep and goats) diets, roasting of grains may be favourable as it results in a slower release of nutrients, thus allowing more crude protein to escape degradation in the rumen. Flame roasting, besides the beneficial aspects of reduction in moisture and mycotoxin levels, seemed to be only moderately beneficial for maize and barley and not beneficial for oats and wheat (McNiven *et al.*, 1994). Due to the lack of accurate temperature control, care must be taken not to exceed the optimal roasting level as at too high temperature nutrients will rapidly become unavailable.

Firik (or frekeh) is a traditional food produced from immature, early wheat at the milky phase (Maskan, 2002). This product is usually homemade but is also commercially manufactured by small-scale producers. It is made by flame roasting the immature spikes in order to burn off the leafy material, after which the spikes are sundried (Özkaya *et al.*, 1999; Maskan, 2002). After sun drying, the spikes are threshed and the kernels are separated from the hulls and cracked (Maskan, 2002). Firik has a characteristic smoked taste which is achieved by roasting. This product is generally used as a substitute for rice. Firik pilav, e.g. consists of firik, meat, tomatoes and butter and is a traditional dish in Middle Eastern countries (Özkaya *et al.*, 1999).

### *Microwave roasting*

Microwave roasting has gained increasing popularity in recent years as an alternative drying or roasting method for a range of agricultural and food products (Vadivambal & Jayas, 2007). There is an increasing trend towards using microwave energy for food processing since it improves the quality of products and leads to considerable energy savings due to the shorter processing times compared to other treatments (Joshi *et al.*, 2014). Rakesh & Datta (2011) developed a model to understand and optimise microwave roasting. To generate the amount of pressure necessary to puff materials, very high temperatures were required. Furthermore, in order for roasting to be successful, an intensive heating source such as microwaves is needed. Other advantages of microwave heating include accurate process control and faster start-up and shut-down times (Uysal *et al.*, 2009). All these factors make microwave treatment an ideal option for puffing or roasting grains (Joshi *et al.*, 2014).

Microwave roasting of barley led to a lower reduction in the bulk density and less puffing in comparison to sand roasting (Sharma & Gujral, 2011). It is a promising alternative to traditional methods due to the high internal heating rates (Altan, 2014). Several studies on the application of microwave roasting has been performed and included peanuts (Megahed, 2001), sunflower seeds (Anjum *et al.*, 2006), coffee (Nebesny & Budryn, 2003) and pumpkin seeds (Yoshida *et al.*, 2006). Microwave roasting did not have any adverse effects on the oil or seed quality of pumpkin seeds and short-term microwave roasting showed to delay deterioration. The antioxidant properties of coffee beans were better protected by microwave roasting (Nebesny & Budryn, 2003). Warchalewski *et al.* (1998) evaluated wheat samples for odour and colour changes during microwave irradiation and observed a burnt odour after an exposure time of 180 s.



### *Gun and oven puffing*

Puffed cereal grains are usually used as ready-to-eat breakfast cereals or as ingredient in snack foods (Mariotti *et al.*, 2006). Ready-to-eat cereals, processed from maize, wheat, oats or rice, are suitable for consumption without the need for any further cooking. Puffed cereals are commonly used because of their lightness, crispness and cellular structure (Peleg, 1997), as well as their degree of expansion (Owusu-Ansah *et al.*, 1984).

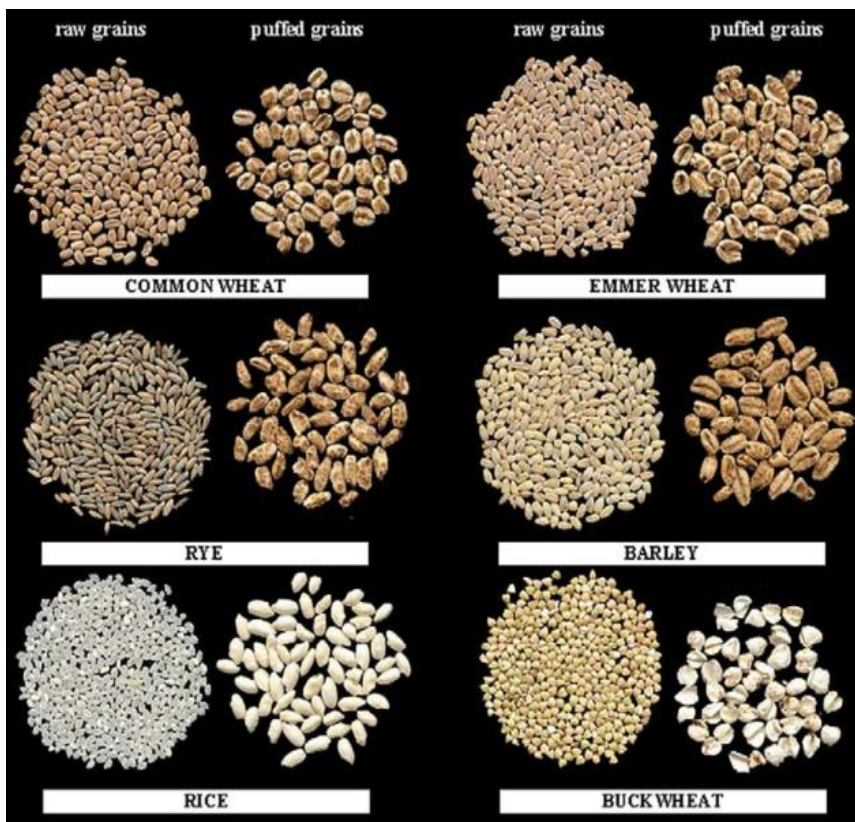
During HTST heating processes sudden expansion of moisture inside the openings between starch granules leads to the puffing of grains (Chandrasekhar & Chattopadhyay, 1989). Puffing is generally described as a pressure drop process or an atmospheric pressure process with a sudden heat application (Pardeshi & Chattopadhyay, 2014). Examples of atmospheric pressure processes include sand, air or oven, oil and roller puffing, whereas gun puffing makes use of a pressure drop process (Chandrasekhar & Chattopadhyay, 1990). Oven and gun puffing are the two methods mostly used (Mariotti *et al.*, 2006). Gun puffing entails the sudden transfer of grain, containing superheated steam, from a high pressure to a low pressure. This allows rapid vaporisation of water and causes expansion. The preferred cereals for gun puffing are whole grain rice and wheat. Maize and oats are sometimes also used. Puffing usually takes place in an expansion chamber, where the grains come into contact with steam that is injected under pressure. After a certain time the chamber is opened and the sudden reduction in pressure leads to immediate evaporation of moisture in the grains. Figure 3.4 provides an illustration of raw and gun puffed grains.

Oven puffing entails sudden heat application at atmospheric pressure. This leads to moisture evaporation and product expansion. Maize and rice are normally used for oven puffing, since they inherently puff in the presence of heat if the moisture content is correctly adjusted. Numerous parameters influence the degree of expansion and these are correlated to the grain composition (Chen & Yeh, 2001; Jones *et al.*, 2000) and the processing conditions (Owusu-Ansah *et al.*, 1984; Chandrasekhar & Chattopadhyay, 1990).

### *Continuous roasting*

Unevenly roasted flakes are the result of roasting in a static position, therefore the advantage of rotary ovens is that the product is suspended in heated air and all the surfaces are exposed uniformly (Murthy *et al.*, 2008). Free flow of the product is ensured by the improved heating system and also product discharge. In the breakfast industry standard ovens with rotary units, that make use of hot air, are normally used for roasting various types of flakes (Fast *et al.*, 1990). The rotating units are made up of an inner rotating cylinder (consisting of carbon steel) and an outer casing (consisting of stainless steel) that is insulated (Murthy *et al.*, 2008). For larger flakes, such as maize, perforated inner shells are used. In these units the conveyor moves through the oven chamber. The oven chambers can be fired indirectly or directly. The direct-fired method is not widely used as the product is directly exposed to the flame temperature. A jet zone unit is very

effective in hot air roasters since the hot air is forced through nozzles, directing it into the product at a high speed (Murthy *et al.*, 2008). Subsequently, uniform roasting and shorter times is the result of this roasting method.



**Figure 3.4.** Raw and puffed cereal grains with the expanded structure clearly visible from the puffed kernels (Mariotti *et al.*, 2006).

#### *Forced convection continuous tumble (FCCT) roasting*

The FCCT roaster is based on a simple working principle in combination with high performance heat transfer (Flinn, 2012). The uniqueness relates to the ease of application and the low production costs (Anonymous, 2014). The working principle entails that hot air is forced right through the product, while the product is continuously mixed and moved through the roaster. According to Flinn (2012) heat transfer to the roasted product is the highest on the market and the product is evenly roasted, not easily matched by other technologies. Other advantages of this roaster include continuous operation, multiple product applications, accurate temperature control and it is based on a simple working principle making it easy to understand and operate. The FCCT roaster requires minimum maintenance and it is easily movable. Superheated steam from the moisture in the product enhances even roasting. Energy is used efficiently as there is continuous recirculation of superheated steam inside the roaster. A further advantage is that electrical interruptions will not cause a serious problem since the roaster automatically shuts off in the case of a power failure and continues roasting when the power supply has been corrected (Anonymous,

2014). The roaster can run 24 hours a day without intensive supervision in comparison to traditional roasting methods. It has been reported that superheated steam processing heats food, while retaining vitamins and other essential nutrients (Pronyk *et al.*, 2004).

The FCCT roaster was initially developed to roast whole soy beans and grains to create feed mixes (Flinn, 2012). It was found that the roaster destroys the trypsin inhibitor in soy beans, without losing any proteins and vital fibre and it increases the digestibility and feed conversion by animals.

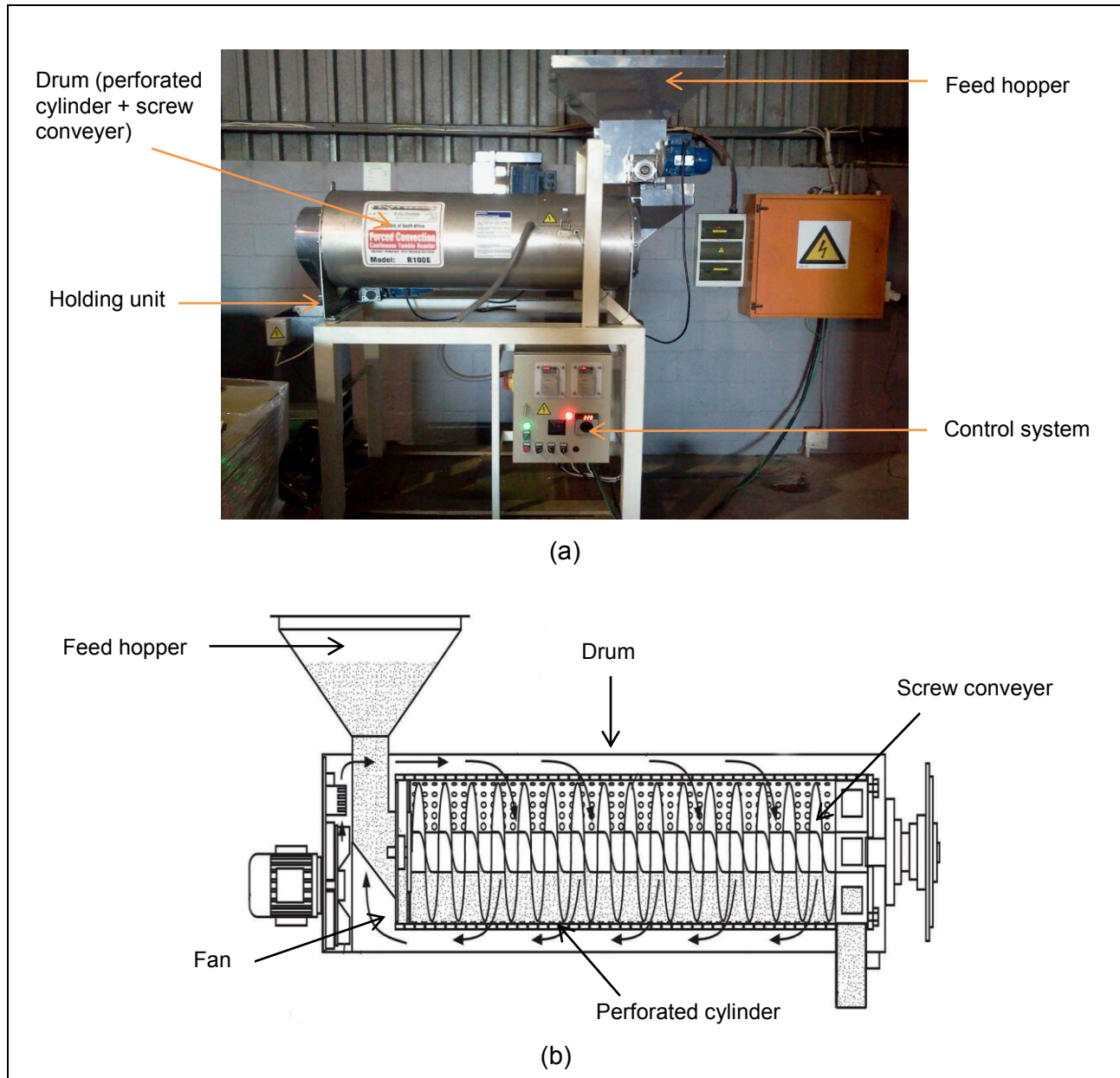
Figure 3.5 illustrates the four main components of the roaster, namely the control system, feed hopper, drum (perforated cylinder and screw conveyor) and holding unit. From the feed hopper the sample is transferred to the drum by gravity, where it is heated with hot air or superheated steam blown by a fan. The air is heated by an electric element and controlled by an adjustable electronic thermostat. The product is conveyed through the roaster by a perforated cylinder with a screw conveyor inside (Fig. 3.5) (Flinn, 2012). In the drum, the rotating perforated cylinder mixes the sample and the screw conveyer (which also mixes the sample) propels the sample forward at a set speed. Thus, continuous uniform heat distribution is ensured and this leads to more effective roasting than in a stationary roaster. An inherent problem associated with conventional methods is the non-uniformity in roasting caused by an uneven distribution of heat. This problem is overcome with the FCCT roaster.

The control system is used to select the optimal roasting time and temperature combination. The speed at which the material moves through the roaster can be manipulated with the variable speed drive to allow different roasting speeds. The speed of the screw conveyer determines the holding time of the product at the set temperature. After speed and temperature conditions are set, roasting conditions will be stable, leading to continuous and precise roasting (Flinn, 2012). The total surface area of each of the particles in the process is used for heat transfer, resulting in an evenly roasted product.

The temperature of the hot air is accurately controlled, so particles will not be exposed to extreme hot surfaces (Flinn, 2012). Moisture from the product replaces the hot air inside the roaster. Thermal insulation leads to less heat loss and effective energy usage. The running cost of this roaster is 20% less than that of conventional gas fired drum-type roasters operating at the same capacity.

In previous studies the FCCT roaster has been used to determine the effect of roasting on the sensory and nutritional quality of marama-sorghum composite flours and porridges (Kayitesi *et al.*, 2010) and to determine the effect on the physicochemical, nutritional and functional characteristics of defatted marama bean flour (Maruatona *et al.*, 2010). Roasting inactivated the trypsin inhibitors in marama beans. Furthermore, it was applied to assess its effectiveness as a pre-treatment in controlling the hard-to-cook (HTC) phenomenon in cowpeas (Ndungu *et al.*, 2012). It was, however, found that micronisation was more effective than FCCT roasting in controlling the HTC defect. This was attributable to a higher degree of phytase inactivation during micronisation.

FCCT roasting technology has already replaced extruders and micronising equipment and it is successfully used commercially for roasting soybeans, maize, coriander, groundnuts, macadamia nuts, rolled oats and for caramelising dehydrated onions (Flinn, 2012). With this roaster no oil is needed for nut roasting and a very evenly roasted product is produced with many health benefits.



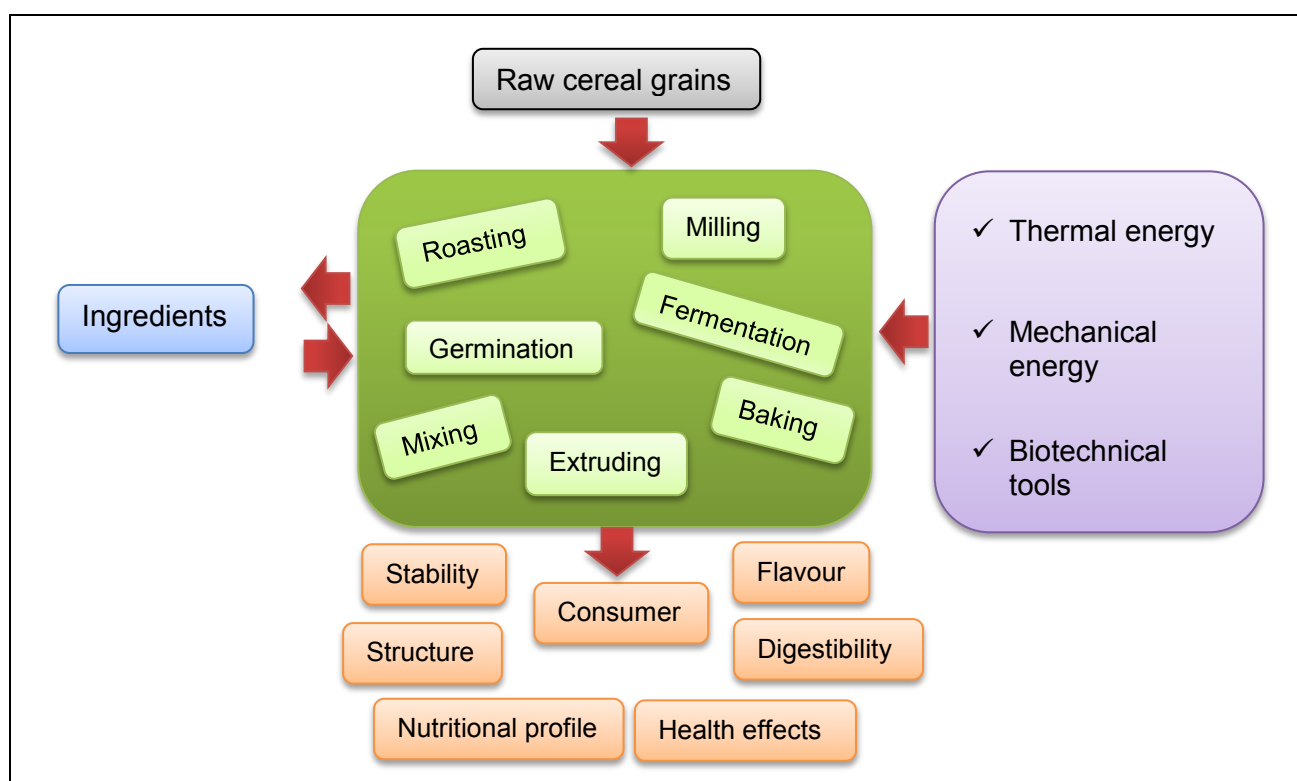
**Figure 3.5.** Illustration of (a) the main components and (b) internal set-up of the forced convection continuous tumble (FCCT) roaster.

### Effect of roasting on cereal grains

Roasted grains, in various forms, are not only consumed in South Asian countries and the Indian subcontinent, but throughout the world (Srivastav *et al.*, 1990). The roasting method will depend on various factors, i.e. locality, availability and type of grains, convenience and food habits. Roasting is classified as a HTST processing technique that makes use of hot air for short time periods to



improve grain characteristics (Sharma & Gujral, 2010; Sharma *et al.*, 2011). It inactivates contaminating microorganisms and growth inhibitors while retaining nutrients (Srivastav *et al.*, 1990). Roasting modifies the nature of starches and proteins by altering the physical, nutritional, functional and chemical properties. Quality changes that takes place during thermal treatment involves optical (appearance and colour), sensory (flavour, odour and taste), structural (density, porosity and volume), texture, rehydration (rate and capacity), functional (thermal and pasting properties) and nutritional (vitamins and proteins) properties (Vadivambal & Jayas, 2007). Figure 3.6 illustrates a general scheme of the unit operations in cereal processing and other factors that affect cereal product quality.



**Figure 3.6.** Key factors influencing cereal product quality. The figure shows the variables involved and the systematic approaches to obtain an optimal procedure that integrates raw materials and processing to obtain an acceptable end product (adapted from Poutanen *et al.* 2014).

### Nutrition

Roasting of cereal grains may be beneficial to ruminant diets as it leads to a slower release of nutrients (McNiven *et al.*, 1994). Feed roasting aims to alter the physical and chemical properties of the raw cereal starch structure in such a way that it results in greater feed availability. Thus roasted feed is more efficient due to the increased digestibility, resulting in increased weight gain and reduced total grain intake (Anonymous, 2014).

In the raw state many protein sources (e.g. soya and linseed) contain toxic enzymes and other anti-nutritional elements that hinder digestion (Anonymous, 2014). Roasting is considered as

one of the most effective and economical answers to consistent eradication of toxic enzymes (Anonymous, 2014). Even though most mycotoxins are moderately heat-stable, variable degrees of destruction can be obtained with high-temperature processing (Kabak, 2009). Data indicate that roasting leads to a decrease in mycotoxin levels in a variety of foods (Kabak, 2009). The reduction levels are dependent on the roasting conditions, i.e. time and temperature and also the type and concentration of the mycotoxin. A previous study reported that roasting maize meal samples (218°C; 15 min) that were either artificially or naturally contaminated caused almost a complete loss of fumonisins (Castelo *et al.*, 1998). Pan roasting at 285°C for 7 min resulted in aflatoxin reductions of up to 81% and was proven to be more effective than boiling (Méndez-Albores *et al.*, 2004). In a study by Gujral *et al.* (2011) oats were subjected to high temperature sand roasting to produce a characteristic flavour by Maillard browning and also to terminate the activity of lipolytic enzymes. The roasted flour had an increased antioxidant activity and  $\beta$ -glucan extractability. Omwamba & Hu (2010) used hot air roasting to optimise the antioxidant capacity in barley.

Flame roasting is especially used to destroy trypsin inhibitors in soybeans (Kunitz, 1947) or to eliminate mycotoxins and moulds in maize (Hamilton & Thompson, 1992). Roasting of maize has a beneficial nutritional aspect as it improves the availability of minerals (Khan *et al.*, 1991). A variety of ethnic groups in Africa, Northern Mexico and Southwest USA consumes the flour from roasted maize as an energy source (Carrera *et al.*, 2015). Roasting leads to a more rapid starch digestion rate. High digestibility is directly linked to the rate of glucose (energy) released resulting in better starch, protein and amino acid digestibility (Anonymous, 2014). Furthermore, studies on starch have revealed that digestibility increased in barley (32 to 98%), wheat (28 to 90%) and maize (43 to 90%) after roasting (Anonymous, 2014). Roasting may either increase or decrease the nutritional and health promoting value, depending on the method and conditions used (Ayatse *et al.*, 1983).

### Sensory

A number of physicochemical alterations, heat exchange and chemical reactions takes place during roasting (Saklar *et al.*, 2001). It is essential to control these changes to optimise the colour, texture and flavour of the roasted product (Cammarn *et al.*, 1990). These changes may lead to an increase in the desirability of a product due to flavour development, hardness reductions and gelatinisation of starch which renders better palatability (Srivastav *et al.*, 1990). Roasting transforms starches to sugars that greatly enhance the grain palatability and flavour (Anonymous, 2014). With roasting, the stringency associated with some cereal grains are replaced with a very agreeable toasted nutty flavour, while preserving the beneficial high energy level with excellent shelf life (Anonymous, 2014).

It is necessary to control the roasting time and temperature to obtain optimal characteristics, without burning the grains and compromising the flavour. In India, cereal grains are traditionally

roasted to improve organoleptic properties and digestibility, to enhance the shelf life, to ease the incorporation into ready-to-eat foods and breakfast cereals and to reduce anti-nutrient elements (Murthy *et al.*, 2008; Gahalawat & Sehgal, 1992). Roasting of grains have shown to deliver an improved texture and crispness and enhanced volume (Hoke *et al.*, 2007). Flours from roasted cereals could, besides from being used as an ingredient in snack formulations, also be used to control moisture migration in baked goods. Staling in bread occurs, among other factors, due to moisture transfer between the bread components (Gray & Bemiller, 2003). The use of small quantities of roasted flour in dough can delay staling and consequently lead to a product that stays softer for longer.

### *Microstructure*

Cereal grains, which have a well-organised microstructure, determines the structure of manufactured foods (Autio & Salmenkallio-Marttila, 2001). The quality of end products is affected by the microstructural modifications that take place during processing. Starch gelatinisation, protein denaturation and fragmentation of the cell walls are some of the structural changes that occur at microscopic level during cereal roasting (Autio & Salmenkallio-Marttila, 2001). Porosity, which is the extent of starch gelatinisation, contributes to the texture and appearance of cereal products. Roasted cereal grains have an increased porosity, which will affect the density and hardness of end products (Murthy *et al.*, 2008). A recent study focussed on the optimisation of chemical and textural properties of roasted expanded purple maize using response surface methodology (Mrad *et al.*, 2014). It was reported that a process called, Intensification of Vaporisation by Decompression to the Vacuum (IVDV), is an interesting texturizing process that can be used as pre-treatment for roasting purple maize and probably other cereal grains, since it preserves antioxidant properties. In a study on the puffing of cereal grains the results demonstrated substantial changes in the starch structure and water holding capacity (Mariotti *et al.*, 2006). Raigar *et al.* (2016) reported that with roasting of wheat puffing took place which diminished the interactions between glutenin and gliadin protein molecules and disrupted the network formation.

## **Roasting applications**

### *General*

During roasting the availability of nutrients can be improved, destruction of undesirable microorganisms and food contaminants takes place and physical attributes can be favourably changed (Ayatse *et al.*, 1983). Roasting improves and adjust the quality and safety of products such as hazelnuts (Saklar *et al.*, 2001; Özdemir & Devres, 2000; Uysal *et al.*, 2009), soybeans (Kato *et al.*, 1981), *Cassia occidentalis* seeds (Medoua & Mbofung, 2007), pistachio nuts (Yazdanpanah *et al.*, 2005), coffee beans (Pittia *et al.*, 2001; Mendes *et al.*, 2001), sesame seeds (Kahyaoglu & Kaya, 2006), wheat (Gahalawat & Sehgal, 1993) and coconuts (Jayalekshmy &

Mathew, 1990). It is considered to be the most important step in the processing of coffee beans and nuts as roasting leads to essential changes regarding physical, chemical, structural and sensorial properties (Kahyaoglu & Kaya, 2006; Pittia *et al.*, 2001). Roasting also forms the basis for the production of sesame products (Kahyaoglu & Kaya, 2006). Here it promotes the flavour, provide the desired colour and lead to textural changes that improves the overall palatability (Kahyaoglu & Kaya, 2006). The optimum roasting conditions for sesame paste production is 90 to 100°C for a few minutes in an electrically heated tunnel (Sawaya *et al.*, 1985). The impact of vacuum, steam, hot plate and hot air roasting on the nutritional characteristics of sesame pastes were investigated in another study, which recommended hot air roasting at 130°C for 1 h (El-Adawy & Mansour, 2000). Roasting of peanuts at lower temperatures and longer time periods delivers a more evenly roasted product with an enhanced flavour (Moss & Otten, 1989). It was also found that at these conditions more even temperature distribution inactivated enzymes and a longer shelf life was exhibited.

Roasting of coffee beans is accompanied by several physical changes such as volume, density, colour and texture (Frisullo *et al.*, 2012). With regards to texture, it is known that the beans will lose their strength and become fragile and brittle (Pittia *et al.*, 2007). The cell structure is dramatically altered by complex chemical and physical reactions during the roasting process such as non-enzymatic browning and dehydration (Frisullo *et al.*, 2012). The modification in structure is mainly caused by released gasses, which create a high internal pressure. Macropore studies on roasted coffee beans have been performed with a combination of electron microscopy and mercury porosimetry (Schenker *et al.*, 2000), whereas micropores have been investigated with light microscopy (LM), transmission and scanning electron microscopy (TEM and SEM) and image analysis (Massini *et al.*, 1990). Roasting conditions have a major influence on the microstructure of coffee beans, since the development of flavour and colour compounds is accompanied by an increase in volume and microstructural changes (Schenker *et al.*, 2000). Using X-ray  $\mu$ CT it was shown that that roasting of coffee beans led to the development of a porous structure with pores varying in shape and size (Pittia *et al.*, 2011). High temperature roasting led to greater pores and bean volumes and larger micropores in the cell walls in comparison to low temperature roasting. The characteristics of the pores depended on the area of the bean as cracks occur predominantly in the external regions.

### *Cereal grains*

Maize kernels are usually treated by boiling, steaming, grilling, milling, fermentation, roasting or puffing and is then consumed directly or as secondary processing products, e.g. cornmeal (Chung *et al.*, 2011; Oboh *et al.*, 2010). In developed countries maize is consumed as popcorn, sweet corn, corn snacks or corn bread (Watson, 1987). Maize roasting has been a traditional preparation method for several centuries (Oboh *et al.*, 2010) and is a popular method to create products like



popcorn, 'elekute', 'guguru', 'aandun' and 'dankuwa' (Ayatse *et al.*, 1983). Roasted maize is widely eaten by Nigerians across high- and low-income groups (Ayatse *et al.*, 1983). The quality and utilisation of roasted maize is reliant on the roasting conditions.

Carrera *et al.* (2015) investigated the *in vitro* digestibility, crystallinity, rheological, thermal, particle size and morphological characteristics of pinole, a traditional energy food that is obtained from roasted ground maize. Roasting increased the hydrolysis rate and digestibility and can thus be used to manufacture food where fast digestibility is desired. Thin porridges, called atoles, produced from roasted maize flour are commonly consumed in Africa and Mexico (Vivas *et al.*, 1987), while mumu, a traditional food product made from roasted maize, is consumed in Nigeria (Ingbian & Adegoke, 2007). For the consumption of mumu, roasted maize is reconstituted in cold water with sugar or honey and consumed as a snack, breakfast porridge or convenience food item. It also has the potential of being utilised as the basis for cooked pastes, in soups and as thickening agent (Ingbian & Adegoke, 2007). Roasting as processing method for pinole or atoles preparation is highly recommended since it has definite nutritional advantages (Méndez-Albores *et al.*, 2004). A traditional maize porridge, known as 'Tom Brown', made from roasted maize flour is commonly consumed in African countries, i.e. Ghana and Nigeria as weaning food (Plahar *et al.*, 2003; Pelto & Armar-Klemesu, 2011; Nagai *et al.*, 2012; Keshinro *et al.*, 1993).

Roasting of white and yellow maize led to a significant increase in the crude fat, magnesium (Mg), sodium (Na), calcium (Ca), zinc (Zn) and carbohydrate content (Obboh *et al.*, 2010). Contradictory, Ayatse *et al.* (1983) reported a 41% loss of Ca and no effect on the Na and Zn content. A significant decrease in crude protein, crude fibre, iron (Fe), potassium (K) and phytate content were also detected (Obboh *et al.*, 2010). On the contrary, Ayatse *et al.* (1983) reported that roasting led to no significant difference between raw and roasted maize in terms of the crude fibre, crude protein, ash and carbohydrate content. Nonetheless, there was a significant difference in the moisture content (Ayatse *et al.*, 1983). Roasting also significantly reduced the extractable flavonoid and phenol content in maize, while a substantial increase in the ferric reducing antioxidant power occurred (Obboh *et al.*, 2010). Even though roasting decreased the protein content in maize, a higher energy value were obtained and an increased antioxidant capacity. The increased antioxidant capacity was correlated with the high reducing power.

In Korea, maize is traditionally roasted and extracted with hot water to prepare extracts that are consumed as a coffee-like beverage. A recent study optimised the roasting conditions (207°C; 24 min) for the preparation of this beverage (Youn & Chung, 2012). The method of processing affects the nutritional value of maize, therefore the health promoting value may either increase or decrease depending on the processing method (Ayatse *et al.*, 1983). Dry heat treatment has mixed effects on the nutritional value of foods. Heat may increase the availability of certain nutrients and it is capable of destroying undesirable enzymes and microorganisms. In maize, roasting has shown to liberate niacin from niacytin. Together with the desirable changes, undesirable modifications

also occur, such as the loss of certain nutrients (Ayatse *et al.*, 1983). Roasting resulted in significant reductions in phytic acid content in maize (Khan *et al.*, 1991) and wheat (Khan *et al.*, 1986; Khan *et al.*, 1988) products. Phytic acid reduces the bioavailability of several metals by chelating it and therefore it has anti-nutritional properties.

In India, roasted whole grains, called sattu, are widely consumed as health food in the form of a refreshing drink or ready-to-eat snack (Sharma & Gujral, 2011). Roasted whole wheat, prepared by pan roasting, called “kavurga”, is consumed as snack food in Turkey where it is milled and mixed with syrup before consumption (Işikli *et al.*, 2014). A range of alternate forms of toasted cereal grains exist, e.g. breakfast cereals, pasta and baked products. Roasted wheat grits can be incorporated with dried milk, in formulation or with other nutritious cereal complements and the roasted flour may be used as basis for beverage products or instant sauces (Mossman *et al.*, 1973).

Table 3.1 lists a few applications of roasted wheat. Optimum roasting conditions for wheat using sand roasting are  $300 \pm 10^\circ\text{C}$  for 25 to 30 s and  $280$  to  $350^\circ\text{C}$  for 45 to 50 s using FBR (Murthy *et al.*, 2008). FBR was reported to be superior to traditional sand roasting as the sample required less energy for size reduction and it also led to more evenly roasted wheat. The roasting conditions can differ depending on the type of roaster used, the degree of roasting required, the moisture content, variety and age of the sample (Mendes *et al.*, 2001). The degree of roasting can be monitored by the colour, weight loss and chemical modifications of certain components (Mendes *et al.*, 2001). Colour is an effective control parameter as there is an increase in brown pigments as the Maillard reaction progresses during roasting (Nicoli *et al.*, 1997). These Maillard reaction products play a role in the oxidative stability of processed food. As the moisture content decreases during roasting the product will begin to darken more rapidly (Moss & Otten, 1989).

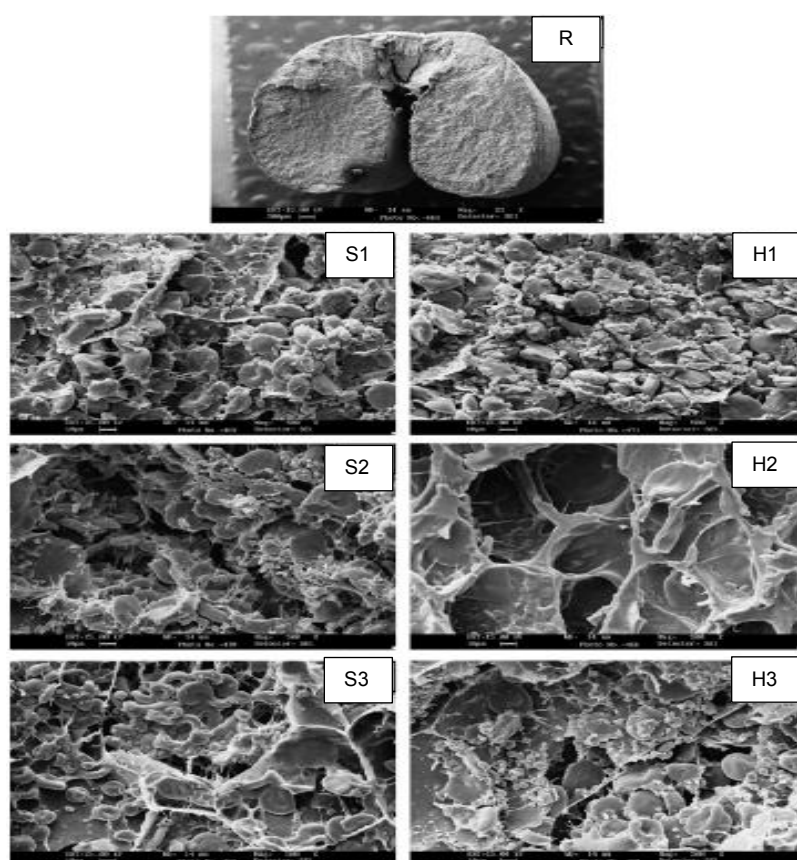
Roasting was found to have little effect on the chemical composition of wheat bran (Caprez *et al.*, 1986). Furthermore, the starch content and total dietary fibre of the wheat bran remained unaffected. A slight increase in the protein content was noted and that might have been due to the formation of protein aggregates that is protease-resistant (Caprez *et al.*, 1986). Roasting wheat bran reduced the moistening ability and consequently delayed water uptake. In the Canary Islands, “gofio”, a combination of roasted maize or wheat flour are acknowledged for its high energy content and excellent digestibility (Hernández *et al.*, 2014).

Apart from enhancing antioxidant activity, roasting prevents oxidation of unsaturated fatty acids and thereby improves the stability of wheat germ (Krings *et al.*, 2000; Krings & Berger, 2001) and generates DNA-protective properties (Krings *et al.*, 2006). The improved antioxidant activity of roasted wheat germ at elevated temperatures ( $160$ – $200^\circ\text{C}$ ) in comparison to raw wheat germ is due to Maillard-type antioxidants that are formed (Krings *et al.*, 2000). Before being added to food products, wheat germ is usually heat processed to develop colour and flavour (Moran Jr *et al.*, 1968). A more intense colour and flavour is observed with severe heat treatments. Furthermore,

heat processing improves the shelf life by means of deactivating enzymes found in the germ (Kent, 1983). Murthy *et al.* (2008) evaluated the microstructure of raw and two types of roasted wheat using SEM. In Figure 3.7 the SEM micrographs indicate the microstructure of raw wheat with a closed structure and roasted wheat with more a porous microstructure. It can be perceived that sand roasted wheat has a denser microstructure in comparison to the hot air roasted samples. Table 3.2 provides a summary of the literature available on cereal roasting and the roasting method and conditions used.

**Table 3.1.** Applications of roasted wheat (Lazar *et al.*, 1974)

Applications	Form in which used
Batters for fish, poultry, meat and vegetables	Flour
Fried specialties, snacks	Flour, extrusions
Bakes specialties, snacks	Flour
Gels	Flour
Thickener (sauces, soups, gravies)	Flour
Gruel	Flour, grits, flakes



**Figure 3.7.** Scanning electron micrographs of raw (R), sand under roasted (S1), hot air under roasted (H1), sand optimum roasted (S2), hot air optimum roasted (H2), sand over roasted (S3) and hot air over roasted (H3) wheat (Murthy *et al.*, 2008).

**Table 3.2.** Summary of the literature available on the roasting methods, conditions and the purpose of roasting cereal grains

Product	Roasting method	Roasting conditions	Purpose	References
Barley	Automatic roasting machine	1 <sup>st</sup> roasting: 434, 446, 458 and 465°C for 48 s 2 <sup>nd</sup> roasting: 327, 332, 335 and 341°C for 60 s	Effect on antioxidant activity	(Duh <i>et al.</i> , 2001)
Barley	Microwave	300-600 Watt; 7-9 min	Optimisation of antioxidant activity	(Omwamba & Hu, 2010)
Barley	Sand	280±5°C; 20 s	Effect on antioxidant activity	(Sharma & Gujral, 2011)
Barley	Sand	280±5°C; 20 s	Effect on $\beta$ -glucan, thermal, textural and pasting properties	(Sharma <i>et al.</i> , 2011)
Barley, maize, oats and wheat	Flame roasted using a propane-fired roaster	Barley and oats: 77, 121 and 168°C, 1 min Maize: 74, 119 and 163°C, 1 min Wheat: 93, 149 and 193°C; 1min	Effect on nutritional quality	(McNiven <i>et al.</i> , 1994)
Buckwheat	Laboratory temperature-controlled cabinet	160°C; 30 min	Effect on structure, functionality and enzyme <i>in vitro</i> susceptibility	(Christa <i>et al.</i> , 2009)
Buckwheat	-	160°C; 30 min	Influence on protein quality and antioxidant properties	(Zielinski <i>et al.</i> , 2009)
Maize	Aluminium frying pan	60-130°C; 14-17min	Effect on nutritive value	(Ayatse <i>et al.</i> , 1983)
Maize	Laboratory model rotary grain roaster	150±2°C; 9 min	Effect on hydration kinetics	(Bhattacharya, 1995)
Maize	Pan	270±2°C; 7 min	Effect on digestibility, crystallinity, rheological, thermal, particle size	(Carrera <i>et al.</i> , 2015)

			and morphological characteristics	
Maize	Electric rotary roaster	160-240°C; 0-50 min	Effect on bulk density, soluble solids, browning index and phenolic compounds	(Chung <i>et al.</i> , 2011)
Maize	Liquid petroleum gas-fired roaster	80, 100, 120, 140 and 160°C; 30-35 s	Effect on nutritive value	(Costa <i>et al.</i> , 1976)
Maize	Liquid propane-fired roaster (flame roasting)	110-140°C; 4-5 min	Effect on chemical and nutrient content	(Hamilton & Thompson, 1992)
Maize	Aluminium frying pan	60-130°C; 17min	Effect on nutritional and antioxidant properties	(Obboh <i>et al.</i> , 2010)
Maize	Electric rotary roaster	160-240°C; 10-50 min	Optimisation of roasting conditions	(Youn & Chung, 2012)
Maize, Bengalgram and soybean	Open aluminium pan	180, 215 and 250°C; 1.5, 2 and 2.5 min	Effect on <i>in vitro</i> protein digestibility	(Srivastav <i>et al.</i> , 1990)
Maize (cornflakes)	Household oven	215°C, three heating stages of 90 s each	Relationship between texture, mechanical properties and structure	(Chaunier <i>et al.</i> , 2007)
Maize (cornflakes)	Batch pilot plant air toasting unit	200-300°C; 5-75 s	Effect on product characteristics	(Sumithra & Bhattacharya, 2008)
Maize meal	Oven	150±5°C; 60 min	Effect on proximate compositions, pasting and rheological properties	(Ingbian & Adegoke, 2007)
Maize (pinole)	Pan	285±2°C; 7 min	Effect on $\beta$ -aflatoxins during pinole preparation	(Méndez-Albores <i>et al.</i> , 2004)
Oats	Convection oven	104°C; 120 min	Influence on viscosity	(Doehlert <i>et al.</i> , 1997)

Oats	Sand	280 ±5°C; 15 s	Effect on beta glucan extractability, physicochemical and antioxidant properties	(Gujral <i>et al.</i> , 2011)
Oats	Oven	115 ±2°C; 3 h	Effect on physical, functional and antioxidant properties	(Sandhu <i>et al.</i> , 2015)
Oats	Oven	105°C; 120 min	Effect on rheological properties	(Zhang <i>et al.</i> , 1998)
Rice	Convective–microwave oven	180, 200, and 220°C; 10-100s	Inspection of puffing characteristics	(Joshi <i>et al.</i> , 2014)
Rice	Sand	270-280°C	Effect on starch characteristics and morphology	(Mahadevamma & Tharanathan, 2007)
Sorghum	Fluidised bed air roasting unit	140-180°C; 5-15 min	Effect on rheological and functional properties	(Ranganathan <i>et al.</i> , 2014)
Wheat	Microwave and jet-sploder type roaster	Microwave: 1000 Watt; 300 s Jet-sploder roaster: 350°C; 15 s	Influence on strength characteristics	(Grochowicz & Zawislak, 2002)
Wheat	Modified direct gas-fired pilot plant toaster	300-500°F; 0-60 s	Effect on functional properties for food applications	(Lazar <i>et al.</i> , 1974)
Wheat	Continuous, gas fired, hot air toaster	620°F; 11-40 s	Effect on organoleptic, physical and nutritional quality	(Mossman <i>et al.</i> , 1973)
Wheat	Sand and fluidised bed	Sand: 300±10°C; 15-18, 25-30 and 80-100 s Fluidised bed: 280–350°C; 30-35, 45-50 and 100-120 s	Effect on moisture content, bulk density, colour, microstructure, texture and acid insoluble ash	(Murthy <i>et al.</i> , 2008)
Wheat	Sand roasting	202°C; 1.80 min	Effect on grinding characteristics, granular morphology and yield	(Raigar <i>et al.</i> , 2016).

Wheat, barley and green gram	Oven	70°C; 2 h	Influence of roasting and malting on total and extractable mineral contents of human weaning mixtures	(Gahlawat & Sehgal, 1993)
Wheat bran	Oven	230°C; 7.5 min	Effect on chemical composition and physical properties	(Caprez <i>et al.</i> , 1986)
Wheat bran	Drum roaster	150°C; 9 min	Effect on rheology, microstructure and quality characteristics of biscuits	(Nandeesh <i>et al.</i> , 2011)
Wheat (durum)	-	-	Production of traditional Italian pasta: chemical, mechanical, sensory and image analyses	(Baiano <i>et al.</i> , 2008)
Wheat (durum)	Tin pans placed on a wood-fire	250°C; 35–45 s	Effect on the physical and mechanical properties of bread loaves	(Baiano <i>et al.</i> , 2009)
Wheat (durum)	Direct contact with a wood-fire	120 s	Protein characterisation	(Lamacchia <i>et al.</i> , 2010)
Wheat germ	Conventional hot air spouted bed dryer	Inlet: 216 °C; Outlet: 150°C for 7min	Optimisation of supercritical carbon dioxide extraction of antioxidants	(Gelmez <i>et al.</i> , 2009)
Wheat germ	Oven	140, 160, 180 and 200°C; 20 min	Effect on antioxidant activity	(Krings <i>et al.</i> , 2000)
Wheat germ	Oven	160°C; 20 min	Effect on <i>in vitro</i> DNA-protective activity	(Krings <i>et al.</i> , 2006)
Wheat, oat, corn, rice and soybean	Oven	180°C; 3, 6 and 10 min - including an additional 2 min pre-heating step	Effect of the Maillard reaction during the toasting process of common flours	(Rufián-Henares <i>et al.</i> , 2009)



## Conclusion

Understanding the effect of roasting on cereal grains is the basis for the development of industrial processes and value-added products. During processing and product development, information is required on the interactions between the product and the effect of processing conditions. The structure-function relationships of raw materials are valuable in order to produce a high quality end product.

Hardness is an important characteristic in the cereal industry as it influences yield, storage and milling properties. Roasting will affect the microstructure of cereal grains and has been linked to an increase in volume and porosity and a decrease in density and thus hardness. It is therefore important to characterise and quantify roasted cereal grains to establish the impact of roasting on the microstructure. Conventionally SEM has been used to investigate microstructure, but the fact that X-ray  $\mu$ CT is non-destructive and allows 3D characterisation makes it a promising alternative to improve the visualisation and quantification of the structural changes induced by roasting. These structural changes will depend on the roasting method and conditions used and can be related to changes in physicochemical, rheological and functional properties.

## References

- Altan, A. (2014). Effects of pretreatments and moisture content on microstructure and physical properties of microwave expanded hull-less barley. *Food Research International*, **56**, 126-135.
- Anjum, F., Anwar, F., Jamil, A. & Iqbal, M. (2006). Microwave roasting effects on the physico-chemical composition and oxidative stability of sunflower seed oil. *Journal of the American Oil Chemists' Society*, **83**, 777-784.
- Anonymous. (1996a). Corn: layers and structures of corn kernel [Internet document]. URL <http://www.britannica.com/EBchecked/topic-art/103350/162/The-outer-layers-and-internal-structures-of-a-kernel-of>. Accessed 24/03/2014.
- Anonymous. (1996b). Wheat: wheat kernel [Internet document]. URL <http://www.britannica.com/EBchecked/topic/103350/cereal-processing/50119/Milling>. Accessed 24/03/2014.
- Anonymous. (2014). Roastech [Internet document]. URL <http://www.roastech.com/contact.html>. Accessed 23/05/2014.
- Asep, E., Jinap, S., Tan, T.J., Russly, A., Harcharan, S. & Nazimah, S. (2008). The effects of particle size, fermentation and roasting of cocoa nibs on supercritical fluid extraction of cocoa butter. *Journal of Food Engineering*, **85**, 450-458.
- Autio, K. & Salmenkallio-Marttila, M. (2001). Light microscopic investigations of cereal grains, doughs and breads. *LWT-Food Science and Technology*, **34**, 18-22.
- Ayatse, J., Eka, O. & Ifon, E. (1983). Chemical evaluation of the effect of roasting on the nutritive value of maize (*Zea mays*, Linn.). *Food Chemistry*, **12**, 135-147.



- Baiano, A., Fares, C., Peri, G., Romaniello, R., Taurino, A.M., Siciliano, P., Gambacorta, G., Lamacchia, C., Pati, S. & Notte, E.L. (2008). Use of a toasted durum whole meal in the production of a traditional Italian pasta: chemical, mechanical, sensory and image analyses. *International Journal of Food Science & Technology*, **43**, 1610-1618.
- Baiano, A., Romaniello, R., Lamacchia, C. & La Notte, E. (2009). Physical and mechanical properties of bread loaves produced by incorporation of two types of toasted durum wheat flour. *Journal of Food Engineering*, **95**, 199-207.
- Bhattacharya, S. (1995). Kinetics of hydration of raw and roasted corn semolina. *Journal of Food Engineering*, **25**, 21-30.
- Cammarn, S., Lange, T. & Beckett, G. (1990). Continuous fluidized-bed roasting. *Chemical Engineering Progress*, **86**, 40-46.
- Cämmerer, B. & Kroh, L.W. (2009). Shelf life of linseeds and peanuts in relation to roasting. *LWT-Food Science and Technology*, **42**, 545-549.
- Campling, R. (1991). Processing cereal grains for cattle—a review. *Livestock Production Science*, **28**, 223-234.
- Caprez, A., Arrigoni, E., Amadò, R. & Neukom, H. (1986). Influence of different types of thermal treatment on the chemical composition and physical properties of wheat bran. *Journal of Cereal Science*, **4**, 233-239.
- Carrera, Y., Utrilla-Coello, R., Bello-Pérez, A., Alvarez-Ramirez, J. & Vernon-Carter, E.J. (2015). In vitro digestibility, crystallinity, rheological, thermal, particle size and morphological characteristics of pinole, a traditional energy food obtained from toasted ground maize. *Carbohydrate Polymers*, **123**, 246-255.
- Castelo, M.M., Sumner, S.S. & Bullerman, L.B. (1998). Stability of fumonisins in thermally processed corn products. *Journal of Food Protection*, **61**, 1030-1033.
- Chandrasekhar, P. & Chattopadhyay, P. (1989). Heat transfer during fluidized bed puffing of rice grains. *Journal of Food Process Engineering*, **11**, 147-157.
- Chandrasekhar, P. & Chattopadhyay, P. (1990). Studies on microstructural changes of parboiled and puffed rice. *Journal of Food Processing and Preservation*, **14**, 27-37.
- Charalampopoulos, D., Wang, R., Pandiella, S. & Webb, C. (2002). Application of cereals and cereal components in functional foods: a review. *International Journal of Food Microbiology*, **79**, 131-141.
- Chaunier, L., Della Valle, G. & Lourdin, D. (2007). Relationships between texture, mechanical properties and structure of cornflakes. *Food Research International*, **40**, 493-503.
- Chen, C.M. & Yeh, A.I. (2001). Effect of amylose content on expansion of extruded rice pellet. *Cereal Chemistry*, **78**, 261-266.

- Christa, K., Soral-Smietana, M. & Lewandowicz, G. (2009). Buckwheat starch: structure, functionality and enzyme in vitro susceptibility upon the roasting process. *International Journal of Food Sciences and Nutrition*, **60**, 140-154.
- Chung, H.S., Chung, S.K. & Youn, K.S. (2011). Effects of roasting temperature and time on bulk density, soluble solids, browning index and phenolic compounds of corn kernels. *Journal of Food Processing and Preservation*, **35**, 832-839.
- Costa, P., Jensen, A., Harmon, B. & Norton, H. (1976). The effects of roasting and roasting temperatures on the nutritive value of corn for swine. *Journal of Animal Science*, **42**, 365-374.
- Delcour, J. & Hosney, R.C. (2010). *Principles of Cereal Science and Technology*. Pp. 1-12. St. Paul, Minnesota, USA: AACC International Press.
- Doehlert, D.C., Zhang, D. & Moore, W.R. (1997). Influence of heat pretreatments of oat grain on the viscosity of flour slurries. *Journal of the Science of Food and Agriculture*, **74**, 125-131.
- Dowsell, C.R., Paliwal, R.L. & Cantrell, R.P. (1996). *Maize in the Third World*. New York, USA: Westview Press.
- Duh, P.-D., Yen, G.-C., Yen, W.-J. & Chang, L.-W. (2001). Antioxidant effects of water extracts from barley (*Hordeum vulgare* L.) prepared under different roasting temperatures. *Journal of Agricultural and Food Chemistry*, **49**, 1455-1463.
- El-Adawy, T.A. & Mansour, E.H. (2000). Nutritional and physicochemical evaluations of tahina (sesame butter) prepared from heat-treated sesame seeds. *Journal of the Science of Food and Agriculture*, **80**, 2005-2011.
- FAOSTAT. (2015). Food and Agriculture Organization of the United Nations. Statistics division [Internet document]. URL <http://faostat3.fao.org/download/Q/QC/E>. Accessed 07/05/2015.
- Fast, R., Shouldice, F., Thomson, W., Taylor, D. & Getgood, S. (1990). Toasting and toasting ovens for breakfast cereals. *Cereal Foods World*, **35**, 299.
- Flinn, B. (2012). New roasting technology! [Internet document]. URL [http://www.agriculture.com/machinery/precision-agriculture/new-roasting-technology\\_234-ar26331?print](http://www.agriculture.com/machinery/precision-agriculture/new-roasting-technology_234-ar26331?print). Accessed 24/02/2014.
- Frisullo, P., Barnabà, M., Navarini, L. & Del Nobile, M. (2012). *Coffea arabica* beans microstructural changes induced by roasting: an X-ray microtomographic investigation. *Journal of Food Engineering*, **108**, 232-237.
- Gahalawat, P. & Sehgal, S. (1992). Phytic acid, saponins, and polyphenol in weaning foods prepared from oven-heated green gram and cereals. *Cereal Chemistry*, **69**, 463-464.
- Gahalawat, P. & Sehgal, S. (1993). The influence of roasting and malting on the total and extractable mineral contents of human weaning mixtures prepared from Indian raw materials. *Food Chemistry*, **46**, 253-256.
- Gelmez, N., Kincal, N.S. & Yener, M.E. (2009). Optimization of supercritical carbon dioxide extraction of antioxidants from roasted wheat germ based on yield, total phenolic and

- tocopherol contents, and antioxidant activities of the extracts. *The Journal of Supercritical Fluids*, **48**, 217-224.
- Gray, J. & Bemiller, J. (2003). Bread staling: molecular basis and control. *Comprehensive Reviews in Food Science and Food Safety*, **2**, 1-21.
- Grochowicz, J. & Zawislak, K. (2002). Changes in strength characteristics of heat-treated wheat grain (communication). *International Agrophysics*, **16**, 167-170.
- Gropper, M., Moraru, C.I. & Kokini, J.L. (2002). Effect of specific mechanical energy on properties of extruded protein-starch mixtures. *Cereal Chemistry*, **79**, 429-433.
- Gujral, H.S., Sharma, P. & Rachna, S. (2011). Effect of sand roasting on beta glucan extractability, physicochemical and antioxidant properties of oats. *LWT-Food Science and Technology*, **44**, 2223-2230.
- Hamilton, R.M. & Thompson, B.K. (1992). Chemical and nutrient content of corn (*Zea mays*) before and after being flame roasted. *Journal of the Science of Food and Agriculture*, **58**, 425-430.
- Hernández, O., Fraga, J., Jiménez, A., Jiménez, F. & Arias, J. (2014). Characterization of toasted cereal flours from the Canary Islands (gofios). *Food Chemistry*, **151**, 133-140.
- Heywood, B. (1978). Continuous vibratory fluid bed drying. *Food Processing Industry*, **47**, 21-25.
- Hoke, K., Houška, M., Průchová, J., Gabrovská, D., Vaculová, K. & Paulíčková, I. (2007). Optimisation of puffing naked barley. *Journal of Food Engineering*, **80**, 1016-1022.
- Hoke, K., Housova, J. & Houska, M. (2005). Optimum conditions of rice puffing. *Czech Journal Food of Science*, **23**, 1-11.
- Huffman, S.L. & Martin, L.H. (1994). First feedings: optimal feeding of infants and toddlers. *Nutrition research*, **14**, 127-159.
- İbanoğlu, E. (2002). Kinetic study on colour changes in wheat germ due to heat. *Journal of Food Engineering*, **51**, 209-213.
- Ingbian, E.K. & Adegoke, G.O. (2007). Proximate compositions, pasting and rheological properties of mumu—a roasted maize meal. *International Journal of Food Science & Technology*, **42**, 762-767.
- Işikli, N.D., Şenol, B. & Çoksöyler, N. (2014). Some physical and mechanical properties of roasted zerun wheat. *Journal of Food Science and Technology*, **51**, 1990-1997.
- Jain, R. & Srivastav, P. (1993). Low-cost traditional and improved devices for roasting and puffing of grains. *Indian Food Industry*, **12**, 33-33.
- Jayalekshmy, A. & Mathew, A. (1990). Changes in the carbohydrates and proteins of coconut during roasting. *Food Chemistry*, **37**, 123-134.
- Jha, S. (2005). Mathematical simulation of roasting of grain. *Journal of Food Engineering*, **71**, 304-310.
- Jones, D., Chinnaswamy, R., Tan, Y. & Hanna, M. (2000). Physiochemical properties of ready-to-eat breakfast cereals. *Cereal Foods World*, **45**, 164-168.

- Joshi, N.D., Mohapatra, D., Joshi, D.C. & Sutar, R. (2014). Puffing characteristics of parboiled milled rice in a domestic convective–microwave oven and process optimization. *Food and Bioprocess Technology*, **7**, 1678-1688.
- Kabak, B. (2009). The fate of mycotoxins during thermal food processing. *Journal of the Science of Food and Agriculture*, **89**, 549-554.
- Kahyaoglu, T. & Kaya, S. (2006). Modeling of moisture, color and texture changes in sesame seeds during the conventional roasting. *Journal of Food Engineering*, **75**, 167-177.
- Kato, H., Doi, Y., Tsugita, T., Kosai, K., Kamiya, T. & Kurata, T. (1981). Changes in volatile flavour components of soybeans during roasting. *Food Chemistry*, **7**, 87-94.
- Kayitesi, E., Duodu, K.G., Minnaar, A. & De Kock, H.L. (2010). Sensory quality of marama/sorghum composite porridges. *Journal of the Science of Food and Agriculture*, **90**, 2124-2132.
- Kent, N.L. (1983). *Technology of Cereals: an Introduction for Students of Food Science and Agriculture*. London: Pergamon Press.
- Keshinro, O., Ogundipe, A., Scot-Emuakpor, M. & Egele, P. (1993). Effects of preparatory procedures on selected nutrient contents of some tropical maize products. *Journal of Cereal Science*, **18**, 287-294.
- Khan, N., Zaman, R. & Elahi, M. (1986). Effect of processing on the phytic acid content of wheat products. *Journal of Agricultural and Food Chemistry*, **34**, 1010-1012.
- Khan, N., Zaman, R. & Elahi, M. (1988). Effect of processing on the phytic acid content of bengal grams (*Cicer arietinum*) products. *Journal of Agricultural and Food Chemistry*, **36**, 1274-1276.
- Khan, N., Zaman, R. & Elahi, M. (1991). Effect of heat treatments on the phytic acid content of maize products. *Journal of the Science of Food and Agriculture*, **54**, 153-156.
- Kikugawa, K., Arai, M. & Kurechi, T. (1983). Participation of sesamol in stability of sesame oil. *Journal of the American Oil Chemists' Society*, **60**, 1528-1533.
- Krings, U. & Berger, R. (2001). Antioxidant activity of some roasted foods. *Food Chemistry*, **72**, 223-229.
- Krings, U., El-Saharty, Y.S., El-Zeany, B.A., Pabel, B. & Berger, R.G. (2000). Antioxidant activity of extracts from roasted wheat germ. *Food Chemistry*, **71**, 91-95.
- Krings, U., Johansson, L., Zorn, H. & Berger, R.G. (2006). In vitro DNA-protective activity of roasted wheat germ and fractions thereof. *Food Chemistry*, **97**, 712-718.
- Kunitz, M. (1947). Crystalline soybean trypsin inhibitor II: general properties. *The Journal of General Physiology*, **30**, 291-310.
- Lamacchia, C., Baiano, A., Lamparelli, S., Notte, E.L. & Luccia, A.D. (2010). Changes in durum wheat kernel and pasta proteins induced by toasting and drying processes. *Food Chemistry*, **118**, 191-198.

- Lazar, M., Mossman, A. & Wallace, J. (1974). Air-fluidized toasting of whole kernel wheat-processing variables and functional properties for food applications. *Journal of Food Science*, **39**, 239-243.
- Mahadevamma, S. & Tharanathan, R. (2007). Processed rice starch characteristics and morphology. *European Food Research and Technology*, **225**, 603-612.
- Manley, M., Williams, P., Nilsson, D. & Geladi, P. (2009). Near infrared hyperspectral imaging for the evaluation of endosperm texture in whole yellow maize (*Zea mays* L.) kernels. *Journal of Agricultural and Food Chemistry*, **57**, 8761-8769.
- Mariotti, M., Alamprese, C., Pagani, M.A. & Lucisano, M. (2006). Effect of puffing on ultrastructure and physical characteristics of cereal grains and flours. *Journal of Cereal Science*, **43**, 47-56.
- Maruatona, G.N., Duodu, K.G. & Minnaar, A. (2010). Physicochemical, nutritional and functional properties of maramba bean flour. *Food Chemistry*, **121**, 400-405.
- Maskan, M. (2002). Effect of processing on hydration kinetics of three wheat products of the same variety. *Journal of Food Engineering*, **52**, 337-341.
- Massini, R., Nicoli, M., Cassarà, A. & Lerici, C. (1990). Study on physical and physico-chemical changes of coffee beans during roasting. *Italian Journal of Food Science*, **2**, 123-130.
- McNiven, M.A., Hamilton, R.M.G., Robinson, P.H. & DeLeeuw, J.W. (1994). Effect of flame roasting on the nutritional quality of common cereal grains for non-ruminants and ruminants. *Animal Feed Science and Technology*, **47**, 31-40.
- Medoua, G.N. & Mbofung, C.M. (2007). Kinetics studies of some physico-chemical substances during roasting and preparation of beverage made by *Cassia occidentalis* seeds. *LWT-Food Science and Technology*, **40**, 730-736.
- Megahed, M. (2001). Microwave roasting of peanuts: effects on oil characteristics and composition. *Food/Nahrung*, **45**, 255-257.
- Mendes, L.C., De Menezes, H.C., Aparecida, M. & Da Silva, A. (2001). Optimization of the roasting of robusta coffee (*C. canephora* conillon) using acceptability tests and RSM. *Food Quality and Preference*, **12**, 153-162.
- Méndez-Albores, A., De Jesús-Flores, F., Castañeda-Roldan, E., Arámbula-Villa, G. & Moreno-Martínez, E. (2004). The effect of toasting and boiling on the fate of B-aflatoxins during pinole preparation. *Journal of Food Engineering*, **65**, 585-589.
- Moore, G., Devos, K., Wang, Z. & Gale, M. (1995). Cereal genome evolution: grasses, line up and form a circle. *Current Biology*, **5**, 737-739.
- Moran Jr, E., Summers, J. & Bass, E. (1968). Heat processing of wheat germ meal and its effect on utilization and protein quality for the growing chick: toasting and autoclaving. *Cereal Chemistry*, **45**, 304-311.

- Moss, J. & Otten, L. (1989). A relationship between colour development and moisture content during roasting of peanuts. *Canadian Institute of Food Science and Technology Journal*, **22**, 34-39.
- Mossman, A., Rockwell, W. & Fellers, D. (1973). Hot air toasting and rolling whole wheat effect on organoleptic, physical and nutritional quality. *Journal of Food Science*, **38**, 879-884.
- Mrad, R., Debs, E., Saliba, R., Maroun, R.G. & Louka, N. (2014). Multiple optimization of chemical and textural properties of roasted expanded purple maize using response surface methodology. *Journal of Cereal Science*, **60**, 397-405.
- Murthy, K.V., Ravi, R., Keshava Bhat, K. & Raghavarao, K.S.M.S. (2008). Studies on roasting of wheat using fluidized bed roaster. *Journal of Food Engineering*, **89**, 336-342.
- Nagai, T., Staatz, J., Bernsten, R., Sakyi-Dawson, E. & Annor, G. (2012). Locally processed roasted-maize-based weaning foods fortified with legumes: factors affecting their availability and competitiveness in Accra, Ghana. *African Journal of Food, Agriculture, Nutrition and Development*, **9**, 1927-1944.
- Nandeesh, K., Jyotsna, R. & Venkateswara Rao, G. (2011). Effect of differently treated wheat bran on rheology, microstructure and quality characteristics of soft dough biscuits. *Journal of Food Processing and Preservation*, **35**, 179-200.
- Ndungu, K.E., Emmambux, M.N. & Minnaar, A. (2012). Micronisation and hot air roasting of cowpeas as pretreatments to control the development of hard-to-cook phenomenon. *Journal of the Science of Food and Agriculture*, **92**, 1194-1200.
- Nebesny, E. & Budryn, G. (2003). Antioxidative activity of green and roasted coffee beans as influenced by convection and microwave roasting methods and content of certain compounds. *European Food Research and Technology*, **217**, 157-163.
- Nicoli, M.C., Anese, M., Manzocco, L. & Lerici, C.R. (1997). Antioxidant properties of coffee brews in relation to the roasting degree. *LWT - Food Science and Technology*, **30**, 292-297.
- Oboh, G., Ademiluyi, A.O. & Akindahunsi, A.A. (2010). The effect of roasting on the nutritional and antioxidant properties of yellow and white maize varieties. *International Journal of Food Science & Technology*, **45**, 1236-1242.
- Omwamba, M. & Hu, Q. (2010). Antioxidant activity in barley (*Hordeum vulgare* L.) grains roasted in a microwave oven under conditions optimized using response surface methodology. *Journal of Food Science*, **75**, C66-C73.
- Owusu-Ansah, J., Van De Voort, F. & Stanley, D. (1984). Textural and microstructural changes in corn starch as a function of extrusion variables. *Canadian Institute of Food Science and Technology Journal*, **17**, 65-70.
- Özdemir, M. & Devres, O. (2000). Kinetics of color changes of hazelnuts during roasting. *Journal of Food Engineering*, **44**, 31-38.



- Özkaya, B., Özkaya, H., Erenb, N., Ünsal, A. & Köksel, H. (1999). Effects of wheat maturation stage and cooking method on physical and chemical properties of firiks. *Food Chemistry*, **66**, 97-102.
- Pardeshi, I. & Chattopadhyay, P. (2014). Whirling bed hot air puffing kinetics of rice-soy ready-to-eat (RTE) snacks. *Journal of Ready to Eat Foods*, **1**, 1-10.
- Peleg, M. (1997). Review: mechanical properties of dry cellular solid foods. *Food Science and Technology International*, **3**, 227-240.
- Pelto, G.H. & Armar-Klemesu, M. (2011). Balancing nurturance, cost and time: complementary feeding in Accra, Ghana. *Maternal & Child Nutrition*, **7**, 66-81.
- Pittia, P., Dalla Rosa, M.D. & Lerici, C.R. (2001). Textural changes of coffee beans as affected by roasting conditions. *LWT-Food Science and Technology*, **34**, 168-175.
- Pittia, P., Nicoli, M.C. & Sacchetti, G. (2007). Effect of moisture and water activity on textural properties of raw and roasted coffee beans. *Journal of Texture Studies*, **38**, 116-134.
- Pittia, P., Sacchetti, G., Mancini, L., Voltolini, M., Sodini, N., Tromba, G. & Zanini, F. (2011). Evaluation of microstructural properties of coffee beans by synchrotron X-ray microtomography: a methodological approach. *Journal of Food Science*, **76**, 222-231.
- Plahar, W., Okezie, B.O. & Gyato, C. (2003). Development of a high protein weaning food by extrusion cooking using peanuts, maize and soybeans. *Plant Foods for Human Nutrition*, **58**, 1-12.
- Pomeranz, Y., Carvajal, M., Hosney, R. & Ward, A. (1970). Wheat germ in breadmaking. I. Composition of germ lipids and germ protein fractions. *Cereal Chemistry*, **47**, 373-380.
- Poutanen, K., Sozer, N. & Della Valle, G. (2014). How can technology help to deliver more of grain in cereal foods for a healthy diet? *Journal of Cereal Science*, **59**, 327-336.
- Pronyk, C., Cenkowski, S. & Muir, W. (2004). Drying foodstuffs with superheated steam. *Drying Technology*, **22**, 899-916.
- Raigar, R.K., Prabhakar, P.K. & Srivastav, P.P. (2016). Effect of different thermal treatments on grinding characteristics, granular morphology and yield of ready-to-eat wheat grits. *Journal of Food Process Engineering*, doi:10.1111/jfpe.12363.
- Rakesh, V. & Datta, A.K. (2011). Microwave puffing: determination of optimal conditions using a coupled multiphase porous media – large deformation model. *Journal of Food Engineering*, **107**, 152-163.
- Ranganathan, V., Nunjundiah, I.T. & Bhattacharya, S. (2014). Effect of roasting on rheological and functional properties of sorghum flour. *Food Science and Technology International*, **20**, 579-589.
- Rufián-Henares, J.A., Delgado-Andrade, C. & Morales, F.J. (2009). Assessing the Maillard reaction development during the toasting process of common flours employed by the cereal products industry. *Food Chemistry*, **114**, 93-99.

- Saklar, S., Katnas, S. & Urgan, S. (2001). Determination of optimum hazelnut roasting conditions. *International Journal of Food Science & Technology*, **36**, 271-281.
- Salmenkallio-Marttila, M., Heiniö, R.L., Myllymäki, O., Lille, M., Autio, K. & Poutanen, K. (2004). Relating microstructure, sensory and instrumental texture of processed oat. *Agricultural and Food Science*, **13**, 124-137.
- Sandhu, K.S., Godara, P., Kaur, M. & Punia, S. (2015). Effect of toasting on physical, functional and antioxidant properties of flour from oat (*Avena sativa* L.) cultivars. *Journal of the Saudi Society of Agricultural Sciences*, <http://dx.doi.org/10.1016/j.jssas.2015.06.004>.
- Sawaya, W.N., Ayaz, M., Khalil, J.K. & Al-Shalhat, A.F. (1985). Chemical composition and nutritional quality of tehneh (sesame butter). *Food Chemistry*, **18**, 35-45.
- Schenker, S., Handschin, S., Frey, B., Perren, R. & Escher, F. (2000). Pore structure of coffee beans affected by roasting conditions. *Journal of Food Science*, **65**, 452-457.
- Schoeman, L., Williams, P., Du Plessis, A. & Manley, M. (2016). X-ray micro-computed tomography ( $\mu$ CT) for non-destructive characterisation of food microstructure. *Trends in Food Science & Technology*, **47**, 10-24.
- Serna-Saldivar, S.O. (2010). *Cereal Grains: Properties, Processing, and Nutritional Attributes*. London, UK: CRC Press Inc.
- Sharma, P. & Gujral, H.S. (2010). Milling behavior of hulled barley and its thermal and pasting properties. *Journal of Food Engineering*, **97**, 329-334.
- Sharma, P. & Gujral, H.S. (2011). Effect of sand roasting and microwave cooking on antioxidant activity of barley. *Food Research International*, **44**, 235-240.
- Sharma, P., Gujral, H.S. & Rosell, C.M. (2011). Effects of roasting on barley  $\beta$ -glucan, thermal, textural and pasting properties. *Journal of Cereal Science*, **53**, 25-30.
- Shelton, P.G. & Niranjana, K. (1993). Fluidization and its applications to food processing. *Food Structure*, **12**, 199-215.
- Shewry, P.R. (2007). Improving the protein content and composition of cereal grain. *Journal of Cereal Science*, **46**, 239-250.
- Srivastava, P., Das, H. & Prasad, S. (1990). Effect of roasting process variables on in-vitro protein digestibility of Bengalgram, maize and soybean. *Food Chemistry*, **35**, 31-37.
- Sumithra, B. & Bhattacharya, S. (2008). Toasting of corn flakes: product characteristics as a function of processing conditions. *Journal of Food Engineering*, **88**, 419-428.
- Uysal, N., Sumnu, G. & Sahin, S. (2009). Optimization of microwave–infrared roasting of hazelnut. *Journal of Food Engineering*, **90**, 255-261.
- Vadivambal, R. & Jayas, D.S. (2007). Changes in quality of microwave-treated agricultural products—a review. *Biosystems Engineering*, **98**, 1-16.
- Vivas, N., Waniska, R. & Rooney, L. (1987). Thin porridges (atole) prepared from maize and sorghum. *Cereal Chemistry*, **64**, 384-389.



- Warchalewski, J.R., Gralik, J., Wojtasiak, R., Zabielski, J. & Kusnierz, R. (1998). The evaluation of wheat grain odour and colour after gamma and microwave irradiation. *Electronic Journal of Polish Agricultural Universities*, **1**, 1-11.
- Watson, S.A. (1987). Structure and Composition. In: *Corn; Chemistry and Technology* (edited by S.A. Watson & P.E. Ramstad). Pp. 53-82. St. Paul, Minnesota, USA: American Association of Cereal Chemists, Inc.
- Wu, F. & Guclu, H. (2013). Global maize trade and food security: implications from a social network model. *Risk Analysis*, **33**, 2168-2178.
- Yazdanpanah, H., Mohammadi, T., Abouhossain, G. & Cheraghali, A.M. (2005). Effect of roasting on degradation of aflatoxins in contaminated pistachio nuts. *Food and Chemical Toxicology*, **43**, 1135-1139.
- Yoshida, H., Tomiyama, Y., Hirakawa, Y. & Mizushima, Y. (2006). Microwave roasting effects on the oxidative stability of oils and molecular species of triacylglycerols in the kernels of pumpkin (*Cucurbita* spp.) seeds. *Journal of Food Composition and Analysis*, **19**, 330-339.
- Youn, K.S. & Chung, H.S. (2012). Optimization of the roasting temperature and time for preparation of coffee-like maize beverage using the response surface methodology. *LWT-Food Science and Technology*, **46**, 305-310.
- Zhang, D., Doehlert, D. & Moore, W. (1998). Rheological properties of (1→3),(1→4)-β-d-glucans from raw, roasted, and steamed oat groats. *Cereal Chemistry*, **75**, 433-438.
- Zielinski, H., Michalska, A., Amigo-Benavent, M., Del Castillo, M.D. & Piskula, M.K. (2009). Changes in protein quality and antioxidant properties of buckwheat seeds and groats induced by roasting. *Journal of Agricultural and Food Chemistry*, **57**, 4771-4776.
- Zzaman, W. & Yang, T.A. (2013). Effect of superheated steam and convection roasting on changes in physical properties of cocoa bean (*Theobroma cacao*). *Food Science and Technology Research*, **19**, 181-186.

**Declaration by the candidate:**

With regard to Chapter 4 (pp. 85-109), the nature and scope of my contribution were as follows:

<b>Nature of contribution</b>	<b>Extent of contribution (%)</b>
Research, analysis and writing of chapter	75

The following co-authors have contributed to Chapter 4 (pp. 85-109):

<b>Name</b>	<b>e-mail address</b>	<b>Nature of contribution</b>	<b>Extent of contribution (%)</b>
Prof Marena Manley	mman@sun.ac.za	Research inputs, editorial suggestions and proofreading	15
Dr Anton du Plessis	anton2@sun.ac.za	Assistance with X-ray $\mu$ CT analysis and proofreading	10

Signature of candidate: L. Schoeman

Date: 30/11/2016

**Declaration by co-authors:**

The undersigned hereby confirm that

1. the declaration above accurately reflects the nature and extent of the contributions of the candidate and the co-authors to Chapter 4 (pp. 85-109),
2. no other authors contributed to Chapter 4 (pp. 85-109) besides those specified above, and
3. potential conflicts of interest have been revealed to all interested parties and that the necessary arrangements have been made to use the material in Chapter 4 (pp. 85-109) of this dissertation.

<b>Signature</b>	<b>Institutional affiliation</b>	<b>Date</b>
Prof Marena Manley	Department of Food Science, Stellenbosch University	30/11/2016
Dr Anton du Plessis	CT Scanner Facility, Stellenbosch University	30/11/2016

Declaration with signature in possession of candidate and supervisor.

## CHAPTER 4

### **Non-destructive characterisation and quantification of the effect of conventional oven and forced convection continuous tumble (FCCT) roasting on the three-dimensional microstructure of whole wheat kernels using X-ray micro-computed tomography ( $\mu$ CT)\***

#### **Abstract**

Food microstructure influences the characteristics of end products. X-ray micro-computed tomography ( $\mu$ CT) enables investigating internal structure of food products non-destructively. High-resolution X-ray  $\mu$ CT, in combination with image analysis, was used to visualise and quantify the impact of conventional oven and forced convection continuous tumble (FCCT) roasting (180°C for 140 s) on the microstructure of whole wheat kernels. After image acquisition, two-dimensional (2D) cross-sectional images were reconstructed into three-dimensional (3D) volumes. Quantitative parameters, i.e. volume, porosity, expansion ratio (ER) and relative density, were calculated. Oven roasting was associated with a significantly ( $P \leq 0.05$ ) larger increase in kernel volume (4.47%) than FCCT roasting (1.57%). Porosity was higher in the oven-roasted samples ( $10.33 \pm 4.63\%$ ), indicating a more destructive impact on the internal structure (FCCT =  $8.29 \pm 2.29\%$ ). Roasting introduced cavities and cracks within the wheat kernels, resulting in a decrease in whole kernel density (oven = 2.76%; FCCT = 0.55%), however the material density remained unaffected during FCCT roasting.

*Keywords:* Microstructure; X-ray micro-computed tomography; Image analysis; Roasting; Porosity

---

\*Published as: Schoeman, L., Du Plessis, A. & Manley, M. (2016). Non-destructive characterisation and quantification of the effect of conventional oven and forced convection continuous tumble (FCCT) roasting on the three-dimensional microstructure of whole wheat kernels using X-ray micro-computed tomography ( $\mu$ CT). *Journal of Food Engineering*, **187**, 1-13.

## Introduction

Worldwide, wheat (*Triticum aestivum* L.) is an important crop, with total annual yields exceeding 700 million tonnes in 2013 (FAOSTAT, 2015). The success of wheat as a raw material can be attributed to its processing properties and its ability to develop cohesive doughs that can be formed into noodles and pasta or baked into bread (Lamacchia *et al.*, 2010). Wheat is a staple food and is used for human consumption in a variety of products, i.e. breads, pastas, noodles, couscous, cakes, biscuits, pastries, breakfast cereals and flour.

Cereal roasting is traditionally practiced in India with the objective of increasing shelf life, enhancing organoleptic properties and to ease integration into breakfast cereals and other ready-to-eat products (Murthy *et al.*, 2008). Most roasters used in India are batch type heated pans, where sand is used as heat transfer medium. This roasting method has various negative aspects since it is unhygienic, tedious to operate, leads to a low productivity, there is a lack of temperature control and the product has non-uniform characteristics (Murthy *et al.*, 2008).

Few investigations focused on the effect of heat treatment on the microstructure of cereal grains; the effect of roasting specifically has been even less investigated. Gun puffing (105-115°C) strongly influenced the kernel morphology and it led to an increased water holding capacity of the flour (Mariotti *et al.*, 2006). Roasted wheat can be roller milled to obtain flour yields as high as 70 to 75% when the moisture content is below 10% (Lazar *et al.*, 1974). Flour from roasted wheat can be included in breads, pastas, baked and fried speciality products, gels, batters, instant sauces, snacks, gruels and it can be used as basis for beverage products (Mossman *et al.*, 1973; Lazar *et al.*, 1974; Baiano *et al.*, 2008).

A few studies reported on the use of a forced convection continuous tumble (FCCT) roaster for agricultural products such as marama beans and cowpeas (Kayitesi *et al.*, 2010; Ndungu *et al.*, 2012; Nyembwe *et al.*, 2015). The FCCT roaster is an energy efficient roasting technique that can be used to modify the microstructure of cereal grains. This roaster employs the moisture inside the sample to generate superheated steam, leading to faster and even heat transfer. The rotating cylinder enables the sample to be suspended in the heated air, thus all the surfaces are exposed evenly to the heat. Thermal insulation results in less heat loss and efficient energy usage (Flinn, 2012).

In food science, it is common to relate physical behaviour to microstructure in order to gain more comprehensive insights into the product or production process. Food microstructure plays an important role in determining the characteristics (physical, textural and sensory) of the final product (Aguilera, 2005). Structural probing of also cereal grains are of great importance to the food industry, since microstructure effects processing, storage, functionality and the end use of products (Dogan, 2007). For example, the microstructure of wheat for bread making significantly influences its quality and baking properties. Traditionally, microstructural investigations involved light microscopy (LM), scanning electron microscopy (SEM) and confocal laser scanning microscopy (CLSM). These destructive methods however have various drawbacks. It requires sectioning which

are likely to disrupt the structure, cause imaging artefacts and is limited to two-dimensional (2D) images (Salvo *et al.*, 2010).

The limitations of 2D, destructive methods have led to the increasing use of a powerful non-destructive and non-invasive high-resolution imaging technique, X-ray micro-computed tomography ( $\mu$ CT), which enables characterisation of three-dimensional (3D) volumes for better understanding of food microstructure (Salvo *et al.*, 2010; Zhu *et al.*, 2012). X-ray  $\mu$ CT makes use of the differences in X-ray attenuation that arises mainly from differences in density within a sample. High density materials will attenuate the beam and areas of high attenuation will appear brighter on the 2D slice images. X-rays are sent around and through the scanned sample, creating projection X-ray images. Consecutive images are accumulated to create 3D volumes that can be manipulated digitally to perform a number of quantitative and qualitative measurements (Ketcham & Carlson, 2001).

Traditional computed tomography (CT) and  $\mu$ CT has been applied in various agricultural commodities e.g. traditional medical CT has been used to evaluate undesirable fibrous tissue in carrots (Donis-González *et al.*, 2015) and to assess internal decay in fresh chestnuts (Donis-González *et al.*, 2014), while  $\mu$ CT has been applied for 3D pore space quantification of apple tissue (Mendoza *et al.*, 2007). Synchrotron X-ray CT was used to characterise the 3D gas exchange pathways in pome fruit (Verboven *et al.*, 2008). Lammertyn *et al.* (2003) performed a comparative study using two non-destructive imaging techniques, X-ray CT and magnetic resonance imaging (MRI), to investigate the spatial distribution of core breakdown in pears.

X-ray  $\mu$ CT (40 kV; 250  $\mu$ A) was recently investigated for real-time 3D visualisation and quantification of the internal structure of single wheat kernels damaged by sprouting and insect infestation (Suresh & Neethirajan, 2015). Other X-ray  $\mu$ CT cereal grain investigations include the characterisation of rice strains by differences in pore shapes (Zhu *et al.*, 2012) and the effect of heat treatment on rice kernel structure (Mohorič *et al.*, 2009; Witek *et al.*, 2010).

It is not possible to examine expanded starch based products by conventional 2D imaging or scanning methods without destroying the structure. Cutting them also leads to disruption of the pores and breakage due to their brittle texture. To avoid these constraints non-destructive X-ray  $\mu$ CT were applied in a few studies for the characterisation of porous cereal products (Van Dalen *et al.*, 2007), extruded products (Agbisit *et al.*, 2007; Horvat *et al.*, 2014), wheat flour dough (Bellido *et al.*, 2006), bread (Wang *et al.*, 2011; Besbes *et al.*, 2013; Demirkesen *et al.*, 2014; Van Dyck *et al.*, 2014), and to explain airflow resistance in wheat (Neethirajan *et al.*, 2006). Furthermore, X-ray  $\mu$ CT has been used widely to analyse porosity in food products, e.g. banana chips (Léonard *et al.*, 2008) and meringues (Licciardello *et al.*, 2012). Kelkar *et al.* (2015) recently described a method to determine the density of foods using X-ray  $\mu$ CT.

Andrejko *et al.* (2011) made use of X-ray radiographic examination to illustrate structural changes in wheat after infrared treatment (exceeding 150°C and 90 s). High temperature roasting of coffee beans led to an increased volume and porosity and a decreased density with increase in

roasting time (Frisullo *et al.*, 2012). The ability to accurately analyse pores makes X-ray  $\mu$ CT an effective technique to study the microstructure of roasted products.

Quality changes occurring during thermal processing include sensory (flavour, odour and taste), optical (colour and appearance), structural (density, volume and porosity), textural, nutritional (proteins and vitamins) and rehydration properties (Vadivambal & Jayas, 2007). Roasting is a time-temperature dependant process that leads to chemical reactions, moisture loss and major changes in volume, shape and density (Hernández *et al.*, 2008).

Wheat endosperm texture influences the energy requirement for milling. Porosity and density are closely related properties (Dobraszczyk *et al.*, 2002) affecting endosperm texture and thus milling yield (Chang, 1988). More dense endosperm ground to larger particles which flows more easily and are easy to handle, whereas more porous endosperm mill to flours that are very fine and results in the blocking of mill sieves (Dobraszczyk *et al.*, 2002). Ideally heat processing or roasting of wheat should have minimum effect on endosperm texture in terms of microstructural changes (porosity, volume and density). Decrease in material density would thus be undesirable. A roasting method resulting in adverse structural changes, i.e. larger cracks, large increase in porosity and loss in material density would be considered destructive.

Wheat kernel microstructural changes occurring during roasting have not been thoroughly studied in the pursuit of understanding the roasting phenomenon. The gap in understanding the mechanism that governs the behaviour of roasted grain microstructure is attributed to the lack of techniques capable of visualising the microstructure non-destructively. The need for 3D characterisation and quantification of microstructure, is now addressed with X-ray  $\mu$ CT which provides datasets that can be analysed for various structural parameters (Chevallier *et al.*, 2014).

This study hypothesises that X-ray  $\mu$ CT is a feasible technique to determine the impact of roasting on wheat kernels. As verification this study presents the application of X-ray  $\mu$ CT in combination with image analysis to non-destructively investigate the impact of conventional oven and FCCT roasting on the microstructure of whole wheat kernels. Qualitatively the internal microstructure and porosity distribution were analysed using X-ray  $\mu$ CT 2D slice images and 3D volume renderings. Quantitative measurements, obtained from 3D volumes, included volume, porosity, expansion ratio (ER) and relative density.

## Material and methods

### *Wheat samples*

Eighteen whole wheat kernels were randomly selected from a wheat sample, kindly provided by PANNAR Seeds (Greytown, South Africa). The same kernels were imaged with X-ray  $\mu$ CT before (control) and after roasting to have a direct comparison. Nine kernels were subjected to oven roasting and nine to FCCT roasting. The kernels were weighed before and after roasting to determine the percentage weight loss. The samples were kept in sealed jars at ambient temperature until used.

### *Roasting*

Wheat samples were roasted at 180°C for 140 s using two roasting methods: conventional convection oven roasting (831 Electric Multifunction Thermofan Solid Plate Oven, Defy Appliances, Durban, South Africa) and FCCT roasting (Roastech, Bloemfontein, South Africa). For the FCCT roaster roasting time is determined by means of speed settings. A speed setting of 80 Hz is equivalent to 140 s and was used for FCCT roasting. This speed setting refers to the rotation speed of the screw conveyor inside the roasting chamber.

For both roasting methods the individual kernels were numbered for direct comparison of the X-ray images before and after roasting. The raw FCCT-roasted wheat kernels were in addition coloured with a heat-stable green dye to easily find the sample in each roasted batch. Each kernel was roasted, mixed in a 200 g rice sample. The nine kernels were roasted individually for each roasting method, thus nine replicates per roasting treatment.

The FCCT roaster had a capacity of 100 kg/h and the roasting chamber a volume of 0.199 m<sup>3</sup>. A temperature of 180°C was chosen since it falls within the thermal processing temperature range commonly used for cereal grains (Andrejko *et al.*, 2011). A 15 min start-up time was allowed for the FCCT roaster to obtain steady-state conditions prior to roasting. The conventional convection oven was pre-heated to 180°C before placing the numbered kernel in the oven together with 200 g of rice. The samples were placed centrally in the oven on a stainless steel baking tray. After roasting the samples were immediately cooled to ambient temperature by spreading it out on a cold flat surface to stop exothermic reactions and prevent excessive roast and further moisture loss. The samples were stored in airtight containers at ambient temperature until X-ray  $\mu$ CT image acquisition.

The main difference between the two roasting methods is that during oven roasting the sample is stationary, whereas during FCCT roasting the sample is continuously moving inside the roasting chamber. During FCCT roasting superheated steam is generated, since the moisture removed from the sample becomes part of the roasting medium (hot air) (Moreira, 2001). In the oven only dry, hot air is used as the moist air is replaced by fresh air that is heated to the desired temperature (Moreira, 2001). Superheated steam has been reported to be cleaner, cause less oxidation and colour deterioration and lead to a higher evaporation rate, thus mitigating the loss of nutritional values in comparison to hot air (Moreira, 2001).

### *X-ray micro-computed tomography ( $\mu$ CT) image acquisition*

The wheat kernels were imaged under identical conditions (Table 4.1). Real-time X-ray  $\mu$ CT scans of the raw and roasted wheat kernels were obtained using a General Electric Phoenix V|Tome|X L240 (General Electric Sensing & Inspection Technologies GmbH, Phoenix, Wunstorf, Germany) high-resolution X-ray computed tomography system with a tungsten target X-ray tube. Due to X-ray  $\mu$ CT being non-destructive, the 3D internal structure of the same kernel could be studied before and after roasting.



Two wheat kernels, e.g. two raw, or one FCCT and one oven-roasted, were scanned together. Thus, for each of the nine oven and nine FCCT-roasted kernels, two scans were performed, firstly raw and then after being roasted. This was done in order to make direct comparisons between the kernels in the raw and roasted state. Various system settings were tested to optimise the scan quality. Instrumental conditions that needed to be considered included beam energy and current, sample-to-detector-distance and exposure time. Parameters were optimised to obtain the shortest possible scanning time while ensuring adequate image contrast. X-ray radiation was thus generated from a source voltage (energy) of 60 kV and an electron current set at 240  $\mu\text{A}$ , resulting in CT scans with a voxel size (resolution) of 12  $\mu\text{m}$ .

The scanning procedures described required no sample preparation, besides mounting of the sample. Each wheat kernel was mounted horizontally (crease facing down) on a piece of oasis (floral foam) and on a polymeric disc (10 mm thickness and 25 mm diameter), obtained from Maizey Plastics (Cape Town, South Africa), and glued to the translation stage (see sample setup in Fig. 4.1). The low density of the oasis made it an appropriate mounting material because it could easily be distinguished from the subject of interest. The density ( $2.15 \text{ g/cm}^3$ ) of the polymeric disc was used as a reference standard for relative density determinations; therefore the plastic was scanned in the field-of-view (FOV).

**Table 4.1.** Summary of the scanning parameters used for image acquisition

Units	Parameter
Voltage (kV)	60
Current ( $\mu\text{A}$ )	240
Magnification	16.67
Pixel size in the X- and Y axes (mm)	0.200
Field-of-view (FOV) (mm)	700
Number of pixels in the X- and Y axes	2024
Resolution/ voxel size ( $\mu\text{m}$ )	12
Spot size ( $\mu\text{m}$ )	5
Scan time (s)	1500
Original image greyscale intensity resolution	16-bit
Grey levels	$2^{16} = 65536$
Number of 2D images	1500
Image acquisition time (ms)	500
Rotation sector ( $^\circ$ )	360

#### *Image processing and analysis*

The 2D image slices, covering the entire sample were attained using a fully automated data acquisition system and saved onto a processing workstation, operated by system-supplied Datos reconstruction software (Datos|x® 2.1, General Electric Sensing & Inspection Technologies GmbH, Phoenix, Wunstorf, Germany). Angular projections generated 2D X-ray images which were reconstructed to create 3D volumes of the external and internal geometries of the sample (see

Appendix A). Reconstruction involved filtered back-projection algorithms. The final product from reconstruction is a raw 3D volume file which was imported directly into the image visualisation and analysis software, Volume Graphics VGStudio Max 2.2 software (Volume Graphics, Heidelberg, Germany).

### Segmentation and defining regions-of-interest (ROIs)

Wheat kernel images were segmented into different ROIs: whole kernel, kernel material (which constitutes the solid phase) and air voids (which forms part of the gaseous phase). ROIs were subjected to the Volume analyser function (VGStudio Max 2.2) to calculate microstructural parameters. A representative slice from the kernels was selected from the dataset to obtain an average grey value for the solid and air components in the kernel. Once a segmented volume has been defined, quantitative measurements were performed.

### Quantitative measurements

Quantitative measurements included volumes-of-interest (VOIs), porosity, expansion ratio (ER) and relative density. In addition, kernel dimensions (length, width and depth) were measured, also using VGStudio Max 2.2 software.

#### i. Volumes-of-interest (VOIs)

VOIs were measured using the Volume analyser tool which automatically calculates the specific volume of the selected ROIs. By creating different VOIs, volume measurements of specific areas (e.g. air) in the sample or the sample as a whole can be determined.

#### ii. Porosity (percentage air volume)

It is the ratio of the intergranular air space to the total space occupied by the kernel (Kheiralipour *et al.*, 2008). Porosity analysis was performed by thresholding the voids and creating and extracting this ROI and calculating the total air volume against the total sample volume (Du Plessis *et al.*, 2014). It should be noted that for this study the porosity were considered as the total air in the sample, thus the entirety of cavities and pores.

$$Porosity (\%) = \frac{Volume\ of\ air\ (mm^3)}{Total\ volume\ (mm^3)} \times 100\% \quad (1)$$

#### iii. Expansion ratio (ER)

$$ER = \frac{Volume\ after\ roasting\ (mm^3)}{Volume\ before\ roasting\ (mm^3)} \quad (2)$$

#### iv. Relative density

In this study relative densities were determined using mean grey values (arbitrary units) which correlate to the X-ray attenuation. Each voxel has a grey value which relies on the

material density. Higher grey values, corresponds with higher attenuation coefficients and thus higher densities (Landis *et al.*, 2003). The grey value histogram provides a diagram of the number and intensity of voxels in the whole image or specific ROI, illustrating the density distribution based on grey values (Landis & Keane, 2010). The y-axis display the number of voxels associated with each grey value, whereas the x-axis indicates the grey values and thus the intensity of the voxels in an image. Relative density was measured in terms of the mean grey value of the ROI in relation to the mean grey value of the reference standard. It was then multiplied with the known density of the reference standard ( $2.15 \text{ g/cm}^3$ ). For each ROI the mean grey value was measured using the Volume analyser tool. The mean grey value of the polymeric disc was attained by selecting a representative area using the Adaptive rectangle tool. The mean grey value of the homogenous polymer disc is thus a measure of its density.

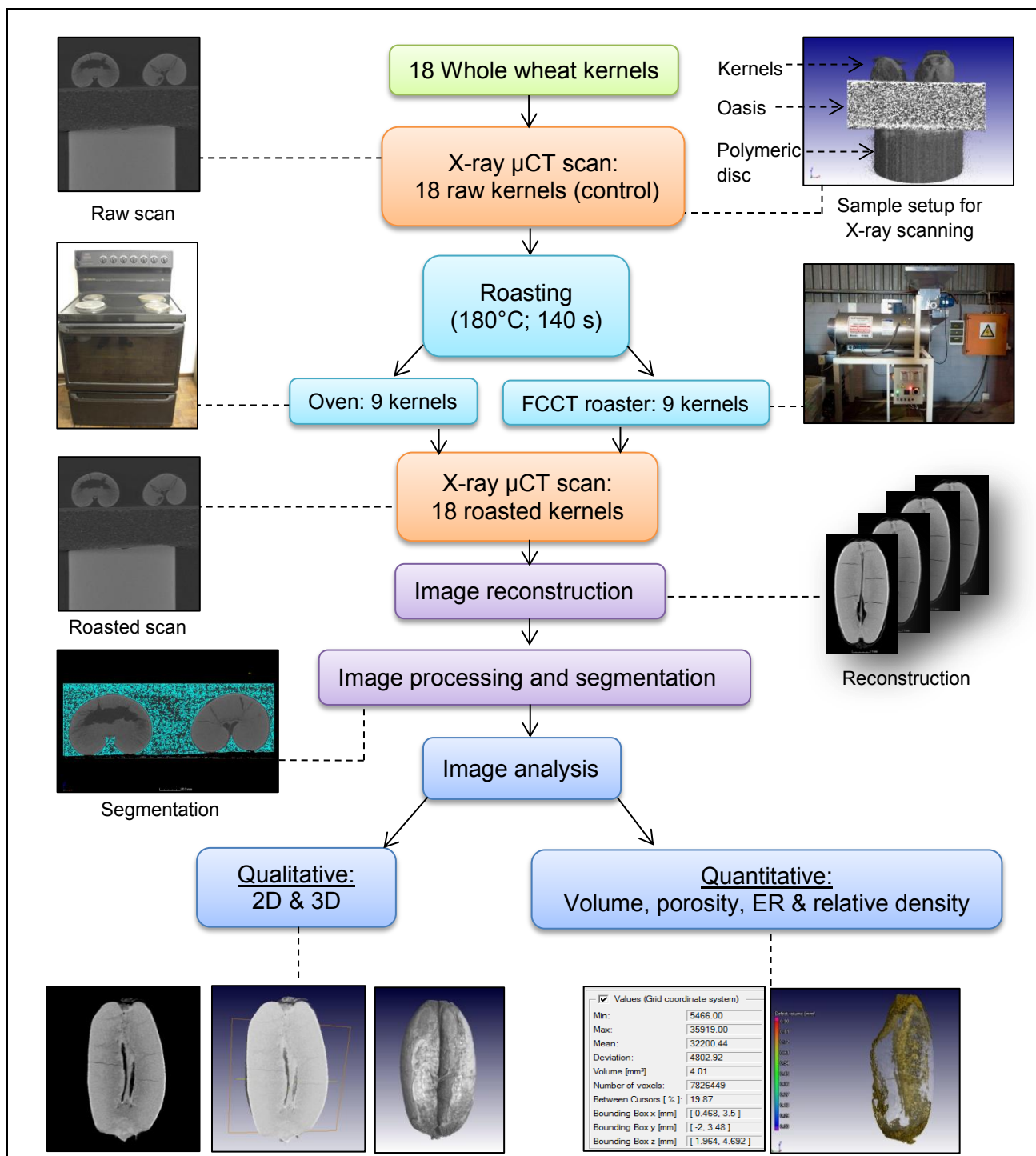
$$\text{Relative density (g/cm}^3\text{)} = \frac{\text{mean greyvalue of ROI}}{\text{mean greyvalue of reference standard}} \times 2.15 \text{ g/cm}^3 \quad (3)$$

#### *Experimental design*

Figure 4.1 details the experimental design for determining the effect of roasting on the microstructure of whole wheat kernels in a non-destructive manner by means of a flow diagram.

#### *Statistical analysis*

One-way analysis of variance (ANOVA) was performed to compare averages for the respective quantitative measurements with respect to the two roasting methods. Data was reported as the mean ( $n=9$ )  $\pm$  standard deviation. Data analyses were performed using STATISTICA version 13 (StatSoft, Inc., Tulsa, USA). The level of confidence required for significance was selected at  $P \leq 0.05$ .



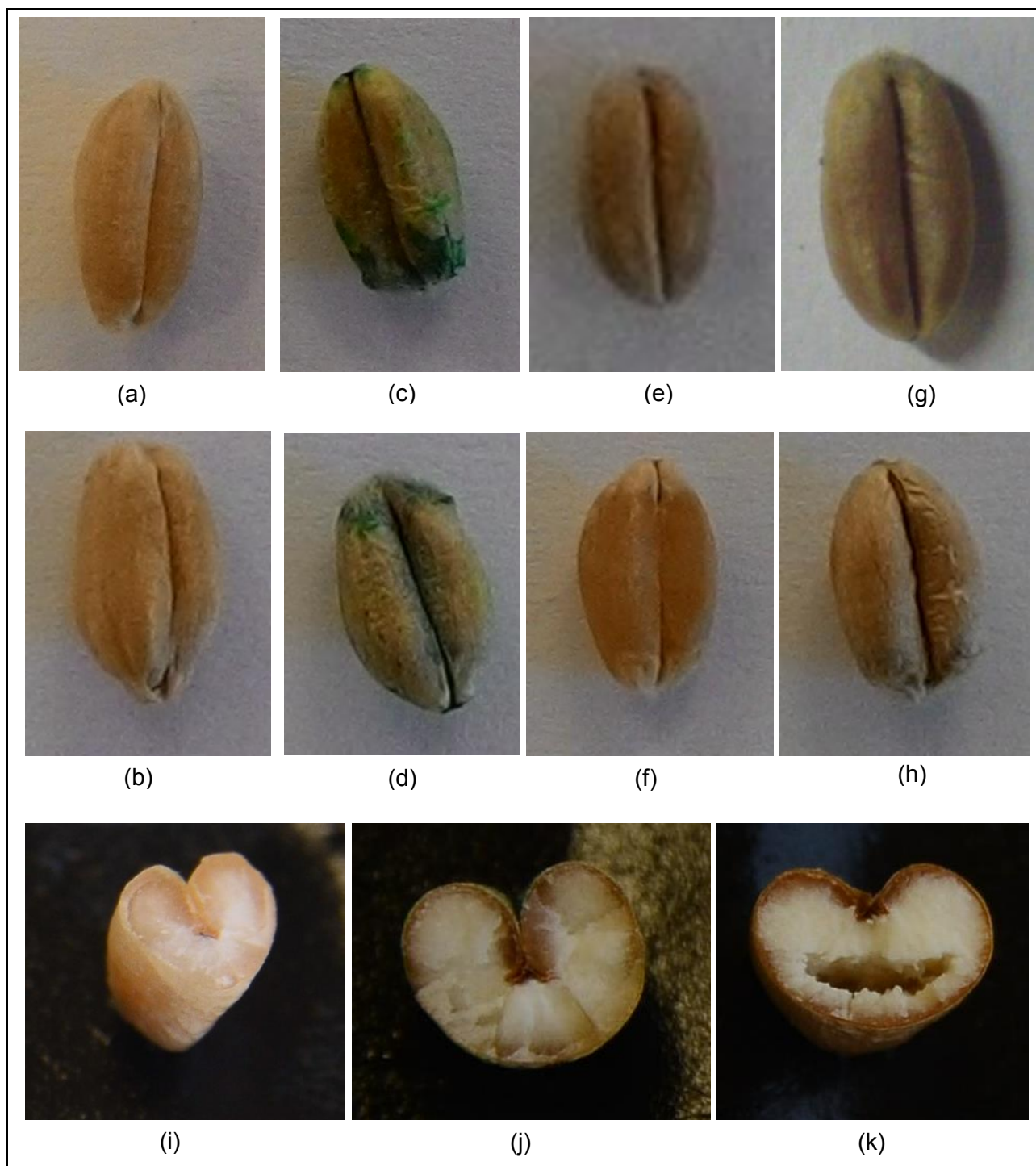
**Figure 4.1.** Flow diagram of experimental design for determining the effect of oven and FCCT roasting on the microstructure of whole wheat kernels using X-ray  $\mu$ CT and image analysis.

## Results and discussion

### Visual assessment

The wheat kernels partially retained a brown/yellowish pigmentation due to the carotenoid content, despite the roasting method (Fig. 4.2). Roasting led to swollen grains with a widened crease, especially during oven roasting. Wheat with a more open crease require less force during milling than those with a closed crease (Evers & Millar, 2002). Furthermore, a more bulged appearance

was observed in the oven-roasted samples, whereas the FCCT-roasted kernels remained more uniform in shape. The bran outer layer, which surrounds the germ and endosperm, remained intact.



**Figure 4.2.** Digital (Canon SX40 digital camera, Canon, Ohtaku, Tokyo, Japan) images of the same wheat kernels before and after roasting with (a) and (b) raw, (c) and (d) FCCT-roasted, (e) and (f) raw, and (g) and (h) oven-roasted. The cross-sectional digital images of (i) raw, (j) FCCT-roasted and (k) oven-roasted kernels reveals the internal structure.

The digital images in Fig. 4.2 depict the cross-sectional views of raw, FCCT and oven-roasted wheat kernels. Since similar results were obtained, images of only one of the kernels for each



roasting method are shown. The raw kernel had no visible internal cracks, whereas the FCCT-roasted kernel revealed thin cracks. In the oven-roasted kernel a large irregular internal void developed in the dorsal (non-crease) region. The appearance of the oven-roasted sample was similar to the internal structure obtained after roasting with a direct gas-fired pilot plant toaster (Lazar *et al.*, 1974). The development of large internal voids resulted in a reduced toasted quality. The large cavity scatters the light reflected from the endosperm (Dobraszczyk *et al.*, 2002) causing the oven-roasted wheat kernel to have a mealy and opaque appearance. Opaqueness is usually correlated with softness in wheat kernels since the air spaces leads to a decreased density (Almeida-Dominguez *et al.*, 1997). The raw kernel appeared more translucent and the oven-roasted kernel was more opaque, whilst the FCCT-roasted sample maintained a degree of translucency. The endosperm of the raw sample appeared white, while those of the FCCT and oven-roasted samples were greyish brown and yellowish white, respectively. Oven roasting resulted in a much darker, yellow-brown, external colour, while the FCCT-roasted sample retained a light brownish colour. This indicated the more intense degree of roasting using the oven roasting method, under similar conditions.

#### *Qualitative image analysis*

Qualitative analysis (also see Appendix B) enables visualisation of the internal structure of the raw, FCCT and oven-roasted wheat kernels. A representation of the grey level 2D cross-sectional images, virtually cut in the middle for the three orthogonal views, i.e. frontal, horizontal and sagittal, is presented for the kernels before and after roasting in Fig. 4.3. Images of only one of the kernels for each roasting method are shown, since similar qualitative results were obtained.

#### Porosity, internal cracks and cavities (2D analysis)

The qualitative results illustrated considerable structural changes during roasting, especially in the oven-roasted kernels (Fig. 4.3). The raw samples were compact (dense) with few thin cracks and small cavities detectable. FCCT-roasted kernels contained slightly more and wider cracks, whereas the oven-roasted kernels had large cavities in the endosperm tissue especially near the centre of the kernel. These adverse changes resulted in the endosperm becoming completely unstructured. The endosperm is especially a crack sensitive region (Dobraszczyk *et al.*, 2002). Small voids in the raw kernels are planes of weakness, which leads to the concentration of stresses, in this case internal pressure, and acts as sites where cracks or cavities initiate (Dobraszczyk *et al.*, 2002). In the crease region, the wheat endosperm adheres peripherally to adjacent tissue, where a void (known as the endosperm cavity) exists (Evers & Millar, 2002). This endosperm cavity in the raw kernel can clearly be observed in the frontal views.

For both roasting methods, the bran remained intact, in spite of internal cracks (FCCT-roasted) and cavities (oven-roasted) formed in the endosperm. From the images, the aleurone layer appeared to be the densest constituent being the brightest region.

The germ remained intact as the cracks did not propagate into this region. From the sagittal orientation (Fig. 4.3), fissures can be observed as vertical lines in the oven-roasted endosperm. From this view, expansion of the roasted kernels is clear with oven roasting revealing much greater expansion compared to FCCT roasting. FCCT roasting had a less invasive impact on the internal structure in comparison to oven roasting which led to larger fissures.

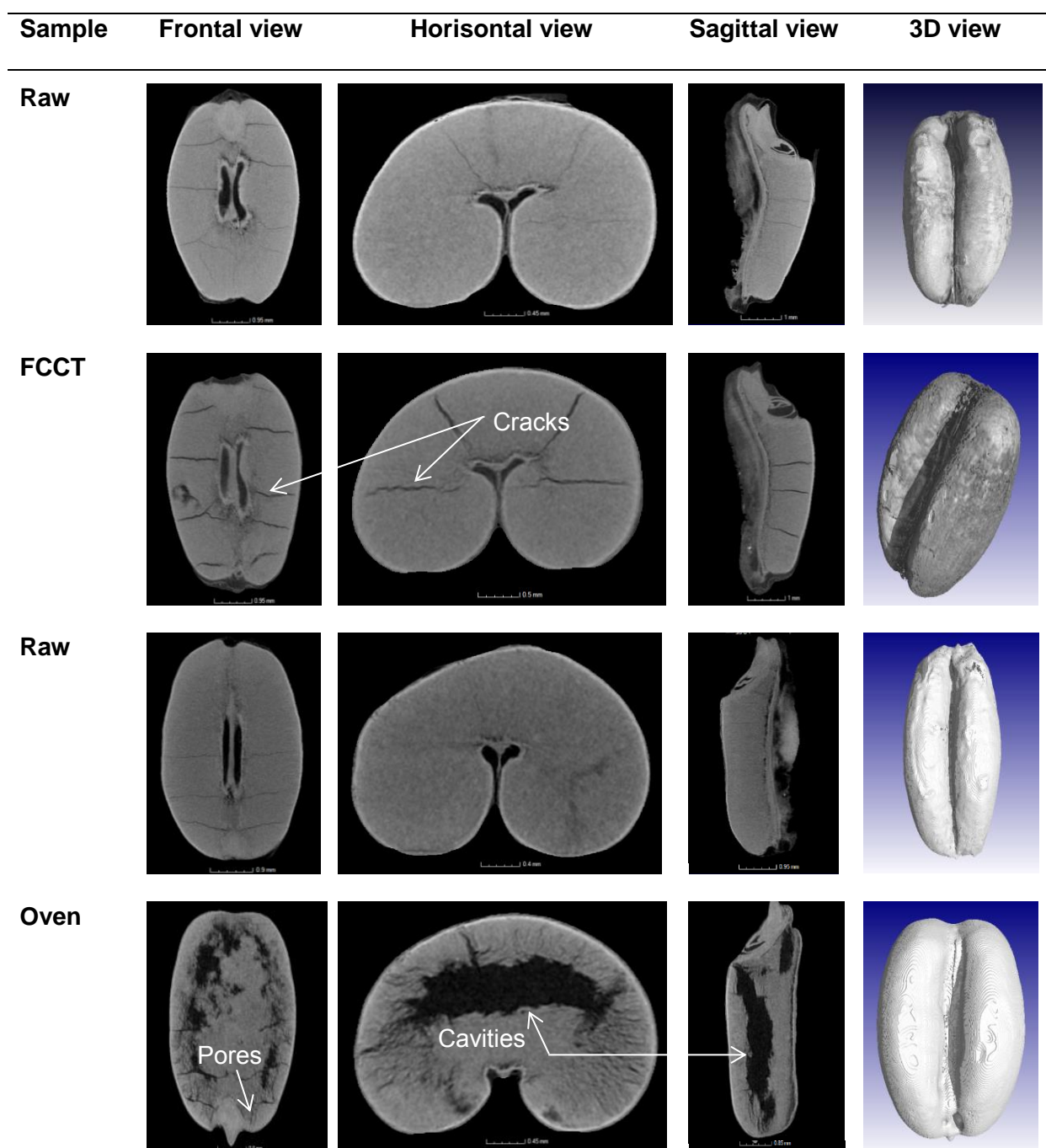
During roasting air is incorporated into the structure due to physical and chemical changes taking place (Köksel *et al.*, 1998). Internal moisture is transformed into the vapour state and the dense structure of the wheat kernel leads to an increase in vapour pressure resulting in the generation of steam and consequently expansion in structure. In the oven-roasted kernels sufficient pressure was generated to create large cavities in the cellular matrix. An inherent problem associated with oven roasting is non-uniform heating due to the uneven distribution of heat, in comparison to FCCT roasting where more uniform roasting is achieved.

The different modes of heat transfer in the roasting methods could be considered as the main factor responsible for the structural differences between the samples, since the roasting conditions (time and temperature) were similar. Continuous movement of the kernels in the rotating cylinder of the roasting drum of the FCCT roaster resulted in more uniform heat transfer. In contrast, during oven roasting the kernels were stationary and only the dry air was moving. FCCT roasting can be controlled by means of the rotating speed of the cylinder; a higher speed results in a faster roasting time. The internal steam generated inside the roaster together with the rotating movement of the cylinder lead to a more homogenous roasting process, where the superheated steam generated forms part of the heat transfer medium and is more evenly dispersed around the sample.

Figure 4.4 illustrates the three orthogonal views of the porosity in raw and roasted samples with the voids as ROI. Porosity describes the overall open structure of a desiccated material, where it comprises the fraction of empty volume. Raw wheat kernels displayed a dense internal structure with low porosity and more homogeneous distribution of the grey values (Fig. 4.4). The few small pores or cracks could be attributed to the drying process after harvesting. In the oven-roasted kernels fissures extended to close to the bran, however the outer layer remained intact, supporting the pores and large cavities. The large irregular distributed and partially interconnected cavities and cracks form a porous structure. The internal structure of the FCCT-roasted wheat kernels were characterised by multiple thin cracks.

Oven roasting had a more detrimental effect on porosity being the more severe roasting method due to more direct heat penetration. This is in agreement with a wheat study where SEM images indicated that hot air roasted wheat has a greater porosity resulting in a reduced energy requirement for grinding (Murthy *et al.*, 2008).

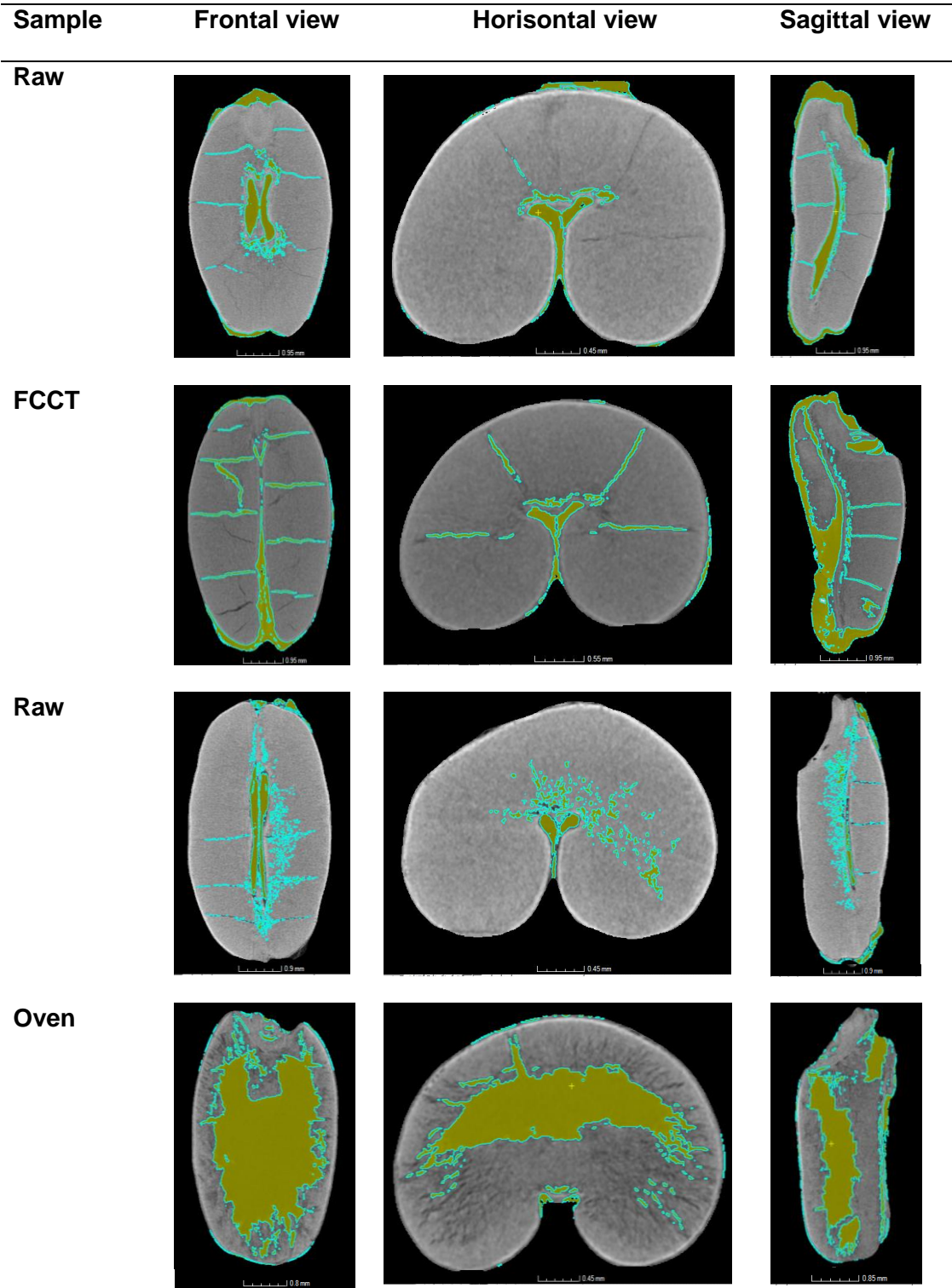




**Figure 4.3.** Grey scale 2D tomographic images of the different views (frontal, horisontal and sagittal) of whole wheat kernels before and after FCCT and oven roasting (average dimensions: length= $6.02 \pm 0.38$  mm; width= $3.32 \pm 0.27$  mm; depth= $3.22 \pm 0.32$  mm).

Cavities are like excavated cells, which are structured in a skeleton made by partial thermally degraded structures and the complete loss of the cell walls in some points. During roasting it can be assumed that smaller pores and cracks (FCCT-roasted) were formed due to the internal pressure created, and then ultimately the coalescence of these pores led to the development of larger asymmetric voids that resembles interconnected cavities (oven-roasted) (Pittia *et al.*, 2011). These cavities are generated by a flash of superheated steam, which partially damages the structure (Sumithra & Bhattacharya, 2008). Cracks propagated from the centre outwards, with the

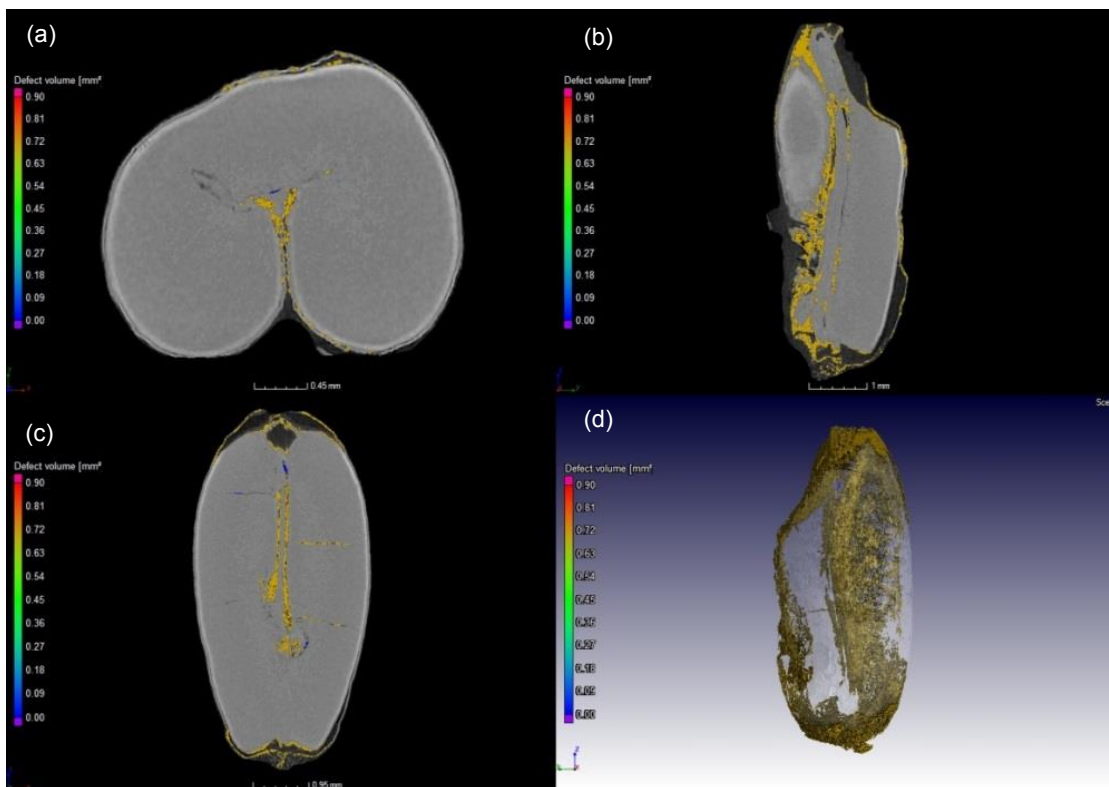
largest areas of porosity towards the centre of the kernel, especially in the oven-roasted samples. This confirms that the thermal centre is localised in the centre of the wheat kernel (Andrejko *et al.*, 2011).



**Figure 4.4.** 2D slice images (centre slice) of the spatial distribution of the porous network in wheat kernels before and after roasting, with the voids (total air) selected as ROI. The air filled pores and cavities are displayed in yellow and outlined with blue, while the kernel matrix is grey (average dimensions: length=6.02±0.38 mm; width=3.32±0.27 mm; depth=3.22±0.32 mm).

### Porosity, internal cracks and cavities (3D analysis)

Determining defects such as voids and cracks in a sample would typically require destructive testing. Volume rendering in 3D is required to understand the overall structure of samples and to visualise the internal microstructure (Suresh & Neethirajan, 2015). X-ray  $\mu$ CT scanning enables the detection of internal features and flaws by displaying this information in 3D without destroying the sample. In Fig. 4.5 the 2D images (a-c) and a 3D volume rendering (d), illustrates the internal porosity in a raw wheat kernel. The degree of porosity can be incorrectly interpreted from the 2D images as disconnected cavities. In the 3D volume rendering the path of the fissures or cracks are illustrated as tortuous and it contains multiple branching which creates an interconnected porous network throughout the kernel.



**Figure 4.5.** 2D images (a-c) [(a) horizontal, (b) sagittal and (c) frontal views] and 3D volume rendering (d) of the porosity in a raw wheat kernel. In the 3D volume the visualisation of the porosity volume size distribution is characterised in yellow and the kernel structure (material) is represented as transparent (kernel dimensions: length=5.46 mm; width=2.59 mm; depth=2.70 mm).

### *Quantitative analysis*

Quantitative information on the internal structure can be obtained as volume, porosity and relative density whereas the geometry can be quantified in terms of size, shape, orientation and position. For quantitative density and volume measurements it is assumed that wheat kernels are a two-phase system with a solid phase (kernel structure) and a gas phase (voids).

Volumes-of-interest (VOIs)

Whole kernel and air volumes increased during roasting (Table 4.2). The increase in whole kernel volume (1.57%) was not significant ( $P>0.05$ ) during FCCT roasting in comparison to a significant ( $P\leq 0.05$ ) increase of 4.47% during oven roasting. Both roasting methods resulted in a significant ( $P\leq 0.05$ ) increase in air volume. The larger increase in whole kernel volume was due to the larger increase in air volume during oven roasting (103.38%). The increase in air volume was much lower for the FCCT-roasted samples (38.86%). The increase in whole kernel volume for both methods were lower than in a previous study where wheat roasted in a steel pan led to a 8.30% increase in kernel volume (Işikli *et al.*, 2014). The increase in volume is due to the release of water, CO<sub>2</sub> and volatile organic compounds from the kernel to the gas phase (Dutra *et al.*, 2001).

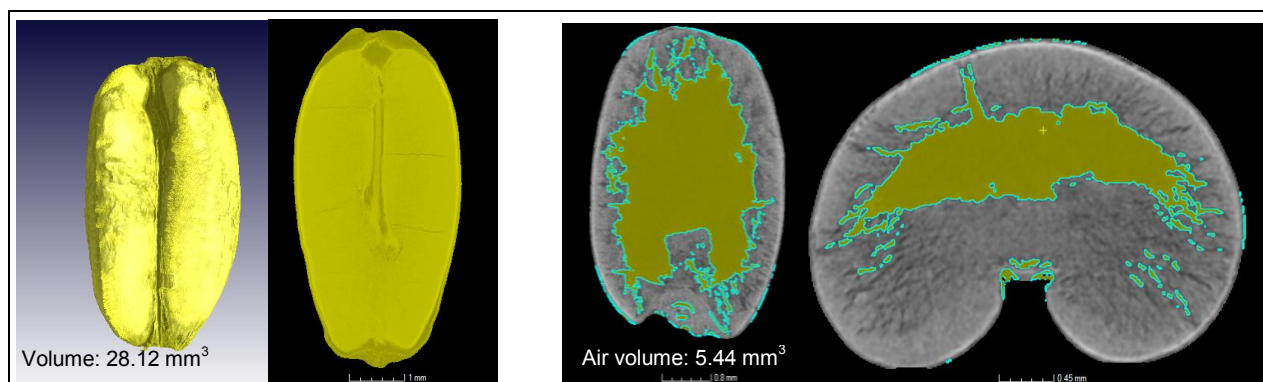
Thermal treatment of whole wheat kernels is typically associated with an increase in volume and a negative change in density (Bayram *et al.*, 2004), with the large fissures contributing significantly to the increased volume of the expanded kernel (Pardeshi & Chattopadhyay, 2010). Figure 4.6 displays the wheat kernel ROIs (whole kernel and air) to obtain the whole kernel and air volumes, respectively in a raw and oven-roasted sample.

**Table 4.2.** Mean and percentage increase/decrease in microstructural parameters of wheat kernels before and after roasting

Parameter	FCCT			Oven		
	Raw (n=9)	Roasted (n=9)	% Increase/Decrease	Raw (n=9)	Roasted (n=9)	% Increase/Decrease
<b>Whole kernel VOI (mm<sup>3</sup>)</b>	29.24±3.04 <sup>ab</sup>	29.70±3.12 <sup>ab</sup>	1.57	28.40±6.03 <sup>b</sup>	29.67±5.66 <sup>a</sup>	4.47
<b>Air VOI (mm<sup>3</sup>)</b>	1.75±0.41 <sup>b</sup>	2.43±0.58 <sup>a</sup>	38.86	1.48±0.55 <sup>b</sup>	3.01±1.27 <sup>a</sup>	103.38
<b>Porosity (%)</b>	6.04±1.54 <sup>cb</sup>	8.29±2.29 <sup>ab</sup>	2.25	5.28±1.57 <sup>c</sup>	10.33±4.63 <sup>a</sup>	5.05
<b>Expansion ratio (ER)</b>	1.02±0.01 <sup>a</sup>		-	1.05±0.06 <sup>b</sup>		-
<b>Whole kernel relative density (g/cm<sup>3</sup>)</b>	1.81±0.03 <sup>a</sup>	1.80±0.03 <sup>ab</sup>	-0.55	1.81±0.04 <sup>a</sup>	1.76±0.07 <sup>b</sup>	-2.76
<b>Material relative density (g/cm<sup>3</sup>)</b>	1.84±0.03 <sup>a</sup>	1.84±0.04 <sup>a</sup>	0	1.84±0.04 <sup>a</sup>	1.79±0.06 <sup>b</sup>	-2.72
<b>Weight loss (%)</b>	3.50±3.68 <sup>a</sup>		-	6.04±4.42 <sup>a</sup>		-

Values are means ± standard deviation, of nine replicates. Different letters in the same row indicate significant differences ( $P\leq 0.05$ ).





**Figure 4.6.** Illustration of the use of the Volume analyser tool on a (a) raw sample where the whole kernel was selected as VOI (28.12 mm<sup>3</sup>) and (b) oven-roasted sample where the air (yellow) was selected as VOI (5.44 mm<sup>3</sup>) (kernel dimensions: length=6.24 mm; width=3.56 mm; depth=3.27 mm).

### Porosity analysis

Voids are inherent to wheat kernels and other cereal grains because of the porous nature of the endosperm (Chang, 1988). Thus, an increase in the existing porosity and development of additional voids were expected due to roasting. Understanding the contribution of air to the total wheat kernel is relevant because it affects the yield, which is a highly desirable property for the milling industry.

Porosity did not change significantly ( $P > 0.05$ ) during FCCT roasting, however increased significantly ( $P \leq 0.05$ ) during oven roasting. The porosity in the FCCT-roasted samples was  $6.04 \pm 1.54\%$  and  $8.29 \pm 2.29\%$  for the raw and roasted kernels respectively, resulting in a much lower increase (2.25%) than in the oven-roasted (5.05%) samples which ranged from  $5.28 \pm 1.57\%$  to  $10.33 \pm 4.63\%$ . FCCT roasting will result in a better quality roasted product in terms of endosperm texture (too soft kernels are undesirable). The increased porosity during oven roasting can be ascribed to a bigger puffing effect occurring due to the higher internal vapour pressure generated. The greater porosity was consistent with the larger distributed internal network of cavities observed during qualitative analysis.

### Expansion ratio (ER)

The ER is also known as the puffing index (PI) (Lazar *et al.*, 1974). Larger ERs implies a larger difference in kernel volume before and after roasting. Greater air volumes correspond to greater ERs in cereal products (Jones *et al.*, 2000; Sumithra & Bhattacharya, 2008). The oven-roasted kernels had the highest ER ( $1.05 \pm 0.06$ ) and porosity ( $10.33 \pm 4.63\%$ ), compared to the FCCT-roasted samples (ER =  $1.02 \pm 0.01$ ; porosity =  $8.29 \pm 2.29\%$ ) under similar roasting conditions (Table 4.2).

In infrared treated wheat (100-180 °C; 30-150 s) a negative relationship occurred between ER and density (Andrejko *et al.*, 2011). This trend was also observed during oven roasting, where

higher expansion was correlated to a higher relative density decrease (2.76%), while the FCCT-roasted kernels had a lower ER and a lower density decrease (0.55%).

A PI (using a gas fired hot air toaster) of 1.3 was obtained for wheat kernels (15% moisture content) roasted at 204°C for 17 s, whereas 40 s resulted in a PI of 1.5 (Lazar *et al.*, 1974). The differences in ER values obtained can be attributed to the different roasting methods and conditions, and also to the moisture content. In the present study lower ERs were obtained due to the lower moisture content since no tempering was performed before roasting. Although roasting was conducted at a low moisture content, the combination of high temperature for a short duration will rapidly release steam resulting in an expanded structure (Sumithra & Bhattacharya, 2008). When the moisture content is too low, insufficient superheated vapour is generated, resulting in even lower ERs (Lee *et al.*, 2000). This is, however, also dependent on the roasting method and conditions. The pericarp may also limit the degree of expansion (Mariotti *et al.*, 2006).

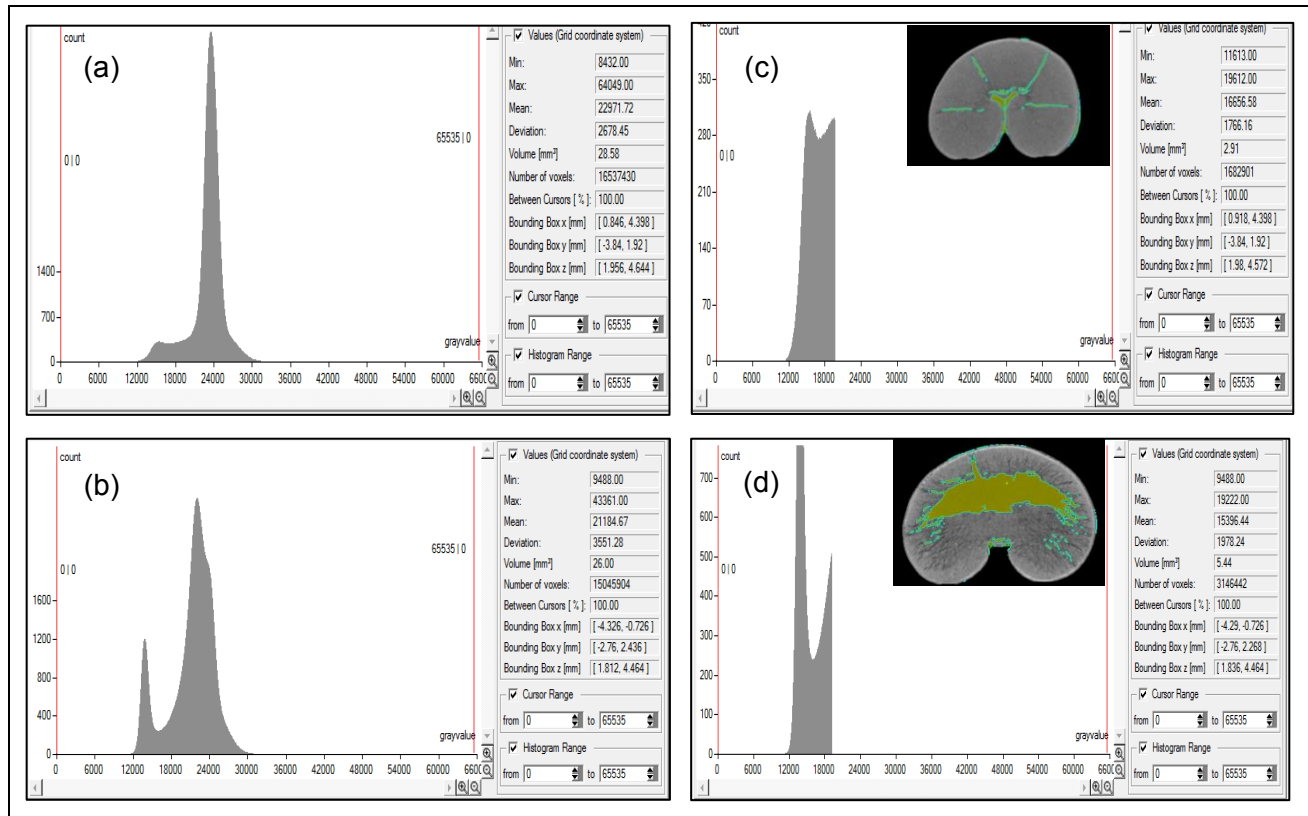
### Density analysis

Density determinations usually performed in industry include hectolitre mass, which provides limited information since only the average apparent density of the bulk is measured and it is influenced by the degree of packing and the shape and size of the crease (Dobraszczyk *et al.*, 2002). Wheat density can also be measured using a pycnometer (Chang, 1988; Ohm *et al.*, 1998; Nelson, 2015). Chang (1988) documented the mean true density of wheat to be 1.47 g/cm<sup>3</sup> and the mean apparent (inclusion of air) density as 1.39 g/cm<sup>3</sup>. As some intercellular spaces are inaccessible to the gas or mercury, the volume determined using a pycnometer may include these air spaces and thus the density determined might not be the true density (Chang, 1988). Kelkar *et al.* (2015) developed a method, using both X-ray digital radiography and computed tomography (CT) to directly determine the apparent density of foods. X-ray CT gave results comparable with conventional methods.

Figure 4.7 demonstrates the grey value histograms for FCCT and oven-roasted wheat kernels. Two histograms are displayed for each roasting method (Fig 4.7): whole kernel and the air as ROI. A histogram with a wide distribution (Fig. 4.7a) indicates more contrast in the image, whereas a narrow distribution (Fig. 4.7c) correlates with less contrast (Umbaugh, 2011). If grey values are concentrated at the lower end of the graph (Fig. 4.7d), the image appears darker and vice versa. The whole kernel grey value histogram illustrate different peaks (corresponding to different phases), recognising that lower grey values correspond to internal air and higher values correspond to the kernel structure.

The mean grey values for the FCCT and oven-roasted samples were 22971.72 and 21184.67 respectively (Fig. 4.7a and b). The mean grey value intensity is a measure of brightness and density, where roasting resulted in lower mean grey values relating to lower densities of the roasted kernels. In the histograms the grey value range was smaller for the oven-roasted (9488-43361) sample than for the FCCT-roasted (8432-64049). The histogram of the oven-roasted kernel

had more distinct peaks, indicating the increase in porosity due to the increase in the lower grey value peak (Fig. 4.7b). This large distribution of low grey values was also observed in the histogram where the air was selected as ROI (Fig. 4.7d) and is associated with more voids. Changes in the grey values associate with changes in the microstructure as observed during qualitative analysis.



**Figure 4.7.** Histograms illustrating the grey value distribution in images of whole (a) FCCT-roasted and (b) oven-roasted kernels and the air selected as ROI in (c) FCCT-roasted and (d) oven-roasted kernels. The top three values in the tables indicate the minimum, maximum and mean grey values, respectively.

Whole kernel density is the density of the kernel including air voids and thus it is a function of the air volume proportion (Vadivambal & Jayas, 2007), whereas the material density reports the density of the kernel material per se, excluding all the air, and is thus more representative of the true density. Whole kernel density decreased with 0.55% ( $P>0.05$ ) and 2.76% ( $P\leq 0.05$ ) during FCCT and oven roasting, respectively (Table 4.2). In contrast, the material density remained unaffected during FCCT roasting while a significant ( $P\leq 0.05$ ) decrease of 2.72% occurred during oven roasting. The significantly larger decrease in whole kernel density during oven roasting was due to the higher porosity that developed using this method. These results were in agreement with previous studies that suggested lower densities were due to higher porosities, expansion (volume increase) and as a result of moisture loss (Fang & Campbell, 2000; Jha, 2005; Al-Mahasneh & Rababah, 2007). Whole kernel densities were lower than material densities because it included the contribution of air which lowered the density. The weight loss for the oven-roasted samples was



much higher with an average of  $6.04 \pm 4.42\%$ , whereas FCCT roasting contributed to a loss of  $3.50 \pm 3.68\%$  (Table 4.2).

Murthy *et al.* (2008) investigated the impact of fluidised bed roasting (FBR) ( $280\text{--}350^\circ\text{C}$  for 30–120 s), using hot flue gas as fluidising medium and traditional pan roasting ( $300^\circ\text{C}$  for 15–100 s), using sand as heat transfer method on the quality of wheat kernels. Roasting was correlated with a decrease in wheat density. FBR demonstrated to be a superior roasting method in terms of product quality, since these samples indicated a better heat transfer and more uniform texture than sand roasted kernels. A previous study on grain roasting (both sand and microwave) indicated that decreased bulk densities were due to a loss in structural integrity between starch-protein and starch-starch matrices and this was attributed to the formation of air spaces in the endosperm (Sharma & Gujral, 2011). The higher puffing effect that occurred during oven roasting resulted in larger air volumes (porosity) and lower relative densities in comparison to FCCT roasting. Decreased densities was an indication of pore formation due to volumetric expansion (Kahyaoglu *et al.*, 2010). This study confirmed the negative relationship between porosity and density.

## Conclusion

It was possible to successfully illustrate distinct changes and differences in the microstructure of wheat kernels induced by the two roasting methods from the 2D projection images, which could be rendered into 3D volumes to perform quantitative analysis. The degree of cracking and cavities in the wheat kernels provided an indication of the complexity and interconnectedness of the porous network. Cavities were much larger in the oven-roasted samples resulting in more open porous and expanded structure in relation to FCCT roasting, which had a less destructive impact. The qualitative results observed in the 2D images were confirmed with quantitative measurements. Roasting resulted in an increase in volume, porosity and ER and a decrease in relative density. These measurements were higher during oven roasting. Oven roasting, in a static position, resulted in unevenly roasted kernels, thus the advantage of FCCT roasting is that the product continuously rotating in the superheated steam and the kernel surface is exposed uniformly. Therefore FCCT roasting is preferable in terms of minimal structural alteration caused during roasting, resulting in a more acceptable internal structure. The material density also remained constant during FCCT roasting which will lead to less affected milling yields.

X-ray  $\mu\text{CT}$  is increasingly being used as a research tool to study the microstructure of agricultural produce since it enables non-destructive capturing of high-resolution images, permitting fine details to be studied. This technique has been demonstrated to be a powerful tool to investigate and characterise the microstructure of roasted wheat.

## References

- Agbisit, R., Alavi, S., Cheng, E., Herald, T. & Trater, A. (2007). Relationships between microstructure and mechanical properties of cellular cornstarch extrudates. *Journal of Texture Studies*, **38**, 199-219.
- Aguilera, J.M. (2005). Why food microstructure? *Journal of Food Engineering*, **67**, 3-11.
- Al-Mahasneh, M.A. & Rababah, T.M. (2007). Effect of moisture content on some physical properties of green wheat. *Journal of Food Engineering*, **79**, 1467-1473.
- Almeida-Dominguez, H.D., Suhendro, E.L. & Rooney, L.W. (1997). Factors affecting Rapid Visco Analyser curves for the determination of maize kernel hardness. *Journal of Cereal Science*, **25**, 93-102.
- Andrejko, D., Grochowicz, J., Goździewska, M. & Kobus, Z. (2011). Influence of infrared treatment on mechanical strength and structure of wheat grains. *Food and Bioprocess Technology*, **4**, 1367-1375.
- Baiano, A., Fares, C., Peri, G., Romaniello, R., Taurino, A.M., Siciliano, P., Gambacorta, G., Lamacchia, C., Pati, S. & Notte, E.L. (2008). Use of a toasted durum whole meal in the production of a traditional Italian pasta: chemical, mechanical, sensory and image analyses. *International Journal of Food Science & Technology*, **43**, 1610-1618.
- Bayram, M., Öner, M.D. & Eren, S. (2004). Effect of cooking time and temperature on the dimensions and crease of the wheat kernel during bulgur production. *Journal of Food Engineering*, **64**, 43-51.
- Bellido, G.G., Scanlon, M.G., Page, J.H. & Hallgrimsson, B. (2006). The bubble size distribution in wheat flour dough. *Food Research International*, **39**, 1058-1066.
- Besbes, E., Jury, V., Monteau, J.-Y. & Le Bail, A. (2013). Characterizing the cellular structure of bread crumb and crust as affected by heating rate using X-ray microtomography. *Journal of Food Engineering*, **115**, 415-423.
- Chang, C. (1988). Measuring density and porosity of grain kernels using a gas pycnometer. *Cereal Chemistry*, **65**, 13-15.
- Chevallier, S., Réguerre, A.L., Le Bail, A. & Della Valle, G. (2014). Determining the cellular structure of two cereal food foams by X-ray micro-tomography. *Food Biophysics*, **9**, 219-228.
- Demirkesen, I., Kelkar, S., Campanella, O.H., Sumnu, G., Sahin, S. & Okos, M. (2014). Characterization of structure of gluten-free breads by using X-ray microtomography. *Food Hydrocolloids*, **36**, 37-44.
- Dobraszczyk, B., Whitworth, M., Vincent, J. & Khan, A. (2002). Single kernel wheat hardness and fracture properties in relation to density and the modelling of fracture in wheat endosperm. *Journal of Cereal Science*, **35**, 245-263.
- Dogan, H. (2007). Nondestructive imaging of agricultural products using X-ray microtomography. *Microscopy and Microanalysis*, **13**, 1316-1317.

- Donis-González, I.R., Guyer, D.E., Fulbright, D.W. & Pease, A. (2014). Postharvest noninvasive assessment of fresh chestnut (*Castanea* spp.) internal decay using computer tomography images. *Postharvest Biology and Technology*, **94**, 14-25.
- Donis-González, I.R., Guyer, D.E., Chen, R. & Pease, A. (2015). Evaluation of undesirable fibrous tissue in processing carrots using Computed Tomography (CT) and structural fiber biochemistry. *Journal of Food Engineering*, **153**, 108-116.
- Du Plessis, A., Seifert, T., Booysen, G. & Els, J. (2014). Microfocus X-ray computed tomography (CT) analysis of laser sintered parts. *South African Journal of Industrial Engineering*, **25**, 39-49.
- Dutra, E., Oliveira, L., Franca, A., Ferraz, V. & Afonso, R. (2001). A preliminary study on the feasibility of using the composition of coffee roasting exhaust gas for the determination of the degree of roast. *Journal of Food Engineering*, **47**, 241-246.
- Evers, T. & Millar, S. (2002). Cereal grain structure and development: some implications for quality. *Journal of Cereal Science*, **36**, 261-284.
- Fang, C. & Campbell, G.M. (2000). Effect of measurement method and moisture content on wheat kernel density measurement. *Food and Bioproducts Processing*, **78**, 179-186.
- FAOSTAT. (2015). Food and Agriculture Organization of the United Nations. Statistics division [Internet document]. URL <http://faostat3.fao.org/download/Q/QC/E>. Accessed 07/05/2015.
- Flinn, B. (2012). New Roasting Technology! [Internet document]. URL [http://www.agriculture.com/machinery/precision-agriculture/new-roasting-technology\\_234-ar26331?print](http://www.agriculture.com/machinery/precision-agriculture/new-roasting-technology_234-ar26331?print). Accessed 24/02/2014.
- Frisullo, P., Barnabà, M., Navarini, L. & Del Nobile, M. (2012). *Coffea arabica* beans microstructural changes induced by roasting: an X-ray microtomographic investigation. *Journal of Food Engineering*, **108**, 232-237.
- Hernández, J.A., Heyd, B. & Trystram, G. (2008). Prediction of brightness and surface area kinetics during coffee roasting. *Journal of Food Engineering*, **89**, 156-163.
- Horvat, M., Guthausen, G., Tepper, P., Falco, L. & Schuchmann, H.P. (2014). Non-destructive, quantitative characterization of extruded starch-based products by magnetic resonance imaging and X-ray microtomography. *Journal of Food Engineering*, **124**, 122-127.
- Işikli, N.D., Şenol, B. & Çoksöyler, N. (2014). Some physical and mechanical properties of roasted zerun wheat. *Journal of Food Science and Technology*, **51**, 1990-1997.
- Jha, S. (2005). Mathematical simulation of roasting of grain. *Journal of Food Engineering*, **71**, 304-310.
- Jones, D., Chinnaswamy, R., Tan, Y. & Hanna, M. (2000). Physiochemical properties of ready-to-eat breakfast cereals. *Cereal Foods World*, **45**, 164-168.
- Kahyaoglu, L.N., Sahin, S. & Sumnu, G. (2010). Physical properties of parboiled wheat and bulgur produced using spouted bed and microwave assisted spouted bed drying. *Journal of Food Engineering*, **98**, 159-169.

- Kayitesi, E., Duodu, K.G., Minnaar, A. & De Kock, H.L. (2010). Sensory quality of marama/sorghum composite porridges. *Journal of the Science of Food and Agriculture*, **90**, 2124-2132.
- Kelkar, S., Boushey, C.J. & Okos, M. (2015). A method to determine the density of foods using X-ray imaging. *Journal of Food Engineering*, **159**, 36-41.
- Ketcham, R.A. & Carlson, W.D. (2001). Acquisition, optimization and interpretation of X-ray computed tomographic imagery: applications to the geosciences. *Computers & Geosciences*, **27**, 381-400.
- Kheiralipour, K., Karimi, M., Tabatabaeefar, A., Naderi, M., Khoubakht, G. & Heidarbeigi, K. (2008). Moisture-depend physical properties of wheat (*Triticum aestivum* L.). *Journal of Agricultural Technology*, **53**, 53-64.
- Köksel, H., Sivri, D., Scanlon, M. & Bushuk, W. (1998). Comparison of physical properties of raw and roasted chickpeas (leblebi). *Food Research International*, **31**, 659-665.
- Lamacchia, C., Baiano, A., Lamparelli, S., Notte, E.L. & Luccia, A.D. (2010). Changes in durum wheat kernel and pasta proteins induced by toasting and drying processes. *Food Chemistry*, **118**, 191-198.
- Lammertyn, J., Dresselaers, T., Van Hecke, P., Jancsó, P., Wevers, M. & Nicolai, B. (2003). MRI and X-ray CT study of spatial distribution of core breakdown in 'Conference' pears. *Magnetic Resonance Imaging*, **21**, 805-815.
- Landis, E.N. & Keane, D.T. (2010). X-ray microtomography. *Materials Characterization*, **61**, 1305-1316.
- Landis, E.N., Nagy, E.N. & Keane, D.T. (2003). Microstructure and fracture in three dimensions. *Engineering Fracture Mechanics*, **70**, 911-925.
- Lazar, M., Mossman, A. & Wallace, J. (1974). Air-fluidized toasting of whole kernel wheat-processing variables and functional properties for food applications. *Journal of Food Science*, **39**, 239-243.
- Lee, E.Y., Lim, K.I., Lim, J.K. & Lim, S.T. (2000). Effects of gelatinization and moisture content of extruded starch pellets on morphology and physical properties of microwave-expanded products. *Cereal Chemistry*, **77**, 769-773.
- Léonard, A., Blacher, S., Nimmol, C. & Devahastin, S. (2008). Effect of far-infrared radiation assisted drying on microstructure of banana slices: an illustrative use of X-ray microtomography in microstructural evaluation of a food product. *Journal of Food Engineering*, **85**, 154-162.
- Licciardello, F., Frisullo, P., Laverse, J., Muratore, G. & Del Nobile, M.A. (2012). Effect of sugar, citric acid and egg white type on the microstructural and mechanical properties of meringues. *Journal of Food Engineering*, **108**, 453-462.
- Mariotti, M., Alamprese, C., Pagani, M.A. & Lucisano, M. (2006). Effect of puffing on ultrastructure and physical characteristics of cereal grains and flours. *Journal of Cereal Science*, **43**, 47-56.

- Mendoza, F., Verboven, P., Mebatsion, H.K., Kerckhofs, G., Wevers, M. & Nicolai, B. (2007). Three-dimensional pore space quantification of apple tissue using X-ray computed microtomography. *Planta*, **226**, 559-570.
- Mohorič, A., Vergeldt, F., Gerkema, E., Van Dalen, G., Van den Doel, L.R., Van Vliet, L.J., Van As, H. & Van Duynhoven, J. (2009). The effect of rice kernel microstructure on cooking behaviour: a combined  $\mu$ -CT and MRI study. *Food Chemistry*, **115**, 1491-1499.
- Moreira, R.G. (2001). Impingement drying of foods using hot air and superheated steam. *Journal of Food Engineering*, **49**, 291-295.
- Mossman, A., Rockwell, W. & Fellers, D. (1973). Hot air toasting and rolling whole wheat effect on organoleptic, physical and nutritional quality. *Journal of Food Science*, **38**, 879-884.
- Murthy, K.V., Ravi, R., Keshava Bhat, K. & Raghavarao, K.S.M.S. (2008). Studies on roasting of wheat using fluidized bed roaster. *Journal of Food Engineering*, **89**, 336-342.
- Ndungu, K.E., Emmambux, M.N. & Minnaar, A. (2012). Micronisation and hot air roasting of cowpeas as pretreatments to control the development of hard-to-cook phenomenon. *Journal of the Science of Food and Agriculture*, **92**, 1194-1200.
- Neethirajan, S., Karunakaran, C., Jayas, D. & White, N. (2006). X-ray computed tomography image analysis to explain the airflow resistance differences in grain bulks. *Biosystems Engineering*, **94**, 545-555.
- Nelson, S. (2015). Closely related physical properties data for grain and seed. In: *Dielectric Properties of Agricultural Materials and Their Applications*. Pp. 260-261. London: Academic Press.
- Nyembwe, P., Minnaar, A., Duodu, K.G. & De Kock, H.L. (2015). Sensory and physicochemical analyses of roasted marama beans [*Tylosema esculentum* (Burchell) A. Schreiber] with specific focus on compounds that may contribute to bitterness. *Food Chemistry*, **178**, 45-51.
- Ohm, J., Chung, O. & Deyoe, C. (1998). Single-kernel characteristics of hard winter wheats in relation to milling and baking quality 1. *Cereal Chemistry*, **75**, 156-161.
- Pardeshi, I. & Chattopadhyay, P. (2010). Hot air puffing kinetics for soy-fortified wheat-based ready-to-eat (RTE) snacks. *Food and Bioprocess Technology*, **3**, 415-426.
- Pittia, P., Sacchetti, G., Mancini, L., Voltolini, M., Sodini, N., Tromba, G. & Zanini, F. (2011). Evaluation of microstructural properties of coffee beans by synchrotron X-ray microtomography: a methodological approach. *Journal of Food Science*, **76**, 222-231.
- Salvo, L., Suéry, M., Marmottant, A., Limodin, N. & Bernard, D. (2010). 3D imaging in material science: application of X-ray tomography. *Comptes Rendus Physique*, **11**, 641-649.
- Sharma, P. & Gujral, H.S. (2011). Effect of sand roasting and microwave cooking on antioxidant activity of barley. *Food Research International*, **44**, 235-240.
- Sumithra, B. & Bhattacharya, S. (2008). Toasting of corn flakes: product characteristics as a function of processing conditions. *Journal of Food Engineering*, **88**, 419-428.

- Suresh, A. & Neethirajan, S. (2015). Real-time 3D visualization and quantitative analysis of internal structure of wheat kernels. *Journal of Cereal Science*, **63**, 81-87.
- Umbaugh, S.E. (2011). *Digital Image Processing and Analysis: Human and Computer Vision Applications With CVIPtools*. Pp. 456-463. Boca Raton: CRC Press.
- Vadivambal, R. & Jayas, D.S. (2007). Changes in quality of microwave-treated agricultural products—a review. *Biosystems Engineering*, **98**, 1-16.
- Van Dalen, G., Nootenboom, P. & Van Vliet, L.J. (2007). 3D imaging, analysis and modelling of porous cereal products using X-ray microtomography. *Image Analysis and Stereology*, **26**, 169-177.
- Van Dyck, T., Verboven, P., Herremans, E., Defraeye, T., Van Campenhout, L., Wevers, M., Claes, J. & Nicolaï, B. (2014). Characterisation of structural patterns in bread as evaluated by X-ray computer tomography. *Journal of Food Engineering*, **123**, 67-77.
- Verboven, P., Kerckhofs, G., Mebatsion, H.K., Ho, Q.T., Temst, K., Wevers, M., Cloetens, P. & Nicolaï, B.M. (2008). Three-dimensional gas exchange pathways in pome fruit characterized by synchrotron X-ray computed tomography. *Plant Physiology*, **147**, 518-527.
- Wang, S., Austin, P. & Bell, S. (2011). It's a maze: the pore structure of bread crumbs. *Journal of Cereal Science*, **54**, 203-210.
- Witek, M., Węglarz, W.P., De Jong, L., Van Dalen, G., Blonk, J.C.G., Heussen, P., Van Velzen, E., Van As, H. & Van Duynhoven, J. (2010). The structural and hydration properties of heat-treated rice studied at multiple length scales. *Food Chemistry*, **120**, 1031-1040.
- Zhu, L.J., Dogan, H., Gajula, H., Gu, M.H., Liu, Q.Q. & Shi, Y.C. (2012). Study of kernel structure of high-amylose and wild-type rice by X-ray microtomography and SEM. *Journal of Cereal Science*, **55**, 1-5.

**Declaration by the candidate:**

With regard to Chapter 5 (pp. 111-145), the nature and scope of my contribution were as follows:

<b>Nature of contribution</b>	<b>Extent of contribution (%)</b>
Research, analysis and writing of chapter	80

The following co-authors have contributed to Chapter 5 (pp.111-145):

<b>Name</b>	<b>e-mail address</b>	<b>Nature of contribution</b>	<b>Extent of contribution (%)</b>
Prof Marena Manley	mman@sun.ac.za	Research inputs, editorial suggestions and proofreading	20

Signature of candidate: L. Schoeman

Date: 30/11/2016

**Declaration by co-authors:**

The undersigned hereby confirm that

1. the declaration above accurately reflects the nature and extent of the contributions of the candidate and the co-authors to Chapter 5 (pp. 111-145),
2. no other authors contributed to Chapter 5 (pp. 111-145) besides those specified above, and
3. potential conflicts of interest have been revealed to all interested parties and that the necessary arrangements have been made to use the material in Chapter 5 (pp. 111-145) of this dissertation.

<b>Signature</b>	<b>Institutional affiliation</b>	<b>Date</b>
Prof Marena Manley	Department of Food Science, Stellenbosch University	30/11/2016

Declaration with signature in possession of candidate and supervisor.



## CHAPTER 5

### Oven and forced convection continuous tumble (FCCT) roasting: effect on physicochemical, structural and functional properties of wheat

#### Abstract

Wheat roasting is generally performed to enhance flavour and improve organoleptic properties. This study investigated the physicochemical, structural and functional properties of whole wheat kernels after being roasted at 180°C for 140 s using a conventional oven and a more homogeneous and energy efficient roasting method, referred to as a forced convection continuous tumble (FCCT) roaster. Wheat kernels tend to puff upon roasting and the weight, bulk density, moisture content, flour yield, protein content and hardness decreased significantly ( $P \leq 0.05$ ) for both roasting methods compared to the unroasted control. The A-type crystalline structure of the wheat starch was only slightly affected after roasting with no significant ( $P > 0.05$ ) change in crystallinity content. Scanning electron microscopy (SEM) micrographs of the starch granules explains the minor influence of roasting on the structure and functionality. Roasting introduced pores and cavities within the intact cell walls of the endosperm, together with a disintegrated protein matrix, with these changes being more profound for the oven-roasted samples. Both roasting methods resulted in an increase in functional properties, i.e. water absorbance capacity (WAC) and pasting properties, whereas the water solubility index (WSI) and flour dispersibility (FD) remained unaffected ( $P > 0.05$ ). Limited gelatinisation occurred during roasting, due to limited water available in the samples. This was also confirmed in the SEM micrographs. The two roasting treatments caused different changes in structure and these changes had diverse impacts, although not significantly different ( $P > 0.05$ ), on the degree of gelatinisation (FCCT=10.14%; oven=17.16%). Differential scanning calorimetry (DSC) demonstrated an increase ( $P \leq 0.05$ ) in the thermal transition temperatures of both roasted samples, while the gelatinisation enthalpy ( $\Delta H$ ) decreased ( $P \leq 0.05$ ) after roasting. Rheological characteristics, measured with the Alveograph, were not affected ( $P > 0.05$ ) by either roasting methods, whereas the peak time, measured with the Mixograph, increased significantly ( $P \leq 0.05$ ). The roasting conditions used will have no detrimental effect on the baking quality of bread and may even delay staling. Thus, the results of this study may assist in potential future applications and the development of value-added products.

#### Introduction

Wheat is the most important cereal crop in the world with regard to cultivation areas and total production. The cultivation, consumption and uses thereof are worldwide and it constitutes one of the staple food commodities. Wheat plays a vital role in human diets, due to its agronomical adaptability and its sustained nutritional qualities during storage (Raigar *et al.*, 2016). It is extensively used as prime energy source and is utilised for the production of a wide range of food products, i.e. bread, pasta, fortified cereals and confectionary products. At present, dietary

guidelines recommend an increase in the consumption of whole grain cereal products, since they are commonly associated with a better quality diet and play an important role in reducing the risk of cardiovascular diseases, hypertension, certain cancers, type-2 diabetes and obesity (Işikli *et al.*, 2014). Commercial wheat flour are not pre-gelatinised and do not contain bran and germ. Removal of the bran and germ deprives consumers of the nutritional value thereof since these components are sources of dietary fibre, vitamins and minerals, phytochemicals, essential amino acids and unsaturated fatty acids (Bolade, 2009). To maintain these vital substances in end-products, whole grain flours are recommended for the production of functional foods (Ragaei & Abdel-Aal, 2006).

Technologies used to process whole grains into intermediate and end products commonly involve heat (Bolade, 2009). Different thermal processing treatments, e.g. parboiling, flaking, puffing, pressure cooking, extrusion and roasting can be used to prepare wheat products. Roasting is a high-temperature-short-time (HTST) thermal processing method which entails numerous physical, nutritional and chemical changes which can either be desirable or undesirable (Oboh *et al.*, 2010). Some desirable alterations reported for cereal grains include enhancing antioxidant activity and nutrient availability, which supports their potential as a natural functional food (Chung *et al.*, 2011; Muyonga *et al.*, 2014). Roasting can extend the shelf life and safety of products by lowering the water activity which reduces the rate of microbial growth (Ranganathan *et al.*, 2014). Roasting of cereal grains plays a vital role in improving sensory properties by increasing the overall palatability, enhancing flavour, colour, texture and appearance and makes it easier to integrate into ready-to-eat products (Murthy *et al.*, 2008). Wheat roasting can serve as a pre-processing step to enable the use of less energy for milling and to produce value-added products. It is considered one of the most effective methods to inactivate destructive enzymes and reduce mycotoxin levels (Kabak, 2009; Griffith & Castell-Perez, 1998). Moreover, roasting leads to starch gelatinisation and protein denaturation, hence improving digestibility (Sharma *et al.*, 2011). This has contributed to the renewed interest in using roasted cereal grains as ingredient for formulating value-added food products. In contrast, undesirable changes include decreases in nutritive values and loss in vitamins and minerals (Ayatse *et al.*, 1983). A significant reduction in crude protein, dietary fibre, phenolic and flavonoid content of maize was reported by Oboh *et al.* (2010) after roasting.

Roasting whole wheat followed by milling are an economically viable approach to prepare products, i.e. instant rolled wheat for breakfast cereals, puffed snacks, pasta, grits or pre-gelatinised flour for baked goods, flour blends or soup mixes (Mossman *et al.*, 1973). In Central and Eastern Europe and Asia the consumption of roasted buckwheat as breakfast cereal or as processed flour, are of increasing popularity (Zielinski *et al.*, 2009). Roasted wheat flour is commonly incorporated into pasta (Baiano *et al.*, 2008) and bread (Baiano *et al.*, 2009) in Italy. The addition of roasted flour into bread resulted in a decreased bread volume and detrimental effects on mechanical properties due thermal denaturation of gluten-forming proteins (Baiano *et al.*, 2009).

The effect of roasting on end product properties will, however, depend on the roasting method and conditions under which processing is performed. Traditional roasting technologies, i.e. sand

roasting should be improved by looking at the following factors: economics (increase capacity, reduce equipment size and energy consumption and increase ease of control), environmental considerations (reduce emissions and increase operators' safety) and improve product quality (uniform roasting and minimal physical, chemical and nutritional degradation) (Pronyk *et al.*, 2004). Modern superheated steam processing uses a clear, colourless gas attained by the application of heating ordinary steam under normal pressure to a higher temperature (Head *et al.*, 2010). The reuse of latent heat of evaporation during superheated steam roasting makes it a more energy efficient process compared to conventional hot air (Zzaman & Yang, 2013). In contrast to hot air, superheated steam creates an oxygen free environment which means no oxidative or combustion reactions occur and this results in improved product quality (no scorching) (Pronyk *et al.*, 2004). Furthermore, superheated steam roasting results in the preservation of more desirable food characteristics in terms of colour and microstructure in comparison to oven roasting, under similar time and temperature roasting conditions (Idrus & Yang, 2012).

A recent study by Schoeman *et al.* (2016b) used X-ray micro-computed tomography ( $\mu$ CT) to characterise and quantify the effect of conventional oven and innovative forced convection continuous tumble (FCCT) roasting on the microstructure of whole wheat kernels. Using the same roasting parameters, oven roasting resulted in more substantial microstructural (e.g. volume, porosity and relative density) changes when compared to FCCT roasting. Besides microstructural changes, it is likely that roasting will also affect other properties which will have a great influence in determining the use thereof for food purposes. This has spurred the need for this study since physicochemical, structural (starch-protein morphology and crystallinity) and functional information is required by food scientists to obtain a better understanding of food properties.

Physicochemical and functional properties of food are strongly influenced by structure-property relationships (Frisullo *et al.*, 2012). Changes in physicochemical and functional properties induced by roasting have been reported for cereals, i.e. oats (Sandhu *et al.*, 2015), quinoa (Rothschild *et al.*, 2015) and barley (Sharma *et al.*, 2011). Physical properties of roasted wheat, like those of other grains, are important for the design of equipment for processing, packing and transportation (Işikli *et al.*, 2014). Thermal changes induced by roasting affect the internal matrix of wheat (Schoeman *et al.*, 2016a) and this may be reflected in the hardness, milling and flour yield and end product quality (Raigar *et al.*, 2016). Milling yield is an essential wheat quality trait that defines the profits for milling industries (Kong & Baik, 2016). Thus, the milling industry prefers harder wheat due to the greater yield and higher quality flour produced, resulting in higher economic value. Hectolitre mass (HLM) is an important indicator of wheat quality and is often correlated with milling yield and hardness.

Particle size index (PSI) provides an indication of hardness, where softer kernels yielding finer flours has a higher PSI. Murthy *et al.* (2008) reported that fluidised bed roasted wheat was softer than sand roasted wheat, indicating lower energy requirements for further processing such as grinding. PSI influence the dry flour flow characteristics and sensory and baking quality, since

softer damaged starch granules can absorb more water and are also more susceptible to amylase action than intact starch granules (Griffith & Castell-Perez, 1998). Bread baked from fine particle size flour generally results in lower loaf volume than breads baked from coarse PSI flours. This is attributed to the reduced gas retention in the dough as a result of the large amount of fine particles present in the flour (Zhang *et al.*, 1998). Bulk density is an index of the extent of puffing during roasting, thus expressed as the puffing index (PI) (Lazar *et al.*, 1974). According to Hoke *et al.* (2007) roasted grains display enhanced crispiness and volume and improved texture because of puffing.

Ranganathan *et al.* (2014) attributed swelling and deformation of roasted sorghum starch granules to partial gelatinisation. Thus, it is important to investigate the starch-protein morphology of the roasted sample using scanning electron microscopy (SEM). A study on maize found that the crystallinity content, determined using X-ray diffraction (XRD), decreased ( $P \leq 0.05$ ) after roasting resulting in positive effects on starch availability and digestibility (Carrera *et al.*, 2015).

Water absorption capacity (WAC) provides an indication of the ability of starch to absorb water (swelling behaviour) and is an indirect measure of starch gelatinisation (Zhu *et al.*, 2010). A previous study reported that FCCT roasting (150°C for 20 min) increased the WAC and *in vitro* protein digestibility of marama bean flour which was then used in combination with sorghum to produce a value-added composite porridge (Maruatona *et al.*, 2010). An increase in WAC can be attributed to an increase in starch gelatinisation (Zhu *et al.*, 2010). Roasted flours with an increased the WAC is useful for the preparation of instant mixes and porridges (Ranganathan *et al.*, 2014). Water solubility index (WSI) is an indicator of the degradation of molecular components, since it is a measure of the quantity of soluble components released from starch (Ding *et al.*, 2006). Flour dispersibility (FD) refers to the ability to reconstitute in water (Edema *et al.*, 2005).

In certain food preparations, i.e. bread making, an optimum level of damaged starch is desirable as it improves the hydration rate and enhances the fermentation capability (Mahadevamma & Tharanathan, 2007). Nonetheless, excessive starch damage is detrimental as it will result in unwanted functional and rheological properties (Mahadevamma & Tharanathan, 2007). Raigar *et al.* (2016) found that roasting influences the final characteristics and end product quality in terms of protein and starch digestibility, which is related to the extent of gelatinisation. During roasting starch can be modified to different extents and this can contribute to important effects on the functionality, especially the thermal properties, of products. Thermal properties and gelatinisation characteristics can be examined using differential scanning calorimetry (DSC). The level of gelatinisation, partial or complete, will depend on the processing method and conditions, as well as the moisture available (Holm *et al.*, 1988). Andrejko *et al.* (2011) observed starch gelatinisation in wheat when infrared heating was performed at temperatures above 150°C for more than 90 s.

Viscosity is one of the most important functional properties since a Rapid Visco Analyser (RVA) profile provides information on the starting temperature of gelatinisation, peak viscosity and

retrogradation. Since wheat contains almost 60% starch, it is likely that starch modification will have a major influence on the consistency of roasted products (Mossman *et al.*, 1973).

Good gluten quality produces bread with a high volume and good crumb texture. Strong wheat flours with a desirable gluten quality result in good dough properties, i.e. a high water absorption and stability time during mixing, as well as high resistance and extensibility (Van Hung *et al.*, 2006). In contrast, dough from soft wheat flours result in inferior gluten quality which exhibits low water absorption and less stability during mixing and less extensibility. Roasted whole wheat can be beneficial in terms of its functional and rheological effects, as it can be used to generate products with specific rheological and functional properties to meet the needs of specific applications. Zhang *et al.* (1998) reported that a combination of roasting and steaming (105°C, 20 min) of oats improved the bread baking potential of oat flours.

Roasting as a form of wheat processing is scarcely studied. The effects of roasting on the antioxidant activity (Gelmez *et al.*, 2009; Hernández-Borges *et al.*, 2005), extractable mineral and phytic acid content (Gahlawat & Sehgal, 1993; Khan *et al.*, 1986), hydration kinetics (Maskan, 2002), chemical composition and physical, organoleptic and nutritional properties (Caprez *et al.*, 1986; Mossman *et al.*, 1973) of wheat were investigated earlier. Some food applications of air-fluidised roasted wheat were investigated by Lazar *et al.* (1974). Applications that showed promise were the use of roasted wheat as breaders for fish and meat or as thickeners in soups, sauces or gravies. Raigar *et al.* (2016) examined the effect of different thermal treatments on the grinding characteristics, granular morphology and yield of ready-to-eat wheat grits. Roasting was found to be desirable in terms of protein digestibility, granular morphology and hardness.

Currently there is increasing interest in the use of roasted grains in food products due to numerous health benefits and improved product quality (Carrera *et al.*, 2015). To date no studies have been undertaken to investigate the physicochemical, structural and functional properties of wheat after conventional oven and novel FCCT roasting. Keeping in view the aforesaid discussion, the aim of this study was to examine the effect of these two roasting methods, using similar roasting conditions, with regards to changes in physicochemical, structural and functional properties of whole wheat. This will provide baseline information, which would identify potential applications for roasted whole wheat and its flour as functional ingredient in food systems.

## Materials and methods

### *Wheat samples*

A commercial wheat cultivar (30 kg) was procured from Pioneer Foods (Paarl, South Africa). Impurities and broken kernels were removed from the wheat sample using a Carter Day Dockage Tester (Carter Day International, Minneapolis, MN). The sample was then thoroughly mixed by pouring it three times through a Boerner Divider (Seedburo Equipment Co., Chicago, USA) after which it was divided into nine batches of 2.2 kg each. Three of the batches remained unroasted and served as the control, whereas the other six batches were roasted using oven or FCCT

roasting, respectively. Each sample was stored in an airtight plastic container at ambient temperature until further evaluation. The three replicates of the control and two roasting methods were analysed in either triplicate, duplicate or as single measurements as indicated in each method.

#### *Tempering of test run for FCCT roasting*

For the FCCT roasting method, a test run sample (400 g) was tempered with pure deionised water (dH<sub>2</sub>O) to a final moisture content of between 18 and 20%. This was done to generate some initial moisture and superheated steam in the roasting chamber which replaced the dry, hot air prior to roasting, ensuring a more homogenous roasting process. The amount of water added was calculated according to the AACC Method 26-95.01 (AACC, 1999c). This method takes the original moisture content and the mass of the sample into consideration (Eq.1). The tempered sample was kept in an airtight container for 24 h at room temperature with regular shaking intervals to ensure even moisture absorption.

$$\text{Weight of water to add (g)} = \left( \frac{100 - \text{original moisture (\%)}}{100 - \text{desired moisture (\%)}} - 1 \right) \times \text{sample weight (g)} \quad (1)$$

#### *Roasting*

Roasting involved exposure of the wheat samples to either dry, hot air in the conventional convection oven (831 Electric Multifunction Thermofan Solid Plate Oven, Defy Appliances, Durban, South Africa) or superheated steam in the FCCT roaster (Roastech, Bloemfontein, South Africa) at 180°C for 140 s. A temperature of 180°C is commonly used for roasting cereal grains (Chung *et al.*, 2011). The retention time of the wheat in the roasting chamber is determined by the rotary velocity of the screw conveyer inside the roasting chamber. A screw speed setting of 80 Hz resulted in a roasting time of 140 s. The actual samples were not tempered as tempering is not typically applied in the production of roasted wheat (Işikli *et al.*, 2014). For each roasting method three batches of 2.2 kg were roasted according to the procedure described by Schoeman *et al.* (2016). After roasting the samples were immediately spread on a cold flat surface to stop further exothermic reactions. The cooled samples were stored in airtight containers at ambient temperature until being milled.

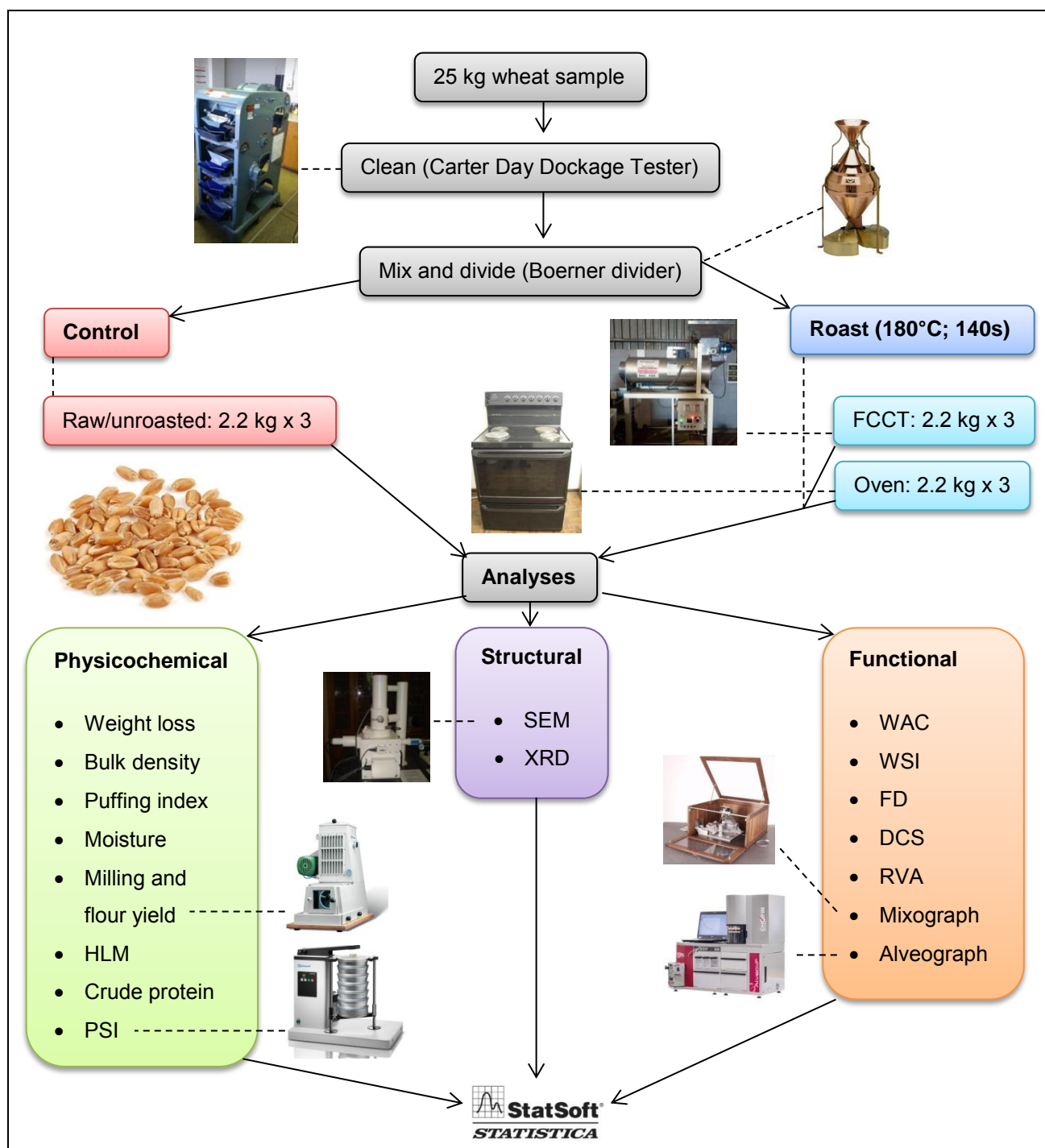
#### *Grinding of wheat samples*

To obtain whole wheat flour, the control and roasted samples (300 g each) were pulverised separately in a hammer-type cyclone Laboratory Mill 3100 (Perten, Hägersten, Sweden) fitted with a 1 mm sieve. The whole wheat flour samples were stored in airtight containers (at ambient temperature) from which required quantities was removed for further analyses.



*Experimental design*

A schematic diagram of the experimental setup and analyses procedures is illustrated in Figure 5.1.



**Figure 5.1.** A simplified flow diagram of the roasting and analyses procedures used. HLM= hectolitre mass; PSI= particle size index; SEM= scanning electron microscopy; XRD= X-ray diffraction; WAC= water absorption capacity; WSI= water solubility index; FD= flour dispersibility; DSC= differential scanning calorimetry; RVA= Rapid Visco Analyser.



## Physicochemical analyses

### Weight loss

The percentage weight loss of each sample was recorded in triplicate by measuring the initial (before roasting) and final (after roasting) weights.

### Bulk density and puffing index (PI)

Bulk density was determined in triplicate according to the method of Sandhu *et al.* (2015). The wheat samples were filled in a 100 mL graduated cylinder (previously tared). The bottom of the cylinder was gently tapped until there was no further diminution of the sample after filling it to the 100 mL mark. The bulk density of the control and roasted wheat samples was calculated as the weight of the sample per unit volume ( $\text{g}/\text{cm}^3$ ) using Equation 2. The PI was calculated by dividing the bulk density of the control with the bulk density of the roasted sample (Sandhu *et al.*, 2015).

$$\text{Bulk density (g/cm}^3\text{)} = \frac{\text{Weight of sample (g)}}{\text{Volume occupied (cm}^3\text{)}} \quad (2)$$

### Moisture content

Moisture content of the control and roasted flours was determined in triplicate using the air-oven drying Method 44-19.01 (AACC, 1999d) immediately after grinding was performed. Wheat flour ( $2 \text{ g} \pm 1 \text{ mg}$ ) was heated in aluminium moisture dishes for 2 h at  $135^\circ\text{C}$  in an oven, model EM10 (CHOPIN Technologies, Cedex, France). Moisture loss was used to calculate the percentage moisture (Eq.3).

$$\text{Moisture (\%)} = \frac{\text{Moisture loss (g)}}{\text{Sample weight (g)}} \times 100 \quad (3)$$

### Milling and flour yield

Experimental milling was performed at the research and development facility of Sasko (Essential Foods, Division of Pioneer Foods (Pty) Ltd., Paarl, South Africa) using the Brabender Quadrumat Jr. (Quadruplex) mill (C.W. Brabender Instruments Inc., South Hackensack, NJ) according to the AACC method 26-50.01 (AACC, 1999b). The aspirator was adjusted to give maximum airflow without excessive loss of fine flour. The wheat (1 kg of each sample) was tempered to a moisture content of 15-16% for 24 h using the AACC Method 26-95.01 (AACC, 1999c). Before milling, the mill was run empty for half an hour after which a test sample was run in order to bring the mill to operating temperature. Then 1 kg sample was poured into the feed hopper. The feed rate was 75 g/min. The continuous reel sifter automatically separates the ground product into flour and by-product (bran and large endosperm particles). Milling yield was calculated on the basis of total recovered products (comprising bran and flour) after milling the tempered whole wheat sample. Flour yield is the weight of the flour extracted, expressed as a percentage of the total tempered grain weight milled (Kong & Baik, 2016). The bran was discarded and the flour was stored in airtight containers for further use.

### Hectolitre mass (HLM)

HLM (kg hL<sup>-1</sup>) determinations were performed in duplicate at the research and development facility of Sasko using the German Kern 220/222 Grain Sampler (KERN & SOHN GmbH, Balingen-Frommern, Germany). This test was performed according to the method described by Guelpa *et al.* (2015).

### Crude protein

Crude protein content of the control and roasted wheat flour was assayed in duplicate using the Dumas combustion AACC Approved Method 46-30.01 (AACC, 1999e). A LECO TruMac N (LECO Corporation, Saint Joseph, Michigan, USA) nitrogen analyser was used. Combustion at high temperature in pure oxygen sets nitrogen free, which is measured by thermal conductivity detection. The crude protein content was determined at 12% moisture base (mb) and a conversion factor of 5.7 was used to determine the crude protein (%) from the nitrogen.

### Particle size index (PSI)

PSI was determined in duplicate according to the AACC Approved Method 55-30.01 (AACC, 1999h) to give an indication of relative wheat kernel hardness. The PSI of 10 g ground flour was obtained by sieving using a Retsch AS 200 Tap Sieve Shaker (Retsch, Haan, Germany). Approximately 50 g of whole wheat kernels were also placed on the sieve. Each sample was shaken for 10 min with the Sieve Shaker which was operated electrically and provided with a timer to control sieving time. Two sets of pans and sieves were stacked on top of each other and sieved simultaneously. The fine particles of wheat flour passing through the 75 µm size were collected in the receiving pan. The fine material adhering to the bottom of the sieve was brushed into the receiving pan and weighed to obtain the weight of the throughs (W). Equation 4 was used to determine the PSI. The PSI (%) obtained was converted to relative hardness using Table 5.1. Hard wheat results in lower PSI values and *vice versa*.

$$\text{PSI (\%)} = \frac{W \text{ (g)}}{\text{Sample weight (g)}} \times 100 \quad (4)$$

**Table 5.1.** Relative wheat hardness scale

Category	PSI (%)
Extra hard	Up to 7
Very hard	8-12
Hard	13-16
Medium hard	17-20
Medium soft	21-25
Soft	26-30
Very soft	31-35
Extra soft	Over 35

## Structural analyses

### Scanning electron microscopy (SEM)

The microstructure of the control and roasted wheat were analysed at an accelerating voltage of 7 kV and current of 11  $\mu$ A using a LEO 1430VP scanning electron microscope (Zeiss, Germany). A spot size of 150 was used. Two control, two FCCT-roasted and two oven-roasted wheat kernels were sectioned into half along the transverse axis with a Solingen blade. The sectioned kernels were mounted on aluminium specimen stubs with double-sided carbon tape and coated with a thin layer of gold palladium employing a 5150A sputter-coater (HHV, Crawley, United Kingdom). The granular morphology and surface structure of the samples were identified with secondary electron images. Representative micrographs of the kernels were obtained using variable magnifications to observe the endosperm packing density and starch granule morphology. At least four micrographs were obtained for each sample.

### X-ray diffraction (XRD)

X-ray diffractometry was performed at room temperature on the control and roasted flour samples using a D8 Advance Bruker X-ray powder diffractometer (BRUKER AXS, Germany) as described by Carrera *et al.* (2015), with slight modifications. The instrument was equipped with a water-cooled rotating copper anode that produces Cu-K $\alpha$  radiation ( $\lambda = 1.5406$ ). The X-ray tube operated at a current of 10 mA and an accelerating voltage of 30 kV. The scanning region of the diffraction angle ( $2\theta$ ) was 5–40° with an exposure time of 1285 s, step size of 0.016° and measuring time of 0.5 s per point. One diffractogram was collected for each sample and the average of the three replicates was reported. Crystalline and amorphous areas were quantified using EVA software (BRUKER AXS, Germany). Crystallinity (%) was determined as the integrated area of the upper region of the curve (crystalline peaks) divided by the total integrated area under the curve and above the straight baseline (amorphous + crystalline peaks), multiplied by 100 (Yoo & Jane, 2002).

## Functional analyses

### Water absorption capacity (WAC), water solubility index (WSI) and flour dispersibility (FD)

WAC of the flour samples was determined in triplicate according to the AACC method 56-20.01 (AACC, 1999i). Two grams of flour was weighed into a pre-weighed 50 mL centrifuge tube. To this 40 mL dH<sub>2</sub>O was added and it was mixed thoroughly. The suspension was left to stand for 10 min and mixed by inverting at the end of 5 and 10 min periods. The samples were centrifuged (TJ-25 Centrifuge, Beckman Coulter, South Kraemer Boulevard, US) for 15 min at 1000x gravity at 20°C. After pouring the supernatant liquid into tared evaporating dishes the centrifuge tubes with remaining residue (sediment) were weighed (Mwangwela *et al.*, 2007). WAC (g water/g flour) was calculated as the weight of sediment obtained after removal of supernatant per unit weight of the original dry solids (Eq. 5).

$$\text{WAC (g/g)} = \frac{(\text{weight of tube + sediment}) - \text{weight of tube}}{\text{sample weight (dry basis)}} \quad (5)$$

The supernatant liquid from the WAC procedure was oven-dried for 24 h at 100°C (Hafsa *et al.*, 2015). WSI, defined as the water-soluble fraction in the sample, was determined from the weight of dried solids recovered by evaporating the supernatant and was expressed as percent dry solids or WSI (%) (Eq. 6).

$$\text{WSI (\%)} = \frac{\text{weight of dry solids in supernatant}}{\text{sample weight (dry basis)}} \times 100 \quad (6)$$

FD determinations were performed in triplicate according to the method of Edema *et al.* (2005). A flour sample (10 g) was weighed into a 100 mL measuring cylinder and filled to the 100 mL mark with dH<sub>2</sub>O. The sample was vigorously stirred and then allowed to settle for 3 h. The volume of the settled particles was recorded and subtracted from 100 to obtain the percentage FD.

#### Differential scanning calorimetry (DSC)

Thermal characteristics of the whole wheat flours (control and roasted) were analysed using a differential scanning calorimeter (DSC Q20, TA Instruments, New Castle, USA), equipped with a thermal analysis data station. Thermal data were obtained by carefully weighing the flour sample (5 mg, dry basis) into an 40 µL aluminium pan and dH<sub>2</sub>O (15 µL) was added with a micropipette. The pan was hermetically sealed before heating. The instrument was calibrated using indium and an empty aluminium pan was used as reference. The reference pan and sample pan were each placed on a separate heater and heated in the DSC cell from 20 to 140°C at a heating rate of 10°C/min. The calorimeter was equipped with a controlled cooling accessory, using liquid nitrogen with a flow rate of 50 mL/min as cooling agent. DSC analysis generated a profile of injected/extracted heat flow from the analysed sample as a function of temperature (Carrera *et al.*, 2015). Any transitions, i.e. starch gelatinisation and protein denaturation were recorded, finding in the thermograms the onset ( $T_o$ ), peak ( $T_p$ ) and endset ( $T_e$ ) temperatures of the endotherm (Guzmán *et al.*, 2009). The gelatinisation enthalpy ( $\Delta H$ ) of the transitions was estimated from the area of the endotherm using Matlab™ 2014b software (Mathworks, Natick, MA, USA) (Ahmed *et al.*, 2007). The gelatinisation temperature range ( $\Delta T$ ) was calculated as  $T_e - T_o$ . The average values of three replicates were reported. The degree of gelatinisation (%) was determined as reported by Sharma *et al.* (2011) (Eq. 7):

$$\text{Degree of gelatinisation (\%)} = \left[ 1 - \left( \frac{\Delta H \text{ of roasted sample}}{\Delta H \text{ of control sample}} \right) \right] \times 100 \quad (7)$$

#### Pasting properties and $\alpha$ -amylase activity

Pasting properties of the whole wheat flours were determined using a Rapid Visco Analyser (RVA) model 4500 (Perten Instruments, Eden, Australia) according to the AACC method 76-21.01 (AACC, 1999j). Triplicate runs were conducted for each sample. The RVA instrument contained its own microprocessor, which carried out internal control and monitoring functions. Milled flour (3.5 g  $\pm$  0.01 g on a 14% mb) was placed in the aluminium test canister together with 25 mL dH<sub>2</sub>O (corrected to compensate for 14% mb). The suspension was thoroughly mixed with a plastic

paddle to prevent lump formation. Standard profile 1 was used to capture rheological information. The measurement cycle of the pre-programmed profile was initiated by depressing the motor tower of the instrument. The test was then allowed to proceed and terminate automatically after 13 min. The procedure involved an initial holding stage at 50°C for 1 min, a heating step from 50 to 95°C for 3 min and 42 s, a holding phase at 95°C for 2 min and 30 s, a cooling step from 95°C to 50°C for 3 min and 48 s and a final holding stage at 50°C for 2 min. The suspension was stirred at 960 rpm for 10 s, followed by a constant rotating speed of 160 rpm throughout the analysis. The peak ( $V_p$ ), breakdown ( $V_b$ ), final ( $V_f$ ), setback ( $V_s$ ) and through ( $V_t$ ) viscosity, as well as the peak time and pasting temperature ( $P_{temp}$ ) were reported by *Thermocline for Windows™* (Version 3) software. For each RVA measurement the viscosity (measured in centipoise; cP), temperature (°C) and speed (rpm) were recorded every four seconds.

In a separate experiment, the stirring number (SN, viscosity at 3 min) was measured in triplicate with the RVA according to the AACC method 22-08.01 (AACC, 1999a) using the SN profile. This method is based on the ability of  $\alpha$ -amylase to liquefy a starch gel and is an indication of amylase activity. Flour (3.5 g corrected to 14% mb) and water (25 mL corrected to 14% mb) was measured into a test canister. The stirring paddle was placed in the canister and vigorously jogged up and down ten times to remove any lumps. The canister with the paddle was placed into the RVA and the measurement cycle was initiated by depressing the motor tower of the instrument. The SN (recorded in cP) was displayed as the final viscosity after termination of the test. Higher SN values is an indication of less  $\alpha$ -amylase activity (Ragaei & Abdel-Aal, 2006).

#### Rheology: Mixograph and Alveograph

Rheological analyses were conducted as single measurements for each of the three replicates using the flour obtained from the Brabender Quadrumat Jr. (Quadruplex) mill (C.W. Brabender Instruments Inc., South Hackensack, NJ). The resistance of the dough to mixing was measured using a Mixograph (National Mfg Co., Lincoln, Nebraska, USA) according to the AACC method 54-40.02 (AACC, 1999g). The Mixograph comprises two pairs of relatively thin pins rotating in a planetary motion and three fixed pins in the mixing bowl to oppose the action of the moving pins. A flour sample of 35 g (14% mb) was weighed and placed in a Mixograph bowl. Water was dispensed to the flour from a burette after which the bowl was inserted into the Mixograph. The flour and water was mixed for 7 min to form dough. As the dough is mixed the Mixograph automatically recorded a graph on the computer. The graph was used to determine the optimum development time (min) and to estimate the water absorption (amount of water required for dough to reach a defined consistency).

The resistance of dough to extension was determined following the AACC method 54-30.02 (AACC, 1999f), using an Alveograph MA 82 (Chopin, Tripette ed Renaud, France) where dough with a definite thickness was prepared under specific conditions and expanded by air pressure until it ruptures. The internal pressure in the bubble is graphically recorded. Alveographic indices

recorded included: resistance to extension (tenacity) or stability measured as the height of the curve (P, mm); dough extensibility measured as the length of the curve (L, mm); deformation energy (W,  $\times 10^{-4}$  J), strength ( $S = W/6.54$ ,  $\text{cm}^2$ ) and the curve configuration ratio (P/L).

### *Statistical analysis*

Statistical analysis was carried out using STATISTICA version 13 (StatSoft, Inc., Tulsa, USA). The data was analysed using one-way analysis of variance (ANOVA) to test for differences between the control and the two roasting methods. Mean differences were evaluated at the 5% significance level ( $P \leq 0.05$ ) using the least significant difference test. Data was reported as mean  $\pm$  standard deviation for roasting experiments performed in triplicate.

## **Results and discussion**

### *Physicochemical properties*

The physicochemical properties of the control and roasted whole wheat samples are summarised in Table 5.2.

### Weight loss

Roasting evoked significant ( $P \leq 0.05$ ) changes in weight loss with oven roasting resulting in almost double (1.02%) the loss compared to FCCT roasting (0.53%) (Table 5.2). Weight loss is mainly attributed to moisture loss (due to dehydration), but also in a lesser extend to thermal degradation of organic compounds (sugars, polysaccharides and proteins) and non-enzymatic and pyrolytic reactions (Alessandrini *et al.*, 2008). In conventional oven roasting the sample is stationary, whereas in the FCCT roaster the rotary motion of the roasting drum agitates the sample which ensures that the kernels are continuously stirred and all the surfaces are exposed evenly while propelling the sample through the roasting chamber. The internal superheated steam generated by the moisture from the sample inside the FCCT roaster, together with the rotating movement of the cylinder, results in uniform heat transfer and thus more homogenous roasting.

**Table 5.2.** Effects of roasting on the physicochemical characteristics of whole wheat

Sample	Weight loss (%)	Bulk density (g/cm <sup>3</sup> )	PI <sup>b</sup>	Moisture (%)	Milling yield (%) <sup>*</sup>	Flour yield (%) <sup>*</sup>	HLM (kg hL <sup>-1</sup> ) <sup>c**</sup>	Crude protein (%) <sup>a**</sup>	PSI (%) <sup>d**</sup>
<b>Control</b>	0 <sup>c</sup>	0.83±0.003 <sup>a</sup>	0 <sup>c</sup>	10.72±0.10 <sup>a</sup>	98.74±0.12 <sup>a</sup>	55.17±3.26 <sup>a</sup>	82.23±0.15 <sup>a</sup>	11.77±0.06 <sup>a</sup>	23.10±1.67 <sup>c</sup>
<b>FCCT</b>	0.53±0.11 <sup>b</sup>	0.81±0.003 <sup>b</sup>	1.03±0.004 <sup>b</sup>	10.12±0.25 <sup>b</sup>	98.70±0.21 <sup>a</sup>	49.58±0.37 <sup>b</sup>	82.13±0.21 <sup>a</sup>	11.60±0 <sup>b</sup>	36.86±0.75 <sup>b</sup>
<b>Oven</b>	1.02±0.07 <sup>a</sup>	0.77±0.001 <sup>c</sup>	1.08±0.005 <sup>a</sup>	9.92±0.19 <sup>b</sup>	98.61±0.35 <sup>a</sup>	46.65±1.33 <sup>b</sup>	81.90±0.26 <sup>a</sup>	11.58±0.03 <sup>b</sup>	41.37±0.49 <sup>a</sup>

Values are presented as mean ± standard deviation of three replicates (n=3). Values followed by different superscripts in a column differ significantly (P≤0.05). <sup>a</sup>Crude protein are expressed as N x 5.7 on a 12% mb; <sup>b</sup>Puffing index; <sup>c</sup>Hectolitre mass; <sup>d</sup>Particle size index; <sup>\*</sup>Mean values of single measurements from three replicates <sup>\*\*</sup>Mean values of duplicate measurements from three replicates.



### Bulk density and puffing index (PI)

A significant ( $P \leq 0.05$ ) difference was observed between the bulk density of the FCCT ( $0.81 \text{ g/cm}^3$ ) and oven-roasted ( $0.77 \text{ g/cm}^3$ ) sample (Table 5.2.). The decrease in bulk density after roasting is due to two factors: weight (moisture) loss and volume increase (expansion) giving rise to the typical porous structure of a roasted product (Alessandrini *et al.*, 2008). Low bulk densities after roasting is an indication of internal pore or cavity formation in the endosperm and this in concurrence with the results reported by Schoeman *et al.* (2016a), where oven roasting resulted in a higher wheat kernel porosity and lower relative density compared to FCCT roasting. The decrease in bulk density can also be due to changes in cellular structure attributed to a loss of structural integrity between the starch–starch and starch–protein matrix (Chandrasekhar & Chattopadhyay, 1990). Murthy *et al.* (2008) reported that the bulk density decreased from  $833 \text{ kg/m}^3$  ( $0.83 \text{ g/cm}^3$ ) for raw wheat to  $526 \text{ kg/m}^3$  ( $0.53 \text{ g/cm}^3$ ) and  $555 \text{ kg/m}^3$  ( $0.56 \text{ g/cm}^3$ ) for sand and fluidised bed roasted wheat, respectively. The raw bulk density of the wheat was the same as the control ( $0.83 \text{ g/cm}^3$ ) reported in the current study (Table 5.2), however the much lower roasted values reported by Murthy *et al.* (2008) can be due to the different roasting methods used as well as the higher roasting temperatures.

Roasting resulted in a PI of 1.03 and 1.08 for FCCT and oven roasting, respectively. These values were lower than the PI of 1.5 reported by Mossman *et al.* (1973) using hot air roasting. A decrease in bulk density during roasting results in an increase in PI due to volumetric expansion. The driving force for puffing has been hypothesised to be the vaporisation of water present in the interstices of the starch granules during HTST heating (Boischot *et al.*, 2003). During roasting, internal moisture, entrapped in the kernels, is converted from a liquid to vapour state. The condensed structure of the raw kernels and rapid evaporation of the moisture generates vapour, which exerts internal pressure resulting in a porous, puffed kernel with a lower density (Altan, 2014). These results are in concurrence with previous studies that reported a decrease in bulk density and increase in PI after roasting oats (Sandhu *et al.*, 2015) and barley (Sharma & Gujral, 2011).

### Moisture content

Moisture content is one of the most critical indices for the keeping quality of cereal grains and its products. The roasted wheat was characterised by a significantly ( $P \leq 0.05$ ) lower moisture content. The lower moisture content helps to prevent, or reduce microbial and enzymatic reactions which ensure that the product will have a good keeping quality. The moisture content of all the samples (Table 5.2) falls within and below the recommended safe moisture level of 10–12% for grains and flour products (Ingbian & Adegoke, 2007). Although not of significance ( $P > 0.05$ ), oven roasting resulted in a lower moisture content compared to FCCT roasting. A previous study also observed that convection oven roasting results in a higher moisture loss in cocoa beans compared to superheated steam roasting when using the same temperature and time combination (Zzaman &

Yang, 2013). Khan *et al.* (1986) reported a decrease from 10.6% to 9.6% after sand roasting whole wheat kernels, while the moisture content decreased from 10% to 3% for sand as well as fluidised bed roasted wheat (Murthy *et al.*, 2008). Thus, different roasting conditions and methods, relying on different modes and rates of heat transfer, will have diverse effects on moisture content.

#### Milling and flour yield

Roasting had no significant ( $P>0.05$ ) effect on the milling yield, however, reduced the flour yield significantly ( $P\leq 0.05$ ) to 49.58% (FCCT roasting) and 46.65% (oven roasting) compared to the control (Table 5.2). Schoeman *et al.* (2016a) illustrated that the porosity of the oven-roasted samples was much higher than for the FCCT-roasted samples. This is attributed to the softer kernels with a lower flour yield. Wheat characteristics, i.e. hardness, density, kernel size and test weight are known to affect flour yield (Kong & Baik, 2016). Van Hung *et al.* (2006) reported that wheat flour, recovered around 60% yield by weight of whole wheat grain after removal of germ and bran fractions using modern milling techniques.

Kong & Baik (2016) found a significantly positive correlation between wheat hardness and flour yield, as hard wheat tend to give clean separation of bran during milling, resulting in increased flour yield. During roasting the internal structure of wheat is weakened because of internal moisture diffusion, resulting in increased levels of porosity (Schoeman *et al.*, 2016a) and reduction in mechanical strength. This will in turn influence the breaking line which cause more endosperm to remain on the bran and thus decrease the flour yield (Kahyaoglu *et al.*, 2010). Due to the reduction in mechanical strength of the roasted samples they are easily converted into powdery form and will result in less energy consumption during milling (Raigar *et al.*, 2016). Roasting leads to finer particles during milling which can result in more milling loss (Raigar *et al.*, 2016). Lazar *et al.* (1974) reported that flour yields as high as 70-75% can be obtained from roasted whole wheat if the moisture content is below 10%.

#### Hectolitre mass (HLM)

HLM provides a measure of the bulk density of grain and is also a useful indication of soundness and potential milling extraction (SAGL, 2016). Roasting had no ( $P>0.05$ ) effect on HLM and resulted in a HLM of 82.13 kg hL<sup>-1</sup> and 81.90 kg hL<sup>-1</sup> for the FCCT and over-roasted samples, respectively (Table 5.2). It can thus be assumed that the PI determined from the HLM will also not be affected. The bulk density reported earlier (Table 5.2) decreased significantly ( $P\leq 0.05$ ) after roasting, resulting in the higher ( $P\leq 0.05$ ) PI. The difference between these two bulk density methods can be attributed to the sample size used, as well as the accuracy of the procedure. In industry HLM is the preferred method for determining bulk density, since it is more precise and uses a larger sample size resulting in a more representative representation of the sample. The HLM of the control and roasted samples was similar to the average HLM of 81.1 kg hL<sup>-1</sup> reported

by the South African Grain Laboratory (SAGL) for the 2015/2016 season, also measured using the Kern 222 instrument (SAGL, 2016).

#### Crude protein

Roasting resulted in decrease ( $P \leq 0.05$ ) in protein content with no significant ( $P > 0.05$ ) difference between the two roasting methods (Table 5.2). The results fall within the range of 8.6-15.5% (mean of 11.1%) reported by Ohm *et al.* (1998) and compared favourably with the 11.8% reported by the SAGL for the 2015/2016 season (SAGL, 2016). Previously roasting also decreased ( $P \leq 0.05$ ) the protein content of oats (Sandhu *et al.*, 2015) and buckwheat (Zielinski *et al.*, 2009). Similarly, Oboh *et al.* (2010) reported that roasting caused a decrease ( $P \leq 0.05$ ) in the protein content of maize, suggesting protein quality depletion due to thermal degradation and formation of insoluble brown polymers (melanoidins). The reduction in protein content after roasting can thus be ascribed to denaturation and loss of protein due to the involvement of amino acids in the Maillard reaction (Oboh *et al.*, 2010).

#### Particle size index (PSI)

The control sample had a PSI of 23.10% (Table 5.2) falling into the medium soft category according to the relative hardness scale (Table 5.1). The two roasted samples differed significantly ( $P \leq 0.05$ ) from the control and from each other (Table 5.2). Both roasted samples were classified as extra soft according to Table 5.1. A decrease in hardness upon roasting can be attributed to grain expansion, starch gelatinisation and the development of fissures (Sharma *et al.*, 2011). Hardness reductions in the roasted kernels is indicative of the extent of structural changes, i.e. porosity that occur during roasting, which was illustrated earlier using X-ray  $\mu$ CT (Schoeman *et al.*, 2016a) and also confirmed in the subsequent section by the modified endosperm texture and packing density in the SEM micrographs.

Softer kernels (high PSI), with a high degree of porosity will reduce milling efficiency and yield due to a finer flour being produced. However, the milling yield reported in Table 5.2 showed that roasting had no significant ( $P > 0.05$ ) effect on this property. An increase in porosity weakens the endosperm structure and consequently voids in the porous endosperm concentrate stresses and results in a decrease in mechanical strength (Dobraszczyk *et al.*, 2002). Oven roasting brought about a greater decrease in hardness compared to FCCT roasting, which corresponds with the greater decrease in bulk density and weight loss, as well as the lower flour yield of this sample. An earlier comparative study between the effect of superheated steam and oven roasting on the physical properties of cocoa beans found that hardness was also more affected by oven roasting (Zzaman & Yang, 2013). Griffith & Castell-Perez (1998) reported that roasting increased the PSI of cereal grains. Finer flours milled from roasted wheat can be beneficial for infant feeding, since infants require smoother, softer foods due to their poorly developed oral motor skills (Griffith & Castell-Perez, 1998).

## Structural properties

### Scanning electron microscopy (SEM)

From the whole kernel cross-sectional micrographs, taken at a low magnification, the endosperm of the control (Fig. 5.2a1) is tightly packed (dense) with no air spaces. In the FCCT-roasted sample (Fig. 5.2b1) a few thin cracks are detectable, whereas in the oven-roasted kernel (Fig. 5.2ac1) a large cavity appeared. According to Lazar *et al.* (1974), the formation of large irregular voids and internal fissures reduces the roasting quality. Similarly, Murthy *et al.* (2008) reported SEM micrographs of raw wheat to have closed structure and roasted wheat to be more porous.

There was no clear difference among the endosperm of the control (Fig. 5.2a2) and FCCT-roasted (Fig. 5.2b2) wheat. In the higher magnification micrographs more voids and larger air spaces are clearly noticeable in the endosperm of the oven-roasted kernel (Fig. 5.2c2). This is in concurrence with the X-ray  $\mu$ CT results reported earlier (Schoeman *et al.*, 2016a), where a higher degree of porosity was observed for the oven-roasted samples. In the oven-roasted sample the presence and expansion of cavities in the endosperm appear more adverse than for the FCCT-roasted sample. These observations are in agreement with the physicochemical results (Table 5.2), where oven roasting resulted in a reduced ( $P \leq 0.05$ ) bulk density and kernel hardness in comparison to FCCT roasting. FCCT roasting had a less invasive impact on the starch-protein morphology due to the method of heat transfer. In this method the sample is continuously moving in the roasting chamber, resulting in a more uniform heat transfer in comparison to oven roasting where the sample is static and the heat penetration is more intense.

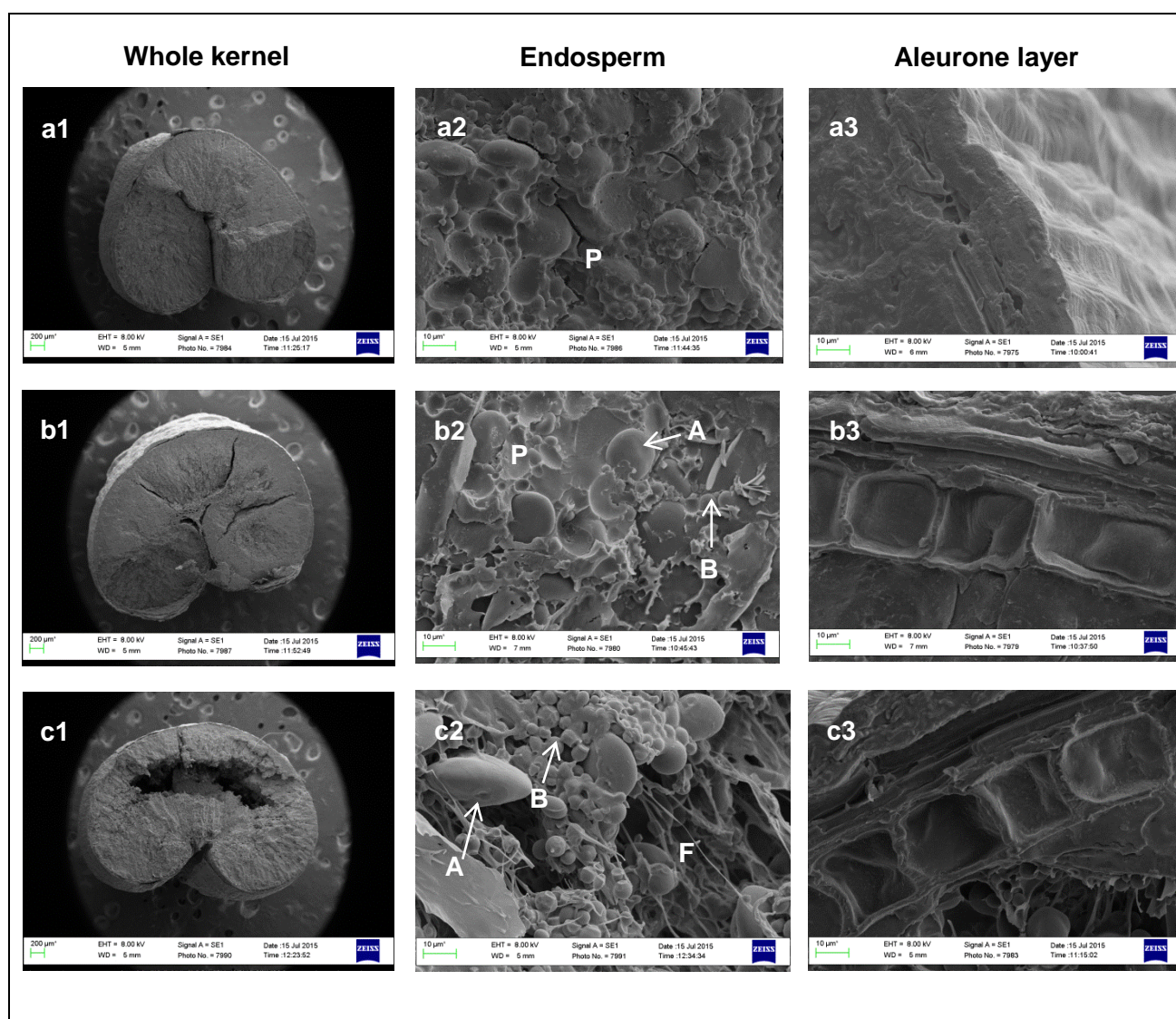
The aleurone layer plays an important role during milling, since this is where separation of the endosperm and bran takes place (Kong & Baik, 2016). The aleurone layer of the control and FCCT-roasted samples (Figs. 5.2a3 and b3) is mainly intact and unmodified. In the oven-roasted kernel (Figs. 5.2c3) the loss in subcellular organisation resulted in some degree of detachment from the aleurone layer.

Under the higher magnification micrographs (Figs. 5.2a2, b2 and c2) of the endosperm region two starch granule size distributions can be observed: large, lenticular A-type (18-33  $\mu$ m) and small, spherical B-type (2-5  $\mu$ m) starch granules which are embedded in a protein matrix (Yoo & Jane, 2002). In contrast to the control and FCCT-roasted samples (with a dense endosperm) the starch granules of the oven-roasted sample became swollen, loosely packed and deformed, but still distinguishable. Damaged starch granules typically exhibit granular distortion, irregularity and less uniformity (Barrera *et al.*, 2013). During oven roasting the internal vapour generated enough pressure to cause large voids in the cellular matrix of the endosperm. In Fig 5.2c2 some starch granules appear molten and connected with each other (partially fused), illustrating some degree of gelatinisation. Most of the starch granules from the oven-roasted sample have been separated from the protein matrix. This separation of the starch granules are caused by dehydration during roasting (Kong & Baik, 2016). In Fig. 5.2a2 the protein matrix appear intact, whereas in Figs. 5.2b2 and c2 partial disappearance (breakdown and disintegration) of the protein matrix is observed as



thin, fragmented strands which can be an indication of protein denaturation. Again this was more evident in the oven-roasted sample where thin glue-like filaments were detected. Similar results were obtained for wheat in an earlier study after 90 s of microwave roasting (Błaszczak *et al.*, 2002).

Although the roasting temperature (180°C) used exceeds the gelatinisation temperature range (51-60°C) of wheat starch, the starch granules did not gelatinise completely (Delcour & Hosney, 2010). The limited amount of moisture in the wheat samples and short roasting time was probably the reason complete gelatinisation did not occur (Raigar *et al.*, 2016). To support this hypothesis, further investigation using DSC was employed in a subsequent section to determine the degree of gelatinisation.

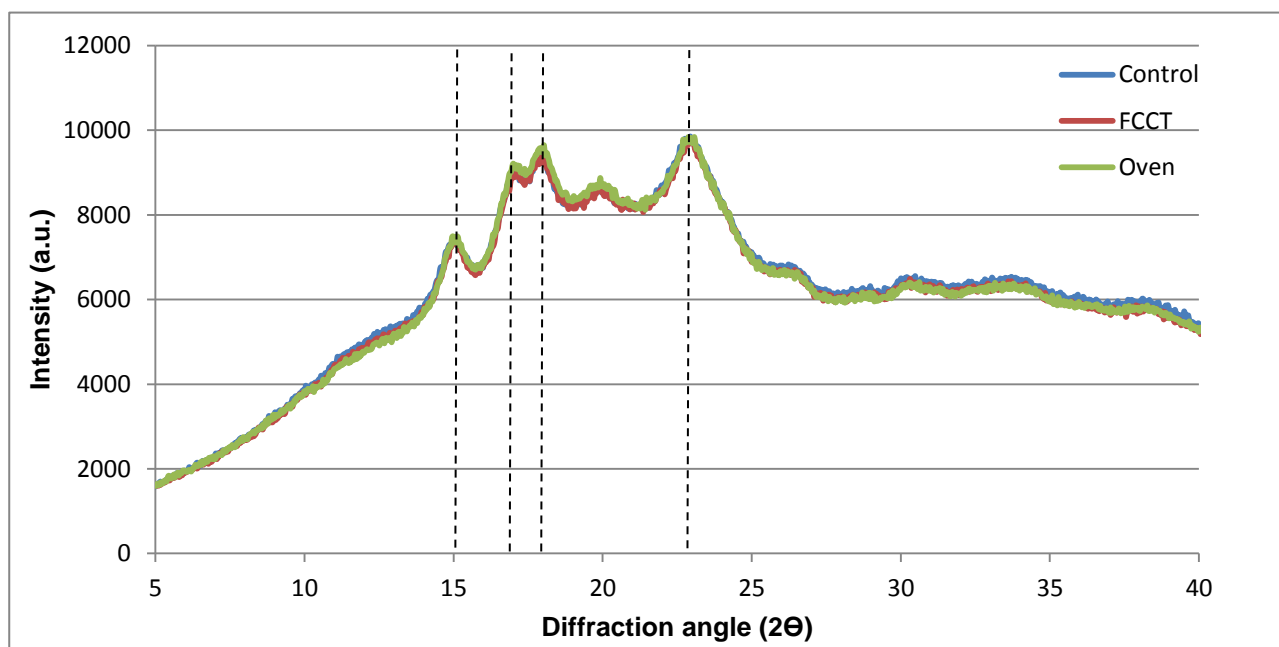


**Figure 5.2.** Scanning electron micrographs of a cross section of (a) control, (b) FCCT-roasted and (c) oven-roasted wheat kernels, illustrating the (1) whole kernel at a lower magnification (scale bar = 200 µm) and (2) endosperm and (3) aleurone layer at a higher magnification (scale bar = 10 µm). Large A-type and small B-type starch granules are identified with arrows in the endosperm region. P=protein matrix; F= fragmented protein strands.

### X-ray diffraction (XRD)

The control and roasted samples exhibited the characteristic A-type crystalline pattern of cereal starches (Fig. 5.3). Distinct peaks were positioned at around  $2\theta = 15^\circ$ ,  $16.9^\circ$ ,  $17.6^\circ$  and  $22.7^\circ$ , which are representative of a A-type crystalline structure (Dries *et al.*, 2014). Both roasting methods applied elicited only slight changes in crystallinity, with very little variation from the control, which was ascertained based on the XRD patterns (Fig. 5.3). Within the XRD trace of the oven-roasted sample a minor peak V-type peak at around  $20^\circ$  became slightly more apparent, which may reflect the presence of a amylose-lipid complex (Yoo & Jane, 2002). The intensity of the diffractions are dependent on the extent of starch gelatinisation and moisture content (Mahadevamma & Tharanathan, 2007).

Roasting had no significant ( $P>0.05$ ) effect on the crystallinity content. The crystallinity of the control, FCCT and oven-roasted sample was  $10.50\pm0.41\%$ ,  $10.38\pm0.33\%$  and  $10.34\pm0.48\%$ , respectively. The crystallinity content results are in agreement with the XRD pattern obtained, illustrating that crystallinity was preserved after roasting. This little disruption in crystallinity can be due to a combination of low initial moisture content of the wheat samples and the short roasting time. Likewise, Christa *et al.* (2009) also reported that roasting did not modify ( $P>0.05$ ) the crystalline structure of buckwheat starch. This observation was rather astonishing, due to the fact that thermal treatment typically results in a decrease in crystallinity. Thermal damage to starch granules cause a progressive loss of order and therefore a decrease in crystallinity is usually observed.



**Figure 5.3.** XRD traces of the control, FCCT and oven-roasted wheat flour samples. The prominent peaks for A-type crystallinity are indicated with dashed vertical lines.

*Functional properties*Water absorption capacity (WAC), water solubility index (WSI) and flour dispersibility (FD)

Both roasting methods resulted in an increase in WAC, this increase being significant ( $P \leq 0.05$ ) only for the oven-roasted sample (Table 5.3). The lower WAC of the FCCT-sample, compared to the oven-roasted sample, can be attributed to a more compact structure (SEM) due to less starch damage and fragmentation, leading to the inaccessibility of water (Lee *et al.*, 2006). Mossman *et al.* (1973) reported a WAC of 2.1 g/g for raw wheat, whereas hot air roasting increased the WAC to a range of 2.8-4.5 g/g. Damaged or disrupted starch has the ability to absorb more water than native granules due to partial gelatinisation of the starch (Barrera *et al.*, 2013).

The increase in WAC can also be explained by the structure of the endosperm. SEM micrographs of the oven-roasted kernel (Fig. 5.2c) illustrated more and larger voids in the endosperm which increase the water contact area and thus facilitate water absorption. WAC also depends on the availability of hydrophilic groups which can bind water molecules. It can be postulated that roasting increased the accessibility of polar amino acids of the denatured proteins. During roasting the proteins unfold, thereby exposing previously concealed hydration sites; making them more available to interact with water, following increased WAC (Maruatona *et al.*, 2010). An increase in WAC after roasting of cereals and legumes has been reported in previous studies (Gujral *et al.*, 2011; Griffith & Castell-Perez, 1998; Sandhu *et al.*, 2015; Mariotti *et al.*, 2006). Caprez *et al.* (1986) found that roasting had no ( $P \leq 0.05$ ) effect on the WAC of wheat.

Roasting resulted in a decrease, although not significant ( $P > 0.05$ ), in WSI (Table 5.3). This is in agreement with previous studies who also reported a decrease in WSI after roasting buckwheat (Christa *et al.*, 2009) and oats (Gujral *et al.*, 2011). Structural changes within the endosperm and starch granules after roasting may be accountable for the reduction in WSI (Olayinka *et al.*, 2008). Gujral *et al.* (2011) ascribed a reduction in WSI to the formation of amylose–lipid complexes within the starch granules during roasting. A decreased WSI may also be due to a loss of low molecular weight glucosaccharides, i.e. maltose (Holm *et al.*, 1988). The WSI values obtained in Table 5.3 were in agreement with the range of 7 to 10% reported for hot air roasted wheat (Mossman *et al.*, 1973). The inverse trend of increasing WAC and decreasing WSI after thermal treatment was also observed by Zhu *et al.* (2010). FD increased marginally after roasting ( $P > 0.05$ ). Based on earlier work better FD indices (Onilude *et al.*, 1999) were expected.

**Table 5.3.** WAC, WSI and FD of the control and roasted whole wheat flours

Sample	WAC (g/g)	WSI (%)	FD (%)
Control	2.48±0.03 <sup>b</sup>	7.45±0.044 <sup>a</sup>	72.50±0.29 <sup>a</sup>
FCCT	2.50±0.02 <sup>ab</sup>	7.09±0.16 <sup>a</sup>	72.56±0.10 <sup>a</sup>
Oven	2.53±0.01 <sup>a</sup>	7.31±0.06 <sup>a</sup>	72.67±0.17 <sup>a</sup>

Results are mean values ± standard deviation of triplicate determinations (n=3) from three replicates. Mean values followed by different superscripts in each column are significantly different at  $P \leq 0.05$ . WAC= water absorbance capacity; WSI = water solubility index; FD= flour dispersibility.



### Differential scanning calorimetry (DSC)

The DSC thermograms exhibited one distinct endotherm which corresponded to the gelatinisation of the crystalline structure of the control sample and residual structure of the roasted sample (Maache-Rezzoug *et al.*, 2008). The control displayed an endotherm at a  $T_o = 55.10^\circ\text{C}$ ,  $T_p = 59.93^\circ\text{C}$  and  $T_e = 66.60^\circ\text{C}$ , which was comparable to the FCCT and oven-roasted sample, indicating that starch was only partially gelatinised during roasting (Table 5.4). The endothermic peak at  $59.93^\circ\text{C}$  in the control corresponded to the gelatinisation temperature range of  $51$  to  $60^\circ\text{C}$  for wheat (Delcour & Hosney, 2010). The thermal characteristics of the control sample (Table 5.4) were in agreement with the results for native wheat reported earlier (Holm *et al.*, 1988; Yoo & Jane, 2002).

Khan & Yu (2013) studied the thermal degradation behaviour of heat-induced cereal grains when autoclaved (moist heating) and dry-heated (roasted) at  $121^\circ\text{C}$  for 80 min. The endothermic peak of dry-heated cereals shifted towards a higher temperature than for the control and moist-heated sample, indicating the high thermal stability of dry-heated cereals. Similarly, in this study dry hot air oven roasting ( $T_p = 64.73^\circ\text{C}$ ) shifted the endothermic peak towards a higher ( $P \leq 0.05$ ) temperature than for the control ( $T_p = 59.93^\circ\text{C}$ ). FCCT roasting, showed a lower ( $P \leq 0.05$ ) endothermic peak position of  $T_p = 62.77^\circ\text{C}$ . The endotherm transition peak is dependent on moisture content, since moisture causes the endothermic peak to shift to a lower position (Khan & Yu, 2013). Because FCCT roasting uses superheated steam, a lower  $T_p$  was obtained than for oven roasting.

Moisture plays an important role in the overall thermal characteristics, since water exerts a plasticising effect, resulting in a decrease in gelatinisation temperature and increase in  $\Delta H$  values (Mahadevamma & Tharanathan, 2007). The opposite is, however, true for limited moisture situations. With roasting  $\Delta H$  decreased,  $\Delta T$  increased and the gelatinisation endotherm shifted towards higher temperatures than for native starch (Table 5.4). Similar results were reported in the literature for thermally treated maize (Dries *et al.*, 2014) and wheat (Holm *et al.*, 1988). In agreement with the results in Table 5.4, Hoover & Manuel (1996) noted a broadening of the  $\Delta T$  of about  $4$  to  $6^\circ\text{C}$  after thermal treatment of maize. The lower ( $P \leq 0.05$ )  $\Delta H$  of the roasted samples indicates partial starch gelatinisation or pre-gelatinisation (Holm *et al.*, 1988), which was confirmed by the degree of gelatinisation (%) results.

Gelatinisation enthalpy ( $\Delta H$ ) is the energy required to gelatinise starch and is also an indication of the loss of molecular order within starch granules (Dharmaraj *et al.*, 2015). The control sample required more energy for gelatinisation, due to its more crystalline structure. Roasted wheat is partially gelatinised and thus required less energy, which agrees with the observed decrease in  $\Delta H$ . A decrease in  $\Delta H$  also indicate partial loss of protein structure (Ahmed *et al.*, 2007) and are in agreement with the decrease ( $P \leq 0.05$ ) in protein (Table 5.1) reported for the roasted samples. Thus, the decrease in  $\Delta H$  cannot solely be ascribed to starch gelatinisation or protein denaturation, but rather a combination thereof (Ahmed *et al.*, 2007). According to

Bhattacharya & Choudhury (1994) an increase in gelatinisation results in an increase in PI and decrease in bulk density. A similar trend was observed in this study.

The degree of gelatinisation was 10.14% and 17.16% for the FCCT and oven-roasted samples, respectively. The FCCT roasting transition temperatures were more comparable to that of the control, suggesting less starch are gelatinised during FCCT roasting (Table 5.4). Oven roasting resulted in more starch damage, resulting in a higher degree of gelatinisation. This confirmed the SEM observations. Gelatinisation predominates at a moisture content above 20%, with maximum gelatinisation occurring at 28-29% moisture (Case *et al.*, 1992). The low moisture content of the wheat may thus be the contributing factor to the limited degree of gelatinisation (Pronyk *et al.*, 2006), together with the short roasting time. Holm *et al.* (1988) reported only partial gelatinisation in both steam-flaked (22.4%) and dry-autoclaved (48.6%) wheat.

**Table 5.4.** DSC thermal characteristics of the control and roasted whole wheat flours

Sample	T <sub>o</sub> (°C)	T <sub>p</sub> (°C)	T <sub>e</sub> (°C)	ΔH (J/g)	ΔT (°C)	% Gelatinisation
Control	55.10±0.70 <sup>b</sup>	59.93±1.25 <sup>c</sup>	66.60±0.92 <sup>c</sup>	11.83±0.35 <sup>a</sup>	11.50±0.26 <sup>b</sup>	0 <sup>b</sup>
FCCT	58.53±1.01 <sup>a</sup>	62.77±0.70 <sup>b</sup>	70.73±0.55 <sup>b</sup>	10.63±0.38 <sup>b</sup>	12.20±1.55 <sup>b</sup>	10.14±4.34 <sup>a</sup>
Oven	59. ±0.98 <sup>a</sup>	64.73±0.21 <sup>a</sup>	74.17±0.42 <sup>a</sup>	9.80±0.30 <sup>c</sup>	15.17±1.36 <sup>a</sup>	17.16±4.98 <sup>a</sup>

Values are means ± standard deviation of three replicates (n=3). Different letters in the same column indicate significant differences (P≤0.05). T<sub>o</sub>, T<sub>p</sub>, and T<sub>e</sub> indicate onset, peak and endset temperatures, respectively; ΔH = enthalpy of gelatinisation; ΔT (T<sub>e</sub> – T<sub>o</sub>) = gelatinisation temperature range.

#### Pasting properties and α-amylase activity

The RVA profiles for a representative control, FCCT and oven-roasted sample are shown in Figure 5.4. Both roasting methods increased, although non-significantly (P>0.05), the P<sub>temp</sub>, peak time, V<sub>f</sub>, and V<sub>t</sub> (Table 5.5). The V<sub>s</sub> and SN decreased (P>0.05) after roasting. A low V<sub>s</sub>, as observed for the roasted samples, indicate a low rate of starch retrogradation and syneresis (Ragae & Abdel-Aal, 2006). V<sub>p</sub> and V<sub>b</sub> increased (P≤0.05) after oven-roasting and only V<sub>b</sub> increased (P≤0.05) after FCCT roasting. Pasting properties, especially V<sub>p</sub>, influences the texture, quality and acceptability of the end product (Ragae & Abdel-Aal, 2006). Viscosity depends to a large extent on the degree of gelatinisation, where a higher V<sub>p</sub> reflect more degradation and starch gelatinisation (Gupta *et al.*, 2008). The higher V<sub>p</sub> of the oven-roasted sample can be attributed to the higher WAC and degree of gelatinisation reported. V<sub>b</sub> provides an indication of the degree of starch disintegration or paste stability during heating (Bolade, 2009).

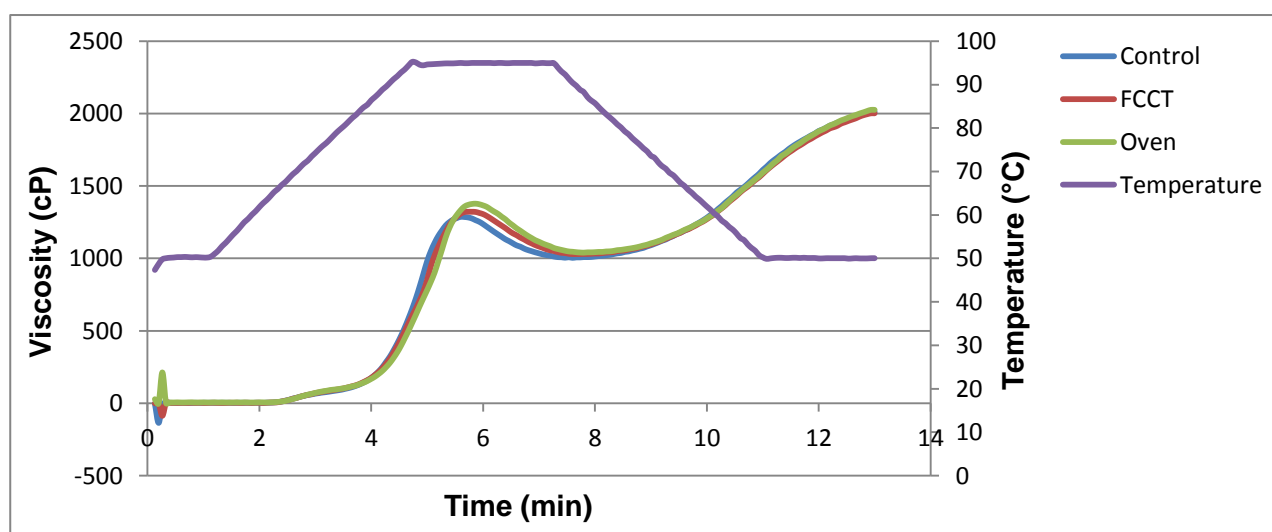
A high V<sub>p</sub> are related to a high V<sub>b</sub>, which are in turn associated with the degree of swelling during heating (Ragae & Abdel-Aal, 2006). This was the case for the roasted samples, which had higher V<sub>p</sub> and V<sub>b</sub> values, in contrast to the control. This trend is explained by the fact that all these properties are reliant on the speed and level of starch granule disintegration, where the control is more resistant and contain less disintegrated starch granules (Muyonga *et al.*, 2014). Damaged starch granules can absorb more water, swell and leach out amylose, resulting in an increased

viscosity (Barrera *et al.*, 2013). Griffith & Castell-Perez (1998) also reported that roasting increased the viscosity of cereals grains. The reduced moisture content in the roasted flours allows a larger concentration of solids by weight, leading to an increased viscosity. The  $V_p$  and  $V_f$  results reported in Table 5.5 falls within the appropriate semiliquid consistency for infant weaning foods which is 1000–3000 cP (Griffith & Castell-Perez, 1998).

In agreement with the results in Table 5.5 and Fig. 5.4, Mossman *et al.* (1973) and Lazar *et al.* (1974) reported that roasting increased the viscosity of wheat flour. This was attributed to partial gelatinisation which enables starch to absorb more water, than in the unprocessed sample. Both FCCT and oven-roasted flours contain partially gelatinised starch (as reported in the DSC section), which hydrates rapidly and contributes to increased viscosities.

Wheat kernel hardness influences gelatinisation and hydration rates and will thus also play a role in viscosity. The harder control sample, which mill to coarse particles, will lead to less water diffusion and limited starch swelling. In contrast the softer, roasted samples, which mill to smaller and finer particles with a larger surface area, will lead to more rapid hydration and thus a higher viscosity (Almeida-Dominguez *et al.*, 1997). Ragae & Abdel-Aal (2006) reported soft whole wheat flour to have higher  $V_p$ ,  $V_t$  and  $V_f$  values, compared to harder wheat.

The level of  $\alpha$ -amylase activity in wheat starch has an effect on the pasting properties of their flours (Ragae & Abdel-Aal, 2006). Sharma *et al.* (2011) reported that starch become more susceptible to enzymatic breakdown after roasting. This was also observed from the results in Table 5.5 where the SN (indicative of the  $\alpha$ -amylase activity) decreased after roasting, indicating more amylase activity. An increase in amylase activity, which promoted gel-like properties of the starch granules, was also reported in a previous study for thermally treated wheat (Błaszczak *et al.*, 2002). Damaged (roasted) starch granules are more susceptible to amylase activity than intact (control) starch granules.



**Figure 5.4.** RVA pasting profiles of a representative (a) control, (b) FCCT-roasted and (c) oven-roasted whole wheat flour. The RVA viscometers reports the viscosity as a function of time together with the temperature ramp.

**Table 5.5.** RVA pasting properties of the control and roasted whole wheat flours

Sample	P <sub>temp</sub> (°C)	Peak time (min)	V <sub>p</sub> (cP)	V <sub>b</sub> (cP)	V <sub>f</sub> (cP)	V <sub>t</sub> (cP)	V <sub>s</sub> (cP)	SN (cP)
Control	86.27±0.42 <sup>a</sup>	5.70±0.01 <sup>a</sup>	1272.56±9.67 <sup>b</sup>	262.12±12.89 <sup>b</sup>	2011.78±21.72 <sup>a</sup>	1010.44±6.19 <sup>a</sup>	1001.34±14.99 <sup>a</sup>	1101.89±68.29 <sup>a</sup>
FCCT	86.26±0.63 <sup>a</sup>	5.79±0.09 <sup>a</sup>	1321.33±47.95 <sup>ab</sup>	293.33±37.63 <sup>a</sup>	2011.89±27.22 <sup>a</sup>	1028.00±27.30 <sup>a</sup>	983.89±6.17 <sup>a</sup>	1074.00±22.52 <sup>a</sup>
Oven	86.59±0.64 <sup>a</sup>	5.78±0.06 <sup>a</sup>	1356.44±15.33 <sup>a</sup>	323.22±20.98 <sup>a</sup>	2019.78±19.46 <sup>a</sup>	1033.22±11.21 <sup>a</sup>	986.56±9.10 <sup>a</sup>	1059.00±16.52 <sup>a</sup>

Results are mean values ± standard deviation of triplicate determinations (n=3). Mean values followed by different superscripts in each column are significantly different at P≤0.05. P<sub>temp</sub>= pasting temperature; V<sub>p</sub>= peak viscosity; V<sub>b</sub> = breakdown viscosity; V<sub>f</sub>= final viscosity; V<sub>t</sub>= trough viscosity; V<sub>s</sub>= setback viscosity and SN= stirring number.

**Table 5.6.** Mixographic and Alveographic indices of the control and roasted whole wheat flours

Dough	Mixographic indices			Alveographic indices			
	Peak time (min)	Water absorption (%)	P (mm)	L (mm)	P/L	W (10 <sup>-4</sup> J)	S (cm <sup>2</sup> )
Control	3.19±0.04 <sup>b</sup>	61.82±0.08 <sup>a</sup>	88.67±3.21 <sup>a</sup>	131.67±3.21 <sup>a</sup>	0.67±0.04 <sup>a</sup>	310.33±11.55 <sup>a</sup>	47.45±5.32 <sup>a</sup>
FCCT-roasted	3.81±0.27 <sup>a</sup>	61.69±0.07 <sup>b</sup>	99.67±8.08 <sup>a</sup>	107±14 <sup>a</sup>	0.95±0.19 <sup>a</sup>	322.67±14.19 <sup>a</sup>	49.34±3.98 <sup>a</sup>
Oven-roasted	3.50±0.43 <sup>a</sup>	61.73±0 <sup>ab</sup>	89.33±8.50 <sup>a</sup>	123.33±22.85 <sup>a</sup>	0.75±0.23 <sup>a</sup>	311±7.94 <sup>a</sup>	47.55±4.75 <sup>a</sup>

Results are mean values ± standard deviation of triplicate determinations (n=3). Mean values followed by different superscripts in each column are significantly different at P≤0.05. P= resistance to extension or tenacity; L= extensibility; P/L= curve configuration ratio, W= deformation energy, S= strength.

### Rheology: Mixograph and Alveograph

Table 5.6 reports the Mixographic and Alveographic indices of dough prepared from the control and roasted flours. During mixing the resistance of dough increases, reaches a maximum and then finally decreases, which can be monitored using a Mixograph. The peak time, indicating the optimum mixing time, increased ( $P \leq 0.05$ ) for the roasted samples. This increase was unexpected since weak gluten flour has a shorter peak time than strong gluten flour. Thus, flour with good breadmaking properties usually have a longer mixing time. It seems as if roasting increased the gluten strength. Longer mixing times can be explained by the significantly ( $P \leq 0.05$ ) lower protein content of the roasted samples, since mixing time increases as protein content decrease (SAGL, 2016). Flour behaviour during mixing is thus a function of protein quality. Caprez *et al.* (1986) also reported that roasting of wheat prolonged the dough mixing time.

The amount of water absorption influences the position of the curve, where less water increases the dough consistency and results in an upward shift of the curve. There was no significant ( $P > 0.05$ ) difference between the water absorption of the FCCT and oven-roasted samples (Table 5.6). The control and roasted flours fall within the acceptable water absorption range of 60.0–64.0% for white bread flour (SAGL, 2016). The water absorption also compares favourably with the 60.8% reported by the SAGL for the 2015/2016 season (SAGL, 2016). Flour with higher water absorption is preferred by bakers since it increases dough yields. Water absorption is influenced by protein content and quality, where a higher protein content results in higher water absorption.

A previous study reported that the addition of roasted/steamed oat flour to wheat flour increased water absorption and resulted in longer mixing times and greater mixing stabilities (Zhang *et al.*, 1998). This improved phenomenon was explained by the ability of roasting to inactivate endogenous enzymes, resulting in less residual endogenous enzymes or other bioactive reducing agents, which can be involved in the dough-weakening effect.

There was no significant ( $P > 0.05$ ) difference between any of the samples in terms of the Alveographic indices (Table 5.6). Acceptable ranges for the Alveographic indices are a P (stability) of 65 – 120 mm, L (extensibility) 80 – 120 mm and P/L of 0.70 – 1.50 (SAGL, 2016). All the measurements were within the requirements except the control and oven-roasted L values and the P/L of the control. Both roasting methods resulted in an increase ( $P > 0.05$ ) in P, P/L, W and S and a decrease ( $P > 0.05$ ) in L. L decrease and P increase with higher levels of damaged starch, which was observed for the roasted samples.

P relates to resistance to deformation. Stronger dough requires more force to break the bubble, resulting in a higher P value and *vice versa*. A high L value indicates a higher extensibility, which is an indication of the ability to stretch before breaking. A low P and W and high L value is indicative of weak gluten flour and is usually preferred for confectionary products, whereas strong gluten flours, preferred for bread, have a high P and W value. A too low L value, indicated by a high P/L, can result in a lower loaf volume. A too high L value are indicative of soft doughs with

excess stretching properties and can also result in low loaf volumes due to poor gas retention (SAGL, 2016). The shorter L of the roasted dough and the slightly higher P value resulted in the observed increase in P/L, indicating that the roasted samples were more resistant to extension.

The FCCT-roasted sample had a P/L very close to one, indicating a good balance between extensibility and elasticity (Table 5.6). A decrease in L after wheat roasting was also observed by Baiano *et al.* (2008) and was attributed to aggregation of wheat proteins and starch induced by roasting. The W and S increased ( $P>0.05$ ) after roasting, representing an increase in dough strength and thus baking strength (SAGL, 2016). W is a measure of the energy required to inflate the bubble until it ruptures. All the samples had a W value of more than 300; which is representative of a very strong flour and better baking quality (Table 5.6).

Baiano *et al.* (2008) reported that roasted whole wheat results in a low W value and a weak gluten network due to protein denaturation and the presence of bran and germ components that interfere with dough development. In contrast, the results reported in Table 5.6 illustrates that roasting resulted in favourable changes and will thus not have a detrimental effect on the rheological properties and might even improve the baking quality.

## Conclusion

The physicochemical, structural and functional properties of whole wheat kernels were examined as a basis for evaluating the effect of FCCT and oven roasting. In terms of the physicochemical properties both roasting methods resulted in a decrease ( $P\leq 0.05$ ) in weight, bulk density, moisture content, flour yield, crude protein and hardness, with these changes being more profound for the oven roasting method. Milling yield and HLM (commercially used for measuring bulk density) was not significantly ( $P>0.05$ ) affected by roasting. The results were in concurrence with Chapter 4 which reported oven roasting to result in more adverse microstructural changes.

SEM illustrated that the starch-protein morphology differed depending on the roasting treatment. Less structural interference were observed in the FCCT-roasted kernel, since there were smaller and less cracks and voids and the granular integrity was maintained, whereas oven roasting resulted in large intergranular voids and disruption of the orderly structure of the endosperm. XRD reported no significant ( $P>0.05$ ) differences in the crystallinity after roasting and this was also illustrated by the similar A-type XRD patterns for the control and roasted samples.

WAC increased ( $P\leq 0.05$ ) after oven roasting, while WSI and FD was not significantly ( $P>0.05$ ) influenced by either roasting methods. DSC provided evidence of changes associated with starch gelatinisation, where the degree of starch gelatinisation was higher during oven roasting. Thermal transition temperatures increased ( $P\leq 0.05$ ), while  $\Delta H$  decreased ( $P\leq 0.05$ ) for both roasted samples. The occurrence of partial gelatinisation was attested by the decrease in gelatinisation enthalpy. DSC results confirmed the SEM observations. Viscosity depends to a large extent on the degree of starch gelatinisation. Pasting behaviour was only moderately affected by roasting, since  $V_p$  and  $V_b$  were the only properties that increased ( $P\leq 0.05$ ). Roasted wheat with increased



viscosities can be used as thickening or gelling agent. The increase ( $P \leq 0.05$ ) in dough development time of the roasted flours can be attributed to protein denaturation as observed by the decrease ( $P \leq 0.05$ ) in protein content. Both roasting methods did not alter ( $P > 0.05$ ) the Alveographic indices, thus the roasted flours will not have detrimental effects on the baking quality.

From all the results it is clear that under similar roasting conditions, oven roasting had more adverse effects. The biggest challenge encountered in oven roasting is uneven heat distribution within the product. This was overcome with the FCCT roaster, as the roasting drum containing the sample was continuously rotating resulting in even heat transfer and thus uniformly roasted wheat which will result in a more acceptable final product. The improved functional properties of the roasted samples, i.e. the higher WAC can be used to delay the staling phenomenon, resulting in softer bread with an extended shelf life. Morphological changes observed could potentially have positive effects on starch availability and digestibility. Roasted flour samples displayed a decrease in gluten extensibility (L), which can improve the baking quality of bread and cakes in terms of the texture, height and volume. Although not significant in all cases, the physicochemical properties were less affected after FCCT roasting, thus FCCT roasting has proven to be the superior roasting method for the production of roasted whole wheat kernels and flour. Further research is, however, required on the development of roasted wheat products and their storage stability as well as the nutritional and sensory characteristics.

## References

- AACC (1999a). AACC International Approved Methods of Analysis, 11th ed. Method 22-08.01. Measurement of  $\alpha$ -amylase Activity with the Rapid Visco Analyser. Approved November 3, 1999. St. Paul, Minnesota, USA: American Association of Cereal Chemists.
- AACC (1999b). AACC International Approved Methods of Analysis, 11th ed. Method 26-50.01. Brabender Quadrumat Jr. (Quadruplex) Method. Approved November 3, 1999. St. Paul, Minnesota, USA: American Association of Cereal Chemists.
- AACC (1999c). AACC International Approved Methods of Analysis, 11th ed. Method 26-95.01. Experimental Milling: Temper Table. Approved November 3, 1999. St. Paul, Minnesota, USA: American Association of Cereal Chemists.
- AACC (1999d). AACC International Approved Methods of Analysis, 11th ed. Method 44-19.01. Moisture- Air-Oven Method, Drying at  $135^\circ$ . Approved November 3, 1999. St. Paul, Minnesota, USA: American Association of Cereal Chemists.
- AACC (1999e). AACC International Approved Methods of Analysis, 11th ed. Method 46-30.01. Crude Protein-Combustion Method. Approved November 3, 1999. St. Paul, Minnesota, USA: American Association of Cereal Chemists.
- AACC (1999f). AACC International Approved Methods of Analysis, 11th ed. Method 54-30.02. Alveograph Method for Soft and Hard Wheat Flour. Approved November 3, 1999. St. Paul, Minnesota, USA: American Association of Cereal Chemists.

- AACC (1999g). AACC International Approved Methods of Analysis, 11th ed. Method 54-40.02. Mixograph Method. Approved November 3, 1999. St. Paul, Minnesota, USA: American Association of Cereal Chemists.
- AACC (1999h). AACC International Approved Methods of Analysis, 11th ed. Method 55-30.01. Particle Size Index for Wheat Hardness. Approved November 3, 1999. St. Paul, Minnesota, USA: American Association of Cereal Chemists.
- AACC (1999i). AACC International Approved Methods of Analysis, 11th ed. Method 56-20.01. Hydration Capacity of Pregelatinized Cereal Products. Approved November 3, 1999. St. Paul, Minnesota, USA: American Association of Cereal Chemists.
- AACC (1999j). AACC International Approved Methods of Analysis, 11th ed. Method 76-21.01. General Pasting Method for Wheat or Rye Flour or Starch Using the Rapid Visco Analyser. Approved November 3, 1999. St. Paul, Minnesota, USA: American Association of Cereal Chemists.
- Ahmed, J., Ramaswamy, H.S., Ayad, A., Alli, I. & Alvarez, P. (2007). Effect of high-pressure treatment on rheological, thermal and structural changes in basmati rice flour slurry. *Journal of Cereal Science*, **46**, 148-156.
- Alessandrini, L., Romani, S., Pinnavaia, G. & Rosa, M.D. (2008). Near infrared spectroscopy: an analytical tool to predict coffee roasting degree. *Analytica Chimica Acta*, **625**, 95-102.
- Almeida-Dominguez, H.D., Suhendro, E.L. & Rooney, L.W. (1997). Factors affecting Rapid Visco Analyser curves for the determination of maize kernel hardness. *Journal of Cereal Science*, **25**, 93-102.
- Altan, A. (2014). Effects of pretreatments and moisture content on microstructure and physical properties of microwave expanded hull-less barley. *Food Research International*, **56**, 126-135.
- Andrejko, D., Grochowicz, J., Goździewska, M. & Kobus, Z. (2011). Influence of infrared treatment on mechanical strength and structure of wheat grains. *Food and Bioprocess Technology*, **4**, 1367-1375.
- Ayatse, J., Eka, O. & Ifon, E. (1983). Chemical evaluation of the effect of roasting on the nutritive value of maize (*Zea mays*, Linn.). *Food Chemistry*, **12**, 135-147.
- Baiano, A., Fares, C., Peri, G., Romaniello, R., Taurino, A.M., Siciliano, P., Gambacorta, G., Lamacchia, C., Pati, S. & Notte, E.L. (2008). Use of a toasted durum whole meal in the production of a traditional Italian pasta: chemical, mechanical, sensory and image analyses. *International Journal of Food Science & Technology*, **43**, 1610-1618.
- Baiano, A., Romaniello, R., Lamacchia, C. & La Notte, E. (2009). Physical and mechanical properties of bread loaves produced by incorporation of two types of toasted durum wheat flour. *Journal of Food Engineering*, **95**, 199-207.
- Barrera, G.N., Bustos, M.C., Iturriaga, L., Flores, S.K., León, A.E. & Ribotta, P.D. (2013). Effect of damaged starch on the rheological properties of wheat starch suspensions. *Journal of Food Engineering*, **116**, 233-239.

- Bhattacharya, S. & Choudhury, G.S. (1994). Twin-screw extrusion of rice flour: effect of extruder length-to-diameter ratio and barrel temperature on extrusion parameters and product characteristics. *Journal of Food Processing and Preservation*, **18**, 389-406.
- Błaszczak, W., Gralik, J., Klockiewicz-Kamińska, E., Fornal, J. & Warchalewski, J. (2002). Effect of  $\gamma$ -radiation and microwave heating on endosperm microstructure in relation to some technological properties of wheat grain. *Food/Nahrung*, **46**, 122-129.
- Boischot, C., Moraru, C. & Kokini, J. (2003). Factors that influence the microwave expansion of glassy amylopectin extrudates. *Cereal Chemistry*, **80**, 56-61.
- Bolade, M.K. (2009). Effect of flour production methods on the yield, physicochemical properties of maize flour and rheological characteristics of a maize-based non-fermented food dumpling. *African Journal of Food Science*, **3**, 288-298.
- Caprez, A., Arrigoni, E., Amadò, R. & Neukom, H. (1986). Influence of different types of thermal treatment on the chemical composition and physical properties of wheat bran. *Journal of Cereal Science*, **4**, 233-239.
- Carrera, Y., Utrilla-Coello, R., Bello-Pérez, A., Alvarez-Ramirez, J. & Vernon-Carter, E.J. (2015). In vitro digestibility, crystallinity, rheological, thermal, particle size and morphological characteristics of pinole, a traditional energy food obtained from toasted ground maize. *Carbohydrate Polymers*, **123**, 246-255.
- Case, S., Hamann, D. & Schwartz, S. (1992). Effect of starch gelatinization on physical properties of extruded wheat and corn based products. *Cereal Chemistry*, **69**, 401-404.
- Chandrasekhar, P. & Chattopadhyay, P. (1990). Studies on microstructural changes of parboiled and puffed rice. *Journal of Food Processing and Preservation*, **14**, 27-37.
- Christa, K., Soral-Smietana, M. & Lewandowicz, G. (2009). Buckwheat starch: structure, functionality and enzyme in vitro susceptibility upon the roasting process. *International Journal of Food Sciences and Nutrition*, **60**, 140-154.
- Chung, H.S., Chung, S.K. & Youn, K.S. (2011). Effects of roasting temperature and time on bulk density, soluble solids, browning index and phenolic compounds of corn kernels. *Journal of Food Processing and Preservation*, **35**, 832-839.
- Delcour, J. & Hosene, R.C. (2010). *Principles of Cereal Science and Technology*. 3rd ed. St. Paul, Minnesota, USA: AACC International Press.
- Dharmaraj, U., Meera, M., Reddy, S.Y. & Malleshi, N.G. (2015). Influence of hydrothermal processing on functional properties and grain morphology of finger millet. *Journal of Food Science and Technology*, **52**, 1361-1371.
- Ding, Q.-B., Ainsworth, P., Plunkett, A., Tucker, G. & Marson, H. (2006). The effect of extrusion conditions on the functional and physical properties of wheat-based expanded snacks. *Journal of Food Engineering*, **73**, 142-148.

- Dobraszczyk, B., Whitworth, M., Vincent, J. & Khan, A. (2002). Single kernel wheat hardness and fracture properties in relation to density and the modelling of fracture in wheat endosperm. *Journal of Cereal Science*, **35**, 245-263.
- Dries, D., Gomand, S., Goderis, B. & Delcour, J. (2014). Structural and thermal transitions during the conversion from native to granular cold-water swelling maize starch. *Carbohydrate Polymers*, **114**, 196-205.
- Edema, M.O., Sanni, L.O. & Sanni, A.I. (2005). Evaluation of maize-soybean flour blends for sour maize bread production in Nigeria. *African Journal of Biotechnology*, **4**, 911-918.
- Frisullo, P., Laverse, J., Barnabà, M., Navarini, L. & Del Nobile, M. (2012). Coffee beans microstructural changes induced by cultivation processing: an X-ray microtomographic investigation. *Journal of Food Engineering*, **109**, 175-181.
- Gahlawat, P. & Sehgal, S. (1993). The influence of roasting and malting on the total and extractable mineral contents of human weaning mixtures prepared from Indian raw materials. *Food Chemistry*, **46**, 253-256.
- Gelmez, N., Kincal, N.S. & Yener, M.E. (2009). Optimization of supercritical carbon dioxide extraction of antioxidants from roasted wheat germ based on yield, total phenolic and tocopherol contents, and antioxidant activities of the extracts. *The Journal of Supercritical Fluids*, **48**, 217-224.
- Griffith, L. & Castell-Perez, M. (1998). Effects of roasting and malting on physicochemical properties of select cereals and legumes. *Cereal Chemistry*, **75**, 780-784.
- Guelpa, A., Bevilacqua, M., Marini, F., O'Kennedy, K., Geladi, P. & Manley, M. (2015). Application of Rapid Visco Analyser (RVA) viscograms and chemometrics for maize hardness characterisation. *Food Chemistry*, **173**, 1220-1227.
- Gujral, H.S., Sharma, P. & Rachna, S. (2011). Effect of sand roasting on beta glucan extractability, physicochemical and antioxidant properties of oats. *LWT-Food Science and Technology*, **44**, 2223-2230.
- Gupta, M., Bawa, A.S. & Semwal, A.D. (2008). Effect of barley flour on development of rice-based extruded snacks. *Cereal Chemistry*, **85**, 115-122.
- Guzmán, A.Q., Flores, M.E.J., Escobedo, R.M., Guerrero, L.C. & Feria, J.S. (2009). Changes on the structure, consistency, physicochemical and viscoelastic properties of corn (*Zea mays* sp.) under different nixtamalization conditions. *Carbohydrate Polymers*, **78**, 908-916.
- Hafsa, I., Mandato, S., Ruiz, T., Schuck, P., Jeantet, R., Mejean, S., Chevallier, S. & Cuq, B. (2015). Impact of the agglomeration process on structure and functional properties of the agglomerates based on the durum wheat semolina. *Journal of Food Engineering*, **145**, 25-36.
- Head, D., Cenkowski, S., Arntfield, S. & Henderson, K. (2010). Superheated steam processing of oat groats. *LWT-Food Science and Technology*, **43**, 690-694.

- Hernández-Borges, J., González-Hernández, G., Borges-Miquel, T. & Rodríguez-Delgado, M.A. (2005). Determination of antioxidants in edible grain derivatives from the Canary Islands by capillary electrophoresis. *Food Chemistry*, **91**, 105-111.
- Hoke, K., Houška, M., Průchová, J., Gabrovská, D., Vaculová, K. & Paulíčková, I. (2007). Optimisation of puffing naked barley. *Journal of Food Engineering*, **80**, 1016-1022.
- Holm, J., Björck, I. & Eliasson, A.C. (1988). Effects of thermal processing of wheat on starch: I. Physico-chemical and functional properties. *Journal of Cereal Science*, **8**, 249-260.
- Hoover, R. & Manuel, H. (1996). The effect of heat-moisture treatment on the structure and physicochemical properties of normal maize, waxy maize, dull waxy maize and amylomaize v starches. *Journal of Cereal Science*, **23**, 153-162.
- Idrus, N.F.M. & Yang, T.A. (2012). Comparison between roasting by superheated steam and by convection on changes in colour, texture and microstructure of peanut (*Arachis hypogaea*). *Food Science and Technology Research*, **18**, 515-524.
- Ingbian, E.K. & Adegoke, G.O. (2007). Proximate compositions, pasting and rheological properties of mumu—a roasted maize meal. *International Journal of Food Science & Technology*, **42**, 762-767.
- Işikli, N.D., Şenol, B. & Çoksöyler, N. (2014). Some physical and mechanical properties of roasted zerun wheat. *Journal of Food Science and Technology*, **51**, 1990-1997.
- Kabak, B. (2009). The fate of mycotoxins during thermal food processing. *Journal of the Science of Food and Agriculture*, **89**, 549-554.
- Kahyaoglu, L.N., Sahin, S. & Sumnu, G. (2010). Physical properties of parboiled wheat and bulgur produced using spouted bed and microwave assisted spouted bed drying. *Journal of Food Engineering*, **98**, 159-169.
- Khan, M.M.R. & Yu, P. (2013). Thermal stability and molecular microstructure of heat-induced cereal grains, revealed with Raman molecular microspectroscopy and differential scanning calorimetry. *Journal of Agricultural and Food Chemistry*, **61**, 6495-6504.
- Khan, N., Zaman, R. & Elahi, M. (1986). Effect of processing on the phytic acid content of wheat products. *Journal of Agricultural and Food Chemistry*, **34**, 1010-1012.
- Kong, L. & Baik, B.K. (2016). Degree of starchy endosperm separation from bran as a milling quality trait of wheat grain. *Journal of Cereal Science*, **69**, 49-56.
- Lazar, M., Mossman, A. & Wallace, J. (1974). Air-fluidized toasting of whole kernel wheat-processing variables and functional properties for food applications. *Journal of Food Science*, **39**, 239-243.
- Lee, K.M., Bean, S.R., Alavi, S., Herrman, T.J. & Waniska, R.D. (2006). Physical and biochemical properties of maize hardness and extrudates of selected hybrids. *Journal of Agricultural and Food Chemistry*, **54**, 4260-4269.



- Maache-Rezzoug, Z., Zarguili, I., Loisel, C., Queveau, D. & Buleon, A. (2008). Structural modifications and thermal transitions of standard maize starch after DIC hydrothermal treatment. *Carbohydrate Polymers*, **74**, 802-812.
- Mahadevamma, S. & Tharanathan, R. (2007). Processed rice starch characteristics and morphology. *European Food Research and Technology*, **225**, 603-612.
- Mariotti, M., Alamprese, C., Pagani, M.A. & Lucisano, M. (2006). Effect of puffing on ultrastructure and physical characteristics of cereal grains and flours. *Journal of Cereal Science*, **43**, 47-56.
- Maruatona, G.N., Duodu, K.G. & Minnaar, A. (2010). Physicochemical, nutritional and functional properties of marama bean flour. *Food Chemistry*, **121**, 400-405.
- Maskan, M. (2002). Effect of processing on hydration kinetics of three wheat products of the same variety. *Journal of Food Engineering*, **52**, 337-341.
- Mossman, A., Rockwell, W. & Fellers, D. (1973). Hot air toasting and rolling whole wheat effect on organoleptic, physical and nutritional quality. *Journal of Food Science*, **38**, 879-884.
- Murthy, K.V., Ravi, R., Keshava Bhat, K. & Raghavarao, K.S.M.S. (2008). Studies on roasting of wheat using fluidized bed roaster. *Journal of Food Engineering*, **89**, 336-342.
- Muyonga, J.H., Andabati, B. & Ssepuuya, G. (2014). Effect of heat processing on selected grain amaranth physicochemical properties. *Food Science & Nutrition*, **2**, 9-16.
- Mwangwela, A.M., Waniska, R.D. & Minnaar, A. (2007). Effect of micronisation temperature (130 and 170°C) on functional properties of cowpea flour. *Food Chemistry*, **104**, 650-657.
- Oboh, G., Ademiluyi, A.O. & Akindahunsi, A.A. (2010). The effect of roasting on the nutritional and antioxidant properties of yellow and white maize varieties. *International Journal of Food Science & Technology*, **45**, 1236-1242.
- Ohm, J., Chung, O. & Deyoe, C. (1998). Single-kernel characteristics of hard winter wheats in relation to milling and baking quality 1. *Cereal Chemistry*, **75**, 156-161.
- Olayinka, O.O., Adebawale, K.O. & Olu-Owolabi, B.I. (2008). Effect of heat-moisture treatment on physicochemical properties of white sorghum starch. *Food Hydrocolloids*, **22**, 225-230.
- Onilude, A., Sanni, A. & Ighalo, M. (1999). Effect of process improvement on the physico-chemical properties of infant weaning food from fermented composite blends of cereal and soybeans. *Plant Foods for Human Nutrition*, **54**, 239-250.
- Pronyk, C., Cenkowski, S. & Abramson, D. (2006). Superheated steam reduction of deoxynivalenol in naturally contaminated wheat kernels. *Food Control*, **17**, 789-796.
- Pronyk, C., Cenkowski, S. & Muir, W. (2004). Drying foodstuffs with superheated steam. *Drying Technology*, **22**, 899-916.
- Ragaei, S. & Abdel-Aal, E.S.M. (2006). Pasting properties of starch and protein in selected cereals and quality of their food products. *Food Chemistry*, **95**, 9-18.
- Raigar, R.K., Prabhakar, P.K. & Srivastav, P.P. (2016). Effect of different thermal treatments on grinding characteristics, granular morphology and yield of ready-to-eat wheat grits. *Journal of Food Process Engineering*, doi:10.1111/jfpe.12363.



- Ranganathan, V., Nunjundiah, I.T. & Bhattacharya, S. (2014). Effect of roasting on rheological and functional properties of sorghum flour. *Food Science and Technology International*, **20**, 579-589.
- Rothschild, J., Rosentrater, K.A., Onwulata, C., Singh, M., Menutti, L., Jambazian, P. & Omary, M.B. (2015). Influence of quinoa roasting on sensory and physicochemical properties of allergen-free, gluten-free cakes. *International Journal of Food Science & Technology*, **50**, 1873-1881.
- SAGL. (2016). 2015-2016 Wheat Crop Report- SAGL [Internet document]. URL [www.sagl.co.za](http://www.sagl.co.za) › Wheat › Wheat reports. Accessed 09/09/2016.
- Sandhu, K.S., Godara, P., Kaur, M. & Punia, S. (2015). Effect of toasting on physical, functional and antioxidant properties of flour from oat (*Avena sativa* L.) cultivars. *Journal of the Saudi Society of Agricultural Sciences*, <http://dx.doi.org/10.1016/j.jssas.2015.06.004>.
- Schoeman, L., Du Plessis, A. & Manley, M. (2016a). Non-destructive characterisation and quantification of the effect of conventional oven and forced convection continuous tumble (FCCT) roasting on the three-dimensional microstructure of whole wheat kernels using X-ray micro-computed tomography ( $\mu$ CT). *Journal of Food Engineering*, **187**, 1-13.
- Schoeman, L., Williams, P., Du Plessis, A. & Manley, M. (2016b). X-ray micro-computed tomography ( $\mu$ CT) for non-destructive characterisation of food microstructure. *Trends in Food Science & Technology*, **47**, 10-24.
- Sharma, P. & Gujral, H.S. (2011). Effect of sand roasting and microwave cooking on antioxidant activity of barley. *Food Research International*, **44**, 235-240.
- Sharma, P., Gujral, H.S. & Rosell, C.M. (2011). Effects of roasting on barley  $\beta$ -glucan, thermal, textural and pasting properties. *Journal of Cereal Science*, **53**, 25-30.
- Van Hung, P., Maeda, T. & Morita, N. (2006). Waxy and high-amylose wheat starches and flours- characteristics, functionality and application. *Trends in Food Science & Technology*, **17**, 448-456.
- Yoo, S.-H. & Jane, J.-L. (2002). Structural and physical characteristics of waxy and other wheat starches. *Carbohydrate Polymers*, **49**, 297-305.
- Zhang, D., Moore, W. & Doehlert, D. (1998). Effects of oat grain hydrothermal treatments on wheat-oat flour dough properties and breadbaking quality. *Cereal Chemistry*, **75**, 602-605.
- Zhu, L.-J., Shukri, R., De Mesa-Stonestreet, N.J., Alavi, S., Dogan, H. & Shi, Y.-C. (2010). Mechanical and microstructural properties of soy protein-high amylose corn starch extrudates in relation to physiochemical changes of starch during extrusion. *Journal of Food Engineering*, **100**, 232-238.
- Zielinski, H., Michalska, A., Amigo-Benavent, M., Del Castillo, M.D. & Piskula, M.K. (2009). Changes in protein quality and antioxidant properties of buckwheat seeds and groats induced by roasting. *Journal of Agricultural and Food Chemistry*, **57**, 4771-4776.

Zzaman, W. & Yang, T.A. (2013). Effect of superheated steam and convection roasting on changes in physical properties of cocoa bean (*Theobroma cacao*). *Food Science and Technology Research*, **19**, 181-186.

**Declaration by the candidate:**

With regard to Chapter 6 (pp. 147-174), the nature and scope of my contribution were as follows:

Nature of contribution	Extent of contribution (%)
Research, analysis and writing of chapter	71

The following co-authors have contributed to Chapter 6 (pp. 147-174):

Name	e-mail address	Nature of contribution	Extent of contribution (%)
Prof Marena Manley	mman@sun.ac.za	Research inputs, editorial suggestions and proofreading	15
Dr Anton du Plessis	anton2@sun.ac.za	Assistance with skeletonization and proofreading	5
Prof Pieter Verboven	pieter.verboven@kuleuven.be	Editorial suggestions and proofreading	3
Prof Bart Nicolaï	bart.nicolai@kuleuven.be	Editorial suggestions and proofreading	3
Dennis Cantre	dennis.cantre@kuleuven.be	Assistance with skeletonization	3

Signature of candidate: L. Schoeman

Date: 30/11/2016

**Declaration by co-authors:**

The undersigned hereby confirm that

1. the declaration above accurately reflects the nature and extent of the contributions of the candidate and the co-authors to Chapter 6 (pp. 147-174),
2. no other authors contributed to Chapter 6 (pp. 147-174) besides those specified above, and
3. potential conflicts of interest have been revealed to all interested parties and that the necessary arrangements have been made to use the material in Chapter 6 (pp. 147-174) of this dissertation.

Signature	Institutional affiliation	Date
Prof Marena Manley	Department of Food Science, Stellenbosch University	30/11/2016
Dr Anton du Plessis	CT Scanner Facility, Stellenbosch University	30/11/2016
Prof Pieter Verboven	Division of Mechatronics, Biostatistics and Sensors (MeBioS), KU Leuven	30/11/2016
Prof Bart Nicolaï	Division of Mechatronics, Biostatistics and Sensors (MeBioS), KU Leuven	30/11/2016
Dennis Cantre	Division of Mechatronics, Biostatistics and Sensors (MeBioS), KU Leuven	30/11/2016

Declaration with signature in possession of candidate and supervisor.

## CHAPTER 6

### Effect of oven and forced convection continuous tumble (FCCT) roasting on the microstructure and dry milling properties of white maize\*

#### Abstract

The effect of oven and forced convection continuous tumble (FCCT) roasting on the microstructure of whole maize kernels was characterised and quantified using X-ray micro-computed tomography ( $\mu$ CT). The three-dimensional (3D) volumes, reconstructed from the two-dimensional (2D) images, were segmented into regions-of-interest (ROIs), i.e. air, germ, floury and vitreous endosperm, and each region quantified. Oven roasting was associated with a larger increase in total kernel volume (10.76%) than FCCT roasting (3.41%) as well as a significant ( $P \leq 0.05$ ) decrease in whole kernel relative density (oven = 6.33%; FCCT = 1.92%). FCCT roasting had almost no effect on material density, in contrast to a significant ( $P \leq 0.05$ ) decrease of 4.97% during oven roasting. The less destructive nature of FCCT roasting was probably due to the continuous rotation of the grains, resulting in even heat transfer and more homogenous roasting. Subsequent validation of the dry milling properties, i.e. percentage hominy chop, milling yield and hectolitre mass (HLM), indicated no significantly ( $P > 0.05$ ) detrimental effect by either roasting methods.

*Industrial relevance:* Roasting of maize can improve sensory, shelf life, nutritional and antioxidant properties with subsequent use in ready-to-eat foods and breakfast cereals. Roasting will inevitably affect the structure of maize which in turn will impact end product quality. This prompted the demand for non-destructive techniques that directly measures microstructural properties of food in order to link structure with quality. X-ray  $\mu$ CT in combination with image analysis uniquely illustrated the microstructural changes occurring during conventional oven and innovative FCCT roasting, respectively. Furthermore, dry milling properties are important indicators of quality characteristics for the dry milling industry. The method described in this paper can be applied to any food material to investigate structural properties.

*Keywords:* Maize kernels; Roasting; Microstructure; Dry milling properties; X-ray micro-computed tomography; Image analysis

---

\*Submitted for publication as: Schoeman, L., Du Plessis, A., Verboven, P., Nicolai, B., Cantre, D. & Manley, M. (2016). Effect of oven and forced convection continuous tumble (FCCT) roasting on the microstructure and dry milling properties of white maize. *Innovative Food Science & Emerging Technologies*.

## Introduction

Maize (*Zea mays* L.) is one of the largest and most important crops produced worldwide contributing to an annual yield of over 1 milliard ton in 2013 (FAOSTAT, 2015). A maize kernel consists of four main parts, i.e. endosperm (80-85%), germ (10-14%), pericarp (5-6%) and aleurone layer (2-3%) (Delcour & Hoskeney, 2010). Typical processed foods produced from maize include breads, breakfast cereals, tortillas, corn chips and snack bars. Depending on the locality and ethnic group, maize can also be prepared and consumed in a variety of other ways, i.e. sundried, fermented, cooked, pounded or roasted (Obboh *et al.*, 2010). Lately there is an increasing demand for crunchy snack products and competition for improved products is developing in the industrial sector (Mrad *et al.*, 2014). Roasting is a dry thermal treatment, traditionally and still being used today for the preparation of healthy, crunchy maize snacks (Mrad *et al.*, 2014). Flour obtained from roasted ground maize is also consumed by diverse ethnic groups in Northern Mexico and Southern USA (Carrera *et al.*, 2015). Roasted cereal grains, with improved organoleptic, shelf life, nutritional as well as antioxidant properties, can easily be incorporated into ready-to-eat foods and breakfast cereals (Obboh *et al.*, 2010; Murthy *et al.*, 2008; Chung *et al.*, 2011; Gujral *et al.*, 2013). On the other hand, severe roasting conditions could cause damage to chemical components (i.e. polyphenols and anthocyanin) thereby decreasing their anti-oxidative activity (Mrad *et al.*, 2014).

In Southern Africa dry milling is used to produce products such as samp, maize grits and meal for human consumption. Roasting could potentially serve as a pre-processing step to enable the use of less energy for milling, to produce value-added products, or to extend the shelf life of products. Roasting of sorghum grains increased the water absorbing capacity for the preparation of instant mixes and porridges (Ranganathan *et al.*, 2014). In a recent study, pinole, a traditional energy food obtained from toasted ground maize, was shown to result in a significant increase in total available starches and *in vitro* hydrolysis rate (Carrera *et al.*, 2015), making it a suitable ingredient for specialised energy cereal bar products.

Roasting influences cereal grains by making kernels softer due to the loss of endosperm structure and increased porosity (Murthy *et al.*, 2008), which could be beneficial depending on the processing method and desired final product. There has been an increasing interest in the use of roasted grains in food products due to potential health benefits such as improved digestibility (Krings & Berger, 2001) and bioavailability of minerals because of the greater loss in phytic acid during roasting (Khan *et al.*, 1991). Roasting is considered one of the most effective methods of reducing aflatoxin levels (Kabak, 2009). It does, however, affect the quality and structure of grains, as their functional, technological, physiochemical and nutritional properties are strongly affected by structure-property relationships (Frisullo *et al.*, 2012). This has spurred the need for non-destructive techniques to characterise and quantify microstructural changes.

Microscopic techniques such as scanning electron microscopy (SEM) and transmission electron microscopy (TEM) are usually used to examine the internal structure of products (Suresh & Neethirajan, 2015). These methods are, however, invasive and destructive as they require

sample preparation, which may in addition lead to the formation of artefacts. Three-dimensional (3D) microstructural information of foods is more suited to a better understanding of food properties to, from an engineering perspective, correctly determine processing parameters. X-ray micro-computed tomography ( $\mu$ CT) is a non-destructive and non-invasive imaging technique that can be used for high-resolution 3D visualisation and characterisation of the internal morphology of a wheat sample (Suresh & Neethirajan, 2015). X-ray  $\mu$ CT is less costly and more convenient than MRI (Lammertyn *et al.*, 2003; Herremans *et al.*, 2014). Although both methods do not require sample preparation or chemical fixation, X-ray  $\mu$ CT, in addition, enables analysing and visualising the structural design of cellular materials down to a few micrometres (Maire & Withers, 2014) and now also into the submicron range (nano-tomography) (Withers, 2007). Furthermore, X-ray  $\mu$ CT measures density whereas MRI provides information on the water content and mobility (Herremans *et al.*, 2014).

Lately, X-ray  $\mu$ CT has been the subject of numerous research articles on non-invasive quantitative and qualitative analysis of the internal quality of agricultural products (Herremans *et al.*, 2013). It has also been used to study the structure of porous cereal products (Van Dalen *et al.*, 2007), rice (Zhu *et al.*, 2012; Witek *et al.*, 2010), foams (Lim & Barigou, 2004), extruded products (Zhu *et al.*, 2010), bread (Lassoued *et al.*, 2007), wheat flour dough (Bellido *et al.*, 2006), fruit tissue (Mendoza *et al.*, 2007; Verboven *et al.*, 2008; Cantre *et al.*, 2014a; Cantre *et al.*, 2014b; Herremans *et al.*, 2015), chocolate (Haedelt *et al.*, 2007) and processed meat (Frisullo *et al.*, 2010). Individual maize kernel volume and density could be accurately measured using this technique (Gustin *et al.*, 2013; Guelpa *et al.*, 2015b). An earlier study comprehensively reviewed the use of X-ray  $\mu$ CT for characterisation of food microstructure (Schoeman *et al.*, 2016b).

A recent study demonstrated the effectiveness of X-ray  $\mu$ CT to non-destructively evaluate the effect of forced convection continuous tumble (FCCT) and oven roasting on the microstructure of wheat (Schoeman *et al.*, 2016a). Oven roasting resulted in more adverse microstructural changes (increased porosity and decreased relative density) observed in the endosperm, when whole wheat grains were roasted at the same time and temperature combination. In contrast to wheat, maize endosperm comprises two types, i.e. vitreous and floury. Hard maize kernels with a larger proportion of the denser vitreous endosperm are favoured by the dry milling industry as it produces greater milling yield and higher quality meals and grits than softer maize. Large intact grits, which are essentially the vitreous endosperm removed from the kernel, are required for cornflake production. In the case of maize it is thus important to evaluate the effect of roasting on the two respective endosperm matrices separately.

Dry milling quality is determined by percentage hominy chop, milling yield and hectolitre mass (HLM). The percentage hominy chop is considered to be one of the most appropriate methods to determine milling quality (Guelpa *et al.*, 2015a). Good milling characteristics are indicated by a small percentage hominy chop. Hominy chop (containing pericarp, tip cap, germ and some endosperm) is of lesser value than maize meal and grits and it is mainly used as animal feed. A



large hominy chop (above 30%) is delivered by maize that mill poorly (typically soft maize kernels) since floury endosperm breaks down easily and is also included into the chop. A good milling quality maize would have a hominy chop below 22%.

Milling yield or extraction is the percentage of meal obtained after dry milling and is one of the most important factors for millers. A higher value indicates a higher extraction of high-grade and most profitable products e.g. samp and grits (de-germed products) that are manufactured from the vitreous part of the endosperm (SAGL, 2016). Kernel hardness affects the quality and quantity of the milled products. Roasted cereal grains may influence milling yield since they are generally characterised by decreased kernel hardness due to the increased internal porosity of the endosperm (Raigar *et al.*, 2016). HLM gives a good indication of potential milling quality as there is a positive correlation between HLM, milling yield and kernel hardness (Guelpa *et al.*, 2015a).

The aim of this study was to quantify and visualise the effect of oven and FCCT roasting on the microstructure of whole maize kernels in terms of volume, porosity and relative density of whole maize kernels, the vitreous and floury endosperm and other selected regions-of-interest (ROIs). Analytical validation of the effect of roasting on dry milling properties was illustrated by means of HLM, hominy chop and milling yield.

## Materials and methods

### *Maize samples*

Twenty whole maize kernels were randomly selected from a white maize sample, kindly provided by PANNAR Seeds (Greytown, South Africa). To allow direct comparison, the same kernels were imaged with X-ray  $\mu$ CT before (control) and after roasting. Ten kernels were subjected to oven roasting and ten to FCCT roasting. The kernels were weighed before and after roasting to determine the percentage weight loss and stored in airtight containers at ambient temperature.

### *Roasting*

Maize samples were roasted at 180°C for 140 s (see Appendix C) using two roasting techniques: conventional convection oven roasting (831 Electric Multifunction Thermofan Solid Plate Oven, Defy Appliances, Durban, South Africa) and patented FCCT roasting (Roastech, Bloemfontein, South Africa). A temperature of 180°C is commonly used for roasting cereal grains (Chung *et al.*, 2011).

During FCCT roasting the roasting time can be controlled by means of the rotating speed of the screw conveyer inside the roasting chamber. A speed setting of 80 Hz is equivalent to 140 s. The individual kernels were numbered for direct comparison of the X-ray images before and after roasting for both methods. Each white maize kernel was roasted, mixed in a 200 g yellow maize sample. The ten kernels were roasted individually for each roasting method, thus ten replicates per roasting treatment. High thermal efficiency is achieved during FCCT roasting since the steam is circulated and re-used during the roasting operation.

For the FCCT roaster a 15 min start-up time was permitted to obtain steady-state conditions before roasting. The conventional convection oven was pre-heated to 180°C before placing the numbered kernel together with 200 g of yellow maize on a stainless steel baking tray and into the oven. The fan of the convection oven circulated the heat throughout the interior of the oven and a portable thermometer was placed inside the oven to measure the air temperature. After roasting the samples were immediately cooled to ambient temperature by spreading it on a cold surface to stop exothermic reactions and further moisture loss. The samples were stored in airtight containers (at ambient temperature) until X-ray  $\mu$ CT image acquisition.

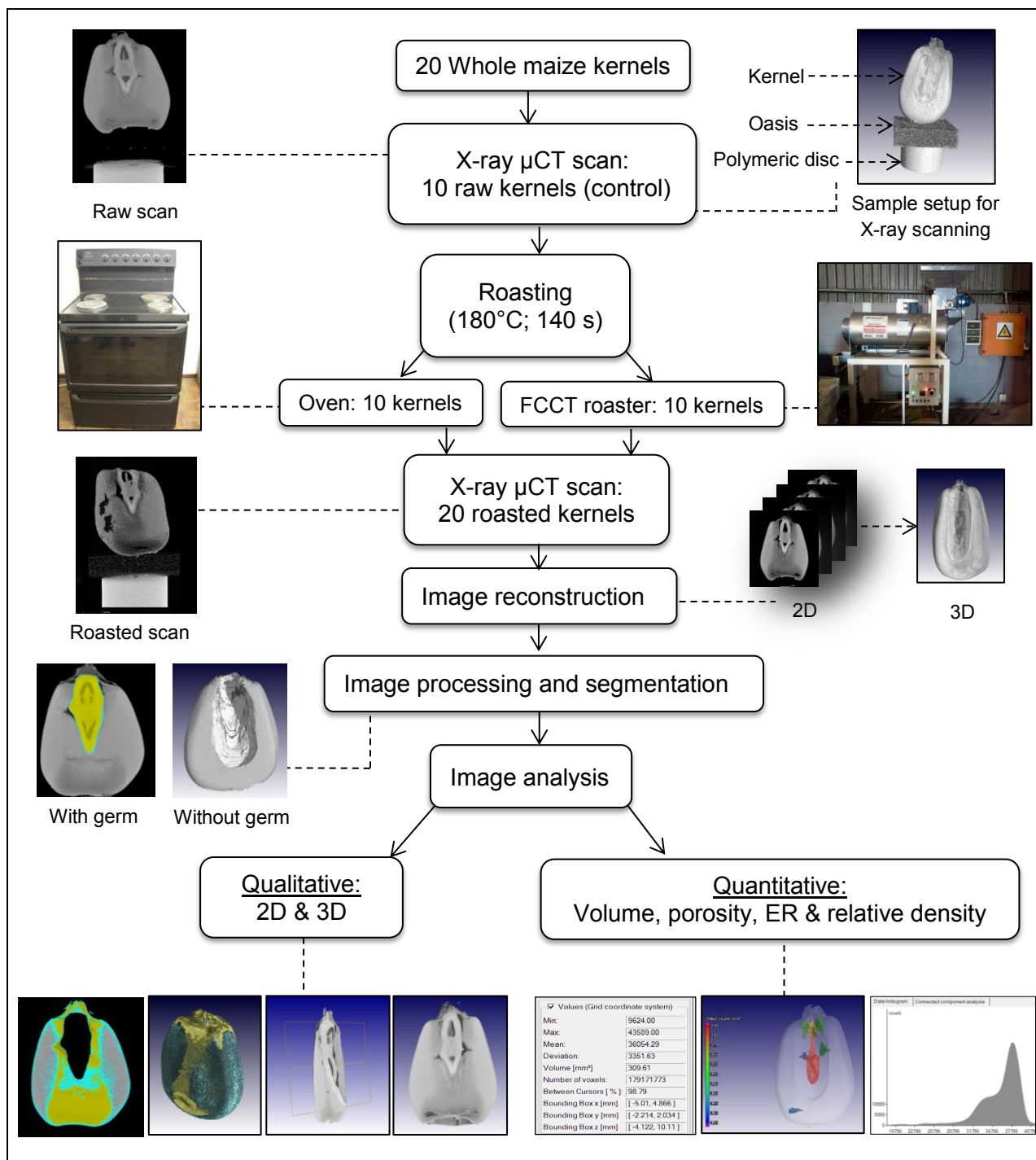
#### *X-ray micro-computed tomography ( $\mu$ CT) image acquisition*

All maize kernels were individually imaged under identical conditions. X-ray  $\mu$ CT scans of the raw and roasted whole maize kernels were obtained using a General Electric Phoenix V|Tome|X L240 (General Electric Sensing & Inspection Technologies GmbH, Phoenix, Wunstorf, Germany) high-resolution X-ray computed tomography (CT) system (see Appendix D). CT scans (tomograms) with a voxel size (resolution) of 12  $\mu$ m were obtained using the scanning parameters described by Schoeman *et al.* (2016a). See Appendix E for optimisation of X-ray  $\mu$ CT scanning parameters. These settings were used since it resulted in high quality images while considering both resolution and scanning time. Images were captured using a 16-bit flat-panel X-ray detector (2048 x 2048 pixels). A series of 2D radiographic X-ray images were acquired during rotation, with 500 milliseconds (ms) exposure time per image, recording 1500 images in one rotation. Detector shift was activated to minimise ring artefacts. Background calibration was performed and the scan time was approximately 25 min per scan.

Figure 6.1 details the experimental design for determining the effect of roasting on the microstructure of whole maize kernels. Each maize kernel was mounted vertically on a piece of oasis (floral foam) and a polytetrafluoroethylene (PTFE) polymer disc (10 mm thickness and 25 mm diameter), obtained from Maizey Plastics (Cape Town, South Africa), on the translation stage (see sample setup in Fig. 6.1). The polymeric disc (density of 2.15 g/cm<sup>3</sup>) was used as reference standard for relative density determinations and was thus scanned in the field-of-view (FOV).

#### *Image processing and analyses*

Image processing and analyses were performed as described by Schoeman *et al.* (2016a). Reconstruction was done using system-supplied Datos reconstruction software (Datos|x® 2.1, General Electric Sensing & Inspection Technologies GmbH, Phoenix, Wunstorf, Germany). This software reconstructs the 2D X-ray projection images into a 3D volume (Fig. 6.1), which consisted of individual voxels (3D pixels) that was mapped to a 16-bit grey value scale (see Appendix F).



**Figure 6.1.** Flow diagram of experimental design for determining the effect of oven and FCCT roasting on the microstructure of whole maize kernels using X-ray  $\mu$ CT and image analysis.

Low density materials attenuate X-rays less than high density components which correspond to low and high grey scale values, respectively (also see Appendix G). In this case the grey values depended on the densest object in the scan volume, which is the polymer disc. Gauss filtering and beam-hardening correction steps were applied to suppress random noise and beam hardening artefacts, respectively. Image analysis was performed with Volume Graphics VGStudio Max 2.2 software (Volume Graphics, Heidelberg, Germany). Before quantification of microstructural parameters, the following image analysis steps were performed: creation of axial images (cross-

sectional slices); segmentation of grey level images; defining and extraction of ROIs; and lastly 3D analysis to calculate structural properties and morphological descriptors.

Additional high resolution scans were performed on the interface section between the two endosperm matrices of three respective raw, FCCT and oven-roasted maize kernels using a Phoenix Nanotom S system (General Electric Sensing and Inspection Technologies / Phoenix X-ray, Wunstorf, Germany). An accelerating voltage of 60 kV and current of 200  $\mu$ A was required to obtain a resolution of 2  $\mu$ m. The resulting scan time was 1 h. Skeletonization was performed on these images using Avizo 9.0 software (VSG, Bordeaux, France). The skeletonization algorithm was applied to a binary smoothed version of the segmented image to generate a 3D spatial distribution which indicates the topology, geometry and connectivity of the porous network in the extracted skeleton. The software computes (model) the skeleton by generating points (nodes) at every porous region and then interconnects these nodes by lines, referred to as segments. This algorithm find, label and track the medial axis of the porous network and is therefore a simplified representation of the centre lines of the air paths. The segments were colour coded based on their thickness.

#### Segmentation and defining ROIs

The Simple registration tool was used to align cross-sectional slice images in VGStudio Max 2.2 software. A cleaning step, using an Adaptive gauss filter was applied to remove pixels not of interest (noise). Grey value based segmentation, including removal of background, was performed using the Region growing and Adaptive rectangle tools. Once the background was removed, ROIs (air, germ, vitreous and floury endosperm) were virtually segmented from the original reconstructed volumes using the Region growing tool (see Appendix H). The germ and vitreous endosperm densities were very similar and prevented accurate segmentation of the endosperm; therefore the germ was virtually removed (Fig. 6.1) using the Drawing tool.

#### Quantitative measurements

Quantitative measurements (also see Appendix I) were performed using VGStudio Max 2.2 software. These included volume-of-interest (VOI;  $\text{mm}^3$ ), percentage object volume (POV; %); porosity (%); expansion ratio (ER); vitreous-to-floury endosperm ratio (V:F); and relative density ( $\text{g/cm}^3$ ) determinations. The unit for all volume measurements were  $\text{mm}^3$ .

##### i. Volumes-of-interest (VOIs)

VOIs were measured using the Volume analyser tool which automatically calculates the volume of the selected ROI. By creating different VOIs, volume measurements of specific kernels constituents (e.g. germ or floury endosperm) or the whole sample can be determined.

## ii. Percentage object volume

$$POV = \frac{VOI}{\text{Total volume}} \times 100\% \quad (1)$$

## iii. Porosity (total air volume fraction)

$$\text{Porosity} = \frac{\text{Air volume}}{\text{Total volume}} \times 100\% \quad (2)$$

Porosity refers to the total air volume and was subdivided into larger cavities and smaller pores. Cavities referred to large air spaces (due to fusion of pores) and pores were regarded as small intergranular air pockets with air pore volumes smaller than  $0.100 \text{ mm}^3$  and comprising more than 8 adjacent dark voxels ( $12 \text{ }\mu\text{m}$ ), that is not always visible with the eye and are created by dehydration during drying. The Defect detection tool was used to perform a Custom defect mask to colour code cavities according to size and to illustrate their arrangement. To determine the volume of pores, Defect detection tool (VGStudio Max 2.2) was applied after the exclusion of the cavities (Guelpa *et al.*, 2015b). For each maize kernel the volumes of cavities (percentage cavities) and pores (percentage pores) were calculated as a percentage of the total kernel volume.

## iv. Expansion ratio (ER)

$$ER = \frac{\text{Volume after roasting}}{\text{Volume before roasting}} \quad (3)$$

## v. Vitreous-to-floury endosperm ratio (V:F)

$$V:F = \frac{\text{Volume of vitreous endosperm}}{\text{Volume of floury endosperm}} \quad (4)$$

## vi. Relative density

$$\text{Relative density} = \frac{\text{Mean greyvalue of ROI}}{\text{Mean greyvalue of reference standard}} \times 2.15 \quad (5)$$

where 2.15 is the density ( $\text{g/cm}^3$ ) of the polymer disc

*Dry milling properties*

A 25 kg commercial white maize variety provided by Sasko (Essential Foods, Division of Pioneer Foods (Pty.) Ltd., Paarl, South Africa) was used to determine the effect of roasting on dry milling properties. The measurements were performed at the research and development facility of Sasko. The sample was cleaned using a Carter Day Dockage Tester and then mixed and divided into nine batches with a Boerner Divider (Seedburo Equipment Co., Chicago, USA). Three of the batches were treated as control samples and remained unroasted, while FCCT and oven roasting were respectively performed, as described above, in triplicate on the remaining six batches. The non-destructive HLM analysis was performed in duplicate, whereas milling yield and hominy chop were

determined as single measurements due to the large sample size required for these destructive measurements.

The HLM (in kg hL<sup>-1</sup>) of the samples was determined using a German Kern 220/222 Grain Sampler (KERN & SOHN GmbH, Balingen-Frommern, Germany). This test was performed according to the method described by Guelpa *et al.* (2015a).

Maize was de-germed using a pilot plant scale de-germer and subjected to the milling process. Hominy chop (blend of pericarp, tip cap, germ and to a lesser extent floury endosperm) was calculated as a percentage of the total sample mass (Guelpa *et al.*, 2015a).

For milling yield determinations, de-germed maize was subjected to dry milling using the Buhler MLU 202 Laboratory Mill (Buhler, Switzerland). The maize (900 g of each sample) was tempered to 15-16% moisture for 24 h before milling. Milling yield was assessed as the percentage of total weight accounted for by the combination of the following milling fractions: semolina, special and super.

### *Statistical analysis*

One-way analysis of variance (ANOVA) was performed to compare averages for the respective quantitative measurements with respect to the two roasting methods. Data was reported as the mean (n=10) ± standard deviation for X-ray  $\mu$ CT results and mean (n=3) ± standard deviation for milling property analyses. Data analyses were performed using STATISTICA version 13 (StatSoft, Inc., Tulsa, USA). The level of confidence required for significance was selected at  $P \leq 0.05$ .

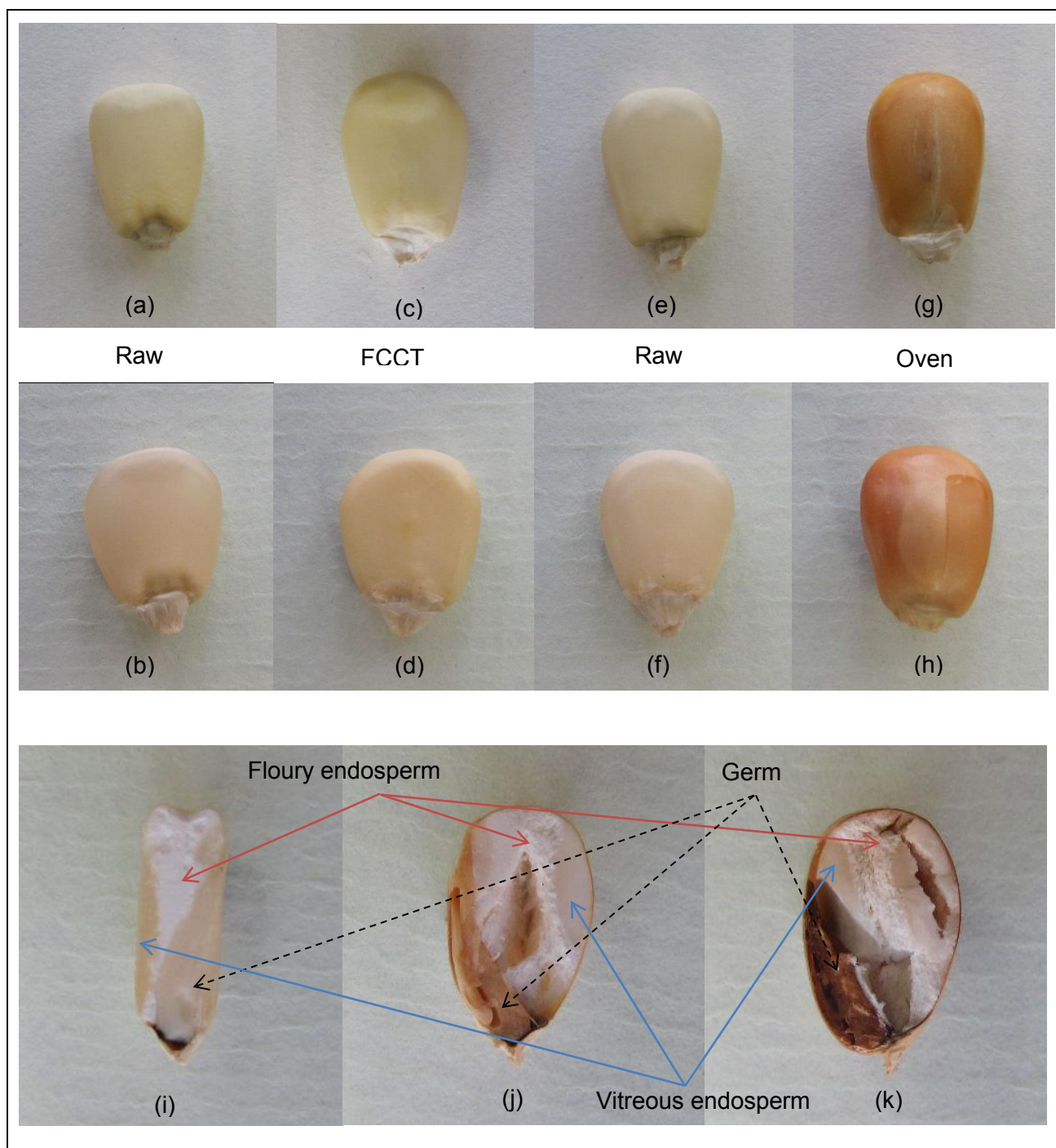
## **Results and discussion**

### *Visual assessment*

All roasted maize kernels partially retained the light yellowish pigmentation due to the carotenoid content, despite the roasting method (Fig. 6.2), as was also observed by Carrera *et al.* (2015). Oven roasting, however, led to a much darker, yellow-brown, external colour compared to FCCT roasting. A previous study illustrated that superheated steam roasting is associated with less colour deterioration and increased drying and evaporation rates, resulting in smaller losses regarding nutritional value in comparison to hot air, under similar conditions (Moreira, 2001). This could be attributed to less oxidation occurring during FCCT roasting using superheated steam (Schoeman *et al.*, 2016a). Furthermore, oven-roasted samples had a bulged appearance, whereas FCCT-roasted samples were more uniform in shape. This indicates a more intense degree of roasting with the oven method. The Maillard reaction occurs when reducing sugars are heated in the presence of free amino groups (e.g., amino acids, amines and proteins) (Odjo *et al.*, 2012). This gave rise to the colour development during roasting. The floury and vitreous endosperm regions are situated as opaque and translucent regions near the centre and towards the outside of the kernels, respectively (Fig. 6.2). The raw kernel had no visible internal cracks, whereas internal



cracks were observed in the floury endosperm of the FCCT-roasted and both endosperm regions of oven-roasted samples. The oven-roasted sample had a much darker internal colour.



**Figure 6.2.** Digital images (Canon SX40 digital camera, Canon, Ohtaku, Tokyo, Japan) of the same maize kernels before and after roasting: (a) and (b) raw, (c) and (d) FCCT-roasted, (e) and (f) raw, and (g) and (h) oven-roasted kernels. The cross-sectional digital images of (i) raw, (j) FCCT-roasted and (k) oven-roasted kernels reveals the internal structure, depicting the floury and vitreous endosperm regions as well as the germ (dashed arrow).

### *Qualitative image analysis*

Roasting is a time-temperature dependent process in which maize kernels undergo a series of reactions leading to several changes in their microstructure. Figure 6.3 illustrates the central plane of the sagittal and horizontal views of the 2D cross-sectional maize kernel images, acquired before and after roasting. As similar results were obtained, images of only one of the kernels are shown for each roasting method.

### Internal cracks, cavities, pores and porosity (2D analysis)

Differences in grey level intensities (image contrast) correlate to density variations within the kernel. Black areas represent air voids, since it has a lower absorption coefficient with respect to kernel structure (also see Appendix J, K and L). In the raw kernels, the germ and vitreous endosperm are thus more dense components illustrated by a brighter region (Fig. 6.3). The softer floury endosperm is related to a less dense region portrayed by a darker grey scale.

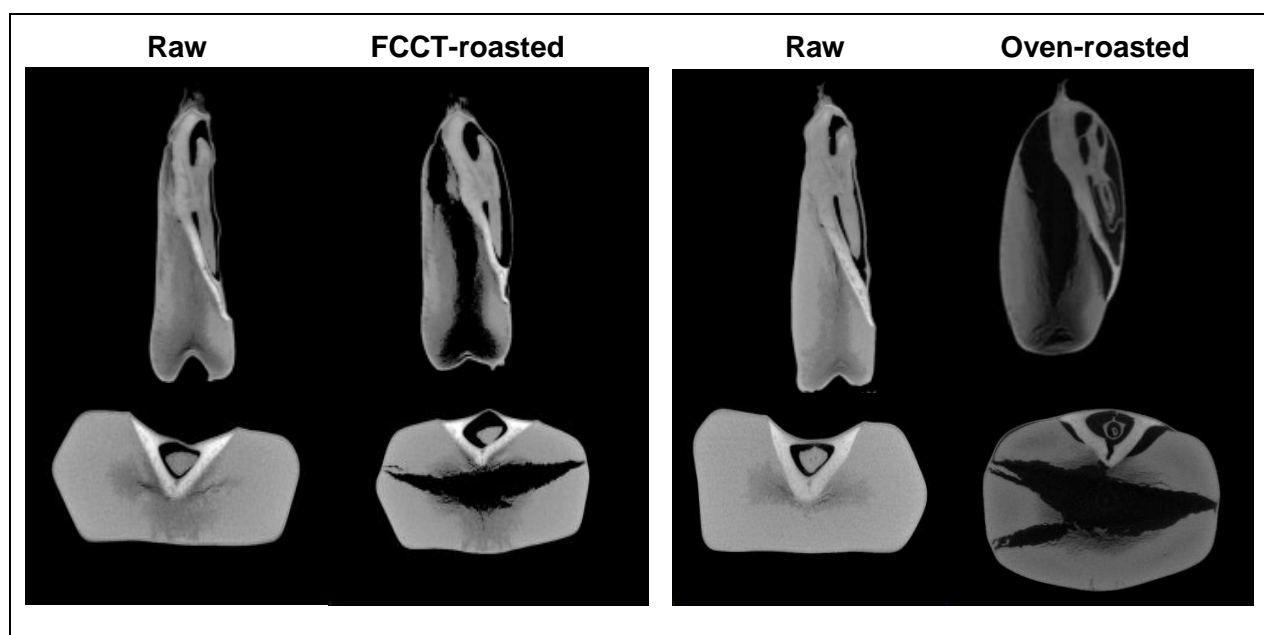
Large internal cracks developed in the floury endosperm of both the oven-roasted and FCCT-roasted samples (Fig. 6.3). These cracks were larger and extended well into the vitreous endosperm, however, not reaching the pericarp, in the case of oven roasting. The pericarp remained intact and acts as a pressure vessel. When the internal water vapour pressure is greater than the material strength, internal cracks develop (Song & Litchfield, 1994). It is also more likely that crack development is initiated by differential expansion due to thermal or moisture gradients. The cracks seemed to initiate at the centre of the kernel since it narrowed when approaching the kernel surface. More voids were present in the floury endosperm, especially around the germ, for both roasted samples. Less structural interference in the vitreous endosperm region might be due to it being harder and having less intercellular spaces, making this region less susceptible to crack formation. An earlier study also observed stress cracks (see Appendix M) in maize during high temperature processing (Shoughy *et al.*, 2009). Non-destructive light reflectance measurement and ultrasonic imaging were unsuitable to detect the presence of stress cracks, whereas 2D X-ray imaging was used successfully (Gunasekaran & Paulsen, 1986).

Figure 6.4 illustrates the complexity and interconnectedness of the crack network by means of internal cavities (or cracks) and pores. The raw kernels had a dense internal structure with small cavities and only a few pores around the germ and in the floury endosperm (Fig. 6.4a). The roasted kernels had inconsistently distributed and partially interconnected cracks and large elongated cavities in the centre of the kernels, whereas smaller pores were particularly observed in the bottom region of the floury endosperm (Figs. 6.4b and c). The size of the cavities was much larger in the oven-roasted samples, resulting in an open porous structure. As expected, the floury endosperm had more cavities since the softer regions have more intercellular spaces between the starch granules and is thus more prone to form cracks. The oven-roasted kernels revealed much greater expansion and more air resulting in a lower density (as discussed later in the quantitative results section) in comparison to the FCCT-roasted samples (Fig. 6.3; sagittal view).

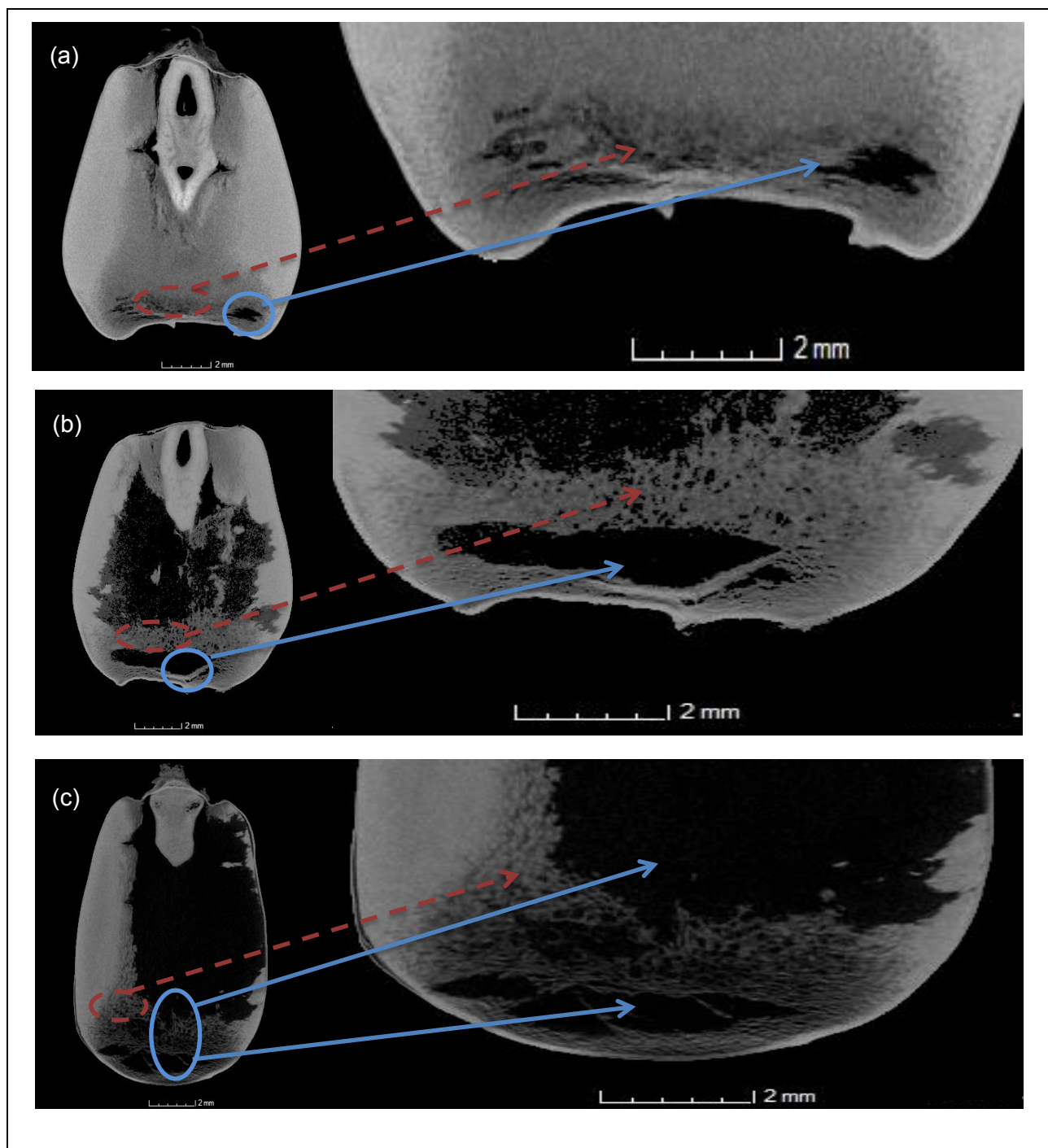
Cavities may have resulted from the fusion of a number of pores. During heat processing coalescence of two or more pores takes place leading to the formation of larger, asymmetric voids, resembling interconnected cavities (Pittia *et al.*, 2011). Even though some researchers consider pore size as a quality evaluator (Gonzales-Barron & Butler, 2008), to date it has not been confirmed that pore characteristics can affect the final quality as perceived by the consumer. Air voids will, however, affect the density and hardness of the maize kernels, which will in turn, affect milling quality (Guelpa *et al.*, 2015b).

The germ was generally intact as the cracks did not propagate into this region (Fig. 6.3). Even though the outer layer of the germ, the scutellum, is in contact with the endosperm, it is still separate and discontinued from the endosperm (Wolf *et al.*, 1952). A thin hyaline band of non-cellular material occupies the space between the endosperm and the scutellum. It is possible that this structural discontinuity inhibits the propagation of cracks in the germ region. This will enable efficient degermination of also roasted samples before milling. The germ is also a more flexible tissue since it grows during germination.

Roasting causes the conversion of the moisture entrapped within a kernel into vapour and this results in the development of ruptures and a puffing effect or expansion in volume (Pardeshi & Chattopadhyay, 2014). This vapour exerts pressure from within the kernel and leads to the development of cracks or fissures. It is through these cracks that the moisture ultimately escapes. Consequently, the cell walls separating pores get fractured and the pores increase in size, forming larger cavities illustrated as irregular black voids (Figs. 6.3 and 6.4). These zones are probably created by a flash of superheated steam that partially damages the structure (Sumithra & Bhattacharya, 2008).



**Figure 6.3.** Grey scale tomographic images of the different views (sagittal and horizontal) of the whole maize kernels, before and after FCCT and oven roasting. Differences in the grey level intensities indicate density variations (light grey = high density; darker grey = low density) while the black areas represent air voids.



**Figure 6.4.** Detailed 2D tomogram representations of pores (dashed arrow) and cavities (solid arrow) as observed in the frontal slice images of a (a) raw, (b) FCCT-roasted and (c) oven-roasted maize kernel.

#### Porosity, cavities and pores (3D analysis)

Figure 6.5 illustrates the porosity (subdivided into cavities and pores) before and after roasting in 3D volume rendered images and thus provides an indication of the cavity and pore size distribution. During roasting the porosity increased. In the raw samples separate cavities and pores were observed, whereas in the roasted samples the cavities and pore networks were interconnected, respectively. Most of the cavities in the raw samples were located near the middle



of the kernel, along the embryonic axis with pores in the floury endosperm. Pores as small as 41  $\mu\text{m}$  in diameter (FCCT-roasted; blue) could be detected, whereas the largest cavity was visible in the oven-roasted sample (dark red) (Fig. 6.5).

The oven-roasted sample had the highest porosity and a widely dispersed pore network, with the cavities contributing to the majority of the air present. Variations in the distribution of pores and cavities in the roasted kernels could be due to the effect of heat and mass (water vapour) transfer during volume expansion mechanisms that occurs in the different regions (Pittia *et al.*, 2011). It is implied that during roasting the increased internal pressure, due to the formation of water vapour, gave rise to the open porous structure. X-ray  $\mu\text{CT}$  analysis offers a more precise estimate of the porosity and the effect of roasting on the internal microstructure.

Figure 6.6 illustrates the three skeletonized models of raw, FCCT and oven-roasted maize kernels, respectively. Skeletonization displays the thickness as well as the connectivity of the air paths inside the maize kernels. Compared to the raw skeleton (Fig. 6.6a), the FCCT-roasted (Fig. 6.6b) skeleton was similar in density and thickness when observing the skeleton segments. In contrast, the oven-roasted sample yielded a complex skeleton (Fig. 6.6c) with a denser porous network of multiple twisting paths and interconnected segments of various thicknesses. The oven-roasted skeleton was also distinctly different from the other skeletons, since a cavity initiation site could be observed as a spider web structure.

#### *Quantitative microstructural analysis*

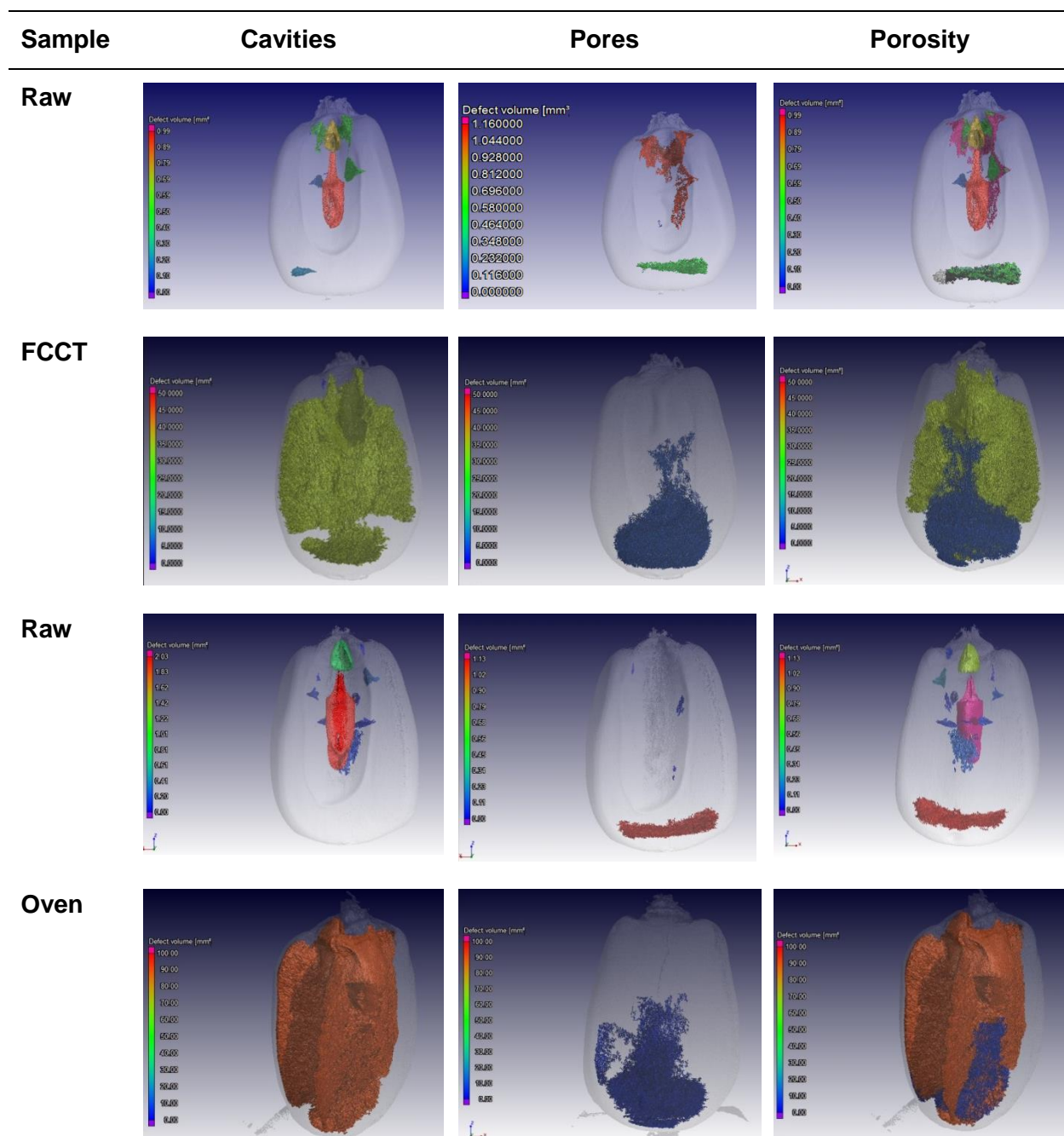
The germ, that remained intact during roasting, was virtually excluded to enable more accurate segmentation of the vitreous and floury endosperm.

#### Volume-of-interest (VOI)

When hand dissection was used to quantify the volumes of the different endosperm types, the vitreous endosperm was determined to be approximately double the volume of the floury endosperm (Wolf *et al.*, 1952). The mean volumes-of-interest (VOIs) for the different maize kernels constituents determined using X-ray  $\mu\text{CT}$  is presented in Table 6.1. Oven roasting had a significant ( $P \leq 0.05$ ) effect on the air (porosity), more specifically the cavities, and also the floury endosperm. FCCT roasting resulted in no significant ( $P > 0.05$ ) volume changes. In the roasted kernels air was the component contributing to the largest increase in volume with an increase of 74.34% and 462.79% during FCCT and oven roasting, respectively.

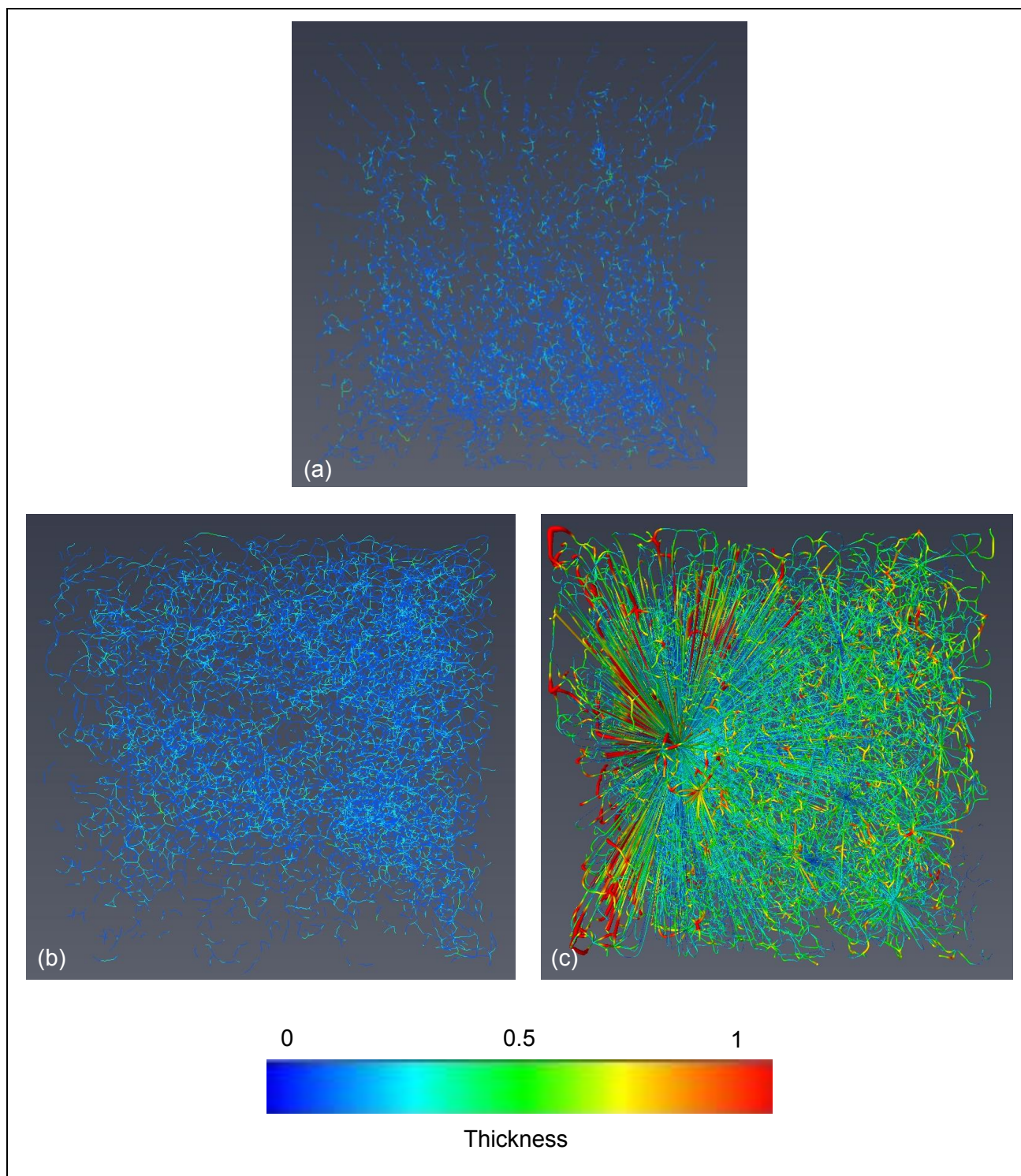
Roasting had a greater impact on the floury endosperm (increase of 9.96% and 60.44% for FCCT and oven roasting, respectively) due to it being softer and closer to the centre of the maize kernel where internal cracks initiated. The vitreous endosperm volume increased with 1.60% (FCCT) and decreased with 0.50% (oven) (Table 6.1). The decrease could be due to the vitreous endosperm becoming softer during roasting and thus the greyscale values decreased and were

regarded as softer, floury endosperm. Roasting had no significant ( $P>0.05$ ) effect on the total endosperm volume.



**Figure 6.5.** Semi-transparent 3D X-ray  $\mu$ CT volumes (12  $\mu$ m resolution) of cavities, pores and porosity (cavities and pores combined) before and after roasting. The colour scale bar indicates the volume size distribution ( $\text{mm}^3$ ) of the cavities and pores, where larger voids are magenta and smaller ones blue. In the raw kernels cavities and pores are separate (shown by different colours) whereas in the roasted kernels the voids are interconnected (shown as one colour).





**Figure 6.6.** Three-dimensional (3D) skeletonization images illustrating the topology and thickness of the pore network in (a) raw, (b) FCCT-roasted and (c) oven-roasted maize kernels. The segments of the skeletons are colour coded based on their thickness, according to the colour scale bar ranging from 0 (dark blue) to 1 (red). Blue represents thin segments and red thick segments, where a thickness of 1 is equal to 10 μm.

The germ was not significantly ( $P>0.05$ ) affected during roasting and increases of 1.94% and 5.53% were observed for FCCT and oven roasting, respectively. The increase in whole kernel volume during FCCT roasting was only 3.41% in comparison to the 10.76% increase during oven

roasting. This was due to the large increase in air volume related to oven roasting and the formation of a more open crack network. In a previous study oven roasting also resulted in an almost threefold increase in whole wheat kernel VOI compared to FCCT roasting (Schoeman *et al.*, 2016a). X-ray  $\mu$ CT enables faster and more accurate analysis of total kernel volume as well as the different internal components compared to volume displacement and manual hand dissection.

**Table 6.1.** Mean volumes-of-interest (VOIs), percentage object volumes (POVs), expansion ratios (ERs) and vitreous-to-floury endosperm ratios (V:F<sub>s</sub>) of the two roasting methods

Properties	FCCT			Oven		
	Raw (n=10)	Roasted (n=10)	% Increase/decrease	Raw (n=10)	Roasted (n=10)	% Increase/decrease
<b>VOIs (mm<sup>3</sup>)</b>						
Whole kernel	336.8±43.0 <sup>a</sup>	348.3±43.5 <sup>a</sup>	3.41	344.7±27.7 <sup>a</sup>	381.8±46.6 <sup>a</sup>	10.76
Total air	11.3±5.7 <sup>b</sup>	19.7±8.4 <sup>b</sup>	74.34	8.6±6.7 <sup>b</sup>	48.4±43.1 <sup>a</sup>	462.79
Cavities	9.2±6.1 <sup>b</sup>	17.1±9.2 <sup>b</sup>	85.87	6.9±6.7 <sup>b</sup>	47.0±43.2 <sup>a</sup>	581.16
Pores	2.1±1.6 <sup>a</sup>	2.7±2.4 <sup>a</sup>	28.57	1.8±1.0 <sup>a</sup>	1.4±0.79 <sup>a</sup>	-22.22
Germ	46.4±7.4 <sup>a</sup>	47.3±6.9 <sup>a</sup>	1.94	47.0±6.6 <sup>a</sup>	49.6±6.9 <sup>a</sup>	5.53
Floury endosperm	71.3±19.2 <sup>ab</sup>	78.4±34.5 <sup>ab</sup>	9.96	59.4±10.7 <sup>b</sup>	95.3±53.3 <sup>a</sup>	60.44
Vitreous endosperm	219.1±39.6 <sup>a</sup>	222.6±37.0 <sup>a</sup>	1.60	238.2±22.3 <sup>a</sup>	237.0±19.2 <sup>a</sup>	-0.50
Total endosperm	290.4±36.9 <sup>a</sup>	301.0±39.7 <sup>a</sup>	3.65	297.6±21.8 <sup>a</sup>	332.3±47.4 <sup>a</sup>	11.66
<b>POV (%)</b>						
Material	96.6±1.6 <sup>a</sup>	94.3±2.0 <sup>a</sup>	-2.30	97.5±2.0 <sup>a</sup>	87.3±8.5 <sup>b</sup>	-10.20
Air (porosity)	3.4±1.6 <sup>b</sup>	5.7±2.0 <sup>b</sup>	2.30	2.5±2.0 <sup>b</sup>	12.7±8.5 <sup>a</sup>	10.20
Cavities	2.7±1.7 <sup>b</sup>	4.9±2.3 <sup>b</sup>	2.20	2.0±2.0 <sup>b</sup>	12.3±8.5 <sup>a</sup>	10.30
Pores	0.63±0.42 <sup>a</sup>	0.76±0.72 <sup>a</sup>	0.13	0.51±0.25 <sup>a</sup>	0.37±0.20 <sup>a</sup>	-0.14
ER	1.03±0.07 <sup>a</sup>	-	-	1.11±0.17 <sup>b</sup>	-	-
V:F	3.3±0.98 <sup>ab</sup>	3.2±0.98 <sup>b</sup>	-3.03	4.2±0.95 <sup>a</sup>	3.0±1.2 <sup>b</sup>	-28.57

Values are means ± standard deviation of ten replicates (n=10). Different letters in the same row indicate significant differences (P≤0.05).

### Percentage object volume (POV)

POV is an indication of the percentage volume of a specific component in the kernel relative to the entire kernel. Since yield is a highly desirable property for the milling industry, understanding the relative contribution of the material (excluding all cavities and pores) to the total maize kernel is relevant. The decrease in material POV was significantly (P≤0.05) higher for oven roasting (10.20%) compared to FCCT roasting (2.30%) (Table 6.1).

### Porosity (cavities and pores)

Pores and voids are inherent to maize kernels due to the porous nature of the endosperm (Chang, 1988). Oven-roasted samples had a significantly (P≤0.05) higher porosity (12.7%) than FCCT-

roasted samples (5.7%) (Table 6.1). Due to the lower porosity, FCCT roasting is expected to deliver a higher quality kernel in terms of milling yield. Little is known about the development of cavities and pores during roasting. In order to obtain a better understanding of the size distribution of the air inside maize kernels the total porosity was further subdivided into larger cavities and smaller pores, quantified as percentage cavities and percentage pores (also see Appendix N, O and P). Figure 6.4 demonstrates the difference between pores and cavities as depicted in 2D. A recent study on wheat considered the porosity as the total air in the sample, thus the entirety of cavities and pores (Schoeman *et al.*, 2016a). Here it was also reported that the porosity of wheat kernels was significantly ( $P \leq 0.05$ ) higher after oven roasting.

The percentage cavities for the raw samples were  $2.7 \pm 1.7\%$  (FCCT) and  $2.0 \pm 2.0\%$  (oven) (Table 6.1). Guelpa *et al.* (2015b) reported the percentage cavities and percentage pores ( $n=16$ ) of raw whole maize kernels as 1.8% and 0.012%, respectively. The percentage cavities in the oven-roasted ( $12.3 \pm 8.5\%$ ) samples were significantly ( $P \leq 0.05$ ) higher than for the FCCT-roasted ( $4.9 \pm 2.3\%$ ) samples. In expanded cereal products, more cavities are formed due to less structural integrity. During oven roasting large cavities are created by coalescence of adjacent cells when the cell walls rupture.

The percentage pores were not significantly ( $P > 0.05$ ) affected during roasting. The percentage pores of the oven-roasted samples decreased with 0.14%, while it increased with 0.13% for the FCCT-roasted samples (Table 6.1). It is likely that during FCCT roasting some new pores developed, whereas during oven roasting the existing pores fused to form larger cavities. Rapid evaporation of moisture inside the maize kernels, results in the formation of new pores. Due to moisture loss, these pores grow and fuse, especially during oven roasting, with neighbouring pores to create larger cavities (Sumithra & Bhattacharya, 2008). The minimum detectable pore size was 41  $\mu\text{m}$  in diameter detectable in a FCCT-roasted sample. Pores in popped popcorn are usually 30 to 60  $\mu\text{m}$  in diameter, whereas pore diameters of maize puffed using puffing guns are usually in the 50 to 200  $\mu\text{m}$  range (Schwartzberg *et al.*, 1995).

Harder maize kernels, having less cavities and pores, will have a better dry milling quality and yield compared to softer kernels (Guelpa *et al.*, 2015b). During wet milling, kernels with a high cavity percentage will steep more rapidly and lose part of their starch in the steep water (Gunasekaran *et al.*, 1985). Also, the protein is case-hardened in highly porous kernels which may lead to difficulty in separating the protein and starch, resulting in less recoverable starch.

Using gas pycnometry, it was shown that adjacent cells that are closed and not interconnected might be counted as interconnected regions if there is a small crack in the cell wall that can allow gas to penetrate. X-ray  $\mu\text{CT}$  is thus more accurate as it can distinguish between adjacent closed cells and interconnected regions (Trater *et al.*, 2005).

### Expansion ratio (ER)

A larger ER is associated with greater air volumes and a higher density decrease (Sumithra & Bhattacharya, 2008). Oven roasting produced kernels with a significantly ( $P \leq 0.05$ ) higher sectional expansion ( $1.11 \pm 0.17$ ) than FCCT roasting ( $1.03 \pm 0.07$ ) indicating a much larger difference in the volumes of the oven-roasted kernels before and after roasting (Table 6.1). Visual assessment also indicated a bulged effect, especially toward the middle region, indicating localised high expansion, in the oven-roasted kernels. This is attributed to the fracturing of the cell walls that separates pores leading to an increase in cavity volume. In a study by Mrad *et al.* (2014), on the textural properties of roasted purple maize, the ER was in the range of 1.44-3.13. The most acceptable ER was found to be approximately 1.5 as kernels at this level were expanded without being deformed. This will however depend on the roasting method and conditions used. There are a large number of parameters that affect the degree of expansion in cereals, which are connected to both the compositional characteristics of the raw material (Jones *et al.*, 2000) and the processing conditions (Mariotti *et al.*, 2006).

The internal pressure created inside the kernel causes expansion. Even though the roasting process is conducted at a low moisture content, the use of high temperature for a short time suddenly releases steam, leaving behind an expanded structure (Sumithra & Bhattacharya, 2008). Greater air volumes (oven-roasted samples) were synonymous with greater expansion ratios. The expansion of a sample is primarily reliant on the development of air pockets which are formed when vapour expands. A relationship exists between porosity and the expanded volume since the entrapped air plays an important role in expansion (Boischot *et al.*, 2003).

The mechanism that governs cereal expansion is similar for all thermal processes (Boischot *et al.*, 2003). During heating, the starch matrix in the presence of water undergoes a phase transition from a glassy to a rubbery state that allows expansion and formation of the final structure (Boischot *et al.*, 2003). Furthermore, moisture content plays a critical role in cereal expansion due to its ability to generate the driving force (vaporisation of water) during the roasting process and also through its impact on the extensional viscosity and phase transitions of the food matrix. Oven roasting had a significant ( $P \leq 0.05$ ) effect on kernel weight and resulted in a loss of 2.64%, while the weight remained almost unaffected during FCCT roasting (Table 6.2). Oven roasting relies on only air movement while the sample is stationary, imparting a higher internal pressure and resulting in more moisture loss.

A previous study comparing roasted peanuts using superheated steam and conventional oven (without steam) roasting demonstrated that during oven roasting the rate of decrease in moisture content is much higher compared to the superheated steam method (Idrus & Yang, 2012). This study also suggested that as a novel method for food processing, superheated steam roasting is more convenient and at the same time and temperature conditions favourable characteristics i.e. colour, texture and microstructure, are maintained.



### Endosperm ratios

Guelpa *et al.* (2016) reported a V:F of 0.69 to 7.18 for good milling hybrids and a range of 0.20 to 3.17 for poor milling hybrids and indicated V:F to be a good descriptor of maize milling quality. According to Table 6.1 the V:F decreased from  $3.3 \pm 0.98$  to  $3.2 \pm 0.98$  for FCCT-roasted samples and from  $4.2 \pm 0.95$  to  $3.0 \pm 1.2$  for oven-roasted samples. The significant ( $P \leq 0.05$ ) decrease of the V:F in the oven-roasted samples is due to the larger increase in floury endosperm and decrease in vitreous endosperm VOI.

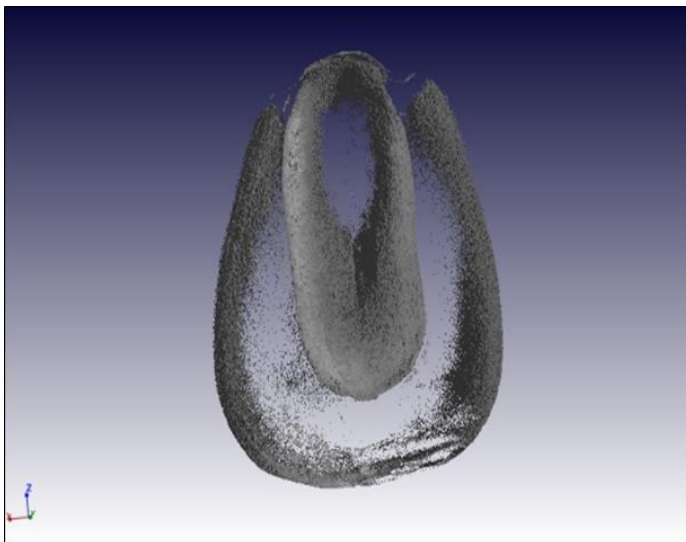
Previously a dissecting microscope and electronic planimeter was used to quantify the F:V (range of 0.12 to 0.30) in popped maize kernels (Pordesimo *et al.*, 1991). Expansion was generally higher when the F:V was lower. In contrast, in this study kernels with a higher ER (oven-roasted) had the lowest V:F (or highest F:V). It can be hypothesised that, because the floury endosperm had a less dense structure, the vapour that was generated internally, diffused into the voids leading to an increase in internal pressure (Pordesimo *et al.*, 1991). This caused the floury endosperm volume to increase more and this region thus underwent more structural alteration in comparison to the vitreous endosperm. Therefore a lower V:F was indicative of an increase in floury endosperm volume.

Blandino *et al.* (2010) determined the V:F (range of 0.2 to 4.8) of maize kernels using hand dissection in combination with an image analysis system. These methods are destructive and time-consuming and thus not practical for large sample sizes. X-ray  $\mu$ CT enabled more accurate and non-destructive segmentation of the vitreous and floury endosperm into specific ROIs in order to quantify the volumes and determine the V:F. X-ray  $\mu$ CT is unfortunately time-consuming with cost implications when analysing a large number of samples. However, a recent paper demonstrated a high-throughput approach where 150 maize kernels were scanned simultaneously (Guelpa *et al.*, 2016). Although this resulted in reduced resolution scans, sufficient segmentation and quantification of ROIs was still possible.

### Relative density analysis

Density is an important property, which depends on the internal structure of food (Kelkar *et al.*, 2015). For porous foods, accurate density measurements is challenging because conventional methods are tedious, operator-dependent and incapable of precise volume measurements. Kelkar *et al.* (2015) overcome such limitations by developing a methodology, using both X-ray digital radiography and computed tomography (CT) to directly determine the apparent density of foods. X-ray CT was more efficient giving results comparable with conventional methods.

X-ray  $\mu$ CT enables images to be generated that maps variances in X-ray attenuation within a sample and this relates closely to density (Schoeman *et al.*, 2016b). Each voxel in an image has a specific grey value which is reliant on density. The higher the grey values, the higher the attenuation coefficients and the higher the material density. Figure 6.7 represents a 3D volume illustrating relative density differences in a maize kernel.



**Figure 6.7.** A semi-transparent 3D volume illustrating the density differences of the maize constituents, where the less dense area (floury endosperm) is shown with partial transparency and the more dense regions (germ and vitreous endosperm) in grey.

The mean relative densities of all the constituents decreased during roasting (Table 6.2). In contrast to wheat, here again it was important to evaluate both endosperm types, since a greater decrease in vitreous endosperm will have a significant effect on milling yield. It should be noted that the relative densities of the individual tissues e.g. floury endosperm include the air in that region. Oven roasting resulted in a significant ( $P \leq 0.05$ ) decrease in whole kernel and material relative density, while no significant ( $P > 0.05$ ) density decreases were observed for FCCT roasting. During oven roasting a 6.33% decrease in whole kernel relative density were obtained in comparison to a 1.92% decrease by FCCT roasting. This can be attributed to the large increase in air volume that is accounted for in the whole kernel density of the oven-roasted kernels. These results are in accordance with a previous study that found a significant decrease in density due to an increase in the air volume after roasting coffee beans (Dutra *et al.*, 2001).

Voids in roasted kernels made up a large volume of the kernel, suggesting that whole kernel density may not be as informative of kernel hardness as material density (Gustin *et al.*, 2013). The material density (also known as true density), which excludes all air voids, remained almost unaffected (decrease of 0.63%) during FCCT roasting, but decreased significantly ( $P \leq 0.05$ ) with 4.97% during oven roasting. Similarly Schoeman *et al.* (2016a) reported FCCT roasting to have no effect on the material density of wheat.

Larger relative density decreases took place during oven roasting for the germ (3.13%) and vitreous endosperm (2.47%), in comparison to FCCT roasting (germ = 1.27%; vitreous endosperm = 1.25%). The floury endosperm was the component contributing most to the relative density decrease, resulting in a 6.25% and 4.83% decrease in the FCCT and oven-roasted kernels, respectively. The absence of a thick protein matrix that covers the starch granules in the floury endosperm led to formation of cracks, which ultimately developed into larger cavities when



moisture loss was experienced during roasting. Less intracellular air spaces were found in the tightly packed vitreous endosperm as opposed to the loosely packed floury endosperm, explaining the higher density.

Gustin *et al.* (2013) correlated maize kernel density with kernel volume and internal air space. Similarly, in this study the whole kernel density was affected by the increased porosity during roasting. The relative density results corresponded well with the results obtained by Guelpa *et al.* (2015b), whom made use of a X-ray  $\mu$ CT density calibration for raw maize kernels ( $n=16$ ) where the density ranges were 1.28 to 1.62 g/cm<sup>3</sup>, 1.60 to 1.75 g/cm<sup>3</sup> and 1.21 to 1.53 g/cm<sup>3</sup> for material, vitreous endosperm and floury endosperm, respectively.

Jha (2005) found that the density of grains decreased during roasting due to expansion, development of pores and as a result of moisture loss. Chung *et al.* (2011) also reported a decrease in maize density due to puffing. A previous study on maize roasting (using a gas operated roaster) reported a density decrease of 41.9% at 137°C (Felsman *et al.*, 1976). This decrease was much higher in comparison with the results presented in Table 6.2. Oven and FCCT roasting (both using electric heat) utilised in this study made use of a higher roasting temperature and shorter time. This indicates that differences in the roasting method and conditions may account for this discrepancy.

Conventional density measurements, i.e. floating tests (Blandino *et al.*, 2010) might lead to misleading results as internal cavities will greatly influence the results (Guelpa *et al.*, 2015b). Conventional density methods overlook the influence of pores and cavities while with X-ray  $\mu$ CT it is possible to determine only the material density. X-ray  $\mu$ CT is capable of disregarding cavities that could have a negative influence on the results (Gustin *et al.*, 2013). The ability of  $\mu$ CT to divide the maize kernel into biological material and air, for volume and density measurements, provides higher resolution information about kernel characteristics than either pycnometer or floating tests.

**Table 6.2.** Mean relative densities of the different maize kernel constituents and the weight of the raw, FCCT and oven-roasted kernels

Properties	FCCT			Oven		
	Raw (n=10)	Roasted (n=10)	% decrease	Raw (n=10)	Roasted (n=10)	% decrease
<b>Relative density (g/cm<sup>3</sup>)</b>						
Whole kernel	1.56±0.30 <sup>a</sup>	1.53±0.20 <sup>a</sup>	1.92	1.58±0.60 <sup>a</sup>	1.48±0.80 <sup>b</sup>	6.33
Material	1.58±0.30 <sup>a</sup>	1.57±0.30 <sup>ab</sup>	0.63	1.61±0.50 <sup>a</sup>	1.53±0.60 <sup>b</sup>	4.97
Germ	1.58±0.50 <sup>a</sup>	1.56±0.50 <sup>a</sup>	1.27	1.60±0.60 <sup>a</sup>	1.55±0.90 <sup>a</sup>	3.13
Floury endosperm	1.44±0.40 <sup>a</sup>	1.35±0.60 <sup>a</sup>	6.25	1.45±0.50 <sup>a</sup>	1.38±0.90 <sup>a</sup>	4.83
Vitreous endosperm	1.60±0.50 <sup>a</sup>	1.58±0.40 <sup>a</sup>	1.25	1.62±0.60 <sup>a</sup>	1.58±0.80 <sup>a</sup>	2.47
<b>Weight (mg)</b>	424.1±54.0	420.78±55.		449.32±33.	437.48±35.	
	8 <sup>ab</sup>	51 <sup>ab</sup>	0.78	73 <sup>a</sup>	26 <sup>b</sup>	2.64

Values are means ± standard deviation of ten replicates ( $n=10$ ). Different letters in the same row indicate significant differences ( $P \leq 0.05$ ).

*Dry milling properties*

No significant ( $P>0.05$ ) differences were observed between the HLM of the raw ( $78.47 \text{ kg hL}^{-1}$ ), FCCT ( $78.40 \text{ kg hL}^{-1}$ ) and oven-roasted ( $78.23 \text{ kg hL}^{-1}$ ) samples. The values were similar to the average HLM of  $78.30 \text{ kg hL}^{-1}$  reported for the 2014/2015 maize season (SAGL, 2016). Milling yield of the control ( $77.06\pm0.49\%$ ), FCCT ( $76.05\pm1.37\%$ ) and oven-roasted ( $75.79\pm0.56\%$ ) samples was not significantly ( $P>0.05$ ) different (Table 6.3). Oven-roasted samples had the lowest milling yield and this might be attributed to the higher porosity (Table 6.1) and lower density (Table 6.2). The porosity level cause reductions in mechanical strength, yielding softer, finer flour compared to FCCT roasting. These results are in agreement with the average extraction of 78.7% reported for white maize during the 2014/2015 season (SAGL, 2016). The hominy chop was also not significantly ( $P>0.05$ ) influenced (Table 6.3). The raw, FCCT and oven-roasted samples had a hominy chop of  $22.94\pm0.49\%$ ,  $23.95\pm1.37\%$  and  $24.21\pm0.56\%$ , respectively and all the samples could be classified within the good intermediate range.

**Table 6.3.** Dry milling properties of the raw and roasted maize samples

Sample	HLM ( $\text{kg hL}^{-1}$ )*	Milling yield (%)*	Hominy chop (%)**
Raw	$78.47\pm0.29^a$	$77.06\pm0.49^a$	$22.97\pm0.50^a$
FCCT	$78.40\pm0.44^a$	$76.05\pm1.37^a$	$23.97\pm1.34^a$
Oven	$78.23\pm0.55^a$	$75.79\pm0.56^a$	$24.20\pm0.53^a$

Values are presented as mean  $\pm$  standard deviation of three replicates ( $n=3$ ). Mean values with different superscripts in a column differ significantly ( $P\leq0.05$ ). \*Mean values of single measurements from three replicates; \*\*mean values of duplicate measurements from three replicates.

**Conclusion**

Raw, sound maize kernels have a compact and homogenous internal microstructure. Roasting was associated with an increase in kernel volume and decrease in relative density, with the changes being more profound during oven roasting. Roasting increased the porosity of maize kernels comprising cavities and pores of different sizes. Kernel density and porosity were shown to be inversely correlated, with the oven-roasted samples having the highest density decrease and highest porosity increase. FCCT roasting had almost no effect on the material density of the samples, in contrast to oven roasting. Although structural changes occurred during roasting the milling properties were not significantly ( $P>0.05$ ) influenced, indicating that roasting did not comprise milling yield and quality. Maize with good milling properties contain a higher proportion of vitreous endosperm and will thus result in greater yields with higher economic value. Further investigations are needed to assess the functional characteristics of roasted maize.

Although this study was motivated by an innovative roasting method, FCCT roasting, the results also contributed to improved understanding of the effect of high-temperature processing on the internal microstructure of cereal grains in general. Taking all the measurements into account, the FCCT roaster, with the rotating cylinder, was a more effective roasting method. The qualitative

results also illustrated the less invasive impact on the kernel microstructure. FCCT roasting could thus be a more suitable roasting method for food applications. Even though X-ray  $\mu$ CT is ideal as a non-invasive tool for microstructural analysis, it is currently mainly used as a research tool and the application thereof for in-line measurements still needs further development. In the food industry 2D X-ray images could be used for rapid and real-time quality control analyses.

## References

- Bellido, G.G., Scanlon, M.G., Page, J.H. & Hallgrimsson, B. (2006). The bubble size distribution in wheat flour dough. *Food Research International*, **39**, 1058-1066.
- Blandino, M., Mancini, M.C., Peila, A., Rolle, L., Vanara, F. & Reyneri, A. (2010). Determination of maize kernel hardness: comparison of different laboratory tests to predict dry-milling performance. *Journal of the Science of Food and Agriculture*, **90**, 1870-1878.
- Boischot, C., Moraru, C. & Kokini, J. (2003). Factors that influence the microwave expansion of glassy amylopectin extrudates. *Cereal Chemistry*, **80**, 56-61.
- Cantre, D., East, A., Verboven, P., Trejo Araya, X., Herremans, E., Nicolaï, B.M., Pranamornkith, T., Loh, M., Mowat, A. & Heyes, J. (2014a). Microstructural characterisation of commercial kiwifruit cultivars using X-ray micro computed tomography. *Postharvest Biology and Technology*, **92**, 79-86.
- Cantre, D., Herremans, E., Verboven, P., Ampofo-Asiama, J. & Nicolaï, B. (2014b). Characterization of the 3-D microstructure of mango (*Mangifera indica* L. cv. Carabao) during ripening using X-ray computed microtomography. *Innovative Food Science & Emerging Technologies*, **24**, 28-39.
- Carrera, Y., Utrilla-Coello, R., Bello-Pérez, A., Alvarez-Ramirez, J. & Vernon-Carter, E.J. (2015). In vitro digestibility, crystallinity, rheological, thermal, particle size and morphological characteristics of pinole, a traditional energy food obtained from toasted ground maize. *Carbohydrate Polymers*, **123**, 246-255.
- Chang, C. (1988). Measuring density and porosity of grain kernels using a gas pycnometer. *Cereal Chemistry*, **65**, 13-15.
- Chung, H.S., Chung, S.K. & Youn, K.S. (2011). Effects of roasting temperature and time on bulk density, soluble solids, browning index and phenolic compounds of corn kernels. *Journal of Food Processing and Preservation*, **35**, 832-839.
- Delcour, J. & Hosney, R.C. (2010). *Principles of Cereal Science and Technology*. 3rd ed. St. Paul, Minnesota, USA: AACC International Press.
- Dutra, E., Oliveira, L., Franca, A., Ferraz, V. & Afonso, R. (2001). A preliminary study on the feasibility of using the composition of coffee roasting exhaust gas for the determination of the degree of roast. *Journal of Food Engineering*, **47**, 241-246.
- FAOSTAT. (2015). Food and Agriculture Organization of the United Nations. Statistics division [Internet document]. URL <http://faostat3.fao.org/download/Q/QC/E>. Accessed 07/05/2015.

- Felsman, R., Harvey, R., Linnerud, A. & Smith, F. (1976). Effect of roasting temperature on corn grain characteristics. *Journal of Animal Science*, **42**, 476-480.
- Frisullo, P., Barnabà, M., Navarini, L. & Del Nobile, M. (2012). *Coffea arabica* beans microstructural changes induced by roasting: an X-ray microtomographic investigation. *Journal of Food Engineering*, **108**, 232-237.
- Frisullo, P., Marino, R., Laverse, J., Albenzio, M. & Del Nobile, M. (2010). Assessment of intramuscular fat level and distribution in beef muscles using X-ray microcomputed tomography. *Meat Science*, **85**, 250-255.
- Gonzales-Barron, U. & Butler, F. (2008). Discrimination of crumb grain visual appearance of organic and non-organic bread loaves by image texture analysis. *Journal of Food Engineering*, **84**, 480-488.
- Guelpa, A., Bevilacqua, M., Marini, F., O'Kennedy, K., Geladi, P. & Manley, M. (2015a). Application of Rapid Visco Analyser (RVA) viscograms and chemometrics for maize hardness characterisation. *Food Chemistry*, **173**, 1220-1227.
- Guelpa, A., Du Plessis, A., Kidd, M. & Manley, M. (2015b). Non-destructive estimation of maize (*Zea mays* L.) kernel hardness by means of an X-ray micro-computed tomography ( $\mu$ CT) density calibration. *Food and Bioprocess Technology*, **8**, 1419-1429.
- Guelpa, A., Du Plessis, A. & Manley, M. (2016). A high-throughput X-ray micro-computed tomography ( $\mu$ CT) approach for measuring single kernel maize (*Zea mays* L.) volumes and densities. *Journal of Cereal Science*, **69**, 321-328.
- Gujral, H.S., Sharma, P. & Sharma, R. (2013). Antioxidant properties of sand roasted and steam cooked Bengal gram (*Cicer arietinum*). *Food Science and Biotechnology*, **22**, 183-188.
- Gunasekaran, S., Deshpande, S., Paulsen, M. & Shove, G. (1985). Size characterization of stress cracks in corn kernels. *Transactions of the ASAE*, **28**, 1668-1672.
- Gunasekaran, S. & Paulsen, M.R. (1986). Automatic, nondestructive detection of corn kernel defects. *International Advances in Nondestructive Testing*, **12**, 95-115.
- Gustin, J.L., Jackson, S., Williams, C., Patel, A., Armstrong, P., Peter, G.F. & Settles, A.M. (2013). Analysis of maize (*Zea mays*) kernel density and volume using microcomputed tomography and single-kernel near-infrared spectroscopy. *Journal of Agricultural and Food Chemistry*, **61**, 10872-10880.
- Haedelt, J., Beckett, S. & Niranjana, K. (2007). Bubble-included chocolate: relating structure with sensory response. *Journal of Food Science*, **72**, 138-142.
- Herremans, E., Melado-Herreros, A., Defraeye, T., Verlinden, B., Hertog, M., Verboven, P., Val, J., Fernández-Valle, M.E., Bongaers, E. & Estrade, P. (2014). Comparison of X-ray CT and MRI of watercore disorder of different apple cultivars. *Postharvest Biology and Technology*, **87**, 42-50.

- Herremans, E., Verboven, P., Bongaers, E., Estrade, P., Verlinden, B.E., Wevers, M., Hertog, M.L. & Nicolai, B.M. (2013). Characterisation of 'Braeburn' browning disorder by means of X-ray micro-CT. *Postharvest Biology and Technology*, **75**, 114-124.
- Herremans, E., Verboven, P., Verlinden, B.E., Cantre, D., Abera, M., Wevers, M. & Nicolaï, B.M. (2015). Automatic analysis of the 3-D microstructure of fruit parenchyma tissue using X-ray micro-CT explains differences in aeration. *BMC Plant Biology*, **15**, 1-14.
- Idrus, N.F.M. & Yang, T.A. (2012). Comparison between roasting by superheated steam and by convection on changes in colour, texture and microstructure of peanut (*Arachis hypogaea*). *Food Science and Technology Research*, **18**, 515-524.
- Jha, S. (2005) Mathematical simulation of roasting of grain. *Journal of Food Engineering*, **71**, 304-310.
- Jones, D., Chinnaswamy, R., Tan, Y. & Hanna, M. (2000). Physiochemical properties of ready-to-eat breakfast cereals. *Cereal Foods World*, **45**, 164-168.
- Kabak, B. (2009). The fate of mycotoxins during thermal food processing. *Journal of the Science of Food and Agriculture*, **89**, 549-554.
- Kelkar, S., Boushey, C.J. & Okos, M. (2015). A method to determine the density of foods using X-ray imaging. *Journal of Food Engineering*, **159**, 36-41.
- Khan, N., Zaman, R. & Elahi, M. (1991). Effect of heat treatments on the phytic acid content of maize products. *Journal of the Science of Food and Agriculture*, **54**, 153-156.
- Krings, U. & Berger, R. (2001). Antioxidant activity of some roasted foods. *Food Chemistry*, **72**, 223-229.
- Lammertyn, J., Dresselaers, T., Van Hecke, P., Jancsó, P., Wevers, M. & Nicolaï, B. (2003). MRI and X-ray CT study of spatial distribution of core breakdown in 'Conference' pears. *Magnetic Resonance Imaging*, **21**, 805-815.
- Lassoued, N., Babin, P., Della Valle, G., Devaux, M.-F. & Réguerre, A.-L. (2007). Granulometry of bread crumb grain: contributions of 2D and 3D image analysis at different scale. *Food Research International*, **40**, 1087-1097.
- Lim, K.S. & Barigou, M. (2004). X-ray micro-computed tomography of cellular food products. *Food Research International*, **37**, 1001-1012.
- Maire, E. & Withers, P.J. (2014). Quantitative X-ray tomography. *International Materials Reviews*, **59**, 1-43.
- Mariotti, M., Alamprese, C., Pagani, M.A. & Lucisano, M. (2006). Effect of puffing on ultrastructure and physical characteristics of cereal grains and flours. *Journal of Cereal Science*, **43**, 47-56.
- Mendoza, F., Verboven, P., Mebatsion, H.K., Kerckhofs, G., Wevers, M. & Nicolaï, B. (2007). Three-dimensional pore space quantification of apple tissue using X-ray computed microtomography. *Planta*, **226**, 559-570.
- Moreira, R.G. (2001). Impingement drying of foods using hot air and superheated steam. *Journal of Food Engineering*, **49**, 291-295.

- Mrad, R., Debs, E., Saliba, R., Maroun, R.G. & Louka, N. (2014). Multiple optimization of chemical and textural properties of roasted expanded purple maize using response surface methodology. *Journal of Cereal Science*, **60**, 397-405.
- Murthy, K.V., Ravi, R., Keshava Bhat, K. & Raghavarao, K.S.M.S. (2008). Studies on roasting of wheat using fluidized bed roaster. *Journal of Food Engineering*, **89**, 336-342.
- Oboh, G., Ademiluyi, A.O. & Akindahunsi, A.A. (2010). The effect of roasting on the nutritional and antioxidant properties of yellow and white maize varieties. *International Journal of Food Science & Technology*, **45**, 1236-1242.
- Odjo, S., Malumba, P., Dossou, J., Janas, S. & Béra, F. (2012). Influence of drying and hydrothermal treatment of corn on the denaturation of salt-soluble proteins and color parameters. *Journal of Food Engineering*, **109**, 561-570.
- Pardeshi, I. & Chattopadhyay, P. (2014). Whirling bed hot air puffing kinetics of rice-soy ready-to-eat (RTE) snacks. *Journal of Ready to Eat Foods*, **1**, 1-10.
- Pittia, P., Sacchetti, G., Mancini, L., Voltolini, M., Sodini, N., Tromba, G. & Zanini, F. (2011). Evaluation of microstructural properties of coffee beans by synchrotron X-ray microtomography: a methodological approach. *Journal of Food Science*, **76**, 222-231.
- Pordesimo, L.O., Anantheswaran, R.C. & Mattern, P.J. (1991). Quantification of horny and floury endosperm in popcorn and their effects on popping performance in a microwave oven. *Journal of Cereal Science*, **14**, 189-198.
- Pronyk, C., Cenkowski, S., & Muir, W. (2004). Drying foodstuffs with superheated steam. *Drying Technology*, **22**, 899-916.
- Raigar, R.K., Prabhakar, P.K. & Srivastav, P.P. (2016). Effect of different thermal treatments on grinding characteristics, granular morphology and yield of ready-to-eat wheat grits. *Journal of Food Process Engineering*, doi:10.1111/jfpe.12363.
- Ranganathan, V., Nunjundiah, I.T. & Bhattacharya, S. (2014). Effect of roasting on rheological and functional properties of sorghum flour. *Food Science and Technology International*, **20**, 579-589.
- SAGL. (2016). Maize reports 2014-2015 season - SAGL [Internet document]. URL [www.sagl.co.za](http://www.sagl.co.za)  
› Maize › Maize reports. Accessed 09/09/2016.
- Schoeman, L., Du Plessis, A. & Manley, M. (2016a). Non-destructive characterisation and quantification of the effect of conventional oven and forced convection continuous tumble (FCCT) roasting on the three-dimensional microstructure of whole wheat kernels using X-ray micro-computed tomography ( $\mu$ CT). *Journal of Food Engineering*, **187**, 1-13.
- Schoeman, L., Williams, P., Du Plessis, A. & Manley, M. (2016b). X-ray micro-computed tomography ( $\mu$ CT) for non-destructive characterisation of food microstructure. *Trends in Food Science & Technology*, **47**, 10-24.
- Schwartzberg, H.G., Wu, J.P.C., Nussinovitch, A. & Mugerwa, J. (1995). Modelling deformation and flow during vapor-induced puffing. *Journal of Food Engineering*, **25**, 329-372.



- Shoughy, M.I., Marey, S.A. & Abbas, A. (2009). Effect of drying temperatures on stress cracks and breakage susceptibility of corn grains. *Process Engineering*, **26**, 453-468.
- Song, H.P. & Litchfield, J.B. (1994). Measurement of stress cracking in maize kernels by magnetic resonance imaging. *Journal of Agricultural Engineering Research*, **57**, 109-118.
- Sumithra, B. & Bhattacharya, S. (2008). Toasting of corn flakes: product characteristics as a function of processing conditions. *Journal of Food Engineering*, **88**, 419-428.
- Suresh, A. & Neethirajan, S. (2015). Real-time 3D visualization and quantitative analysis of internal structure of wheat kernels. *Journal of Cereal Science*, **63**, 81-87.
- Trater, A.M., Alavi, S. & Rizvi, S.S.H. (2005). Use of non-invasive X-ray microtomography for characterizing microstructure of extruded biopolymer foams. *Food Research International*, **38**, 709-719.
- Van Dalen, G., Nootenboom, P. & Van Vliet, L.J. (2007). 3D imaging, analysis and modelling of porous cereal products using X-ray microtomography. *Image Analysis and Stereology*, **26**, 169-177.
- Verboven, P., Kerckhofs, G., Mebatsion, H.K., Ho, Q.T., Temst, K., Wevers, M., Cloetens, P. & Nicolaï, B.M. (2008). Three-dimensional gas exchange pathways in pome fruit characterized by synchrotron X-ray computed tomography. *Plant Physiology*, **147**, 518-527.
- Witek, M., Węglarz, W.P., De Jong, L., Van Dalen, G., Blonk, J.C.G., Heussen, P., Van Velzen, E., Van As, H. & Van Duynhoven, J. (2010). The structural and hydration properties of heat-treated rice studied at multiple length scales. *Food Chemistry*, **120**, 1031-1040.
- Withers, P.J. (2007). X-ray nanotomography. *Materials Today*, **10**, 26-34.
- Wolf, M., Buzan, C., Macmasters, M.M. & Rist, C. (1952). Structure of the mature corn kernel. 1. Gross anatomy and structural relationships. *Cereal Chemistry*, **29**, 321-333.
- Zhu, L.-J., Dogan, H., Gajula, H., Gu, M.-H., Liu, Q.-Q. & Shi, Y.-C. (2012). Study of kernel structure of high-amylose and wild-type rice by X-ray microtomography and SEM. *Journal of Cereal Science*, **55**, 1-5.
- Zhu, L.-J., Shukri, R., De Mesa-Stonestreet, N.J., Alavi, S., Dogan, H. & Shi, Y.-C. (2010). Mechanical and microstructural properties of soy protein–high amylose corn starch extrudates in relation to physiochemical changes of starch during extrusion. *Journal of Food Engineering*, **100**, 232-238.

**Declaration by the candidate:**

With regard to Chapter 7 (pp. 176-208), the nature and scope of my contribution were as follows:

<b>Nature of contribution</b>	<b>Extent of contribution (%)</b>
Research, analysis and writing of chapter	75

The following co-authors have contributed to Chapter 7 (pp. 176-208):

<b>Name</b>	<b>e-mail address</b>	<b>Nature of contribution</b>	<b>Extent of contribution (%)</b>
Prof Marena Manley	mman@sun.ac.za	Research inputs, editorial suggestions and proofreading	25

Signature of candidate: L. Schoeman

Date: 30/11/2016

**Declaration by co-authors:**

The undersigned hereby confirm that

1. the declaration above accurately reflects the nature and extent of the contributions of the candidate and the co-authors to Chapter 7 (pp. 176-208),
2. no other authors contributed to Chapter 7 (pp. 176-208) besides those specified above, and
3. potential conflicts of interest have been revealed to all interested parties and that the necessary arrangements have been made to use the material in Chapter 7 (pp. 176-208) of this dissertation.

<b>Signature</b>	<b>Institutional affiliation</b>	<b>Date</b>
Prof Marena Manley	Department of Food Science, Stellenbosch University	30/11/2016

Declaration with signature in possession of candidate and supervisor.

## CHAPTER 7

### Physicochemical, structural and functional properties of oven and forced convection continuous tumble (FCCT) roasted maize

#### Abstract

Roasted maize flour is widely consumed as an energy source by certain ethnic groups. Previous work reported that both oven and forced convection continuous tumble (FCCT) roasting changes the microstructure of maize; where oven roasting resulted in a more invasive impact, i.e. a decrease in density and increased porosity. From a food scientist's perspective, information on the effect of roasting on the physicochemical, structural and functional properties is also essential for the development of value-added products. This study found that weight loss, bulk density, puffing index, moisture, crude protein and hardness were more affected by oven roasting in comparison to FCCT roasting, when using the same time-temperature (140 s; 180°C) combination. Furthermore, scanning electron microscopy (SEM) illustrated that oven roasting resulted in central ruptures in the starch granules of the vitreous endosperm and led to the development of larger cavities in the floury endosperm. X-ray diffraction (XRD) demonstrated a decrease in crystallinity, being 14.32%, 13.87% ( $P>0.05$ ) and 12.49% ( $P\leq 0.05$ ) in the control, FCCT and oven-roasted samples, respectively. The thermal properties, measured using differential scanning calorimetry (DSC), of both FCCT and oven-roasted maize starch increased; while the enthalpy decreased after roasting, indicating partial gelatinisation and unfolding of the proteins. The peak viscosity, examined using the Rapid Visco Analyser (RVA), of the roasted flours increased significantly ( $P\leq 0.05$ ) with 20.64% and 21.89% after FCCT and oven roasting, respectively. The results of this study revealed that FCCT roasting resulted in less weight loss and lower hardness reductions and thus indicate that FCCT roasting is the most desirable roasting method.

#### Introduction

Maize (*Zea mays* L.) is one of the most important crops in the developing world as it is used for human consumption and as animal feed (Fox & Manley, 2009). The word maize literally means "that which sustains life" (Mrad *et al.*, 2014a). In Africa, maize which is a highly nutritious staple food, is processed in various ways, i.e. roasting, boiling, fermenting, cooking, milling or a combination of these (Kayode *et al.*, 2013). In its processed form maize is consumed as breads, muffins, wafers, biscuits, infant foods, tortillas, corn chips, snack bars and breakfast cereals (Velu *et al.*, 2006). In poorer regions, where subsistence farming practices produces maize, this staple food undergoes limited processing and is consumed as porridges and flat-style breads (Fox & Manley, 2009). In Nigeria roasted maize snacks include fritters and cakes (Kayode *et al.*, 2013).

Cereal products, especially whole grain, are important in the diets of people worldwide and are a major contributor to good health (Köksel *et al.*, 1998). New and more appealing products are, however, required in the market to increase the consumption of these foods (Köksel *et al.*, 1998).

The utilisation of cereal grains should not be limited to regional or ethnic preferences and consumers worldwide should learn about new ingredients and processing methods (Köksel *et al.*, 1998). Hence, research on roasted maize, which is usually an ethnic food, might broaden the base of this product in the international market. Whole grain flour and products are desirable because of its taste and nutritional benefits. However, after milling, raw whole grain flour rapidly deteriorates due to enzymatic activities, i.e. lipase, peroxidase and lipoxygenase. To overcome this problem and extend storage stability maize can be heat-treated to deactivate enzymes. Thermal treatment will however modify functional, structural and physicochemical properties (Žilić *et al.*, 2010).

Cereal roasting has been reported to improve organoleptic properties, texture, palatability and nutritional and energy value by starch gelatinisation, protein denaturation, increased nutrient availability and inactivation of heat labile toxic compounds and other enzyme inhibitors (Sandhu *et al.*, 2015; Oboh *et al.*, 2010). Roasted whole grains exhibit enhanced crispiness and volume and have improved digestibility and flavour (Sandhu *et al.*, 2015; Cämmerer & Kroh, 2009). Roasting also results in products with an extended shelf life and improved antioxidant properties (Gujral *et al.*, 2013) and can easily be included into ready-to-eat foods and breakfast cereals (Murthy *et al.*, 2008). Roasting can potentially serve as a pre-processing step to reduce the energy consumption required for milling and to improve the processing efficiency of a subsequent milling step (Youn & Chung, 2012). These advantages are however decisively influenced by the roasting conditions (i.e. time and temperature), which are dependent on the roasting method (Youn & Chung, 2012).

Roasting, as a form of maize processing is scarcely studied (Carrera *et al.*, 2015; Oboh *et al.*, 2010; Ayatse *et al.*, 1983). The effects of maize roasting on the nutritive value, hydration kinetics, physicochemical, rheological and textural properties were addressed in some earlier studies (Ayatse *et al.*, 1983; Bhattacharya, 1995; Chung *et al.*, 2011; Ingbian & Adegoke, 2007). The influence of roasting on the antioxidant properties (Oboh *et al.*, 2010) and  $\beta$ -aflatoxins (Méndez-Albores *et al.*, 2004) were also evaluated.

Roasting is a rapid processing method that uses dry heat for short time periods (Mrad *et al.*, 2014b). Roasted maize flour can be processed into a snack, beverage, an oatmeal-type paste, breakfast porridge or baked into a cake or bread (Carrera *et al.*, 2015). It can also be used as the basis for cooked pastes, in soups and as thickening agent (Ingbian & Adegoke, 2007). Pinole, a traditional energy food attained from roasted ground maize, was shown to result in a significant increase in total available starches and *in vitro* hydrolysis rate (Carrera *et al.*, 2015), making it a suitable ingredient for specialised energy cereal bar products. This study provided insights for understanding the extensive use of pinole, as an energy food, by impoverished ethnic groups and also more recently by ultra-runners. Athletes regard pinole as an all-natural energy booster (Carrera *et al.*, 2015). Pinole is widely eaten in Nigeria, across low- and high-income groups (Ayatse *et al.*, 1983) and is also consumed by diverse ethnic groups in Northern Mexico and Southern USA (Carrera *et al.*, 2015; Méndez-Albores *et al.*, 2004). At the household level of production, the process of roasting and milling small quantities of grains in commercial mills is

inconvenient and not cost effective. The solution lies in small-scale enterprise development to handle the preparation and distribution of these products as a commercial venture (Plahar *et al.*, 2003).

Forced convection continuous tumble (FCCT) roasting has been shown to have a less invasive impact on the microstructure of maize in comparison to conventional oven roasting when using the same time and temperature combination (Schoeman *et al.*, 2016b). Oven roasting makes use of dry heat treatment, whereas FCCT roasting utilises superheated steam. Furthermore, during FCCT the sample is continuously moving inside the roasting chamber, resulting in a more homogenous roasting process, in comparison to oven roasting where the sample is static. Both roasting methods did not significantly ( $P > 0.05$ ) influence the dry milling properties. However, from a food scientist's perspective, the effect on physicochemical, structural (in terms of the starch-protein morphology and crystallinity) and functional properties is essential for the development of value-added products.

Roasting can be monitored by physicochemical changes occurring during this thermal treatment (Mendes *et al.*, 2001). Information on these changes may help in controlling the roasting process to obtain a better quality product. Maize hardness is an important quality feature for the milling industry as it influences several stages of grain handling and processing and gives an estimated idea of the overall milling characteristics (Raigar *et al.*, 2016). In South Africa dry milling is used for the production of maize meal, grits and samp and adequate hardness is necessary to obtain an optimum yield and high quality product (O'Kennedy, 2011). Harder kernels are associated with more resistance to breakage, while softer kernels are more susceptible to mechanical damage as well as pathogen attack (Blandino *et al.*, 2010). Softer kernels can reduce milling yield and milling efficiency (Fox & Manley, 2009) and also require less time for steeping for wet milling and are more amenable to separating the storage proteins from the starch (Blandino *et al.*, 2010). The coarse-to-fine ratio (c/f) defines kernel hardness by providing an indirect but precise estimation of the hard and soft portions of maize endosperm (Blandino *et al.*, 2010). Bulk density is also considered an important physical property of pre-processed cereals in terms of storage and transportation.

In maize, starch is laid down in the endosperm tissue (which comprises 80% of the kernel volume) where it serves as the main storage carbohydrate (Delcour & Hosney, 2010). The endosperm is formed by clusters of starch granules, packed differently and covered by a protein matrix (Gustin *et al.*, 2013). Two types of starch granules embedded within a complex protein matrix are present in the endosperm: densely packed polygonal starch granules (7-18  $\mu\text{m}$  in diameter) are associated with the outer region (near aleurone) of the kernel, i.e. the vitreous (hard) endosperm; while the granules in the kernel centre (floury/soft endosperm) tend to be spherical with many intergranular spaces (loosely packed) (Delcour & Hosney, 2010). The region where the two endosperms meet is referred to as the junction or transition phase (O'Kennedy, 2011).

Schoeman *et al.* (2016b) demonstrated that roasting induce changes in the volume and relative density of the two different endosperm regions, with the floury endosperm being more adversely affected than the vitreous endosperm. It is however, important to illustrate the starch-protein morphology, using scanning electron microscopy (SEM), in order to understand these changes. Furthermore, X-ray diffraction (XRD) can identify the crystalline material in maize samples, based on their unique crystal structure (Carrera *et al.*, 2015). When irradiated with X-rays, starch granules behave like crystals and form distinctive patterns according to their crystal structure. Cereal starches typically yields an A-type pattern. Carrera *et al.* (2015) showed that the crystallinity content of maize starch decreased after roasting, which resulted in an improved hydrolysis rate and *in vitro* starch digestibility.

Microstructural changes in the endosperm may result in changes in functionality. Water absorption capacity (WAC), is a measure of the quantity of water absorbed by starch (index of gelatinisation), while water solubility index (WSI) is an indicator of the degree of degradation of molecular components as it measures the amount of soluble components released from starch (Hernández-Nava *et al.*, 2011). Flour dispersibility (FD) in water indicates the ability to reconstitute and is also known as the reconstitution index (RI) (Edema *et al.*, 2005). Changes in structure induced by roasting may also influence thermal transitions and gelatinisation characteristics. Differential scanning calorimetry (DSC) endotherms can be used to determine the temperature range over which the crystal structure is being melted as well as the degree of gelatinisation.

Pasting properties are key to understanding physical characteristics and potential utilisation (Olayinka *et al.*, 2008). Changes in the consistency of the starch pastes can be attributed to changes in structure (Guzmán *et al.*, 2009). The effect of roasting on the functional properties has been reported for oats (Doehlert *et al.*, 1997; Gujral *et al.*, 2011), quinoa (Rothschild *et al.*, 2015), barley (Sharma *et al.*, 2011) and sorghum (Ranganathan *et al.*, 2014). Sharma *et al.* (2011) found that roasting significantly affected the pasting and thermal properties of barley flour. From this work it was postulated that structural changes during roasting could be in great extent responsible for changes in functionality.

Conventional oven roasting used presently in food industries has a number of shortcomings as it is less energy efficient, more costly and may adversely affect not only physicochemical properties but also nutritional quality of the end product (Zzaman & Yang, 2013). Convection oven roasting contributed to increased bitterness, loss of aroma and higher hardness reductions in cocoa beans. In contrast, superheated steam roasting resulted in lower moisture losses and less discolouration (Zzaman & Yang, 2013). Thus, superheated steam roasting can be applied as new thermal processing method because of its convenience, flexibility and more desirable food characteristics. Superheated steam is a type of unsaturated (dry) steam that is generated by the addition of sensible heat to saturated (wet) steam (Head *et al.*, 2010). This method is more energy efficient since it reuses the latent heat during evaporation in comparison to conventional hot air roasting (Zzaman & Yang, 2013). Superheated steam as a drying medium for foodstuff retains vitamins and



other essential nutrients and are thus regarded as healthy, while it results in the preservation of more desirable food characteristics in terms of colour and microstructure (Pronyk *et al.*, 2004; Idrus & Yang, 2012).

Increasing interest in roasted whole grains in food products is arising due to the potential health benefits and bioavailability of minerals because of the greater loss in phytic acid during roasting (Khan *et al.*, 1991; Carrera *et al.*, 2015). In a review article factors affecting the physicochemical, morphological and functional properties of starch from different sources have been published (Singh *et al.*, 2007). However, few studies on the effect of roasting on the physicochemical properties, structure and functionality of maize are found in literature (Carrera *et al.*, 2015; Bhattacharya, 1995). Maize kernels undergo a series of structural changes, e.g. volume, porosity and relative density, during roasting which will affect the final product (Schoeman *et al.*, 2016b). Chemical reactions, i.e. protein denaturation, starch gelatinisation and Maillard reactions are also induced during roasting (Idrus & Yang, 2012).

The aim of this research was to evaluate the physicochemical, structural and functional properties of oven and FCCT-roasted maize kernels. This was achieved by analysing weight loss, bulk density, puffing index, moisture content, crude protein and particle size index (hardness). Structural evaluation included examination of the starch-protein morphology and crystallinity using SEM and XRD, respectively. Determination of WAC, WSI, FD and thermal and pasting properties formed part of the functional analyses.

## Materials and methods

### *Maize samples*

A 19.8 kg commercial white maize variety was kindly provided by Sasko (Essential Foods, Division of Pioneer Foods (Pty.) Ltd., Paarl, South Africa). The maize was cleaned using a Carter Day Dockage Tester (Carter Day International, Minneapolis, MN) to remove foreign materials and broken kernels and then thoroughly mixed and divided into nine batches of 2.20 kg each using a Boerner Divider (Seedburo Equipment Co., Chicago, USA). Each sample was stored in an airtight plastic container at ambient temperature prior to use.

### *Tempering of test run sample before FCCT roasting*

Before FCCT roasting was performed, a test run sample (400 g) was tempered with pure deionised water (dH<sub>2</sub>O) to a final moisture content of between 18 and 20%. This was required for the FCCT roaster to create some initial moisture and generate superheated steam in the roasting chamber to result in a more homogenous roasting process. The quantity of water (Eq. 1) to add was calculated from the original moisture content and mass of the sample (400 g) according to the AACC Method 26-95.01(AACC, 1999b). The test sample was shaken regularly during tempering (24 h at room temperature) in an airtight container to ensure even distribution of the water.

$$\text{Weight of water to add (g)} = \left( \frac{100 - \text{original moisture (\%)}}{100 - \text{desired moisture (\%)}} - 1 \right) \times \text{sample weight (g)} \quad (1)$$

### *Roasting*

Maize samples were roasted at 180°C for 140 s using conventional convection oven roasting (831 Electric Multifunction Thermofan Solid Plate Oven, Defy Appliances, Durban, South Africa) and forced convection continuous tumble (FCCT) (model R100E, Roastech, Bloemfontein, South Africa) roasting, respectively. A temperature of 180°C is commonly used for roasting maize (Chung *et al.*, 2011; Bhattacharya, 1995). Three batches of 2.20 kg each were roasted according to the roasting procedure described earlier (Schoeman *et al.*, 2016a). After roasting the samples were immediately cooled to ambient temperature by spreading it out on a cold flat surface to prevent excessive roast and further moisture loss. Both roasting methods were performed in triplicate. The samples were stored in airtight plastic containers at ambient temperature until being milled and used for further analyses.

### *Grinding of maize samples*

The control and roasted maize samples (300 g of each sample) were milled separately into flour using a hammer-type cyclone Laboratory Mill 3100 (Perten, Hägersten, Sweden) fitted with a 1 mm sieve. The whole grain flour samples were stored in airtight containers (at ambient temperature) from which the required quantities were removed for further analyses.

### *Experimental design*

Figure 7.1 demonstrates the experimental design used for this study. The physiochemical, structural and functional properties of the control and roasted maize, respectively were examined.

### *Physicochemical analyses*

#### Weight loss

The weight of the samples was recorded before and after roasting to determine the percentage weight loss.

#### Bulk density and puffing index (PI)

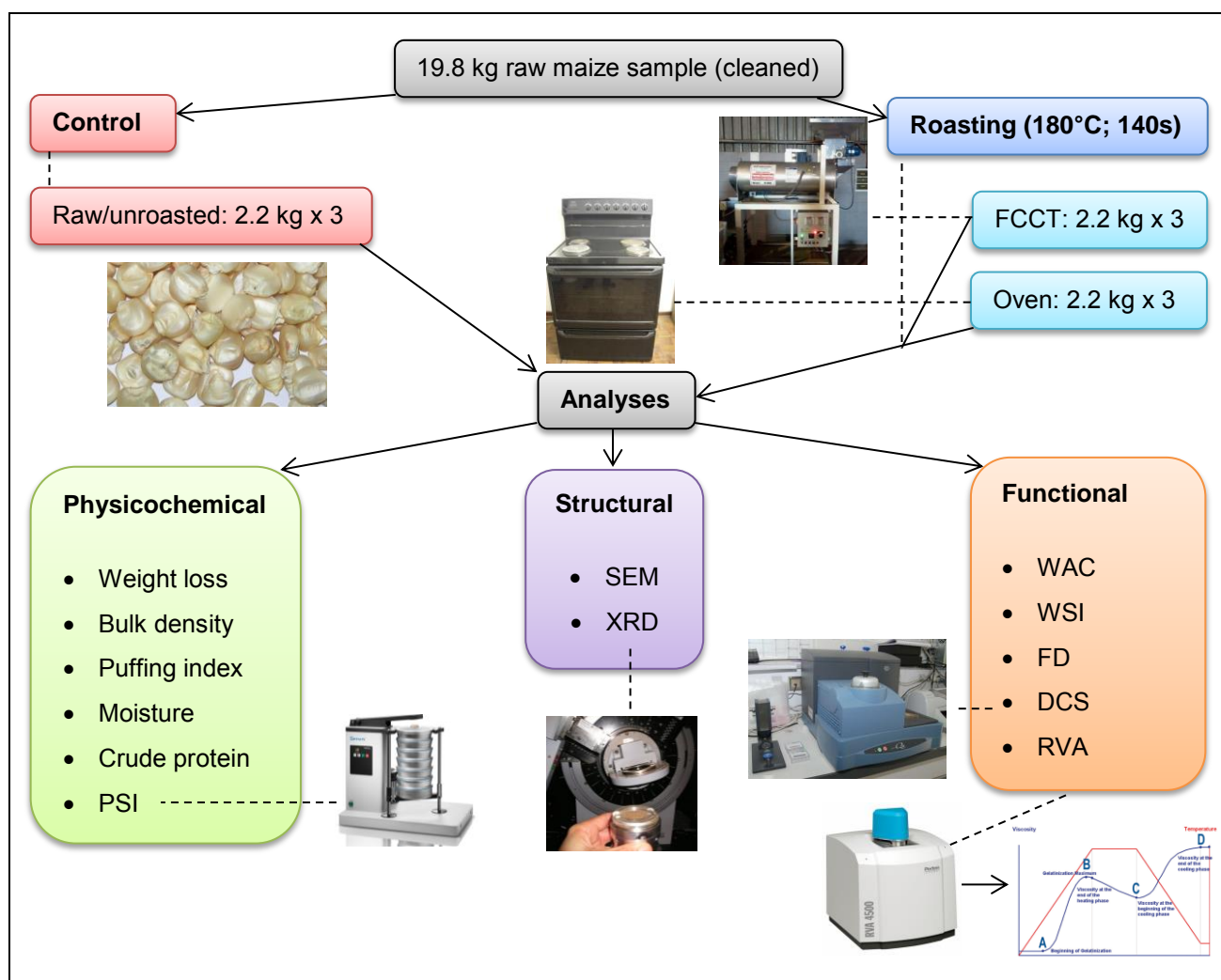
Bulk density and PI were determined in triplicate according to the method described in Chapter 5.

#### Moisture content

Moisture content determinations were performed in triplicate using air-oven drying according to the AACC Method 44-19.01 (AACC, 1999c). Maize flour (2 g ± 1 mg) was heated in aluminium moisture dishes for 2 h at 135°C in an Oven, model EM10 (CHOPIN Technologies, Cedex, France). Moisture loss was used to calculate the percentage moisture (Eq.2).

$$\text{Moisture (\%)} = \frac{\text{Moisture loss (g)}}{\text{Sample weight (g)}} \times 100$$

(2)



**Figure 7.1.** Illustration of a simplified flow diagram of the roasting and analyses procedures used. PSI= particle size index; SEM= scanning electron microscopy; XRD= X-ray diffraction; WAC= water absorption capacity; WSI= water solubility index; FD= flour dispersibility; DSC= differential scanning calorimetry; RVA= Rapid Visco Analyser.

### Crude protein

Crude protein content of the control and roasted maize flour was determined in duplicate using the Dumas combustion method according to the AACC Approved Method 46-30.01 (AACC, 1999d). A LECO TruMac N (LECO Corporation, Saint Joseph, Michigan, USA) instrument was used to determine the crude protein content at 12% moisture base (mb). A protein conversion factor of 6.25 was used to calculate the crude protein (%) from the nitrogen.

### Particle size index (PSI)

PSI was determined to give an indication of maize kernel hardness. The control and roasted samples (50 g of each sample) were milled using a cyclone Laboratory Mill 3100 (Perten,

Hägersten, Sweden) fitted with a 1 mm sieve. The two-sieve method reported by Guelpa *et al.* (2015) was used, where the 150 µm sieve was placed on a 75 µm sieve, fitted with a receiving pan and a lid. The two sets of pans and sieves (Retsch, Haan, Germany) were stacked on top of each other and placed in a Retsch AS 200 Tap Sieve Shaker (Retsch, Haan, Germany) for 10 min. This delivered three fractions:  $PSI_1$ ,  $PSI_2$  and  $PSI_3$  from which a c/f was calculated. To determine  $PSI_1$ , the 150 µm sieve was weighed ( $W_{150 \mu m \text{ sieve}}$ ). Hereafter,  $10 \pm 0.01$  g of ground maize was weighed ( $W_{maize}$ ) into the 150 µm sieve along with  $10 \pm 0.01$  g whole wheat kernels ( $W_{wheat \text{ on } 150 \mu m \text{ sieve}}$ ). The whole wheat kernels were added for more efficient sieving. After the sieving and tapping process, the fine maize meal adhering to the bottom of the 150 µm sieve was brushed off into the 75 µm sieve and the 150 µm sieve was weighed ( $W_1$ ). Equation 3 was used to determine  $PSI_1$ :

$$PSI_1 = \frac{(W_1 - (W_{150 \mu m \text{ sieve}} + W_{wheat \text{ on } 150 \mu m \text{ sieve}}))}{W_{maize}} \quad (3)$$

Next, the fine maize meal adhering to the bottom of the 75 µm sieve was brushed off into the receiving pan and the 75 µm sieve was weighed ( $W_2$ ). The empty 75 µm sieve weight ( $W_{75 \mu m \text{ sieve}}$ ) was recorded as well as the weight of the whole wheat kernels  $10 \pm 0.01$ g placed on the 75 µm sieve ( $W_{wheat \text{ on } 75 \mu m \text{ sieve}}$ ).  $PSI_2$  was determined according to equation 4:

$$PSI_2 = \frac{(W_2 - (W_{75 \mu m \text{ sieve}} + W_{wheat \text{ on } 75 \mu m \text{ sieve}}))}{W_{maize}} \quad (4)$$

Equation 5 was used to determine  $PSI_3$ . The empty receiving pan was weighed ( $W_{pan}$ ) and deducted from the weighed of the pan obtained after sieving ( $W_3$ ).

$$PSI_3 = \frac{(W_3 - W_{pan})}{W_{maize}} \quad (5)$$

Three fractions were determined:  $PSI_1$  (particles > 150 µm),  $PSI_2$  (particles <150 µm, but > 75 µm) and  $PSI_3$  (particles < 75 µm). High  $PSI_1$  values are indicative of harder kernels, whilst high  $PSI_2$  and  $PSI_3$  values relates to softer kernels. Equation 6 was used to calculate the c/f which gives the ratio between the larger ( $PSI_1$ ) and smaller ( $PSI_2 + PSI_3$ ) particle sizes (Guelpa *et al.*, 2015). A high c/f indicates a harder or denser sample and vice versa.

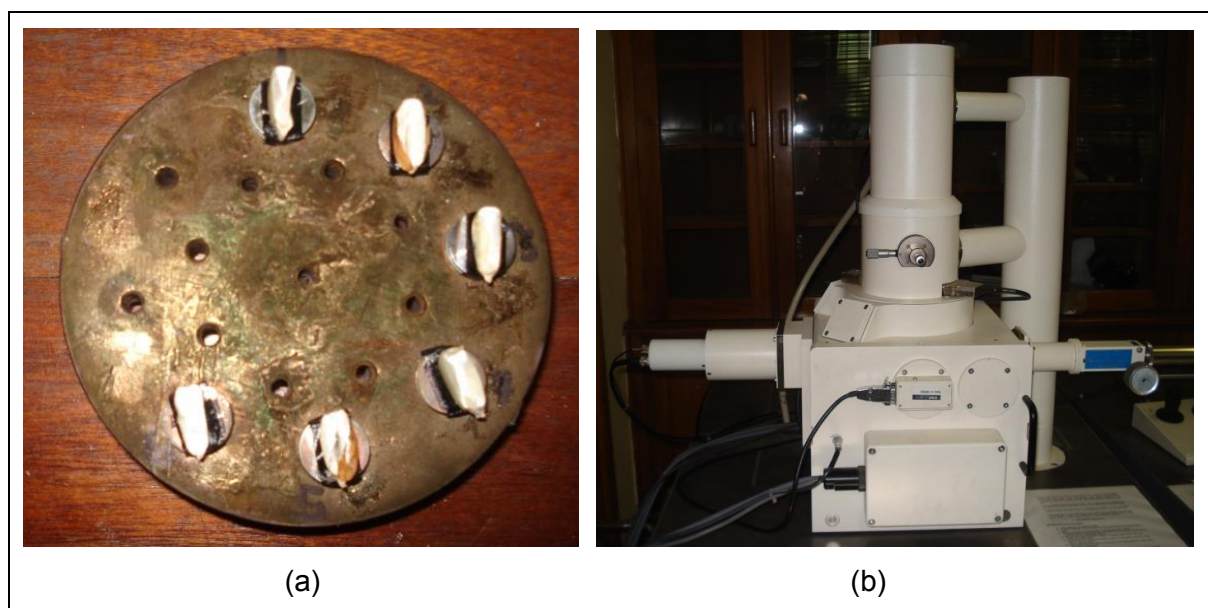
$$c/f = \frac{PSI_1}{(PSI_2 + PSI_3)} \quad (6)$$

## Structural analyses

### Scanning electron microscopy (SEM)

Two control, two FCCT-roasted and two oven-roasted whole maize kernels were cut with a Solingen blade along the transverse axis. The cut kernels were mounted on aluminium stubs with double-sided carbon tape (Fig. 7.2a) and coated with a thin layer of gold dust using a 5150A sputter-coater (HHV, Crawley, United Kingdom). The samples were imaged, using a LEO 1430VP scanning electron microscope (Zeiss, Germany) (Fig 7.2b), under high vacuum conditions at an accelerating voltage of 7 kV and a current of 11µA. The surface structure of the samples was identified with secondary electron images. Representative micrographs of cross-sections of the kernels were obtained at a 500 and 1500 x magnification, respectively to observe the starch

granule morphology within the vitreous and floury endosperm matrices. At least four SEM micrographs were obtained for each maize kernel.



**Figure 7.2.** Photograph of (a) the maize kernels mounted on aluminium stubs with double-sided carbon tape and placed into the sample holder; (b) the LEO 1430VP scanning electron microscope (Zeiss, Germany).

#### X-ray diffraction (XRD)

XRD traces of the flour samples were measured at room temperature using a D8 Advance Bruker X-ray powder diffractometer (BRUKER AXS, Germany) according to the method reported by Carrera *et al.* (2015), with slight modifications. The instrument was equipped with a water-cooled rotating copper anode that produces Cu-K $\alpha$  radiation ( $\lambda = 1.5406$ ) with an accelerating voltage of 30 kV and tube current of 10 mA. Intensities were measured in the 5-40° range 2 $\theta$  with a 0.016° step size and measuring time of 0.5 seconds per point. The total effect time was 1285 s. The scattered intensities are given in arbitrary units (a.u.). The scan mode was continuous PSD fast and a Lynx Eye PSD detector type was used. One diffractogram was collected for each of the nine samples and the average of three replicates was reported. The crystalline and amorphous areas were quantified using EVA software (BRUKER AXS, Germany). To determine the degree of crystallinity the integrated area of the upper region of the curve (crystalline peaks) was divided by the total integrated area under the curve and above the straight baseline (amorphous + crystalline peaks) (Yoo & Jane, 2002). Equation 7 was used to calculate the percentage crystallinity.

$$\text{Crystallinity (\%)} = \frac{A_c}{(A_c + A_a)} \times 100 \quad (7)$$

where  $A_c$  is the crystalline area on the X-ray diffractogram and  $A_a$  is the amorphous area on the X-ray diffractogram.



## Functional analyses

### Water absorption capacity (WAC) and water solubility index (WSI)

The WAC of the control and roasted flour samples was determined in triplicate using centrifugation according to the AACC method 56-20.01 (AACC, 1999e), with slight modifications as reported by Mwangwela *et al.* (2007). The WSI was determined in triplicate according to the method reported by Hafsa *et al.* (2015). These methods were described earlier in Chapter 5. WAC (g water/g flour) was expressed as the weight of water absorbed/bound per gram of dry flour. WSI was calculated as the ratio of the weight of dried solids recovered by evaporation of the supernatant over the initial sample weight and was expressed as percent dry solids.

### Flour dispersibility (FD)

FD analysis was performed in triplicate following the method of Edema *et al.* (2005). For each sample, 10 g of flour was weighed into a 100 mL measuring cylinder and filled to the 100 mL mark with dH<sub>2</sub>O. The sample was vigorously stirred and then allowed to settle. After 3 h the volume of the settled particles was recorded and subtracted from 100 to give a difference that is recorded as percentage dispersibility.

### Differential scanning calorimetry (DSC)

The thermal properties of the control and roasted maize flour samples were analysed using a differential scanning calorimeter (DSC Q20, TA Instruments, New Castle, USA), following the procedure described by Carrera *et al.* (2015). The DSC cell and a universal thermal analysis data station was used to measure endothermal changes. On the thermograms the heat flow (W/g) was measured as a function of temperature (°C). The operating procedure was previously described in Chapter 5. Onset, peak and endset temperatures ( $T_o$ ,  $T_p$  and  $T_e$ ) correspond to the onset, peak and offset of the heat flow with respect to the baseline and were calculated from the DSC thermograms (Carrera *et al.*, 2015). The average values of three replicates were reported. The gelatinisation range ( $\Delta T$ ) was calculated as  $T_e - T_o$ . The change in enthalpy ( $\Delta H$ ) of the transitions (associated with starch gelatinisation and protein denaturation) was determined by calculating the peak areas under the endotherm (curve) using Matlab™ 2014b software (Mathworks, Natick, MA, USA) (Ahmed *et al.*, 2007). The degree of gelatinisation (%) was calculated as reported by Sharma *et al.* (2011) (Eq. 8):

$$\text{Degree of gelatinisation (\%)} = \left[ 1 - \left( \frac{\Delta H \text{ of roasted sample}}{\Delta H \text{ of control sample}} \right) \right] \times 100 \quad (8)$$

### Pasting properties and $\alpha$ -amylase activity using the RVA

The pasting properties of the control and roasted maize flour samples were determined according to the AACC method 76-21.01 (AACC, 1999f) using the Rapid Visco Analyser (RVA) model 4500 (Perten Instruments, Eden, Australia). The *Thermocline for Windows*™ (Version 3) software was used to accept configuration information and test profiles from the operator. Standard profile 1 was



used to capture rheological information (RVA curves). The details of this profile is summarised in Table 7.1. The method has been described earlier in Chapter 5. The viscosity was measured in centipoise (cP) and triplicate runs were conducted for each sample. Pasting properties of the samples were characterised using the parameters recorded on the viscosity trace: pasting temperature ( $P_{temp}$ ) (temperature where viscosity first increases by at least 25 cP over a 20 s period), peak time (time at which peak viscosity occurred), peak viscosity ( $P_v$ ) (maximum hot paste viscosity), trough viscosity ( $V_t$ ) (trough at the minimum hot paste viscosity), final viscosity ( $V_f$ ) (viscosity at the end of test after cooling to 50°C and holding at this temperature), breakdown viscosity ( $V_b$ ) (peak viscosity –trough viscosity) and setback viscosity ( $V_s$ ) (final viscosity – trough viscosity) (Ragae & Abdel-Aal, 2006).

**Table 7.1.** Details of the RVA standard profile 1

Stage	Standard profile 1
Initial temperature (°C)	50
Initial holding time (min)	1:00
Heating time (min)	3:42
Maximum temperature (°C)	95
Hold at max temperature (min)	2:30
Cooling time (min)	3:48
Final temperature (°C)	50
Final holding time (min)	2:00
Total test time (min)	13:00

In a separate experiment, stirring number (SN) was measured by the RVA, as described in the the AACC method 22-08.01 (AACC, 1999a). The SN is an indication of amylase activity and is defined as the apparent viscosity at the 180<sup>th</sup> second of stirring a hot aqueous flour suspension undergoing liquefaction. The SN profile, reported in Table 7.2 was used. After termination of the test the SN, displayed as the final viscosity, were recorded in cP.

**Table 7.2.** Details of the RVA stirring number profile

Stage	Stirring number profile
Idle temperature (°C)	95
Idle tolerance temperature (°C)	1
1: 960 rpm	0 sec
2: 160 rpm	10 sec
3: 95 °C	3 min
End of test	3 min

### Statistical analysis

One-way analysis of variance (ANOVA) was performed to compare averages of the respective quantitative measurements with respect to the control and the two roasting methods. Data was reported as mean  $\pm$  standard deviation for procedures performed in triplicate. Statistical analysis was carried out using STATISTICA version 13 (StatSoft, Inc., Tulsa, USA). The level of confidence required for significance was selected at  $P \leq 0.05$ .

## Results and discussion

### Physicochemical analyses

Table 7.3 illustrates the physicochemical properties of the control and roasted maize samples. Information about changes in physicochemical properties may help in controlling the roasting process in order to obtain a better quality roasted product.

**Table 7.3.** Physicochemical properties of the control and roasted maize samples

Sample	Weight loss (%)	Bulk density (g/cm <sup>3</sup> )	PI	Moisture (%)	Crude protein (%) <sup>a**</sup>	PSI (c/f) <sup>b**</sup>
Control	0 <sup>c</sup>	0.73 $\pm$ 0.001 <sup>a</sup>	0 <sup>c</sup>	12.78 $\pm$ 0.18 <sup>a</sup>	7.21 $\pm$ 0.03 <sup>a</sup>	2.17 $\pm$ 0.19 <sup>a</sup>
FCCT	0.61 $\pm$ 0.03 <sup>b</sup>	0.69 $\pm$ 0.004 <sup>b</sup>	1.05 $\pm$ 0.007 <sup>b</sup>	12.43 $\pm$ 0.08 <sup>b</sup>	6.97 $\pm$ 0.32 <sup>a</sup>	1.07 $\pm$ 0.07 <sup>b</sup>
Oven	1.21 $\pm$ 0.25 <sup>a</sup>	0.66 $\pm$ 0.002 <sup>c</sup>	1.11 $\pm$ 0.00 <sup>a</sup>	11.91 $\pm$ 0.18 <sup>c</sup>	6.54 $\pm$ 0.16 <sup>b</sup>	0.90 $\pm$ 0.10 <sup>b</sup>

Values are presented as mean  $\pm$  standard deviation of three replicates (n=3). Mean values with different superscripts in a column differ significantly ( $P \leq 0.05$ ). <sup>a</sup>Crude protein are expressed as (N x 6.25) on a 12% moisture basis; <sup>b</sup>Particle size index (course-to-fine ratio); <sup>\*\*</sup>Mean values from duplicate measurements of three replicates.

### Weight loss

Weight loss was significantly ( $P \leq 0.05$ ) higher for oven roasting (1.21%) in comparison to the 0.61% loss by FCCT roasting (Table 7.3). Weight loss is mainly due to moisture evaporation during roasting (Chung *et al.*, 2011) and therefore the difference between the weight losses of the two roasting methods may be explained by the difference in evaporation rate. FCCT roasting generates superheated steam from the moisture inside the product and this together with the continuous rotation of the sample in the roasting chamber results in more homogenous roasting. In contrast oven roasting uses dry air and the sample remains in a static position during roasting. Sharma *et al.* (2011) reported much higher weight losses of 2.1-13.7% for barley when using traditional sand roasting at 280°C for 20 s.

### Bulk density and puffing index (PI)

Bulk density is an index of the extent of puffing (Gupta *et al.*, 2008) and thus used to measure the PI. Higher reduction in bulk density and more puffing (larger PI) was achieved by oven roasting (Table 7.3). The significant ( $P \leq 0.05$ ) decrease in bulk density during roasting can be due to a combination of factors i.e. loss in cellular structure, weight and moisture, volume increase (kernel

expansion) and the development of internal pores and cavities (Jha, 2005; Pittia *et al.*, 2001; Schoeman *et al.*, 2016a). The bulk density obtained, for both roasting methods, in this study was comparable to that of roasted maize (0.52 to 0.79 g/cm<sup>3</sup>) reported by Chung *et al.* (2011) using an electric rotary roaster. Chung *et al.* (2011) reported that roasting time and temperature significantly affected ( $P \leq 0.05$ ) the bulk density of maize kernels, with an increase in roasting temperature and time resulting in a decrease in bulk density. Sandhu *et al.* (2015) similarly observed that toasting oats resulted in a decreased bulk density and increased puffing and ascribed this phenomenon to the loss of structural integrity between starch–starch and starch–protein matrices and/or due to the formation of air spaces in the endosperm. Bulk density decreases and PI index increases as starch gelatinisation and the volume of products increases (Case *et al.*, 1992).

### Moisture content

For the same time-temperature roasting conditions, oven roasting had a greater impact on moisture content compared to FCCT roasting (Table 7.3). Again this can be attributed to the more homogenous roasting process of FCCT roasting. Vivas *et al.* (1987) reported a decrease in moisture content from 9.6% to 7.2% when maize was oven-roasted at 232°C for 10 min. Oboh *et al.* (2010) reported that pan roasting (120-130°C; 17 min) of white maize resulted in moisture reductions between 14.31-16.92%. In our case, lower moisture reductions were expected since a shorter roasting time (140 s) was used.

Studying the effect of superheated steam and convection oven roasting on cocoa beans, the results demonstrated that moisture loss were lower at each temperature in superheated steam roasting (Zzaman & Yang, 2013). Similarly, when roasting peanuts, Idrus & Yang (2012) reported oven roasting to result in greater moisture loss than superheated steam roasting. This illustrates that the rate of decrease in moisture content during oven roasting was higher compared to superheated steam roasting. These results are in concurrence with the results obtained from the two roasting methods applied in this study.

Moisture content plays a vital role in the shelf-life of products and is associated with microbial spoilage. Fungal growth are inhibited at moisture contents below 14% (Hoseney, 1994), while a moisture content of less than 13.5% is recommended for proper storage of maize and its products (Humpf & Voss, 2004). The values obtained in this study were below the recommended 13.5% (Table 7.3).

### Crude protein

The crude protein content of the maize samples was not significantly ( $P > 0.05$ ) affected by FCCT roasting, in contrast to oven roasting which resulted in a significant ( $P \leq 0.05$ ) decrease (Table 7.3). The reduction in protein content after roasting can be ascribed to the denaturation and loss of protein due to participation of amino acids in the Maillard reaction (Oboh *et al.*, 2010). During roasting the application of high temperature ( $>180^\circ\text{C}$ ) together with low moisture ( $<15\%$ ) favour the

development of a reaction between the free amino groups of the amino acids and reducing sugar aldehyde groups, giving rise to Maillard reaction (Rufián-Henares & Delgado-Andrade, 2009). This reaction is capable of producing insoluble brown polymers called melanoidins.

Bala (2016) reported that FCCT roasting did not significantly ( $P>0.05$ ) affect the protein content, which agreed with the present finding. This can be attributed to the use of superheated steam instead of dry hot air. Similarly, flame roasting (74-160°C) of maize had no ( $P>0.05$ ) effect on protein content (Costa *et al.*, 1976; McNiven *et al.*, 1994). Oboh *et al.* (2010) reported a significant ( $P\leq 0.05$ ) decrease in the protein content of roasted maize suggesting protein quality depletion due to thermal degradation and formation of melanoidins. Contrary to this, Ingbian & Adegoke (2007) reported a significant ( $P\leq 0.05$ ) increase in protein content during maize roasting. These contrasting findings could be due to differences in the roasting conditions and methods used.

### PSI (c/f)

Raw (harder) grains had a coarser particle size (higher c/f) than the softer, roasted maize (Table 7.3). The significantly ( $P\leq 0.05$ ) smaller c/f of both roasted samples, more specifically the oven-roasted sample, is attributed to the sample being more finely milled and the coarse particles were removed by sieving. These results are in concurrence with previous studies that reported a reduction in hardness after cereal roasting (Murthy *et al.*, 2008; Sharma *et al.*, 2011). This has been attributed to volumetric expansion and starch gelatinisation. The decreasing trend in hardness during roasting were also observed for peanuts when superheated steam and oven roasting (250°C) were compared (Idrus & Yang, 2012). The rate of hardness reduction during convection oven roasting was higher than for superheated steam roasting (Idrus & Yang, 2012). Hence, hardness was more affected during oven roasting. This trend, also observed in this study, was however, not statistically significant ( $P>0.05$ ) for the two roasting methods.

Roasting caused a decrease in hardness, which can be attributed to the increased porosity and cavity development (Schoeman *et al.*, 2016a) as well as structural modifications caused by chemical and physical changes (Schenker *et al.*, 2000). A study on roasting oats attributed changes in physical properties e.g. hardness to grain expansion that occurred as a result of the development of cavities and disorganisation of the endosperm (Gujral *et al.*, 2011).

### *Structural analyses*

#### Scanning electron microscopy (SEM)

Figure 7.3 depicts the longitudinal digital slice images and SEM micrographs of (a) control, (b) FCCT and (c) oven-roasted maize kernels. The floury (opaque) and vitreous (glassy) endosperm matrices are illustrated as white and translucent regions, respectively (Fig. 7.3a). The control kernel has no visible internal cracks and it is closely packed in a honeycomb structure, whereas the roasted kernels reveal internal cracks and cavity development (Fig. 7.3b and c). The transition

region (Fig. 7.3 a), illustrates the polygonal shape of the starch granules and the tightly compacted structure of the vitreous endosperm and the opaque, floury endosperm is seen as spherical shaped starch granules with a loosely packed structure. The starch granules in the vitreous endosperm have an adhering thick continuous protein matrix (P) surrounding it. The floury endosperm contains thin sheets of protein and many intergranular air spaces (Dombrink-Kurtzman & Knutson, 1997).

Roasting resulted in some transformation of the starch granules and disintegration of the protein network (Fig. 7.3b and c). Roasting temperature is the leading factor for structural alterations in the endosperm and breakage of polysaccharide bonds (Oboh *et al.*, 2010). In the floury endosperm of the FCCT-roasted samples very few cavities could be detected, but the starch matrix appeared disordered. The lack of a thick protein matrix covering the starch granules in the floury endosperm, led to the formation of cavities. Proportionally, the vitreous endosperm starch granules remained densely packed and held intact by a thick protein matrix.

The oven-roasted sample (Fig. 7.3c) has a much darker internal colour, especially the germ, indicating a more intense degree of roasting. Larger fissures and cavities observed in the oven-roasted kernels contributed significantly to kernel expansion. More intergranular air spaces during oven roasting relates to the lower bulk density and hardness reported (Table 7.3) in comparison to FCCT roasting. In the oven-roasted kernels, a loss of endosperm structure occurred with ruptures (due to high internal pressure) in the centre of the vitreous endosperm starch granules and numerous large, irregular cavities in the floury endosperm. Hosene *et al.* (1983) reported that the voids around the starch in the floury endosperm provide an alternative site to which the internal steam vaporises. Thus, no ruptures occurred in the floury endosperm as was observed in the vitreous endosperm.

The pericarp acts as a vessel that allows pressure built-up in the endosperm (Hosene *et al.*, 1983). Since no intergranular cavities developed in the vitreous endosperm, the build-up of internal pressure in the starch granules forced ruptures to occur in the centre of the granules. The starch granules, however, maintained their polygonal shape. Starch granules contain a microscopic pore (hilum) in the centre (Schwartzberg *et al.*, 1995). The hilum acts as a nucleation site to which water vapour (internal steam) diffuses in the process of expansion (Hosene *et al.*, 1983). Evidence proposes that the development of cavities at the hilum can be attributed to dehydration, which involves moisture loss, usually at high temperatures (Baldwin *et al.*, 1994). The hilum is believed to be the least organised region because gelatinisation, acid-catalysed hydrolysis, enzymatic attack and cavitation originates here (Fuwa *et al.*, 1978). In a study by Zhang *et al.* (2012) on the characterisation of gelatinised starches it was observed that starch granules started to burst from the centre, where the hilum is located.

Both roasting methods resulted in disintegration of the protein network into thin elongated strands in the floury endosperm. These fragmented glue-like strands are possibly composed of a mixture of melted starch and denatured protein matrix. The shape of the starch granules

predominantly remained intact and the granule boundaries were still visible in both roasting methods. It can be postulated that the starch partially melts during roasting since maize starch begin to melt at approximately 150°C, with a peak at 180 to 186°C (Schwartzberg *et al.*, 1995).

Even though the roasting temperature exceeds the gelatinisation temperature (62-72°C) of maize starch, most starch granules maintained their polygonal or round shape (Delcour & Hosney, 2010). Thus, the majority of the starch granules seemed not to have gelatinised during roasting. Further evaluation using DSC was performed to support these conclusions. The low moisture content may be the contributing factor to the limited gelatinisation (Köksel *et al.*, 1998). Usually during gelatinisation, swelling and melting of starch granules will occur and the molten starch granules will fuse with each other (Srikaeo *et al.*, 2006). This phenomenon was not observed for either of the roasting methods. According to Case *et al.* (1992) gelatinisation predominates at moisture contents above 20% and maximum gelatinisation occurs at 28-29% moisture. It can thus be assumed that the limited amount of moisture (Table 7.3) along with the short roasting time, did not allow complete starch gelatinisation to occur.

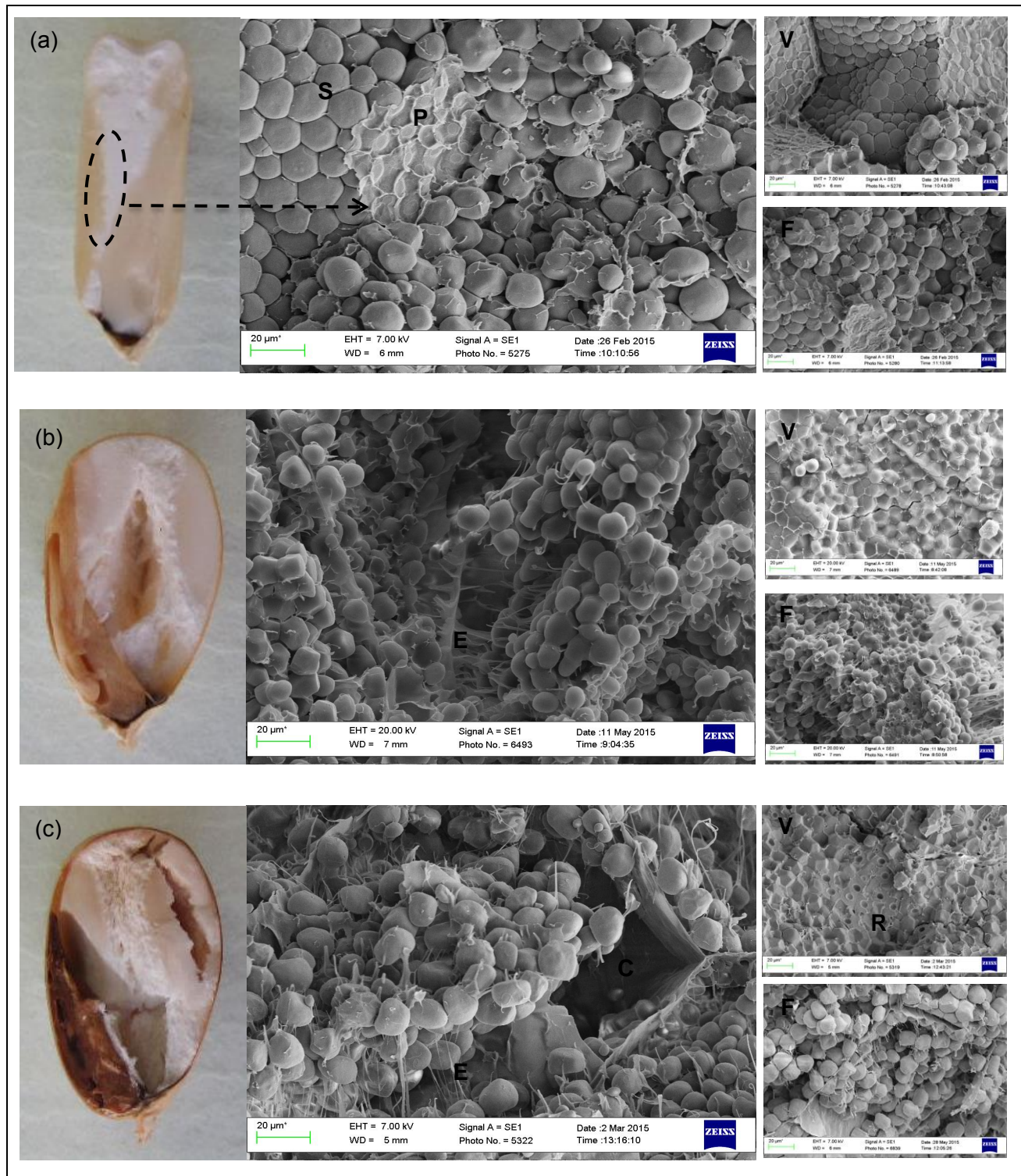
The structural configuration (not the starch granules itself, but rather the spatial distribution thereof) of the vitreous endosperm was less affected than that of the floury endosperm. This could be explained by the vitreous endosperm cells having thinner cell walls but a thicker protein network (Gunasekaran *et al.*, 1985). Due to the thicker protein network, more force is required to break the cell walls in comparison to the floury endosperm. Thus, the vitreous endosperm is more resistant to the formation of large voids. During roasting the floury endosperm structure is disrupted, tearing the thin protein matrix and resulting in loosely bound starch granules and large voids.

Even though the roasting temperature exceeds the gelatinisation temperature (62-72°C) of maize starch, most starch granules maintained their polygonal or round shape (Delcour & Hosney, 2010). Thus, the majority of the starch granules seemed not to have gelatinised during roasting. Further evaluation using DSC was performed to support these conclusions. The low moisture content may be the contributing factor to the limited gelatinisation (Köksel *et al.*, 1998). Usually during gelatinisation, swelling and melting of starch granules will occur and the molten starch granules will fuse with each other (Srikaeo *et al.*, 2006). This phenomenon was not observed for either of the roasting methods. According to Case *et al.* (1992) gelatinisation predominates at moisture contents above 20% and maximum gelatinisation occurs at 28-29% moisture. It can thus be assumed that the limited amount of moisture (Table 7.3) along with the short roasting time, did not allow complete starch gelatinisation to occur.

The structural configuration (not the starch granules itself, but rather the spatial distribution thereof) of the vitreous endosperm was less affected than that of the floury endosperm. This could be explained by the vitreous endosperm cells having thinner cell walls but a thicker protein network (Gunasekaran *et al.*, 1985). Due to the thicker protein network, more force is required to break the cell walls in comparison to the floury endosperm. Thus, the vitreous endosperm is more resistant to



the formation of large voids. During roasting the floury endosperm structure is disrupted, tearing the thin protein matrix and resulting in loosely bound starch granules and large voids.



**Figure 7.3.** Representation of a longitudinal digital slice image and SEM micrograph of (a) a control maize kernel revealing the transition (encircled region) phase from the vitreous (left) to the floury (right) endosperm. Figures (b) and (c) represent a digital longitudinal slice image and SEM micrograph of a FCCT and oven-roasted kernel, respectively. S= starch granules; P= protein matrix; V= vitreous endosperm; F= floury endosperm; E= elongated strands; C= cavity and R= ruptures. The scale bar (20 µm) is given in the lower left corner of the micrographs.

Both roasting methods resulted in disintegration of the protein network into thin elongated strands in the floury endosperm (Fig. 7.3). These fragmented glue-like strands are possibly composed of a mixture of melted starch and denatured protein matrix. The shape of the starch granules predominantly remained intact and the granule boundaries were still visible in both roasting methods. It can be postulated that the starch partially melts during roasting since maize starch begin to melt at approximately 150°C, with a peak at 180 to 186°C (Schwartzberg *et al.*, 1995).

Even though the roasting temperature exceeds the gelatinisation temperature (62-72°C) of maize starch, most starch granules maintained their polygonal or round shape (Delcour & Hosney, 2010). Thus, the majority of the starch granules seemed not to have gelatinised during roasting. Further evaluation using DSC was performed to support these conclusions. The low moisture content may be the contributing factor to the limited gelatinisation (Köksel *et al.*, 1998). Usually during gelatinisation, swelling and melting of starch granules will occur and the molten starch granules will fuse with each other (Srikaeo *et al.*, 2006). This phenomenon was not observed for either of the roasting methods. According to Case *et al.* (1992) gelatinisation predominates at moisture contents above 20% and maximum gelatinisation occurs at 28-29% moisture. It can thus be assumed that the limited amount of moisture (Table 7.3) along with the short roasting time, did not allow complete starch gelatinisation to occur.

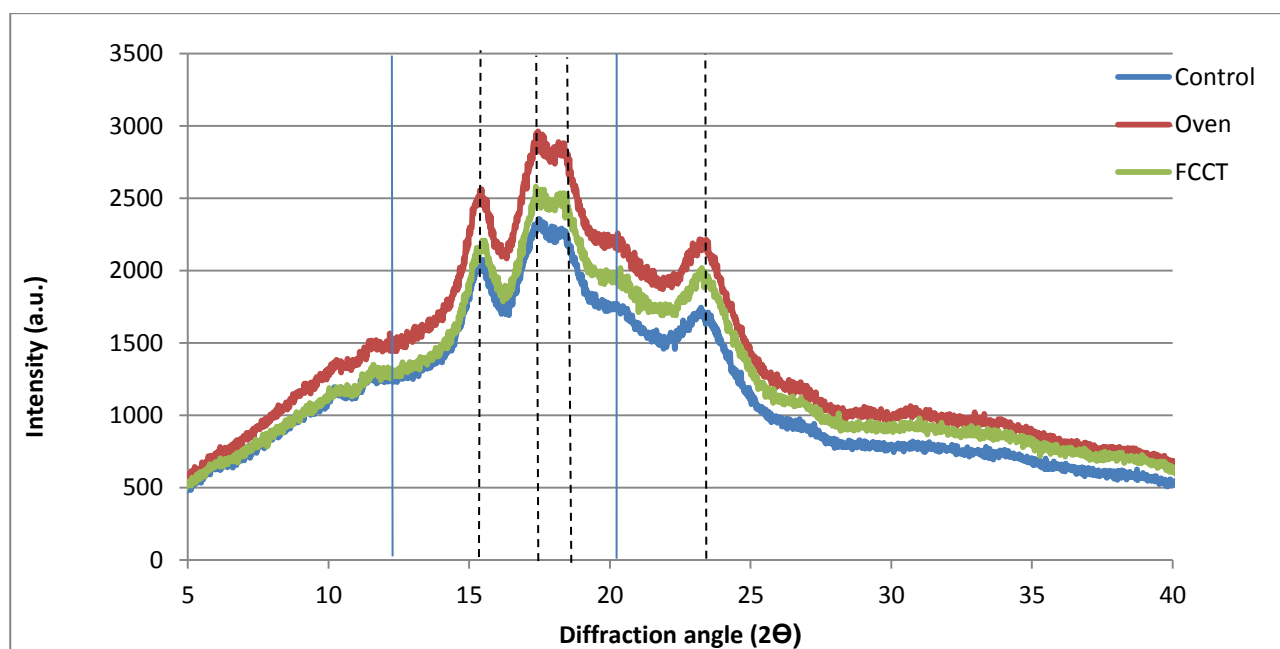
The structural configuration (not the starch granules itself, but rather the spatial distribution thereof) of the vitreous endosperm was less affected than that of the floury endosperm. This could be explained by the vitreous endosperm cells having thinner cell walls but a thicker protein network (Gunasekaran *et al.*, 1985). Due to the thicker protein network, more force is required to break the cell walls in comparison to the floury endosperm. Thus, the vitreous endosperm is more resistant to the formation of large voids. During roasting the floury endosperm structure is disrupted, tearing the thin protein matrix and resulting in loosely bound starch granules and large voids.

#### X-ray diffraction (XRD)

The characteristic A-type XRD pattern was only slightly disturbed when the maize starch was subjected to roasting. Figure 7.4 illustrates the XRD patterns of the control and roasted maize flours. The dashed vertical lines are used to highlight the four prominent intensity peaks at about 15°, 17°, 18° and 23° in 2 $\Theta$ , which indicates A-type crystallinity (Carrera *et al.*, 2015). It can be observed that all the maize samples showed typical A-type patterns. The most prominent peak was the doublet at 17-18° and the broadest peak occurred at 23°. These peaks appeared in both the control and roasted flours. It can be noted that small intensity peaks appeared at 12° and 20° for the roasted samples. These peaks can be indicative of V-type crystallinity, indicating that amylose is complexed with other non-carbohydrate substances, i.e. proteins and lipids. The results compare favourably with that of Carrera *et al.* (2015) for roasted maize. Pre-gelatinisation processes induces the formation of V-amylose–lipid complexes (Mohorič *et al.*, 2009). Several other studies

suggested that thermal treatment induces a V-type crystalline structure of cereal starches and rice (Witek *et al.*, 2010; Mahadevamma & Tharanathan, 2007). Figure 7.4 illustrates that the X-ray intensity peaks of the roasted samples were higher than for the control sample. Previous studies also reported the intensity peaks on the X-ray diffractogram of roasted samples to be higher than those of the raw sample (Köksel *et al.*, 1998; Christa *et al.*, 2009; Hoover & Manuel, 1996). The increase in X-ray intensities of the thermally treated starches are due to shifting of the double helical chains, due to thermal energy and also due to the decreased moisture content (Hoover & Manuel, 1996).

The crystallinity of starch decrease as the content of damaged starch increase (Barrera *et al.*, 2013). The double helical and crystalline patterns are disrupted during roasting. This was confirmed by the crystallinity (%) determinations. Roasting manifested changes in the crystalline structure, since the crystallinity content of the control samples was  $14.32 \pm 0.22\%$  and after roasting it decreased to  $13.87 \pm 0.21\%$  ( $P > 0.05$ ) and  $12.49 \pm 0.25\%$  ( $P \leq 0.05$ ) for FCCT and oven roasting, respectively. Carrera *et al.* (2015) also reported that the crystallinity decreased from 17.16% to 15.63% after roasting of white maize. Roasting induces partial material melting (mainly amylose), which causes disruption of the ordered structure (i.e. double helices) within and over the starch granules (Fig 7.3 b and c). Loss in crystallinity with conversion to an amorphous structure is due to partial starch gelatinisation but can also be attributed to starch-protein and starch-lipid interactions (Guzmán *et al.*, 2009). A decrease in the crystallinity content after maize roasting could greatly improve the *in vitro* starch digestibility, since the roasting process disrupts the order within the starch granules, thereby increasing the action of enzymatic digestion (Carrera *et al.*, 2015).



**Figure 7.4.** XRD traces of the control, FCCT and oven-roasted maize flour samples. Dashed vertical lines indicate the location of the prominent peaks for A-type crystallinity. Solid lines indicate the development of new peaks that resembles V-type crystallinity in the roasted samples.



### *Functional analyses*

#### Water absorption capacity (WAC) and water solubility index (WSI)

Although not significant ( $P > 0.05$ ) for FCCT roasting, both roasting methods resulted in an increased WAC (Table 7.4). It can be postulated that as the starch granule structure (Fig. 7.3 b and c) is disrupted during roasting more water is bound, resulting in increased WAC. The increase in WAC is thus attributed to starch damaged due to partial gelatinisation and formation of pores and cavities in the endosperm, which imbibes and holds water by capillary action (Mariotti *et al.*, 2006). The increased WAC, may also be due to the loss in crystallinity, as already discussed, that increases water penetration within the starch granules (Maache-Rezzoug *et al.*, 2008). These results are in concurrence with previous studies that also reported an increase in WAC after roasting cereals and legumes (Sharma *et al.*, 2011; Gujral *et al.*, 2011; Griffith & Castell-Perez, 1998; Ranganathan *et al.*, 2014). Starches with enhanced WAC can be used in soups, sauces, puddings, pie fillings and gravies as thickening agents (Dries *et al.*, 2014). A high WAC is a desirable functional property in food such as dough, since it should absorb water without dissolution of proteins to attain a viscous texture.

Lee *et al.* (2006) stated that hardness also plays a role in WAC, where softer samples usually display a higher WAC. This can be explained by the higher degree of structural order (crystallinity) and less starch damage (e.g. control samples), resulting in the inaccessibility of water to the compact structure. Roasting ( $150^{\circ}\text{C}$ ; 20 min), using the FCCT roaster, of whole marama beans increased the WAC from 1.5 to 2.4 g/g (Maruatona *et al.*, 2010). This was attributed to unfolding of protein molecules upon roasting, which exposed previously concealed hydration sites. Thus, these sites were made available to interact with water, which increased the WAC. Oven roasting could have resulted in more available hydrophilic binding sites for water holding.

Upon roasting, the WSI decreased ( $P > 0.05$ ) from 10.26% to 7.34 and 7.64% for FCCT and oven roasting, respectively. These results were in concurrence with Gujral *et al.* (2011) and Bhattacharya (1995) who also reported a decrease in WSI during roasting of oats and maize semolina, respectively. This decrease in WSI can be attributed to the formation of amylose-lipid complexes during roasting, which have been reported to reduce water solubility (Gujral *et al.*, 2011). A decrease in WSI is an indication that the protein present in the sample lost its solubility by denaturation when subjected to roasting (Hernández-Nava *et al.*, 2011). Furthermore, since FCCT roasting involves moist heating by steam, this had an increased effect in reducing the solubility when compared to dry roasting (Maruatona *et al.*, 2010). The inverse trend of increasing WAC and decreasing WSI were also observed by Zhu *et al.* (2010).

#### Flour dispersibility (FD)

FCCT roasting had no significant ( $P \leq 0.05$ ) effect on FD, while oven roasting resulted in a significant ( $P \leq 0.05$ ) increase. PSI is an important feature of any granular mix that requires reconstitution with water. The smaller the PSI, the more surface area is available for water

absorption (Kulkarni, 1991). Thus for the oven-roasted samples, with the lower PSI, the FD increased (Table 7.4). The percentage dispersibility of weaning food ingredients range from 63 to 79 (Kulkarni, 1991). The results obtained in this study fall within this range. A previous study observed that cereal roasting resulted in better reconstitution indices compared to unroasted samples (Onilude *et al.*, 1999).

**Table 7.4.** WAC, WSI and FD properties of the control and roasted whole maize flours

Sample	WAC (g/g)	WSI (%)	FD (%)
Control	2.02±0.24 <sup>b</sup>	10.26±2.94 <sup>a</sup>	76.22±0.25 <sup>b</sup>
FCCT	2.22±0.05 <sup>ab</sup>	7.34±1.76 <sup>a</sup>	76.22±0.09 <sup>b</sup>
Oven	2.34±0.08 <sup>a</sup>	7.64±2.29 <sup>a</sup>	77.28±0.35 <sup>a</sup>

Results are mean values of triplicate determinations (n=3). Mean values followed by different superscripts in each column are significantly different at  $P \leq 0.05$ . WAC= water absorbance capacity; WSI = water solubility index; FD= flour dispersibility.

#### Differential scanning calorimetry (DSC)

The control sample had an endotherm with onset ( $T_o$ ), peak ( $T_p$ ) and endset ( $T_e$ ) temperatures of 53.54, 68.12 and 82.09°C, respectively and a  $\Delta H$  of 10.29 J/g (Table 7.5). A previous study reported similar results for maize starch with a gelatinisation temperature ( $T_p$ ) of 70°C and corresponding heat absorbed as 10.2 J/g (Li *et al.*, 2007). The  $T_p$  and gelatinisation enthalpy values were in agreement with others studies (Carrera *et al.*, 2015; Dries *et al.*, 2014; Guzmán *et al.*, 2009; Maache-Rezzoug *et al.*, 2008) and might be considered typical of normal maize starch. The  $T_o$ ,  $T_p$  and  $T_e$  increased for both roasting methods, where the  $T_p$  and  $T_e$  were significantly ( $P \leq 0.05$ ) higher for the oven-roasted samples. The high  $T_e$  (116.30°C) of the oven-roasted sample could be an indication of protein denaturation (Köksel *et al.*, 1998) and corresponded with the decreased crude protein content reported earlier. Differences in the transition peak position of the control and roasted samples are dependent on moisture content (Khan & Yu, 2013). In general, higher moisture content (control sample) causes a shifting endothermic peak at a lower position. Since FCCT roasting was performed in a moist atmosphere, the endothermic transition was shifted at a lower temperature than for oven roasting. Both roasting methods showed a gelatinisation endotherm occurring at a higher temperature than the control sample. These findings were in concurrence with Dries *et al.* (2014) whom reported thermal treatment to show a gelatinisation endotherm at higher temperatures than native maize starch.

Roasting resulted in a decrease ( $P > 0.05$ ) in  $\Delta H$  and the residual starch gelatinised at higher temperatures, with these changes being more profound for the oven-roasted sample. A decrease in  $\Delta H$  after roasting suggest disruption of the double helices within the amorphous regions of the granules and partial loss of protein structure (Mahadevamma & Tharanathan, 2007). The  $\Delta H$  of gelatinisation primarily reflect the loss of double helical order and corresponded the with crystallinity results reported in the previous section. However, the observed reduction in  $\Delta H$  cannot

be attributed solely to partial gelatinisation or unfolding of proteins; it is rather due to a combination of these factors (Ahmed *et al.*, 2007). The endothermic heat of starch gelatinisation represents the energy required for disruption of the native molecular organisation to gelatinised starch (Dries *et al.*, 2014). In the roasted samples the starch is partially gelatinised, thus less energy is required (Dharmaraj *et al.*, 2015).

Liu *et al.* (2009) also displayed an increasing  $T_o$  and  $T_p$ , and decreasing  $\Delta H$  after thermal treatment of maize starch. Hoover & Manuel (1996) reported that gelatinisation transition temperatures ( $T_o$ ,  $T_p$  and  $T_e$ ) of maize starch increased after thermal treatment, while the  $\Delta H$  remained unchanged. This suggested that identical amounts of double helices in the control and heat-treated sample unravelled and melted during gelatinisation (Hoover & Manuel, 1996). Khan & Yu (2013) studied the thermal degradation behaviour of cereal grains treated by autoclaving (moist heating) and roasting at 121°C for 80 min. The position of the major endothermic peak of the control sample shifted toward a higher temperature after treatment suggesting the high thermal stability of the cereals. Heating with moisture, comparable to FCCT roasting, had a lower endothermic transition peak than dry roasting (comparable with oven roasting) (Khan & Yu, 2013).

The transition temperature range ( $\Delta T$ ) decreased ( $P \leq 0.05$ ) for FCCT (17.31°C) roasting but increased ( $P \leq 0.05$ ) for oven roasting (61.96°C). A previous study comparing the effect of roasting on the thermal properties of white and blue maize also reported an opposite trend for the  $\Delta T$  since it increased for white maize but decreased for blue maize (Carrera *et al.*, 2015). Maache-Rezzoug *et al.* (2008) reported a decrease in  $\Delta T$  after thermal treatment, while Hoover and Manuel (1996) reported a broadening of the  $\Delta T$ . Since roasting is the loss of order, it causes different effects in starch granules (Carrera *et al.*, 2015).

An endotherm at lower temperatures corresponds to gelatinisation-melting of crystalline lamellae, whereas an endotherm at higher temperatures resembles disintegration of amylose–lipid complexes (Maache-Rezzoug *et al.*, 2008). Amylose–lipid complexes seldom exist in native cereal starches and are generally formed upon heating or gelatinisation. According to the XRD results new peaks appeared at 12° and 20° in the roasted samples, indicating the formation of amylose–lipid complexes (Maache-Rezzoug *et al.*, 2008). The loss of structural order and decrease in crystallinity (previously discussed) during roasting explains why the roasted samples are more prone to starch gelatinisation (Witek *et al.*, 2010). The occurrence of partial gelatinisation was clearly attested by the decrease in gelatinisation enthalpy (Maache-Rezzoug *et al.*, 2008).

Previous research have found that the occurrence of transition endotherms in starch is dependent on both temperature and moisture (Köksel *et al.*, 1998). Thus, the limited degree of gelatinisation (FCCT=16.23%; oven=25.27%) during roasting can be attributed to the limited water available. The moisture content (Table 7.3) of all the samples were below the range (28-29%) at which gelatinisation is expected (Case *et al.*, 1992). SEM micrographs confirmed that complete gelatinisation did not occur.



**Table 7.5.** DSC thermal characteristics of the control and roasted maize flours

Sample	T <sub>o</sub> (°C)	T <sub>p</sub> (°C)	T <sub>e</sub> (°C)	ΔH (J/g)	ΔT (°C)	% Gelatinisation
<b>Control</b>	53.54±0.57 <sup>b</sup>	68.12±0.77 <sup>b</sup>	82.09±0.72 <sup>b</sup>	10.29±2.74 <sup>a</sup>	28.55±1.25 <sup>b</sup>	-
<b>FCCT</b>	67.96±5.93 <sup>a</sup>	73.85±3.80 <sup>b</sup>	85.27±1.24 <sup>b</sup>	8.62±0.17 <sup>a</sup>	17.31±5.72 <sup>c</sup>	16.23±20.04 <sup>a</sup>
<b>Oven</b>	54.33±4.09 <sup>b</sup>	97.91±5.40 <sup>a</sup>	116.30±5.04 <sup>a</sup>	7.69±0.37 <sup>a</sup>	61.96±3.40 <sup>a</sup>	25.27±17.29 <sup>a</sup>

Values are means ± standard deviation of three replicates (n=3). Different letters in the same column indicate significant differences (P≤0.05). T<sub>o</sub>, T<sub>p</sub>, and T<sub>e</sub> indicate onset, peak and endset temperatures, respectively; ΔH = enthalpy of gelatinisation; ΔT (T<sub>e</sub> – T<sub>o</sub>) = gelatinisation temperature range.

#### Pasting properties and α -amylase activity using the RVA

The pasting properties of the control and roasted samples are presented in Table 7.6, while a representative RVA viscogram is shown in Figure 7.5. Both roasting methods increased the pasting viscosities (V<sub>p</sub>, V<sub>b</sub>, V<sub>f</sub>, V<sub>t</sub> and V<sub>s</sub>) significantly (P≤ 0.05). The increase in viscosity (Table 7.6) may be attributed to the smaller PSI (Table 7.3) of the roasted flours. The control (harder) sample produces coarser particles once milled, while the roasted samples produce finer particles. Thus, there will be differences in the gelatinisation and hydration rates (Almeida-Dominguez *et al.*, 1997). Coarse particles have slow water diffusion and limited starch swelling, resulting in slow viscosity development (Narváez-González *et al.*, 2006). Smaller or finer particles, obtained from roasted samples, have a larger surface area and will result in rapid hydration and thus higher viscosity. Vivas *et al.* (1987) reported that the apparent viscosity of roasted maize was higher than for the raw sample because of the smaller PSI of the roasted flours.

A previous study using FCCT roasting also observed significant increases in the pasting viscosities of whole grain maize flour (Bala, 2016). In the roasted samples the starch granules are loosely packed and partially gelatinised and can thus hydrate and swell more rapidly in the presence of heat, resulting in increased viscosities (Fig 7.5). According to Griffith & Castell-Perez (1998) the reduction in moisture due to roasting allows a larger concentration of solids by weight, thus causing an increased viscosity. Differences in the V<sub>p</sub> can be attributed to differences in the rates of WAC of the starch granules (Ragaei & Abdel-Aal, 2006). Starch granules of thermally treated maize can bind more water and thus become thick and viscous at low concentrations (Žilić *et al.*, 2010).

Žilić *et al.* (2010) found that micronisation (140°C for 40s) significantly increased the V<sub>p</sub> of maize flour and this was attributed to changes in protein and starch properties and also the formation of both hydrophobic and disulphide bonds during thermal treatment. Higher V<sub>b</sub> were obtained after roasting, indicating a weaker ability to withstand stress during cooking. Breakdown is a measure of the ease with which the swollen starch granule can disintegrate and thus an indication of the degree of its organisation (Olayinka *et al.*, 2008). Final viscosity is an indication of the stability of the cooked paste. Food products, especially baked goods, may benefit from using a blend of roasted and raw flours for products that require gelatinisation (Rothschild *et al.*, 2015). The decrease in P<sub>temp</sub> (though, not significant) and significant (P≤0.05) increase in pasting

viscosities of the roasted maize flour compared to the control is an indication of better gelling quality. The  $P_{temp}$  of the roasted samples were slightly lower than that of the control sample. A low  $P_{temp}$  indicates that fewer associate forces and crosslinks are present within the starch granule; thus the roasted samples will gelatinise faster.

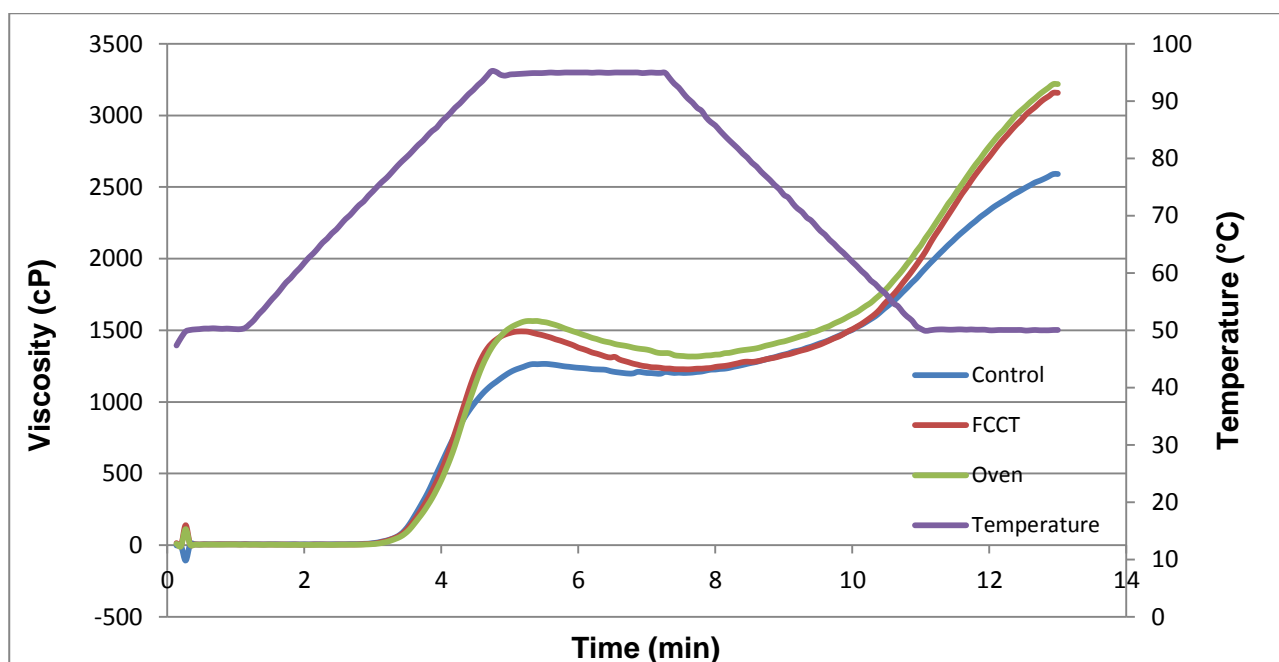
The pasting properties of both control and roasted samples were well within the ranges reported by Sandhu *et al.* (2007) for maize. This study inferred that harder maize has tightly packed starch granules (e.g. control sample) and thus developed lower viscosity levels (Fig. 7.5). The degree of gelatinisation achieved during roasting dictates the rheological properties (Ahmed *et al.*, 2007). This is in agreement with a previous report on roasted maize meal (Ingbian & Adegoke, 2007), which demonstrated that starch gelatinisation results in an increased  $V_p$ . Oven roasting resulted in a higher degree of gelatinisation, thus a higher  $V_p$  than FCCT roasting.

The stimulated enzymes (due to lower SN) in the roasted samples are capable of breaking down the matrix that embeds the starch granules and this allows the granules to swell more freely and gelatinise faster (Bolade, 2009). This relates to the increased pasting properties. SN of cereals flours provides an indirect measurement of amylase activity and the level of activity has an influence on viscosity (Ragae & Abdel-Aal, 2006). The SN decreased significantly ( $P \leq 0.05$ ) as a result of roasting (Table 7.6). The higher SN of the control samples is an indication of lower amylase activity. The oven-roasted sample has the lowest SN (1290.67cP) and thus the highest amylase activity. This can be attributed to the leaching of amylose during roasting.

**Table 7.6.** RVA pasting properties of the control and roasted whole maize flours

Sample	$P_{temp}$ (°C)	Peak time (min)	$V_p$ (cP)	$V_b$ (cP)	$V_f$ (cP)	$V_t$ (cP)	$V_s$ (cP)	SN (cP)
<b>Control</b>	78.31±0.57 <sup>a</sup>	5.49±0.11 <sup>a</sup>	1251.67±10.69 <sup>b</sup>	122.00±17.52 <sup>c</sup>	2564.33±19.73 <sup>b</sup>	1129.67±17.79 <sup>c</sup>	1434.66±2.08 <sup>b</sup>	1490.00±47.95 <sup>a</sup>
<b>FCCT</b>	77.73±0.96 <sup>a</sup>	5.22±0.03 <sup>b</sup>	1510.00±5.57 <sup>a</sup>	307.67±41.57 <sup>a</sup>	3120.67±244.92 <sup>a</sup>	1202.33±6.51 <sup>b</sup>	1918.34±230.61 <sup>a</sup>	1378.67±20.98 <sup>b</sup>
<b>Oven</b>	77.99±0.51 <sup>a</sup>	5.11±0.02 <sup>b</sup>	1525.67±19.04 <sup>a</sup>	272.00±18.61 <sup>b</sup>	3210.00±72.67 <sup>a</sup>	1253.67±30.99 <sup>a</sup>	1956.33±44 <sup>a</sup>	1290.67±39.72 <sup>c</sup>

Results are mean values of triplicate determinations (n=3). Mean values followed by different superscripts in each column are significantly different at  $P \leq 0.05$ .  $P_{temp}$ = pasting temperature;  $V_p$ = peak viscosity;  $V_b$  = breakdown viscosity;  $V_f$ = final viscosity;  $V_t$ = trough viscosity;  $V_s$ = setback viscosity and SN= stirring number.



**Figure 7.5.** RVA pasting profiles of a representative control, FCCT-roasted and oven-roasted maize flour. The RVA viscometer reports the viscosity as a function of time together with the temperature ramp.

## Conclusion

Maize flour is a staple food in a country like Southern Africa where it forms one of the most important pre-processed products for the production of 'Mielie pap'. Since roasted maize flour has been reported to deliver many health benefits, it is also important to understand the physicochemical, structural and functional properties if a potential value-added product is to be developed.

Significant ( $P \leq 0.05$ ) differences were observed between the weight loss, bulk density, PI and crude protein content of the oven and FCCT-roasted samples, when using the same roasting conditions ( $180^\circ\text{C}$ ; 140s). These results revealed that the physicochemical properties were negatively affected during oven roasting. Hardness decreased significantly ( $P \leq 0.05$ ) during both roasting methods which will result in lower energy consumption during milling.

SEM revealed that structural disruption was more pronounced for oven roasting, where it resulted in a less dense endosperm texture and modified starch granules by causing central ruptures in the vitreous endosperm. XRD revealed a significant ( $P \leq 0.05$ ) decrease in the crystallinity (%) of the oven-roasted sample, which indicated a disruption in the crystalline organisation of the starch granules. A decrease in crystallinity content could eventually have a positive effect on the starch availability and digestibility, since it can be exploited for the fabrication of food where fast digestibility is desired, i.e. energy cereal bars. DSC revealed that partial gelatinisation of oven-roasted maize occurred at a higher temperature and required less energy (lower enthalpy) compared to the FCCT-roasted and control samples. Both roasting methods resulted in only partial starch gelatinisation, with the degree of gelatinisation being higher after

oven roasting. The SEM observations confirmed the DSC results that only partial gelatinisation occurred and that the degree of gelatinisation was more pronounced for the oven roasting method. Partially gelatinised starch can be used as a thickening or gelling agent. Roasting resulted in beneficial functional changes, i.e. increased WAC and pasting behaviour. Thus the roasted flour enhances gel formation and can be widely used in different food preparations such as instant mixes, porridge and starch-thickened sauces.

The results supported the hypothesis that the more destructive microstructural changes induced by oven roasting also resulted in more adverse changes in the physical, structural and functional properties of maize. FCCT roasting, using superheated steam, resulted in more homogenous roasting and was more effective in maintaining these properties. It will thus not compromise the quality of the end product when used to develop potential value-added products. It is recommended that future studies examine the nutritional and sensory characteristics of the roasted product, as well as explore various time-temperature roasting combinations to determine the optimum conditions for a specific end-product use.

## References

- AACC (1999a). AACC International Approved Methods of Analysis, 11th ed. Method 22-08.01. Measurement of  $\alpha$ -amylase Activity with the Rapid Visco Analyser. Approved November 3, 1999. St. Paul, Minnesota, USA: American Association of Cereal Chemists.
- AACC (1999b). AACC International Approved Methods of Analysis, 11th ed. Method 26-95.01. Experimental Milling: Temper Table. Approved November 3, 1999. St. Paul, Minnesota, USA: American Association of Cereal Chemists.
- AACC (1999c). AACC International Approved Methods of Analysis, 11th ed. Method 44-19.01. Moisture- Air-Oven Method, Drying at 135°. Approved November 3, 1999. St. Paul, Minnesota, USA: American Association of Cereal Chemists.
- AACC (1999d). AACC International Approved Methods of Analysis, 11th ed. Method 46-30.01. Crude Protein-Combustion Method. Approved November 3, 1999. St. Paul, Minnesota, USA: American Association of Cereal Chemists.
- AACC (1999e). AACC International Approved Methods of Analysis, 11th ed. Method 56-20.01. Hydration Capacity of Pregelatinized Cereal Products. Approved November 3, 1999. St. Paul, Minnesota, USA: American Association of Cereal Chemists.
- AACC (1999f). AACC International Approved Methods of Analysis, 11th ed. Method 76-21.01. General Pasting Method for Wheat or Rye Flour or Starch Using the Rapid Visco Analyser. Approved November 3, 1999. St. Paul, Minnesota, USA: American Association of Cereal Chemists.
- Ahmed, J., Ramaswamy, H.S., Ayad, A., Alli, I. & Alvarez, P. (2007). Effect of high-pressure treatment on rheological, thermal and structural changes in basmati rice flour slurry. *Journal of Cereal Science*, **46**, 148-156.

- Almeida-Dominguez, H.D., Suhendro, E.L. & Rooney, L.W. (1997). Factors affecting Rapid Visco Analyser curves for the determination of maize kernel hardness. *Journal of Cereal Science*, **25**, 93-102.
- Ayatse, J., Eka, O. & Ifon, E. (1983). Chemical evaluation of the effect of roasting on the nutritive value of maize (*Zea mays*, Linn.). *Food Chemistry*, **12**, 135-147.
- Bala, S.M. (2016). Effect of forced convection roasting on physicochemical and antioxidant properties of whole grain maize (*Zea mays* L.) and optimisation of roasting conditions. PhD Thesis in Food Science. Stellenbosch University, South Africa.
- Baldwin, P.M., Adler, J., Davies, M.C. & Melia, C.D. (1994). Holes in starch granules: confocal, SEM and light microscopy studies of starch granule structure. *Starch-Stärke*, **46**, 341-346.
- Barrera, G.N., Calderón-Domínguez, G., Chanona-Pérez, J., Gutiérrez-López, G.F., León, A.E. & Ribotta, P.D. (2013). Evaluation of the mechanical damage on wheat starch granules by SEM, ESEM, AFM and texture image analysis. *Carbohydrate Polymers*, **98**, 1449-1457.
- Bhattacharya, S. (1995). Kinetics of hydration of raw and roasted corn semolina. *Journal of Food Engineering*, **25**, 21-30.
- Blandino, M., Mancini, M.C., Peila, A., Rolle, L., Vanara, F. & Reyneri, A. (2010). Determination of maize kernel hardness: comparison of different laboratory tests to predict dry-milling performance. *Journal of the Science of Food and Agriculture*, **90**, 1870-1878.
- Bolade, M.K. (2009). Effect of flour production methods on the yield, physicochemical properties of maize flour and rheological characteristics of a maize-based non-fermented food dumpling. *African Journal of Food Science*, **3**, 288-298.
- Cämmerer, B. & Kroh, L.W. (2009). Shelf life of linseeds and peanuts in relation to roasting. *LWT-Food Science and Technology*, **42**, 545-549.
- Carrera, Y., Utrilla-Coello, R., Bello-Pérez, A., Alvarez-Ramirez, J. & Vernon-Carter, E.J. (2015). In vitro digestibility, crystallinity, rheological, thermal, particle size and morphological characteristics of pinole, a traditional energy food obtained from toasted ground maize. *Carbohydrate Polymers*, **123**, 246-255.
- Case, S., Hamann, D. & Schwartz, S. (1992). Effect of starch gelatinization on physical properties of extruded wheat and corn based products. *Cereal Chemistry*, **69**, 401-404.
- Christa, K., Soral-Smietana, M. & Lewandowicz, G. (2009). Buckwheat starch: structure, functionality and enzyme in vitro susceptibility upon the roasting process. *International Journal of Food Sciences and Nutrition*, **60**, 140-154.
- Chung, H.S., Chung, S.K. & Youn, K.S. (2011). Effects of roasting temperature and time on bulk density, soluble solids, browning index and phenolic compounds of corn kernels. *Journal of Food Processing and Preservation*, **35**, 832-839.
- Costa, P., Jensen, A., Harmon, B. & Norton, H. (1976). The effects of roasting and roasting temperatures on the nutritive value of corn for swine. *Journal of Animal Science*, **42**, 365-374.

- Delcour, J. & Hosney, R.C. (2010). *Principles of Cereal Science and Technology*. 3rd ed. St. Paul, Minnesota, USA: AACC International Press.
- Dharmaraj, U., Meera, M., Reddy, S.Y. & Malleshi, N.G. (2015). Influence of hydrothermal processing on functional properties and grain morphology of finger millet. *Journal of Food Science and Technology*, **52**, 1361-1371.
- Doehlert, D.C., Zhang, D. & Moore, W.R. (1997). Influence of heat pretreatments of oat grain on the viscosity of flour slurries. *Journal of the Science of Food and Agriculture*, **74**, 125-131.
- Dombrink-Kurtzman, M. & Knutson, C. (1997). A study of maize endosperm hardness in relation to amylose content and susceptibility to damage. *Cereal Chemistry*, **74**, 776-780.
- Dries, D., Gomand, S., Goderis, B. & Delcour, J. (2014). Structural and thermal transitions during the conversion from native to granular cold-water swelling maize starch. *Carbohydrate Polymers*, **114**, 196-205.
- Edema, M.O., Sanni, L.O. & Sanni, A.I. (2005). Evaluation of maize-soybean flour blends for sour maize bread production in Nigeria. *African Journal of Biotechnology*, **4**, 911-918.
- Fox, G. & Manley, M. (2009). Hardness methods for testing maize kernels. *Journal of Agricultural and Food Chemistry*, **57**, 5647-5657.
- Fuwa, H., Sugimoto, Y., Tanaka, M. & Glover, D. (1978). Susceptibility of various starch granules to amylases as seen by scanning electron microscope. *Starch-Stärke*, **30**, 186-191.
- Griffith, L. & Castell-Perez, M. (1998). Effects of roasting and malting on physicochemical properties of select cereals and legumes. *Cereal Chemistry*, **75**, 780-784.
- Guelpa, A., Du Plessis, A., Kidd, M. & Manley, M. (2015). Non-destructive estimation of maize (*Zea mays* L.) kernel hardness by means of an X-ray micro-computed tomography ( $\mu$ CT) density calibration. *Food and Bioprocess Technology*, **8**, 1419-1429.
- Gujral, H.S., Sharma, P. & Rachna, S. (2011). Effect of sand roasting on beta glucan extractability, physicochemical and antioxidant properties of oats. *LWT-Food Science and Technology*, **44**, 2223-2230.
- Gujral, H.S., Sharma, P. & Sharma, R. (2013). Antioxidant properties of sand roasted and steam cooked Bengal gram (*Cicer arietinum*). *Food Science and Biotechnology*, **22**, 183-188.
- Gunasekaran, S., Deshpande, S., Paulsen, M. & Shove, G. (1985). Size characterization of stress cracks in corn kernels. *Transactions of the ASAE*, **28**, 1668-1672.
- Gupta, M., Bawa, A.S. & Semwal, A.D. (2008). Effect of barley flour on development of rice-based extruded snacks. *Cereal Chemistry*, **85**, 115-122.
- Gustin, J.L., Jackson, S., Williams, C., Patel, A., Armstrong, P., Peter, G.F. & Settles, A.M. (2013). Analysis of maize (*Zea mays*) kernel density and volume using microcomputed tomography and single-kernel near-infrared spectroscopy. *Journal of Agricultural and Food Chemistry*, **61**, 10872-10880.



- Guzmán, A.Q., Flores, M.E.J., Escobedo, R.M., Guerrero, L.C. & Feria, J.S. (2009). Changes on the structure, consistency, physicochemical and viscoelastic properties of corn (*Zea mays* sp.) under different nixtamalization conditions. *Carbohydrate Polymers*, **78**, 908-916.
- Hafsa, I., Mandato, S., Ruiz, T., Schuck, P., Jeantet, R., Mejean, S., Chevallier, S. & Cuq, B. (2015). Impact of the agglomeration process on structure and functional properties of the agglomerates based on the durum wheat semolina. *Journal of Food Engineering*, **145**, 25-36.
- Head, D., Cenkowski, S., Arntfield, S. & Henderson, K. (2010). Superheated steam processing of oat groats. *LWT-Food Science and Technology*, **43**, 690-694.
- Hernández-Nava, R., Bello-Pérez, L., San Martín-Martínez, E., Hernández-Sánchez, H. & Mora-Escobedo, R. (2011). Effect of extrusion cooking on the functional properties and starch components of lentil/banana blends: response surface analysis. *Revista Mexicana de Ingeniería Química*, **10**, 409-419.
- Hoover, R. & Manuel, H. (1996). The effect of heat-moisture treatment on the structure and physicochemical properties of normal maize, waxy maize, dull waxy maize and amylomaize v starches. *Journal of Cereal Science*, **23**, 153-162.
- Hoseney, R. (1994). *Principles of Cereal Science and Technology*. St. Paul, Minnesota, USA: American Association of Cereal Chemists. Inc.
- Hoseney, R.C., Zeleznak, K. & Abdelrahman, A. (1983). Mechanism of popcorn popping. *Journal of Cereal Science*, **1**, 43-52.
- Humpf, H.U. & Voss, K.A. (2004). Effects of thermal food processing on the chemical structure and toxicity of fumonisin mycotoxins. *Molecular Nutrition & Food Research*, **48**, 255-269.
- Idrus, N.F.M. & Yang, T.A. (2012). Comparison between roasting by superheated steam and by convection on changes in colour, texture and microstructure of peanut (*Arachis hypogaea*). *Food Science and Technology Research*, **18**, 515-524.
- Ingbian, E.K. & Adegoke, G.O. (2007). Proximate compositions, pasting and rheological properties of mumu—a roasted maize meal. *International Journal of Food Science & Technology*, **42**, 762-767.
- Jha, S. (2005). Mathematical simulation of roasting of grain. *Journal of Food Engineering*, **71**, 304-310.
- Kayode, O., Sulyok, M., Fapohunda, S., Ezekiel, C., Krska, R. & Oguntona, C. (2013). Mycotoxins and fungal metabolites in groundnut-and maize-based snacks from Nigeria. *Food Additives & Contaminants: Part B*, **6**, 294-300.
- Khan, M.M.R. & Yu, P. (2013). Thermal stability and molecular microstructure of heat-induced cereal grains, revealed with Raman molecular microspectroscopy and differential scanning calorimetry. *Journal of Agricultural and Food Chemistry*, **61**, 6495-6504.
- Khan, N., Zaman, R. & Elahi, M. (1991). Effect of heat treatments on the phytic acid content of maize products. *Journal of the Science of Food and Agriculture*, **54**, 153-156.

- Köksel, H., Sivri, D., Scanlon, M. & Bushuk, W. (1998). Comparison of physical properties of raw and roasted chickpeas (leblebi). *Food Research International*, **31**, 659-665.
- Kulkarni, K.D., Kulkarni, D. N., & Ingle, U. M. (1991). Sorghum malt-based weaning food formulations: preparation, functional properties and nutritive value. *Food and Nutrition Bulletin*, **13**, 322-327.
- Lee, K.-M., Bean, S.R., Alavi, S., Herrman, T.J. & Waniska, R.D. (2006). Physical and biochemical properties of maize hardness and extrudates of selected hybrids. *Journal of Agricultural and Food Chemistry*, **54**, 4260-4269.
- Li, J.-Y., Yeh, A.-I. & Fan, K.-L. (2007). Gelation characteristics and morphology of corn starch/soy protein concentrate composites during heating. *Journal of Food Engineering*, **78**, 1240-1247.
- Liu, H., Yu, L., Simon, G., Dean, K. & Chen, L. (2009). Effects of annealing on gelatinization and microstructures of corn starches with different amylose/amylopectin ratios. *Carbohydrate Polymers*, **77**, 662-669.
- Maache-Rezzoug, Z., Zarguili, I., Loisel, C., Queveau, D. & Buleon, A. (2008). Structural modifications and thermal transitions of standard maize starch after DIC hydrothermal treatment. *Carbohydrate Polymers*, **74**, 802-812.
- Mahadevamma, S. & Tharanathan, R. (2007). Processed rice starch characteristics and morphology. *European Food Research and Technology*, **225**, 603-612.
- Mariotti, M., Alamprese, C., Pagani, M.A. & Lucisano, M. (2006). Effect of puffing on ultrastructure and physical characteristics of cereal grains and flours. *Journal of Cereal Science*, **43**, 47-56.
- Maruatona, G.N., Duodu, K.G. & Minnaar, A. (2010). Physicochemical, nutritional and functional properties of marama bean flour. *Food Chemistry*, **121**, 400-405.
- McNiven, M.A., Hamilton, R.M.G., Robinson, P.H. & Deleeuw, J.W. (1994). Effect of flame roasting on the nutritional quality of common cereal grains for non-ruminants and ruminants. *Animal Feed Science and Technology*, **47**, 31-40.
- Mendes, L.C., De Menezes, H.C., Aparecida, M. & Da Silva, A. (2001). Optimization of the roasting of robusta coffee (*C. canephora conillon*) using acceptability tests and RSM. *Food Quality and Preference*, **12**, 153-162.
- Méndez-Albores, A., De Jesús-Flores, F., Castañeda-Roldan, E., Arámbula-Villa, G. & Moreno-Martínez, E. (2004). The effect of toasting and boiling on the fate of B-aflatoxins during pinole preparation. *Journal of Food Engineering*, **65**, 585-589.
- Mohorič, A., Vergeldt, F., Gerkema, E., Van Dalen, G., Van Den Doel, L.R., Van Vliet, L.J., Van As, H. & Van Duynhoven, J. (2009). The effect of rice kernel microstructure on cooking behaviour: a combined  $\mu$ -CT and MRI study. *Food Chemistry*, **115**, 1491-1499.
- Mrad, R., Debs, E., Maroun, R.G. & Louka, N. (2014a). Multiple optimization of chemical components and texture of purple maize expanded by IVDV treatment using the response surface methodology. *Food Chemistry*, **165**, 60-69.

- Mrad, R., Debs, E., Saliba, R., Maroun, R.G. & Louka, N. (2014b). Multiple optimization of chemical and textural properties of roasted expanded purple maize using response surface methodology. *Journal of Cereal Science*, **60**, 397-405.
- Murthy, K.V., Ravi, R., Keshava Bhat, K. & Raghavarao, K.S.M.S. (2008). Studies on roasting of wheat using fluidized bed roaster. *Journal of Food Engineering*, **89**, 336-342.
- Mwangwela, A.M., Waniska, R.D. & Minnaar, A. (2007). Effect of micronisation temperature (130 and 170°C) on functional properties of cowpea flour. *Food Chemistry*, **104**, 650-657.
- Narváez-González, E.D., De Dios Figueroa-Cárdenas, J., Taba, S., Tostado, E.C., Peniche, R.Á.M. & Sánchez, F.R. (2006). Relationships between the microstructure, physical features, and chemical composition of different maize accessions from Latin America. *Cereal Chemistry*, **83**, 595-604.
- O'Kennedy, K. (2011). Characterisation of zein from South African maize of varying endosperm texture. Masters Thesis in Food Science. Stellenbosch University, South Africa.
- Oboh, G., Ademiluyi, A.O. & Akindahunsi, A.A. (2010). The effect of roasting on the nutritional and antioxidant properties of yellow and white maize varieties. *International Journal of Food Science & Technology*, **45**, 1236-1242.
- Olayinka, O.O., Adebowale, K.O. & Olu-Owolabi, B.I. (2008). Effect of heat-moisture treatment on physicochemical properties of white sorghum starch. *Food Hydrocolloids*, **22**, 225-230.
- Onilude, A., Sanni, A. & Ighalo, M. (1999). Effect of process improvement on the physico-chemical properties of infant weaning food from fermented composite blends of cereal and soybeans. *Plant Foods for Human Nutrition*, **54**, 239-250.
- Pittia, P., Dalla Rosa, M.D. & Lerici, C.R. (2001). Textural changes of coffee beans as affected by roasting conditions. *LWT-Food Science and Technology*, **34**, 168-175.
- Plahar, W., Okezie, B.O. & Gyato, C. (2003). Development of a high protein weaning food by extrusion cooking using peanuts, maize and soybeans. *Plant Foods for Human Nutrition*, **58**, 1-12.
- Pronyk, C., Cenkowski, S. & Muir, W. (2004). Drying foodstuffs with superheated steam. *Drying Technology*, **22**, 899-916.
- Ragaei, S. & Abdel-Aal, E.-S.M. (2006). Pasting properties of starch and protein in selected cereals and quality of their food products. *Food Chemistry*, **95**, 9-18.
- Raigar, R.K., Prabhakar, P.K. & Srivastav, P.P. (2016). Effect of different thermal treatments on grinding characteristics, granular morphology and yield of ready-to-eat wheat grits. *Journal of Food Process Engineering*, doi:10.1111/jfpe.12363.
- Ranganathan, V., Nunjundiah, I.T. & Bhattacharya, S. (2014). Effect of roasting on rheological and functional properties of sorghum flour. *Food Science and Technology International*, **20**, 579-589.
- Rothschild, J., Rosentrater, K.A., Onwulata, C., Singh, M., Menutti, L., Jambazian, P. & Omary, M.B. (2015). Influence of quinoa roasting on sensory and physicochemical properties of

- allergen-free, gluten-free cakes. *International Journal of Food Science & Technology*, **50**, 1873-1881.
- Rufián-Henares, J.A. & Delgado-Andrade, C. (2009). Effect of digestive process on Maillard reaction indexes and antioxidant properties of breakfast cereals. *Food Research International*, **42**, 394-400.
- Sandhu, K.S., Godara, P., Kaur, M. & Punia, S. (2015). Effect of toasting on physical, functional and antioxidant properties of flour from oat (*Avena sativa* L.) cultivars. *Journal of the Saudi Society of Agricultural Sciences*, <http://dx.doi.org/10.1016/j.jssas.2015.06.004>.
- Sandhu, K.S., Singh, N. & Malhi, N.S. (2007). Some properties of corn grains and their flours I: physicochemical, functional and chapati-making properties of flours. *Food Chemistry*, **101**, 938-946.
- Schenker, S., Handschin, S., Frey, B., Perren, R. & Escher, F. (2000). Pore structure of coffee beans affected by roasting conditions. *Journal of Food Science*, **65**, 452-457.
- Schoeman, L., Du Plessis, A. & Manley, M. (2016a). Non-destructive characterisation and quantification of the effect of conventional oven and forced convection continuous tumble (FCCT) roasting on the three-dimensional microstructure of whole wheat kernels using X-ray micro-computed tomography ( $\mu$ CT). *Journal of Food Engineering*, **187**, 1-13.
- Schoeman, L., Du Plessis, A., Verboven, P., Nicolaï, B., Cantre, D. & Manley, M. (2016b). Effect of oven and forced convection continuous tumble (FCCT) roasting on the microstructure and dry milling properties of white maize. *Innovative Food Science & Emerging Technologies*, **Submitted**.
- Schwartzberg, H.G., Wu, J.P.C., Nussinovitch, A. & Mugerwa, J. (1995). Modelling deformation and flow during vapor-induced puffing. *Journal of Food Engineering*, **25**, 329-372.
- Sharma, P., Gujral, H.S. & Rosell, C.M. (2011). Effects of roasting on barley  $\beta$ -glucan, thermal, textural and pasting properties. *Journal of Cereal Science*, **53**, 25-30.
- Singh, J., Kaur, L. & McCarthy, O. (2007). Factors influencing the physico-chemical, morphological, thermal and rheological properties of some chemically modified starches for food applications—a review. *Food Hydrocolloids*, **21**, 1-22.
- Srikaeo, K., Furst, J.E., Ashton, J.F. & Hosken, R.W. (2006). Microstructural changes of starch in cooked wheat grains as affected by cooking temperatures and times. *LWT-Food Science and Technology*, **39**, 528-533.
- Velu, V., Nagender, A., Prabhakara Rao, P.G. & Rao, D.G. (2006). Dry milling characteristics of microwave dried maize grains (*Zea mays* L.). *Journal of Food Engineering*, **74**, 30-36.
- Vivas, N., Waniska, R. & Rooney, L. (1987). Thin porridges (atole) prepared from maize and sorghum. *Cereal Chemistry*, **64**, 384-389.
- Witek, M., Węglarz, W.P., De Jong, L., Van Dalen, G., Blonk, J.C.G., Heussen, P., Van Velzen, E., Van As, H. & Van Duynhoven, J. (2010). The structural and hydration properties of heat-treated rice studied at multiple length scales. *Food Chemistry*, **120**, 1031-1040.

- Yoo, S.-H. & Jane, J.-L. (2002). Structural and physical characteristics of waxy and other wheat starches. *Carbohydrate Polymers*, **49**, 297-305.
- Youn, K.-S. & Chung, H.-S. (2012). Optimization of the roasting temperature and time for preparation of coffee-like maize beverage using the response surface methodology. *LWT-Food Science and Technology*, **46**, 305-310.
- Zhang, B., Dhital, S., Haque, E. & Gidley, M.J. (2012). Preparation and characterization of gelatinized granular starches from aqueous ethanol treatments. *Carbohydrate Polymers*, **90**, 1587-1594.
- Zhu, L.-J., Shukri, R., De Mesa-Stonestreet, N.J., Alavi, S., Dogan, H. & Shi, Y.-C. (2010). Mechanical and microstructural properties of soy protein–high amylose corn starch extrudates in relation to physiochemical changes of starch during extrusion. *Journal of Food Engineering*, **100**, 232-238.
- Žilić, S., Hadži-Tašković Šukalović, V., Milašinović, M., Ignjatović-Mićić, D., Maksimović, M. & Semenčenko, V. (2010). Effect of micronisation on the composition and properties of the flour from white, yellow and red maize. *Food Technology and Biotechnology*, **48**, 198-206.
- Zzaman, W. & Yang, T.A. (2013). Effect of superheated steam and convection roasting on changes in physical properties of cocoa bean (*Theobroma cacao*). *Food Science and Technology Research*, **19**, 181-186.

## CHAPTER 8

### General discussion and conclusions

Food microstructure is one of the key elements defining the physical, sensory, textural and functional properties, as well as stability of the end product (Frisullo *et al.*, 2009). Thus, microstructural information is of great interest to the food industry (Pinzer *et al.*, 2012). A proper understanding of food microstructure needs to be developed to produce products with desired sensory, physical and functional properties (Frisullo *et al.*, 2009). Microstructural changes in proteins, cell walls and starch of cereal grains is produced during processes such as milling, malting, roasting, baking and extrusion (Salmenkallio-Marttila *et al.*, 2004). Modification of structural features by means of processing can be used to design products with desired properties. There is thus a need for quantitative methods to accurately characterise the microstructure of food to understand and control structure-property relationships (Herremans *et al.*, 2013). Nowadays food microstructure can be studied at almost any microstructural level, in real-time and with minimum interference (Aguilera, 2005).

There is an increasing trend towards the consumption of roasted whole grain products due to its higher dietary content and antioxidant activity (Carrera *et al.*, 2015; Sandhu *et al.*, 2015). This provides a fundamental basis for the incorporation of roasted grains into food as health-enhancing ingredients. In this study the effect of two roasting methods, conventional oven and innovative forced convection continuous tumble (FCCT) roasting, was evaluated on whole wheat and maize and analysed at different scales for assessment of the microstructure, starch-protein morphology and crystallinity, as well as physicochemical and functional properties. The microstructure was investigated using X-ray micro-computed tomography ( $\mu$ CT) and scanning electron microscopy (SEM), whereas the molecular and mesoscopic level were evaluated using X-ray diffraction (XRD) and differential scanning calorimetry (DSC) to characterise the crystalline structure and gelatinisation behaviour, respectively. Furthermore, investigation of the functionality of the roasted whole grains was undertaken by determining the pasting properties using the Rapid Visco Analyser (RVA), water absorbance capacity (WAC), water solubility index (WSI) and flour dispersibility (FD). Wheat rheology was examined using a Micrograph and Alveograph. Knowledge on all these properties of roasted grains would be valuable for the design of equipment and processes, i.e. handling, transportation, separation and storing as well as for applications in different food formulations (İşikli *et al.*, 2014).

X-ray  $\mu$ CT is an elegant imaging technique that has been proven to be capable of investigating microstructural properties of porous roasted products, where it played a major role in understanding the impact of roasting on microstructure (Pittia *et al.*, 2011; Schoeman *et al.*, 2016a). Quantifying X-ray  $\mu$ CT results was a means of demonstrating the relevance of X-ray  $\mu$ CT beyond the mere visualisation of microstructure. X-ray  $\mu$ CT enabled precise microstructural measurements of specific regions-of-interest (ROIs), i.e. volumetric and relative density



measurements and even more advanced analysis such as pore (void) size distributions (Schoeman *et al.*, 2016b). Segmenting kernels into ROIs was a critical; although tedious and time-consuming part of image processing. Nevertheless, with future advancements in software capabilities, manual intervention will be minimised (Singhal *et al.*, 2013).

Understanding the impact of roasting on microstructural, physicochemical and functional properties of cereal grains is of importance because it governs subsequent processes and final product quality. X-ray  $\mu$ CT enabled full three-dimensional (3D) visualisation and quantification of the kernel microstructure and revealed the porosity distribution in raw and roasted kernels. Reconstructed 3D volumes, obtained from a set of 2D images, allowed the spatial visualisation of internal features. 3D characterisation provided a convenient way to obtain both qualitative and quantitative information on the microstructural evolution during roasting, which is not always achievable from 2D image analysis. Quantitative analysis allowed more comprehensive and objective characterisation of the whole samples and extracted ROIs. Cereal grains are heterogeneous materials and the ability to create ROIs, e.g. pores, enables greater visual interpretation and aids in a better appreciation of the differences in pore size, shape and frequency in samples. X-ray  $\mu$ CT posed to be a useful method when a specific region within a sample needed to be excluded (e.g. germ), non-destructively. The two roasting methods resulted in a distinctly different inner grain structure with FCCT roasting being less destructive; resulting in fewer cracks and smaller cavities.

Quantitative X-ray  $\mu$ CT analyses confirmed the qualitative results, reporting an increase in volume, porosity and expansion ratio (ER), and a decrease in relative density (oven: wheat=2.76% and maize=6.33%; FCCT: wheat=0.55% and maize=1.92%) which in turn affected kernel hardness and bulk density (oven: wheat=0.77 g/cm<sup>3</sup> and maize=0.66 g/cm<sup>3</sup>; FCCT: wheat=0.81 g/cm<sup>3</sup> and maize=0.69 g/cm<sup>3</sup>). The higher ER and lower relative density in the oven-roasted samples were consistent with the greater porosity. It was shown that porosity was the microstructural property indicator affected most during roasting. X-ray  $\mu$ CT demonstrated that during roasting the grains experienced the coupled phenomena of expansion and crack development, which resulted in a complex 3D porous structure. The ER results evidenced the effects of volume expansion induced by water vapour generated, which led to the irregular and porous internal structure. Moisture inside the kernels were converted to superheated steam which created internal pressure and provided the driving force for expansion (Altan, 2014). Skeletonization was performed, at a much higher resolution, on the maize samples to demonstrate another means of displaying the connectivity and thickness of the air paths in the extracted skeleton. The raw and FCCT-roasted skeleton was similar in density and thickness, while the oven-roasted sample yielded a complex skeleton with a much denser porous network of multiple interconnected segments of various thicknesses. In the oven-roasted skeleton a cavity initiation site could be observed as a spider web structure.

A potential extension of the X-ray  $\mu$ CT results could be to perform void/pore wall thickness analysis on higher resolution nano-CT (submicron) scans leading to the visualisation of samples in

greater detail and thus providing new insights on the submicron structure. Although ideally larger sample sets should be used, it was limited in this study due to the high cost of performing X-ray  $\mu$ CT acquisition and analysis. The small number of samples used may question the representativeness of the data; nevertheless a definite trend (under similar roasting conditions) was indicated between the two roasting methods, resulting in less structural alteration during FCCT roasting. In this study a roasting temperature of 180°C was used. It is also recommended that additional studies ought to be performed according to an appropriate experimental design to determine the optimal roasting parameters to attain desired properties that are required for optimum end product quality. This work has the potential to be extended to other cereal grains and roasted products, e.g. nuts and cacao.

It is evident that X-ray  $\mu$ CT has been used successfully for 3D characterisation of the microstructure of roasted wheat and maize and provided a unique insight of the microstructural changes during roasting. The capability of X-ray  $\mu$ CT in combination with image analysis could open a new avenue for using this technique to determine roasting conditions and processing parameters and to assess the quality of grains. This study illustrated that the roasting method, using similar roasting conditions, have a direct impact on the microstructure and thus quality of the final product. The results evidenced that X-ray  $\mu$ CT is a feasible technique capable of providing a resolution at micrometer level that are able to characterise and quantify the 3D microstructure of raw and roasted samples.

Unfortunately, X-ray  $\mu$ CT is not without limitations, e.g. limited availability of facilities, high costs involved with image acquisition and analysis, penetration capability of dense samples and 3D rendering is a computationally intensive and requires super computers. The harmful effects of the X-rays are prevented by properly designed shielding. Even though physics limit X-ray CT to a certain extent, the amount of useful information that can be obtained from this technique continues to grow (Landis & Keane, 2010). Despite being an expensive and time-consuming method, the advantages outweigh the limitations. With advances in image acquisition capabilities, availability of advanced CT systems, new detector technologies, high-performance X-ray tubes, real-time imaging, user friendliness of data analysis, computational power, in terms of both hardware and software, increased reconstruction speed, resolution and image quality, and cost diminution, it is anticipated that X-ray CT would become more applicable in the future (Hanke *et al.*, 2008; Kalender, 2011).

Conventional density methods, i.e. floating tests overlook the influence of pores and cavities (Gustin *et al.*, 2013). The feasibility of X-ray  $\mu$ CT was demonstrated by its capability to divide the grains into biological material and air to perform subsequent relative density measurements. This enabled the determination of material density, which excludes all internal air that may influence the results and was thus more representative of the true density (Gustin *et al.*, 2013). It was noteworthy to observe that for both cereal grains the material density remained unaffected during FCCT roasting. This indicated FCCT roasting to be a less destructive process. These results were

in agreement with the physicochemical outcomes, since FCCT also affected weight loss, bulk density, puffing index, moisture, hardness, crude protein and milling properties less than oven roasting. Roasting compromises the structural integrity, increasing the friability of cereal grains before milling, resulting in the potential for reduction in energy costs and milling time (Pronyk *et al.*, 2006). Oven-roasted samples, containing larger fissures, resulted in a greater decrease in hardness (PSI of wheat=41.37%; c/f of maize=0.90). Harder maize is favoured by the milling industry due to higher yield. Hardness, bulk density and milling properties can be useful to evaluate the quality of roasted cereal grains as well as the efficacy of the milling process.

Both starch and protein properties determine the quality of a cereal product. Further investigation of the effect of roasting on the texture and starch granule packing density in the endosperm required destructive testing using SEM. Both roasting methods led to disintegrated protein networks in the wheat and maize (floury endosperm), which resulted in thin elongated strands. The starch granules, however, maintained their shape. Oven roasting led to more dispersed starch granules as well as larger and more cavities between the granules in the endosperm, compared to FCCT roasting. This structural alteration may be attributed to the fusion of pores into larger interconnected cavities, as illustrated for maize with skeletonization, due to the higher internal pressure generated during this roasting method. The region most affected by roasting was the centre, indicating that the thermal centre was localised in the kernels.

Roasting of wheat and maize imparted important effects on the functionality of the flours. The starch in the roasted grains was only partially gelatinised due to inadequate water availability. The limited gelatinisation of the starch granules observed by SEM was thus confirmed by DSC analysis. Partial gelatinisation (oven: wheat=17.16% and maize=25.27%; FCCT: wheat=10.14% and maize=16.23%) was also evidenced by the decrease in crystallinity (oven: wheat=0.16% and maize=1.83%; FCCT: wheat=0.12% and maize=0.45%) and gelatinisation enthalpy. The loss in structural order (SEM and XRD) explains why the roasted grains were more prone to starch gelatinisation. Morphological changes, i.e. a decrease in crystallinity content may have positive effects on starch availability and protein digestibility and it would be worthwhile evaluating these properties in a future study since it can be exploited for the production of food where fast digestibility is desired. Further research should also be conducted to determine the risk/benefit balance of roasting as a food processing method.

Roasting of cereal grains offered beneficial effects, i.e. an increased WAC such that the roasted flour can be used to prepare foods e.g. instant mixes, porridges and soup. Thus roasting enhanced gel formation and strength, a desirable property that can be used in starch-thickened sauces (Olayinka *et al.*, 2008). Furthermore, the RVA results revealed that roasted flour provided increased pasting properties. This illustrated the effectiveness of roasting for value addition to a specific end-use. SEM micrographs indicated that more adverse structural changes occur during oven roasting and these changes are responsible for the more profound changes in the pasting behaviour of oven-roasted samples.

Microscopy is increasingly used in combination with rheology to gain complementary information on food structure (Wilkinson *et al.*, 2000). It was important for its application in food to find that the rheological properties of the whole wheat flour, i.e. the Alveographic indices were not significantly ( $P>0.05$ ) affected by roasting. The Mixographic indices, i.e. peak time increased significantly ( $P\leq 0.05$ ) (FCCT=3.81 min; oven=3.50 min), while the water absorption decreased slightly (FCCT=61.69%; oven=61.73%) after roasting. Both these parameters did not differ significantly ( $P>0.05$ ) between the two roasting methods. Roasting at 180°C for 140 s did not result in detrimental effects in the rheological properties and will thus not have a negative effect on the baking quality.

Food preparations from roasted cereal grains have been rarely considered. Applications of roasted cereal products can include the development of value-added products, e.g. pinole, a traditional energy product obtained from roasted ground maize, which is now also consumed by athletes and ultra-runners as an all-natural rapid energy booster (Carrera *et al.*, 2015). Roasted cereal grains can be used to manufacture modified starches, pre-cooked breakfast cereals, pasta products and dietetic foods. Since roasting decreases the moisture content, roasted cereal grains are a good candidate for incorporation into specialised cereal bars (Carrera *et al.*, 2015). Roasted whole wheat flour can be used as composites for bread production to obtain an aromatic roasted flavour (Baiano *et al.*, 2009). In addition, the increase in WAC observed (oven: wheat=2.02% and maize=15.84%; FCCT roasting: wheat=0.81% and maize=9.90%) suggests that flours from roasted cereal grains can be used as functional ingredient in snack foods and to control moisture migration in baked products (Mariotti *et al.*, 2006). An increased WAC is a result of the development of a porous endosperm structure during roasting which is capable of absorbing and holding water by capillary action (Mariotti *et al.*, 2006). Bread staling occurs due to moisture transfer between the components (Gray & Bemiller, 2003). Hence, the use of roasted flour in bread dough is capable of delaying the staling phenomenon; resulting in softer bread with a longer shelf life.

Although roasting increase shelf life by lowering water activity which reduces microbial growth and enzymatic activity, Lazar *et al.* (1974) reported the development of two types (enzymatic and pyrolytic) of off-odours when storing roasted wheat. Enzymatically induced off-odours typically occur when grains with high initial moisture are roasted at low temperature for a short period, which leave behind great concentrations of enzymes. In contrast, pyrolytic off-odours arise in samples where there is no active enzyme system, but where excess heat exposure resulted in the development of carbonyl compounds, alcohols and free fatty acids (Lazar *et al.*, 1974). Thus, it is recommended that future studies look into storage stability, since it appears that additives might be required to extend the shelf life of roasted products. Little has been published on the health benefits of roasted cereals. The main advantage of roasting continues to be contributions to sensory and storage quality of the end product (Griffith & Castell-Perez, 1998). Despite growing interest towards functional foods from roasted whole grain products which have specific health-

promoting benefits, desirable sensory characteristics still remain a key priority for consumers (Ragaei & Abdel-Aal, 2006). Prospective studies should focus on the effect of roasting on the nutritional and sensory characteristics.

X-ray  $\mu$ CT is considered the most promising tool for food structure characterisation (Van Dalen *et al.*, 2003). Currently interest in 3D food microstructural investigations are increasing and serves as a method of understanding food functionality and to evaluate the impact of processing on structural parameters that relates to quality (Pittia *et al.*, 2011; Frisullo *et al.*, 2012). In future a continuous increase in the applications related to food science is foreseen as evidenced by the large amount of publications dedicated to X-ray  $\mu$ CT (Schoeman *et al.*, 2016c). Most X-ray  $\mu$ CT investigations on food to date have been feasibility studies, executed only on a limited number of samples, due to the costs involved for scanning and analysis. Despite the extensive research effort, internal characterisation are still uncommon in the food industry (Donis-González *et al.*, 2014). Developments in using this technique in food related fields could open the horizon for developing mathematical and computational models capable of linking food microstructure to rheology, texture and sensory related properties or even to design foods based on the information obtained, making CT much more powerful. This technique will become indispensable for food quality evaluation and product development.

Techniques are needed on-line and at-line to non-destructively measure microstructural properties (Herremans *et al.*, 2013). 2D X-ray inspection systems are used on-line in limited applications, e.g. to detect internal defects in fruits and vegetables. In the food industry CT is an emerging technique that can be integrated in packaging lines to monitor the content of vacuum sealed products, to detect contaminants, e.g. glass, metal or stones and in meat processing factories fat and bone content can be tested and meat can be priced accordingly (De Chiffre *et al.*, 2014). However, X-ray  $\mu$ CT is not often used in- and on-line due to the challenge of high throughput requirements that has to be met and the expense of equipment (Chen *et al.*, 2013). The large size of some equipment and the considerable time needed for data acquisition and image analysis makes it impractical for in- and on-line use (Magwaza & Opara, 2014). Similar developments to the CT scanner truck, an on-line X-ray system to measure the meat-fat-distribution in pig carcasses, is foreseen in the future (De Chiffre *et al.*, 2014). Other promising applications include the determination and distribution of ingredients, e.g. berries, nuts or liquid fillings in chocolate bars, which are essential quality considerations for consumers (De Chiffre *et al.*, 2014). A future trend in the food industry will involve the development of high-performance, low-cost imaging equipment (Chen *et al.*, 2013).

A range of image processing algorithms can be employed for reconstruction, image enhancement, segmentation and classification (Kotwaliwale *et al.*, 2014). There is however no standard image processing protocol yet. This may be due to the large diversity of products. In future it is foreseen that tailored protocols will be developed. To date it was not the purpose of X-ray  $\mu$ CT to aid as a fast detection technique for microstructural changes, but rather to serve as a

good research tool to obtain more insight into the microstructure of products. Animations can be created with 3D volumes which clearly illustrate evolutionary processes and assist in microstructural evaluation in a way that 2D analyses are unable to. Although X-ray  $\mu$ CT is still in its nascent stage, the non-destructive nature and flexibility of this technique for many food science applications helps to retain its attractiveness for the food industry. Continuous developments in the technique, instrumentation and analysis will result in increasing implementation to meet the constantly growing requirements of the food industry.

FCCT roasting preserved desirable characteristics better than oven roasting under the same time and temperature conditions, since the FCCT-roasted sample was more comparable to the control in terms of the physicochemical, structural and functional properties. FCCT roasting is a less severe heat treatment than oven roasting, as the latter involve more direct dry heat penetration. One of the most important limitations in using oven roasting is that it is associated with non-uniform heat distribution. During FCCT roasting, the superheated steam generated in combination with the continuous tumbling movement of the screw conveyor inside the roasting drum, resulted in constant agitation of the sample. This results in faster and even heat transfer to the sample, ensuring a uniformly roasted product. In contrast, during oven roasting the samples were stationary. Formerly, superheated steam heating was reported to be associated with improved product quality (no scorching), less loss in nutritional value and to be cleaner and cause less oxidation compared to hot air heating (Moreira, 2001).

Although this study was motivated by an innovative roasting method, FCCT roasting, the results provide insights for even better understanding of the effect of cereal grain roasting in general. FCCT roasting has served to be a promising method to modify the structure of cereal grains without excessive deformation. FCCT roasting provides a promising incentive to utilise this roasting method, due to lower processing costs, energy efficiency, minimal disruption of structural integrity and more acceptable physicochemical and functional alterations. Knowing the different effects of FCCT and oven roasting allow manufacturers to make informed decisions on which roasting method would be most appropriate for a specific product.

In conclusion, this study provided a better understanding of the structural, physicochemical and functional evolution induced by roasting of cereal grains, which can be useful to elucidate their role in the development of new, healthy foods. Among the imaging techniques, the combination of non-destructive X-ray  $\mu$ CT with a more conventional destructive imaging method, SEM, proved to be a valuable method that provided a more comprehensive understanding of the microstructural changes. In this study a small number of samples were X-ray  $\mu$ CT scanned per roasting method, however, high-throughput scans, using multiple kernels in one scan can reduce acquisition time and cost (Guelpa *et al.*, 2016). While X-ray  $\mu$ CT explained the microstructural differences observed in cereal grains using two roasting methods, SEM, XRD, DSC and the RVA provided valuable information on the starch-protein morphology, crystallinity and thermal and pasting properties, respectively. The changes observed in this study may provide a basis for understanding the



efficiency of roasting at an industrial scale. It is hoped that this study provided inspiration for new investigations that will benefit from X-ray  $\mu$ CT as well as guided the utilisation of roasted cereal grains to provide a foundation for further studies.

## References

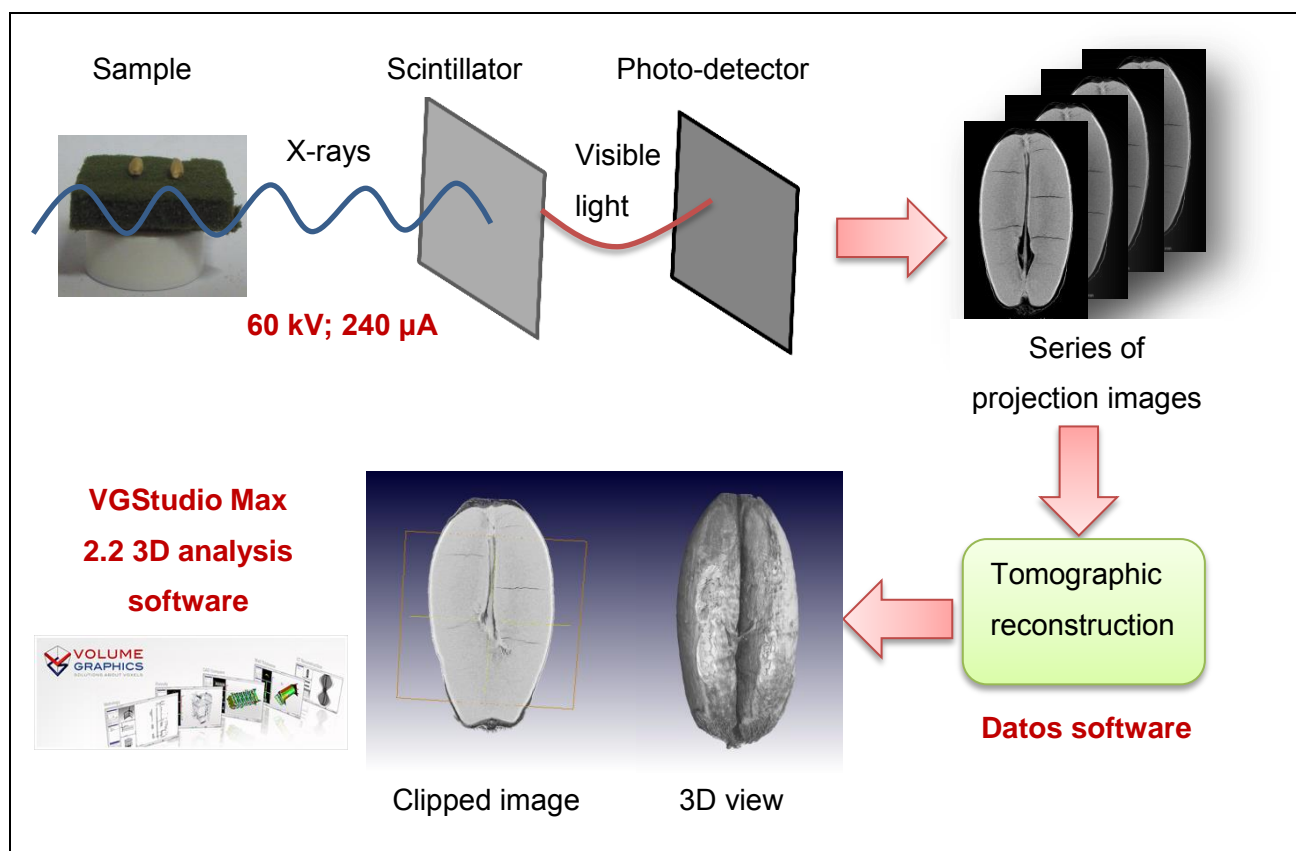
- Aguilera, J.M. (2005). Why food microstructure? *Journal of Food Engineering*, **67**, 3-11.
- Altan, A. (2014). Effects of pretreatments and moisture content on microstructure and physical properties of microwave expanded hull-less barley. *Food Research International*, **56**, 126-135.
- Baiano, A., Romaniello, R., Lamacchia, C. & La Notte, E. (2009). Physical and mechanical properties of bread loaves produced by incorporation of two types of toasted durum wheat flour. *Journal of Food Engineering*, **95**, 199-207.
- Carrera, Y., Utrilla-Coello, R., Bello-Pérez, A., Alvarez-Ramirez, J. & Vernon-Carter, E.J. (2015). In vitro digestibility, crystallinity, rheological, thermal, particle size and morphological characteristics of pinole, a traditional energy food obtained from toasted ground maize. *Carbohydrate Polymers*, **123**, 246-255.
- Chen, Q., Zhang, C., Zhao, J. & Ouyang, Q. (2013). Recent advances in emerging imaging techniques for non-destructive detection of food quality and safety. *Trends in Analytical Chemistry*, **52**, 261-274.
- De Chiffre, L., Carmignato, S., Kruth, J.P., Schmitt, R. & Weckenmann, A. (2014). Industrial applications of computed tomography. *CIRP Annals - Manufacturing Technology*, **63**, 655-677.
- Donis-González, I.R., Guyer, D.E., Pease, A. & Barthel, F. (2014). Internal characterisation of fresh agricultural products using traditional and ultrafast electron beam X-ray computed tomography imaging. *Biosystems Engineering*, **117**, 104-113.
- Frisullo, P., Barnabà, M., Navarini, L. & Del Nobile, M. (2012). *Coffea arabica* beans microstructural changes induced by roasting: an X-ray microtomographic investigation. *Journal of Food Engineering*, **108**, 232-237.
- Frisullo, P., Laverse, J., Marino, R. & Del Nobile, M. (2009). X-ray computed tomography to study processed meat microstructure. *Journal of Food Engineering*, **94**, 283-289.
- Gray, J. & Bemiller, J. (2003). Bread staling: molecular basis and control. *Comprehensive Reviews in Food Science and Food Safety*, **2**, 1-21.
- Griffith, L. & Castell-Perez, M. (1998). Effects of roasting and malting on physicochemical properties of select cereals and legumes. *Cereal Chemistry*, **75**, 780-784.
- Guelpa, A., Du Plessis, A. & Manley, M. (2016). A high-throughput X-ray micro-computed tomography ( $\mu$ CT) approach for measuring single kernel maize (*Zea mays* L.) volumes and densities *Journal of Cereal Science*, **69**, 321-328.
- Gustin, J.L., Jackson, S., Williams, C., Patel, A., Armstrong, P., Peter, G.F. & Settles, A.M. (2013). Analysis of maize (*Zea mays*) kernel density and volume using microcomputed tomography

- and single-kernel near-infrared spectroscopy. *Journal of Agricultural and Food Chemistry*, **61**, 10872-10880.
- Hanke, R., Fuchs, T. & Uhlmann, N. (2008). X-ray based methods for non-destructive testing and material characterization. *Nuclear Instruments and Methods in Physics Research Section A: Accelerators, Spectrometers, Detectors and Associated Equipment*, **591**, 14-18.
- Herremans, E., Bongaers, E., Estrade, P., Gondek, E., Hertog, M., Jakubczyk, E., Nguyen Do Trong, N., Rizzolo, A., Saeys, W., Spinelli, L., Torricelli, A., Vanoli, M., Verboven, P. & Nicolaï, B. (2013). Microstructure–texture relationships of aerated sugar gels: novel measurement techniques for analysis and control. *Innovative Food Science & Emerging Technologies*, **18**, 202-211.
- Işikli, N.D., Şenol, B. & Çoksöyler, N. (2014). Some physical and mechanical properties of roasted zerun wheat. *Journal of Food Science and Technology*, **51**, 1990-1997.
- Kalender, W.A. (2011). *Computed Tomography: Fundamentals, System Technology, Image Quality, Applications*, 3rd ed. Germany: Erlangen Publishing.
- Kotwaliwale, N., Singh, K., Kalne, A., Jha, S.N., Seth, N. & Kar, A. (2014). X-ray imaging methods for internal quality evaluation of agricultural produce. *Journal of Food Science and Technology*, **51**, 1-15.
- Landis, E.N. & Keane, D.T. (2010). X-ray microtomography. *Materials Characterization*, **61**, 1305-1316.
- Lazar, M., Mossman, A. & Wallace, J. (1974). Air-fluidized toasting of whole kernel wheat - processing variables and functional properties for food applications. *Journal of Food Science*, **39**, 239-243.
- Magwaza, L.S. & Opara, U.L. (2014). Investigating non-destructive quantification and characterization of pomegranate fruit internal structure using X-ray computed tomography. *Postharvest Biology and Technology*, **95**, 1-6.
- Mariotti, M., Alamprese, C., Pagani, M.A. & Lucisano, M. (2006). Effect of puffing on ultrastructure and physical characteristics of cereal grains and flours. *Journal of Cereal Science*, **43**, 47-56.
- Moreira, R.G. (2001). Impingement drying of foods using hot air and superheated steam. *Journal of Food Engineering*, **49**, 291-295.
- Olayinka, O.O., Adebawale, K.O. & Olu-Owolabi, B.I. (2008). Effect of heat-moisture treatment on physicochemical properties of white sorghum starch. *Food Hydrocolloids*, **22**, 225-230.
- Pinzer, B., Medebach, A., Limbach, H., Dubois, C., Stampanoni, M. & Schneebeli, M. (2012). 3D-characterization of three-phase systems using X-ray tomography: tracking the microstructural evolution in ice cream. *Soft Matter*, **8**, 4584-4594.
- Pittia, P., Sacchetti, G., Mancini, L., Voltolini, M., Sodini, N., Tromba, G. & Zanini, F. (2011). Evaluation of microstructural properties of coffee beans by synchrotron X-ray microtomography: a methodological approach. *Journal of Food Science*, **76**, 222-231.

- Pronyk, C., Cenkowski, S. & Abramson, D. (2006). Superheated steam reduction of deoxynivalenol in naturally contaminated wheat kernels. *Food Control*, **17**, 789-796.
- Ragaei, S. & Abdel-Aal, E.-S.M. (2006). Pasting properties of starch and protein in selected cereals and quality of their food products. *Food Chemistry*, **95**, 9-18.
- Salmenkallio-Marttila, M., Heiniö, R.-L., Myllymäki, O., Lille, M., Autio, K. & Poutanen, K. (2004). Relating microstructure, sensory and instrumental texture of processed oat. *Agricultural and Food Science*, **13**, 124-137.
- Sandhu, K.S., Godara, P., Kaur, M. & Punia, S. (2015). Effect of toasting on physical, functional and antioxidant properties of flour from oat (*Avena sativa* L.) cultivars. *Journal of the Saudi Society of Agricultural Sciences*, <http://dx.doi.org/10.1016/j.jssas.2015.06.004>.
- Schoeman, L., Du Plessis, A. & Manley, M. (2016a). Non-destructive characterisation and quantification of the effect of conventional oven and forced convection continuous tumble (FCCT) roasting on the three-dimensional microstructure of whole wheat kernels using X-ray micro-computed tomography ( $\mu$ CT). *Journal of Food Engineering*, **187**, 1-13.
- Schoeman, L., Du Plessis, A., Verboven, P., Nicolaï, B., Cantre, D. & Manley, M. (2016b). Effect of oven and forced convection continuous tumble (FCCT) roasting on the microstructure and dry milling properties of white maize. *Innovative Food Science & Emerging Technologies*, **Submitted**.
- Schoeman, L., Williams, P., Du Plessis, A. & Manley, M. (2016c). X-ray micro-computed tomography ( $\mu$ CT) for non-destructive characterisation of food microstructure. *Trends in Food Science & Technology*, **47**, 10-24.
- Singhal, A., Grande, J.C. & Zhou, Y. (2013). Micro/nano-CT for visualization of internal structures. *Microscopy Today*, **21**, 16-22.
- Van Dalen, G., Blonk, H., Van Aalst, H. & Hendriks, C.L. (2003). 3-D imaging of foods using X-ray microtomography. *GIT Imaging and Microscopy*, **3**, 18-21.
- Wilkinson, C., Dijksterhuis, G. & Minekus, M. (2000). From food structure to texture. *Trends in Food Science & Technology*, **11**, 442-450.

## APPENDICES

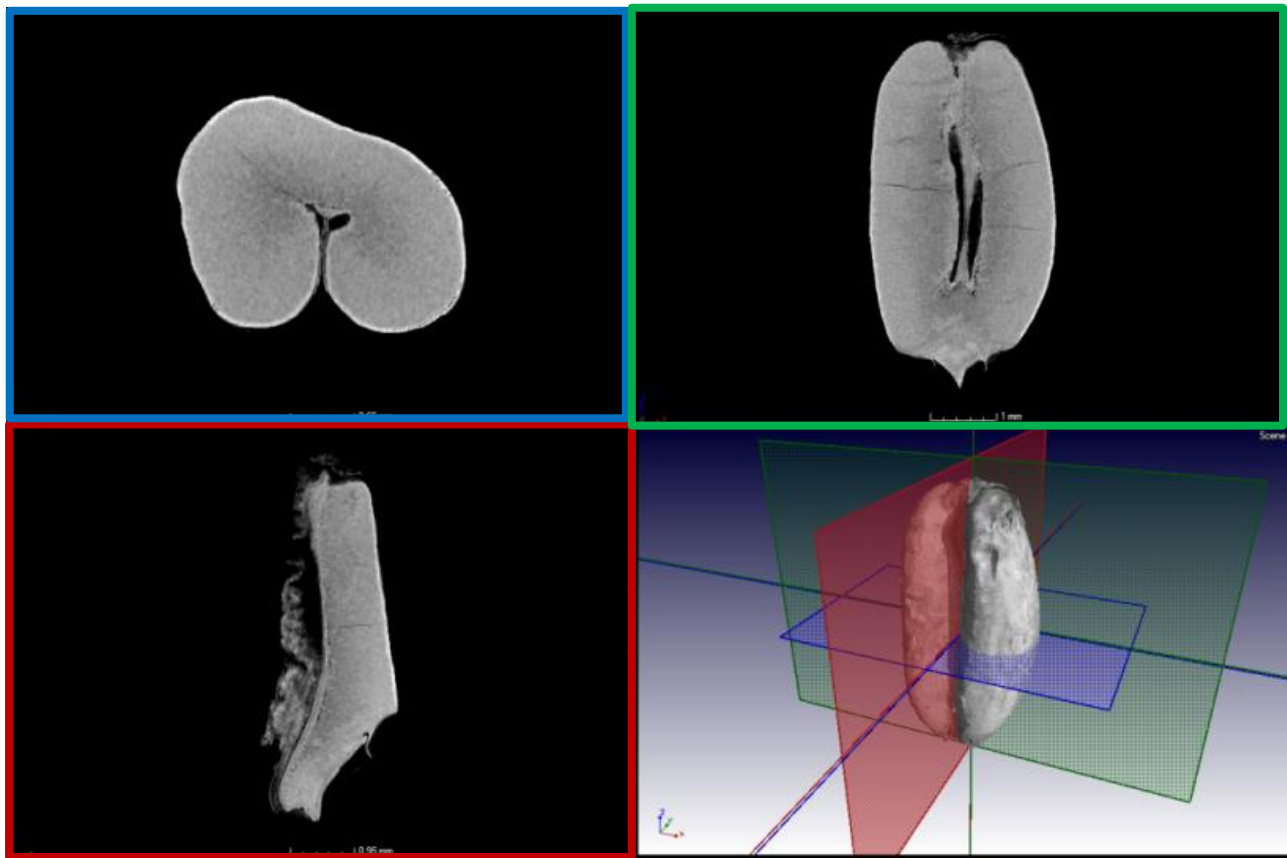
### Appendix A: X-ray $\mu$ CT acquisition and reconstruction process of wheat kernels



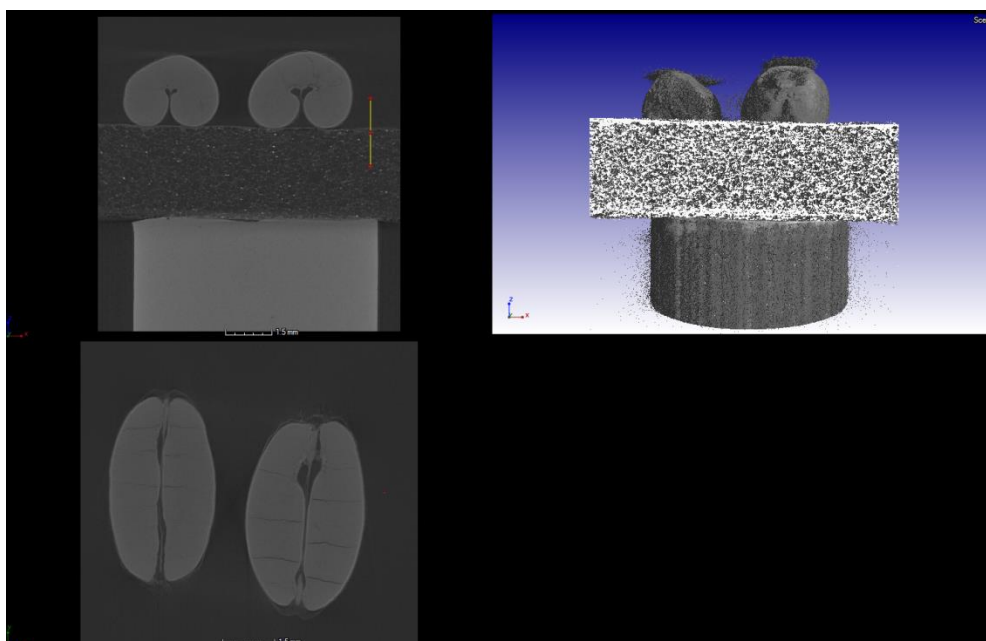
**Figure A.1.** Schematic illustration of the X-ray  $\mu$ CT acquisition and reconstruction process for the wheat kernels. A series of X-ray projection images was acquired and mathematically reconstructed to produce a 3D map of the X-ray absorption in the volume. The 3D volume was constructed from a series of 2D slice images.

## Appendix B: Qualitative image analysis of wheat kernels

Figures B.1 to B.11 illustrates 2D and 3D results of the microstructure of raw and roasted wheat kernels.

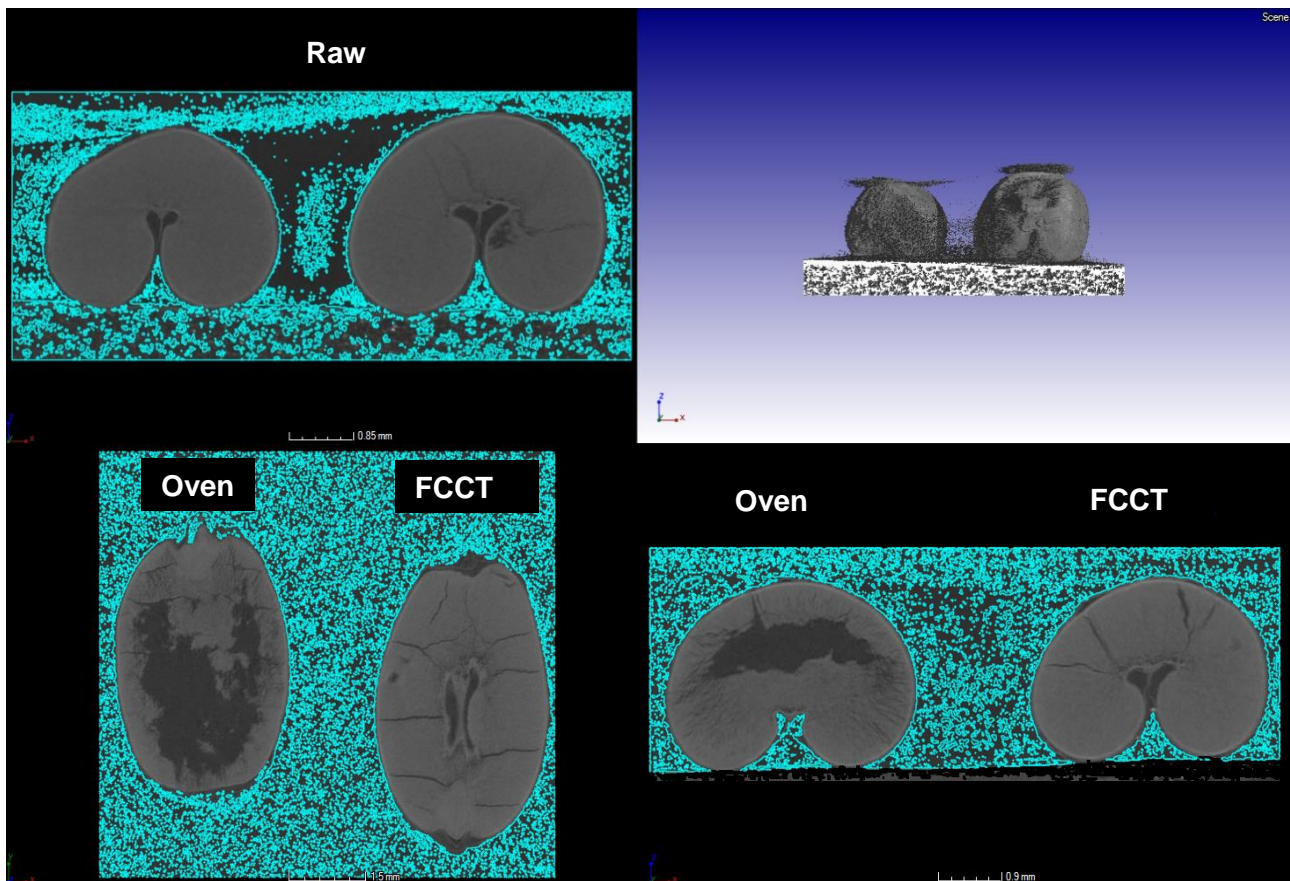


**Figure B.1.** Illustration of the different views of a raw wheat kernel, i.e. horizontal (blue), frontal/coronal (green) and sagittal plane (red) and a 3D rendered volume (bottom right).

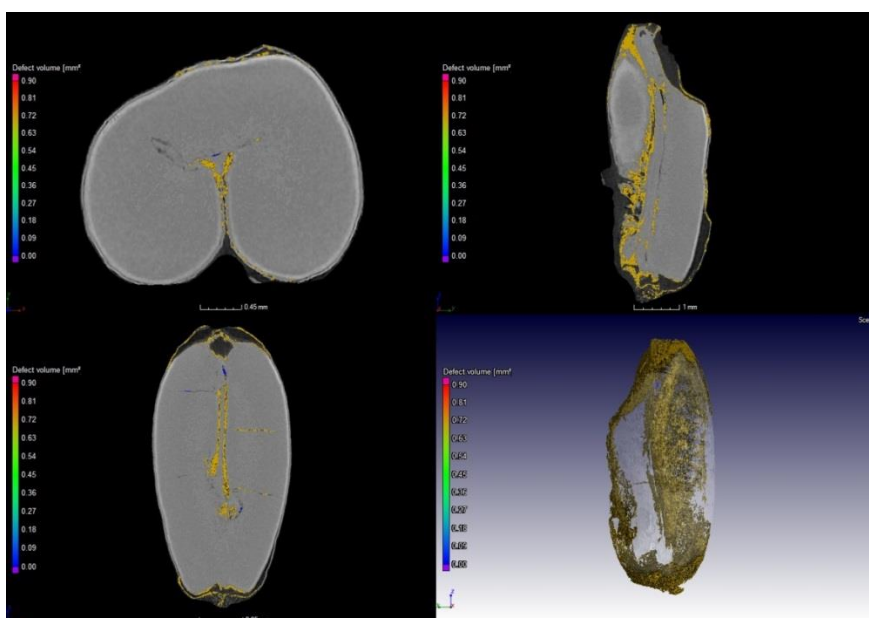


**Figure B.2.** Visualisation of the scan setup where two raw wheat kernels were imaged.



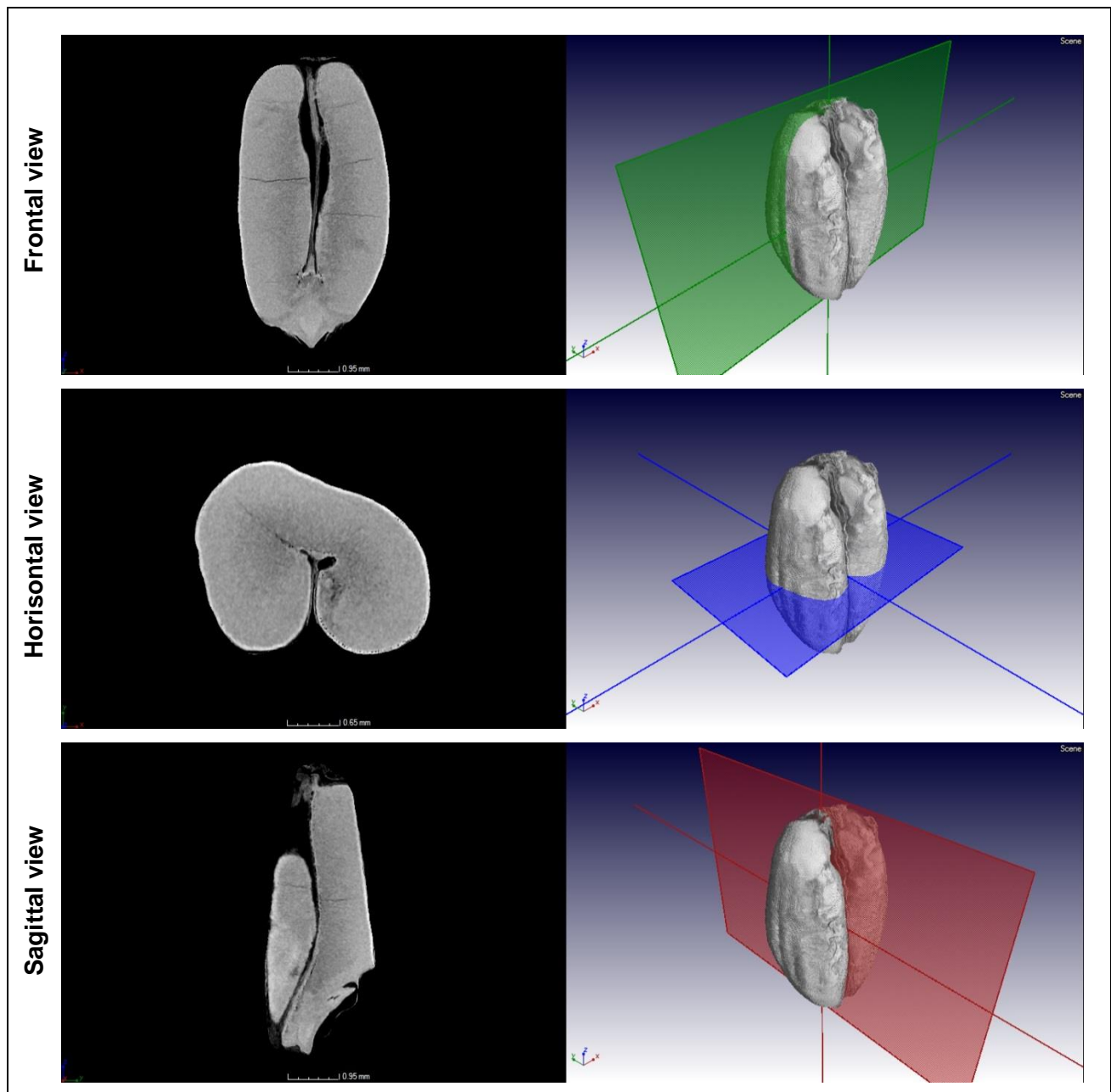


**Figure B.3.** Illustration of the segmentation procedure where the background air was selected and extracted from the image.

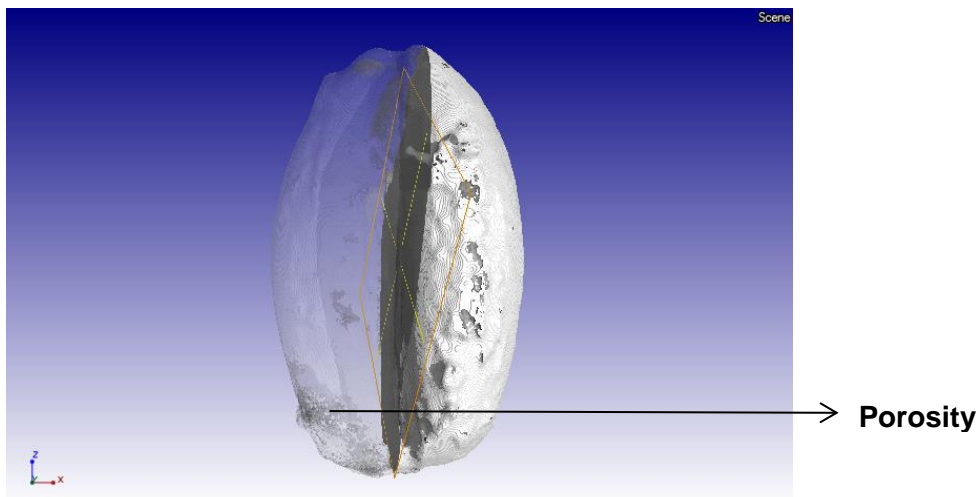


**Figure B.4.** Visualisation of the volume size distribution of the porosity in a raw sample.

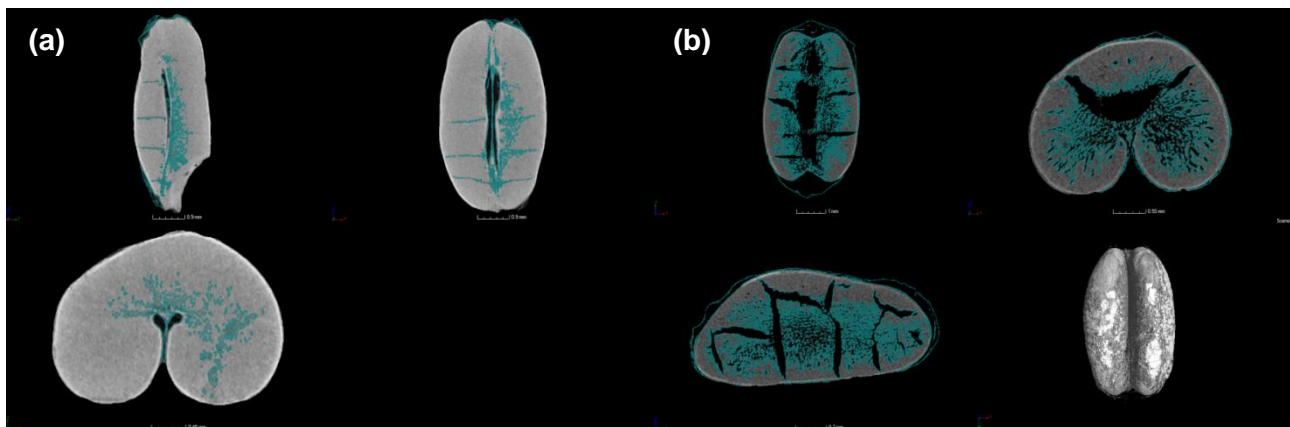




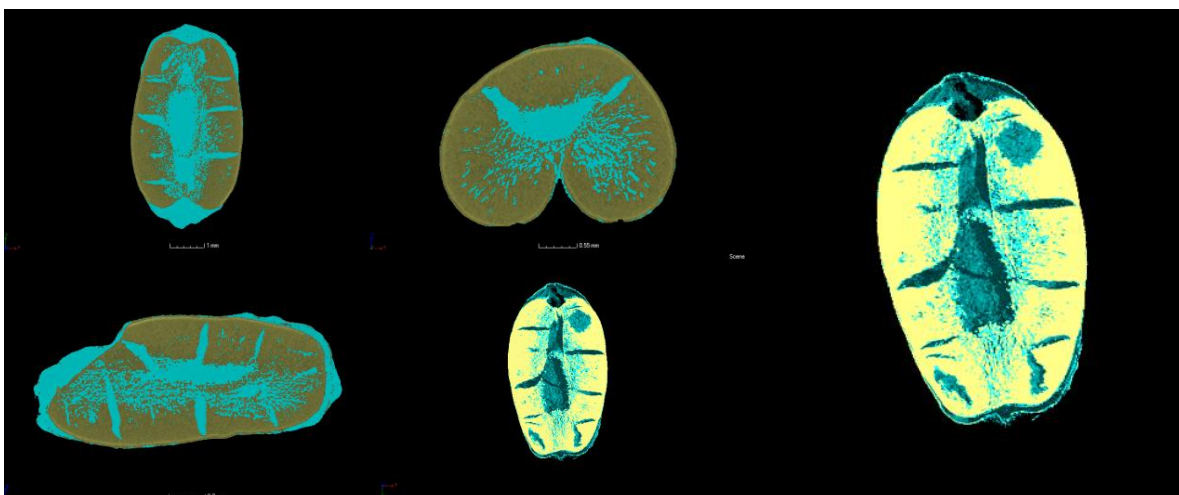
**Figure B.5.** Illustration of the different X-ray image views (horizontal, frontal and sagittal) of a raw wheat kernel. Two-dimensional views are shown on the left and the corresponding section in the 3D view on the right.



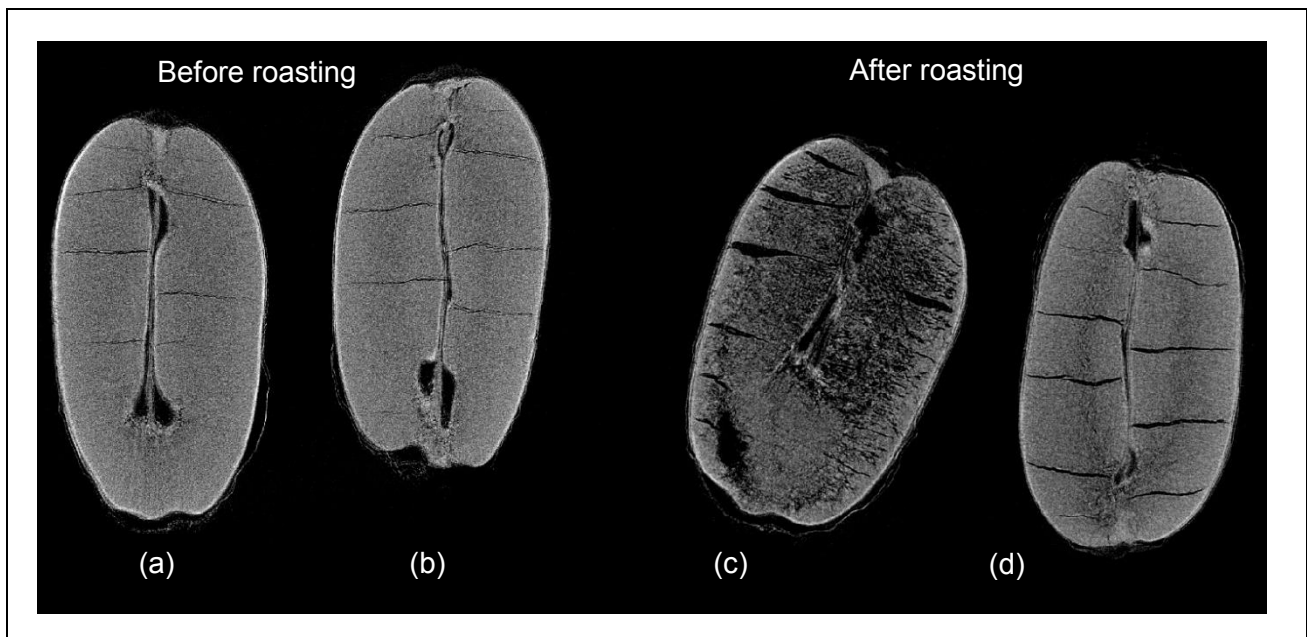
**Figure B.6.** Visualisation of a raw wheat kernel, viewed with partial transparency (left) to illustrate the porosity in grey.



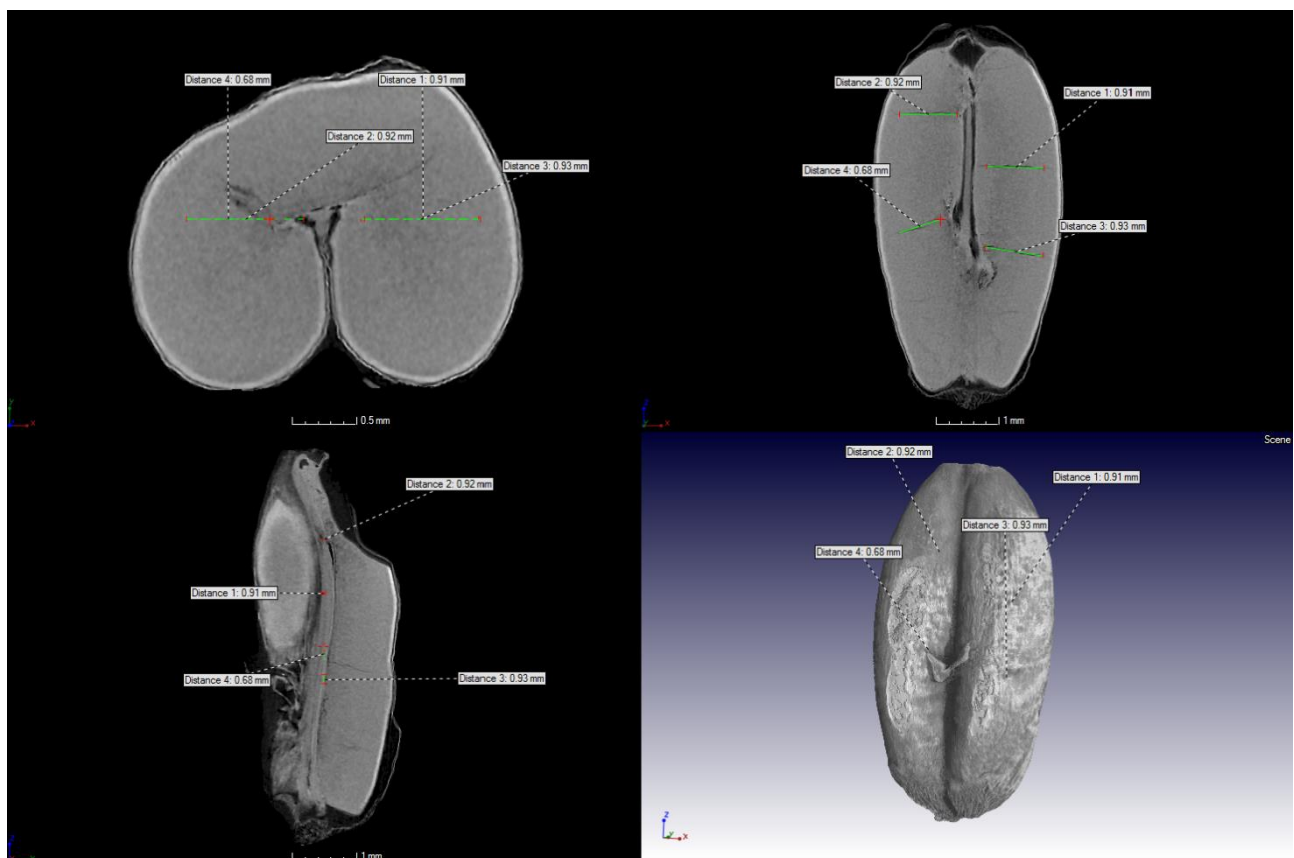
**Figure B.7.** Illustration of a (a) raw and (b) oven-roasted wheat kernel where the porosity is characterised in blue.



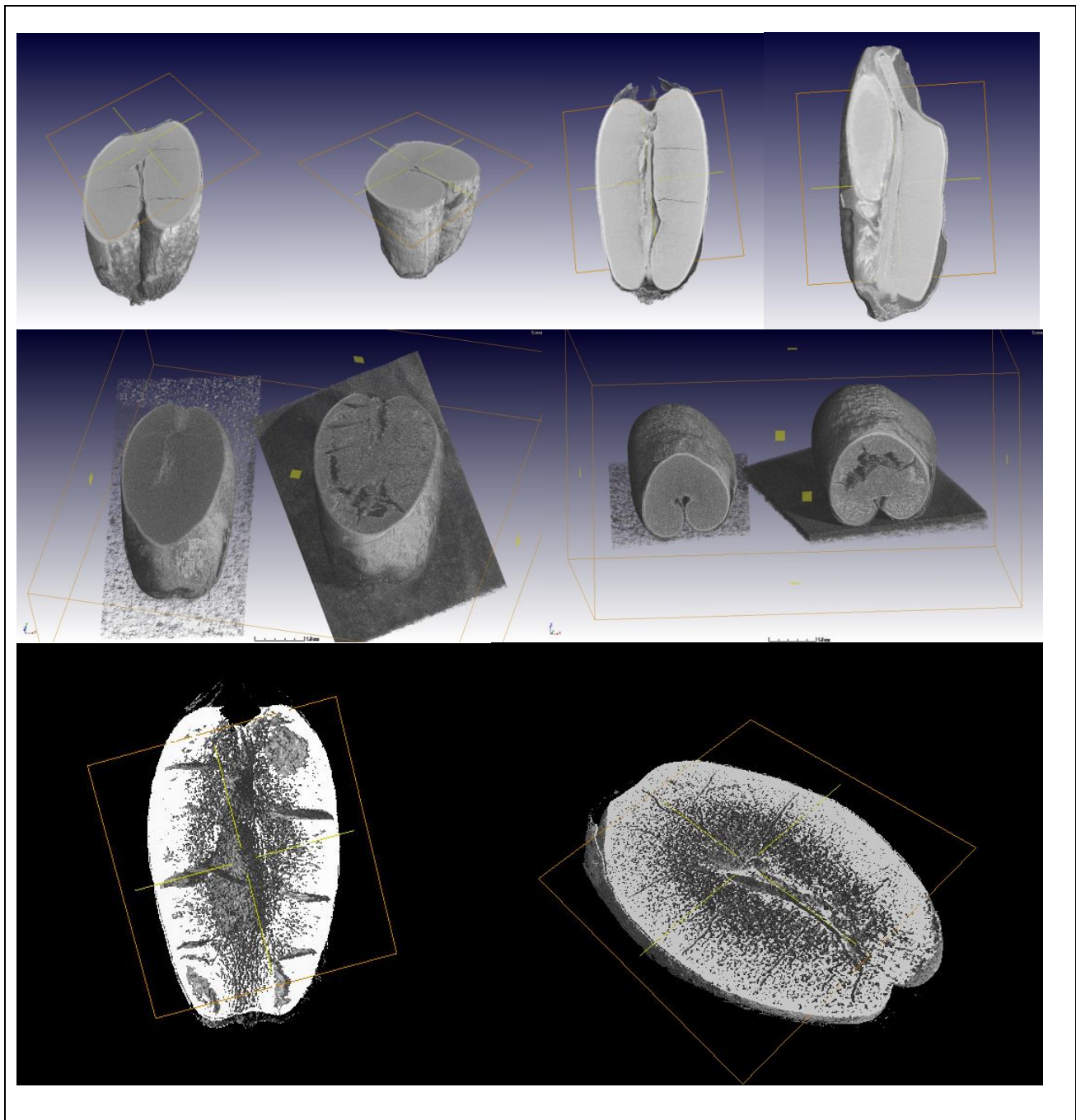
**Figure B.8.** Visualisation of the impact of oven roasting on the microstructure, where air is characterised in blue, while the kernel structure is presented in yellow.



**Figure B.9.** Representations of the frontal slice images of an (a) and (c) oven-roasted and a (b) and (d) FCCT-roasted wheat kernel before and after roasting. The crack and cavity size and distribution can be observed together with the differences in the grey level intensities which represent density variations.



**Figure B.10.** Representation of a raw wheat kernel where dimensional measurements on specific regions-of-interest, i.e. cracks were performed.



**Figure B.11.** Illustration of the different clipping views of raw and oven-roasted wheat kernels, virtually cut to reveal the internal structure.



### Appendix C: Preliminary roasting trails

Roasting trails were performed to select the desired roasting temperature, since the forced convection continuous tumble (FCCT) roaster is a relatively new roasting technique. The independent variables were the roasting speed (which determined the roasting time) and the internal temperature of the roaster at the beginning of the roasting process. Based on preliminary trails (Fig. A.1), temperatures higher than 220°C were rejected due the observation of the popping phenomenon and a temperature of 200°C led to an undesired dark colour and external cracks. Furthermore, temperatures lower than 150°C did not have the desired roasting effect. The roasting conditions was standardised by trials to get maximum grain expansion without burning.

During oven roasting dry hot air was circulated inside the oven by means of a fan (thermofan) which reverses its direction of rotation to ensure a more uniform heat transfer to the product. This enabled the oven roasting method to be more comparable with FCCT roasting.

During roasting the pericarp holds water vapour and allows the internal pressure to build up to a certain point. When this point is exceeded, the pericarp will rupture resulting in popcorn. The water vapour provides the driving force for expansion. Presumably at low moistures there is insufficient superheated water for complete expansion. At high moistures it is assumed that moisture weakens the pericarp causing an early release of pressure.

For FCCT roasting samples were fed into the feed hopper and then transferred to the drum by gravity where it was roasted. The drum comprises of a perforated cylinder and a screw conveyer inside which mixes the sample as it propels it forward at a set speed. Hereby a continuous and uniform heat distribution to the sample is ensured which is more effective than in a stationary roasting method. The screw speed setting of 80 Hz remained constant during roasting. When a sample (at ambient temperature) was fed into the roaster, the temperature dropped with ca. 3°C. The roaster reached the desired temperature of 180°C again within a few seconds.



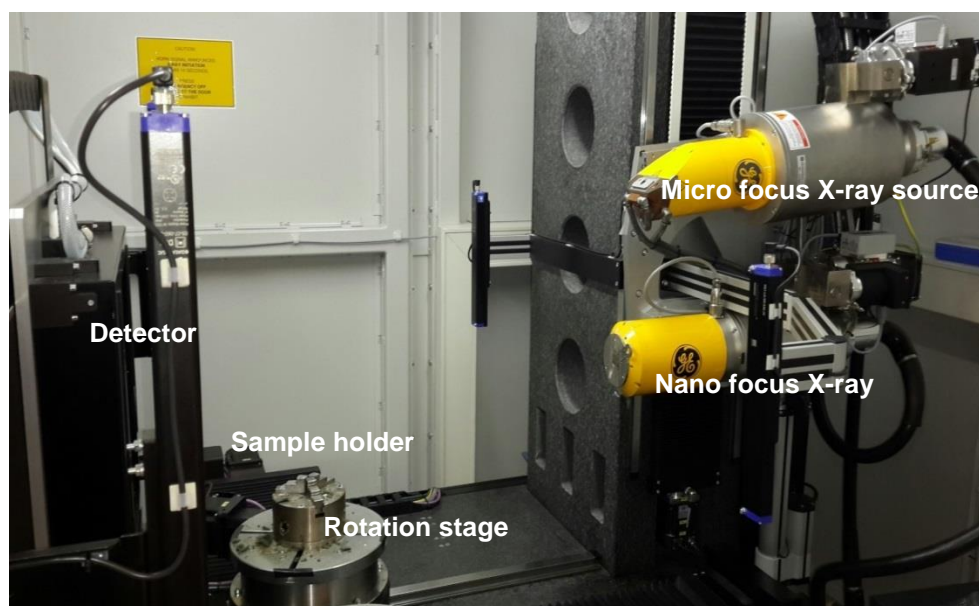
**Figure C.1.** Photograph of undesirable roasted maize kernels obtained from preliminary trails.

## Appendix D: X-ray $\mu$ CT instrumentation

Real-time X-ray  $\mu$ CT scans of the raw and roasted whole maize kernels were obtained using a commercial X-ray computed tomography system, i.e. a General Electric Phoenix V|Tome|X L240 (General Electric Sensing & Inspection Technologies GmbH, Phoenix, Wunstorf, Germany) (Fig. D.1). The high-resolution X-ray  $\mu$ CT imaging system consists of a micro-focus X-ray tube with an additional nano-focus tube (Fig. D.2.). The system comprises of a lead-lined cabinet that houses the X-ray tube, the sample manipulator and the detector. Figure D.3 demonstrates the (a) lead-lined cabinet with the cooling unit and (b) the external control panel.

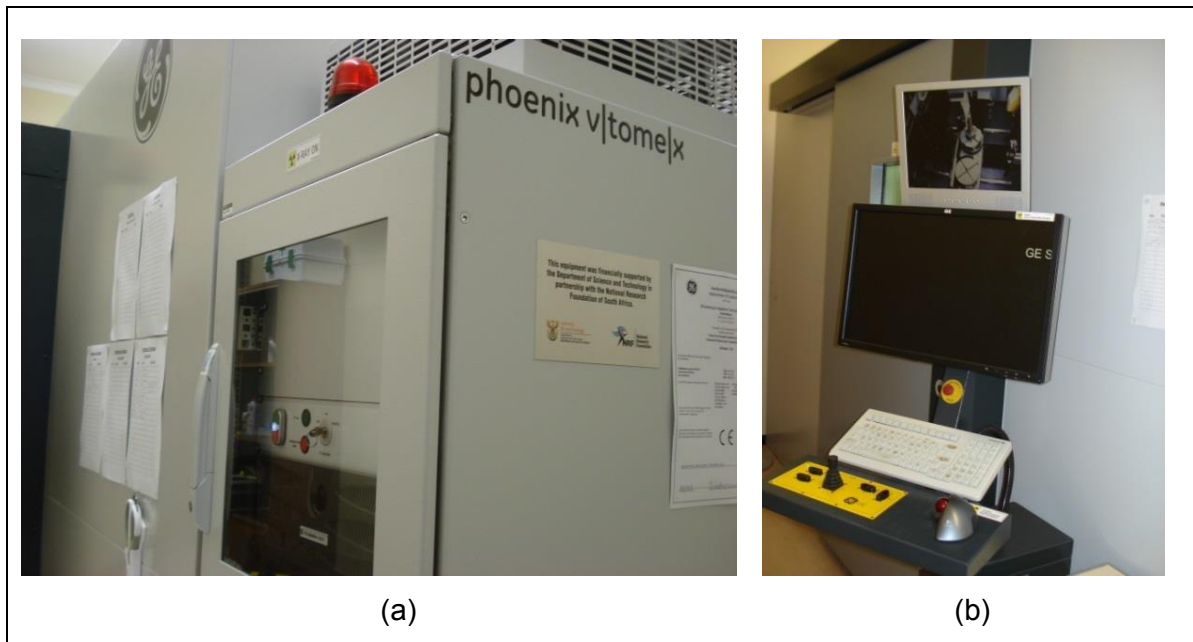


**Figure D.1.** The General Electric Phoenix V|Tome|X L240 X-ray  $\mu$ CT scanner used for acquiring X-ray images.



**Figure D.2.** Photograph of the internal setup of the Phoenix V|Tome|X L240 X-ray  $\mu$ CT scanner, showcasing the X-ray source, rotation stage, sample holder and detector system.



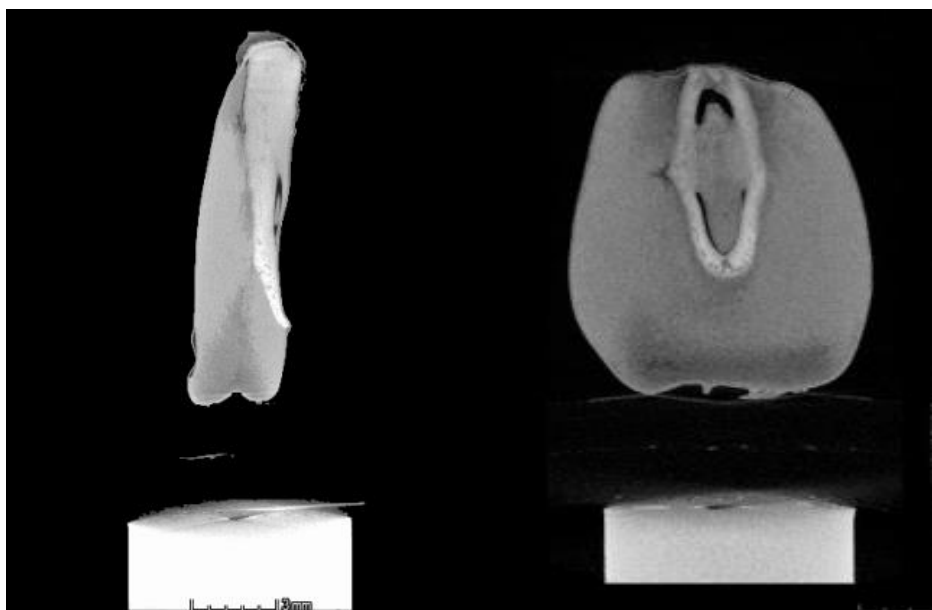


**Figure D.3.** Photograph of the (a) lead-lined cabinet with the cooling unit and (b) the control monitor.

## Appendix E: Optimising X-ray $\mu$ CT scanning parameters

Various system settings were tested to optimise the scan quality. Instrumental conditions that needed to be optimised included beam energy and current, sample-to-detector-distance and exposure time. The energy spectrum (usually between 20 and 100 kV for food) describes the penetrative ability of the X-rays, as well the relative attenuation that is expected as X-rays pass through material varying in density. The current is associated with the number of X-ray photons generated. Higher energy X-rays are more effective in penetrating a sample but it is less sensitive to changes in composition and material density in comparison to lower energy X-rays. An energy value of 60 kV was thus sufficient as the cereal grains did not require a high penetrating power, but rather a higher sensitivity in terms of image contrast.

The only preparation necessary for  $\mu$ CT scanning is to ensure that the sample fits inside the field-of-view (FOV) and that it does not move during the scan. The full scan field is cylindrical (i.e., a stack of circular fields-of-view) and therefore the most efficient geometry to scan is a cylinder. Thus, the sample was stacked onto a polymeric disc in order to take on a cylindrical geometry (Fig. E.1.). Experimental conditions were optimised to allow high quality radiographic projections and were based on the compromise of enhancing both contrast and resolution of the images and using the shortest scanning time of the whole sample volume.

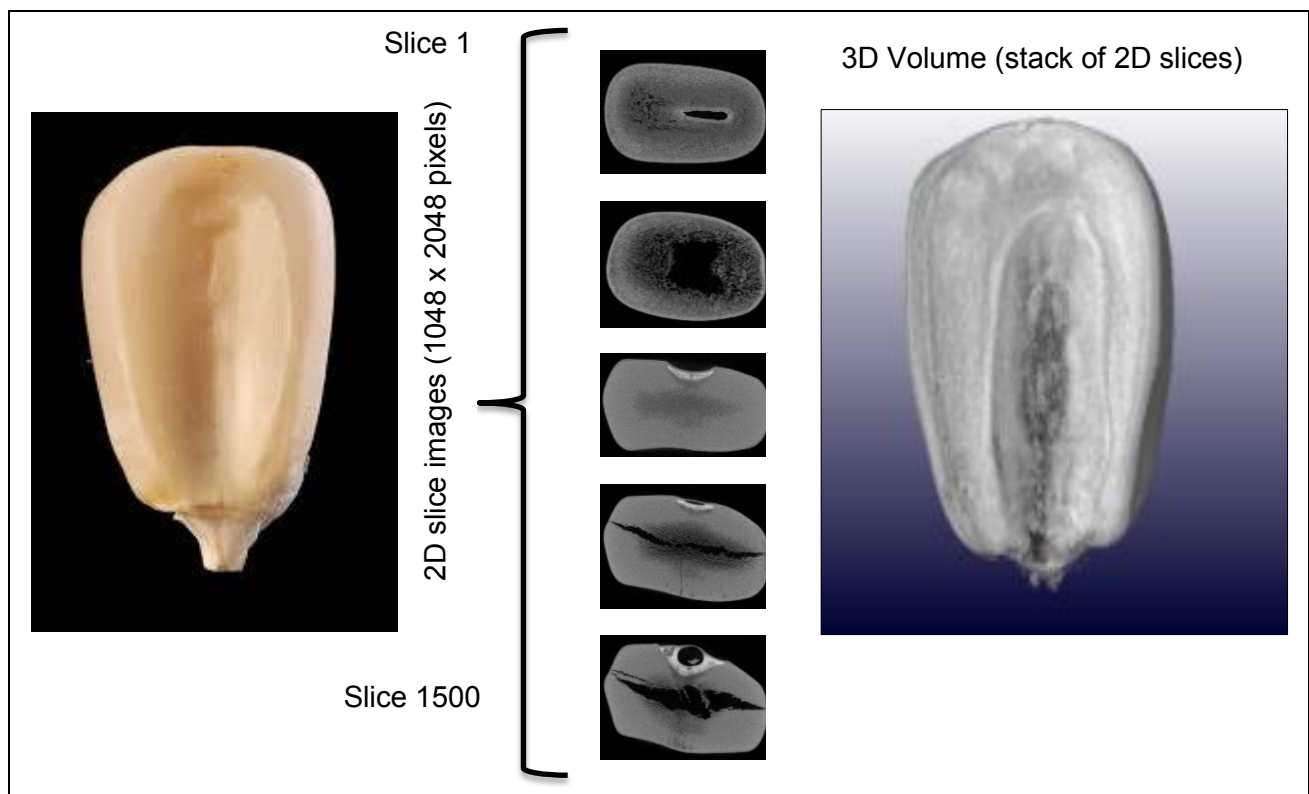


**Figure E.1.** Illustration of a maize kernel mounted on oases and polymeric disc in a 2D side view and frontal view.

## Appendix F: Stacking of X-ray $\mu$ CT slices

The fundamental principle of  $\mu$ CT is to acquire multiple sets of views of a sample over a range of angular orientations. In doing so additional dimensional data are obtained in comparison to conventional X-ray radiography. These data are used to create 2D images, known as tomograms or radiographs and they correspond to what would be seen if the objects were sliced along the scanning plane.

Figure F.1 illustrates the stacking of 2D projection images to obtain a 3D volume. From X-ray  $\mu$ CT images, the brightness is a function of X-ray absorption, where brighter regions correspond to a higher absorption and dark areas correlate to a lower absorption.

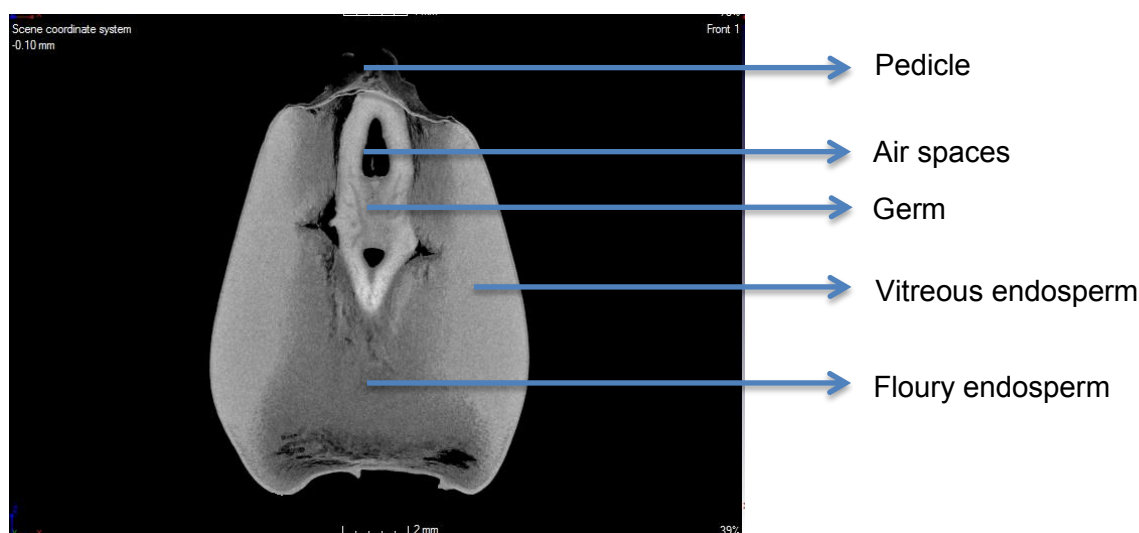


**Figure F.1.** Illustration of the stacking of 2D slice images to obtain a 3D volume.

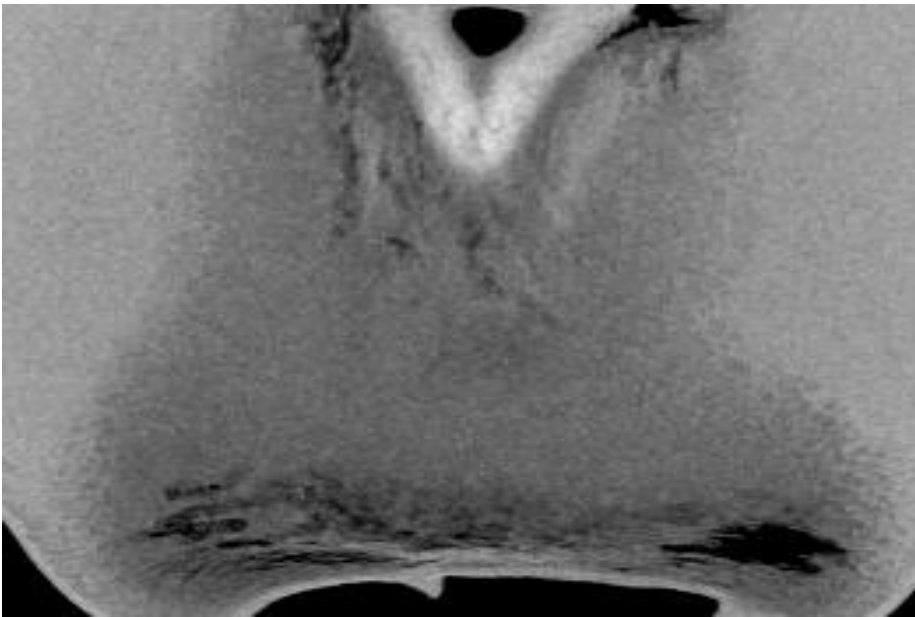
## Appendix G: Image and histogram analysis

Considering the 2D slice image in Figure G.1, a multiphase composition can be observed as the maize kernel is made up of a germ, floury and vitreous endosperm and air spaces. There can be distinguished between these different components based on the difference in the X-ray absorption. This difference manifests itself through the variation in grey scale intensities and therefore it visually appears as distinct phases. Figure G.2 illustrates the spatial distribution of the different density components within a kernel at a higher magnification. Air voids are represented by the black areas as the absorption coefficient is lower with respect to the solid fractions. The black areas indicate that there was no material to interact with the X-ray beams and therefore the beam was not attenuated at all. The grey level intensity within one pixel is a linear function of the local X-ray attenuation coefficient. The brighter grey areas represent the denser germ and vitreous endosperm and these two components have a higher absorption coefficient in comparison with the less dense floury endosperm and the air. Endosperm textural attributes can be obtained from a 2D slice image.

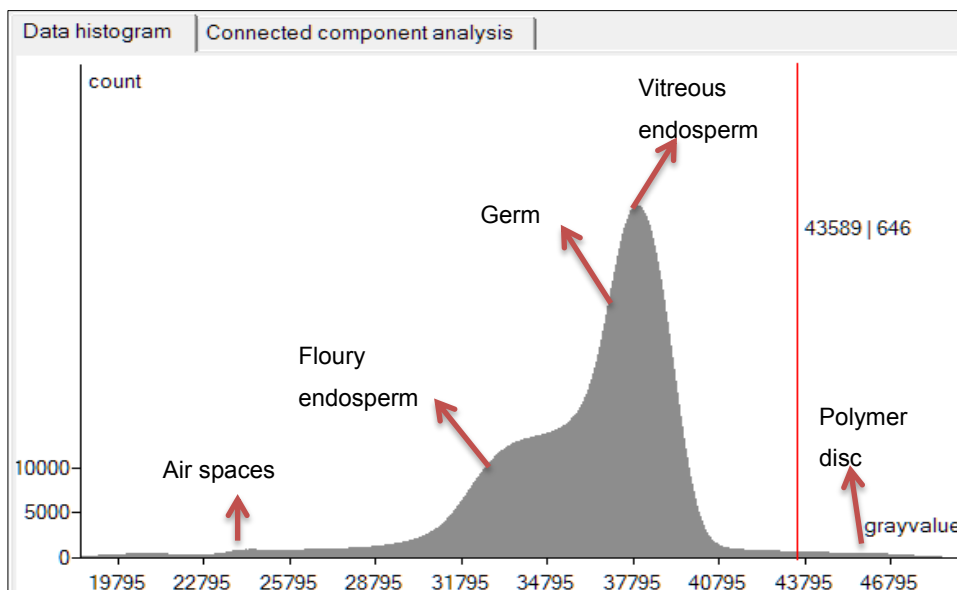
Figure G.3 demonstrates that maize kernel components can be separated based on the grey level distribution in the data histogram. The grey value histogram provides a diagram of the number and intensity of voxels in the whole image or specific regions-of-interest (ROIs), illustrating the density distribution based on grey values. The y-axis displays the number of voxels associated with each grey value, whereas the x-axis indicates the grey values and thus the intensity of the voxels in an image. Lower grey values correspond to internal air space and higher values to solid material. This is valuable for phase analysis and it is often used to segment an image into different ROIs. Separate peaks are observed in Fig. G.3 each corresponding to a different phase, i.e. solid or air.



**Figure G.1.** X-ray  $\mu$ CT image of a maize kernel illustrating the different grey scale intensities of the various components.



**Figure G.2.** An enlarged 2D X-ray  $\mu$ CT image of the endosperm textural properties of a maize kernel. The vitreous endosperm is light grey (more dense), the germ is visible at the top (white) and the less dense floury endosperm with the air spaces (black) is visible in darker grey.



**Figure G.3.** A typical data histogram presenting the grey values for the different maize components.

## Appendix H: Segmentation and defining regions-of-interest

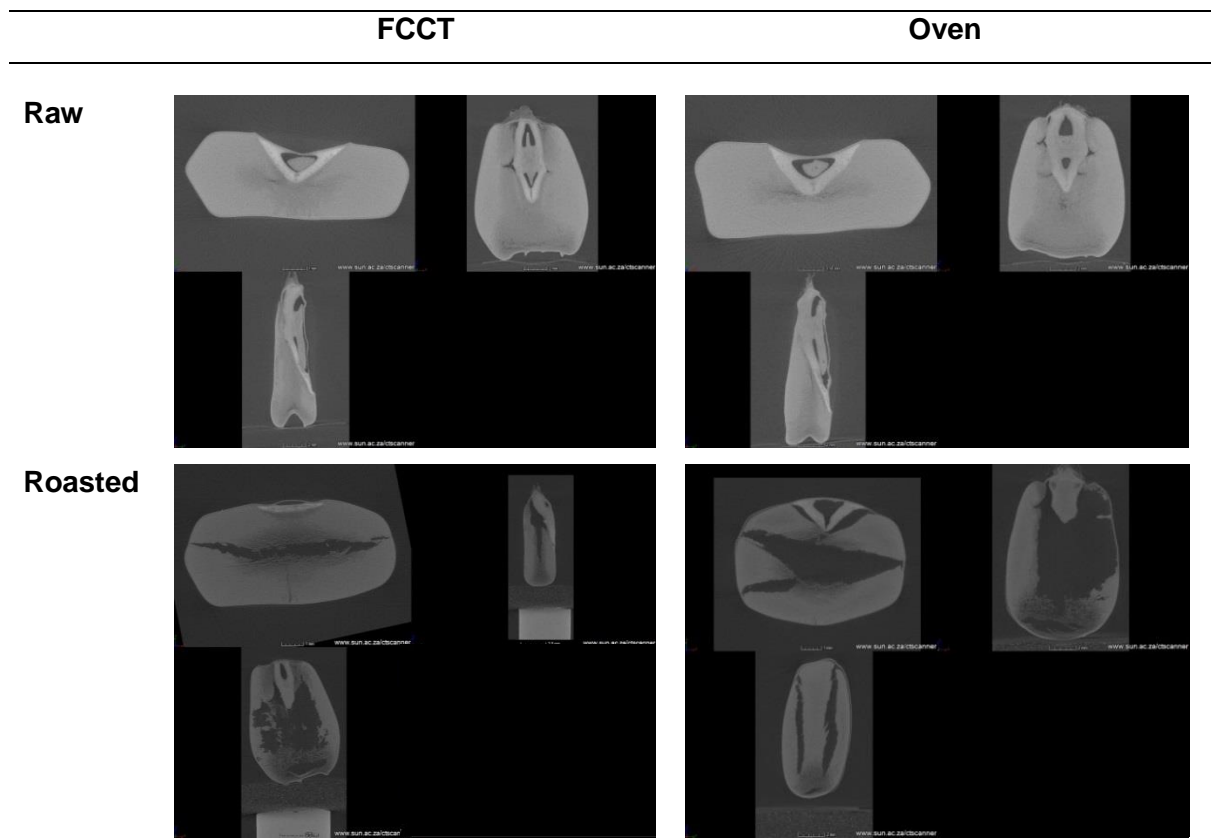
### *Segmentation*

Segmentation entails the process of dividing volume data into different sections, thus the volume is partitioned into different voxel groups called ROIs. Once a ROI has been defined, analyses are restricted to this area. Grey value based segmentation was performed using the Region growing tool where separation of the different ROIs was based on tolerance differences of the associated grey pixels. The threshold value for each sample was established manually based on the distribution in the histogram. In selecting a threshold value, the objective was to separate the kernel into different regions: the germ and vitreous and floury endosperm, which constitutes the solid phase and the cavities and pores which forms the gaseous phase. Image segmentation was carried out on the smoothed 16-bit grey scale images that were obtained from the reconstruction step.

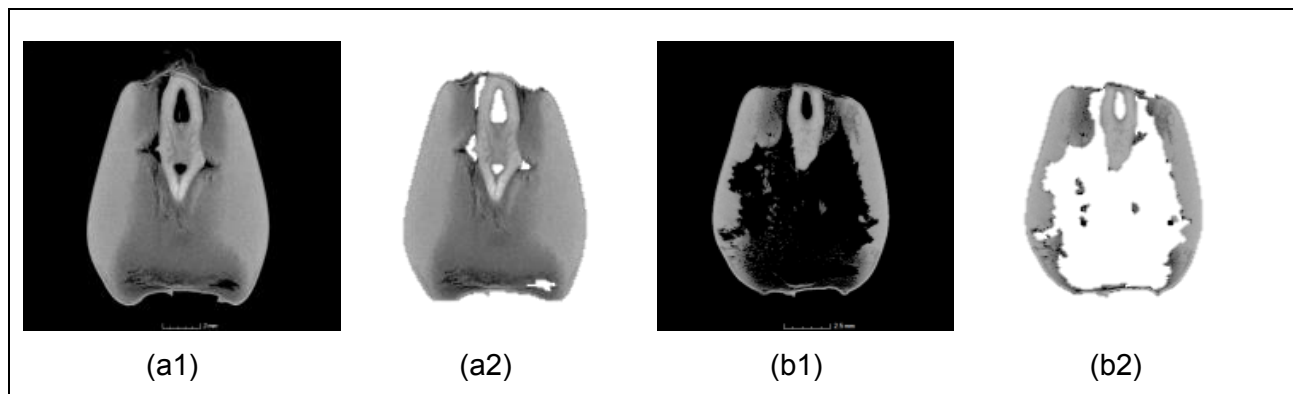
The Adaptive rectangle and Region growing tool was used to remove the background (air) around the kernel. Surface fitting was performed using interactive thresholding of the grey values and observing the fit line on a slice view. Background was removed by creating an ROI of the background and then inverting and extracting the ROI. Figure H.1 illustrates the original, unsegmented images before and after roasting. Figure H.2 represents a raw and roasted kernel with the background and internal air and with the background and internal air removed. Once the background was removed, individual components were virtually segmented from the reconstructed volumes. The Region growing tool propagates through the 3D volume, connecting voxels within a specified grey value range to create a ROI; allowing each voxel of a specific colour to be compared with surrounding voxels. If neighbouring voxels has the same colour, they are considered to be part of the same ROI.

After segmentation a cleaning step were applied to remove small numbers of pixels not of interest (noise) i.e. the partial volume effect. This effect is the result of one pixel containing numerous phases. The cleaning techniques used were an Opening and closing tool and Erode and dilate function. The germ was virtually (in each slice) removed using the Drawing tool in VGStudio Max 2.2 software. Once a segmented volume, with the various ROIs has been defined structural measurements was performed. ROIs were subjected to the Volume analyser function (Fig. H.3) to calculate whole kernel and ROIs volumes and relative densities. A representative slice from the maize kernels was selected from the dataset to obtain a mean grey value for each of the components in the kernel.

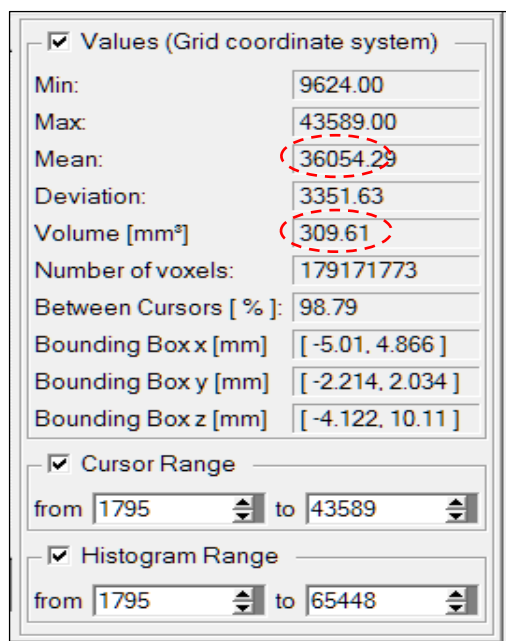




**Figure H.1.** Original, unsegmented X-ray projection images before and after oven and FCCT roasting.



**Figure H.2.** Illustration of (a) raw and (b) FCCT-roasted maize kernels with the background and internal air (a1 and b1) and with the background and internal air removed (a2 and b2).



**Figure H.3.** The Volume analyser function, illustrating the mean grey value and volume of the ROI of a maize kernel (encircled).

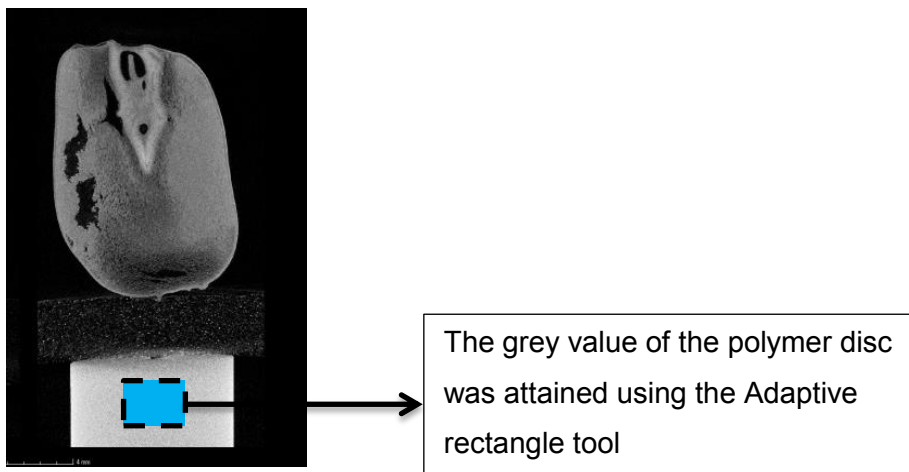
### *Regions-of-interest*

Since a 3D model can be viewed from any angle, it is possible to virtually scroll through the sample to allow visualisation of the internal structure. This feature makes X-ray  $\mu$ CT ideally suited for the non-invasive imaging of internal features of food products, especially foods with a delicate structure, giving X-ray  $\mu$ CT a leading edge over other methods. ROIs can be manipulated by creating intersections or combinations of several ROIs.

Often, with the traditional approach (e.g. hand dissection), it is difficult to properly select a ROI because the target region cannot be identified beforehand and one only has one opportunity for sectioning the sample. By means of 3D reconstruction the selection of a ROI can be repeated as many times as desired and the selection can be changed until the target ROI is attained. Once the ROI is selected in 3D it can be viewed from any arbitrary angle.

### *Reference standard as ROI*

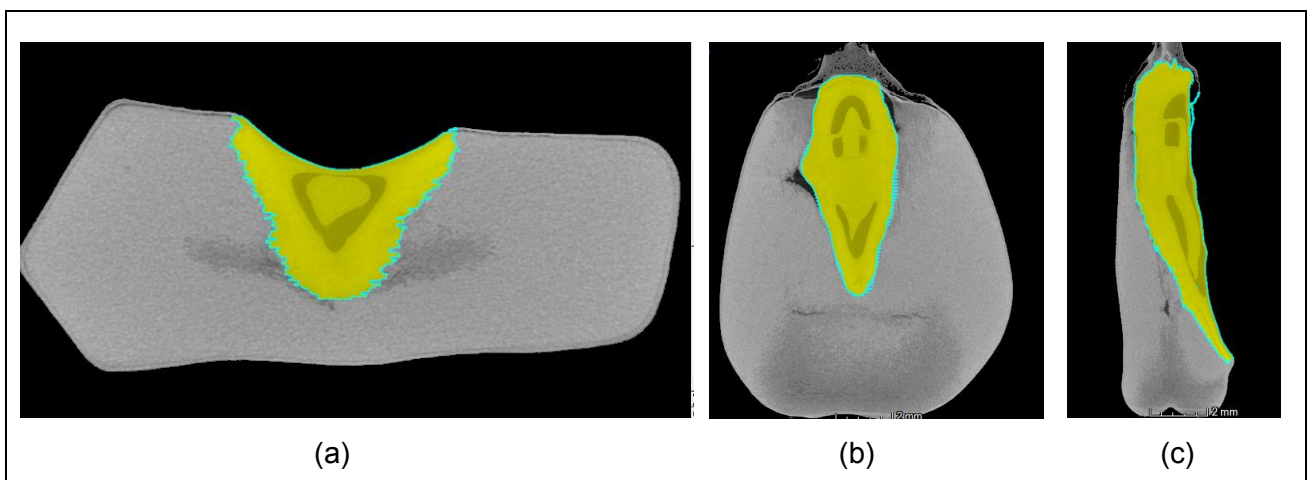
The average grey value of the polymer disc, used as a reference standard, was attained by selecting a representative volume from the disc (Fig. H.4). Each voxel has a certain grey value associated with it, which is dependent on the density and atomic number of the material. The mean grey value of the homogenous polymer disc is thus a measure of its density.



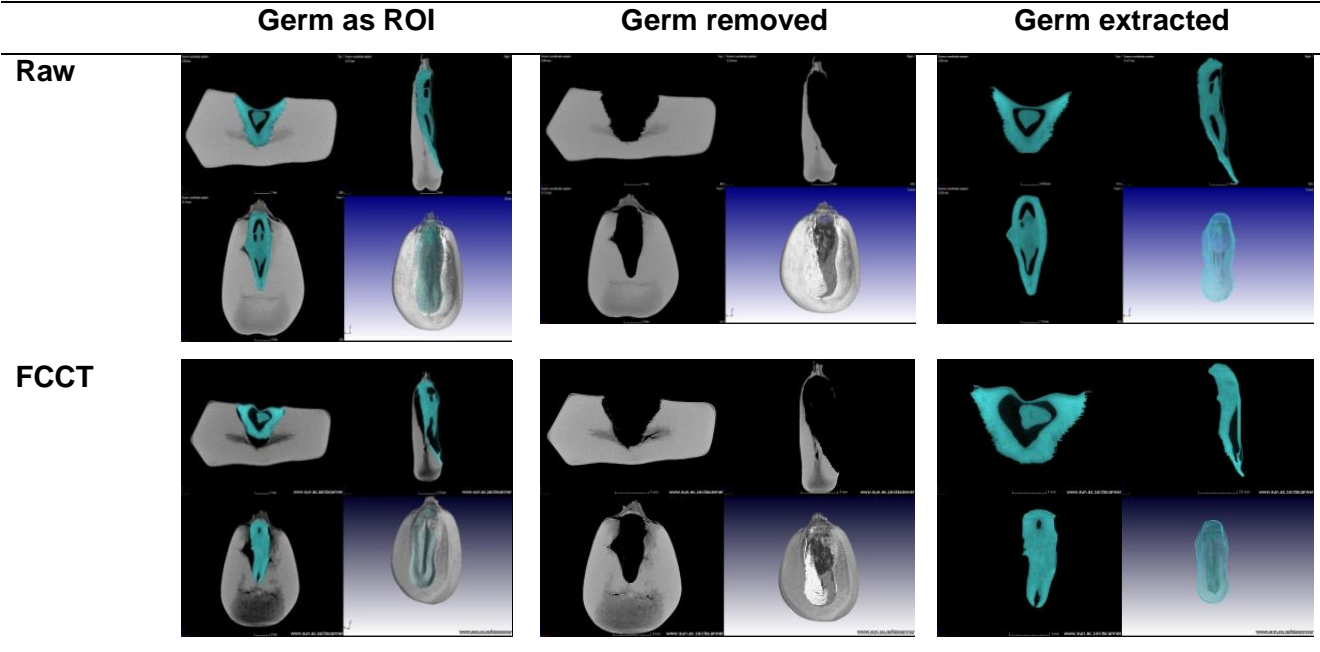
**Figure H.4.** Illustration of the acquisition setup where the polymer disc was scanned in the FOV for relative density determinations.

#### *Germ as ROI*

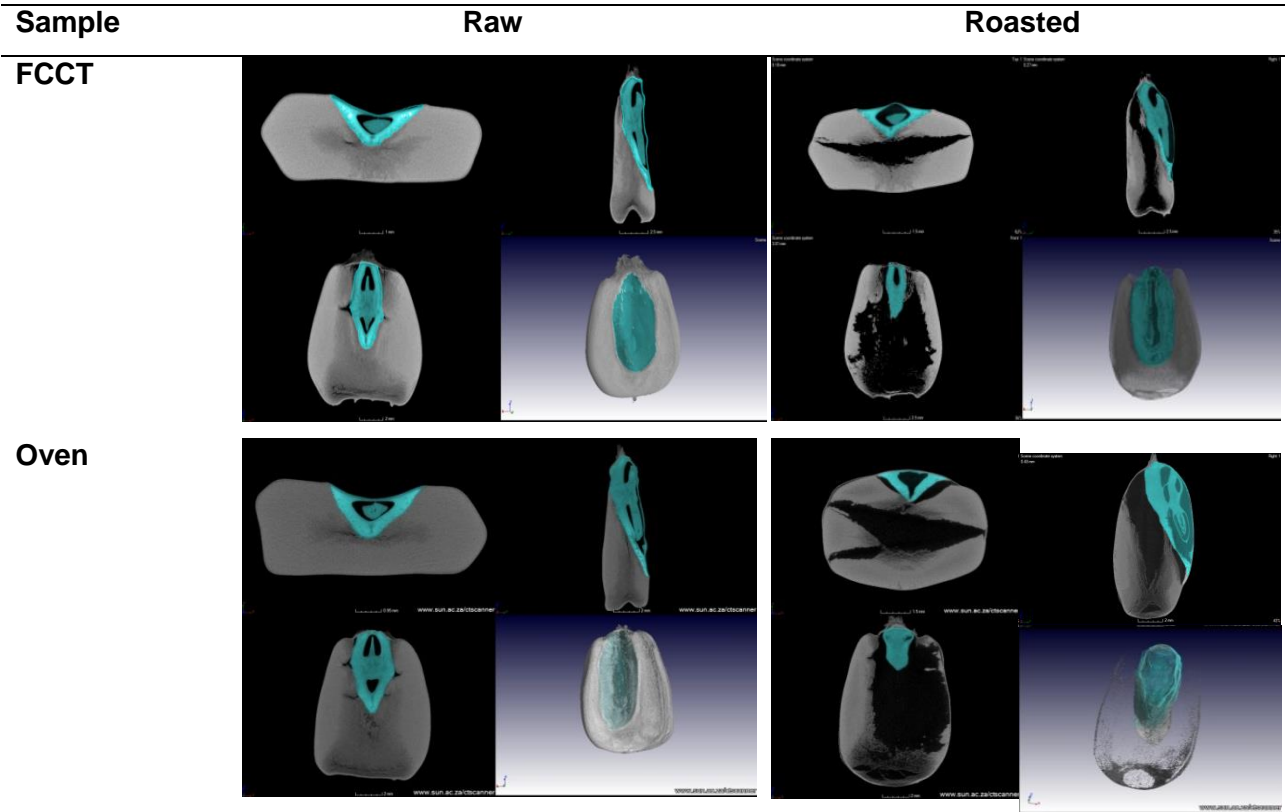
The usefulness of X-ray  $\mu$ CT was illustrated in the ability to exclude certain regions in the maize kernel to facilitate further separation of the ROIs. In this case the germ region was selected as 'n ROI and then removed. This was done to allow more accurate segmentation of the vitreous and floury endosperm. Figures H.5 to H.8 visualises the germ as ROI.



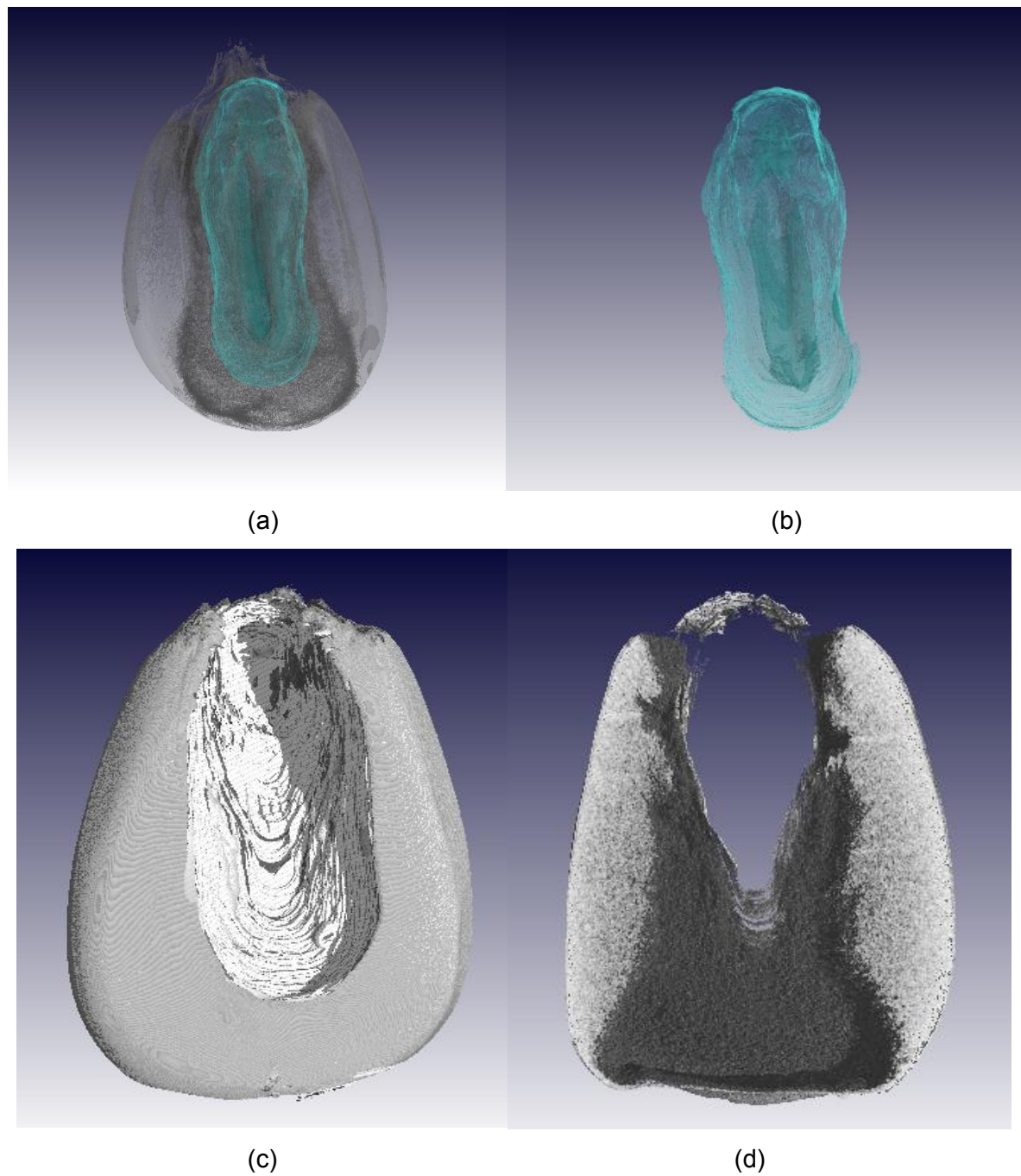
**Figure H.5.** 2D projection images of a raw kernel with the germ selected as ROI in the (a) horizontal, (b) frontal and (c) sagittal view.



**Figure H.6.** Images of raw and FCCT-roasted maize kernels where the germ was selected as ROI, removed and extracted.



**Figure H.7.** Comparison of FCCT and oven roasting, with the germ as ROI before and after roasting.

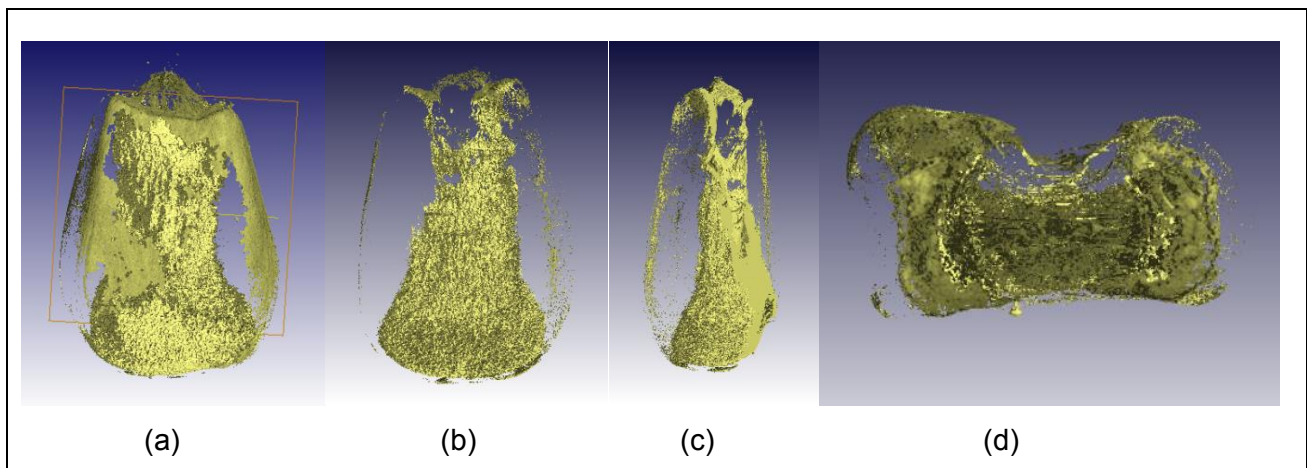


**Figure H.8.** X-ray  $\mu$ CT volumes of a raw kernel where the germ (a) was selected as ROI and (b) was extracted. Volumes (c) and (d) illustrate a 3D reconstructed  $\mu$ CT image with the germ removed in a raw and FCCT-roasted kernel, respectively.

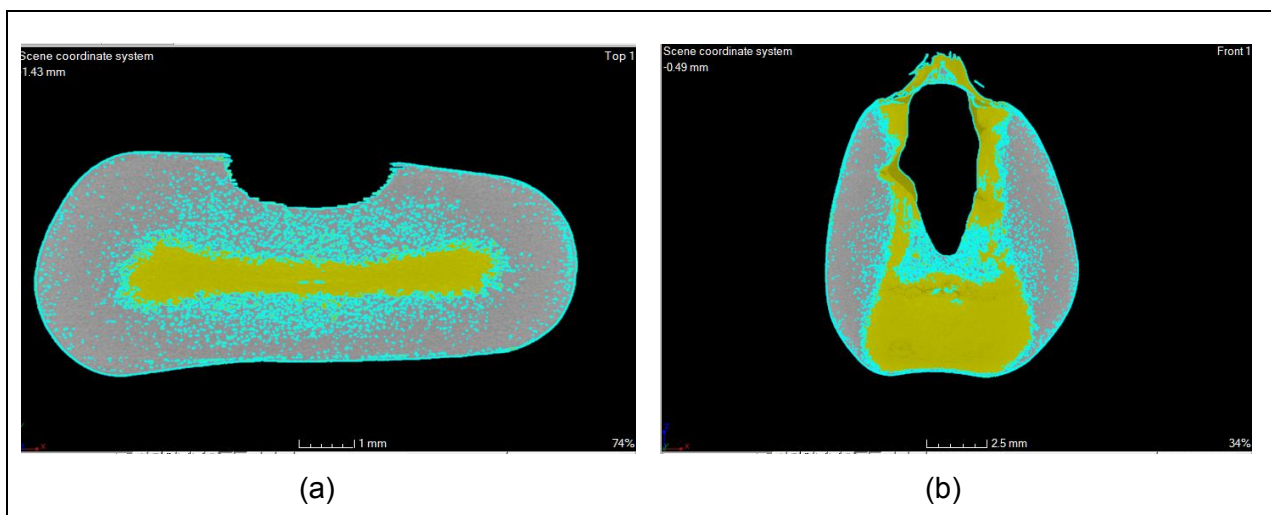
#### *Floury and vitreous endosperm as ROI*

Figures H.9. to H.17 illustrates the endosperm as ROI.

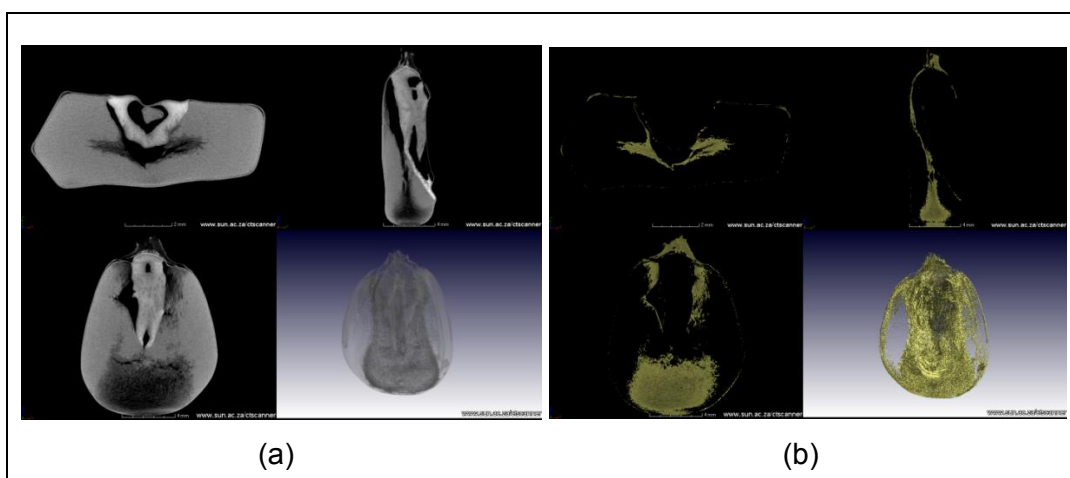




**Figure H.9.** Illustration of the floursy endosperm in a raw maize kernel as viewed from different arbitrary angles: (a) back, (b) frontal, (c) side and (d) bottom 3D view.

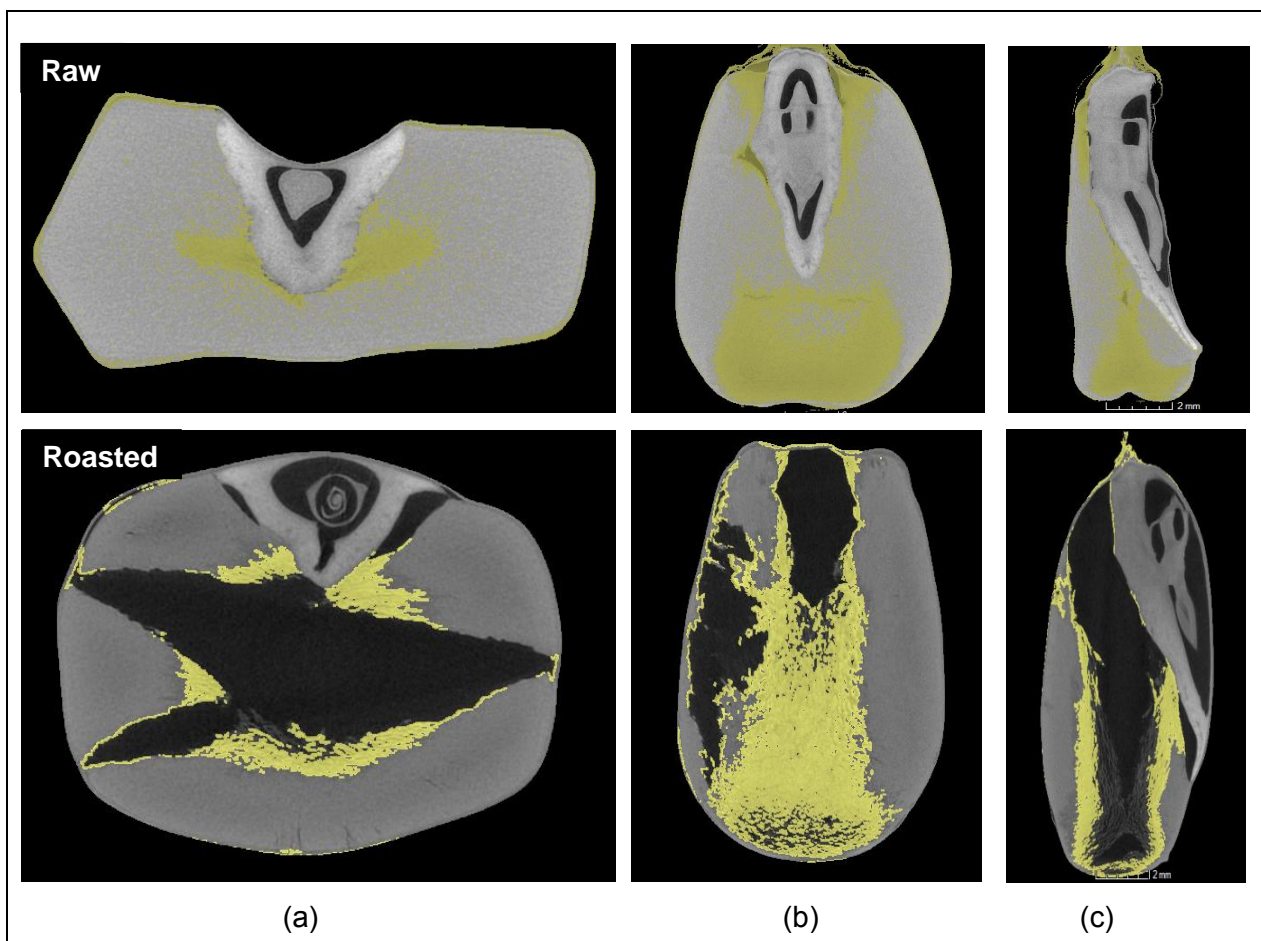


**Figure H.10.** Demonstration of the (a) transverse and (b) frontal slice images of a raw maize kernel where the germ was removed and the floursy endosperm (yellow), vitreous endosperm (grey) and pores (blue) were selected as ROIs.

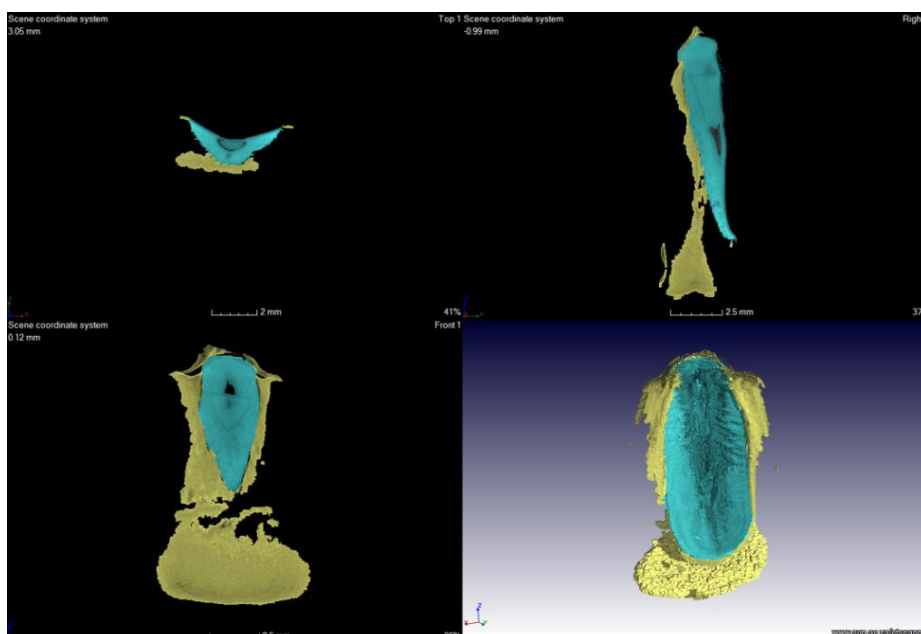


**Figure H.11.** Illustration of (a) the grey scale and (b) floursy endosperm (yellow) extracted views of a FCCT-roasted maize kernel.

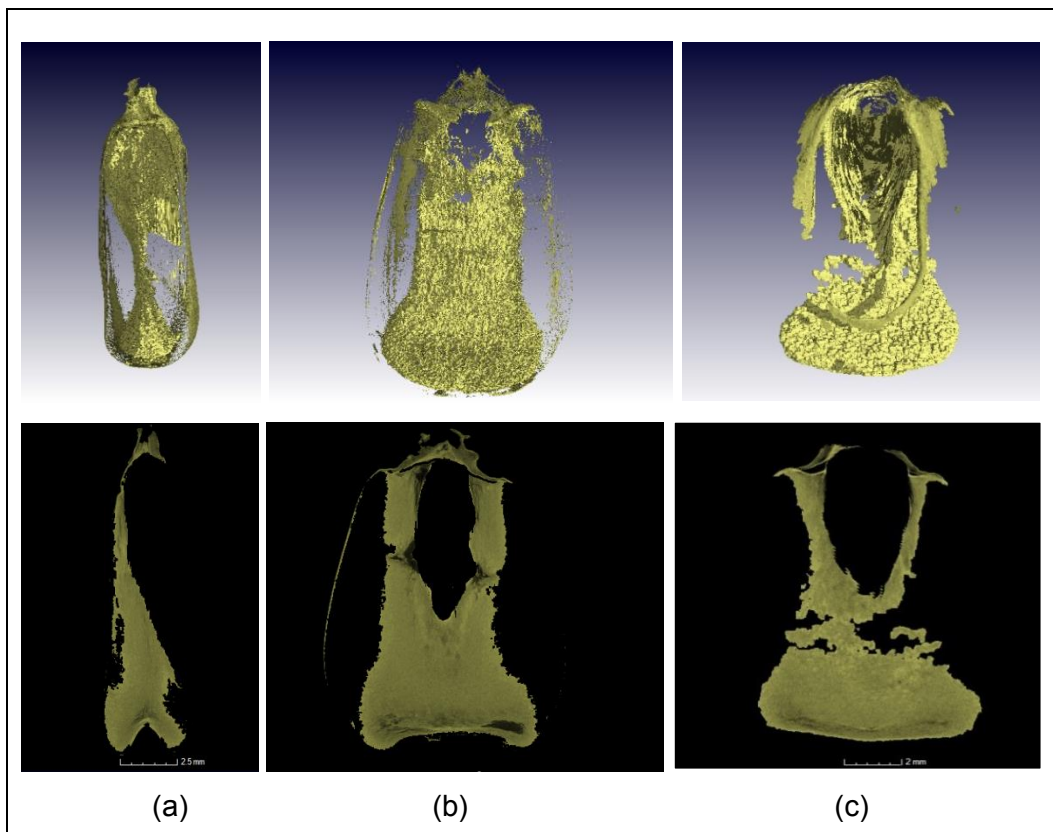




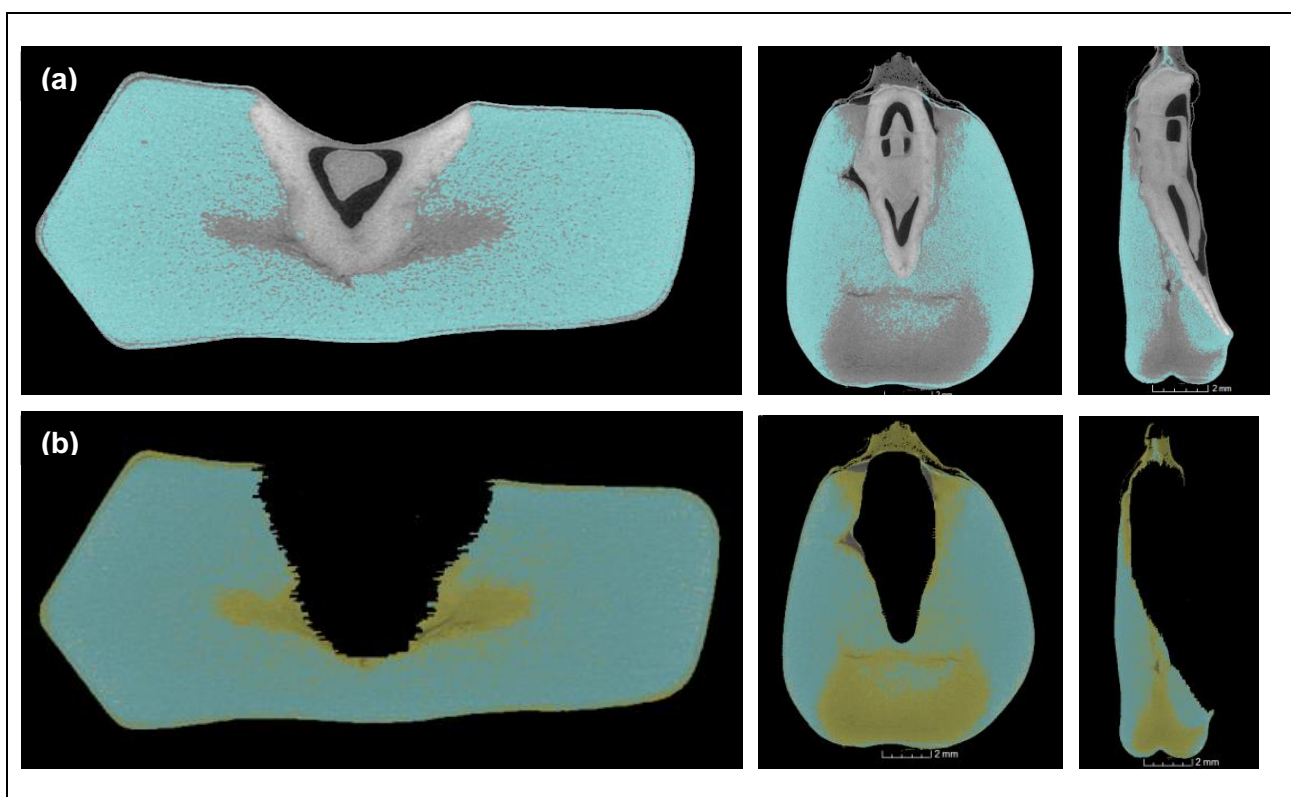
**Figure H.12.** 2D Greyscale images illustrating the floury endosperm in a raw and oven-roasted maize kernel in the (a) transverse, (b) frontal and (c) sagittal view.



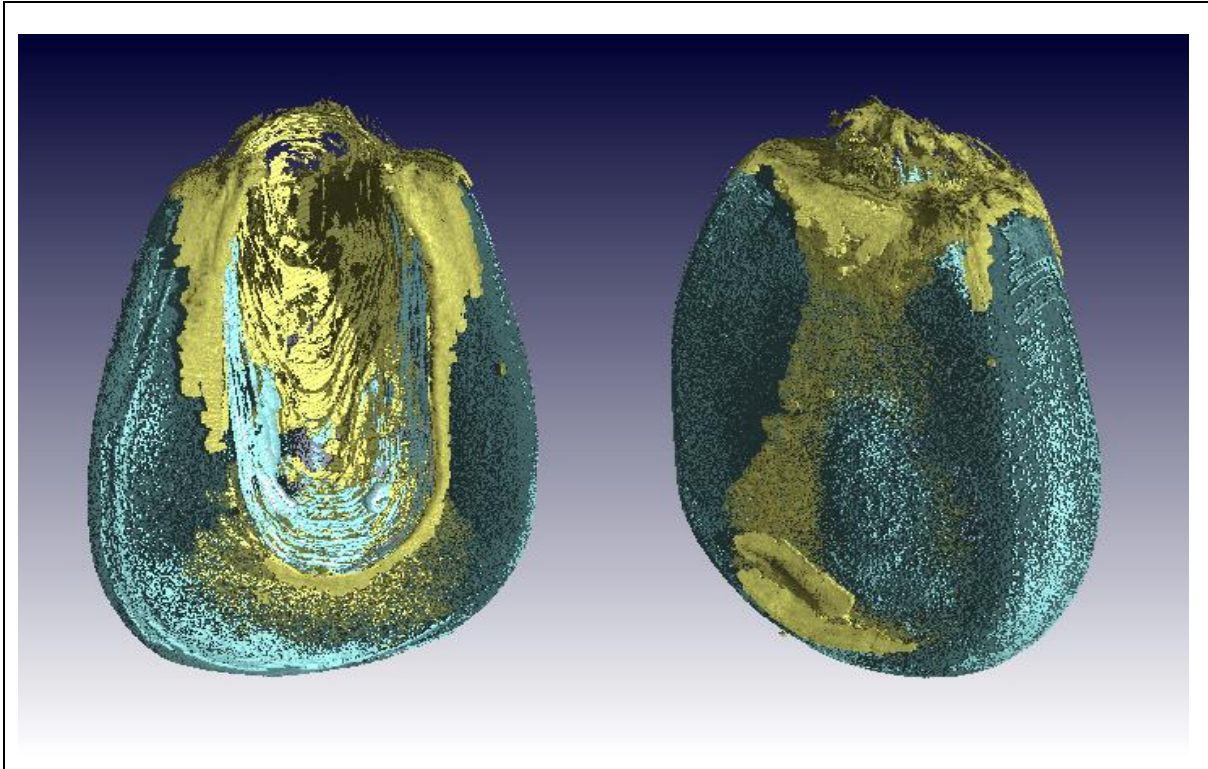
**Figure H.13.** Representation of the 2D and 3D views of the germ (blue) and floury endosperm (yellow) extracted from a raw maize kernel.



**Figure H.14.** 3D and 2D visualisation of the (a) sagittal view, (b) frontal view and (c) back view of the floursy endosperm in a raw maize kernel.

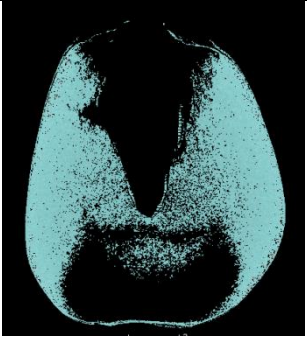
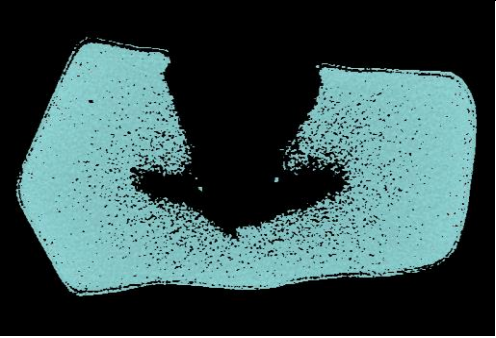


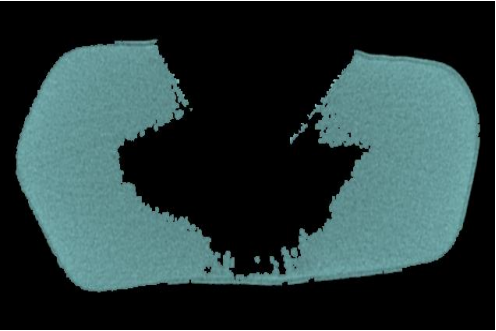

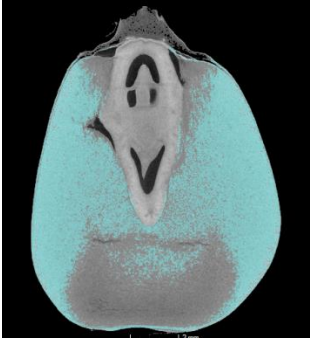
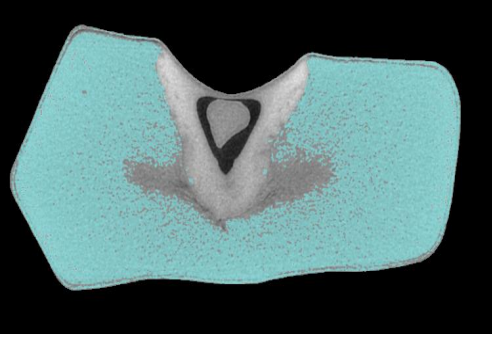
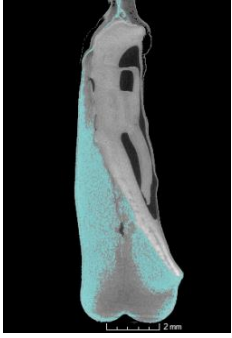

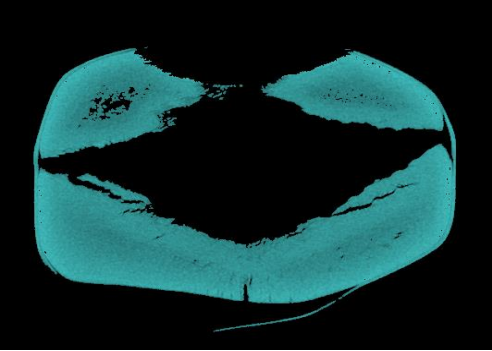



**Figure H.15.** 2D images of a raw maize kernel illustrating the (a) vitreous endosperm (blue) and germ and (b) floursy (yellow) and vitreous (blue) endosperm with the germ removed.



**Figure H.16.** 3D volumes of the floury (yellow) and vitreous (blue) endosperm in a raw maize kernel.



Sample	Frontal view	Transverse view	Sagittal view
Raw			
FCCT			
Raw			
Oven			

**Figure H.17.** 2D images illustrating the vitreous endosperm (blue) in the (a) frontal, (b) transverse and (c) sagittal view in raw and roasted maize kernels.

## Appendix I: Quantitative measurements

- i. Percentage object volume (POV): The proportion of volume-of-interest (VOI) in relation to the total sample (Laverse *et al.*, 2012). The VOI and total volumes were measured using the Volume analyser tool.

$$\text{POV (\%)} = \frac{\text{VOI (mm}^3\text{)}}{\text{Total volume (mm}^3\text{)}} \times 100\% \quad (1)$$

- ii. Porosity: A measure of the volume of air voids (all the black pixels) divided by the total volume of the analysed sample (voids and material) (Gondek *et al.*, 2013). Porosity analysis was performed by thresholding the voids and calculating the total air volume against the total sample volume (Du Plessis *et al.*, 2014). It should be noted that for this study the porosity were considered as the total air in the sample, thus the totality of the cavities and the pores.

$$\text{Porosity (\%)} = \frac{\text{Volume of air (mm}^3\text{)}}{\text{Total volume (mm}^3\text{)}} \times 100\% \quad (2)$$

For the maize cavities were manually selected using the Region growing tool and the volumes were obtained using the Volume analyser function (VGStudio Max 2.2). The Defect detection tool was used to perform a Custom defect mask to colour code the cavities according to size. The %pores is also known as the closed porosity, where a closed pore in 3D is described as a connected assemblage of black voxels that is fully surrounded by white voxels (Gondek *et al.*, 2013). Pore volumes containing more than eight adjacent black voxels were regarded as pores (Guelpa, 2015).

- iii. Expansion ratio (ER): The ratio of the volume after roasting to the volume before roasting (Nath & Chattopadhyay, 2008). The ER was determined in order to quantify the volume increase induced by roasting.

$$\text{ER} = \frac{\text{Volume after roasting (mm}^3\text{)}}{\text{Volume before roasting (mm}^3\text{)}} \quad (3)$$

- iv. Vitreous-to-floury endosperm ratio (V:F): The ratio of vitreous (hard) to floury (soft) endosperm (Guelpa, 2015).

$$\text{V:F} = \frac{\text{volume of vitreous endosperm (mm}^3\text{)}}{\text{volume of floury endosperm (mm}^3\text{)}} \quad (4)$$

- v. Relative density: Measured in terms of the mean grey value of the ROI in relation to the mean grey value of the reference standard. It was then multiplied with the known density of the reference standard (2.15 g/cm<sup>3</sup>). Within the kernel, areas with a different density will result in differences in the X-ray attenuation.

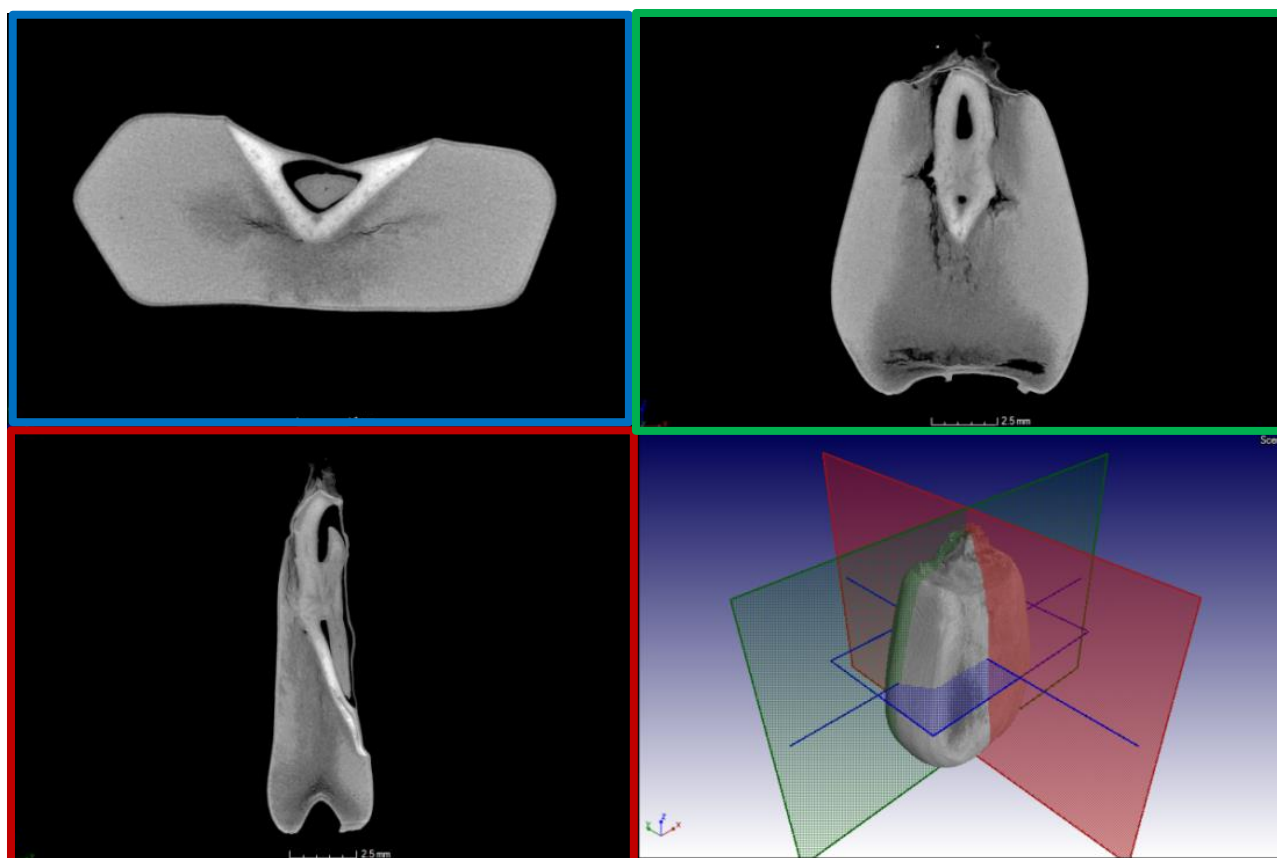
$$\text{Relative density (g/cm}^3\text{)} = \frac{\text{mean greyvalue of ROI}}{\text{mean greyvalue of reference standard}} \times 2.15 \text{ g/cm}^3 \quad (5)$$

The mean grey value of this disc was attained by selecting a representative volume from the disc. Each voxel has a certain grey value associated with it, which is dependent on the density and atomic number of the material. The mean grey value of the homogenous polymer disc is thus a measure of its density. Subsequently the grey values determined for the different ROIs were substituted into formulae (5) to obtain the relative densities.


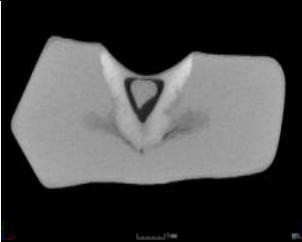


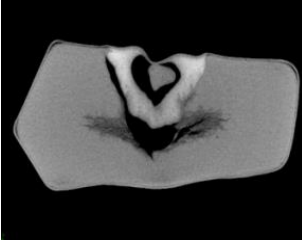





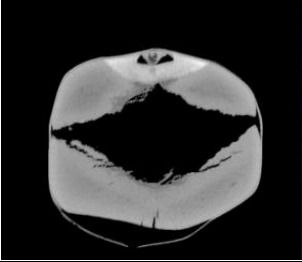



## Appendix J: Qualitative image analysis of maize kernels

Image contrast is based on differences in the absorption of X-rays by the different components of the sample (e.g. germ, endosperm and air voids) as these components have different X-ray absorption coefficients. This contrast is produced by variation in the material density and alteration in sample composition. It is based exclusively on the detection of variations in the amplitude of the X-rays transmitted through the sample itself. The brightness of a voxel is thus proportional to the density: the higher the density, the brighter the image. Figure J.1 presents the different views of a raw maize kernel in VGStudio Max 2.2. One window is a 3D volume, whereas the other three windows are 2D sectional views allowing the visualisation of different orientations (frontal, horizontal and sagittal). In comparison with other microscopic imaging techniques, the virtual inspection of the  $\mu$ CT serial section is easier as semi-automated data analysis is available.



**Figure J.1.** Illustration of the different views of a raw maize kernel, i.e. horizontal/transverse (blue), frontal/coronal (green), sagittal (red) and a 3D rendered image (bottom right).

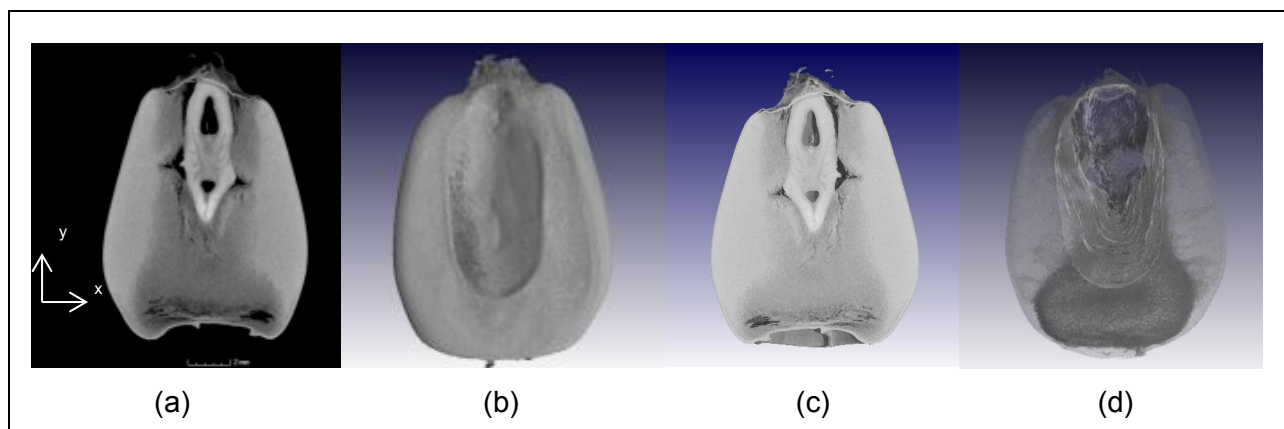
Sample	Frontal view	Horisontal view	Sagittal view
Raw			
FCCT			
Raw			
Oven			

**Figure J.2.** Grey scale tomographic images of the different views (frontal, horisontal and sagittal) of the whole maize kernels, before and after FCCT and oven roasting.

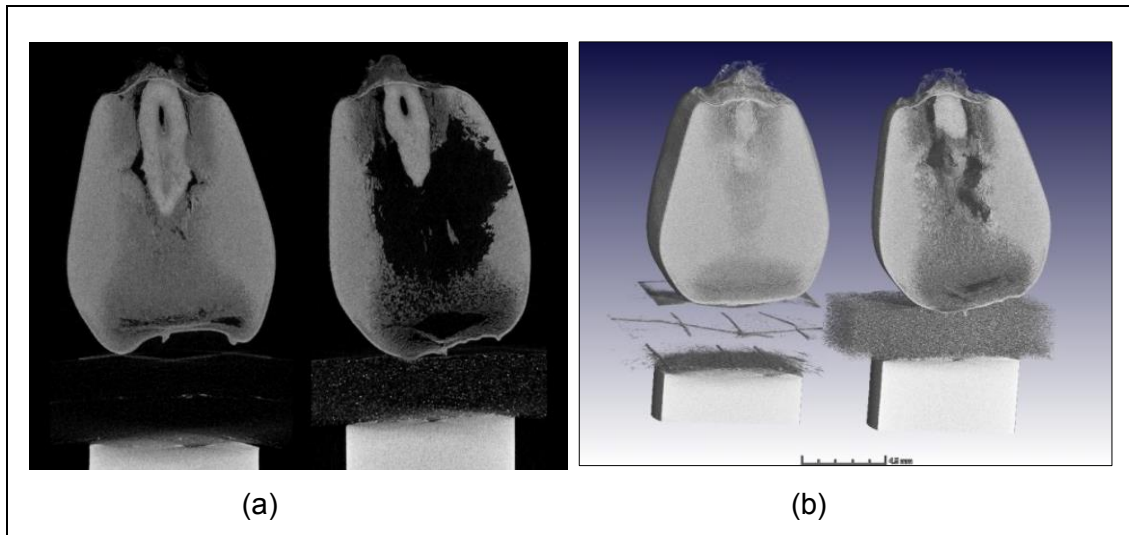
## Appendix K: 2D and 3D interpretation and visualisation of X-ray $\mu$ CT images

Volume data consists of a continuous set of voxels arranged in a 3D grid structure. Voxels are volumetric pixels and thus the 3D equivalent of pixels. The x and y axis represents the horizontal and vertical pixel coordinates (2D), whereas the z axis represents the 3D coordinate. Each voxel represents a specific area in the object and the grey value provides information on the material properties in this area. A 3D map of X-ray absorption can be obtained from 2D projection images. Different features can be identified from these images due to the absorption differences of different materials. Figure K.1 (a) illustrates this approach with a 2D tomographic slice image. The slice represents a series of slices of a complete 3D volume. Figure K.1 (b) illustrates the 3D rendered image of the same kernel, (c) visualises a 3D clipped image, while (d) represents a semi-transparent 3D image.

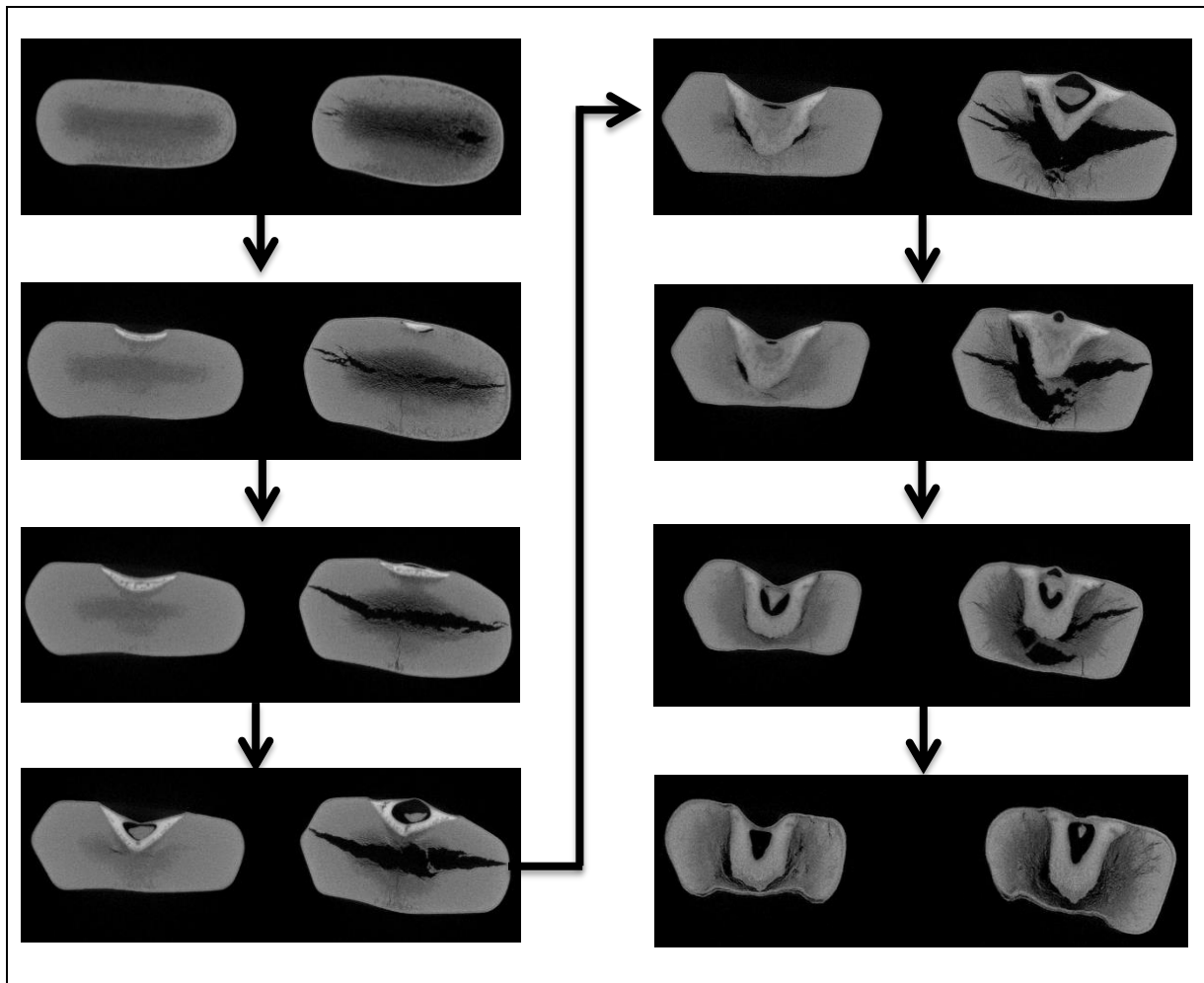
Two-dimensional data is not always fully representative of the true 3D structures, e.g. where the shapes and sizes of pores in a sample are dependent on the location of the 2D section. Images will demonstrate a better change in the size and geometry of the pores or cavities when viewed in 3D. The internal structure of different materials can be studied and the distribution of regions varying in density can be visualised through virtual slicing of a 3D volume rendering (Fig. K.2). This is however only possible if the X-ray attenuation of the ROIs is significantly different to provide adequate contrast. Image analyses is not limited to one individual slice image at a time, but covers the volume in all three dimensions. Figures K.3 and K.4 presents a sequence of snapshots of the internal structure (as seen from the top at various depths) of raw (left) and roasted (right) maize kernels.



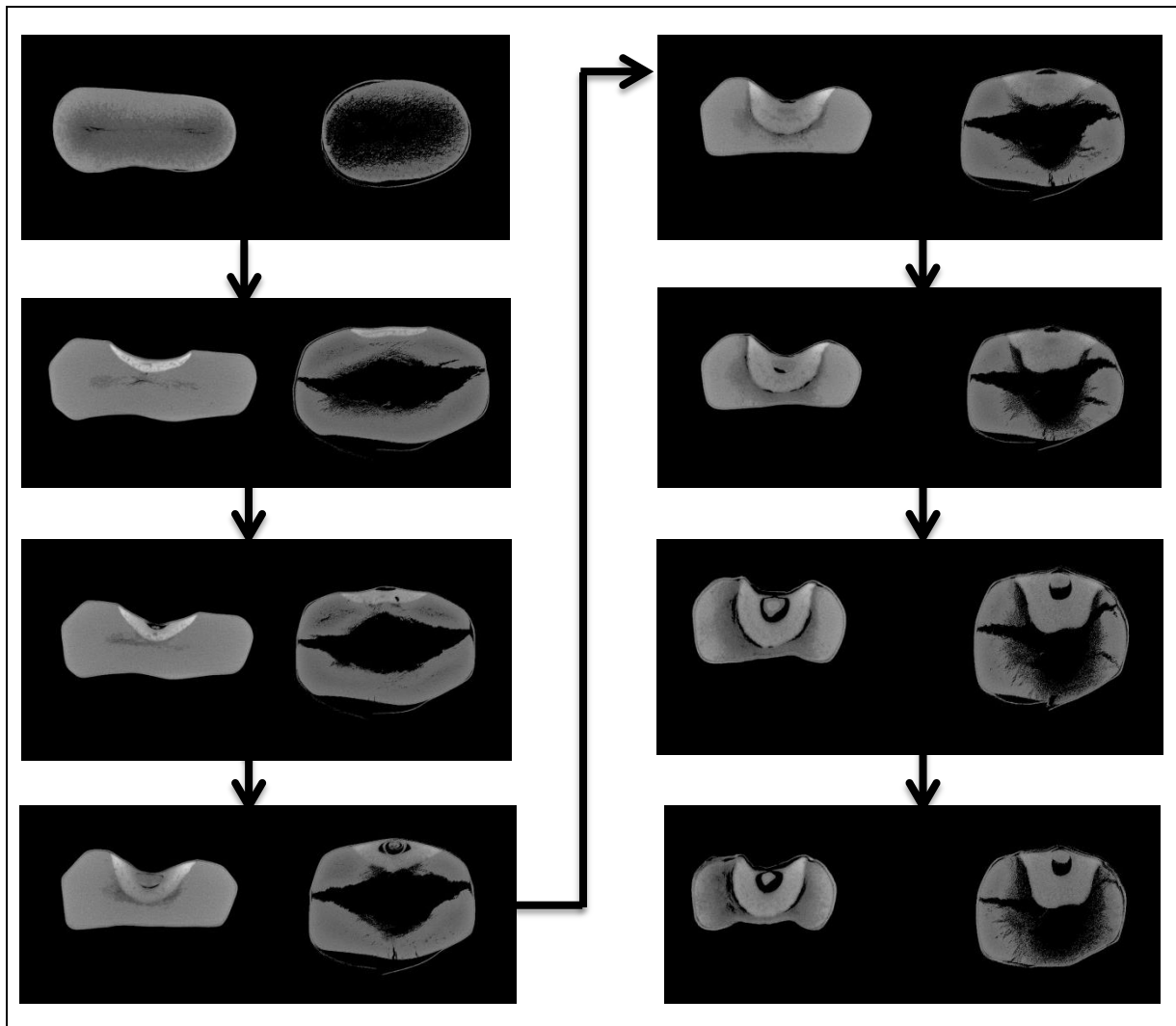
**Figure K.1.** Illustration of a (a) 2D slice image, (b) 3D volume rendering, (c) clipped (sectioned) image and (d) semi-transparent 3D volume of a raw maize kernel.



**Figure K.2.** Illustration of (a) 2D projection images and (b) 3D reconstructed models of maize kernel before (left) and after FCCT roasting (right).

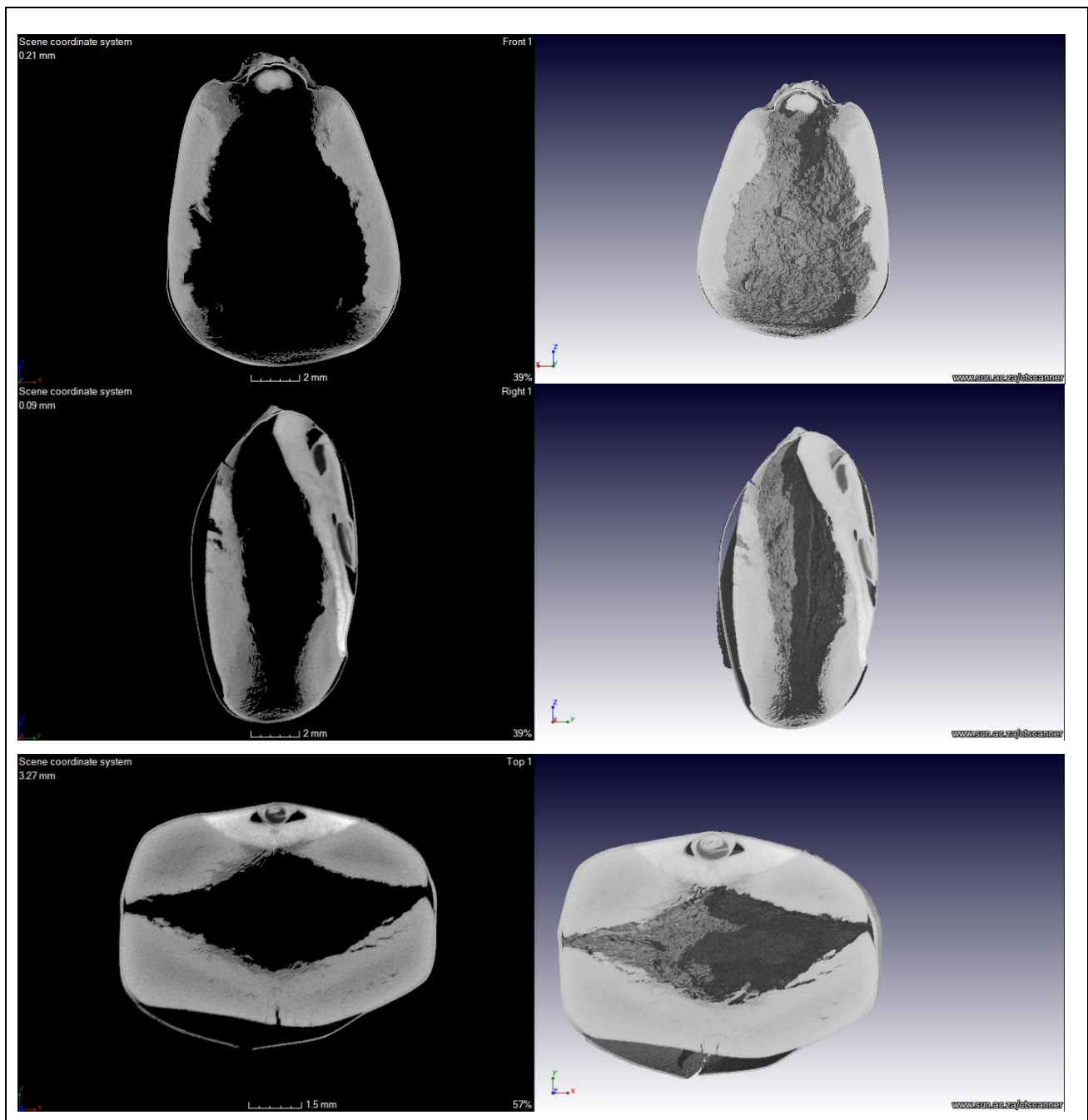


**Figure K.3.** Diagram of the two-dimensional slice-by-slice (traversing the X-Z axis) images of a raw (left) and FCCT-roasted (right) maize kernel.



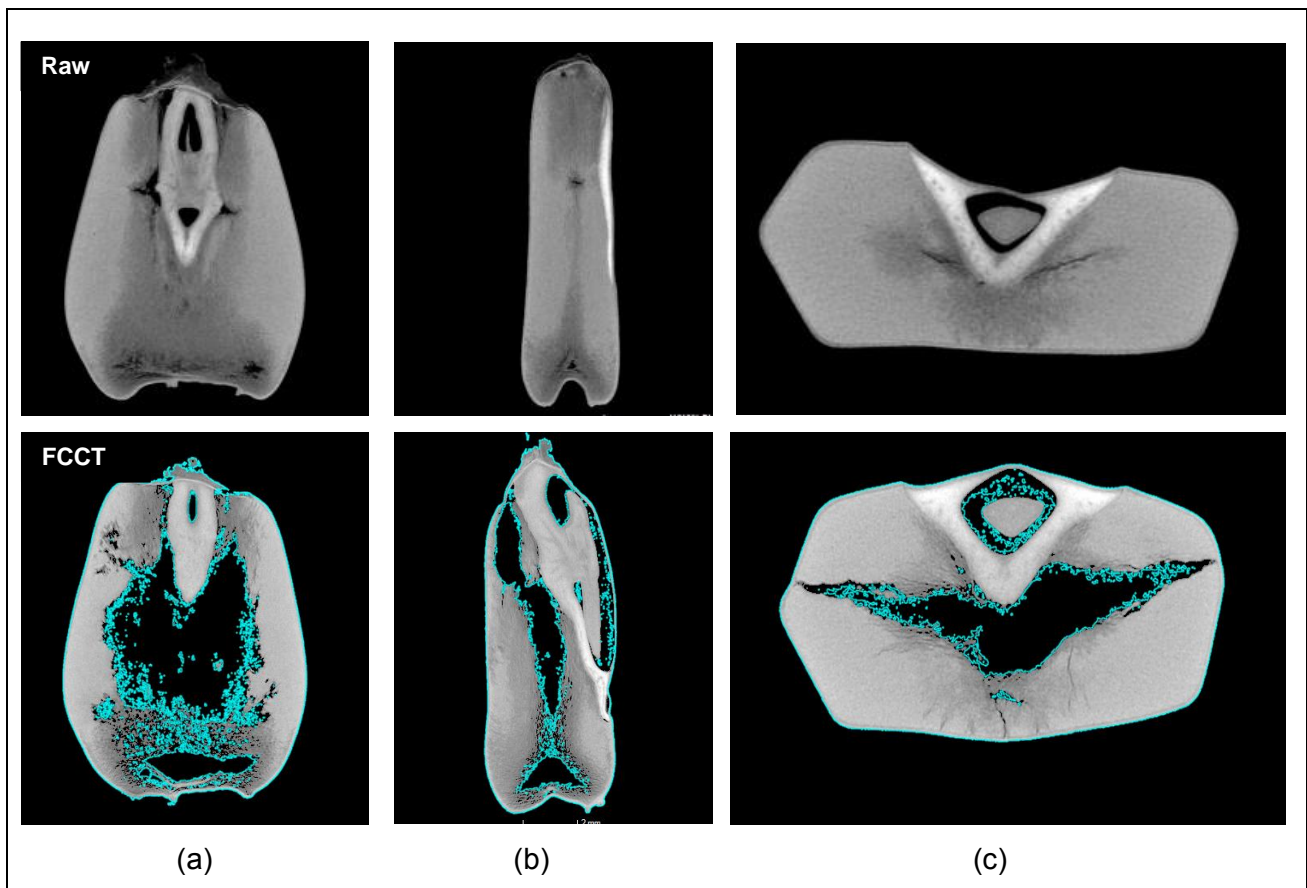
**Figure K.4.** Diagram of the two-dimensional slice-by-slice (traversing the X–Z axis) images of a raw (left) and oven-roasted (right) maize kernel.

In Figure K.5 2D slice images and corresponding 3D models are presented and in Figure K.6 2D views of a raw and roasted kernel are shown to visualise the spatial distribution of voids.



**Figure K.5.** Illustration of the 2D slice images and corresponding 3D reconstructed models through the different planes (frontal, sagittal and horizontal) of an oven-roasted maize kernel.

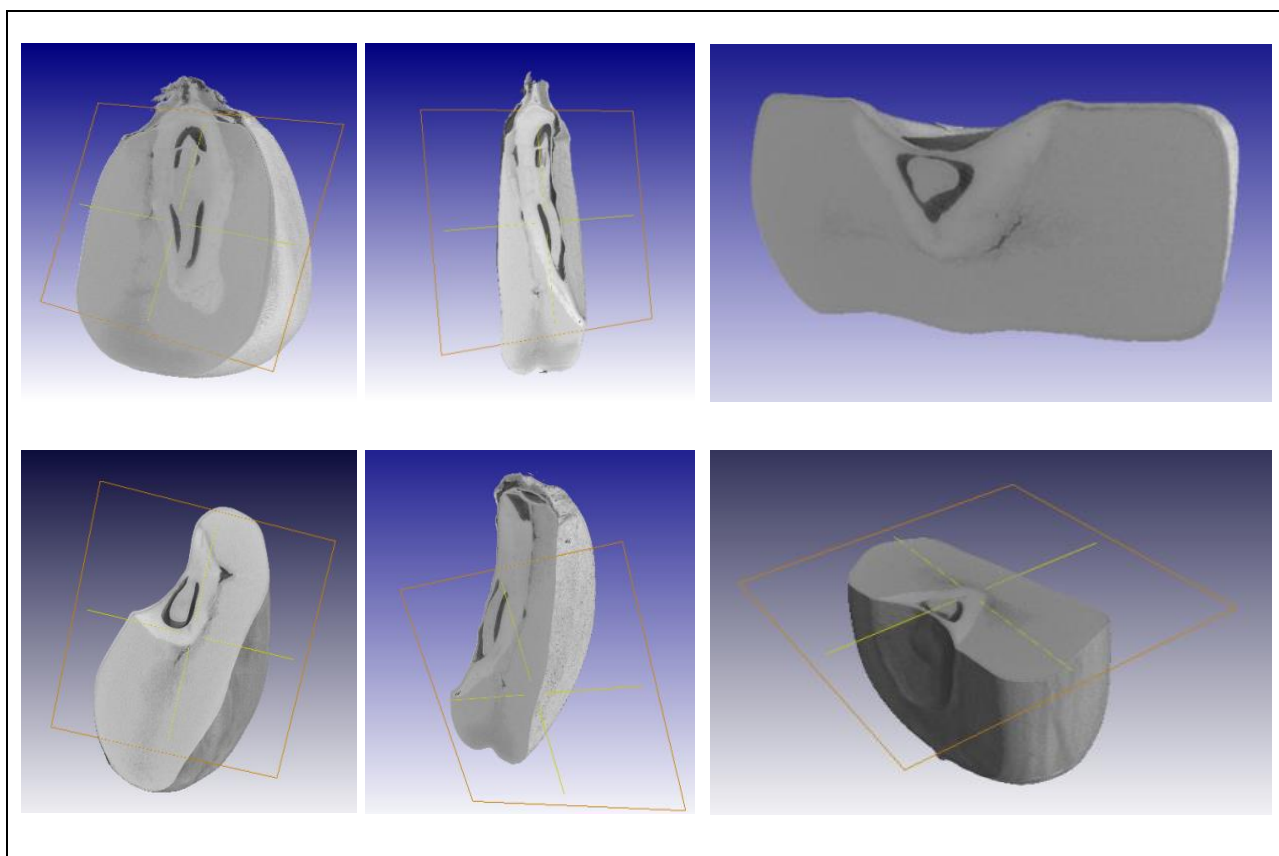




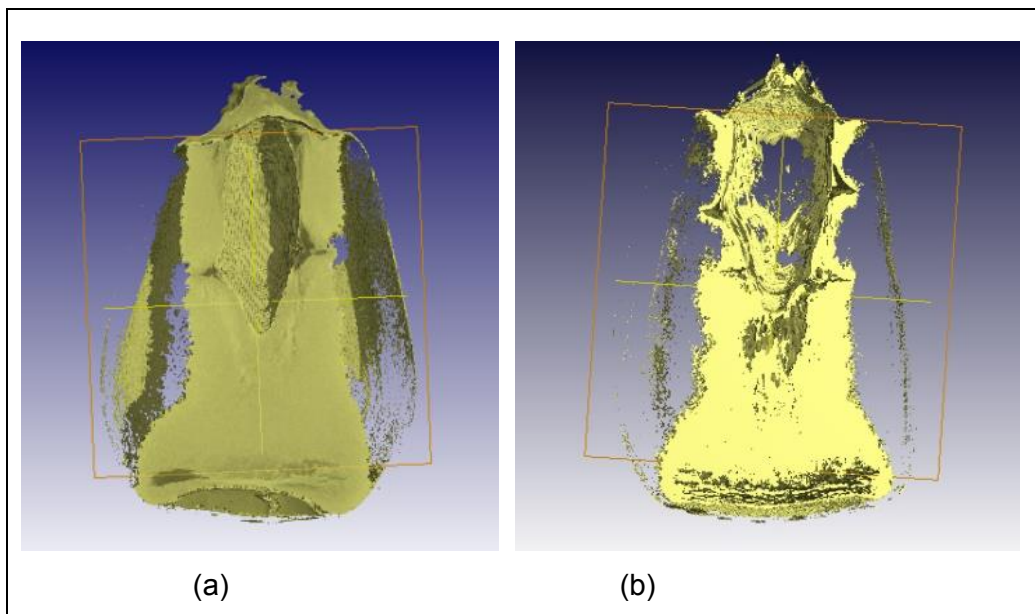
**Figure K.6.** 2D slice images of a raw and FCCT-roasted kernel illustrating the (a) frontal, (b) sagittal and (c) transverse view with the voids (blue) selected as ROI.

## Appendix L: Clipping

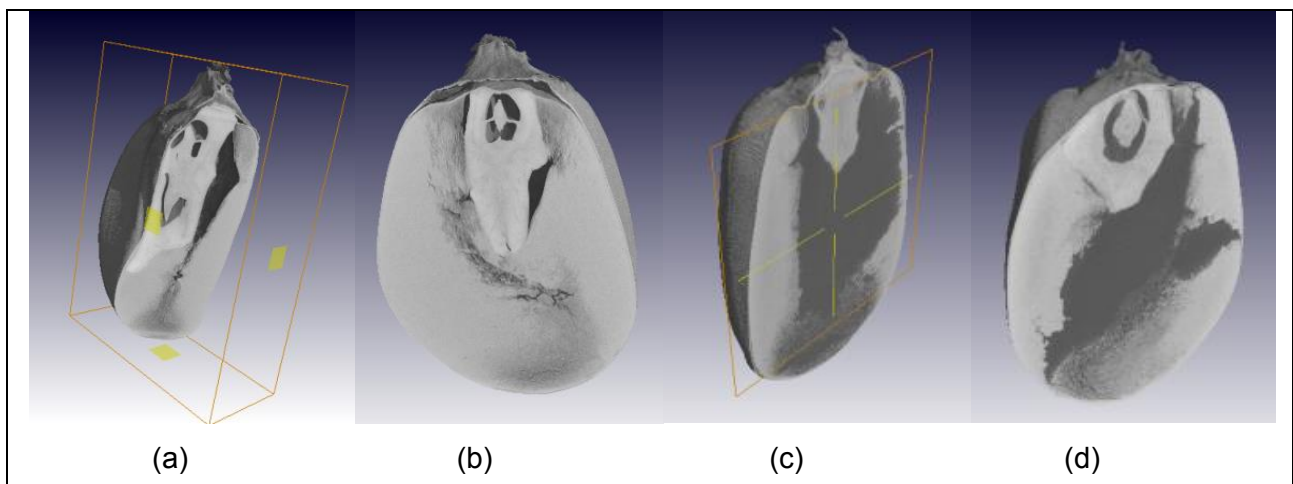
The clipping tool denotes the ability to virtually cut into a sample volume in the 3D window and also to make 2D sections in any orientation. The clipped areas can be made completely transparent to hide them or semi-transparent to illustrate certain features. The samples can also be freely positioned and rotated within the 2D and 3D display areas. The clipping tool enables the sample to be sliced along any arbitrary axis (Figs. L.1-L.4). Analysis software allows one to easily scroll forth and back through a sample. Making use of the 3D cursor tool a certain feature in one window can be marked and then the actual position of this feature will show in all the 2D windows. This tool is helpful, e.g. visualising the orientation of cracks and fractures in maize kernels.



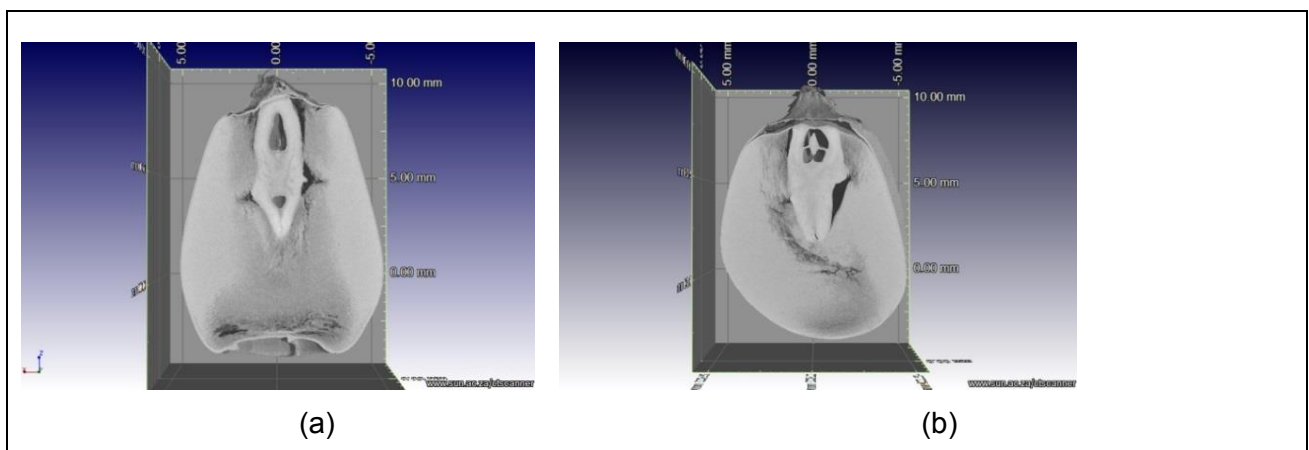
**Figure L.1.** Illustration of the different clipping views of a raw maize kernel, cut to reveal the internal structure.



**Figure L.2.** Illustration of a clipped view of (a) a raw and (b) FCCT-roasted floury endosperm region.



**Figure L.3.** Representation of different clipping views of a (a and b) FCCT-roasted and (c and d) oven-roasted maize kernel.



**Figure L.4.** Illustration of the dimensional analysis of a clipped (a) raw and (b) FCCT-roasted maize kernel.

## Appendix M: Stress cracks

Kim *et al.* (2002) stated that if grains are exposed to high temperature drying, stress cracking levels might increase. The formation of stress cracks is associated with the rapid drying of maize at high temperatures (Gunasekaran *et al.*, 1985). Thus this phenomenon could be assumed for the roasting process. The internal type of damage, referred to as stress cracks, is cracks or fissures that forms on the inside of grains due to excessive compressive or tensile stresses that occur during drying, or in this case roasting (Kim *et al.*, 2002). The extent of the stress cracks are also an indicator of heat damage such as protein denaturation and starch gelatinisation. Even though stress cracking itself does not cause direct physical damage, high stress crack levels leads to higher breakage susceptibility. This will also lead to a lower yield during dry milling and reduce starch recovery during wet milling.

The general method for detecting internal cracks or cavities in maize kernels is visual inspection, by holding the germ side towards a light source (Chowdhury & Buchele, 1976). Internal cracks caused by high temperature during the development of a maize kernel were characterised using visual, X-ray and scanning electron microscopical analysis (Moreira de Carvalho *et al.*, 1999). Analysis with the X-ray machine enabled the visualisation of stress cracks that were not visible with the human eye and, thus, gave a better estimate of the percentage of cracks.

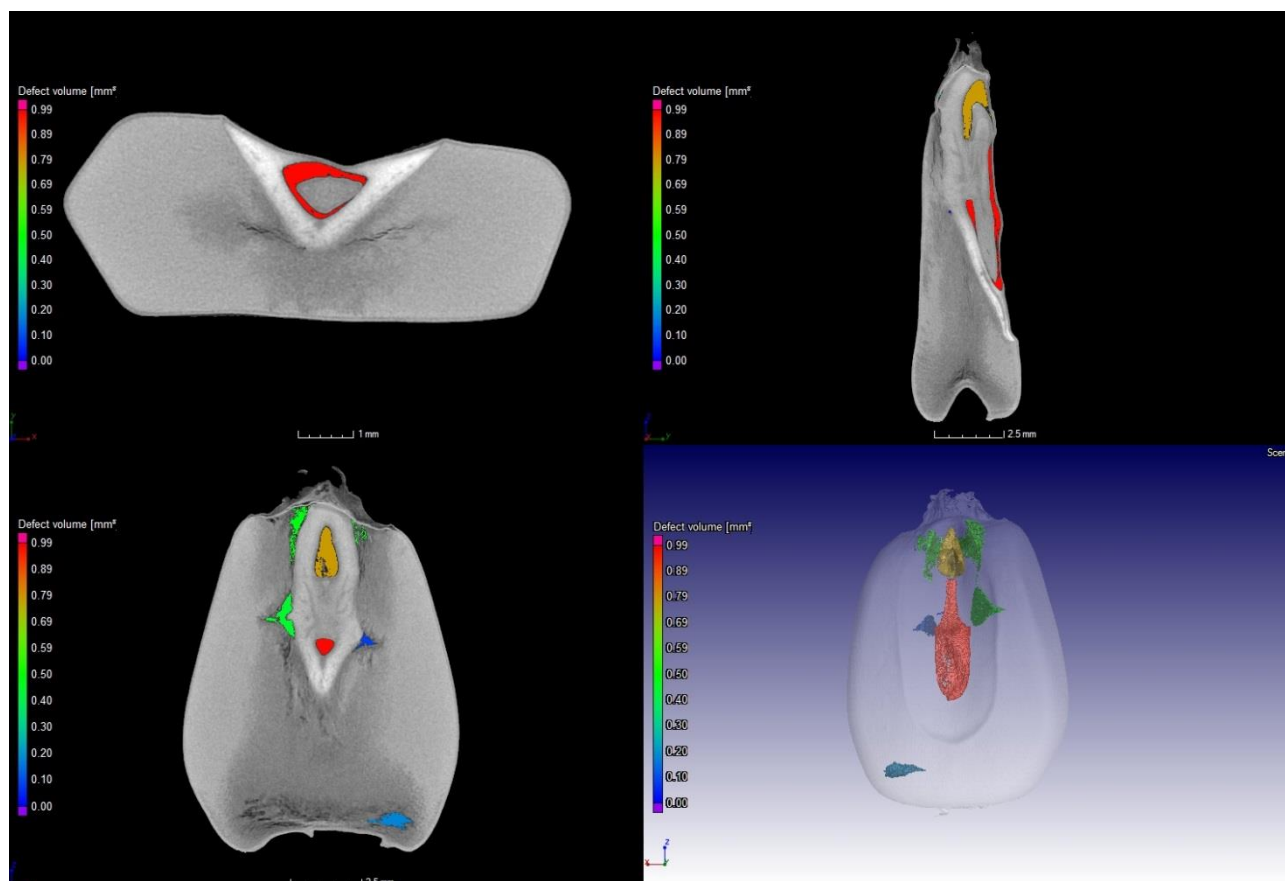
According to Moreira de Carvalho *et al.* (1999) stress cracks differ from external cracks caused by mechanical impact. Defects like pericarp cracks, caused by mechanical stress are easily identified, in contrast to internal cracks caused by thermal stress which are not readily identifiable. It is supposed that if stress cracks are located inside or perpendicular to the embryo axis, it may have an influence on the kernel quality.

In a study by Song & Litchfield (1994) drying induced stress cracks in maize kernels were non-destructively measured during drying and cooling procedures using magnetic resonance imaging (MRI). They observed stress cracks in the vitreous endosperm in areas with a larger moisture gradient and lower moisture content (Song & Litchfield, 1994). Song *et al.* (1992) used 3D microscopic MRI to non-destructively measure the moisture transfer in individual maize kernels during two drying conditions. This study confirmed that the floury endosperm loses moisture faster than the vitreous endosperm.

Gunasekaran *et al.* (1987) developed an image processing algorithm for detecting stress cracks in maize kernels using a commercial vision system and found that stress cracks propagates from the centre of the kernel and does not extend into the pericarp. The same results were found by Balastreire *et al.* (1982), by means of optical microscopy. If cracks are internal and invisible to the human eye, a more accurate and automated method, such as X-ray imaging is desired. Girardin *et al.* (1993) concluded that X-ray radiography was the best method to non-destructively characterise maize kernels characteristics.

## Appendix N: Cavity analysis

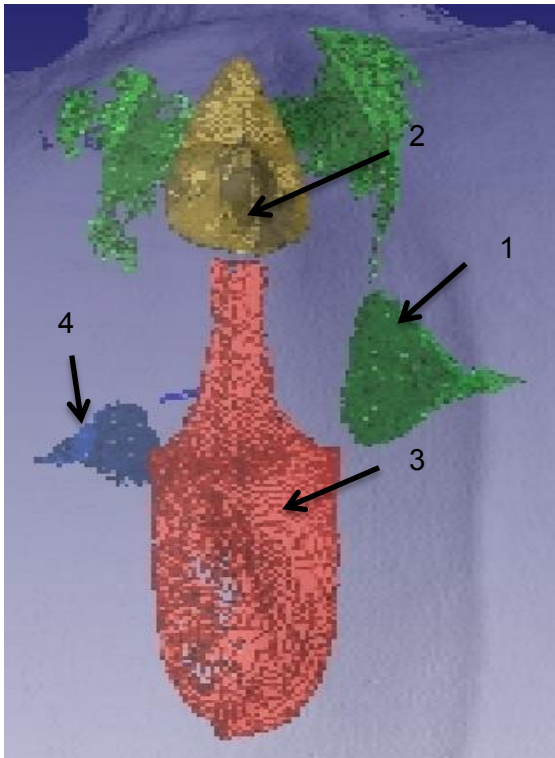
Along with thermal degradation of the structure and organic compounds, non-enzymatic reactions also occur. The high quality of the  $\mu$ CT images reveals details of the microstructure such as internal void shape, size and spatial distribution. Figures N.1 to N.6 reveals the X-ray  $\mu$ CT images obtained at a resolution of 12  $\mu$ m to illustrate the cavities in maize kernels before and after roasting. It should be noted that the colour bar indicates the size ( $\text{mm}^3$ ) of the cavities, where large cavities are magenta and smaller ones purple.



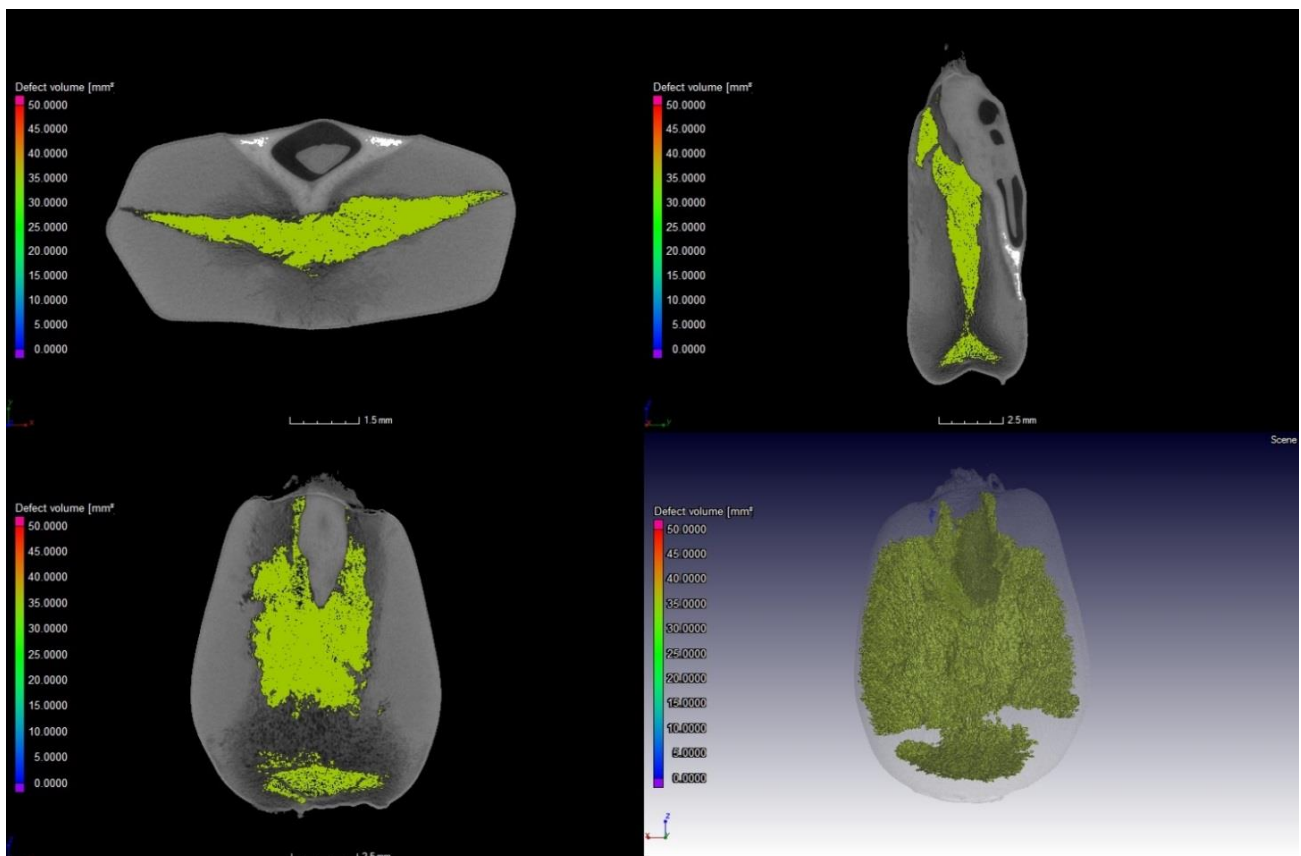
**Figure N.1.** Image of the volume size distribution of the cavities in a raw sample.

Pores and cavities in porous materials can have different structures: (i) interconnected segments or (ii) isolated or non-interconnected segments (Ali *et al.*, 1996). Interconnected spaces are accessible on both ends, while isolated spaces are inaccessible closed pores within the solid material. Thus, interconnected voids are viewed as open apertures, while isolated spaces are closed. The cavities is colour coded according to size, where cavity 1 (green) is  $0.55 \text{ mm}^3$ , cavity 2 (yellow) is  $0.72 \text{ mm}^3$ , cavity 3 (red) is  $0.99 \text{ mm}^3$  and cavity 4 (blue) is  $0.15 \text{ mm}^3$  (Fig. N.2.).



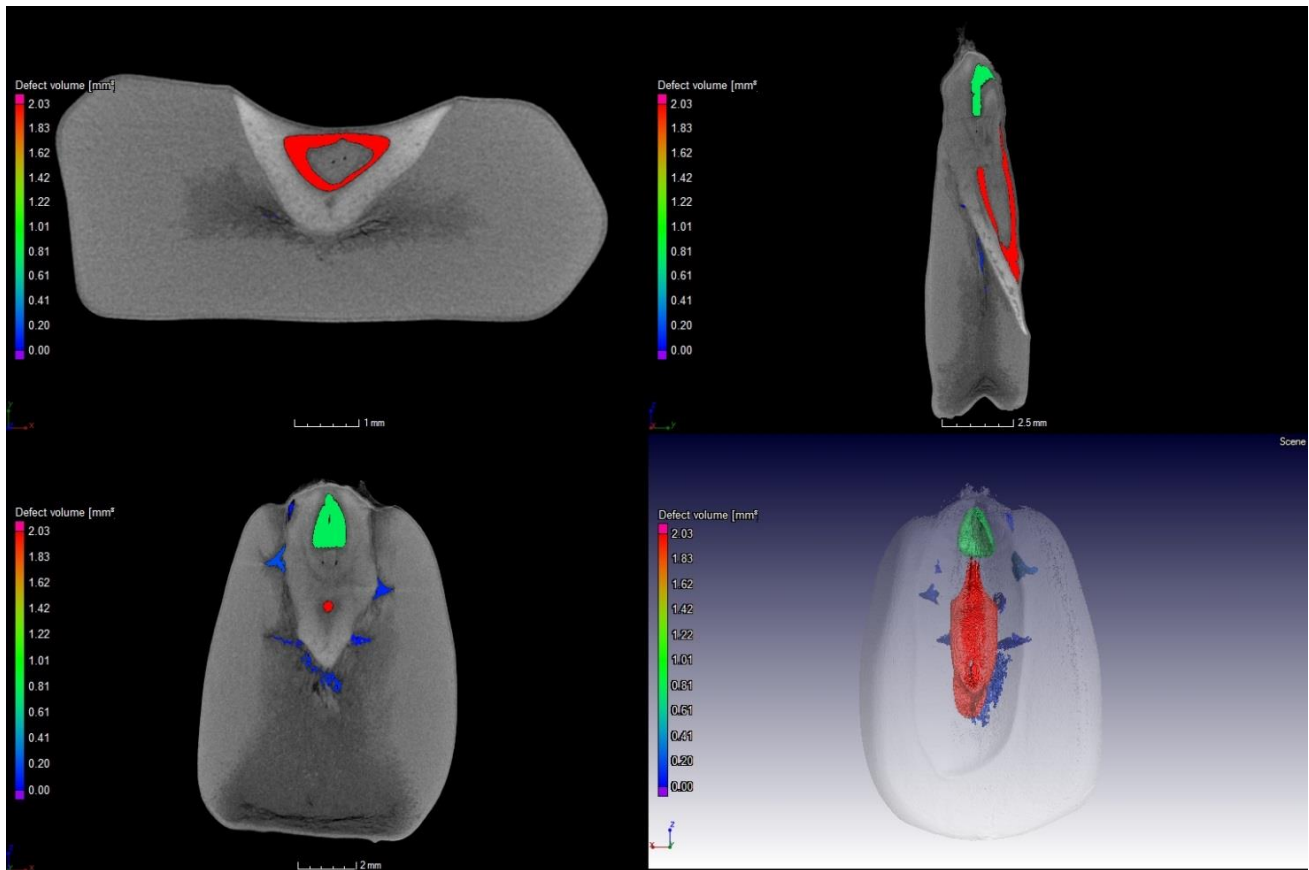


**Figure N.2.** Magnified image of the volume size distribution of the cavities in a raw maize kernel.

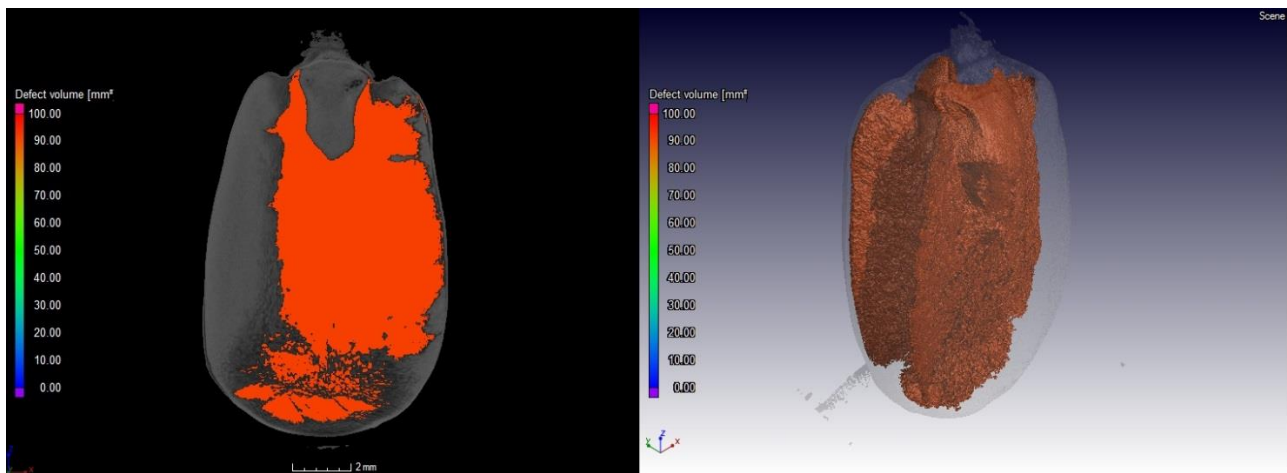


**Figure N.3.** Image of the volume size distribution of the cavities in a FCCT-roasted kernel.

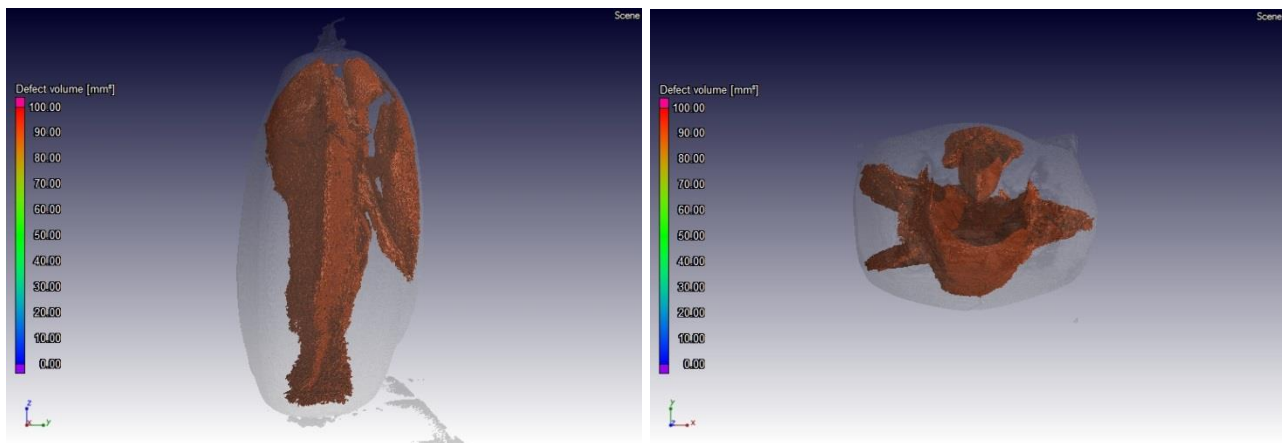




**Figure N.4.** Image of the volume size distribution of the cavities in a raw kernel.



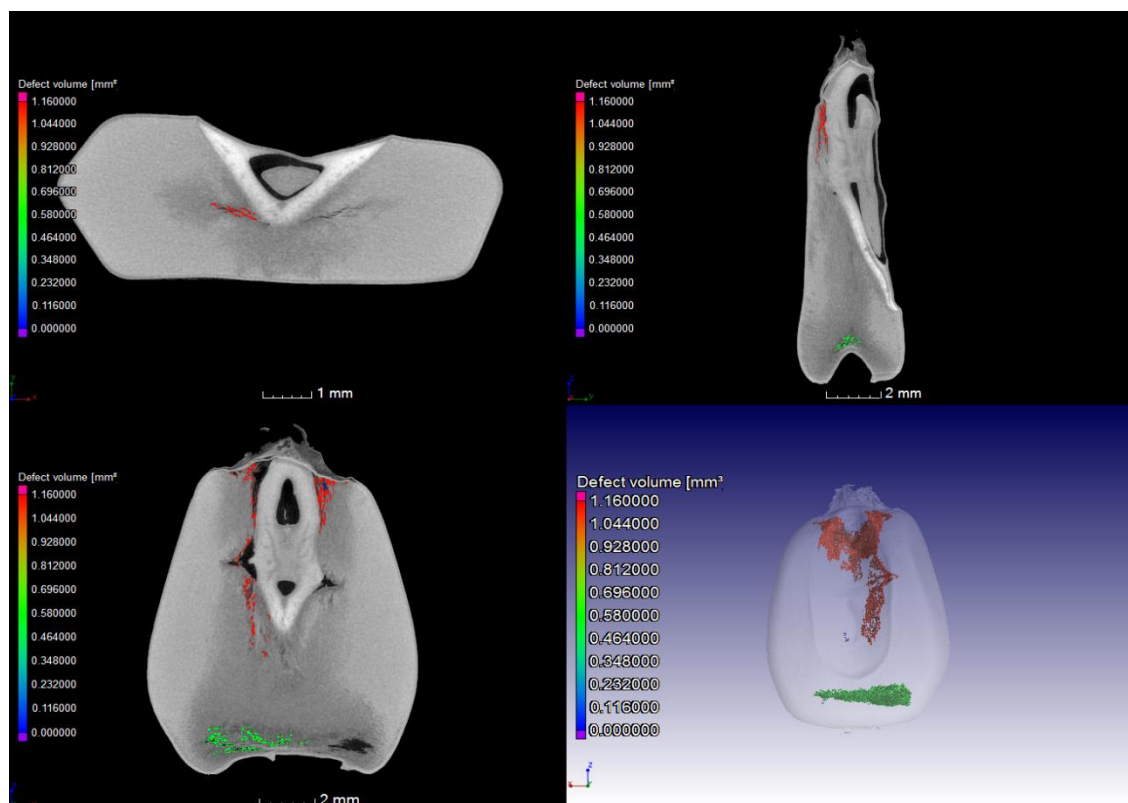
**Figure N.5.** Image of the volume size distribution of the cavities in an oven-roasted kernel.



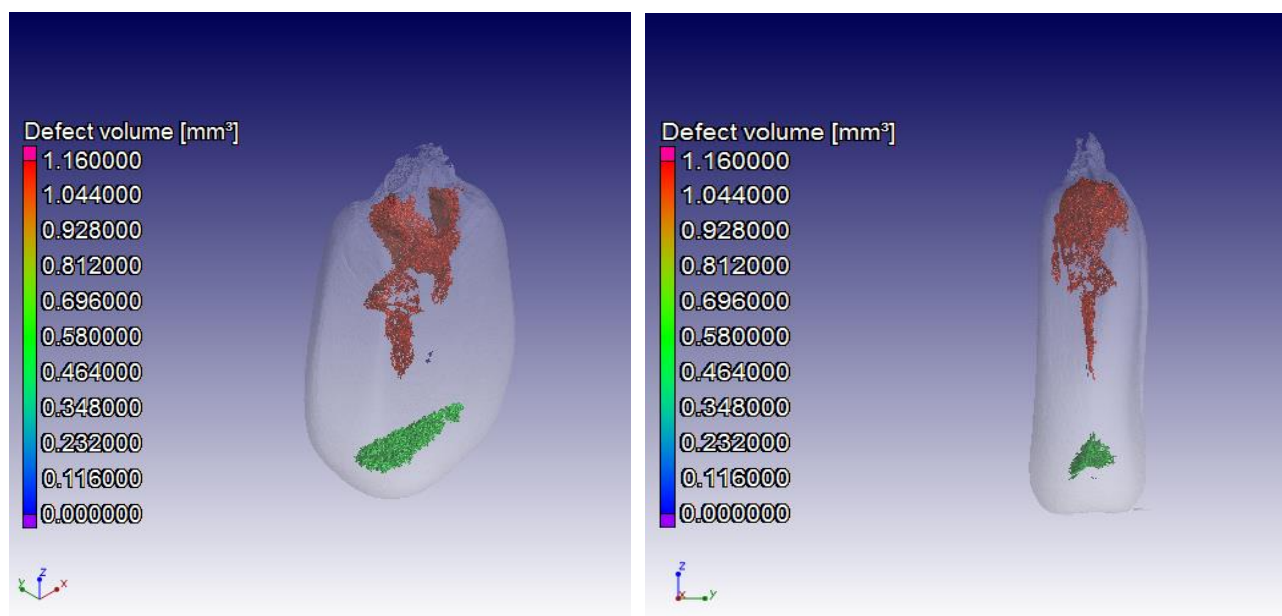
**Figure N.6.** 3D visualisation of the volume size distribution of the cavities in an oven-roasted kernel from the side (left) and form the top (right) view.

## Appendix O: Pore network analysis

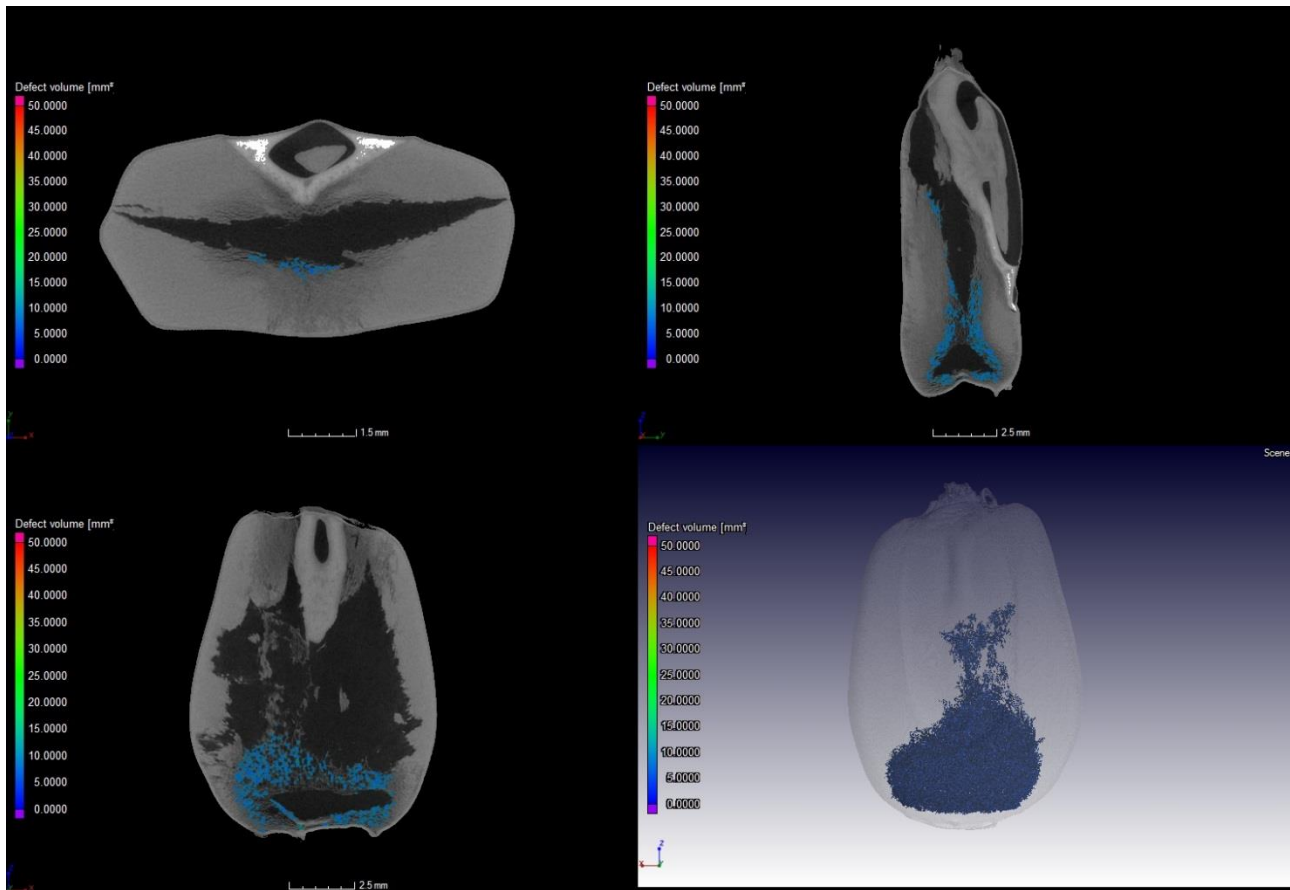
The results of the Defect detection function also allowed pores to be visualised in a clear manner (Fig. O.1-O.5). Comparing the raw and roasted samples separate pore networks are present in the raw samples, illustrated by different colours, whereas in the roasted samples the pores is interconnected forming a pore network illustrated by only one colour.



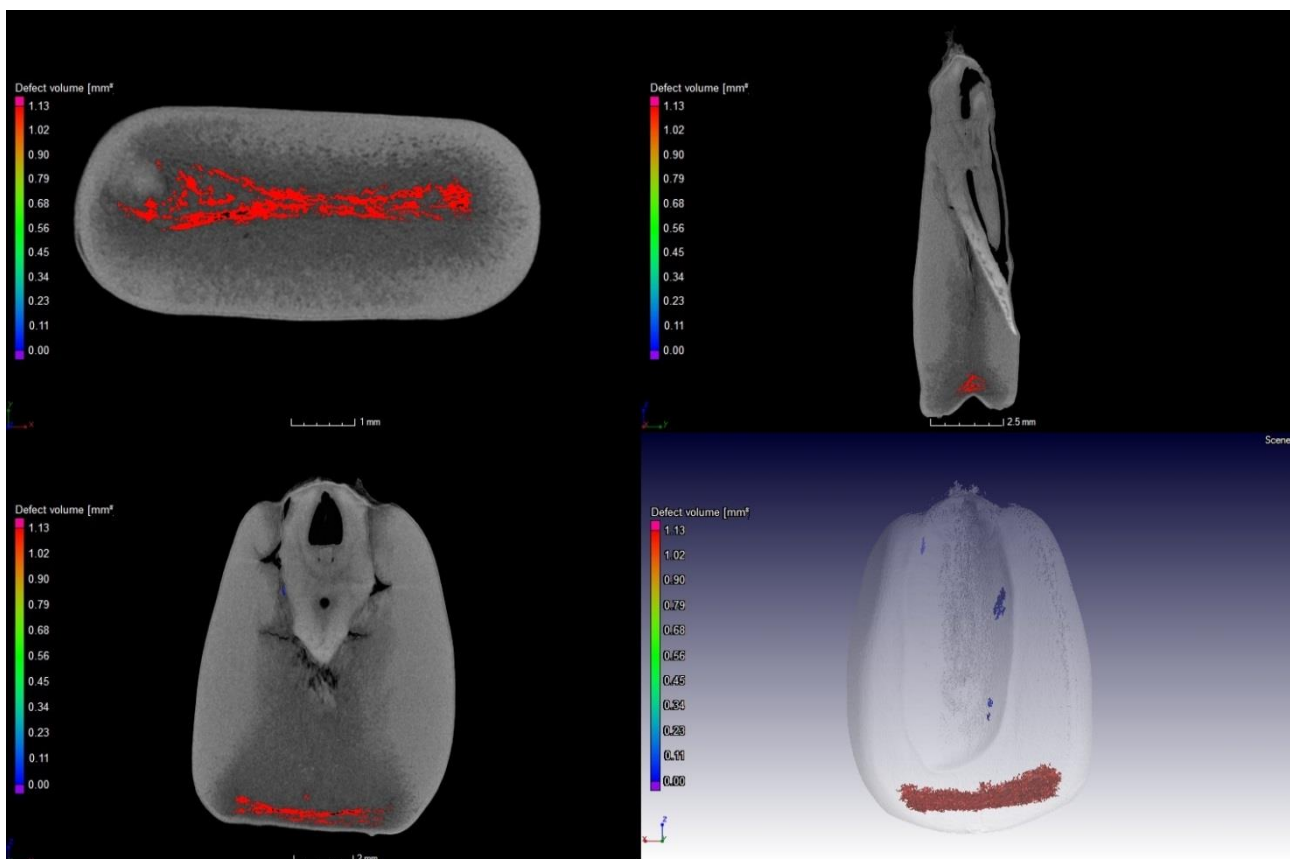
**Figure O.1.** Image of the pore volume size distribution of the pore network in raw sample.



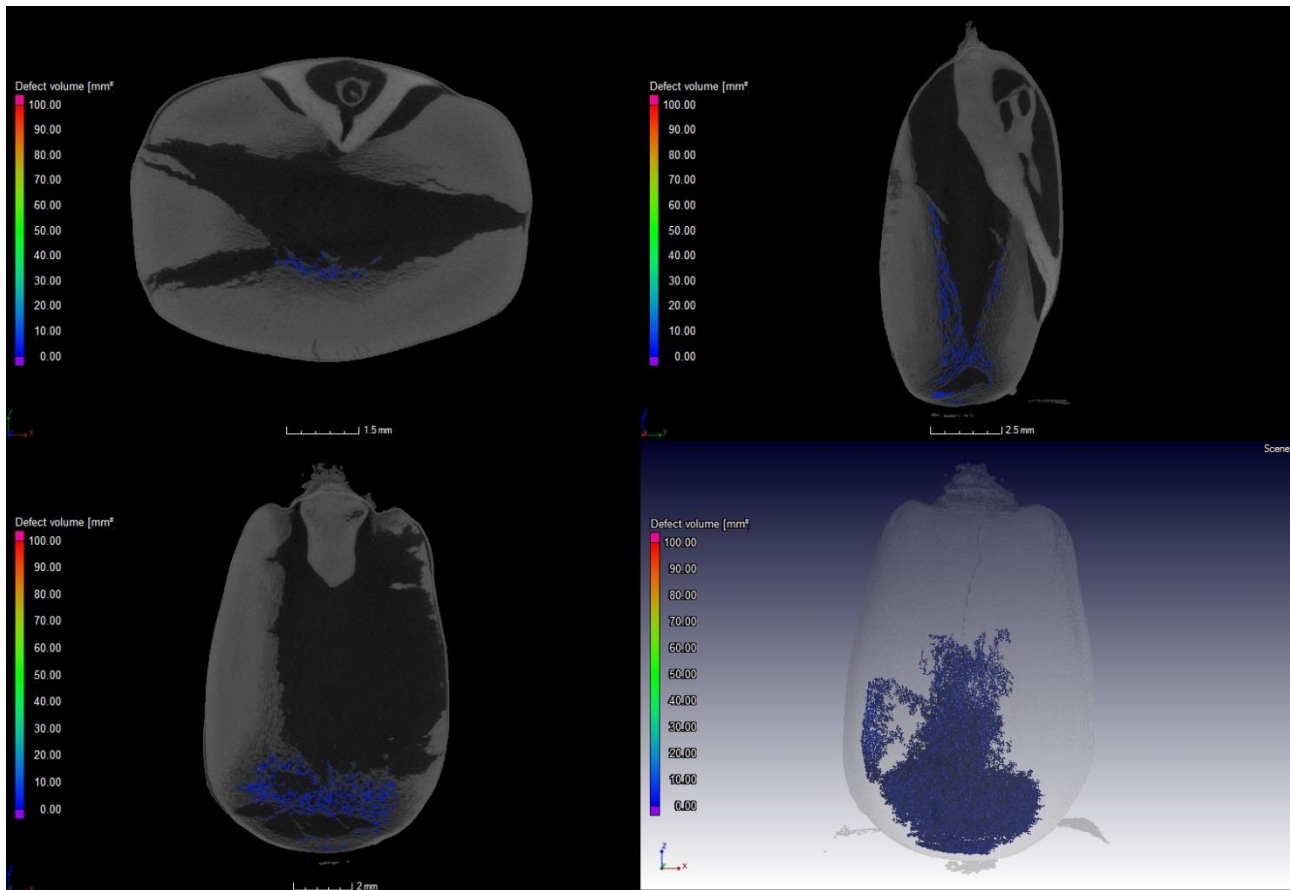
**Figure O.2.** 3D visualisation of the volume size distribution of the pore networks in a raw sample from the back (left) and from the side (right) view.



**Figure O.3.** Image of the volume size distribution of the pores in a FCCT-roasted kernel.



**Figure O.4.** Image of the volume size distribution of the pores in a raw kernel.

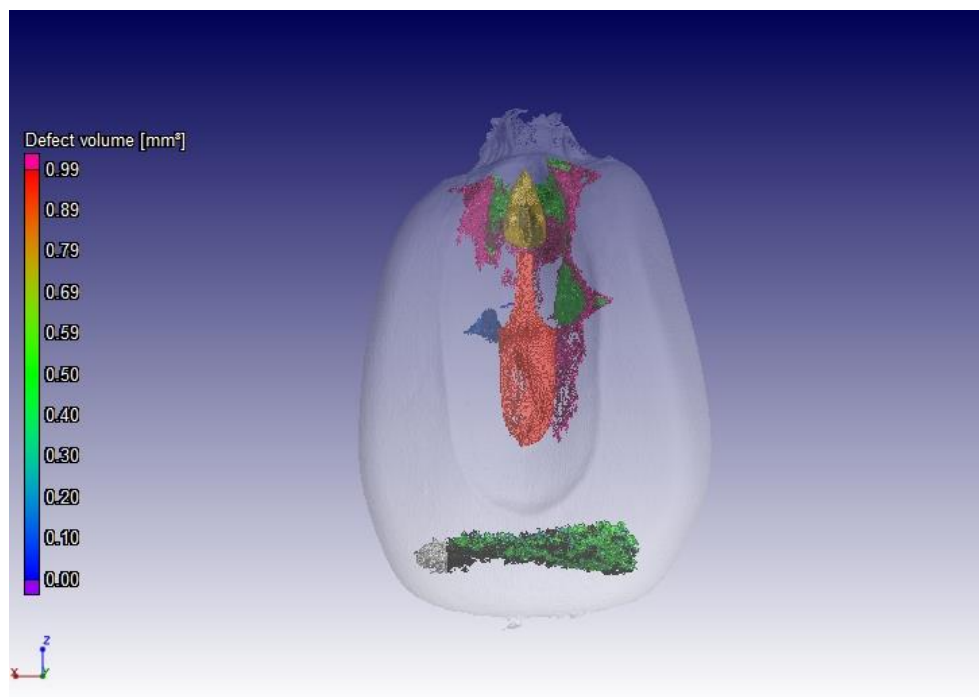


**Figure O.5.** Image of the volume size distribution of the pores in an oven-roasted kernel.

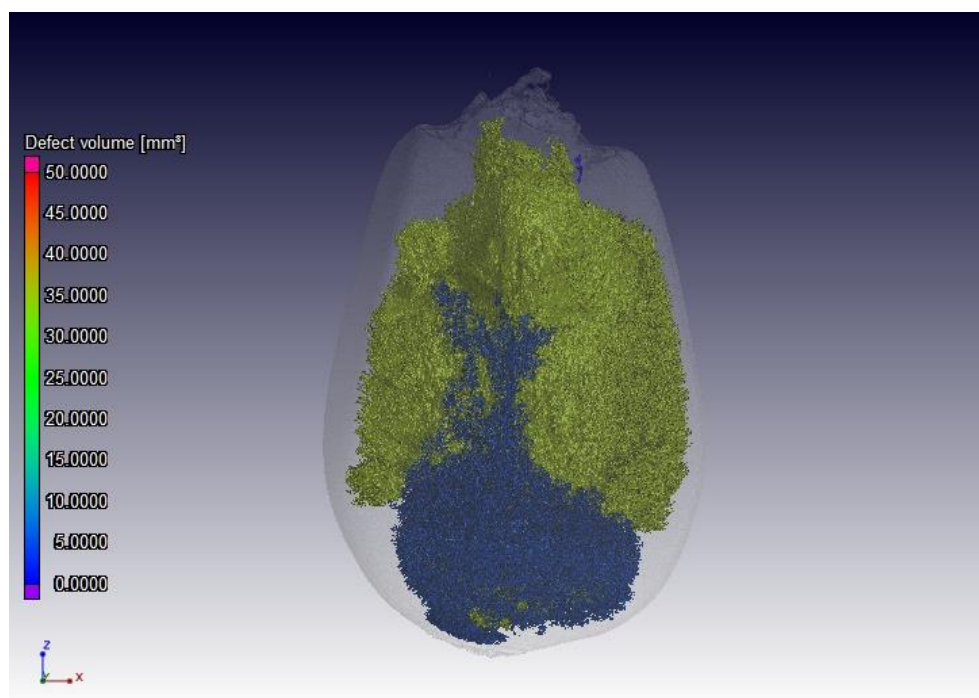


## Appendix P: Porosity (pores and cavities) analysis in three dimensions

Figures P.1 to P.5 showcases porosity (pores and cavities) distribution in 3D volume renderings of the samples reconstructed from the CT slices. The cavities and pores are coloured according to the scale bar to indicate the size and illustrated in one image. The sample is made semi-transparent in order to observe the cavities and pores more clearly.

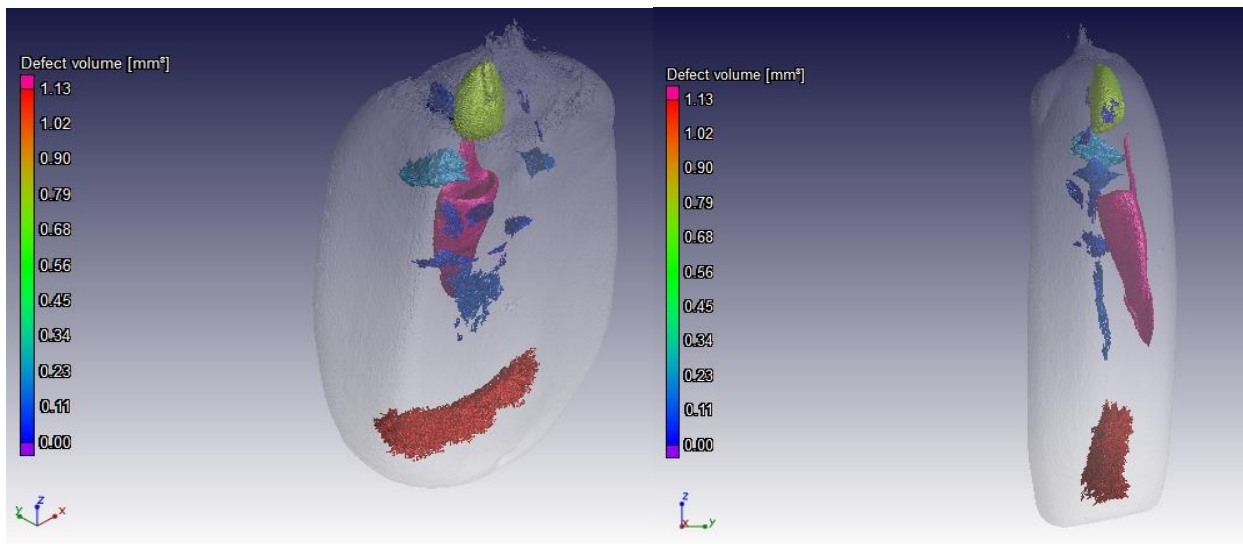


**Figure P.1.** 3D volume of a raw sample illustrating the presence of both the cavities and pores.

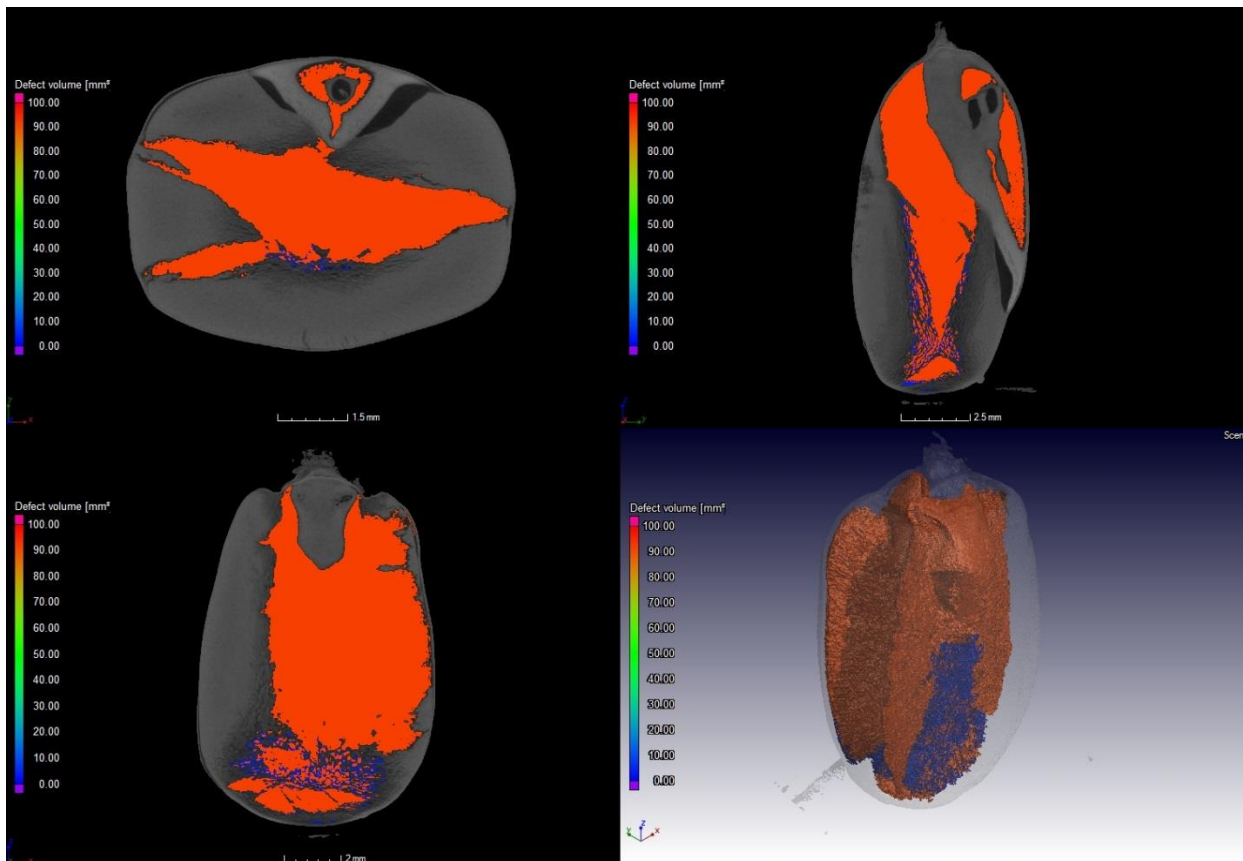


**Figure P.2.** 3D volume of a FCCT-roasted kernel illustrating the cavities (yellow) and pores (blue).

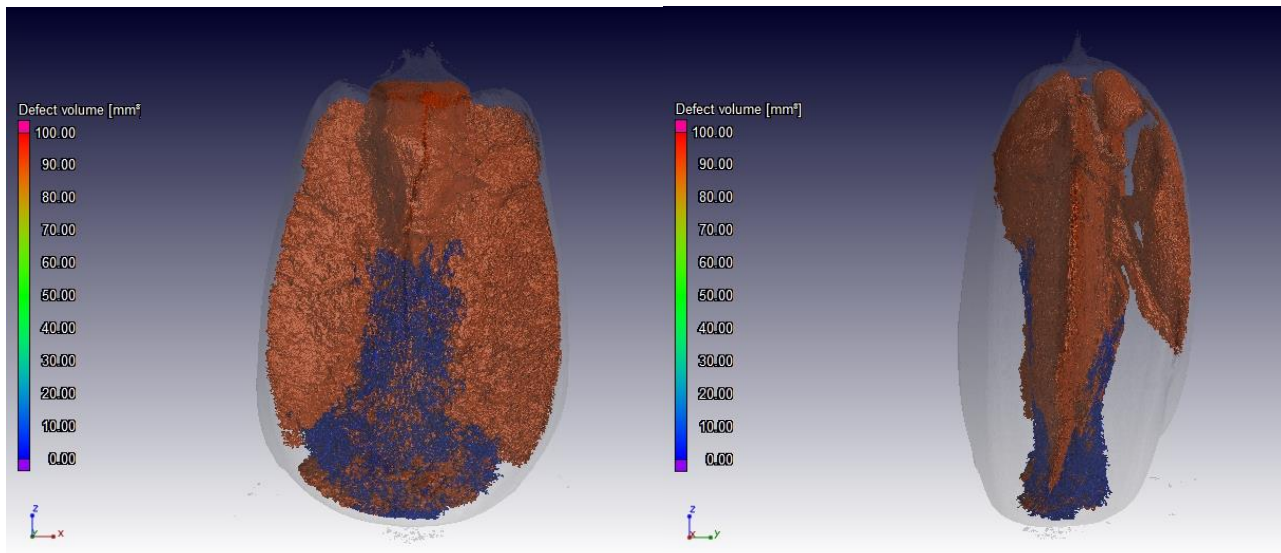




**Figure P.3.** 3D visualisation of the volume size distribution of the cavity and pore networks in a raw sample from the back (left) and from the side (right) view.



**Figure P.4.** Illustration of the presence of both the cavities (dark red) and pores (blue) in a oven-roasted kernel.



**Figure P.5.** 3D visualisation of the volume size distribution of the cavity (dark red) and pore (blue) networks in an oven-roasted sample from the back (left) and from the side (right) view.

## References

- Ali, Y., Hanna, M.A. & Chinnaswamy, R. (1996). Expansion characteristics of extruded corn grits. *LWT-Food Science and Technology*, **29**, 702-707.
- Balastreire, L., Herum, F. & Blaisdell, J. (1982). Fracture of corn endosperm in bending. II. Fracture analysis by fractography and optical microscopy. *Transactions of the ASAE [American Society of Agricultural Engineers]*, **25**, 1062-1065.
- Chowdhury, M.H. & Buchele, W.F. (1976). Development of a numerical damage index for critical evaluation of mechanical damage of corn. *Transactions of the ASAE*, **19**, 428.
- Du Plessis, A., Seifert, T., Booysen, G. & Els, J. (2014). Microfocus X-ray computed tomography (CT) analysis of laser sintered parts. *South African Journal of Industrial Engineering*, **25**, 39-49.
- Girardin, P., Chavagnat, A. & Bockstaller, C. (1993). Determination of seed characteristics of maize (*Zea mays* L.) by use of X-ray radiography. *Seed Science and Technology*, **21**, 545-551.
- Gondek, E., Jakubczyk, E., Herremans, E., Verlinden, B., Hertog, M., Vandendriessche, T., Verboven, P., Antoniuk, A., Bongaers, E., Estrade, P. & Nicolaï, B.M. (2013). Acoustic, mechanical and microstructural properties of extruded crisp bread. *Journal of Cereal Science*, **58**, 132-139.
- Guelpa, A. (2013). Maize endosperm texture characterisation using the Rapid Visco Analyser (RVA), X-ray micro-computed tomography ( $\mu$ CT) and micro-near infrared (microNIR) spectroscopy. PhD in Food Science Thesis, University of Stellenbosch, South Africa.
- Gunasekaran, S., Cooper, T., Berlage, A. & Krishnan, P. (1987). Image processing for stress cracks in corn kernels. *Transactions of the ASAE*, **30**, 266-271.
- Gunasekaran, S., Deshpande, S., Paulsen, M. & Shove, G. (1985). Size characterization of stress cracks in corn kernels. *Transactions of the ASAE*, **28**, 1668-1672.
- Kim, T.H., Hampton, J.G., Opara, L.U., Hardacre, A.K. & Mackay, B.R. (2002). Effects of maize grain size, shape and hardness on drying rate and the occurrence of stress cracks. *Journal of the Science of Food and Agriculture*, **82**, 1232-1239.
- Laverse, J., Frisullo, P., Conte, A. & Nobile, M. (2012). X-ray microtomography for food quality analysis. In: *Food Industrial Processes—Methods and Equipment*. Pp. 339-362. InTech Open Publishers.
- Moreira De Carvalho, M.L., Van Aelst, A.C., Van Eck, J.W. & Hoekstra, F.A. (1999). Pre-harvest stress cracks in maize (*Zea mays* L.) kernels as characterized by visual, X-ray and low temperature scanning electron microscopical analysis: Effect on kernel quality. *Seed Science Research*, **9**, 227-236.
- Nath, A. & Chattopadhyay, P.K. (2008). Effect of process parameters and soy flour concentration on quality attributes and microstructural changes in ready-to-eat potato–soy snack using high-temperature short time air puffing. *LWT - Food Science and Technology*, **41**, 707-715.

- Razzaq, M.R., Anjum, F.M., Khan, M.I., Khan, M.R., Nadeem, M., Javed, M.S. & Sajid, M.W. (2012). Effect of temperature, screw speed and moisture variations on extrusion cooking behavior of maize (*Zea mays* L.). *Pakistan Journal of Food Sciences*, **22**, 12-22.
- Song, H.P. & Litchfield, J.B. (1994). Measurement of stress cracking in maize kernels by magnetic resonance imaging. *Journal of Agricultural Engineering Research*, **57**, 109-118.
- Song, H., Litchfield, J. & Morris, H. (1992). Three-dimensional microscopic MRI of maize kernels during drying. *Journal of Agricultural Engineering Research*, **53**, 51-69.